Communauté
UNIVERSITÉ Grenoble Alpes

THÈSE

Pour obtenir le grade de

DOCTEUR DE LA COMMUNAUTE UNIVERSITE GRENOBLE ALPES

Spécialité : **Physique**

Arrêté ministériel : 25 mai 2016

Présentée par

Boris BOLLIET

Thèse dirigée par **Aurélien BARRAU**, Université Grenoble Alpes

préparée au sein du **Laboratoire de Physique Subatomique et de Cosmologie de Grenoble**
dans **l'École Doctorale de Physique de Grenoble**

Au-delà de la relativité générale : certains aspects de la cosmologie quantique à boucles, des trous noirs et de l'univers sombre

Thèse soutenue publiquement le **24 juillet 2017**,
devant le jury composé de :

Gilles HENRI
Université Grenoble Alpes (Président)

Ruth DURRER
Université de Genève (Rapporteur)

Karim NOUI
Université de Tours (Rapporteur)

Dominique BOUTIGNY
Université Savoie Mont Blanc (Membre)

Patrick PETER
Institut d'Astrophysique de Paris (Membre)

Beyond Einstein's Theory of Gravitation: Some Aspects of Loop Quantum Cosmology, Black Holes and the Dark Universe

Boris Bolliet

Laboratoire de Physique Subatomique et de Cosmologie de Grenoble

Thèse présentée en vue l'obtention du grade de Docteur de l'Université de Grenoble

Directeur de thèse :	Aurélien Barrau	Université de Grenoble
Rapporteurs :	Ruth Durrer	Université de Genève
	Karim Noui	Université de Tours
Examinateurs :	Dominique Boutigny	Université Savoie Mont Blanc
	Gilles Henry	Université de Grenoble
	Patrick Peter	Institut d'Astrophysique de Paris

Aquí me pongo a principiar
sin querer hacer alarde,
de cómo se puso aparte
la tierra del ancho mar.
Habríase que remontar
a un tiempo muy pasado,
en que extraño estado
se hallaba la materia,
en tratando 'e cosa seria
en libros me he informao'.

No les trato del mandiga
ni del gran benefactor,
no hay santo ni pecador
ni hay la virgen encinta.
Escríbalo en fina tinta
sin cuidado en gramática,
yo voy en matemática
a explicar muy certero,
no hay Universo primero
sin mecánica cuántica.

No hallando la explicación
a esta verdad primera,
que así como en la Tierra
así sucede en Orión,
el Hombre con su noción
del espacio reaccionario,
dio en el imaginario
con solución precisa,
este mundo necesita
del Universo inflacionario.

No hay hombre sin su razón,
ni hay causa sin su efecto,
y a quien causó el movimiento
se le llamó el inflatón.
No termino este renglón
sin decir la verdad dura,
a esta esquiva criatura
nadie le ha visto el caracho
ni la ignorancia tiene cura.

Que lindo que seria
en afán de la cultura,
conocer de la natura
su color y geometría.
Cúanto tormento hallaría
el científico en su mente,
mas el sabio muy prudente
se concentra en lo indecible,
pues buscando lo imposible
el Hombre venció a la muerte.

Décimas Por Ciencia,
Del Universo Inflacionario,
Vicente Atal Chomali

Contents

List of Figures

List of Tables

Acknowledgments

I am very grateful to the members of the jury: Dominique Boutigny, Ruth Durrer, Gilles Henri, Karim Noui and Patrick Peter for having accepted to review my work.

Since I started my studies, some people are particularly inspiring and important to me: Louis Bolliet, Joseph Lazjerowicz, Hervé Lauret and my supervisor, Aurélien Barrau.

Je les remercie pour leur grande générosité, pour m'avoir accueilli et enseigné leur savoir, et surtout pour avoir partagé avec moi leur vision de la science et de son rapport avec l'humain.

Aurélien, un très grand merci à toi.

My research also benefited from the guidance of Paul Sorensen, Jerome Lauret, Richard Battye, Ivan Agullo, Eiichiro Komatsu, Julien Grain, Francesca Vidotto, Juan Macias Perez, Barbara Comis and Jakub Mielczarek. Also, I feel extremely lucky to have had the chance to interact with Carlo Rovelli, Abhay Ashtekar, Jorge Pullin, Parampreet Singh, Martin Bojowald, Eugenio Bianchi, Alejandro Perez and Simone Speziale. I am very grateful to them for having taken the time to answer my questions. A special thanks to Ivan who offered me one of nicest opportunities of these last three years: to work with him and Sreenath Vijaykumar on primordial non-gaussianity, during my five months residency at LSU. I thank Bella Leonard and Sylvain Perraud for the preparation they gave me when I was applying to the Fulbright commission.

In my day to day work it was a pleasure to discuss all kinds of ideas with fellow students and Post-docs: Vincent Bonnivard, Alexandre Ghelfi, Linda Linsefors, Susanne Schander, Marcelo Forets Irurtia, Sreenath Vijaykumar, Marios Christodolou, Tommaso De Lorenzo, Jibril Ben Achour, Francesco Pace, Vivian Poulin, Killian Martineau, Florian Ruppin, Flora Moulin, Javier Omedo, Esteban Mato Capurro, Brajesh Gupt and Beatrice Bonga.

I am grateful to ENS de Lyon, LPSC Grenoble and Université Grenoble Alpes for the great administrative and financial support.

The *Laboratoire de Physique Subatomique et de Cosmologie*, in Grenoble, was the best environment to carry out my research. I enjoyed all the discussions with the permanent members of my research group: David Maurin, Laurent Derome, Cécile Renault, Jean-Stéphane Ricol, Céline Combet, Laurence Perotto. I thank Benoit Clément, Frédéric Mayet, Laurent Derome, Jacob Lamblin, Frédéric Faure for their wise guidance over my teaching duties. I also thank the documentalist Emanuelle Vernay for her help regarding my bibliographical researches.

I acknowledge the Fulbright organization, Réseau Franco-Neerlandais, CPTGA, the University of Cracow, the University of Manchester, the organizing committees of the Lindau Nobel Laureate Meeting, the Marcel-Grossman Meeting, the LOOPS conferences, and the SIGRAV foundation for financial support. I am thankful to the departments of Physics at the University of Geneva, Radboud University, Penn-State University, Louisiana State University, Institut Henri Poincaré, Institut d'Astrophysique Spatiale, Insituto Galileo Galilei, and CPT Marseille for their hospitality. The CLASS school held by

Julien Lesgourgues, Thomas Tram and Benjamin Audren in 2014 at Universidad de Barcelona was essential to my apprenticeship of numerical tools for cosmology.

I would like to address a special thanks to Aurélien, Richard, Carlo, Juan, Ivan and Frédéric for supporting my applications to post-doctoral positions. To Jens Chluba and Scott Kay for giving me the opportunity to participate to their research, next year in Manchester.

I thank my family and friends for their support, Yoann Thony, Bella Leonard, Sophie Lapierre and Karim Azouaou, and in particular my mother Catherine Ben Sussan.

Forewords

The objective of my research is to probe the limits (or robustness) of General Relativity, by investigating alternatives to it in the light of the most recent astrophysical and cosmological data. In the beginning of this thesis, I present the historical and scientific context and give an overview of my results. My relevant publications are part of the manuscript. Since there exists a wide literature for both observational and theoretical cosmology, I have decided to discuss, in the accompanying text to the articles, only the key points that have important consequences, or which are particularly enlightening, with respect to the models concerned by my research.

In chapter I, I state the broad motivations that drive the research in the domain, emphasizing on my own personal motivations. Then, Chapter II is dedicated to Loop Quantum Cosmology. The phenomenology of black holes in quantum gravity is studied in Chapter III. Finally, I present my work regarding the phenomenology of dark energy and modified gravity theories in Chapter IV. This chapter contains two main parts, the first one is dedicated to a formalism aimed at describing the landscape of dark sector theories in a unified way. The second part presents the analysis I have done for constraining dark energy models based on the thermal Sunyaev Zel'dovich effect as measured by Planck. I show that the thermal Sunyaev Zel'dovich data from Planck can provide competitive constraints on the equation of state for dark energy.

List of publications

Published:

- Quantum-gravity phenomenology with primordial black holes – A. Barrau, B. Bolliet, M. Shutten, F. Vidotto, C. Weimer, arXiv:1609.02159, Proceedings of the 2015 Karl Schwarzschild Meeting on Gravitational Physics (2016).
- Conceptual issues in loop quantum cosmology – A. Barrau and B. Bolliet, Int.J.Mod.Phys. D25 (2016) no.08, 1642008, arXiv:1602.04452 (2016).
- The Equation of State Approach to Cosmological Perturbations in f(R) Gravity - B. Bolliet, R.A. Battye, J.A. Pearson, arXiv:1601.07585, Proceedings of the XIV Marcel Grossmann Meeting, World Scientific (2016).
- Observational exclusion of a consistent quantum cosmology scenario - B. Bolliet, A. Barrau, J. Grain, S. Schander, Phys.Rev. D93 124011, arXiv:1510.08766 (2016).
- Primordial scalar power spectrum from the Euclidean big bounce - S. Schander, A. Barrau, B. Bolliet, L. Linsefors, J. Mielczarek, J. Grain, Phys.Rev. D93 2, 023531, arXiv:1508.06786 (2016).
- f(R) as a dark energy fluid - R.A. Battye, B. Bolliet, J.A. Pearson, Phys.Rev. D93 4, 044026, arXiv:1508.04569 (2016).
- Phenomenology of bouncing black holes in quantum gravity: a closer look - A. Barrau, B. Bolliet, F. Vidotto, C. Weimer, JCAP 1602, 02 022 arXiv:1507.05424 (2016).
- Comparison of primordial tensor power spectra from the deformed algebra and dressed metric approaches in loop quantum cosmology - B. Bolliet, C. Stahl, J. Grain, L. Linsefors, A. Barrau, Phys.Rev. D91 8, 084035, arXiv:1502.02431 (2015).

Accepted for publication:

- Some clarifications on the duration of inflation in Loop Quantum Cosmology - B. Bolliet, A. Barrau, F. Moulin, K. Martineau, S. Schander, arXiv:1701.02282 (2017).
- Bouncing black holes in quantum gravity and the Fermi gamma-ray excess - A. Barrau, B. Bolliet, M. Schutten, F. Vidotto, arXiv:1609.02159 (2016).

In preparation:

- Probing the acceleration of the universe with the thermal Sunyaev-Zel'dovich power spectrum – B. Bolliet, B. Comis, E. Komatsu. J.-M. Perez.
- A unified framework for studying dark sector theories: the equation of state approach and its numerical implementation – B. Battye, B. Bolliet, F. Pace.
- Primordial non-gaussianity In Loop Quantum Cosmology – I. Agullo, B. Bolliet, V. Sreenath.

Chapter I

Motivations

In 2012, the Higgs boson was discovered at CERN and 2015 saw the first detection of gravitational waves. These are the last successes of quantum mechanics and general relativity. The two theories continue to be surprisingly accurate at describing the observable world: in the past one hundred years, not a single experiment has disproved general relativity or quantum mechanics. However, in the meantime, both theories fail at consistently describing nature on scales larger than the solar system and on scales smaller than the Planck length. For the dynamics of the large scale universe, cosmology, one manifestly needs at least two non standard ingredients in order to explain the observational data, namely dark matter and an additional fundamental constant, Λ.

In section I.1, I recall the main aspects of the paradigm in particle physics and cosmology nowadays. The 'dark universe' is the subject of section I.2 and the cosmological constant is discussed in section I.4.

Other observational data such as the cosmic microwave background temperature anisotropy and black holes are calling for a quantum theory of gravity. However, the fate of general relativity and quantum mechanics at the Planck scale and beyond is still unknown due to conceptual and technical difficulties arising in all attempts to quantize the gravitational field.

We discuss quantum gravity in section I.3. Finally, we close this chapter with section I.5 on 'theory and observation', emphasizing on the need for a unified description of dark sector theories in order to interpret the data of the forthcoming large scale surveys and maybe unveil some aspects of the fundamental theory lying beyond general relativity and the standard model of particle physics.

I.1 The paradigm in particle physics and cosmology

During the first decades of the twentieth century, quantum mechanics and general relativity were developed and brought to a stage of maturity that led to a deep understanding of the vast majority of the natural phenomena observed on Earth and in the cosmos. These two theories emerged from the extraordinary work of Albert Einstein who was the first to give a thorough description of the causal structure of spacetime and gravity, and who laid the basis of quantum mechanics. Of course, the development of the standard model of particle physics and general relativity was made possible by the growing accuracy and variety of experimental evidences, in particular using particle colliders and telescopes.

On Earth, to explain any phenomenon, it seems that one needs three types of elementary particles: leptons, quarks and bosons. These particles may interact through four types of forces: the strong interaction, the weak interaction, the electro-magnetic interaction and gravity. The theoretical framework which describes particles and their interactions, in its most elegant formulation, is written in the language of gauge theories. A symmetry group and a coupling constant corresponds to each one of the fundamental interaction. The standard model of particle physics can be recast as a Yang-Mills theory with total group $\mathrm{SU}(3) \times \mathrm{SU}(2) \times \mathrm{U}(1)$. In general relativity, the symmetry group of gravity

is the group of diffeomorphism. In addition, the underlying causal structure of the standard model is determined by the Lorentz group $\mathrm{SO}(3,1)$.

In the sky, the observations of the dynamics of remote stars and galaxies, the large scale structure of the universe that consists in clusters of galaxies located within a network of filaments, and the measurement of the temperature anisotropy of the cosmic microwave background radiation are all accounted for within a simple cosmological model ruled by Einstein's theory of gravity. The simplest cosmological model, the so-called Λ-Cold-Dark-Matter (ΛCDM) model, consists in a universe filled with standard matter (as described by the standard model of particle physics), dark matter and a scalar field (the inflaton field) which was dominating the energy content of the universe during its primordial era. The cosmological constant Λ can either be thought of as an additional fundamental constant of physics or as the effective outcome of some dark energy component. The dark sector of the universe (dark matter and maybe dark energy), at the level of accuracy of our current experiments, has a single property: it interacts with standard matter only through gravity.

I.2 The dark universe

Present measurements suggest that the matter component of the universe today is made of sixteen percent standard matter and eighty-four percent invisible dark matter, while the total energy density of the universe is being dominated by the cosmological constant (sixty-nine percent). Most of the universe is *dark*. And whatever dark matter is, it is not expected within the standard model of particle physics. The inflaton field could be the Higgs field of the standard model [35], or it could also be a new scalar field. But even if the inflaton field is the Higgs field, some non-standard modification to gravity and the standard model (non-minimal coupling or supersymmetry) are required in order to generate an acceptable inflationary phase.

Dark matter and the inflaton field hypothesis are crucial. On one hand, the necessity of introducing a dark matter component to the universe first arises in astronomy in order to explain the observed velocities of stars. It is also a necessity in cosmology: standard matter *falls* into the gravitational wells formed by dark matter. On the other hand, the inflaton field, thanks to the quantum fluctuations of its vacuum state, is the most successful proposal for explaining the mechanism behind the generation of cosmological perturbations that determines the temperature anisotropy of the CMB and the large scale structure of the universe.

To summarize, as soon as we start probing the cosmos on scales larger than the solar system, the universe is mostly dark and has to include at least an extra scalar field (the inflaton). Considering that the standard model of particle physics gives indeed the correct picture, so we do not expect additional particles, a question naturally comes to our mind: Can Einstein's theory of gravity be trusted on cosmological scales? It is remarkable that Einstein's theory allows to interpret the dark sector component as a modification to general relativity. For instance, in Tensor-Vector-Scalar (TeVeS) gravity proposed by Bekenstein in 2004 [27], the weak field limit yields the famous modified Newton dynamics (MOND) [120] introduced by Milgrom in 1983 to explain the galaxy rotation curves. Another important example is the $\mathcal{R}^2$ modification to general relativity, invented by Starobinsky in 1980 [145], which appears as the inflaton field (after applying a conformal transformation to the metric [68]).

Currently, the most popular view on dark matter is that it is made of exotic particles predicted within supersymmetry (gravitinos and WIMP), extra dimension theories (Kaluza-Klein particles) and Peccei-Quinn theory (axions). Other suitable dark matter candidates, which do not require any modifications to the standard paradigm, are primordial black holes, as we shall see in part III of this thesis. So, there are various possibilities for Einstein's theory not to be blamed for the presence of dark matter if it is due to a new particle. But, there are motivations to look for theories beyond general relativity, if dark matter is actually resulting from a modification to gravity.

I.3 Quantum gravity

The main motivation to look beyond GR certainly comes from quantum gravity: What happens to the gravitational field in the quantum regime? Physics has to address this question. Indeed, the standard cosmological scenario predicts that the universe started from a spacetime singularity, the 'Big Bang', when the gravitational field (or more exactly the Kretschmann scalar, $R_{\mu\nu\sigma\rho}R^{\mu\nu\sigma\rho}$) becomes infinite. In addition, the recent detection of gravitational waves by the LIGO collaboration [60] comes as a strong evidence for the existence of black holes, another type of spacetime singularities. For all of the fields that we know, there is a scale at which one needs to invoke the laws of quantum mechanics to describe their properties. Spacetime, or the gravitational field, shall also become quantum at some scale. The apparent existence of spacetime singularities is a hint that the quantum regime of the gravitational field is realized in nature and it calls for a consistent theoretical description of this regime. Based on Heisenberg's uncertainty principle [85], a famous argument initially stated by Bronstein in 1936 [43] shows that the minimal size at which a particle can be located before being hidden by its own horizon is the Planck length,

$$\ell_{\rm Pl} = \sqrt{G} \sim 10^{-33}\text{cm}. \tag{I.1}$$

Therefore, beyond this scale, the gravitational field has to be described by the quantum theory: particles can no longer be viewed as quantum fields on a smooth background spacetime because spacetime itself, the metric, becomes 'fuzzy'. This led Wheeler to introduce the notion of quantum foam in 1955 [158] and DeWitt in 1966-68 to write down a Schrödinger equation for the wave function describing the quantum states of the gravitational field, known as the Wheeler-DeWitt equation [67]. There are many ways that are being explored to arrive at a consistent quantum description of gravity, with general relativity as the classical limit, but still, none of these proposals has managed to gain a wide acceptance in the community for two reasons: a lack of mathematical consistency and a lack of experimental predictions. Nevertheless, a lot of efforts are being deployed in order to address these two points.

In the first and second part of this thesis, we investigate some of the observational implications of Loop Quantum Gravity (LQG) which is an attractive theory of quantum gravity. It is tempting to believe that the correct description of quantum gravity would lead, at low energy, to a modification to general relativity (such as the one proposed by Starobinsky) suggesting a way to generate inflation without having to add any extra scalar field (or exotic properties to the Higgs field) to the standard model. Very recently, some interesting directions have been explored regarding this point. For instance in [111], Liu, Noui, Wilson-Ewing and Langlois have made a significant contribution in an effort to obtain the effective equation of Loop Quantum Cosmology from more general scalar-tensor theories. And in the latest work of Smolin [143], MOND is identified as the $\hbar \to 0$, $c \to \infty$ regime of quantum gravity.

Apart from dark matter and quantum gravity, there are motivations to look beyond general relativity that can be labeled as *aesthetic* or *unifying* motivations. After the success of the standard model and the discovery of the Higgs boson in 2012 [1, 53], which confirms our understanding of the electroweak symmetry breaking mechanism that dates back to the work by Brout, Englert and Higgs in 1964, one would be keen to try building a unified theory of the four fundamental interactions. Such theory would therefore encompass quantum gravity. The most advanced theory with those ambitions is String Theory. Let us pause for a moment and recall the historical background of String Theory. The unified description of electromagnetism and the weak interaction was proposed more than fifty years ago by Glashow, Salam and Weinberg, starting in 1961 [77]. Soon after, at the time of the first observational evidences for the electroweak interaction (weak neutral currents in neutrino scattering in 1973 and discovery of the W and Z bosons in 1983) the foundations of string theory were laid by Nambu, Nielsen and Susskind. Note that Nambu is also the inventor in 1960 [125] of the spontaneous symmetry breaking scheme that inspired Brout, Englert and Higgs. Today, String Theory relies on a supersymmetric extension of the standard model of particle physics and at least six additional spacetime

dimensions. It has led to mathematical results which are regarded as some of the most important discoveries in theoretical physics in the last few decades, such as the AdS/CFT correspondence found by Maldacena in 1997 [115]. But so far, after these fifty years of continuous effort, no clear experimental predictions have been extracted from String Theory. This is mainly due to the fact that the low energy limit of the theory is unknown. Moreover, String Theory is built on a metric space where gravity appears perturbatively as some excitations of strings, and therefore the core idea that, beyond Planck scale, spacetime itself is quantum can not be addressed as long as String Theory is not written in a non-perturbative manner. Maldacena's result on AdS/CFT is certainly a key step in this direction, however non-perturbative String Theory still remains mysterious and difficult to formulate.

I.4 The cosmological constant

A large part of the recent research dedicated to exploring alternatives to Einstein's theory has been motivated by the observation that the universe is presently in a phase of accelerated expansion. The decisive measurements were made by two teams of astronomers (Supernova Cosmology Project and High-Z Supernova Search Team) and published in 1998 [130, 137]. They observed the luminosity of distant supernovae and concluded that the best way to explain the change of luminosity with the distance was to assume a Λ dominated Friedmann-Lemaître-Roberston-Walker (FLRW) universe. So, as it appears, the universe undergoes a phase of accelerated expansion at both ends of its history: inflation in the primordial era and the contemporary acceleration. This might be a coincidence but one can not exclude that the same mechanism could be at work, allowing to explain both phases in a unified way. Although such unification is very challenging (the energy scale of inflation is more than twenty order of magnitude larger than the temperature of the universe today) some work has been done in this direction, for instance the unified phantom cosmological model where the same scalar field plays the role of the inflaton and the cosmological constant [49]. There could at least be some connections between inflation and the present acceleration. In particular, as inflation is dynamical in the sense that it stopped after some time, one tempting assumption is that the observed acceleration of the universe may also end. These speculations have led to a vast amount of models (quintessence dark energy models) where the present acceleration is driven by a scalar field [152]. Some are exploring the possibility of interacting and decaying dark energy [155] and claim that such models can solve the so-called *coincidence problem*.

The *coincidence problem*, along with the *cosmological constant problem*, are most of the time presented as the main motivations to look for theories beyond general relativity. What is striking is that the new models generally end up not addressing these 'problems', or if they do, some new problems appear. In the unified phantom or quintessence dark energy models, for example, a new scalar field is added and its properties, such as its potential, have to be tuned to mimic the cosmological constant. Details and a standard discussion on the *cosmological constant* and *coincidence problems* can be found in [52]. Here I state them in their simplest versions.

The *coincidence problem* arises when one looks at the history of the universe in terms of its dominating components. As it appears, the universe starts being radiation dominated during a brief phase of 10^4 years, then it is dominated by matter for about 10^9 years, and it is dominated by the cosmological constant for the last ten billion years. Said in this way, there is nothing surprising in the fact that we live in a dark energy dominated epoch, on the contrary the dark energy dominated epoch is the longest. But retracing the history of the universe, not in terms of cosmic time, but in terms of redshift z, the numbers are different. The cosmological constant happens to dominate only since $z \approx 2$, which is an extremely 'short' period compared to, for instance, the eight orders of magnitude of redshift spent since big bang nucleosynthesis. One can bring some probability calculations into the discussion, and find that the fact that we are living precisely when Ω_{m} and Ω_Λ are of the same order is extremely unlikely. This is referred to as the *coincidence problem* and has motivated people to explore

alternatives to the cosmological constant, or invoke an anthropic principle, to explain why we live in such an unlikely era. Personally, I am of the same opinion as Rovelli and Bianchi: "there is nothing rigorous nor convincing in the coincidence problem"[37]. The formulation of the coincidence problem is subject to a large arbitrariness in the choice of the prior probability distribution function for Ω_Λ.

The *cosmological constant problem* refers to the difficulties encountered when trying to explain or predict the value of the measured cosmological constant. The measurements of the accelerated expansion, combined with the CMB data, yield $\Omega_\Lambda = 0.686^{+0.017}_{-0.018}$ (Planck 2015 + JLA, 95% C.L.). The corresponding energy density is

$$\rho_\Lambda \simeq 10^{-120} \mathrm{M}_{\mathrm{Pl}}^4. \tag{I.2}$$

As early as 1968, Zel'dovich realized that the cosmological constant could be related to the vacuum energy of the fields filling the universe [161]. Hence, the measured cosmological constant should in fact be a sum of a contribution coming from vacuum energy and a contribution that simply is the 'bare' cosmological constant of Einstein's equation. The bare cosmological constant is seen as a fundamental constant of Physics and the measured cosmological constant is an effective cosmological constant. Considering that the quantum field theory which describes the standard model of particle physics is valid up to the Planck scale, one concludes that the energy density related to the vacuum energy has to be of the order of $\mathrm{M}_{\mathrm{Pl}}^4$. To accommodate this educated guess with the observed effective cosmological constant, it requires the bare cosmological constant to be adjusted over one hundred and twenty decimal places. This sounds unnatural, but can this really be a motivation for exploring alternatives to Einstein's theory? To me, the underlying problem has to be addressed from the perspective of quantum field theory rather than gravitation, especially because Renormalization and even the concept of vacuum energy are not yet fully understood in flat QFT and even less in QFT on curved spacetime [127, 126, 89, 37]. On this lines, in a very recent article, Wang, Zhu and Unruh have proposed a new calculation of the vacuum energy in cosmology which avoids the cosmological constant problem [156].

So, one could argue that the *cosmological constant problem* and the *coincidence problem* should not be regarded as serious motivations to look for theories beyond Einstein's general relativity. However, the observational evidences for dark matter, inflation and black holes are definitely calling for new ingredients in our present theories.

I.5 Theory and observations

In any cases, whatever the motivations are, there has been a large number of dark energy, modified gravity and quantum gravity models that appeared in the last few years and therefore we do need a coherent phenomenological framework to compare these models to one another and confront them to observational data. This becomes more urgent as the next generations of galaxy surveys and CMB experiments are getting ready to take data. As stated by Planck collaboration, the three main difficulties that were faced in their analysis on dark energy and modified gravity were: (i) a lack of a comprehensive phenomenological framework, (ii) robust constraints on the models can only be achieved with a combination of data sets coming from different probes and the analysis of the degeneracy with systematic errors becomes intricate, (iii) the lack of well tested numerical codes [6].

In the third part of this manuscript, I address the first and the last points thanks to the Equation of State (EoS) approach to cosmological perturbations in the dark sector and its implementation in the Boltzmann code CLASS [105].

The most well-known phenomenological approach for beyond ΛCDM cosmology is certainly the Effective Field Theory (EFT) for inflation introduced in 2007 [54]. It allowed to describe all single field inflationary models in a common language and proved itself to be very efficient for deducing observational constraints related to non-gaussianity [23]. The idea behind an EFT approach is to parametrize all the degrees of freedom of the most general Lagrangian deduced from the symmetries of the physical system. The procedure was applied to dark energy, quite simultaneously by four teams of

cosmologists starting in 2011 leading to: the parametrized post-Friedmann (PPF) formalism [20], the effective field theory of dark energy (EFT for DE) [78, 28] and the EoS approach [25]. The common goal of these approaches is to provide a unified formulation of the dynamics of cosmological perturbations on a Friedmann-Lemaître-Robertson-Walker (FLRW) background.

In the effective field theory for dark energy, five time-dependent functions are required to characterize the evolution of cosmological perturbations, while the EoS approach requires eight time-dependent functions. The parametrized post-Friedmann framework is a direct parametrization of the departure from Einstein's equation given a dark energy or modified gravity model. As we shall see, the three approaches are equivalent: one can be rewritten in the language of the other. The EFT for DE can be seen as a generalization of Horndeski theories (or Generalized Gallileons [65]). Horndeski theories were introduced in [90] as the most general scalar-tensor theories with at most second order equations of motion, while the EFT for DE also includes theories with higher order equations of motion that avoid Ostrogradsky instabilities. In Horndeski theories, or EFT for DE, the starting point is to write the most general action respecting some symmetries and dynamical requirements. This differs from the EoS approach, where, as we shall see, the starting point is to parametrized the anisotropic stress (gravitational shear) and perturbed pressure of the dark energy fluid component. In PPF and EFT for DE, the whole set of Einstein's equations are modified non-trivially, unlike in the EoS approach where the departure from ΛCDM is recast as an effective fluid described by a standard stress-energy tensor. It may seem redundant and unnecessary that three equivalent formalisms are being developed. However, in these early days of dark energy phenomenology, it is healthy to have competing frameworks: the results obtained in one framework can be confirmed in the other.

Chapter II

Towards a consistent description of the early universe: Loop Quantum Cosmology

The Big Bang, a term coined by Fred Hoyle in 1949, is a word used to hide our ignorance regarding the early universe. Mathematical General Relativity predicts that a space-time singularity at early times is unavoidable for a universe filled with standard matter and dark energy. In fact, in the vicinity of the singularity the space-time curvature becomes so high, as the energy density diverges towards infinity, that Einstein's theory can no longer be used on its own to describe the laws of nature. This motivates the search of a quantum theory of gravitation. Once found, this theory will enable us to revisit the high curvature regime of GR and answer the questions: What does nature look like at the Planck scale? Does the notion of 'singularity' survive in this regime, or is it replaced by a different description?

Loop Quantum Gravity (LQG) is a candidate theory of quantum gravity pioneered by Ashtekar, Rovelli and Smolin in the early 80's. In this chapter, I explore its potential phenomenological consequences for the first moments of the universe. In the first section II.1, we present the Hamiltonian constraint in classical GR. The effective equations of LQC and the area gap are introduced in section II.2. Then, from section II.3 to section II.8, we review the technical steps that lead to the modified Friedmann equations of LQC: the Holst action, Ashtekar Variables and loop quantization. Section II.10 and II.11 are dedicated to the background evolution and the duration of inflation in LQC. In section II.12, the key aspects of the theory of cosmological perturbations as developed within the inflationary paradigm are recalled. Two approaches for perturbations in LQC are presented in section II.13. Finally, in section II.14 I have reported my articles and results on the topic.

II.1 The Friedmann equation

Loop quantum cosmology (LQC) refers to a set of cosmological models deduced from the canonical version of Loop quantum gravity (LQG) restricted to homogeneous spacetime. And here we will focus particularly on the flat FLRW spacetime with scale factor $a\,(t)$ and lapse function $N\,(t)$. Due to time re-parametrization invariance the lapse function is only a Lagrange multiplier, so the flat FLRW spacetime has only one dynamical degree of freedom, namely the scale factor. Furthermore, we introduce a minimally coupled scalar field, φ, as the matter content. LQC provides a clear method to arrive at a quantum formulation of this dynamical system.

The phase space is four dimensional, the coordinates are (a, ϕ), and their canonically conjugated momentum are (π_a, π_φ). The expressions of the canonical momenta in terms of the time derivative of the coordinates read: $\pi_\varphi = a^3 \frac{\dot{\varphi}}{N}$, and $\pi_a = -6a\frac{\dot{a}}{N}$, as obtained from the Hamiltonian equations. In GR the Hamiltonian for a free scalar field, minimally coupled to the flat FLRW metric is

$$\mathcal{H}^{\mathrm{GR}} = N\left\{\tfrac{1}{2}a^{-3}\pi_\varphi^2 - \tfrac{1}{12}a^{-1}\pi_a^2\right\}. \tag{II.1}$$

The Euler-Lagrange equation for the lapse function, being a Lagrange multiplier, implies that the Hamiltonian (II.1) vanishes for the solutions to the dynamics. This is the Hamiltonian constraints, which for the flat FLRW universe is equivalent to the *scalar* constraints. In standard GR, the scalar constraint is nothing else than the Friedmann equation,

$$H^2 = \tfrac{1}{3}\rho, \tag{II.2}$$

where $H = \frac{\dot{a}}{a}$, and ρ is the energy density (for the free scalar field, $\rho = \frac{1}{2}\dot{\varphi}^2$).

II.2 The area gap in loop quantum gravity

In the effective approach to LQC, the scalar constraint does not reduce to the Friedmann equation, but to a modified Friedmann equation,

$$H^2 = \tfrac{1}{3}\rho\left(1 - \frac{\rho}{\rho_{\mathrm{B}}}\right), \quad \text{with} \quad \rho_{\mathrm{B}} \equiv \frac{3}{\gamma^2\lambda^2} \tag{II.3}$$

where γ is the Barbero-Immirzi parameter and λ is the so-called area gap. Let us explain the meaning of these two new objects characteristic to LQG, γ and λ, and how one can arrive at this formula.

One of the most important result of LQG, obtained in 1994 by Rovelli and Smolin [138], is that area and volume are represented by operators that have discrete eigenvalues. For instance, the area operator, being algebraically similar to the angular momentum, has eigenvalues $A_j = \gamma\sqrt{j\,(j+1)}$. The area gap, is defined as the smallest non-zero eigenvalue of the area operator, so

$$\lambda^2 \equiv A_{j=\frac{1}{2}} = \tfrac{\sqrt{3}}{2}\gamma. \tag{II.4}$$

To see where the Barbero-Immirzi parameter comes from, we need to take a few steps backward and start from the action for gravity (no scalar field or matter).

II.3 The Holst action

The action for the gravitational field may be written in several different ways which are equivalent to one another, for pure gravity (no fermions) in the classical theory, up to boundary terms.

The Einstein-Hilbert action is written in terms of the metric tensor, $g_{\mu\nu}$, and the Ricci scalar, $\mathcal{R}$, itself being a function of the metric tensor. The connection, ∇_μ, is metric compatible and torsion free, by assumption (Levi-Civita connection). This leads to the well known expressions of the Christoffel symbols, Riemann tensor and Ricci scalar, in terms of the metric tensor. One can then vary the Einstein-Hilbert action with respect to $g_{\mu\nu}$ and obtain Einstein's field equation.

An alternative approach is to view the action as a function of the metric *and* the connection, no longer assuming it metric compatible and torsion free *ab initio*. This yields the *first-order* formulation of GR (in opposition to the *second-order* formulation where the metric is the only variable), the starting point of LQG. In fact, in the first-order formulation, the basic variables are not the metric tensor and the connection but the tetrad, e, and the Lorentz connection, ω. The (Holst) action reads:

$$\mathcal{S}\,[e,\omega] \equiv \int e\wedge e\wedge F^\star + \frac{1}{\gamma}\int e\wedge e\wedge F, \quad \text{with} \quad F = \mathrm{d}\omega + \omega\wedge\omega. \tag{II.5}$$

Had we not written the second term proportional to the inverse of the Barbero-Immirzi parameter, the Holst term, this action would reduce to the so-called Palatini action. The tetrad one-form[1], e^I, are the building blocks of the metric:

$$g = g_{\mu\nu}\mathrm{d}x^\mu\otimes\mathrm{d}x^\nu = \eta_{IJ}e^I_\mu e^J_\nu \mathrm{d}x^\mu\otimes\mathrm{d}x^\nu = \eta_{IJ}e^I\otimes e^J, \tag{II.6}$$

[1] Also called co-tetrad, coframe fields, veirbein, while its associated vector field is known as tetrad, fram field, dreiben.

in other words, they map the tangent space at every point of spacetime to the local inertial frame where the metric is Minkowski, η_{IJ}. The vector fields associated to the tetrad one-forms, defined via $e^I_\mu e^\mu_J = e^I e_J = \delta^I_J$, are therefore orthonormal to one another:

$$g\left(e_I, e_J\right) = \eta_{KL} e^K \otimes e^L\left(e_I, e_J\right) = \eta_{IJ}. \tag{II.7}$$

Having specified a spacetime point, let us apply a local Lorentz transformation, $\Lambda \in \mathrm{SO}\left(3,1\right)$, to the tetrad one-form. So, e^I is mapped to $\Lambda^I_J e^J$ while the metric is invariant under such transformation because, obviously, $\eta_{IJ}\Lambda^I_K\Lambda^J_L = \eta_{KL}$ and so will be the action. Therefore, in the first-order formulation of GR, there is a local Lorentz gauge invariance. From the lessons learned in Yang-Mills theory, a connection is associated to the local gauge invariance in order to define parallel transport with respect to the gauge group of transformations. Here, it is the Lorentz connection (sometimes called the spin connection), ω, which therefore is a one-form with values in the Lie algebra of the Lorentz group:

$$\omega^{IJ} = \omega^{IJ}_\mu \mathrm{d}x^\mu = -\omega^{JI}_\mu \mathrm{d}x^\mu. \tag{II.8}$$

Varying the Holst action (II.5) with respect to the spin connection, one gets that the Lorentz connection has to be metric compatible and torsion free (Levi-Civita), namely

$$\frac{\delta \mathcal{S}}{\delta \omega} = 0 \;\Rightarrow\; \mathrm{d}e^I + \omega^I_J \wedge e^J = 0. \tag{II.9}$$

Using (II.9), the curvature two-form of the Lorentz connection, F, can be expressed in terms of the components of the Riemann tensor,

$$F^{IJ} = e^I_\mu e^J_\nu R^{\mu\nu}_{\rho\sigma} \mathrm{d}x^\rho \wedge \mathrm{d}x^\sigma. \tag{II.10}$$

The variation with respect to the tetrad yields Einstein's field equations. Note that (II.10) implies that the Holst term vanishes:

$$\int e^I \wedge e^J \wedge F_{IJ} = \int \epsilon^{\mu\nu\sigma\rho} R_{\mu\nu\sigma\rho} \sqrt{|g|} \mathrm{d}x^0 \wedge \mathrm{d}x^1 \wedge \mathrm{d}x^2 \wedge \mathrm{d}x^3 = 0, \tag{II.11}$$

in virtue of the fact that the antisymmetric part of the Riemann tensor is zero. This explains why the Holst term plays no role in the classical dynamics. However, it is a crucial ingredient for the quantum theory, like we will see.

II.4 The ADM formalism

Our next step is to follow the prescriptions of the ADM formalism (3+1 split) and use Ashtekar variables to write down the Hamiltonian corresponding to the Holst action. The metric tensor is written as

$$g = \left(-N^2 - N_a N^a\right) \mathrm{d}t \otimes \mathrm{d}t + 2N_a \mathrm{d}t \otimes \mathrm{d}x^a + q_{ab} \mathrm{d}x^b \otimes \mathrm{d}x^a, \tag{II.12}$$

with N the lapse function and N_a the shift function. The 3+1 split induces a 3-metric q_{ab}, and its associated co-frames, the triad one-forms e^i_a:

$$q = q_{ab} \mathrm{d}x^a \otimes \mathrm{d}x^b = \delta_{ij} e^i_a e^j_b \mathrm{d}x^a \otimes \mathrm{d}x^b = \delta_{ij} e^i \otimes e^j. \tag{II.13}$$

The extrinsic curvature of the spatial hyper-surface is

$$K = K_{\mu\nu} \mathrm{d}x^\mu \otimes \mathrm{d}x^\nu = \frac{1}{2N}\left(\dot{q}_{ab} - D_{(a} N_{b)}\right) \mathrm{d}x^a \otimes \mathrm{d}x^b, \tag{II.14}$$

where the dot means a time derivative and D_a is the connection associated with the spatial metric q_{ab}. While the one-form normal to the spatial hyper-surface is

$$n = n_\mu \mathrm{d}x^\mu = -N\mathrm{d}t. \tag{II.15}$$

The Gauss-Codazzi equation enables us to write the Ricci scalar, $\mathcal{R}$, in terms of the Ricci scalar, R , relative to the 3-metric q:

$$\mathcal{R} = R + K_{ab}K^{ab} - K^2 + 2\nabla_\mu \left(Kn^\mu - n^\rho \nabla_\rho n^\mu\right), \text{ with } K = K^a_a \tag{II.16}$$

where ∇_μ is the connection associated with $g_{\mu\nu}$. Then, the Einstein-Hilbert action reads

$$\mathcal{S} = \int N\left(R + K_{ab}K^{ab} - K^2\right)\sqrt{|q|}\mathrm{d}t \wedge \mathrm{d}x^1 \wedge \mathrm{d}x^2 \wedge \mathrm{d}x^3. \tag{II.17}$$

For which the Hamiltonian analysis yields$\mathcal{H} = NC + N^a C_a$,with

$$C = |q|^{-\frac{1}{2}} P^{ab}P_{ab} - \sqrt{|q|}R, \text{ and } C_a = 2D_b P^b_a, \tag{II.18}$$

the so-called scalar (or Hamiltonian) and vector (or diffeomorphism) constraints respectively. We have introduced the canonical momentum of the three-metric,

$$P_{ab} = \frac{\partial \mathcal{L}}{\partial \dot{q}^{ab}} = \frac{\partial \mathcal{L}}{\partial K^{cd}}\frac{\partial K^{cd}}{\partial \dot{q}^{ab}} + \frac{\partial \mathcal{L}}{\partial K}\frac{\partial K}{\partial \dot{q}^{ab}} = \sqrt{|q|}\left(K_{ab} - Kq_{ab}\right), \tag{II.19}$$

where $\mathcal{L}$ is the Lagrangian density which appears as the integrand of the action (II.17). Since the lapse and shift functions are Lagrange multipliers, these constraints have to vanish for the dynamical trajectories.

II.5 The Ashtekar variables

The Hamiltonian analysis of the Holst action, in the first-order formalism, can be done in a similar way. The role of the Lorentz connection, ω, is taken by the torsionless spin connection of the triad, Γ, which therefore satisfies the first Cartan equation with respect to the triad one-form,

$$\mathrm{d}e^i + \epsilon^i_{jk}\Gamma^j \wedge e^k = 0.$$

The spin (or Levi-Civita) connection, $\Gamma^i = \frac{1}{2}\epsilon^i_{jk}\Gamma^{jk}$, is now associated to the gauge group SO (3). It is a one-form with values in the Lie algebra of the three-dimensional group of rotations, that is su (2).

Loop Quantum Gravity started when Sen in 1982 and Ashtekar in 1986 noted that the Hamiltonian analysis of the first-order formalism was greatly simplified when choosing the following canonically conjugated variables:

$$\begin{aligned} A^i &= A^i_a \mathrm{d}x^a &&= \left(\Gamma^i_a + \gamma K^i_a\right)\mathrm{d}x^a, \\ E_i &= E^a_i \partial_a &&= \tfrac{1}{2}\epsilon_{ijk}\epsilon^{abc}e^j_b e^k_c \partial_a = \tfrac{1}{2}|e|\, e^a_i \partial_a. \end{aligned} \tag{II.20}$$

These are respectively the su (2) valued Sen-Ashtekar-Barbero (SAB) connection one-form, and its canonically conjugated variable, the electric field E_i. With these variables, the Hamiltonian and diffeomorphism constraints read

$$C = |e|^{-1} E^a_i E^b_j \left\{\epsilon^{ij}_k F^k_{ab} - 2\left(1+\gamma^2\right)K^i_{[a}K^j_{b]}\right\}, \tag{II.21}$$

$$C_a = F^i_{ab}E^b_i, \tag{II.22}$$

$$G^i = D_a E^{ai}, \tag{II.23}$$

where we have supplemented the set of constraints with the so-called Gauss constraints, G^i, to account for the local SO (3) gauge invariance. We have also introduced the curvature of the SAB connection,

$$F^i_{ab} = \partial_a A^i_b - \partial_b A^i_a + \epsilon^i_{jk} A^j_a A^k_b. \tag{II.24}$$

Again, since the constraints II.21,II.22,II.23 are multiplied by Lagrange multipliers in the Hamiltonian, they have to vanish for the dynamical trajectories. In the next section we apply this procedure to the FLRW universe with a free minimally coupled scalar field.

II.6 The FLRW model with Ashtekar variables

From the results given above, the total FLRW Hamiltonian for a free scalar field may be written as

$$\mathcal{H} = \int \mathrm{d}^3x \left\{ N \left(\tfrac{1}{2} a^{-3} \pi_\varphi^2 - C \right) - N^a C_a - \beta^i G_i \right\}, \tag{II.25}$$

where $\beta = \beta^i \tau_i = -\frac{i}{2}\beta^i \sigma_i$ is a su (2) vector. As we are now considering a spatially flat and homogeneous model, the SAB connection and the electric field must have the form

$$E_i = p \delta^a_i \partial_a \quad \text{and} \quad A^i = c \delta^i_a \mathrm{d}x^a, \quad \text{with} \quad p \equiv a^2 \quad \text{and} \quad c \equiv \gamma \frac{\dot{a}}{N}. \tag{II.26}$$

Indeed, due to homogeneity the (spatial) spin-connection vanishes, $\Gamma^i = 0$, and the extrinsic curvature is $K^i_a = \frac{\dot{a}}{N}\delta^i_a$. Note that the phase space variables (c, p) are canonically conjugated. The vector constraint is automatically satisfied as well as the Gauss constraints, while the scalar 'gravitational' constraint reduces to $C = 3a \left(\frac{\dot{a}}{N}\right)^2$. Hence, one recovers the standard GR Hamiltonian II.1 and the Friedmann equation. The Barbero-Immirzi parameter is still absent in the dynamics.

II.7 Discreteness from loop quantization

To move to the quantum theory, and the original ideas of Rovelli and Smolin, we consider the holonomy of the SAB connection. This provides us with a mathematically well defined operator, and one can proceed to the Dirac quantization of the Poisson brackets. However we do not need to go into these details.

We first observe that the curvature of the SAB connection can be expressed in terms of the holonomy around a closed loop. In classical GR, starting with the holonomy one would need to take the limit in which the loop encompasses a surface whose area tends to zero, in order to evaluate the curvature appropriately. Then, as mentioned above, a prescription from LQG is that the minimal area gap is λ (II.4). Hence, in the limit where the area inside the closed loop tends to λ, the curvature of the SAB connection reads

$$F^i_{ab} = -\frac{\sin^2(\bar{\mu}c)}{\bar{\mu}^2}\epsilon^i_{ab} - \frac{\sin(\bar{\mu}c)\left[1-\cos(\bar{\mu}c)\right]}{\bar{\mu}^2}\left(\delta^i_a - \delta^i_b\right), \quad \text{with} \quad \bar{\mu} = \frac{\lambda}{a} \tag{II.27}$$

the comoving area gap. This can be plugged into (II.21), to obtain the effective 'holonomy corrected' Hamiltonian constraint:

$$N\left\{\frac{\pi_\varphi^2}{2V} - \frac{3}{\gamma^2}\frac{\sin^2(\bar{\mu}c)}{V^{\frac{2}{3}}\bar{\mu}^2}\right\} = \frac{N}{V}\left\{\rho - N^2\rho_{\mathrm{B}}\sin^2(\bar{\mu}c)\right\} = 0 \ \text{ with } \ V = p^{\frac{3}{2}} = a^3, \tag{II.28}$$

where we used $\rho = \frac{N^2}{2V^2}\pi_\varphi^2$. It is easy to see that when λ is artificially taken to zero, or ρ_{B} to infinity, one recovers the standard Hamiltonian constraint (II.1). But in LQG, λ is finite and positive. One finds that the energy density of the scalar field relates to the geometry as follows

$$\rho = \rho_{\mathrm{B}}\sin^2(\bar{\mu}c), \tag{II.29}$$

where we have set $N = 1$. This constraints the energy density to always be smaller than $\rho_{\rm B}$, and suggests that there can not be a singularity such as the big bang, where the energy density is infinite.

II.8 The modified Friedmann equation

In order to derive the modified Friedmann equation given at the beginning of this chapter, we write the Hamilton equation for the variable V,

$$\dot{V} = \{V, C\} = \sqrt{\rho_{\rm B}} V \sin(\bar{\mu}c) \cos(\bar{\mu}c) = V\sqrt{\rho\left(1 - \frac{\rho}{\rho_{\rm B}}\right)}, \tag{II.30}$$

where we used the constraint (II.29) to obtain the last equality. So the volume of a physical region $V \propto a^3$ can not be arbitrarily small in the past. Indeed, when the energy density reaches $\rho_{\rm B}$ the volume is at its minimum value, $\dot{V} = 0$. The effective cosmological model we are considering is in fact a bouncing cosmology.

This is a beautiful results, onto which relies most of the phenomenology of LQC. Two remarks are in order here. First, we note that we could have initially assumed the scalar field to be minimally coupled with a potential and arrive at the same result, by including the potential energy in the definition of the total energy density ρ. Second, is this an original results? Has it been considered in other theoretical frameworks? The only example (I am aware of) were a term quadratic in the energy density appears in the RHS of the Friedmann equation is the Randall-Sundrum model proposed in 1999 [135]. However, in this String Theory motivated model, with extra spacetime dimensions, the quadratic term contributes positively to the spacetime curvature and can not lead to singularity avoidance, or a bounce [59].

II.9 Bouncing cosmologies

In the first part of this section we discuss the issue of trans-Planckian modes. Then, we present a model analogous to the LQC bounce, namely: the de Broglie-Bohm bounce. Finally, we briefly state the main consequences of anisotropy in bouncing models.

II.9.1 Trans-Planckian scales

I refer to Peter and Brandenberger [42] for a recent review on bouncing cosmologies. Bouncing cosmological models are usually presented as alternatives to inflation. Apart from the initial big bang singularity, the main criticism to inflation is that the phase of exponential expansion has to be so long that the scale corresponding to the Hubble horizon today would have been Planckian at roughly sixty e-folds before the end of inflation. This can be seen by a simple calculation. Let $\lambda_{\rm H}$ be the Hubble horizon today, $N_{\rm end} \equiv \ln a$ the number of e-folds between the end of inflation and today, $N_\star$ the number of e-fold before the end of inflation at which we want to evaluate $\lambda_\star$ the scale corresponding to $\lambda_{\rm H}$, and $a_\star$ the scale factor at this time:

$$\lambda_\star = a_\star \lambda_{\rm H} = e^{-(N_\star + N_{\rm end})}\lambda_{\rm H} \quad \text{with} \quad \lambda_{\rm H} = \frac{c}{H_0} \simeq 10^{60}\ell_{\rm Pl} \simeq e^{138}\ell_{\rm Pl}. \tag{II.31}$$

To explain the homogeneity of the CMB temperature anisotropy as well as the small measured value of the spatial curvature, one must have $N_\star \gtrsim N_{\rm end}$. Moreover, as explained by Liddle and Leach, most reasonable assumptions regarding the inflationary mechanism require that inflation lasted at least sixty e-folds [109]. In particular, at $N_\star \simeq 70$ the present Hubble scale was Planckian, and smaller scales (Large scale structure, galaxy clusters) were trans-Planckian. Cosmological perturbations are described by a set of second order differential equations. During inflation, these equations take on a

simple form. The question of initial conditions is generally easy to address too: the inflationary phase is approximately de Sitter; so there is a natural choice for the initial state, *i.e.* initial conditions for the quantum perturbations, the Bunch-Davies vacuum. The Bunch-Davies vacuum refers to the class of state that is invariant under the transformations associated with the isometry group of De Sitter spacetime $\mathrm{O}(1,3)$, and verifies the Hadamard condition so the corresponding stress-energy tensor is protected from infrared divergencies. For short wave-length modes it reduces to the Minkowski vacuum state. Is the Bunch-Davies vacuum the correct initial state for trans-Planckian modes? The answer to this question can certainly not be formulated until we have a clearer understanding of trans-Planckian physics, or quantum gravity. Note that bouncing models, in general, do not have to address this issue because the entire range of cosmological scales observable today were always larger than the Planck scale, even at the bounce.

Finally, we note that the inflationary paradigm owes a large part of its success to the fact that it predicts, from first principles, a primordial power spectrum of cosmological perturbations that is in a very good agreement with CMB and LSS data. Apart from LQC, there are many other bouncing scenarios which can also generate a nearly scale-invariant primordial power spectrum and therefore are serious alternatives to inflation, without initial singularity nor trans-Planckian issues, but which do require some new physics. In these models, the matter sector has to obey particular energy conditions in order to avoid the singularity theorems of Hawking and Penrose. I refer to Battlefeld and Peter for an overview of these models. Here, in order to shed more light on quantum cosmology, I only present a bouncing model based on the de Broglie-Bohm (dBB) interpretation of quantum mechanics.

II.9.2 Another bouncing quantum cosmology

The dBB model was introduced in 2006 by Peter, Pinho and Pinto-Neto [132, 131]. They consider a matter-dominated contracting universe connected to the expanding phase via quantum cosmological effects. As in LQC, the starting point is the ADM formulation of GR, however remaining in the metric framework (not the first-oder formalism). The matter sector is represented by a perfect fluid with equation of state parameter w. In addition to the scale factor, a time variable T , or rather its canonically conjugated momentum, is added by hand to the Hamiltonian. For T to be interpreted as a 'time', one has to set the lapse function appropriately, $N = a^{3w}$. Then T can be related to conformal time through $N\mathrm{d}T = a\mathrm{d}\eta$. With a change of variable $\chi = \frac{2}{3}(1-w)^{-1} a^{3(1-w)/2}$, one can write a Schrödinger equation,

$$i\frac{\partial\Psi}{\partial T} = \frac{1}{4}\frac{\partial^2\Psi}{\partial\chi^2} \tag{II.32}$$

for the wave function $\Psi = \Psi[a, T]$ that shall describe the background quantum Bohmian trajectories. For instance, with the following initial wave-function

$$\Psi = \exp\left(-\chi^2\right), \tag{II.33}$$

one finds the dBB trajectory for the scale-factor

$$a^{\mathrm{dBB}}(T) = a_0\left\{1+T^2\right\}^{\frac{1}{3(1-w)}}. \tag{II.34}$$

The equations of propagation of cosmological perturbations are obtained by considering a 'higher order' version of the wave function. In the dBB framework, although the background is not defined at the classical level (but only in terms of quantum trajectory), the perturbations obey the same evolution equation as in the FLRW model with the difference that the scale factor is replaced by its dBB counterpart (II.34). In this respect, the dBB model is similar to the *dressed metric* approach to cosmological perturbations in LQC (see the articles bellow). A rich phenomenology follows for the primordial power spectra and the CMB, actually analogous to what is presented in this thesis. But

unlike LQC, the dBB model does not have a post-bounce inflationary so the bounce has to occur at significantly low energy density compared to the Planck scale in order to agree with the amplitude of the CMB anisotropy.

II.9.3 A word on spatial anisotropy

In anisotropic homogeneous flat cosmological models, the Friedmann equation is

$$H^2 = \tfrac{1}{3}\left\{\rho_0 a^{-3(1+w)} + \sigma_0 a^{-6}\right\}, \tag{II.35}$$

where ρ_0 is the energy density at some initial time and σ_0 the initial anisotropy term. We have also introduced $w = P/\rho$ the equation of state parameter. As can be seen, as the scale factor decreases, the anisotropy contribution dominates the energy density. Therefore, all bouncing cosmological models have to cope with the issue of large anisotropy in the high curvature regime, near the bounce. An anisotropic bounce is problematic for bouncing models without an inflationary phase in the expanding branch because it leads to an isotropic universe contrary to our measurements. In this case, naively, one can initially assume spatial isotropy from the start, or fine tune the initial shear term in the contracting phase to make sure it does not blow up. (There is one known exception: in the epkyrotic scenario the problem is solved because $w \gg 1$ during the epkyrotic phase so the matter always dominates at high curvature.)

In LQC, having an anisotropic bounce is not problematic because the expanding phase starts with a long inflationary regime, where, as the scale factor increases, the anisotropy is diluted, so the post-inflationary universe is isotropic. The analysis of the dynamics of cosmological perturbations propagating on a bouncing anisotropic background is intricate. But in some studies, the observational consequences of an anisotropic bounce have been investigated [116]. The main conclusion of this work was that the presence of a large shear at the bounce can decrease the length of inflation (provided the potential of the scalar field near the bounce is confining, see the article for details [116]).

II.10 The background evolution in LQC

So far, we have only used the idea of fundamental discreteness from LQG to deduce the effective equations of motion for the scale factor and the scalar field. At the quantum level, these have to be interpreted as operators whose evolution is determined by a wave function. From the Hamiltonian constraint promoted to operator, $\hat{\mathcal{H}}\Psi = 0$, the Schrödinger equation for the wave function Ψ can be written as

$$-\partial_\varphi^2 \Psi\left[V,\varphi\right] = C_-\Psi\left[V_-,\varphi\right] + C_0\Psi\left[V,\varphi\right] + C_+\Psi\left[V_+,\varphi\right], \tag{II.36}$$
$$\text{with } V_\pm = V \pm \gamma\lambda,$$

where $V = a^3$, γ, λ were defined earlier. The particular form of $C_\pm$ can be found in the 2006 seminal work by Ashtekar Pawlowski and Singh [18] or in a more recent version in [10] p 20. Note that here, the scalar field plays explicitly the role of internal (or relational) time. On the RHS one recognizes a difference equation where the step is determined by the Barbero-Immirzy parameter γ and the area gap λ.

Given an initial state, and its associated wave function, this equation can solved numerically. The so-called CHIMERA code has been developed by Diener, Singh and Gupt in 2014 to investigate the behavior of wave-functions propagating across the LQC bounce [69]. It is important to understand that the bounce appearing in this procedure has, a priori, nothing to do with the effective LQC bounce of the previous sections apart from one fact: they originate from the same effect, namely the discreteness of the holonomy around a fundamental space-like loop. Like for the dBB model, the bounce is dictated

by the trajectory of the scale factor with respect to the wave function. The interesting point is that for states whose wave-functions are sharply peaked in V (small dispersion with respect to V), the trajectory of the expectation values of a and φ follows precisely the one corresponding to the effective Friedmann equation. Recently, it was shown that for a more general class of states, some effective equations can also be used to describe the dynamics of the expectation values of a and φ [12]. These generalized effective equations are equivalent to the one derived in the previous section with the only difference that $\rho_{\rm B}$ has a different expression [16]. Therefore, most phenomenological studies, including the one presented in this thesis, have been using the effective modified Friedmann equation.

II.11 Genericity of inflation in LQC

The background dynamics is entirely characterized by the modified Friedmann equation (II.3) and the Klein-Gordon equation for the scalar field

$$\ddot{\varphi} + 3H\dot{\varphi} + V_{\varphi} = 0, \tag{II.37}$$

where a subscript φ means derivative with respect to φ. The Klein-Gordon equation can be obtained in several different ways from the Hamilton equations, the Euler-Lagrange equations or the Bianchi identity. It is equivalent to the continuity equation

$$\dot{\rho} = -3H\left(\rho + P\right), \tag{II.38}$$

were $P \equiv \frac{1}{2}\dot{\varphi}^2 - V$ is the pressure, unaffected by quantum cosmological effects. This is not surprising as our quantum inputs were performed in the geometrical sector (gravitational part of the Hamiltonian), not in the matter sector.

We generally set initial conditions in the pre-bounce contracting branch. There we specify the values of the scale factor a and the scalar field φ, as well as their derivatives, $\dot{a}$ and $\dot{\varphi}$. The choice of the initial scale factor has no physical importance, but, initial conditions must be such that the modified Friedmann equation (Hamiltonian constraints) holds. So, the set of solutions to the background dynamics can be parametrized by two numbers: the initial Hubble parameter, $H_{\rm ini}$, and the initial value value of the scalar field, $\phi_{\rm ini}$. Noting that the energy density at the bounce is necessarily given by $\rho_{\rm B} = \left(3/\lambda^2\gamma^2\right)$, we conclude that the set of solutions is in a one-to-one correspondence with the value of the scalar field at the bounce, $\varphi_{\rm B}$.

Any bouncing cosmological model features three subsequent dynamical regimes, the pre-bounce contracting phase ($\dot{\rho} > 0$), the bounce ($\dot{\rho} = 0$), and the post-bounce expanding phase ($\dot{\rho} > 0$). For the LQC bounce, driven by a scalar field, there is systematically a phase of slow-roll deflation (time-reversal of inflation) preceding the bounce and a phase of slow-roll inflation after the bounce. The durations of both phases depends on the initial conditions. Note that if the bounce was to occur at an energy scale significantly smaller than $\mathrm{M}_{\rm Pl}^4$, by several orders of magnitude, these two slow-roll phases would be absent from the dynamics. However, we shall not consider this possibility and always assume $\rho_{\rm B} \sim \mathrm{M}_{\rm Pl}^4$. Indeed, the area gap is Planckian and there are reasons, motivated by the entropy of black holes, to think that the Barbero-Immirzi should be of order one.

In the phenomenological framework developed by Ashtekar and Gupt, initial conditions are set at the bounce. The pre-bounce history of the universe is ignored and the initial value of the scalar field is tuned so as to yield a phase of slow-roll inflation of about sixty efolds. This is motivated by the fact that in this setting, since inflation starts right after the bounce, the largest wavelength modes are affected by the non-trivial background dynamics at the bounce. Therefore the low-k range of the primordial power spectrum of curvature perturbations is modified and can lead to a better fit to CMB data than the nearly scale invariant inflationary expectation. *In fine*, having set $\varphi_{\rm ini}$ thanks to observational data, they deduce several predictions for other observables such as the CMB polarization spectra [17]. This is similar to the phenomenological approach developed in [132] for the dBB bounce.

I have adopted a quite different strategy, based on the work of Linsefors and Barrau [110], where the background dynamics is not tuned to observational data. We allow for *a prior* any initial conditions in the remote past of the contracting branch ($\rho \ll \rho_{\rm B}$) and ask the following question. For the whole set of initial conditions, is there a common behavior exhibited by the different solutions to the dynamics? In fact, there is one. Strikingly, most solutions have a post-bounce phase of slow-roll inflation lasting about one-hundred and forty efolds[1]. One of my contributions was to explain why. The calculation of Gibbons and Turok showing that the fraction of trajectories, μ, associated with a long slow-roll regime is suppressed by

$$\mu \propto \exp\left(-3N\right), \tag{II.39}$$

where N is the number of e-folds of the slow-roll phase, can be used to conclude that the pre-bounce deflationary phase has to be minimal (for a random choice of the initial value of the scalar field $\phi_{\rm ini}$ on a flat prior probability distribution at fixed energy density). With analytical approximations, one can show that the shortest deflationary phase corresponds to a scalar field value at the bounce given by

$$\varphi_{\rm B} \equiv \sqrt{\tfrac{2}{3}} \ln\left(2\Gamma/\sqrt{\ln\Gamma}\right) \quad \text{with} \quad \Gamma \equiv \sqrt{3\rho_{\rm B}/m}, \tag{II.40}$$

for a quadratic potential with mass m. In turn, this determines the maximal value of the scalar field reached after the bounce,

$$\varphi_{\rm I} = \varphi_{\rm B} + \sqrt{\tfrac{2}{3}}\,\mathrm{arcsinh}\left(\Gamma\sqrt{2/\ln\alpha}\right), \quad \text{with} \quad \alpha \equiv 8\Gamma^2 \exp\left(\sqrt{6}\varphi_{\rm B}\right) \tag{II.41}$$

at the onset of slow-roll inflation, and therefore the length of the inflationary phase $N \approx \left(\varphi_{\rm I}^2/4\right)$.

An important remark here is that such dynamics, with a long inflationary phase $N = \mathcal{O}(100)$, correspond to a kinetic energy dominated bounce. Hence, the evolution in the high curvature regime (the bounce) does not depend on the particular form of the potential. In the case of a kinetic energy dominated bounce, analytical formulas can be derived easily. For the scale factor, in coordinate time, one finds

$$a\left(t\right) = a_{\rm B}\left(1 + 3t^2\right)^{\frac{1}{6}} \tag{II.42}$$

with $t = 0$ at the bounce. So the bounce is 'time symmetric, furthermore it is interesting to note the similarity of this time-dependence with that of the dBB model given in (II.34).

As can be deduced from the Klein-Gordon equation (II.37), at the end of slow-roll inflation in the expanding branch, and before deflation in the contracting phase, the potential energy E_p and kinetic energy E_K of the scalar field oscillate so that their sum remains equal to the total energy density. Hence, the amplitude of the oscillations is determined by the Hubble parameter, while the frequency (with respect to time t) is given by $V_{\phi\phi} = m$, for the massive quadratic potential. The frequency of these oscillations is large compared to the expansion (or contraction) rate, $H \ll m$. So in both stages, the matter content (scalar field) is well modeled by dust. This can be seen by computing an effective equation of state, $w \equiv P/\rho$,

$$w = \frac{\bar{E}_K - \bar{E}_P}{\bar{E}_K + \bar{E}_P} = 0 \quad \text{since} \quad \bar{E}_K = \bar{E}_P, \tag{II.43}$$

where the 'bar' quantities are time averaged values over a time scale large compare to the period of the oscillations. Note that the continuity equation, together with the Friedmann equation (unmodified in this low-curvature regime), implies

$$w \neq -1 \quad \Rightarrow \quad a\left(t\right) \propto t^{\frac{2}{3}\frac{1}{1+w}} \quad \text{and} \quad \rho \propto t^{-2}. \tag{II.44}$$

We shall now review the consequences of the background dynamics, a bounce and a long slow-roll inflationary phase, for the evolution of cosmological perturbations and their implications for the CMB anisotropy power spectra.

[1] For the bounce energy density set to its default value, $\rho_{\rm B} \simeq 0.41 m_{\rm Pl}^4$, and a quadratic potential with mass $m = 10^{-6} m_{\rm Pl}$.

II.12 Dynamics of cosmological perturbations

The dynamics of cosmological perturbations in the quantum regime of the LQC bounce can be formulated in several ways. Predictions can be drastically different from one formalism to the other. I refer to Wilson-Ewing for an overview [159]. Two approaches are particularly appealing due their mathematical consistency: the *effective constraint* (deformed algebra) approach and the *dressed metric* approach. Before presenting them, I recall some important aspects of cosmological perturbations.

II.12.1 Correlation functions

The objective of the study of cosmological perturbations is to arrive at a prediction for the multi-point correlation functions (correlators) of the gauge invariant curvature perturbation, $\mathcal{R}$, in Fourier space. In particular, the two-point and three-point correlators can be written as

$$\langle \mathcal{R}_{\mathbf{k}_1} \mathcal{R}_{\mathbf{k}_2} \rangle = (2\pi)^3 P_{\mathcal{R}}(k_1)\, \delta(\mathbf{k}_1 + \mathbf{k}_2) \tag{II.45}$$

$$\langle \mathcal{R}_{\mathbf{k}_1} \mathcal{R}_{\mathbf{k}_2} \mathcal{R}_{\mathbf{k}_3} \rangle = (2\pi)^3 B_{\mathcal{R}}(k_1, k_2, k_3)\, \delta(\mathbf{k}_1 + \mathbf{k}_2 + \mathbf{k}_3) \tag{II.46}$$

where $P_{\mathcal{R}}$ is the power spectrum and $B_{\mathcal{R}}$ the bispectrum, both directly related to CMB and LSS observables. Here, the curvature perturbation $\mathcal{R}$ is the perturbation to the Ricci scalar of the comoving spatial hyper-surface (which is zero in FLRW). Instead of the comoving curvature perturbation, we may also use the gauge invariant scalar field perturbation. In the comoving Newtonian gauge (CNG), it reads as

$$Q \equiv z_{\mathrm{S}} \mathcal{R} = a\left(\delta\varphi + \frac{\dot{\varphi}}{H}\phi\right) \quad \text{with} \quad z_{\mathrm{S}} \equiv \frac{a}{H}\sqrt{(\rho + P)} = a\frac{\dot{\varphi}}{H}. \tag{II.47}$$

This two quantities, Q and $\mathcal{R}$, are gauge invariant in the sense that their numerical value does not depend on the system of coordinate. In (II.47), ϕ is the scalar degree of freedom of the perturbed metric. In the CNG, the perturbed FLRW metric is

$$\mathrm{g} = -(1+2\psi)\,\mathrm{dt}\otimes\mathrm{dt} + a^2(1-2\phi)\,\delta_{ij}\mathrm{dx}^{\mathrm{i}}\otimes\mathrm{dx}^{\mathrm{j}} + a^2 h_+ \mathrm{e}_+ + a^2 h_\times \mathrm{e}_\times, \tag{II.48}$$

where h_+, $h_\times$ refer to the two tensor components of the perturbation, which are gauge invariant too. We work at linear order in perturbation theory. As a consequence of the linearized Einstein's field equations both gravitational potentials are equal[1], $\phi = \psi$.

Tensor perturbations propagate independently from scalar perturbations. Moreover, as they satisfy the same type of initial conditions, both helicity modes can be treated on the same footing, i.e. $h_+ = h_\times = h$. The two-point correlator of tensor perturbations is also an important quantity because it can generate a B mode in the CMB polarization anisotropy. One can define its associated power spectrum via

$$\langle h_{\mathbf{k}_1} h_{\mathbf{k}_2} \rangle = (2\pi)^3 P_h(k_1)\, \delta(\mathbf{k}_1 + \mathbf{k}_2). \tag{II.49}$$

The cosmological perturbations, Q, $\mathcal{R}$, $\delta\varphi$ and h are treated as statistically homogeneous and isotropic random field. This means that their joint multi-point probability distribution functions are invariant under translation and rotation of the spatial coordinates (see [33] for details). For this reason, the correlators could be written in terms of the absolute value of the wavenumber. In what follows, we use the notations $v_{\mathrm{S}} \equiv Q$, $v_{\mathrm{T}} \equiv h$ and $v \equiv v_{\mathrm{S,T}}$.

II.12.2 Second order Hamiltonian

Mukhanov and Chibishov showed in 1981 that the second-order Hamiltonian in Fourier space is given by

$$\mathcal{H}^{(2)} = \tfrac{1}{2}\int \mathrm{d}^3\mathbf{k}\left\{v_k'^2 + \left(k^2 - \frac{z''}{z}\right)v_k^2\right\}, \tag{II.50}$$

[1] $\delta G_i^j = \partial_i\partial^j(\phi - \psi) \doteq \partial_i\delta\varphi\partial^j\delta\varphi = \mathcal{O}(\delta\varphi^2)$

with $z \equiv z_{\mathrm{S,T}}$ and $z_{\mathrm{T}} \equiv (a''/a)$, where a prime denotes a derivative with respect to conformal time [123]. This is a simple Hamiltonian, analogous to that of an harmonic oscillator with a time-dependent frequency. The equations of motion are easily obtained as

$$v_k'' + \left(k^2 - \frac{z''}{z}\right) v_k = 0. \tag{II.51}$$

During inflation, we start by approximating the evolution as De Sitter ($H = H_\star = \text{cste}$) so $z_{\mathrm{S}} = z_{\mathrm{T}} = a$ and $(z''/z) = -2a^2 H_\star^2 = \left(2/\tau^2\right)$. In terms of the scale factor, the solutions to (II.51) are

$$v_k^{\mathrm{dS}}(a) = A_+ \frac{e^{ik/(aH_\star)}}{\sqrt{2k}} \left(1 + \frac{iaH_\star}{k}\right) + A_- \frac{e^{-ik/(aH_\star)}}{\sqrt{2k}} \left(1 - \frac{iaH_\star}{k}\right), \tag{II.52}$$

where $A_\pm$ are two constants determined by boundary conditions. Note that during the dust-like regimes, i.e. remote past of the contracting branch and post-inflationary stage, $(z_{\mathrm{T}}''/z_{\mathrm{T}}) = (a''/a) = 2/\tau^2$, see *e.g.* Eq. (II.44). Hence for tensor perturbations, the solutions to (II.51) are given by

$$v_{\mathrm{T},k}^{\mathrm{dust}}(a) = \sqrt{\frac{k}{|aH|}} \left\{ A_+ \mathrm{H}_{3/2}\left(\frac{k}{|aH|}\right) + A_- \mathrm{H}_{3/2}^\star\left(\frac{k}{|aH|}\right) \right\}, \tag{II.53}$$

where H_ν is the Hankel function of order $\nu = (3/2)$. For a 'real' matter phase, not a dust-like scalar field, one has $z_{\mathrm{S}} = \pm\sqrt{3}a$ (positive during expansion, negative during contraction) so the scalar perturbation obeys the same equation as the tensor perturbation and the solution to (II.51) is also given by (II.53). However, in our case $z_{\mathrm{S}} = a\frac{\dot\varphi}{H}$ and one can show that $(z_{\mathrm{S}}''/z_{\mathrm{S}})$ is dominated by $-a^2m^2$ during the dust-like phase. Such behavior is problematic, both numerically and conceptually, because the effective frequency in Eq. (II.51) becomes arbitrarily large.

II.12.3 Quantum to classical transition for perturbations

The beauty of the inflationary paradigm (as well as the key aspect of bouncing model with a matter dominated contracting phase) relies in the following step: we interpret the cosmological perturbations as quantum fields. This yields the prediction of a nearly scale invariant power spectrum and a gaussian statistics for the cosmological perturbations, as we explain now.

The Fourier modes v_k are promoted to operators. The position-space perturbation field, $\hat v(\mathbf{x}, \tau)$, is expanded in terms of creation and annihilation operators. In Fourier space, the coefficients in front of the creation and annihilation operators are called the mode functions. One has

$$\hat v_k(\tau) \equiv f_k(\tau)\, \hat a_{\mathbf{k}} + f_{-k}^\star(\tau)\, \hat a_{-\mathbf{k}}^\dagger \quad \text{with} \quad \left[\hat a_{\mathbf{k}_1}, \hat a_{\mathbf{k}_2}^\dagger\right] = (2\pi)^3 \delta(\mathbf{k}_1 + \mathbf{k}_2). \tag{II.54}$$

The canonical commutation relations must be satisfied and therefore, since $[\hat v_k, \hat v_k'] = i$ (canonical commutation between 'position' and 'momentum'), one finds a *normalization* condition:

$$f_k' f_k^\star - f_k f_k^{\star\prime} = i. \tag{II.55}$$

Also, the mode functions obey the same equation of motion as v_k. At sufficiently early time in a De Sitter phase, $a \ll (k/H_\star)$, or in a matter dominated contraction, (z''/z) can be neglected compared to k^2 in (II.51) and Eq. (II.51) reduces to that of a simple harmonic oscillator with time-independent frequency, $f_k'' + k^2 f_k = 0$. Then, like we mentioned in II.9.1, there is a natural choice for the state of perturbations, the minimum energy state (or the Minkowski vacuum):

$$\lim_{k^2 \gg (z''/z)} f_k(a) = \frac{e^{ik/(aH_\star)}}{\sqrt{2k}}, \tag{II.56}$$

where we already took (II.55) into account. This totally determines the form of the mode function, since by matching (II.56) to (II.52) and (II.53) we find $A_+ = 1$ and $A_- = 0$ in the De Sitter case and $A_+ = \sqrt{\pi/4k}$ and $A_- = 0$ for matter-dominated contraction.

Turning to the other limit, when $k^2 \ll (z''/z)$ *i.e.* 'horizon exit', we observe that the mode function becomes well approximated by

$$k^2 \ll \left(z''/z\right) \Rightarrow \;\; f_k\left(a\right) \approx f^{\star}_{-k}\left(a\right) \approx \frac{iaH_{\star}}{\sqrt{2}k^{3/2}} \;\Rightarrow\; \hat{v}_k\left(\tau\right) \approx \frac{iaH_{\star}}{\sqrt{2}k^{3/2}}\left(\hat{a}_{\mathbf{k}} + \hat{a}^{\dagger}_{-\mathbf{k}}\right), \tag{II.57}$$

which means, in virtue of the canonical commutation relations (II.54), that the operators associated with the Fourier mode of the perturbation commute with one another for different wave numbers. Note that this is true for both the De Sitter (II.52)and dust solutions (II.53), however the amplitude of modes which cross the horizon during the dust-like or matter dominated pre-bounce contracting phase is affected by the subsequent evolution of (z''/z). After horizon exit, the quantum nature of the modes $\hat{v}_k$ has disappeared: "*the field $v = z\mathcal{R}, h$ can be seen as a classic stochastic field where ensemble averages $\langle ... \rangle$ identify with vacuum expectation values* " [33]:

$$\left\langle 0 \left| \hat{v}_{\mathbf{k}_1} ... \hat{v}_{\mathbf{k}_{2p}} \right| 0 \right\rangle = \left\langle v_{\mathbf{k}_1} ... v_{\mathbf{k}_{2p}} \right\rangle. \tag{II.58}$$

For the modes for which their exists a time in the past when $k^2 \gg (z''/z)$ and a later time when $k^2 \ll (z''/z)$, a quantum-to-classical transition is realized. When these modes re-enter the horizon much later in the expansion history, they leave their imprints in the perturbed gravitational potential which inherits their 'quantum' statistical properties. In particular, because the $\hat{v}_k$'s commute, the Wick theorem holds:

$$\left\langle v_{\mathbf{k}_1} ... v_{\mathbf{k}_{2p}} \right\rangle = \sum_{\text{all pairs}} \prod_{p \,\text{pairs}(i,j)} \left\langle v_{\mathbf{k}_i} v_{\mathbf{k}_j} \right\rangle \;\text{ and }\; \left\langle v_{\mathbf{k}_1} ... v_{\mathbf{k}_{2p+1}} \right\rangle = 0. \tag{II.59}$$

So the power spectra, in Eq. (II.45) and (II.49) totally determines the statistical properties of the perturbed fields (Gaussian statistics). Classical cosmological perturbations are therefore expected to be *Gaussian* homogeneous random fields.

II.12.4 Predictions of slow-roll inflation

The amplitudes of the dimensionless power spectra, $\mathcal{P}_{\mathrm{S,T}}$, at horizon exit during the inflationary phase (quasi De Sitter) can easily be computed with Eq. (II.57). We obtain

$$\mathcal{P}_{\mathrm{S}}\left(k\right) \;\equiv\; \frac{k^3}{2\pi^2} P_{\mathcal{R}}\left(k\right) = \frac{1}{8\pi^2} \frac{H^2}{\mathrm{M}^2_{\mathrm{Pl}}} \frac{1}{\epsilon_1}\bigg|_{k=aH}, \tag{II.60}$$

$$\mathcal{P}_{\mathrm{T}}\left(k\right) \;\equiv\; \frac{k^3}{\pi^2} P_h\left(k\right) = \frac{2}{\pi^2} \frac{H^2}{\mathrm{M}^2_{\mathrm{Pl}}}\bigg|_{k=aH}, \tag{II.61}$$

where we have introduced the Hubble flow functions (HFF),

$$\epsilon_1 \equiv -\frac{\dot{H}}{H^2}, \quad \epsilon_{i+1} \equiv \frac{\dot{\epsilon}_i}{H\epsilon_i}. \tag{II.62}$$

Taking into account that horizon crossing ($k = aH$) happens at slightly different times for different wavenumbers, one concludes that the primordial power spectra are nearly scale invariant with spectral indices given by

$$n_{\mathrm{S}} - 1 = -2\epsilon_1 - \epsilon_2 + \mathcal{O}\left(\epsilon_i^2\right) \;\text{ and }\; n_{\mathrm{T}} = -2\epsilon_1 + \mathcal{O}\left(\epsilon_i^2\right). \tag{II.63}$$

These appear in the phenomenological parametrization of the dimensionless power spectra

$$\mathcal{P}_{\rm S}(k) = A_{\rm S}\left(\frac{k}{k_\star}\right)^{n_{\rm S}-1} \quad \text{and} \quad \mathcal{P}_{\rm T}(k) = A_{\rm T}\left(\frac{k}{k_\star}\right)^{n_{\rm T}} \tag{II.64}$$

at first order in the HFF, where $k_\star = 0.05\text{Mpc}^{-1}$ is the *pivot scale.*

II.13 Cosmological perturbations in LQC

In LQC, through the Friedmann equation, the curvature at the bounce is associated to a wavenumber

$$k_{\rm B} \equiv a_{\rm B}\sqrt{\rho_{\rm B}}\text{M}_{\rm Pl}^{-1}, \tag{II.65}$$

where $a_{\rm B}$ is the scale factor at the bounce ($a = 1$ at present). I have investigated how $k_{\rm B}$ is related to the pivot scale $k_\star$ depending on the duration of inflation and the post-inflationary expansion history. We arrived at the conclusion that $k_{\rm B}$ is within the observable window of wavenumbers (typical cosmological scales: $10^{-4}\text{Mpc}^{-1} < k < 1\text{Mpc}^{-1}$) only if the duration of inflation is close to its minimal value $N \simeq 60$. This would require a tuning of initial conditions for the scalar field. However, if we let $\varphi_{\rm B}$ be a free parameter, most of the background solutions have a much longer inflationary phase, as discussed in section II.11. In this case, $k_{\rm B}$ is well bellow the observational window so that CMB scales would correspond to wavelengths much smaller than the curvature scale at the bounce, *i.e.* trans-Planckian modes.

For these modes, one has $k^2 \gg (z''/z)$ during the entire contracting branch and the bounce. Horizon crossing happens only once, at about sixty e-folds before the end of the post-bounce inflationary phase and therefore one would expect the nearly scale invariant power spectra given in (II.60) and (II.61), and conclude that cosmology has no chance to probe quantum gravity (at least for the next couple of billions of years or forever if the universe remains Λ dominated).

But such a conclusion holds only if the dynamics of cosmological perturbations, in particular for trans-Planckian modes, remains unaffected by quantum cosmological effects so that the perturbations are still in the Bunch-Davies vacuum state after the bounce. We now review the two main approaches to cosmological perturbations in LQC. Like we shall see, the *dressed metric approach* suggests that the dynamics is still described by Eq. (II.51) in the quantum gravity regime, while the *effective constraint* (or deformed algebra) approach predicts a drastically different behavior. The validity of one or the other approach is still subject to a lively debate in the community. My position has been to take seriously both approaches and confront them with observations.

II.13.1 The dressed metric approach

The dressed metric approach to cosmological perturbations in LQC was developed by Agullo, Ashtekar and Nelson in 2012 [10, 9, 11]. In this framework, they study the dynamics of perturbations $v = z\mathcal{R}, h$ evolving on a background represented by the wave function $\Psi[a, \varphi]$ and find that this evolution is equivalent to that of test perturbations propagating on a dressed metric

$$\tilde{g} = \tilde{a}^2\left(-\text{d}\tilde{\tau}\otimes\text{d}\tilde{\tau} + \delta_{ij}\text{d}x^i\otimes\text{d}x^j\right), \tag{II.66}$$

where $\tilde{a}$ is the dressed scale factor and $\tilde{\tau}$ the dressed conformal time, both obtained via

$$\tilde{a}^4 = \left\langle \hat{H}_0^{-\frac{1}{2}}\hat{a}^4\hat{H}_0^{-\frac{1}{2}}\right\rangle\left\langle \hat{H}_0^{-1}\right\rangle^{-1} \quad \text{and} \quad \text{d}\tilde{\tau} = \tilde{a}^2\left\langle \hat{H}_0^{-1}\right\rangle\text{d}\varphi, \tag{II.67}$$

where $\hat{H}_0$ is the operator associated with half the gravitational part of scalar constraint, $\frac{1}{2}C$, given in (II.21) and the brackets have to be understood as quantum expectation values with respect to the state

corresponding to the wave function $\Psi[a,\varphi]$. These can be explained as follows. In order to interpret the scalar field as a relational time one has to set the lapse function to $N = a^3\pi_\varphi^{-1}$ so the scalar field momentum appears linearly in the Hamiltonian (II.25) and recalling the expression of π_φ, it follows $d\varphi = d\tau$. As the scalar constraints vanishes for solutions to the dynamics, one can identify π_φ^{-1} with $\hat{H}_0^{-1}$ at the quantum level. Then, taking into account the appropriate factor ordering we may write, heuristically,

$$\begin{aligned} dt &= Nd\tau = Nd\phi = a^3\pi_\varphi^{-1}d\phi \\ &= a^3\hat{H}_0^{-1}d\phi = \tilde{a}\tilde{a}^2\left\langle\hat{H}_0^{-1}\right\rangle \mathrm{d}\varphi = \tilde{a}d\tilde{\tau}. \end{aligned} \tag{II.68}$$

See [9] for the rigorous derivation. Finally, by writing the (quantum version of) second order Hamiltonian the equations of motion are obtained as

$$v_k'' + \left(k^2 - \frac{\tilde{z}''}{\tilde{z}}\right)v_k = 0, \tag{II.69}$$

with $\tilde{z}_{\mathrm{T}} = \tilde{a}$ for tensor perturbations. The equation for scalar perturbations is slightly more complicated due to the fact that $z_{\mathrm{S}} = (a\dot{\varphi}/H)$ and so z''/z involves the inflaton potential (see Eq. A8 of [11] for the relevant expressions). Now one may ask about the time evolution of $\tilde{z}$ for a given state $\Psi[a,\varphi]$: does it follow the trajectories obtained with the effective modified Friedmann equation (II.3)? Fortunately, the answer is yes. In general one does not need to solve the full quantum evolution for the wave-function corresponding to Eq. (II.36). It is safe to use the generalized effective equations introduced in [12], as discussed in section II.10.

So, in this approach, the only non-trivial features for the perturbations appear for modes with wavenumbers $k \lesssim k_{\mathrm{B}}$. Indeed, if $k \gg k_{\mathrm{B}}$ the modes do not 'feel' the bounce and exit the horizon during inflation, yielding the standard inflationary power spectra.

II.13.2 Effective constraints for perturbations

The *effective constraints approach*, also known as the deformed algebra approach, was initiated by Bojowald and refined by Cailleteau, Mielczarek, Barrau, Grain and Vidotto in 2012 [47, 45, 46, 48]. This approach is based on the closure of the hyper-surface deformation algebra, or the algebra of constraints, at the level of perturbations. Indeed, the discretization of the curvature, described in section II.7, leads to anomalies in the algebra of constraints. Note that this point is not addressed in the dressed metric approach. Here, I give describe the main steps of the effective constraints approach that lead to a modification of the equations of motion for cosmological perturbations.

We first define the smeared Gauss, scalar and vector constraints

$$G[\beta] \equiv \int \mathrm{d}^3x\beta^i G_i, \quad H[N] \equiv \int \mathrm{d}^3x NC \quad \text{and} \quad D[N^a] \equiv \int \mathrm{d}^3x N^a C_a. \tag{II.70}$$

These correspond to the constraints integrated over the constant time three dimensional slice. A direct consequence of the equations of motion is that the smeared constraints are *first-class*: the Poisson bracket between any two constraints can be expressed in terms of a linear combinations of constraints. Straightforward calculations lead to

$$\begin{aligned}
\{H[N], H[M]\} &= -D\left[S^{ab}\left(N\partial_b M - M\partial_b N\right)\right] \text{ with } S^a_b = |e|^{-1} E^a_i E^i_b, \\
\left\{D[N^a], D\left[M^b\right]\right\} &= D\left[\mathcal{L}_{N^a} M^b\right], \\
\{G[\alpha], G[\beta]\} &= -G[[\alpha,\beta]] \text{ with } \alpha,\beta \in \mathrm{su}(2), \\
\{H[N], D[M^a]\} &= H[\mathcal{L}_{M^a} N], \\
\{H[N], G[\alpha]\} &= 0, \\
\{D[N^a], G[\alpha]\} &= G[\mathcal{L}_{N^a}\alpha],
\end{aligned} \tag{II.71}$$

where for u, v two vector fields, $\mathcal{L}_u v$ is the Lie drag of v along u. The Poisson brackets are $\{..,..\} \equiv \{..,..\}_{c,p} + \{..,..\}_{\varphi,\pi_\varphi}$ where c and p were introduced in (II.26) and are proportional to the extrinsic curvature (or $\dot{a}$) and the scale factor a respectively. Then, the smeared constraints are expanded up to quadratic order with respect to δK^i_a and δE^a_i the perturbed extrinsic curvature and its conjugated momentum, the 'electric' field, as in Eq. (II.20). Due to the effective holonomy correction that we used for the curvature (II.27), the algebra at second order features some anomalies, generically denoted $\mathcal{A}$. It is not closed anymore. For instance, the Poisson brackets are now of the form

$$\left\{H\left[\bar{N}+\delta N\right], D\left[\bar{M}^a+\delta M^a\right]\right\} = H[\mathcal{L}_{M^a} N] + \mathcal{A}(\delta N, \delta M^a). \tag{II.72}$$

A surprising result is that in order to cancel these anomalies, $\mathcal{A}$, and recover a closed algebra of constraints, one can add counter terms to (II.72) (and the other Poisson brackets) which in the end lead to

$$\{H[N], H[M]\} = \Omega D\left[S^{ab}\left(N\partial_b M - M\partial_b N\right)\right] \text{ with } \Omega \equiv 1 - 2\frac{\rho}{\rho_{\mathrm{B}}}, \tag{II.73}$$

for the Poisson bracket of the scalar constraint with itself. For the equations of motions, this implies

$$v_k'' + \left(\Omega k^2 - \frac{z''}{z}\right) v_k = 0. \tag{II.74}$$

Hence, for trans-Planckian modes, *i.e.* $k \gg k_{\mathrm{B}}$, this equation reduces to $v_k'' - k^2 v_k = 0$ near the bounce so that their amplitude is amplified exponentially. At the level of the power spectrum one has

$$\mathcal{P}(k) \underset{k\gg k_{\mathrm{B}}}{\propto} \exp\left(k\int_{\Delta\tau}\sqrt{|\Omega|}d\tau\right), \tag{II.75}$$

where $\Delta\tau$ is the time range around the bounce for which $\Omega < 0$. Such behavior is tremendously different from the nearly scale invariant inflationary expectation. We note that the appearance of the Ω term in the equation of motion for perturbations, in these approach, has been argued to be related to a change of signature of the background metric in the quantum gravitational regime of space-time. A result also obtained in other quantum gravity theories such as Causal Dynamical Triangulation [119].

II.14 Results and articles

In the article "*Some Clarifications on the Duration of Inflation in Loop Quantum Cosmology*", I show how the argument of Turok and Gibbons stating that a long phase of inflation is unlikely (with respect to the variety of possible initial data) can be used to deduce that the contracting branch of the LQC universe must end in a way that minimize deflation (accelerated contraction). This selects a particular phase-space trajectory for the background universe, for which the expanding branch undergoes a phase of inflation lasting around one hundred and forty efolds (in the simplistic model of a massive scalar field dominated universe and a bounce occurring at Planckian energy density). The LQC bounce generically

lead to an inflationary universe. This is the main result obtained in this article. Nevertheless, the goal of the analysis was also to identify the true impact of the LQC modifications to the Friedmann equation on the background dynamics: Is the specific LQC effective equation responsible for a long inflation? or, would one obtain the same conclusions with a different modified dynamics? To address this question, we considered a 'GR-like' bouncing scenario, always driven by the standard Friedmann equation. In the 'GR-like' bounce, the Hubble parameter is change *by hand* from negative to positive as soon as the energy density reaches the Planckian energy scale. This may seem quite audacious, but actually in this 'GR-like' bounce, apart from the Hubble parameter, the other relevant dynamical quantities are continuous, namely the scale factor and the energy density. Surprisingly, the results of the numerical analysis are that the 'GR-like' and the LQC bounce are hardly distinguishable, not only for the background dynamics but for cosmological perturbations too.

The length of inflation is a crucial phenomenological aspect of LQC as it determines wether the features imprinted by the bounce onto the primordial cosmological perturbations can be probed within the temperature and polarization anisotropy of the CMB light, or the large scale structure of the universe.

As deduced from the inflationary paradigm, the characteristics of the present universe are related to the cosmological perturbations whose wavelengths became larger than the Hubble radius during the last sixty efolds of inflation. In particular, the present universe is insensitive to modes of larger wavelengths. If the post-bounce inflation is much longer than sixty e-folds there is no hope for probing quantum gravity with current cosmological data.

The genericity of a long inflation is however an ambiguous results: it depends on the chosen probability measure. So, there is still room for a short inflation and studying the implications of the LQC bounce for cosmological perturbations is definitely an important research topic which may not only help identifying the relevant observational probes of quantum gravity but also shed more light on the phenomenology of trans-Planckian physics in general.

Therefore, in the second article reported here, "*Comparison of primordial tensor power spectra from the deformed algebra and dressed metric approaches in loop quantum cosmology*", we study the behavior of tensor perturbations as they propagate across the LQC bounce, starting their journey in a Minkowski vacuum state in the contracting branch of the universe. Then we compare the predictions of the two main dynamical scenarios for cosmological perturbations in LQC: the dressed metric approach and the deformed algebra (or effective constraint) approach. We find that in both approaches, the resulting power spectra at the end of inflation (primordial power spectra) have three different regimes with respect to the wavelengths of the modes. Since the bounce occurs at Planckian energy density, their are three types of modes: infrared (IR) modes whose wavelengths are very large compared to the Planck length, Planckian modes, and trans-Planckian modes with a small wavelength compared to the Planck length. Had the bounce occurred at a different energy density, the relevant scale for LQC phenomenology would not be the Planck scale but the curvature radius at the bounce, proportional to $\rho_{\mathrm{B}}^{-1/2}$. This leads to what we called the IR regime, the intermediate regime and the ultraviolet regime of the primordial power spectrum. Both the dressed metric and effective constraint approach predict the same features for the tensor power spectrum for the IR and intermediate range of wavenumbers. In the infra-red limit the power spectrum is scale invariant, and for the intermediate (Planckian) modes the amplitude of the power spectrum is oscillatory. However, both approaches differ regarding their predictions for trans-Planckian modes: in the effective constraint approach the power spectrum diverges exponentially while it is nearly scale invariant, undistinguishable from the standard inflationary prediction in the dressed metric approach. In the article, we study the dependency of the power spectrum on the values of different parameters such as the mass of the scalar field and the bounce energy density. We also find that when the contracting branch ends with deflation, the amplitude of the IR plateau of the power spectrum can become very large, depending on the length of the deflationary phase which itself is related to the potential energy at the bounce. All the numerical results are supported and

confirmed by analytical formulas derived in the article.

The dynamics of scalar perturbations presents two difficulties which are absent for tensor perturbations. First, in the remote past of the contracting branch, the 'effective potential' z''/z in the equation of motion diverges. Hence, the Minkowski vacuum state is no longer naturally selected as the initial state for perturbations. This adds a considerable freedom, or ambiguity, as far far as predictions are concerned. Second, the equation of motion for scalar perturbations in the effective constraint approach is singular at the bounce when written with the Mukhanov-Sasaki variables. In the article "*Primordial scalar power spectrum from the Euclidean Big Bounce*", we address these two issues and extract the predictions for the primordial power spectrum of cosmological perturbations in the effective constraints approach. The scalar power spectrum is found to have the same form as the tensor power spectrum in the UV limit (exponential divergence) and intermediate range (oscillations). However, the infrared regime is different: the scalar power spectrum is suppressed (proportional to k^3) while the tensor power spectrum is nearly scale invariant.

With a long phase of inflation, longer than sixty efolds, the modes of observational interest lie in the UV part of the power spectra. They are trans-Planckian modes. Tacking seriously the prediction of the effective constraint approach of an exponential amplification of the power spectrum, it is easy to exclude the model based on observational data. This is what we do in the article "*Observational Exclusion of a Consistent Quantum Cosmology Scenario*". We use the tensor power spectrum and the tensor-to-scalar ratio to show that the effective constraint approach, with initial conditions in the contracting phase, is incompatible with current CMB measurements. Moreover, as an auxiliary result we show that even if one does not regard the exponential growth of the power spectrum as a correct prediction but rather as an artifact of a model that we consider outside its range of validity (trans-Planckian modes), the observational signature associated with the oscillatory part of the power spectrum would hardly be measurable. Indeed, with an inflationary phase of about sixty-efolds, it would affect the low multipole of the CMB anisotropy where the signal is tributary to the cosmic variance.

To summarize, on one hand, according to the work presented in this thesis, the effective constraint approach is excluded if one considers generic initial conditions in the remote past of the pre-bounce contracting phase. Indeed, if one ignores possible issues related to trans-Planckian modes, it predicts an exponential amplification for the modes within the observable window, in total disagreement with observational data.

On the other hand, still with generic initial conditions in the past, the dressed metric approach yields the same prediction as inflation for the observables scales (inflation lasts long, so $k_\star \gg k_{\rm B}$ and the observable modes do not 'feel' the bounce). If the dressed metric approach was to be correct, there might be quantum gravitational effects in the CMB and LSS, which are not in disagreement with present data but still require a higher level of accuracy before being potentially probed, provided inflation is short ($N \simeq 60$). As we said already, this requires a tuning of initial conditions for the inflaton field. Even if we accept this, as a final remark I note that the current project on non-gaussianity I am about to complete with Ivan Agullo and Sreenath Vijayakumar seems to indicate that the bounce leads to a very large curvature three-point correlation function, also in disagreement with observations. In the triangle plot presented in figure 1 I show the non-gaussianity parameter computed in LQC, with a numerical code I had written during my Fulbright residency at Louisiana State University under the supervision of Ivan Agullo. As can be seen, the LQC prediction is three orders of magnitude away from the standard slow-roll expectation, while current data give $f_{\rm NL} = \mathcal{O}\left(10^2\right)$ [3]. Primordial non-gaussianity may therefore be the key observable to constrain quantum gravity models. It is remarkable that, based on the present CMB data, one can already exclude a significant part of the parameter space of LQC, a well defined quantum cosmological proposal that has GR as its low energy limit. This was thought to be impossible only a few years ago.

As a conclusion to this chapter, I have reported my review article with Aurélien Barrau entitled

"*Some Conceptual Issues in Loop Quantum Cosmology*" where we discuss the main open issues in the field and perspective for future research.

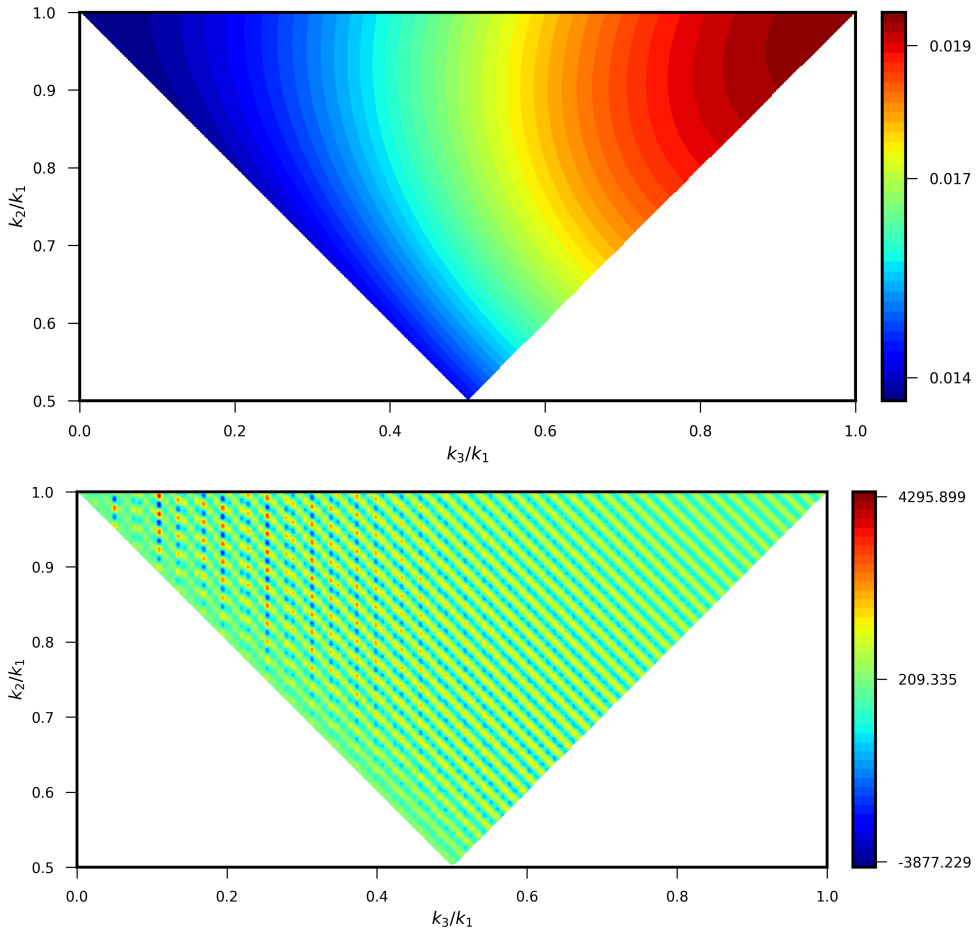

Figure 1: Amplitude of the non-gaussianity parameter $f_{\rm NL}$ as predicted by standard slow-roll inflation with massive quadratic scalar field (top panel) against the prediction of loop quantum cosmology (bottom panel), with an inflationary phase lasting about sixty e-folds. The reference wavenumber was set to $k_1 = 2.5 \times 10^{-3}\text{Mpc}^{-1}$, half the pivot scale of the Planck data. For LQC, we considered a bounce occurring at the Planck energy scale and we set initial condition for perturbations at the first minimum of kinetic energy before the bounce.

Some Clarifications on the Duration of Inflation in Loop Quantum Cosmology

Boris Bolliet,[1,*] Aurélien Barrau,[1] Killian Martineau,[1] and Flora Moulin[1]

[1] *Laboratoire de Physique Subatomique et de Cosmologie, Université Grenoble-Alpes, CNRS/IN2P3 53, avenue des Martyrs, 38026 Grenoble cedex, France*

(Dated: April 24, 2017)

The prediction of a phase of inflation whose number of e-folds is constrained is an important feature of loop quantum cosmology. This work aims at giving some elementary clarifications on the role of the different hypotheses leading to this conclusion. We show that the duration of inflation does not depend significantly on the modified background dynamics in the quantum regime.

Loop quantum gravity (LQG) is a nonperturbative and background-independent quantization of general relativity (GR). It relies on the Sen-Ashtekar-Barbero variables, that is SU(2) valued connections and conjugate densitized triads. The quantization is obtained using holonomies of the connections and fluxes of the densitized triads. Loop quantum cosmology (LQC) is an effective theory based on a symmetry reduced version of LQG. In LQC, the big bang is believed to be replaced by a bounce due to repulsive quantum geometrical effects (see [1] for a review). For the flat homogeneous and isotropic background cosmology that we consider in this work, the effective LQC-modified Friedmann equation is

$$H^2 = \frac{\rho}{3}\left(1 - \frac{\rho}{\rho_{\rm B}}\right), \tag{1}$$

where $H \equiv (\dot{a}/a)$ is the Hubble parameter, ρ is the total energy density and $\rho_{\rm B}$ is the critical density at the bounce (expected to be of the order of the Planck density). The dot refers to a coordinate time derivative. Throughout all this article we use reduced Planck units: $\sqrt{8\pi G} = 1$. So, in these units, the Planck mass is $m_{\rm Pl} \equiv 1/\sqrt{G} = \sqrt{8\pi}$.

We assume that the dominating energy component in the early universe is a scalar field ϕ, with potential $V = \frac{1}{2}m^2\phi^2$. As shown in [2], a massive scalar field is now disfavored by data. This choice however remains interesting so as to compare our study with other results (a quantitative estimate of the effect of choosing, for example, the Starobinsky potential, used in [3], can be found in [4]). The total energy density can be written as $\rho = \frac{1}{2}\dot{\phi}^2 + V$. As explained in details in [5] it should be made clear that the existence of an inflationary phase is not in itself a consequence of LQC, but of the choice of an appropriate scalar field as the content of the Universe. Based on cosmic microwave background (CMB) measurements and under most reasonable assumptions for the length of *observable inflation* (between horizon exit of the pivot scale and the end of the inflationary phase), one obtains $m \simeq 10^{-6} m_{\rm Pl}$. The equation of motion for the scalar field is

$$\ddot{\phi} + 3H\dot{\phi} + m^2\phi = 0. \tag{2}$$

There are different ways to statistically estimate the duration of inflation in this framework.

At a fixed energy density, ρ_0, one can first ask the following question: for a given number of e-folds N, what is the fraction of trajectories, *i.e.* solutions to Eq.(2), that lead to a phase of slow-roll inflation lasting more than N e-folds? It should be noticed that the set of trajectories can be parametrized by $\{a_0, \phi_0\}$. As the energy density has been fixed, the initial time derivative of the scalar field, $\dot{\phi}_0$, is determined in terms of ρ_0 and ϕ_0. This also implies that ϕ_0 can only take values within a finite interval, ranging from $-(\sqrt{2\rho_0}/m)$ to $(\sqrt{2\rho_0}/m)$. In a flat universe, the value of the scale factor has no physical meaning. The number of e-folds of inflation depends on ϕ_0 but not on a_0: $N = N(\phi_0; m, \rho_0)$. So the fraction of trajectories that achieve a phase of inflation lasting more than N e-folds can be written as $\mu = (m\Delta\phi_0)/(2\sqrt{2\rho_0})$, where $\Delta\phi_0$ is the range of initial values of the scalar field that yields the required inflationary phase. It is then necessary to evaluate μ as a function of N. There are two cases in which this can be done analytically: (i) at *low energy*, $\rho_0 \ll m^2$, and (ii) at *high energy* $\rho_0 \gg m^2$. At low energy, the calculation of Gibbons and Turok of the probability for inflation can be used to show that [6]

$$\mu(N) = \mathcal{C} m N^{-\frac{1}{2}} \exp(-3N)\{1 + 1/(6N)\}, \tag{3}$$

where $\mathcal{C}$ is a numerical factor that does not depend on m or ρ_0. For $N \simeq 60$ e-folds, as required to explain the CMB temperature anisotropy, this leads to $\mu(N) \ll 1$. It should be noticed that the conclusions of [6] are to be contrasted with those of [7], which shows the importance of working with well defined probability distribution functions. At high energy, one reaches the opposite conclusion. In this case, one can compute $\Delta\phi_0$ as follows. For a massive quadratic potential the total number of e-folds of inflation can be expressed in terms of the amplitude of the scalar field at the start of the inflationary phase, $\phi_{\rm I}$, as $N \approx (\phi_{\rm I}^2/4)$. In turn, $\phi_{\rm I}$ can be expressed in terms of the initial value of the scalar field as [8]:

$$\phi_{\rm I} = \phi_0 + \mathrm{sgn}(\dot{\phi}_0)\sqrt{(2/3)}\,\mathrm{Arcsinh}\left(\Gamma\sqrt{2/\ln(z)}\right), \tag{4}$$

with $z \equiv 8\Gamma^2 \exp(\sqrt{6}\phi_0)$ and $\Gamma \equiv \sqrt{3\rho_0}/m$. This formula for the amplitude of the scalar field at the start of inflation is valid in LQC, with the modified Friedmann equation given by Eq. (1). For the standard flat

FLRW dynamics, without LQC modifications, the analytical calculations suggest that at the start of inflation the scalar field reaches a maximum value given by (4) minus $(\ln 2/\Gamma)$. In both cases, we find that the range of values of ϕ_0 that do not yield an inflationary phase longer than N e-folds is an interval of size $4\sqrt{N}$ centered on $\phi_0 = 0$. Hence,

$$\mu(N) = 1 - m\sqrt{(2N/\rho_0)}, \tag{5}$$

and $\mu(60) \simeq 0.99999$ (for $\rho_0 = 1$) , which means that all but a tiny fraction of the possible trajectories do not go through a long inflationary phase. It might be tempting to interpret μ as a probability measure. This is however not that simple. The phase space of the flat FLRW universe presents a serious ambiguity: the Liouville measure is proportional to the scale factor and the scale factor can be rescaled arbitrarily. In addition, as explained just before, μ depends on the choice of the surface of initial data. More importantly, the fundamental question to ask is: is there a variable on which a flat (or at least known) probability distribution function (PDF) can be assigned? There is no reason to assume implicitly that the initial values of the field should have a flat PDF.

This work is somehow complementary to what was studied in [9] and sheds a new light on the difference between different predictions made in quantum and classical cosmology.

In [10] it was argued that the two first issues mentioned above can be solved in LQC. It was indeed claimed that the scale factor can be rigorously factored out of the Liouville measure, and that the bounce provides a preferred choice for the surface of initial data. In this study, following [11, 12] we choose a different perspective. We decide, the other way round, to set initial conditions in the remote past of the contracting branch, when the Universe is classical and well understood ($\rho_0 \ll \rho_{\rm B}$). This is not only technically justified but also conceptually necessary if the bounce has to be taken seriously in a causal way. Still, we naturally choose a time which is close enough to the bounce so that it is reasonable to assume a scalar field as the main component of the Universe. The phase of the oscillations of the scalar field in the contracting branch is an obvious variable to which a flat PDF can be assigned [11]. In addition, the key point is that this PDF is preserved over time (as long as one remains in the classical phase when the field oscillates). The numerical analysis of [11] shows that at fixed ρ_0, nearly all possible initial values for the scalar field, ϕ_0, yield an inflationary phase whose number of e-folds is peaked around $N = 142$ e-folds (with $\rho_{\rm B} = 0.41 m_{\rm Pl}^4$).

The procedure to derive this result is simple:

- Consider an initial energy density $\rho_0 = \rho_{\rm Pl}/\alpha^2$, with α large enough so that the evolution starts in the remote past of the contracting phase.
- Choose an initial value for the scalar field and its time derivative by a random sampling of the phase θ_0 between 0 and 2π, where θ_0 is defined such as $\phi_0 = \sqrt{\frac{2}{3}}\frac{\Gamma}{\alpha}\sin\theta_0$.
- Solve the dynamics, across the bounce, until the end of slow-roll inflation in the expanding branch.
- For each θ_0, collect the corresponding number of e-folds.

Finally, one can produce the associated histogram which, in a probabilistic interpretation, is the PDF for the number of e-folds. This is illustrated on the right panel of Fig. 3 where we also present the PDFs for several initial energy densities corresponding to different values of $\alpha \equiv \sqrt{\rho_{\rm Pl}/\rho_0}$ in order to show that for large values of α the PDF becomes independent of the initial energy density, as explained analytically in [11]. Interestingly, the peakedness of the PDF can be understood as follows. The calculation Gibbons and Turok is often considered controversial in standard cosmology because they somehow set "initial conditions" for the *final* state. However, in the case of a bouncing Universe it implies that almost none of all the possible trajectories, starting at low energy in the *contracting* branch, have a significant phase of pre-bounce exponential contraction, that is of so-called *deflation*. A trajectory with deflation in the contracting phase leading to $(\phi_{\rm B}, \dot\phi_{\rm B})$ can be identified with a trajectory with inflation in the expanding phase with $(\phi_{\rm B}, -\dot\phi_{\rm B})$. Equation (4) can be used to calculate the value of the scalar field at the bounce corresponding to the trajectory with no deflation. One simply has to solve Eq. (4) with respect to $\phi_{\rm B}$ for $\phi_{\rm I} = 0$ and $\dot\phi_{\rm B} < 0$. In the limit of large Γ, the solution is well approximated by

$$\phi_{\rm B}^{\rm GT} \equiv \sqrt{(2/3)}\ln\left(2\Gamma/\sqrt{\ln\Gamma}\right). \tag{6}$$

This can then be inserted back into Eq. (4), with $\dot\phi_{\rm B} > 0$, in order to obtain the value of the field at the start of inflation in the expanding phase and the corresponding number of e-folds of inflation. With the standard values for m and $\rho_{\rm B}$, this calculation yields $N = 142$, in excellent agreement with the numerics (Fig. 3). Moreover, a closer look at Gibbons and Turok's PDF for the number of e-folds suggests that most trajectories starting in the remote past have less than one e-folds of deflation, see Fig. 5. This means that nearly all trajectories end up with a value of $\phi_{\rm B}$ that belongs to an interval of size $\Delta\phi_{\rm B} \approx 4$ centered around $\phi_{\rm B}^{\rm GT}$. In terms of number of e-folds this translates into $\Delta N \approx 4\sqrt{N}$, also in agreement with the numerics as can be seen on Fig. 3.

We shall now investigate to which extent the specific modified dynamics is responsible for the peakedness of

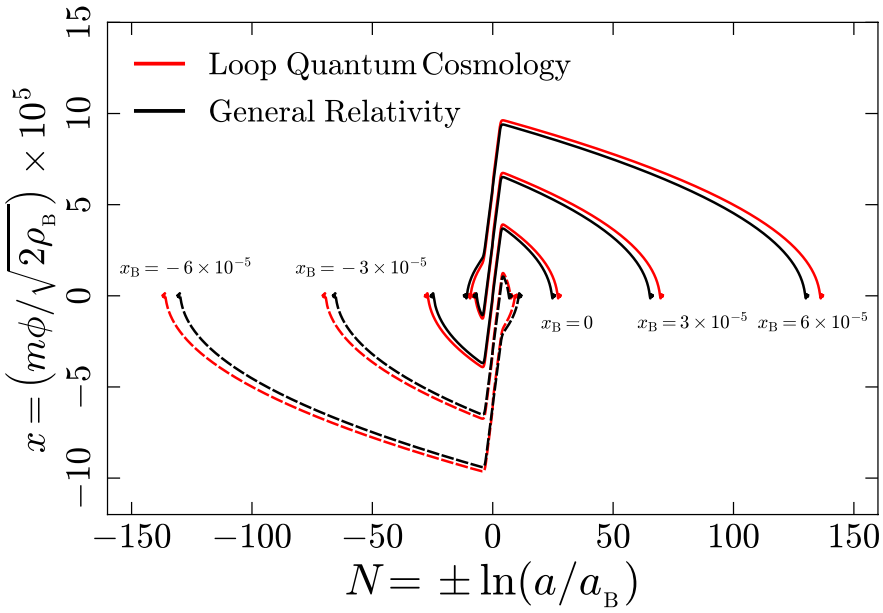

FIG. 1: Evolution of the potential energy parameter in the GR-like scenario (black) compared to loop quantum cosmology (red), for different values of $x_{\rm B}$, linearly distributed between -10^{-6} and 10^{-6}. Dashed lines correspond to negative initial values for $x_{\rm B}$.

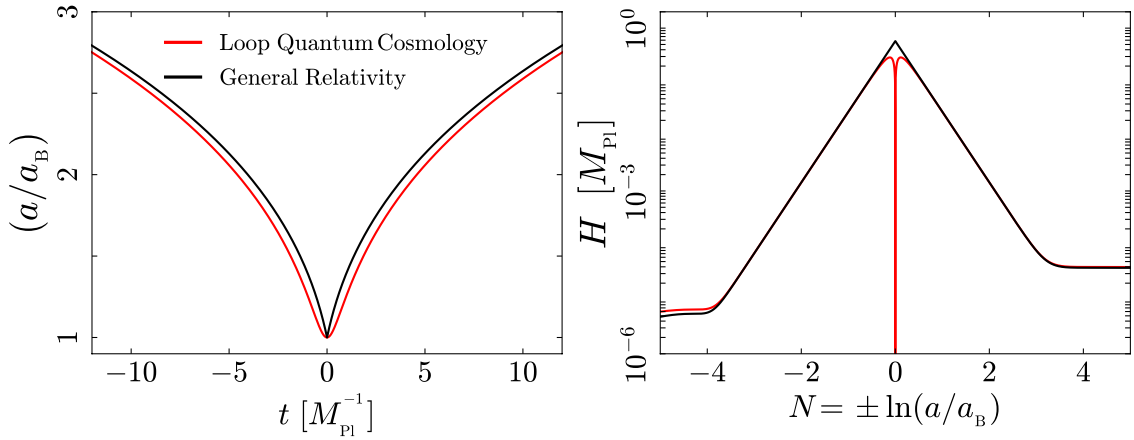

FIG. 2: Evolution of the scale factor (left) and the Hubble parameter (right) in loop quantum cosmology (red) and in the GR-like scenario (black).

the probability density function of the number of e-folds in loop quantum cosmology. The argument we have developed in the previous section did not refer to the modified LQC dynamics. It was essentially based on Gibbons and Turok's analysis combined with the presence of the bounce at Planckian energy density. It can therefore already be guessed that the peakedness does not depend strongly on the LQC modification to the Friedmann equation. To address this question in more details, we consider an artificial bouncing cosmological scenario where the Friedmann equation is left unchanged even at Planckian energy. In this "GR-like" cosmological scenario, initial conditions for a given trajectory are set in the remote past of the contracting branch at the same energy density and with the same values of ϕ_0 and $\dot{\phi}_0$ than for a trajectory which follows the LQC dynamics (as previously considered). The dynamics is divided into two parts: the contracting branch with a negative Hubble parameter and the expanding branch with a positive Hubble parameter. The evolution, starting in the contracting branch, is artificially stopped when the energy density reaches the LQC critical energy density $\rho_{\rm B}$. The values of $\phi_{\rm B}$ and $\dot{\phi}_{\rm B}$ are collected and used as initial conditions for the dynamics in the expanding branch where the

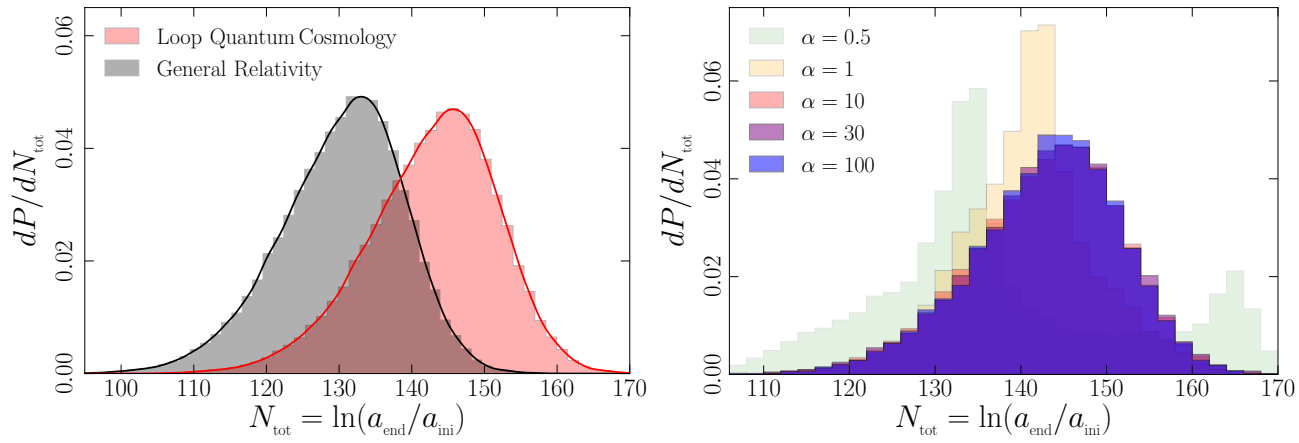

FIG. 3: Probability distribution of the number of inflationary e-folds. On the left panel, the black histograms corresponds to a 'GR' like dynamics (using the standard Friedmann equation throughout the evolution). The red histogram is the prediction of loop quantum cosmology. With the standard Friedmann equation the most likely value is $N_{\rm tot} = 133$, while in LQC we find $N_{\rm tot} = 145$. The right panel shows that the probability density function does not depend on the value of the energy density as long as the surface of initial data is set at $\rho \ll \rho_{\rm Pl}$. The different histograms are labeled by $\alpha = \sqrt{\rho_{\rm Pl}/\rho}$. The probability density function converges as soon as α becomes larger than 10.

initial Hubble parameter is now positive. At the junction between both phases, the Hubble parameter and therefore $\ddot{\phi}$ are discontinuous but a, ϕ and $\dot{\phi}$ are continuous, as illustrated in Fig. 1, 2 and 6.

The numerical result for the PDF of the number of e-folds in the GR-like scenario is plotted against the LQC prediction on the left panel of Fig. 3. The PDF has the same width and shape than in LQC. This confirms that the peakedness does not depend strongly on the specific LQC modified dynamics, and suggests that this feature would remain in case one incorporates additional quantum gravity corrections to the LQC effective equations. Nevertheless, the number of e-folds corresponding to the peak of the PDF is slightly different in the GR-like scenario than in LQC. This can be explained as follows.

First, it should be noticed that the difference between the GR-like scenario and LQC becomes significant when $\rho \approx \rho_{\rm Pl}$. Second, as shown in the previous sections, the fraction of trajectories that have a significant phase of deflation in the contracting branch is tiny. This means that at high energy density, the dynamics of most trajectories is largely kinetic energy dominated. In simplistic terms, deflation can not bring the amplitude of the scalar field to large values because it stops nearly immediately. To inverstigate the difference between the GR-like scenario and LQC, the equation of motion of the scalar field at high energy, and for kinetic energy domination, need to be studied. It is natural to introduce $x \equiv \phi/\sqrt{2\rho_{\rm B}}$ and $y \equiv \dot{\phi}/\sqrt{2\rho_{\rm B}}$, the so-called potential and kinetic energy parameters. As the duration of inflation depends on the scalar field amplitude, it is sufficient to focus on the potential energy parameter. It is easy to show that in the regime compatible with observations

$$x^{\rm GR} \simeq x_{\rm B} + (3/\Gamma)\ln a, \tag{7a}$$
$$x^{\rm LQC} \simeq x_{\rm B} + (3/\Gamma)\ln a + (\ln 2/\Gamma). \tag{7b}$$

In LQC the scalar field is *boosted* by a short phase of super-inflation, $\dot{H} > 0$, during which its amplitude accumulates a surplus of $(\ln 2/\Gamma)$ compared to the standard FLRW dynamics. This yields a difference of $\sqrt{8/3}\ln 2\sqrt{N_{\rm GR}}$ between the number of e-folds in both scenarios. With the standard numerical values of m and $\rho_{\rm B}$, one gets $N_{\rm LQC} - N_{\rm GR} \simeq 13$, in agreement with the numerical results.

Although an exhaustive investigation would in principle be necessary it can be quite safely conjectured that most results derived in this study do not depend on the details of the considered bounce scenario. Actually, the key parameter is the energy density at which the bounce takes place.

One can also study the differences between the primordial power spectra of cosmological perturbations in the GR-like scenario and in LQC (the interested reader can consider [13] for a detailed study in the dressed metric approach and [14] in the deformed algebra approach). As a toy model to focus on the difference between both background dynamics, we set initial conditions for perturbations at an energy density corresponding to the bounce energy density, choosing the Bunch-Davies vacuum as the initial state. This a "true" Minkowski vacuum only for small enough modes and we use arbitrarily the same normalisation as an approximate Minkowski-like vacuum for IR modes. The resulting power spectra are shown on Fig. 4 and compared with the usual slow-roll inflation expec-

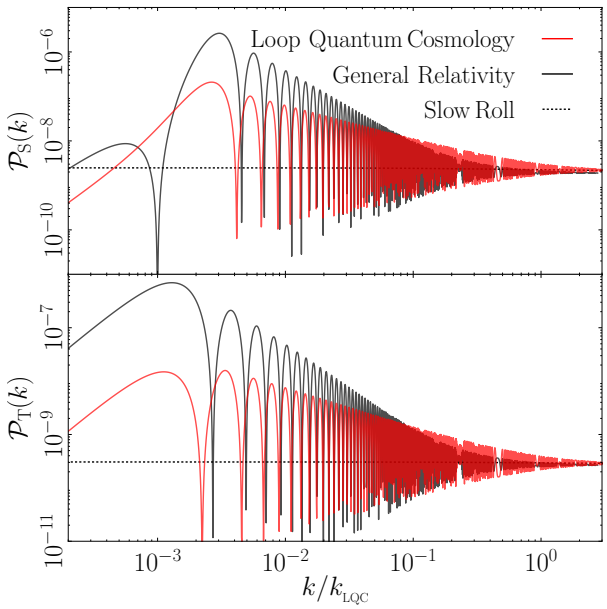

FIG. 4: Primordial power spectra of scalar (top) and tensor (bottom) perturbations for the GR-like dynamics in black (standard Friedmann equation, initial condition at the energy density corresponding to the energy density of the LQC bounce) and LQC dynamics in red (initial conditions at the bounce) plotted against the slow-roll expectation (dotted lines). On the x-axis, $k_{\rm LQC} = a_{\rm B}\sqrt{\rho_{\rm B}}$. The spectrum becomes scale invariant in the UV limit.

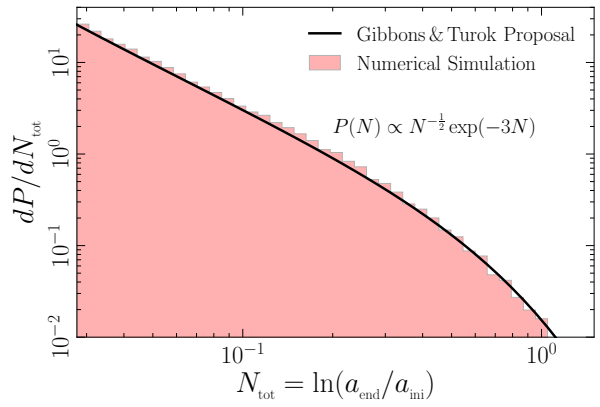

FIG. 5: Probability distribution of the number of e-folds, when the surface of initial data is set at low energy density, in a agreement with the result of Gibbons&Turok.

tation (dotted lines). Such spectra (and their variants including ore subtle LQC effects) are the main observables associated with loop quantum cosmology.

The duration of inflation is crucial because it determines the location of the window of wavenumbers relevant for the cosmic microwave background anisotropy measurements, with respect to the characteristic LQC scale $k_{\rm LQC} \equiv a_{\rm B}\sqrt{\rho_{\rm B}}$. On infrared scales, the mode functions remain in the Bunch-Davies state with $\mathcal{P}(k) \propto k^2$.

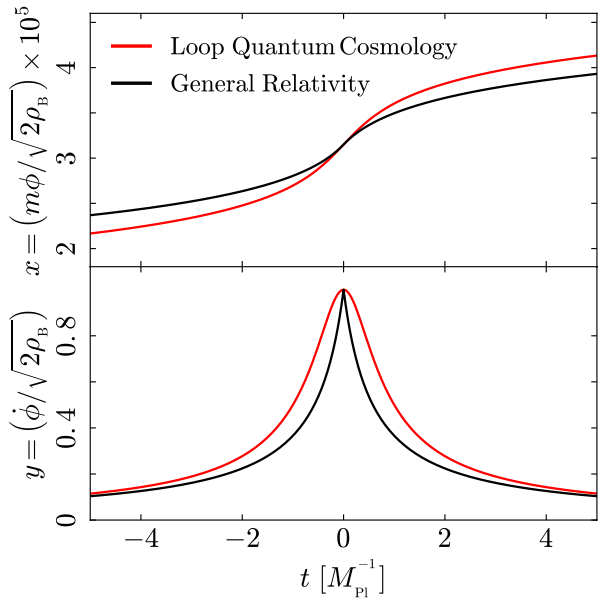

FIG. 6: The fraction of potential and kinetic energy in general relativity (black) and loop quantum cosmology (red).

We see that in both LQC and the GR-like scenario the power spectra agree with the slow-roll expectations in the ultraviolet regime. Oscillations are present in both scenarios in the range $10^{-3} < k/k_{\rm LQC} < 1$. The amplitude is larger in the GR-like scenario than in LQC, however the period of the oscillations does not seem to be affected by the specific modified LQC dynamics. This shows that oscillations in themselves are a bounce feature but not a specific LQC feature. This motivates the search for complementary probes such as primordial non-gaussianity [15]. For a more detailed comparison of the different kinds of power spectra expected in LQC under different assumptions for the mode propagation, see [16].

The most reliable result of loop quantum cosmology is the modified Friedmann equation describing the background dynamics. It receives a quadratic correction in density which prevents the Universe from collapsing into a singularity. In this article, we have investigated the influence of this modified dynamics on the duration of inflation. The conclusion is that the modification of the Friedmann equation has a very small (but non vanishing) impact on the duration of inflation. The key role played by LQC in "predicting" inflation – or more precisely the duration of inflation – is not due to the modified dynamics in itself. It is grounded in two different aspects. First, LQC sets the energy scale. This is the fundamental point. As far as the Universe is assumed to be filled by a massive scalar field, inflation happens naturally if the energy scale "before" inflation is high enough, $\rho \gg m^2$. But whereas starting at the Planck energy density in GR is somehow arbitrary, in LQC the bounce energy density can be calculated (modulo some hypotheses) and derived from the

full theory, providing a natural energy scale. This is the first important aspect. Second, LQC selects favored conditions at the bounce, see formula (6), corresponding to a favored duration of inflation $N \simeq 145$, for $\rho_{\rm B} = 0.41 m_{\rm Pl}^4$. This is an interesting prediction rooted in the existence of a pre-bounce phase where a natural variable to which a known PDF can be assigned was identified. This cannot be produced in standard cosmology and is specific to bouncing models.

ACKNOWLEDGEMENT

The work of BB was supported by a grant from ENS Lyon and a Fulbright Grant from the Franco-American commission.

* Corresponding author: boris.bolliet@lpsc.in2p3.fr

[1] A. Ashtekar and P. Singh, Class. Quant. Grav. **28**, 213001 (2011), 1108.0893.
[2] P. Ade et al. (Planck) (2015), 1502.02114.
[3] B. Bonga and B. Gupt, Gen. Rel. Grav. **48**, 71 (2016), 1510.00680.
[4] K. Martineau, A. Barrau, and S. Schander, Phys. Rev. **D95**, 083507 (2017), 1701.02703.
[5] A. Barrau and B. Bolliet, Int. J. Mod. Phys. **D25**, 1642008 (2016), 1602.04452.
[6] G. W. Gibbons and N. Turok, Phys. Rev. **D77**, 063516 (2008), hep-th/0609095.
[7] L. Kofman, A. D. Linde, and V. F. Mukhanov, JHEP **10**, 057 (2002), hep-th/0206088.
[8] B. Bolliet, A. Barrau, J. Grain, and S. Schander, Phys. Rev. **D93**, 124011 (2016), 1510.08766.
[9] A. Corichi and A. Karami, Phys. Rev. **D83**, 104006 (2011), 1011.4249.
[10] A. Ashtekar and D. Sloan, Gen. Rel. Grav. **43**, 3619 (2011), 1103.2475.
[11] L. Linsefors and A. Barrau, Phys. Rev. **D87**, 123509 (2013), 1301.1264.
[12] L. Linsefors and A. Barrau, Class. Quant. Grav. **32**, 035010 (2015), 1405.1753.
[13] I. Agullo, A. Ashtekar, and W. Nelson, Class.Quant.Grav. **30**, 085014 (2013), 1302.0254.
[14] A. Barrau, M. Bojowald, G. Calcagni, J. Grain, and M. Kagan, JCAP **1505**, 051 (2015), 1404.1018.
[15] I. Agullo, Phys. Rev. **D92**, 064038 (2015), 1507.04703.
[16] B. Bolliet, J. Grain, C. Stahl, L. Linsefors, and A. Barrau, Phys.Rev. **D91**, 084035 (2015), 1502.02431.

Comparison of primordial tensor power spectra from the deformed algebra and dressed metric approaches in loop quantum cosmology

Boris Bolliet,[1,2,*] Julien Grain,[3,4,†] Clément Stahl,[4,3,‡] Linda Linsefors,[2,§] and Aurélien Barrau[2,¶]

[1] *École Normale Supérieure de Lyon, 46 Allée d'Italie, Lyon 69007, France*
[2] *Laboratoire de Physique Subatomique et de Cosmologie, Université Grenoble-Alpes, CNRS/IN2P3 53,avenue des Martyrs, 38026 Grenoble cedex, France*
[3] *CNRS, Orsay, France, F-91405*
[4] *Université Paris-Sud 11, Institut d'Astrophysique Spatiale, UMR8617, Orsay, France, F-91405*

Loop quantum cosmology tries to capture the main ideas of loop quantum gravity and to apply them to the Universe as a whole. Two main approaches within this framework have been considered to date for the study of cosmological perturbations: the dressed metric approach and the deformed algebra approach. They both have advantages and drawbacks. In this article, we accurately compare their predictions. In particular, we compute the associated primordial tensor power spectra. We show – numerically and analytically – that the large scale behavior is similar for both approaches and compatible with the usual prediction of general relativity. The small scale behavior is, the other way round, drastically different. Most importantly, we show that in a range of wavenumbers explicitly calculated, both approaches do agree on predictions that, in addition, differ from standard general relativity and do not depend on unknown parameters. These features of the power spectrum at intermediate scales might constitute a universal loop quantum cosmology prediction that can hopefully lead to observational tests and constraints. We also present a complete analytical study of the background evolution for the bouncing universe that can be used for other purposes.

PACS numbers: 04.60.Pp, 04.60.Bc, 98.80.Qc
Keywords: Quantum gravity, quantum cosmology

I. INTRODUCTION

Loop Quantum Gravity (LQG) is a consistent theory of quantum pseudo-Riemannian geometry that builds on both Einstein gravity and quantum physics, without requiring any fundamentally new principle (like, *e.g.*, extra-dimensions or supersymmetry). Several introductory reviews can be found in [1]. Loop Quantum Cosmology (LQC) is a symmetry reduced version of LQG (see [2] for introductions) which accounts for the basic cosmological symmetries. At this stage, a fully rigorous derivation of LQC from the mother theory is not yet available. In fact, LQC imports the main techniques of LQG in the cosmological sector and uses a "LQG-like" quantization procedure. This so-called polymeric quantization relies on a kinematical Hilbert space that is different from the Wheeler-DeWitt one, and therefore evades the Von Neumann uniqueness theorem. Nonetheless, it has been shown to be well defined when the diffeomorphism invariance is rigorously imposed [3]. Since there is no operator associated with the Ashtekar connection but only with its holonomy, the basic variables of LQC are the holonomy of the Ashtekar connection and the flux of the densitized triad, its conjugate momentum. The main result of LQC is that the Big Bang singularity is removed and replaced by a Big Bounce smooth evolution, so that the total energy density cannot be greater than a critical energy density. Intuitively, for sharply peaked states of the background geometry, the Universe undergoes a quantum tunneling from a classical contracting solution to a classical expanding solution.

At the effective level, LQC can be modeled by two kinds of corrections. The inverse-volume corrections [4] (or inverse-triad, if one relaxes the isotropy hypothesis) are natural cut-off functions of divergences for factors containing inverse powers of densitized triads, arising because of spatial discreetness. The holonomy correction [5] is instead associated with higher powers of the intrinsic and extrinsic spatial curvature components, stemming from the appearance of holonomies of the Ashtekar connection. As the status of inverse-volume correction is less clear –in particular because of a fiducial-cell dependance– we only consider in this article the holonomy corrections.

Even when dealing with holonomy corrections only, there are two main ways of considering the effective theory, leading to a lively debate within the LQC community. This study aims at comparing the predictions for cosmological perturbations of both approaches, setting the initial conditions in the same way (that is at the same time and with the same vacuum), which as not been done to date.

The first approach has been developed in [6–8] and is referred to as the *dressed metric* approach. It relies on a minisuperspace strategy where the homogeneous and isotropic degrees of freedom as well as the inhomogeneous ones (considered as perturbations) are both quantized. The former quantization follows the loop approach

* boris.bolliet@ens-lyon.fr
† julien.grain@ias.u-psud.fr
‡ clement.stahl@icranet.org
§ linsefors@lpsc.in2p3.fr
¶ Aurelien.Barrau@cern.ch

whereas the latter is obtained from a Fock-like procedure on a quantum background. The physical inhomogeneous degrees of freedom are given by the Mukhanov-Sasaki variables derived from the linearized classical constraints. The second order Hamiltonian is promoted to be an operator and the quantization is performed using techniques suitable for the quantization of a test field evolving on a quantum background [9]. The Hilbert space is just the tensor product of a Hilbert space for the background degrees of freedom, with another one for the perturbed degrees of freedom. In the interaction picture, the Schrödinger equation for the perturbations was demonstrated to be formally identical to the Schrödinger equation for the quantized perturbations evolving on a classical background but using a *dressed* metric that encodes the quantum nature of this background.

The second approach, that we refer to as the *deformed algebra*, focuses on the well known problem of the consistency of the effective theory. This basically means that the evolution produced by the model should be consistent with the theory itself. This translates into the requirement that the Poisson bracket between two corrected constraints should be proportional to another constraint. The coefficient of proportionality being a function of the fundamental variables, which makes the situation slightly more subtle than in usual field theories dealing with simple structure constants. The key point is that the closure of the algebra should also be considered off-shell [10]. Interestingly, this closure consistency condition is, after the holonomy correction implementation, basically enough to determine the structure of the quantum Poisson bracket algebra [11–13]. An essential result is that the spacetime structure eventually becomes Euclidean instead of Lorentzian around the bounce, when the total energy density is larger than half the critical energy density. This had been overlooked until spherically symmetric inhomogeneity and cosmological perturbations were studied in an anomaly-free way. Without inhomogeneity, one cannot determine the signature because (i) it is impossible to see the relative sign between temporal and spatial derivatives and (ii) the relevant Poisson bracket trivially equals zero in homogeneous models. The signature change is not a consequence of inhomogeneities, the latter rather being used as a test field. There are hints that in the present context, such an effect could really be interpreted as a deep signature change of space-time rather than a mere tachyonic instability [14].

In this specific study, we do not focus on a specific approach. Both have their advantages and drawbacks. The *dressed metric* approach certainly captures more quantum effects, as it deals with the full wave functions. But it faces a problem. In general relativity (GR), there is in principle an infinite number of dynamical laws, all written with respect to different choices of time coordinates. They are all equivalent one to another because of the symmetries of the classical theory and it is legitimate to pick up an arbitrary choice. In the *dressed metric* approach, one is implicitly making use of several such choices, referred to as a background gauge. The mode dynamic is then written in terms of coordinate-invariant combinations of metric and matter perturbations. Only after these steps, one obtains a specific dynamic for the background variables and perturbations, which is written in a Hamiltonian way. Classically, the resulting dynamic does not depend on the coordinate choice and the procedure is valid. But as some degrees of freedom are quantized here, the equations are modified by quantum corrections of different kinds, and nothing still guarantees that the results do not depend on the arbitrary choices made before (that is, the theory may not be covariant or anomaly-free). What is important is the fact that the classical theory enjoys a strong symmetry which is often used in order to simplify the analysis. When one quantizes or modifies the theory, this symmetry must not be violated, or else one may obtain meaningless (gauge-dependent) results. When the dynamics (including dynamical equations and symmetries) is formulated as a constrained system, one gains access to powerful canonical methods by which the consistency of the theory can be easily analyzed. It is of course possible to use another formalism, but not to ignore the problem of potential violations of crucial symmetries [14]. The *deformed algebra* approach does not suffer from this problem and is certainly more obviously consistent. But it does suffer from other difficulties, namely the shape of the modifications is not strictly speaking entirely determined by the anomaly-free condition, there is a kind of tension with the Hojman, Kuchar and Teitelboim theorem [15] making the geometrical interpretation difficult, and the fact that the fields are normalized *after* the effective quantum corrections were applied to the background, leading to a kind of possibly artificial "re-quantization" of the theory.

The first part of this article is devoted to analytical investigations of the background evolution that were already known but not expressed in such a systematic way. This material will also be very useful for the rest of the study, as the shape of the primordial tensor power spectrum depends mainly on the cosmic history. The second part is devoted to the calculation of the infrared and ultraviolet limits of the primordial tensor power spectrum for sharply peaked states in the dressed metric approach. The third part deals with the same issues in the deformed algebra model. In both cases, the initial conditions are set in the same way, in the contracting phase, in order to make a meaningful comparison. The fourth part shows the results of the numerical computations of the full power spectra and some universal features are underlined. In the conclusion, we outline the main differences and similarities between both approaches before giving some perspectives towards observational tests and constraints.

II. BACKGROUND EVOLUTION: ANALYTICAL SOLUTIONS

In this section we study the background evolution at the effective level. Although this has already been studied (see [2]), our purpose here is to provide analytic solutions which are accurate approximations of the cosmic history over different regions. Our scope is twofold. First, this can give further insights on the effective dynamics of the background, potentially useful for further investigations. Second, these analytic results are developed in the scope of the forthcoming investigation of tensor perturbations since their equation of motion obviously involves background quantities such as the scale factor and the total energy density. Here we focus on the most probable dynamics as in [16, 17].

A. Overview of the background dynamics

The background evolution of the quantum universe is described using the effective, semiclassical dynamics, as derived in loop quantum cosmology with holonomy corrections. In this article, the background geometry is described by the unperturbed metric tensor $\mathrm{g} = -\mathrm{dt} \otimes \mathrm{dt} + a^2 \delta_{ij} \mathrm{dx^i} \otimes \mathrm{dx^j}$, where a is the scale factor. Dots denote derivatives with respect to the cosmic time, $\dot{a} \equiv \frac{\partial a}{\partial t}$, and primes denote derivatives with respect to conformal time, related to the cosmic time by $dt = a d\eta$. The content of the universe is modelled by a single massive scalar field, ϕ, with a quadratic potential, $V(\phi) = m^2\phi^2/2$. In order to characterize the field evolution we use two dynamical parameters, the potential energy parameter, x, and the kinetic energy parameter, y, defined by

$$x \equiv \frac{m\phi}{\sqrt{2\rho_{\mathrm{c}}}}, \qquad y \equiv \frac{\dot{\phi}}{\sqrt{2\rho_{\mathrm{c}}}}, \tag{1}$$

where ρ_{c} is the critical density, *i.e.* the maximum value of the total energy density that can be express as $\rho = \rho_{\mathrm{c}}\left(x^2 + y^2\right)$. The modified Friedmann equation, as predicted in LQC from the Hamiltonian constraint and the Hamilton equations, is

$$H^2 = \frac{8\pi G\rho}{3}\left(1 - \frac{\rho}{\rho_{\mathrm{c}}}\right), \tag{2}$$

where $H \equiv \frac{\dot{a}}{a}$ is the Hubble parameter. The Klein-Gordon equation for the scalar field is

$$\ddot{\phi} + 3H\dot{\phi} + m^2\phi = 0. \tag{3}$$

Equations (2) and (3) are recast into

$$\begin{cases} \dot{H} &= -8\pi G\rho_{\mathrm{c}} y^2\left(1 - 2x^2 - 2y^2\right), \\ \dot{x} &= my, \\ \dot{y} &= -3Hy - mx. \end{cases} \tag{4}$$

There are two time scales involved in this system of equations. One is given by $1/m$ and corresponds to the classical evolution of the field. The other time scale is $1/\sqrt{G\rho_{\mathrm{c}}}$ and corresponds to the quantum regime of the evolution. Modulo a numerical factor, relevant for the following calculations, the ratio of these two time-scales is

$$\Gamma \equiv \frac{m}{\sqrt{24\pi G\rho_{\mathrm{c}}}}. \tag{5}$$

If we assume $\Gamma \ll 1$, and start with a negative Hubble parameter (contracting universe), the background dynamics splits into three subsequent phases:

(i) Pre-bounce contracting phase,

(ii) Bouncing phase,

(iii) Slow-roll inflation.

In each phase, it is possible to get analytical expressions for all the background variables. Note that the value of the inflaton mass preferred by Cosmic Microwave Background (CMB) observations is $m \simeq 10^{-6} m_{\mathrm{Pl}}$. Furthermore, calculations of the black hole entropy suggests $\rho_{\mathrm{c}} = 0.41 m_{\mathrm{Pl}}^4$, leading to $\Gamma \simeq 2 \times 10^{-7}$. Therefore, asserting $\Gamma \ll 1$ is not a strong assumption at all.

B. Initial conditions

The initial conditions $\{a_0, x_0, y_0\}$ are set in the remote past, when $H_0 < 0$ and

$$\sqrt{\tfrac{\rho_0}{\rho_{\mathrm{c}}}} \ll \Gamma. \tag{6}$$

The subscript '0' means that the variables are evaluated at $t = 0$. The condition (6) ensures that initially the dynamic is not dominated by the amplification due to the term '$3H$' in (3). We often use polar coordinates for x and y:

$$\begin{cases} x(t) = \sqrt{\frac{\rho(t)}{\rho_{\mathrm{c}}}}\sin\left(mt + \theta_0\right), \\ y(t) = \sqrt{\frac{\rho(t)}{\rho_{\mathrm{c}}}}\cos\left(mt + \theta_0\right). \end{cases} \tag{7}$$

The initial value of the energy density is specified with the two numbers α and θ_0:

$$\sqrt{\tfrac{\rho_0}{\rho_{\mathrm{c}}}} = \frac{\Gamma}{\alpha}\left\{1 - \frac{\sin(2\theta_0)}{4\alpha}\right\}^{-1}. \tag{8}$$

For a given $\alpha \gg 1$, such that (6) is valid, there is a one-to-one correspondence between the family of solutions to (4) and the interval $\{\theta_0 |\, 0 \leq \theta_0 < 2\pi\}$. The choice for this parametrization is clarified in the next section.

C. The pre-bounce classical contracting phase

As long as (6) holds for $\rho(t)$, the system (4) can be solved analytically. In the third line of (4), the term '$3Hy$' can be neglected, compared to mx', as their ratio is of order $\mathcal{O}(1/\alpha)$ initially. Then, x and y behave simply as the phase variables of the harmonic oscillator (*i.e.* (7) with constant amplitude). The solution for y can be injected into the equation for $\dot{H}$ in (4) where one neglects '$-2x^2-2y^2$' in comparison to unity in the bracket. The Hubble parameter is replaced by its expression in terms of the energy density (2) where the correction $\rho/\rho_{\rm c}\ll 1$ is neglected. After these replacements, one is left with a first order differential equation over $\rho(t)$ which can be integrated into

$$\sqrt{\tfrac{\rho(t)}{\rho_{\rm c}}}=\frac{\Gamma}{\alpha}\left\{1-\frac{1}{2\alpha}\left[mt+\tfrac{1}{2}\sin(2mt+2\theta_0)\right]\right\}^{-1}. \quad (9)$$

This solution exhibits an oscillatory behavior due to the sine function in the denominator. The oscillations have a period of order $1/m$, much smaller than the time scale of the growth, α/m. Moreover, their amplitude is also smaller than the averaged amplitude $\sqrt{\rho/\rho_{\rm c}}$ by a factor α. When these small and fast oscillations are neglected, the Hubble parameter can be expressed as

$$H(t)=H_0\left(1+\tfrac{3}{2}H_0 t\right)^{-1}, \quad (10)$$

where the initial Hubble parameter is $H_0=-m/(3\alpha)$. With the parametrization (9), solutions with the same α but different θ_0's are all corresponding to the same averaged behavior (there is only a phase difference between them). From (10), the scale factor can be computed as a function of cosmic time, and as a function of conformal time after another integration. As the value of the initial conformal time η_0 can be set arbitrarily, we choose $\eta_0=2/(H_0a_0)$. With such a choice, the expression for the scale factor simply reads

$$a(\eta)=\lambda_0\eta^2 \quad \text{with} \quad \lambda_0\equiv\frac{a_0^3H_0^2}{4}, \quad (11)$$

so that the expression of the comoving Hubble radius during the contracting phase is

$$aH(\eta)=\frac{2}{\eta}. \quad (12)$$

This is the same behavior as with a universe filled with dust-like matter. When $H\simeq -m/3$, the amplification term '$3H$' in (4) becomes dominant. It corresponds to the end of the pre-bounce contracting phase and the start of the bouncing phase. The contracting phase ends when $\rho_{\rm A}=\Gamma^2\rho_{\rm c}$, so at this stage there is no significant quantum effects.

D. The bouncing phase

Let us define $t_{\rm A}$, the time such that $H(t_{\rm A})=-m/3$. One finds $t_{\rm A}=2(\alpha-1)/m$. Moreover, at $t_{\rm A}$, if the small and fast oscillations of the field are neglected, the fractions of potential and kinetic energy are given by

$$x_{\rm A}=\Gamma\sin\theta_{\rm A} \quad \text{and} \quad y_{\rm A}=\Gamma\cos\theta_{\rm A}, \quad (13)$$

with $\theta_{\rm A}\equiv 2(\alpha-1)+\theta_0$. The Hubble parameter keeps increasing (in modulus) until it reaches a maximum, $H_{\rm max}\equiv\sqrt{24\pi G\rho_{\rm c}}/6$. The inverse of $H_{\rm max}$ has the dimension of a time and gives an estimate of the time scale of this amplification. As a first analysis, in the second equation of the system (4), the time derivative can be replaced by a factor $H_{\rm max}$. Then, we find that the ratio between the fraction of potential and kinetic energy is of order $\sim 6\Gamma$, and therefore very small in comparison to unity. This suggests that at the start of the bouncing phase, the kinetic energy parameter grows very quickly, while the fraction of potential energy remains of order $\sim\Gamma$. When the kinetic energy is dominant, the system of equations (4) reduces to

$$\begin{cases}\dot{y}=\sqrt{24\pi G\rho_{\rm c}}\,y^2\sqrt{1-y^2},\\ \dot{x}=my,\end{cases} \quad (14)$$

which can be solved analytically. The solutions to (14) shall be valid as long as the kinetic energy dominates over the potential energy. In particular, they are valid at the bounce when the energy density reaches $\rho_{\rm c}$, or equivalently when $y(t_{\rm B})=1$. For the time $t_{\rm B}$, at which the bounce occurs, one finds $t_{\rm B}=t_{\rm A}+\frac{1}{m|\cos\theta_{\rm A}|}$.

The fractions of kinetic and potential energy during the bouncing phase can be expressed as

$$y(t)=\left[1+24\pi G\rho_{\rm c}(t-t_{\rm B})^2\right]^{-\frac{1}{2}}, \quad (15a)$$

$$x(t)=x_{\rm B}+\varepsilon\Gamma\,\mathrm{arcsinh}\left(\sqrt{24\pi G\rho_{\rm c}}(t-t_{\rm B})\right), \quad (15b)$$

where $\varepsilon\equiv\mathrm{sgn}(\cos\theta_{\rm A})$, and the value of the potential energy parameter at the bounce is given by

$$x_{\rm B}=x_{\rm A}-\varepsilon\Gamma\ln\left(\tfrac{1}{2}\Gamma\left|\cos\theta_{\rm A}\right|\right). \quad (16)$$

The case $\cos\theta_{\rm A}\ll 1$ may appear problematic. Actually it corresponds to a different evolution of the background, with a phase of *deflation* before the bounce. Here we focus on cases –statistically much more frequent and therefore relevant for phenomenology [17]– where a sufficiently long phase of inflation is achieved. During the bouncing phase, the Hubble parameter and the scale factor take on a very simple form. The scale factor is related to the kinetic energy parameter by $a=a_{\rm B}|y|^{-\frac{1}{3}}$. Consequently, the expression for the scale factor at $t_{\rm A}$ is

$$a_{\rm A}=a_{\rm B}\left|\Gamma\cos\theta_{\rm A}\right|^{-\frac{1}{3}}. \quad (17)$$

Using (12), we can find the conformal time $\eta_{\rm A}$ that corresponds to $t_{\rm A}$. Then, we can use (17) and (11) in order to write $\eta_{\rm A}$ in terms of λ_0. We get

$$\eta_{\rm A}=-\left(\frac{6}{m\lambda_0}\right)^{1/3}. \quad (18)$$

After the bounce, the fraction of potential energy increases. Meanwhile, the fraction of kinetic energy decreases and eventually becomes smaller than the fraction of potential energy. This corresponds to the start of slow-roll inflation.

E. The classical slow-roll inflation

The total energy density $\rho = \rho_{\rm c}\left(x^2+y^2\right)$, with $x\left(t\right)$ and $y\left(t\right)$ given by (15a) and (15b), reaches a minimum at time $t_{\rm i}$. According to these analytical expressions the total energy density increases for $t > t_{\rm i}$. Obviously, this is irrelevant in an expanding universe without energy sources: the total energy density must always decrease. The time $t_{\rm i}$ can be computed analytically by solving $\dot{\rho}\left(t_{\rm i}\right) = 0$. One gets $t_{\rm i} = t_{\rm B} + \left(f/m\right)$, where f is expressed in terms of the Lambert W function (defined as the solution to $z = W(z)e^{W(z)}$), and $x_{\rm B}$ is given by

$$f \equiv \sqrt{\frac{2}{W\left(z\right)}} \quad \text{with} \quad z = \frac{8}{\Gamma^2}\exp\left(\frac{2\left|x_{\rm B}\right|}{\Gamma}\right). \tag{19}$$

In general, f is of order $\mathcal{O}(1)$. For instance, when $\cos\theta_{\rm A} = 1$ and $\Gamma = 2\times10^{-7}$, one gets $f \simeq 0.18$. At $t_{\rm i}$, the fraction of potential energy is calculated with (15a), (15b) and (16). We find

$$x_{\rm i} = x_{\rm A} - 2\varepsilon\Gamma\ln\left(\tfrac{1}{2}\Gamma\sqrt{\tfrac{\left|\cos\theta_{\rm A}\right|}{f}}\right). \tag{20}$$

Shortly after $t_{\rm i}$ (in a time of order $1/(m\ln\Gamma)$), one can show that the fraction of kinetic energy ends up being almost constant. One then has $y_{\rm i} \equiv -\varepsilon\Gamma$ and the slow-roll conditions are fulfilled. Actually, for the quadratic potential it is enough to check that $\epsilon_{\rm H} \equiv -\dot{H}/H^2$ is small in comparison to unity for the slow-roll conditions to be valid. We find

$$\epsilon_{\rm H} = 3\left|\frac{\Gamma}{x_{\rm i}}\right|^2, \tag{21}$$

which is generally a small number. For $\cos\theta_{\rm A} = 1$ and $\Gamma = 2\times10^{-7}$ one gets $\epsilon_{\rm H} \simeq 0.003$. Slow-roll inflation can start, the system of equation (4) reduces to

$$\begin{cases} y = -\varepsilon\Gamma, \\ \dot{x} = my, \end{cases} \tag{22}$$

and the Hubble parameter becomes

$$H(t) = H_{\rm i}|1 - \varepsilon\tfrac{\Gamma}{x_{\rm i}}m(t-t_{\rm i})|. \tag{23}$$

where $H_{\rm i} = \sqrt{8\pi G\rho_{\rm c}/3}\,|x_{\rm i}|$. We can also use (23) to compute the scale factor at $t_{\rm i}$ with $|y_{\rm i}| = \Gamma$. We get

$$a_{\rm i} = a_{\rm B}\Gamma^{-\frac{1}{3}}. \tag{24}$$

Note that at the start of slow-roll inflation the total energy density is smaller than the critical energy density by a factor Γ^2. Therefore, when slow-roll inflation starts, the universe is already classical (since quantum corrections are negligible).

We stress that all the analytical approximations derived above have been checked against numerical integrations of equation (4). This has been done for each one of the three subsequent phases as well as for the matching between them.

III. POWER SPECTRUM IN THE DRESSED METRIC APPROACH

A. Preliminaries on the dressed metric approach

The dressed metric approach for both scalar and tensor cosmological perturbations in LQC has been developed in [6–8]. Focusing on the tensor modes, the primordial power spectrum at the end of inflation is defined in terms of the mode functions of the Mukhanov-Sasaki variables, denoted v_k, as[1]

$$\mathcal{P}_{\rm T}(k) = \frac{32Gk^3}{\pi}\left|\frac{v_k(\eta_{\rm e})}{a(\eta_{\rm e})}\right|^2, \tag{25}$$

with $\eta_{\rm e}$ standing for the end of inflation.

It is worth mentioning that the precise knowledge of $\eta_{\rm e}$ is not mandatory for the derivation of the primordial power spectrum in both the infrared (IR) and ultraviolet (UV) limits. For the IR limit, this is because infrared modes are (by definition) mainly amplified during the contraction and the contribution of inflation is suppressed as compared to the previous phases. In the UV, this is because we focus on modes that crossed the horizon during inflation, so that their amplitude has remained constant after a few e-folds.

In order to obtain the power spectrum, one has to solve the equation of motion for the mode functions, $v_k(\eta)$, with given initial conditions. In conformal time, this equation takes the form of a Schrödinger equation

$$v_k''(\eta) + \left(k^2 - \frac{\langle\tilde{a}''\rangle}{\langle\tilde{a}\rangle}\right)v_k(\eta) = 0, \tag{26}$$

where $\tilde{a}$ is a *dressed* scale factor and $\langle.\rangle$ refers to the quantum expectation value on background states. This takes into account the width of the background wave function and has *a priori* no reason to be equal to the scale factor, $a(t)$, solution to the modified Friedmann equation (corresponding to the scale factor traced by the *peak* of the

[1] This model is parity invariant and the two helicity states of the tensor mode are equally amplified. The summation over the helicity states is implicitly done in our definition of the primordial power spectrum.

sharply peaked wave function). However, it is argued in [8] that for sharply peaked background states, the dressed effective potential term, $\langle\tilde{a}''\rangle / \langle\tilde{a}\rangle$, is very well approximated by its peaked value, a''/a, from the bounce up to the entire expanding phase. We expect this approximation to be valid from the bounce down to the classical contracting phase since this also corresponds to a more and more classical universe when going backward in time from the bounce. With this approximation, (26) becomes

$$v_k''(\eta) + \left(k^2 - \frac{a''}{a}\right) v_k(\eta) = 0, \tag{27}$$

where the scale factor is now solution to the modified Friedmann equation, and the analytical results derived in Sec. II can be used for the background variables.

B. Calculation of the IR limit

1. Definition of the IR regime

The IR limit of the primordial power spectrum is obtained by considering the modes which stopped oscillating with time and were frozen during the pre-bounce contracting phase. The freezing of a mode happens when its wavenumber becomes smaller than the effective potential, $\sqrt{a''/a}$. With the analytical expressions given in the previous section, one finds that during the contraction,

$$\frac{a''}{a} = \frac{2}{\eta^2}. \tag{28}$$

Thus, an infrared mode with a wavenumber k crosses the effective potential at a conformal time $|\eta_k| \equiv \sqrt{2}/k$. Its amplitude is frozen from that time up to the end of inflation, as k^2 remains smaller than a''/a. Since $-\infty < \eta < \eta_A$ (with $\eta_A < 0$), the modes that crossed the potential during the contracting phase are in the range $0 < k < k_{\rm IR}$, with $k_{\rm IR}$ defined by the mode that crossed the effective potential at the beginning of the bouncing phase. With (28), (17), (11) and (18) we find

$$k_{\rm IR} = \frac{a_{\rm B}}{3\sqrt{2}} \left(\frac{m^2\sqrt{24\pi G\rho_{\rm c}}}{|\cos\theta_{\rm A}|}\right)^{1/3}. \tag{29}$$

The IR limit stands for the modes such that $k \ll k_{\rm IR}$.

2. Primordial power spectrum in the IR regime

For infrared modes, from the potential crossing η_k to the end of inflation $\eta_{\rm e}$, the solution to the equation of motion (27) is therefore well approximated by

$$v_k^{\rm IR}(\eta) = \alpha_k a(\eta) + \beta_k a(\eta) \int_{\eta_\star}^{\eta} \frac{d\eta'}{a^2(\eta')} + \mathcal{O}((k/k_{\rm IR})^2), \tag{30}$$

where α_k and β_k are two constants to be determined. The value of $\eta_\star$ can be conveniently set by requiring the term proportional to α_k to be solely decaying, and the term proportional to η_k to be solely growing. During the contracting phase, the term proportional to α_k is clearly decaying since $a(\eta)$ is decreasing. A convenient choice for $\eta_\star$ is such that the term proportional to β_k must be solely growing. Since $a(\eta) = \lambda_0\eta^2$, the term proportional to β_k has a time dependance $\sim \eta^2(\eta^{-3} - \eta_\star^{-3})$, in which the part proportional to $\eta^2/\eta_\star^3$ is decaying ($\eta < 0$) and we send $\eta_\star$ to $(-\infty)$ to remove it[2].

From (30) and (25), the expression of the IR limit of the spectrum reads

$$\mathcal{P}_{\rm T}(k)^{\rm IR} = \frac{32Gk^3}{\pi} \left|\alpha_k + \beta_k I(\eta_{\rm e})\right|^2, \tag{31}$$

where $I(\eta_{\rm e})$ is the integral defined as

$$I(\eta_{\rm e}) \equiv \int_{-\infty}^{\eta_{\rm e}} \frac{d\eta}{a^2}. \tag{32}$$

The calculation of the IR limit proceeds in two steps. First, we compute α_k and β_k by matching (30) to a set of solutions defined in the contracting phase. As we shall see, this determines the scale dependence of the primordial power spectrum in the infrared regime. The second step is the calculation $I(\eta_{\rm e})$ using the analytical solutions for the background, obtained in Sec. II. This second step sets the amplitude of the power spectrum. The expression of the primordial spectrum is finally obtained by gathering the expressions of α_k, β_k and $I(\eta_e)$.

In order to derive the expressions of α_k and β_k, the approximate solution given in (30) (valid in the IR only but from η_k to $\eta_{\rm e}$) has to be matched with a set of solutions to the equation (27), during the contracting phase. With $a''/a = 2/\eta^2$, this set of solutions corresponds to the linear combinations of the Hankel functions of order $\nu = 3/2$:

$$v_k^{\rm C}(\eta) = \sqrt{-k\eta}\left[A_k H_{3/2}(-k\eta) + B_k H^\star_{3/2}(-k\eta)\right], \tag{33}$$

where the superscript 'C' recalls that (33) is valid only during the contracting phase. In order to specify A_k and B_k we match (33) with the Minkowski vacuum in the remote past, *i.e.* $v_k(\eta \to -\infty) = e^{-ik\eta}/\sqrt{2k}$. This requirement leads to

$$A_k = \sqrt{\frac{\pi}{4k}} \quad \text{and} \quad B_k = 0, \tag{34}$$

[2] During the contracting phase, the identification of the growing and decaying modes differs from that identification during inflation. Because the Universe is expanding during inflation, the term $\alpha_k a(\eta)$ is solely growing (while it is solely decaying during contraction). Then the term $\beta_k \int_{\eta_\star}^{\eta} d\eta'/a^2(\eta')$ can be made solely decaying in an inflationary universe by setting $\eta_\star = \eta_{\rm e}$ (while it is made solely growing during contraction by setting $\eta_\star \to -\infty$).

up to a phase which is has no importance here[3]. A set of solutions valid in the range $-\infty < \eta < \eta_A$, and corresponding to the Minkowski vacuum, is thus

$$v_k^{\rm C}(\eta) = \tfrac{1}{2}\sqrt{-\pi\eta}\,H_{3/2}(-k\eta). \tag{35}$$

Since $\eta_k \ll \eta_{\rm A}$ for infrared modes, the IR limit of (35) has to coincide with (30) in the interval $\eta_k \lesssim \eta \lesssim \eta_{\rm A}$. At a given η in this interval, we calculate the asymptotic limit of the Hankel function when $k \to 0$. This leads to

$$\lim_{k\to 0} v_k^{\rm C}(\eta) = \frac{i}{\sqrt{2}k^{3/2}\eta} + \mathcal{O}(k^{3/2}). \tag{36}$$

The term of order $\mathcal{O}(k^{3/2})$ has a time dependence given by $a(\eta) \propto \eta^2$, and corresponds to the term proportional to α_k in (30).

Eventually, we have to match (36) with the explicit expression of (30) that one obtains with $a(\eta) = \lambda_0\eta^2$ and $\eta_\star = -\infty$:

$$v_k^{\rm IR}(\eta) = \alpha_k\lambda_0\eta^2 - \frac{\beta_k}{3\lambda_0\eta}. \tag{37}$$

By comparing (37) with (36), one finds

$$\alpha_k = \mathcal{O}(k^{3/2}) \quad \text{and} \quad \beta_k = (3i/\sqrt{2})\lambda_0 k^{-3/2}. \tag{38}$$

For infrared modes the contribution of α_k is negligible, so that (31) simplifies to

$$\mathcal{P}_{\rm T}(k)^{\rm IR} = \frac{144G}{\pi}\lambda_0^2|I(\eta_{\rm e})|^2. \tag{39}$$

Therefore, in the IR limit we expect the power spectrum to be *scale invariant* (at least at the order of validity of our approximations).

The amplitude of the power spectrum in the IR regime is obtained by evaluating the integral $I(\eta_{\rm e}) = \int_{-\infty}^{\eta_{\rm e}} d\eta/a^2$. In order to do this, we split the integral into three parts

$$I(\eta_{\rm e}) = I(-\infty,\eta_{\rm A}) + I(\eta_{\rm A},\eta_{\rm i}) + I(\eta_{\rm i},\eta_{\rm e}). \tag{40}$$

The first part corresponds to the contracting phase, the second part corresponds to the bouncing phase, and the last part gives the contribution of the inflationary phase. With $a(\eta) = \lambda_0\eta^2$ during the contracting phase, and recalling that $\eta_{\rm A} = -[6/(m\lambda_0)]^{1/3}$, the first part of the integral is easy to compute:

$$I(-\infty,\eta_{\rm A}) = \frac{m}{18\lambda_0}. \tag{41}$$

The second part of the integral is first written in cosmic time, $I(\eta_{\rm A},\eta_{\rm i}) = \int_{t_{\rm A}}^{t_{\rm i}} a(t)^{-3}dt$. During the bouncing phase we have found that $a = a_{\rm B}|y|^{-\frac{1}{3}}$. Then, with $y = \dot{x}/m$, the integrand is proportional to $\dot{x}$ and the integral itself is proportional to the difference $|x_{\rm i} - x_{\rm A}|$ (which is given in (20)). Eventually, one gets

$$I(\eta_{\rm A},\eta_{\rm i}) = -\frac{m}{18\lambda_0}\frac{1}{|\cos\theta_{\rm A}|}\ln\left(\tfrac{1}{2}\Gamma\sqrt{\tfrac{|\cos\theta_{\rm A}|}{f}}\right). \tag{42}$$

The last part of the integral corresponds to the slow-roll inflation as obtained from a massive scalar field. The calculations are well known in this case, leading to

$$I(\eta_{\rm i},\eta_{\rm e}) = \left(\frac{1}{3a_{\rm i}^3H_{\rm i}} - \frac{1}{3a_{\rm e}^3H_{\rm e}}\right)[1 + \mathcal{O}(\epsilon_{\rm H})], \tag{43}$$

where $\epsilon_{\rm H} \equiv -\dot{H}/H^2$ is the slow-roll parameter which remains small in comparison to unity (except in the neighbourhood of $t_{\rm e}$). It will be neglected in the forthcoming calculations. During slow-roll inflation, the Hubble parameter decreases linearly with cosmic time while the scale factor grows exponentially. The second term, $1/(a_{\rm e}^3H_{\rm e})$, can be safely neglected as it is suppressed by a factor $\sim \exp(-3N_{\rm e})$, where $N_{\rm e}$ denotes the number of e-folds from $\eta_{\rm i}$ to $\eta_{\rm e}$. This also means that the detailed dynamic of inflation is not needed here, since its contribution is rapidly negligible after a few e-folds. With the expressions of $a_{\rm i}$ and $H_{\rm i}$ given in (23), $I(\eta_{\rm i},\eta_{\rm e})$ evaluates to

$$I\left(\eta_{\rm i},\eta_{\rm e}\right) = \frac{m}{12\sqrt{3}\lambda_0}\frac{\Gamma}{|x_{\rm i}\cos\theta_{\rm A}|}, \tag{44}$$

with x_i given in (20).

Gathering the results (41), (42) and (44), the integral $I(\eta_{\rm e})$ can be written as $I\left(\eta_{\rm e}\right) = \frac{m}{18\lambda_0}\left(1 + \mathcal{I} + \mathcal{J}\right)$, so that the IR limit of the power spectrum (39) reads

$$\mathcal{P}_{\rm T}(k)^{\rm IR} = \frac{4G}{9\pi}m^2|1 + \mathcal{I} + \mathcal{J}|^2, \tag{45}$$

where

$$\mathcal{I} \equiv -\frac{1}{|\cos\theta_{\rm A}|}\ln\left(\tfrac{1}{2}\Gamma\sqrt{\tfrac{|\cos\theta_{\rm A}|}{f}}\right), \tag{46}$$

$$\mathcal{J} \equiv \frac{\Gamma\sqrt{3}}{2\,|x_{\rm i}\cos\theta_{\rm A}|}. \tag{47}$$

In general, $\mathcal{J}$ is much smaller than $\mathcal{I}$, suggesting that the contribution to the amplitude of the spectrum in the IR that corresponds to inflation is negligible (for instance with $\cos\theta_{\rm A} = 1$ and $\Gamma = 2\times10^{-7}$, one gets $\mathcal{J}/\mathcal{I} \simeq 0.002$).

The scale-invariance of the IR limit of the spectrum is a direct consequence of the fact that the infrared modes crossed the effective potential, a''/a, during the contracting phase whose dynamics is equivalent to that of a dust-like matter dominated era. No further assumption on the detailed dynamics of the bounce is needed to get the scale invariance (though the detailed dynamics is needed to get the amplitude of the power spectrum). The amplitude

[3] This also fits with the appropriate Wronskian condition as required for the quantization *à la* Fock of the tensor perturbations field.

only depends on three parameters: the critical energy density, the mass of the scalar field, and the phase $\theta_{\rm A}$, between $x = m\phi/\sqrt{2\rho_{\rm c}}$ and $y = \dot{\phi}/\sqrt{2\rho_{\rm c}}$ at the start of the bouncing phase. The first two parameters are fundamental. The phase $\theta_{\rm A}$ depends on θ_0 which is a contingent parameter whose value sets the initial conditions (see [17] for a more detailed discussion). The case $\cos\theta_{\rm A} \ll 1$ may appear problematic (as it would lead to a divergent power spectrum), however in this case the dynamic of the background would be different (with *deflation* before the bounce) and our analytical results would not be valid.

C. Calculation of the UV limit

1. Definition of the UV regime

By definition, the ultraviolet modes have remained well inside the Hubble radius until the phase of slow-roll inflation. They are insensitive to the background curvature during the contracting and the bouncing phase. The effective potential a''/a can be written in terms of the Hubble parameter and its time derivative as $a''/a = a^2\left(\dot{H}+2H^2\right)$. During the bounce, this expression becomes

$$\frac{a''}{a} = \frac{8\pi G\rho_{\rm c}}{3}a_{\rm B}^2 y^{\frac{4}{3}}\left(4y^2-1\right). \tag{48}$$

It is clear in (48) that the effective potential reaches its maximum at the bounce, when $y = 1$. This feature sets a scale, $k_{\rm UV} \equiv \max\sqrt{a''/a}$, which evaluates to

$$k_{\rm UV} = a_{\rm B}\sqrt{8\pi G\rho_{\rm c}}. \tag{49}$$

All modes with a wavenumber larger than $k_{\rm UV}$ crossed the potential during slow-roll inflation. The UV limit of the power spectrum is defined by the modes with a wavenumber $k \gg k_{\rm UV}$.

2. Primordial power spectrum in the UV regime

In the dressed metric approach, the calculation of the UV limit of the power spectrum is straightforward. As during the bouncing phase the mode functions do not feel the curvature of space-time, they are well approximated by

$$v_k^{\rm UV}(\eta) = \frac{1}{\sqrt{2k}}e^{ik\eta} \quad \text{for } \eta < \eta_{\rm i}. \tag{50}$$

Once the Universe enters inflation, the term a''/a cannot be neglected anymore and behaves as $(2+3\epsilon_{\rm H})/\eta^2$. The mode functions are now given by a linear combination of the Hankel functions of order $3/2+\epsilon_{\rm H}$. At this stage, the derivation of the primordial spectrum is simple: we have to match the Minkowski vacuum (well defined within the Hubble radius for $k \gg k_{\rm UV}$) with the mode functions commonly used in slow-roll inflation. The power spectrum in the UV regime is then given by the standard red-tilted power spectrum of slow-roll inflation (see [23–25]),

$$\mathcal{P}_{\rm T}(k)^{\rm UV} = \frac{16G}{\pi}H^2\left[1-2\epsilon_{\rm H}\left(2C+1\right)\right], \tag{51a}$$

$$\frac{{\rm d}\ln\mathcal{P}_{\rm T}(k)^{\rm UV}}{{\rm d}\ln k} = -2\epsilon_{\rm H}, \tag{51b}$$

where H is the Hubble parameter evaluated when $k = aH$, and $C \simeq -0.73$. At the order of validity of our approximation ($\Gamma \ll 1$) and neglecting $\epsilon_{\rm H}$ in the amplitude, these expressions become

$$\mathcal{P}_{\rm T}(k)^{\rm UV} = \frac{16G}{\pi}m^2\left|\frac{x_{\rm i}}{\Gamma}\right|^2, \tag{52a}$$

$$\frac{{\rm d}\ln\mathcal{P}_{\rm T}(k)^{\rm UV}}{{\rm d}\ln k} = -6\left|\frac{\Gamma}{x_{\rm i}}\right|^2, \tag{52b}$$

where $\Gamma \equiv m/\sqrt{24\pi G\rho_{\rm c}}$ and $x_{\rm i}$ is given by (20). This prediction of a slightly red tilted spectrum matches the standard inflationary model. The amplitude scales with m^2 and depends on the critical energy density in a non-trivial way. With $\cos\theta_{\rm A} = 1$ for simplicity, one gets $\mathcal{P}_{\rm T}(k)^{\rm UV} \propto m^2\ln^2(m/\sqrt{G\rho_{\rm c}})$. Moreover, with the standard value $\Gamma = 2\times10^{-7}$ we find that the spectral index at the start of inflation, given by (52b), is $n_{\rm T}-1 \simeq -0.007$.

IV. POWER SPECTRUM IN THE DEFORMED ALGEBRA APPROACH

A. The deformed algebra approach

The calculations presented above can be extended to the case of the tensor power spectrum in the deformed algebra approach [10–14]. The equation of motion for the mode functions of the Mukhanov-Sasaki variables also takes the form of a Schrödinger equation. However, the frequency term is time-dependent and the effective potential is different:

$$v_k''(\eta) + \left(\Omega k^2 - \frac{z_{\rm T}''}{z_{\rm T}}\right)v_k(\eta) = 0, \tag{53}$$

where

$$\Omega \equiv 1 - 2\frac{\rho}{\rho_{\rm c}} \quad \text{and} \quad z_{\rm T} \equiv \frac{a}{\sqrt{\Omega}}. \tag{54}$$

The region with $\Omega > 0$, corresponding to $\rho < \rho_{\rm c}/2$, is Lorentzian whereas the region with $\Omega < 0$, corresponding to $\rho > \rho_{\rm c}/2$, is Euclidean. Here, the mode functions are related to the amplitude of the tensor modes of the metric perturbation, h_k, via $v_k = z_{\rm T}h_k/\sqrt{32\pi G}$, so that the power spectrum is now defined as

$$\mathcal{P}_{\rm T}(k) = \frac{32Gk^3}{\pi}\left|\frac{v_k(\eta_{\rm e})}{z_{\rm T}(\eta_{\rm e})}\right|^2, \tag{55}$$

where $\eta_{\rm e}$ denotes the conformal time at the end of slow-roll inflation. Actually, this definition is equivalent to (25) because during slow-inflation $z_{\rm T} \simeq a$ (as a consequence of $\rho_{\rm i} \ll \rho_{\rm c}$).

B. Calculation of the IR limit

The IR limit is defined exactly in the same way as in the dressed metric approach. From the expression of a and ρ as functions of conformal time, one easily notices that $\Omega k^2 - z_{\rm T}''/z_{\rm T} \simeq k^2 - 2/\eta^2 + \mathcal{O}(\Gamma^2/\eta^8)$. In the contracting phase, there is therefore no noticeable difference between the deformed algebra and the dressed metric approaches. The IR limit still corresponds to modes with $k \ll k_{\rm IR}$, where $k_{\rm IR}$ is given in (29).

The calculation of the IR limit of the spectrum proceeds in the same way as for the dressed metric approach. We first write the approximate solution to (53) in the infrared regime,

$$v_k^{\rm IR}(\eta) = \alpha_k z_{\rm T}(\eta) + \beta_k z_{\rm T}(\eta) \int_{-\infty}^{\eta} \frac{d\eta'}{z_{\rm T}^2(\eta')} + \mathcal{O}(k^2), \quad (56)$$

from which the general expression of the IR limit of the power spectrum directly follows:

$$\mathcal{P}_{\rm T}(k)^{\rm IR} = \frac{32Gk^3}{\pi} \left| \alpha_k + \beta_k \int_{-\infty}^{\eta_{\rm e}} \frac{d\eta}{z_{\rm T}^2} \right|^2. \quad (57)$$

With the definition of $z_{\rm T}$, the integral on the RHS is simply given by the sum of $I(\eta_{\rm e}) + I_\Omega(\eta_{\rm e})$, with $I(\eta_{\rm e})$ defined in (32), and

$$I_\Omega(\eta_{\rm e}) \equiv -2 \int_{-\infty}^{\eta_{\rm e}} \frac{\rho}{\rho_{\rm c}} \frac{d\eta}{a^2}. \quad (58)$$

As before, the two constants α_k and β_k in (57) are obtained by matching the solution (56) with a set of solutions valid for any wavenumber k during the contracting phase. During the contracting phase the difference between $(\Omega k^2 - z_{\rm T}''/z_{\rm T})$ and $(k^2 - a''/a)$ can be neglected. Consequently, the two constants α_k and β_k take the same value as before: $\alpha_k = \mathcal{O}(k^{3/2})$ and $\beta_k = (3i/\sqrt{2})\lambda_0 k^{-3/2}$. With these expressions, the IR limit of the power spectrum becomes

$$\mathcal{P}_{\rm T}(k)^{\rm IR} = \frac{144G}{\pi} \lambda_0^2 \left| I(\eta_{\rm e}) + I_\Omega(\eta_{\rm e}) \right|^2. \quad (59)$$

Note that all the differences between the deformed algebra and the dressed metric approach are encoded in the integral $I_\Omega(\eta_{\rm e})$.

Now, we will show that $I_\Omega(\eta_{\rm e})/I(\eta_{\rm e}) = \mathcal{O}(\Gamma^2)$, so that the contribution of $I_\Omega(\eta_{\rm e})$ to the IR limit of the spectrum can be neglected. First, we split the integral into three parts: $I_\Omega(\eta_{\rm e}) = I_\Omega(-\infty, \eta_{\rm A}) + I_\Omega(\eta_{\rm A}, \eta_{\rm i}) + I_\Omega(\eta_{\rm i}, \eta_{\rm e})$. The proof is straightforward for the first and the third parts of the integral. Indeed, recalling that before $\eta_{\rm A}$ the energy density remains smaller than $\rho_{\rm A} = \Gamma^2 \rho_{\rm c}$, we have

$$I_\Omega(-\infty, \eta_{\rm A}) \equiv -2 \int_{-\infty}^{\eta_{\rm A}} \frac{\rho}{\rho_{\rm c}} \frac{d\eta}{a^2} \leq -2\Gamma^2 I(-\infty, \eta_{\rm A}). \quad (60)$$

The same holds for $I_\Omega(\eta_{\rm i}, \eta_{\rm e})$, with $\rho_{\rm i}$ instead of $\rho_{\rm A}$. The remaining part of the integral is

$$I_\Omega(\eta_{\rm A}, \eta_{\rm i}) \equiv -2 \int_{\eta_{\rm A}}^{\eta_{\rm i}} \frac{\rho}{\rho_{\rm c}} \frac{d\eta}{a^2}. \quad (61)$$

During the bouncing phase, $\rho = \rho_{\rm c} y^2$ and $a = a_{\rm B}|y|^{-\frac{1}{3}}$ so when we switch to cosmic time, the integral becomes

$$I_\Omega(\eta_{\rm A}, \eta_{\rm i}) = -(2/a_{\rm B}^2) \int_{t_{\rm A}}^{t_{\rm i}} |y(t)|^3 dt. \quad (62)$$

The last step is to express dt in terms of dy with (14). Then the integration can be performed analytically and leads to

$$I_\Omega(\eta_{\rm A}, \eta_{\rm i}) = -\frac{m}{36\lambda_0} \frac{\sin^2\theta_{\rm A}}{\cos\theta_{\rm A}} \Gamma^2. \quad (63)$$

Therefore, at order $\mathcal{O}(\Gamma^2)$, we predict no difference for the IR limits of the power spectra in both approaches. The IR limit of the power spectrum in the deformed algebra approach is still given by (45).

C. Calculation of the UV limit

The UV limit of the power spectrum in the deformed algebra approach has already been discussed in [27], here we recall the conclusion of this previous work. Thanks to numerical integrations for the equation of motion as well as WKB based arguments, it is shown that the primordial power spectrum exponentially grows with the wavenumber k, for large values of k. Actually, oscillations are still superimposed to this exponential envelope. During the bouncing phase, the term $z_{\rm T}''/z_{\rm T}$ reaches a maximum $|z_{\rm T}''/z_{\rm T}|_{t_B} = 40\pi G\rho_{\rm c}$. This means that for modes such that $k^2 \gg 40\pi G\rho_{\rm c}$, the time-dependent frequency in the equation of motion, $\Omega k^2 - z_{\rm T}''/z_{\rm T}$, is dominated by Ωk^2 during most of the cosmic history prior to inflation. The Euclidean phase around the bounce, $\Omega < 0$, leads to an instability in the equation of motion so the amplitude of tensor modes recieves a real exponential contribution, *i.e.* $v_{k\to\infty} \propto \exp(k \times \int_{\Delta\eta} \sqrt{|\Omega|}\, d\eta)$, where the integration is performed over the interval $\Delta\eta$ corresponding to the Euclidean phase.

V. POWER SPECTRUM AT ALL SCALES: NUMERICAL RESULTS

Deriving the primordial power spectrum for tensor modes at all scales requires a numerical integration of

both the equation of motion of the mode functions ((27) or (53) depending on the approach) *and* the equations of motion for the background (gathered in the system of equations (4)). The numerical integration is performed starting in the contracting phase, when $\rho_0/\rho_c \ll \Gamma^2$. For the background, the initial conditions are set by choosing the value of θ_0, the initial phase between the share of potential energy and kinetic energy in the total energy density. For the perturbations, the initial conditions are set during the contracting phase when the modes are well inside the horizon. The initial state of the perturbation can then be identified with the usual Minkowski vacuum.

The detailed dynamics of the background (*e.g.* the value of x at the bounce, or the number of e-folds during inflation) and subsequently the detailed shape of $\mathcal{P}_{\mathrm{T}}(k)$, are fully determined by two types of parameters: the mass of the scalar field and the critical energy density on one hand, and the phase θ_0 on the other hand.

The mass of the scalar field and the critical energy density can be seen as fundamental constants of the model. Though their values are not known, some particular values are favored by CMB observations and theoretical considerations. Even if the details of the calculation using the minimal area gap of LQG still need clarification, some dimensional arguments lead to believe that the value of ρ_{c} should not be far from the Planck scale. Note that ρ_{c} is the only parameter linked to LQG (via its dependence on the Immirzi parameter, γ). The value commonly accepted is $\rho_{\mathrm{c}} = 0.41 m_{\mathrm{Pl}}^4$, and we shall use it as the standard choice in our numerical simulation. The value of the mass of the scalar field, as deduced from the CMB observations, is generally chosen to be $m \simeq 1.2\times10^{-6} m_{\mathrm{Pl}}$ [19].

The parameter θ_0 has a different status since it is totally *contingent*. Its value can vary between 0 and 2π (actually the range $0 < \theta_0 < \pi$ is enough as the equations remain unchanged under the transformation $\theta_0 \to \theta_0 + \pi$). As underlined in [17], most of the values of θ_0 lead to a universe with a phase of inflation shortly after the bounce (and no deflation before the bounce). We have restricted ourselves to this kind of solutions since they are the most probable, and the more in line with our current knowledge of the cosmic history (believed to have underwent a phase of primordial inflation).

Qualitatively, we can already anticipate the global shape of the primordial power spectrum. Irrespective of any approach, its shape is driven by the background evolution through the functions a and Ω (in the deformed algebra approach) and their time derivatives. Our analysis is restricted to the wide range of cosmic histories that split into three main eras: a classical (dust-like) contracting phase, a bouncing phase where quantum effects are significant, and a classical inflationary phase. We anticipate the shape of the primordial power spectrum to be *qualitatively* unaffected by the values of m, ρ_{c}, and θ_0. (Obviously, the precise values of these parameters will affect the scales and amplitudes involved in the spectrum at a *quantitative* level). We can also anticipate three regimes in the power spectra, corresponding to: the modes that have left the horizon during the contracting phase (large scales); the modes that have left the horizon during the bouncing phase (intermediate scales); the modes that have remained within the horizon until the start of the inflationary phase (small scales). For the large and small scales, we should recover the IR and UV limit derived analytically in the previous sections.

In the next three sections we present the primordial power spectra obtained within each approach. We study the influence of the three parameters, m, ρ_c, and θ_0. For each varying parameter, we present the primordial power spectra as predicted by each approach, thus facilitating the comparison.

We use Planck units hereafter, with the following definition of the Planck mass, $m_{\mathrm{Pl}} = 1/\sqrt{G}$. For simplicity, we normalize the scale factor at the time of the bounce, setting $a_{\mathrm{B}} = 1$. The power spectra are depicted as functions of the comoving wavenumber k.

A. Varying the mass of the scalar field

The primordial power spectrum for different values of the mass of the scalar field is presented in Fig. 1. The upper panel corresponds to the dressed metric approach and the lower panel to the deformed algebra approach. The mass takes three different values: $m = 10^{-3} m_{\mathrm{Pl}}$ (triangles), $m = 10^{-2.5} m_{\mathrm{Pl}}$ (open disks), and $m = 10^{-2} m_{\mathrm{Pl}}$ (black disks). For numerical convenience, these values are larger than the preferred value. However, the results can be extrapolated and the associated phenomenology shall be studied with values closer to $10^{-6} m_{\mathrm{Pl}}$ [28]. The critical energy density is set equal to $0.41 m_{\mathrm{Pl}}^4$ and $\cos\theta_{\mathrm{A}} \simeq 1$.

In the dressed metric approach (upper panel of Fig. 1), there are three regimes in the primordial power spectrum:

(i) At the largest scales, for $k < k_{\mathrm{IR}}$ with

$$k_{\mathrm{IR}} = \frac{1}{3\sqrt{2}} \left(\frac{m^2 \sqrt{24\pi G \rho_{\mathrm{c}}}}{|\cos\theta_{\mathrm{A}}|} \right)^{1/3},$$

the power spectrum is scale invariant in agreement with the analytical calculations of Sec. III. This corresponds to modes that were amplified mainly during the classical contracting phase. In Fig. 1, the scale corresponding to k_{IR} is depicted with vertical dotted lines. At this scale, there is a transition in the numerical results that is in perfect agreement with the analytical formula (especially its $m^{2/3}$ dependence). Moreover, it is clear on the figure that the numerical IR limit of the spectrum behaves as m^2, again in perfect agreement with (45).

(ii) For intermediate scales, such that $k_{\rm IR} < k < k_{\rm UV}$, with

$$k_{\rm UV} = \sqrt{8\pi G\rho_{\rm c}}\,,$$

the amplitude of the power spectrum is oscillating. This part of the spectrum corresponds to modes that were amplified during the bouncing phase. The first peak corresponds to a maximum of the power spectrum, that reaches $100 \times {\mathcal{P}_{\rm T}}^{\rm IR}$ approximately. Then, the amplitude of the oscillations is damped for increasing values of the wavenumber. Intuitively, these oscillations can be understood as due to quasi-bound states in the effective Schrödinger equation. The second transition scale, $k_{\rm UV}$, is depicted in Fig. 1 as a vertical dashed line and is in agreement with the transition scale found numerically.

(iii) At the smallest scales, $k > k_{\rm UV}$, the power spectrum is a power law with a slightly red spectral index, just as predicted by the standard inflationary paradigm. This part of the power spectrum corresponds to modes that have remained inside the horizon until the start of the inflationary phase. The numerical results are in agreement with the UV limit derived analytically in Sec. III, see Fig. 3.

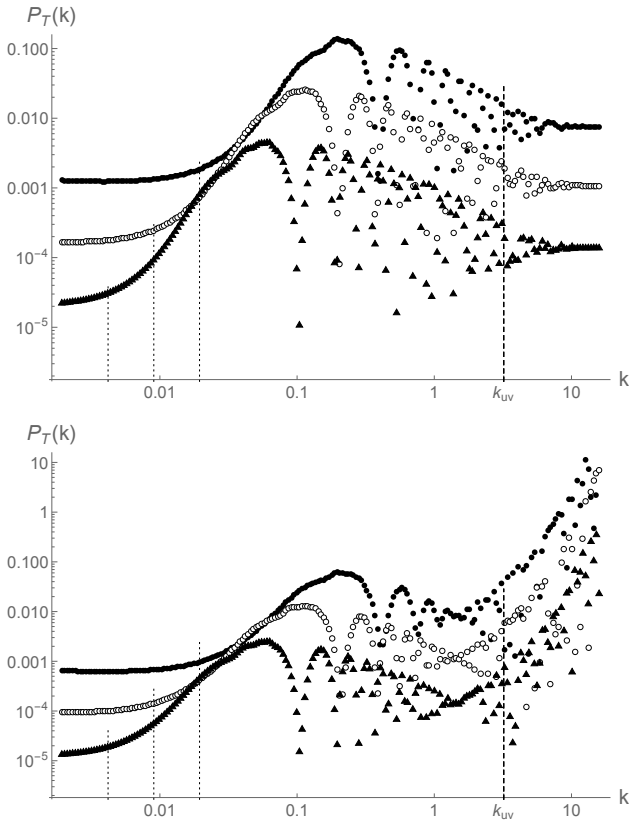

Figure 1. Primordial power spectra for tensor modes in the dressed metric approach (upper panel) and in the deformed algebra approach (lower panel) for different values of the mass of the scalar field. The critical energy density is $\rho_{\rm c} = 0.41 m_{\rm Pl}^4$ and $\cos\theta_{\rm A} \simeq 1$. The mass of the scalar field takes three values: $m = 10^{-3} m_{\rm Pl}$ (triangles), $m = 10^{-2.5} m_{\rm Pl}$ (open disks), and $m = 10^{-2} m_{\rm Pl}$ (black disks). The dashed vertical line at large k, corresponds to $k_{\rm UV}$ (which does not depend on m). The dotted vertical lines at smaller k correspond to $k_{\rm IR}$ (which scales as $m^{2/3}$).

In the deformed algebra approach the primordial tensor power spectrum also features three different regimes (see the lower panel of Fig. 1). The first two regions (*i.e.* the large scales, $k < k_{\rm IR}$, and the intermediate scales, $k_{\rm IR} < k < k_{\rm UV}$), are almost identical to the power spectrum derived in the dressed metric approach. The scale-dependence of the power spectrum and the transition scales are the same. This is because the impact of Ω is subdominant for these modes. However, within these two regions the numerical results suggest that for $k < k_{\rm UV}$ the amplitude of the spectrum in the deformed algebra approach is slightly smaller than in the dressed metric approach (by less than a factor 2). (This feature could not be explained by our analytics.)

At smaller scales, $k > k_{\rm UV}$, the primordial power spectrum in the deformed algebra approach strongly differs from the one predicted by the dressed metric approach. As already suggested by our analytical considerations (see Sec. IV), the power spectrum is exponentially increasing with the wavenumber (as a result of the instability generated by Ω which is negative-valued around the bounce), with superimposed oscillations. Note that the numerical results confirm once again that the scale defining the transition between the intermediate scales (oscillations) and the large scales (exponential growth) does not depend on m.

The UV behavior of the spectrum clearly raises questions. The first one is related to the fundamentally trans-Planckian nature of these modes. As demonstrated in [6], this is not a problem when considering the appropriate length operator in loop quantum gravity. A more serious issue is related to the use of the perturbation theory when the spectrum increases exponentially. Obviously, backreaction should be taken into account in this regime and the results shown here are not fully reliable anymore. They just give a general trend and not the accurate shape of the spectrum. However, we believe that this is basically enough for the phenomenological purposes we are interested in. The most interesting region, that is the oscillatory one, is under control and the C_ℓ CMB spectrum can be safely calculated [28]. If the observational window of wavenumber was to fall on the exponentially rising part, this would anyway lead to a situation incompatible with data (as the tensor to scalar ratio is small). The perturbation theory breaks at a level where tensor modes are anyway excluded by current data.

B. Varying the critical energy density

The critical energy density depends on the Immirzi parameter, a fundamental parameter in LQG, whose value is traditionally deduced from a calculation of the black holes entropy. Nonetheless, it has been recently argued [20] that the formula for the entropy of black holes can be recovered, in the framework of LQG, without specifying the value of the Immirzi parameter. Recently, a quasi-local description of a black hole [30] was indeed shown to allow one to recover at the semi-classical limit the expected thermodynamical behaviors of a black hole for all values of γ [31], assuming the existence of a non trivial chemical potential conjugate to the number of horizon punctures. A detailed microscopic mechanism was also put forward in [32] and [33] where the area degeneracy was analytically continued from real γ to complex γ and evaluated at the complex values $\gamma = \pm i$. This motivates us to consider other values for the critical energy density and discuss how it can affect the primordial tensor power spectrum.

In Fig. 2, we show the primordial tensor power spectra for different values of $\rho_{\rm c}$. Here, the mass of the scalar field is set equal to $m = 10^{-3} m_{\rm Pl}$, and $\cos\theta_{\rm A} \simeq 1$. The upper panel corresponds to the dressed metric approach and the lower panel to the deformed algebra approach. The different values of the critical energy density are $\rho_{\rm c} = 0.0041 m_{\rm Pl}^4$ (triangles), $\rho_{\rm c} = 0.041 m_{\rm Pl}^4$ (open disks), and $\rho_{\rm c} = 0.41 m_{\rm Pl}^4$ (black disks) which is the theoretically favored value.

The global shape of the primordial power spectrum is recovered for both approaches, with three different regions. The positions of the transition scales, $k_{\rm IR}$ and $k_{\rm UV}$, clearly depend on $\rho_{\rm c}$ irrespectively of the approach. The IR transition scale, $k_{\rm IR}$, mildly decreases for smaller values of $\rho_{\rm c}$, in agreement with the analytical calculations that led to $k_{\rm IR} \propto (G\rho_{\rm c})^{1/6}$. The UV transition scale, $k_{\rm UV}$, is more strongly dependent on the value of the critical energy density, also in agreement with the scaling derived analytically, $k_{\rm UV} \propto \sqrt{G\rho_{\rm c}}$.

For the dressed metric approach, a decrease of $\rho_{\rm c}$ yields a slight decrease of the amplitude of the primordial power spectrum at *all* scales. This feature is also suggested by the analytical results, as both formulae for the UV and IR limits depend on the critical energy density as $\sim \ln^2(m/\sqrt{G\rho_{\rm c}})$.

For the deformed algebra approach, a decrease of $\rho_{\rm c}$ leads to a slight decrease of the amplitude of the spectrum at large and intermediate scales as in the dressed metric approach. At smaller scales, $k > k_{\rm UV}$, the smallest value of $\rho_{\rm c}$ corresponds to the fastest divergence of the spectrum. Analytically, we expect this divergence to scale as $\propto \exp(k \int_{\Delta\eta} \sqrt{|\Omega|}\, d\eta)$, where the interval $\Delta\eta$ corresponds to the euclidean phase. Therefore we can define the rate of growth of the spectrum in the UV as $k_\Omega \equiv 1/\int_{\Delta\eta} \sqrt{|\Omega|}\, d\eta$.

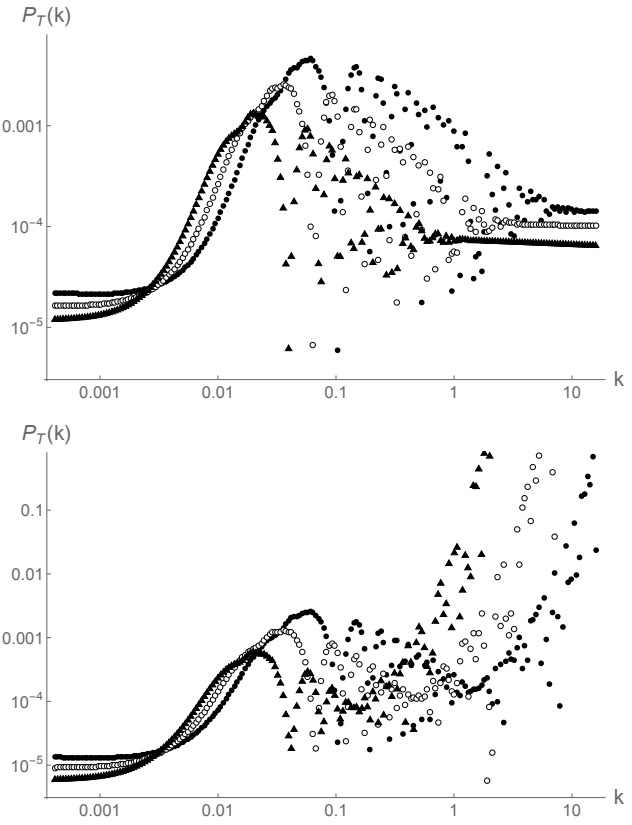

Figure 2. Primordial power spectra for the tensor modes in the dressed metric approach (upper panel) and in the deformed algebra approach (lower panel) for different values of $\rho_{\rm c}$. The mass of the scalar field is $m = 10^{-3} m_{\rm Pl}$ and $\cos\theta_{\rm A} \simeq 1$. The critical energy density is $\rho_{\rm c} = 0.0041 m_{\rm Pl}^4$ (triangles), $\rho_{\rm c} = 0.041 m_{\rm Pl}^4$ (open disks) and $\rho_{\rm c} = 0.41 m_{\rm Pl}^4$ (black disks).

This integral can be computed, leading to

$$k_\Omega \simeq 0.8\sqrt{24\pi G\rho_{\rm c}}\,. \tag{64}$$

So, small values of the critical energy density indeed correspond to a quicker divergence of the power spectrum in the UV.

C. Dependence on θ_0

The primordial power spectra for different choices of θ_0 are shown in Fig. 3, in the dressed metric approach (upper panel) and in the deformed algebra approach (lower panel). The mass of the scalar field is $m = 10^{-3} m_{\rm Pl}$, and the critical energy density is $\rho_{\rm c} = 0.41 m_{\rm Pl}^4$. We chose five values of θ_0, equally spaced between $(\pi/2 - 1)$ and $(\pi/2 + 1)$, ensuring that the background goes through a phase of inflation after the bounce. In the numerical simulations we have always set $\alpha = 17\pi/4 + 1$, so that

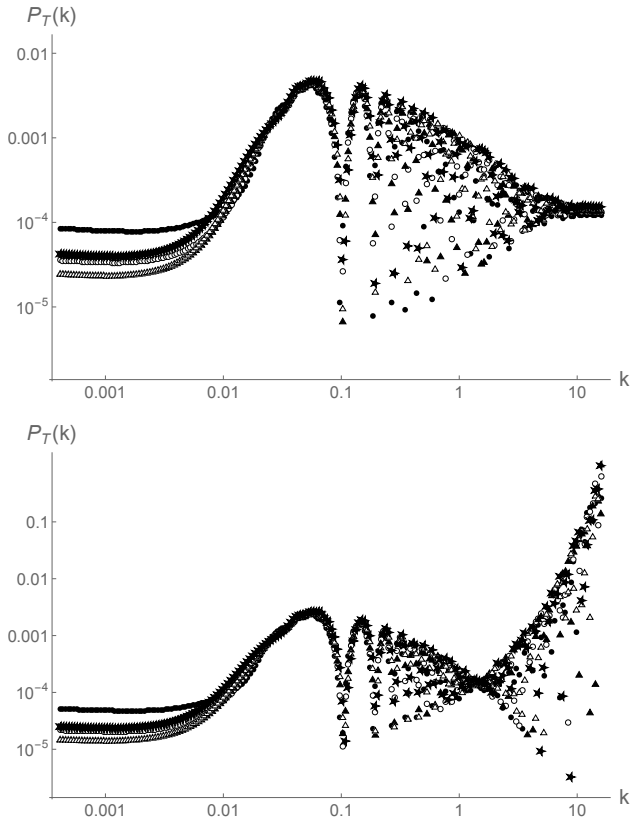

Figure 3. Primordial power spectra for the tensor modes in the dressed metric approach (upper panel), and in the deformed algebra approach (lower panel). The parameter θ_0 varries from $(\pi/2-1) \simeq 0.18\times\pi$ to $(\pi/2+1) \simeq 0.81\times\pi$. The exact values are: plain disks for $\theta_0 = (\pi/2-1)$, open disks for $\theta_0 = (\pi/2-1/2)$, plain triangles for $\theta_0 = \pi/2$, open triangles for $\theta_0 = (\pi/2+1/2)$, and plain stars for $\theta_0 = (\pi/2+1)$. The mass of the field is $m = 10^{-3}m_{\rm Pl}$, and the critical energy density is $\rho_c = 0.41m_{\rm Pl}^4$.

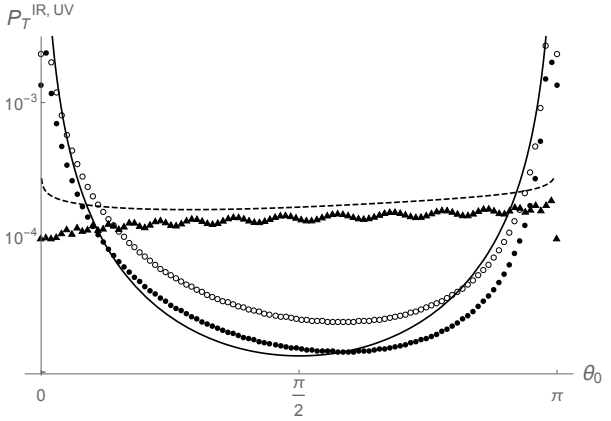

Figure 4. The infrared limit (disks) and the ultraviolet limit (triangles) of the primordial power spectrum as a function of θ_0. The solid black curve corresponds to the analytical calculations for $\mathcal{P}_{\rm T}{}^{\rm IR}$, see (45). The IR limit from a numerical simulation is displayed with open disks for the dressed metric approach, and black disks in the deformed algebra approach. The dashed black curve stands for the analytical UV limit in the dressed metric approach, see (52a). The UV limit in the dressed metric approach, as derived from the numerics, corresponds to the black triangles. The mass of the scalar field is $m = 10^{-3}m_{\rm Pl}$, and the critical energy density is $\rho_c = 0.41m_{\rm Pl}^4$.

$\cos\theta_{\rm A} = 0$ (with $\theta_{\rm A} = 2(\alpha-1)+\theta_0$) corresponds to $\theta_0 = 0$ and α is significantly larger than one.

The main impact of θ_0 is in the IR regime. Both the infrared transition scale $k_{\rm IR}$ (varying as $\sim |\cos(\theta_{\rm A})|^{-1/3}$) and the amplitude of the IR limit of the spectrum are significantly depending on θ_0. This is true in both approaches. At intermediate and smaller scales, the power spectra are nearly independent of the choice of θ_0, again irrespectively of the considered approach. The numerical results confirm that the ultraviolet transition scale $k_{\rm UV}$ is independent of θ_0. Moreover, in the deformed algebra approach the growth rate of the spectrum in the UV appears to be independent on θ_0 too, in agreement with (64).

In order to highlight the dependence of the IR limit as a function of θ_0, Fig. 4 shows this limit in both approaches and for different choices of θ_0, with $m = 10^{-3}m_{\rm Pl}$, and $\rho_c = 0.41m_{\rm Pl}^4$. The solid black curve corresponds to the analytical calculation for $\mathcal{P}_{\rm T}{}^{\rm IR}$, see (45). This analytical curve is valid for both the dressed metric and the deformed algebra approaches at first order in $\Gamma \equiv m/\sqrt{24\pi G\rho_c}$. The numerical derivation of the IR limit is displayed as open disks for the dressed metric approach, and as black disks in the deformed algebra approach. We observe a fairly good agreement between analytical and numerical results. Although there are some differences in the amplitude of the IR limit[4], the behavior as a function of θ_0 is consistent between the analytics and the numerics. This shows that $\mathcal{P}_{\rm T}{}^{\rm IR}$ strongly depends on θ_0, the former varying by more than one order of magnitude from its minimal value at $\theta_0 = \pi/2$ (thus giving $\cos\theta_{\rm A} = 1$), to its maximal value reached when θ_0 tends to 0 or π.

In the restricted case of the dressed metric approach, the UV limit as a function of θ_0 is also displayed in Fig. 4. The dashed black curve stands for the analytical calculation presented in (52a). The UV limit obtained from the numerical simulation is displayed with triangles. A good agreement is also observed here. Nonetheless, the

[4] The discrepancy is not surprising. First of all, the analytic result is based on some approximations for the time dependence of a and $\mathbf{\Omega}$. Second, the numerical evaluation fo $\mathcal{P}_{\rm T}{}^{\rm IR}$ cannot be exactly obtained for $k = 0$ since this would require to start the numerical integration at $\eta \to -\infty$ which is unfeasible. We believe that these features are at the origin of the disagreement between the numerics and the analytics.

remaining difference between the analytical and numerical results certainly comes from the approximations involved in the determination of $x_{\rm i}$, on which the UV limit depend.

VI. CONCLUSION AND DISCUSSION

In this work, we have compared the dressed metric and deformed algebra approaches to loop quantum cosmology. In order to compare them efficiently, we have set the initial conditions in the same way for both approaches (in the remote past of the classical contracting branch). This is consistent and arguably the most obvious choice if the word *initial* is to be taken literally. It is however fair to mention that this is not the only choice one could have made. As far as the dressed metric approach is concerned, the authors who developed the strategy have preferred to set the initial conditions at the bounce [6–8]. Then the initial state for tensor perturbations is given by a 4th-order WKB vacuum defined for $k \geq k_{\rm UV}$. In fact, their results seem to be very similar to ours (for the range of scales covered by both choices of initial conditions). As far as the deformed algebra approach is concerned, it should be underlined that it is also possible to set initial conditions at the surface of signature change. This has been investigated in [29] and leads to a different spectrum. If these issues are left for future considerations and if we focus on the comparison with similar initial conditions, several important conclusions can already be drawn.

First, it is remarkable that for both approaches the IR limit is the same and basically agrees with the prediction of standard general relativity. Therefore at the largest scales, the primordial tensor power spectrum cannot be used to probe quantum gravity (at least in this setting).

Second, there is a strong difference between the approaches in the ultraviolet regime. Whereas the dressed metric simply leads to the slightly red-tilted power spectrum, as predicted in standard inflationary cosmology, the deformed algebra leads to an exponentially increasing spectrum (modulated by oscillations).

Third, at intermediate scales, a very interesting behavior appears. Not only because it is substantially different from the predictions of the standard inflationary models but also because both predictions are in agreement with each other! This region seems to exhibit a *universal LQC effect* that has been searched for during the last decade. In addition, the phase of the oscillations that appear at these intermediate scales, does *not* depend on the unknown (and fundamentally random) phase parameter, θ_0. This opens an interesting avenue in the perspective of testing the predictions of effective LQC.

In the future, this work should be extended in two directions. One is to consider not only the tensor modes, that have not yet been observed, but also the well known scalar modes. The relevant equations have already been derived for the dressed metric approach but are still to be investigated into more details in the deformed algebra approach. The reason for this difficulty is related to divergences (at the bounce and at the change of signature) that should be regularized. The difficulty is however more technical than conceptual and should be solved soon.

The second path to follow is naturally to go more deeply into the phenomenology of this comparison and calculate the corresponding cosmic microwave background C_ℓ spectra which are already constrained by observations. Two main tasks will have to be pursued. The first is related to the number of e-folds that the Universe underwent since the bounce. This number depends, among other parameters, on θ_0 and on the reheating temperature. Once the number of e-folds since the bounce will be specified, the range of wavenumbers considered in this study that falls within our observable window will be completely determined. The second important task is to investigate how the oscillations at intermediate scales shall be washed out by the transfer phenomena that occur between the end of inflation and the decoupling.

ACKNOWLEDGMENTS

BB is supported by a grant form ENS Lyon. L.S. is supported by the Labex ENIGMASS, initiative d'excellence.

[1] P. Dona & S. Speziale, arXiv:1007.0402V1;
A. Perez, arXiv:gr-qc/0409061v3;
R. Gambini & J. Pullin, *A First Course in Loop Quantum Gravity*, Oxford, Oxford University Press, 2011;
C. Rovelli, Living Rev. Relativity **1**, 1, 1998;
C. Rovelli, *Quantum Gravity*, Cambridge, Cambridge University Press, 2004;
C. Rovelli, arXiv:1102.3660v5 [gr-qc];
C. Rovelli & F. Vidotto, *Covariant loop quantum gravity*, Cambridge, Cambridge University Press, 2014 L. Smolin, arXiv:hep-th/0408048v3;
T. Thiemann, Lect. Notes Phys. **631**, 41, 2003;
T. Thiemann, *Modern Canonical Quantum General Relativity*, Cambridge, Cambridge University Press, 2007

[2] A. Ashtekar, M. Bojowald, and J. Lewandowski, Adv. Theor. Math. Phys. 7, 233, 2003;
A. Ashtekar, Gen. Rel. Grav. **41**, 707, 2009;
A. Ashtekar & P. Singh, Class. Quantum Grav. **28**, 213001, 2011;
M. Bojowald, Living Rev. Rel. **11**, 4, 2008;

M. Bojowald, Class. Quantum Grav. **29**, 213001, 2012;
K. Banerjee, G. Calcagni, and M. Martin-Benito, SIGMA **8**, 016, 2012;
G. Calcagni, Ann. Phys. (Berlin) **525**, 323, 2013;
I. Agullo & A. Corichi, in "The Springer Handbook of Spacetime," edited by A. Ashtekar and V. Petkov., Springer-Verlag, arXiv:1302.3833 [gr-qc];
A. Barrau, T. Cailleteau, J. Grain, and J. Mielczarek, Class. Quantum Grav. **31**, 053001, 2014
A. Barrau & J. Grain, arXiv:1410.1714

[3] A. Ashtekar, M. Campuglia, Class. Quantum. Grav **29**, 242001, 2012

[4] T. Thiemann, Class. Quantum. Grav **15**, 839, 1998;
C. Rovelli & L. Smolin, Phys. Rev. Lett **72**, 446, 1994

[5] T. Thiemann, Class. Quantum. Grav **15**, 1281, 1998

[6] I. Agullo, A. Ashtekar, and W. Nelson, Phys. Rev. Lett. **109**, 251301, 2012

[7] I. Agullo, A. Ashtekar, and W. Nelson, Phys. Rev. D **87**, 043507, 2013

[8] I. Agullo, A. Ashtekar, and W. Nelson, Class. Quantum Grav. **30**, 085014, 2013

[9] A. Ashtekar, W. Kaminski, and J. Lewandowski, Quantum field theory on a cosmological, quantum space-time, *Phys. Rev. D* **79** 064030 (2009)

[10] M. Bojowald, G.M. Hossain, M. Kagan, and S. Shankaranarayanan, Phys. Rev. D, 78, 063547, 2008

[11] J. Mielczarek, T. Cailleteau, A. Barrau, and J. Grain, Class. Quantum Grav. **29**, 085009, 2012

[12] T. Cailleteau, J. Mielczarek, A. Barrau, and J. Grain, Class. Quantum Grav. **29**, 095010, 2012

[13] T. Cailleteau, A. Barrau, J. Grain, and F. Vidotto, Phys. Rev. D **86**, 087301, 2012

[14] A. Barrau, M. Bojowald, G. Calcagni, J. Grain, and M. Kagan, arXiv:1404.1018

[15] S. A. Hojman, K. Kuchar and C. Teitelboim, Geometrodynamics regained, Ann. Phys. **96**, 88, 1976

[16] A. Ashtekar & D. Sloan, Phys. Lett. B **694**, 108, 2010

[17] L. Linsefors & A. Barrau, Phys. Rev. D **87**, 123509, 2013

[18] B. Bolliet, Master Thesis, ENS-Lyon, 2013

[19] A. R. Liddle, P. Parsons, and J. D. Barrow, Phys. Rev. D **50**, 7222, 1994

[20] E. Bianchi, arXiv:1204.5122

[21] E. Wilson-Ewing, JCAP **03**, 026, 2013

[22] J. Grain, A. Barrau, T. Cailleteau, and J. Mielczarek, Phys. rev. D **82**, 123520, 2010

[23] D. Lyth & E. D. Stewart, Phys. Lett. B **302**, 171, 1993

[24] E. D. Stewart & J.-O. Gong, Phys. Lett. B **510**, 1, 2001

[25] J. Martin & D. Schwarz, Phys. Rev. D **62**, 103520, 2000

[26] J. Grain & A. Barrau, Phys. Rev. Lett. **102**, 081301, 2009

[27] L. Linsefors, T. Cailleteau, A. Barrau, and J. Grain, Phys. Rev. D **87**, 107503, 2013

[28] B. Bolliet, A. Barrau, and J. Grain, in preparation.

[29] J. Mielczarek, L. Linsefors, and A. Barrau, arXiv:1411.0272

[30] Ernesto Frodden, Amit Ghosh, and Alejandro Perez. Quasilocal first law for black hole thermodynamics. Phys.Rev., D87:121503.

[31] Amit Ghosh and Alejandro Perez. Black hole entropy and isolated horizons thermodynamics. Phys.Rev.Lett., 107:241301.

[32] Ernesto Frodden, Marc Geiller, Karim Noui, and Alejandro Perez. Black Hole Entropy from complex Ashtekar variables. Europhys.Lett., 107:10005, 2014.

[33] Jibril Ben Achour, Amaury Mouchet and Karim Noui. Analytic continuation of black hole entropy in Loop Quantum Gravity. arXiv:1406.6021, 2014.

Primordial scalar power spectrum from the Euclidean Big Bounce

Susanne Schander*
Technische Universität Kaiserslautern, D-67653 Kaiserslautern, Germany and
Laboratoire de Physique Subatomique et de Cosmologie, Université Grenoble-Alpes, CNRS-IN2P3
53, avenue des Martyrs, 38026 Grenoble cedex, France

Aurélien Barrau,† Boris Bolliet,‡ Linda Linsefors,§ and Jakub Mielczarek¶
Laboratoire de Physique Subatomique et de Cosmologie, Université Grenoble-Alpes, CNRS-IN2P3
53, avenue des Martyrs, 38026 Grenoble cedex, France

Julien Grain**
CNRS, Orsay, France, F-91405 and
Université Paris-Sud 11, Institut d'Astrophysique Spatiale, UMR8617, Orsay, France, F-91405
(Dated: January 18, 2016)

In effective models of loop quantum cosmology, the holonomy corrections are associated with deformations of space-time symmetries. The most evident manifestation of the deformations is the emergence of an Euclidean phase accompanying the non-singular bouncing dynamics of the scale factor. In this article, we compute the power spectrum of scalar perturbations generated in this model, with a massive scalar field as the matter content. Instantaneous and adiabatic vacuum-type initial conditions for scalar perturbations are imposed in the contracting phase. The evolution through the Euclidean region is calculated based on the extrapolation of the time direction pointed by the vectors normal to the Cauchy hypersurface in the Lorentzian domains. The obtained power spectrum is characterized by a suppression in the IR regime and oscillations in the intermediate energy range. Furthermore, the speculative extension of the analysis in the UV reveals a specific rise of the power leading to results incompatible with data.

PACS numbers: 98.80.Qc, 98.80.Jk

I. INTRODUCTION

Loop quantum gravity (LQG) is a simple, consistent, non-perturbative and background-independent quantization of general relativity. It uses Ashtekar variables, namely the SU(2)-valued connections and the conjugate densitized triads. The quantization is obtained through holonomies of the connections and fluxes of the densitized triads. No heavy hypothesis is required. Introductions can be found in Refs. [1].
Loop quantum cosmology (LQC) is an application of LQG-inspired quantization methods to a gravitational system with cosmological symmetries. In LQC, the big bang is generically replaced by a big bounce due to repulsive quantum geometrical effects when the density approaches the Planck density and interesting predictions can be made about the duration of inflation when a given matter content is assumed. It is, however, important to underline that LQC has not yet been rigorously derived from LQG and remains an attempt to use LQG-like methods in the cosmological sector. Introductions can be found in Refs. [2, 3].

The confrontation of LQG with available empirical data is crucial in order to check the physical validity of this approach to quantum gravity. The most promising option in this direction is currently given by the exploration of the cosmological sector of LQG. The present state of advancement, however, does not allow for a derivation of the cosmological dynamics directly from the full theory. Because of this, LQC models are considered to fill the existing gap. These models suffer from quantum ambiguities, which are believed to be fixed by the cosmological dynamics regained from LQG.

This study is based on the effective LQC dynamics, which allow to address various cosmological issues. In particular, numerous studies have been devoted to the computation of tensor power spectra and their significance in the light of the future observations (see, *e.g.*, Refs. [4–7]). In this work, we will focus on scalar modes, which are more relevant from the observational point of view but which are more demanding to deal with at the theoretical level because of subtle gauge-invariance issues and hypersurface deformation algebra closure conditions.
Two main types of quantum corrections are expected at the effective level of LQC. The first one comes from the fact that loop quantization is based on holonomies, *i.e.* using exponentials of the connection rather than direct connection components. The second type of corrections arises for inverse powers of the densitized triad, which, when quantized, becomes an operator without zero

* schander@lpsc.in2p3.fr
† Aurelien.Barrau@cern.ch
‡ boris.bolliet@ens-lyon.fr
§ linsefors@lpsc.in2p3.fr
¶ jakub.mielczarek@uj.edu.pl
** julien.grain@ias.u-psud.fr

eigenvalue in its discrete spectrum, thus avoiding the divergence. As the status of "inverse volume" corrections is not fully clear, due to the fiducial volume dependence, this work focuses on the holonomy term alone which has a major influence on the background equations and is better controlled [8]. In this framework, we will consider the Euclidean phase predicted by LQC [9, 10], and put, as advocated in Ref. [11], initial conditions in the remote past of the contracting branch of the universe (this choice can be questioned and other proposals have been considered [12, 13]).
It is worth noticing, that an alternative attempt regarding the cosmological perturbations in LQC have recently been presented (see Refs. [14]). In this approach, quantum fields are considered on a homogeneous quantum background, based on the methods developed in Ref. [15]. Because the gauge-invariant variables for perturbations are fixed to be the classical ones, the Euclidean phase characterized by the elliptic nature of the equations of motion does not occur. However, the consistency of the effective dynamics emerging from this formulation remains an open issue.

The key ingredient of this work is the existence of an Euclidean phase around the bounce. A completely rigorous study of the physical consequences would require a full understanding of quantum field theory (QFT) in curved Euclidean spaces and at the junction hypersurface with the Lorentzian manifold. This is obviously far beyond the scope of this article. Especially when taking into account that even on a well behaved Lorentzian dynamical space, QFT is not without ambiguities and many issues remain open. The central methodology of this study is to define physical quantities in the initial classical Lorentzian space (the contracting branch before the bounce), to evolve them in a mathematically rigorous way through the Euclidean zone, and to calculate observables in the second Lorentzian phase (the expanding branch we live in) where the physical meaning is clear again. Although, by definition, there is no time anymore in the Euclidean phase, one can still rely on general covariance and the corresponding structure has a well-defined canonical formulation using hypersurface deformations. We don't claim that this is the only way to address this situation. There are clearly other possible ways to deal with this speculative new phenomenon. However, it seems to be a quite natural and reasonable first assumption. In addition, this is the methodology that has been used up to now to evaluate the tensor spectrum in the deformed algebra approach to LQC. It is therefore important to also derive the scalar spectrum following the very same methodology, at least for a meaningful comparison.

In the following section, we first remind the basis of the deformed algebra approach used in this study. In section III, we summarize some important features of the background dynamics in LQC. The equation of motion for scalar perturbations is derived in section IV. In section V, different ways of choosing initial conditions for perturbations are presented. Section VI is devoted to the analysis of the scalar power spectrum. Concluding remarks are given in section VII.

II. DEFORMED ALGEBRA

In the canonical formulation of general relativity, the Hamiltonian is a sum of three constraints,

$$H_{\rm G}[N^i,N^a,N]=\frac{1}{2\kappa}\int_\Sigma d^3x\left(N^iC_i+N^aC_a+NC\right)\approx 0,$$

where $\kappa=8\pi G$, (N^i,N^a,N) are Lagrange multipliers, C_i is the Gauss constraint, C_a is the diffeomorphism constraint and C is the scalar constraint. The equality denoted as "$\approx$" is to be understood as an equality on the surface of constraints (*i.e.* a weak equality). It is convenient to define the corresponding smeared constraints,

$$\mathcal{C}_1=G[N^i]=\frac{1}{2\kappa}\int_\Sigma d^3x\ N^iC_i, \tag{1}$$

$$\mathcal{C}_2=D[N^a]=\frac{1}{2\kappa}\int_\Sigma d^3x\ N^aC_a, \tag{2}$$

$$\mathcal{C}_3=S[N]=\frac{1}{2\kappa}\int_\Sigma d^3x\ NC, \tag{3}$$

such that $H_{\rm G}[N^i,N^a,N]=G[N^i]+D[N^a]+S[N]$. The Hamiltonian is a total constraint which vanishes for all multiplier functions (N^i,N^a,N). The time derivative of the Hamiltonian constraint vanishes also weakly and therefore the Hamilton equation, $\dot{f}=\{f,H_{\rm G}[M^i,M^a,M]\}$, leads to

$$\left\{H_{\rm G}[N^i,N^a,N],H_{\rm G}[M^i,M^a,M]\right\}\approx 0. \tag{4}$$

As the Poisson brackets are linear, the condition (4) is satisfied if the smeared constraints belong to a first class algebra,

$$\{\mathcal{C}_I,\mathcal{C}_J\}=f^K{}_{IJ}(A^j_b,E^a_i)\mathcal{C}_K, \tag{5}$$

where the $f^K{}_{IJ}(A^j_b,E^a_i)$ are structure functions which depend on the Ashtekar variables (A^j_b,E^a_i). The algebra closure is fulfilled at the classical level due to general covariance. The algebra must also be closed at the quantum level. Otherwise the system might escape from the surface of constraints, leading to an unphysical behavior. In addition, as shown in Ref. [16], the algebra of effective quantum constraints should be strongly closed (that is, off shell closure must be considered). This means that the relation (5) should hold in the whole kinematical phase space, and not only on the surface of constraints (corresponding to on shell closure). When the constraints are quantum-modified by the holonomy corrections, the resulting Poisson algebra might not be closed,

$$\{\mathcal{C}^Q_I,\mathcal{C}^Q_J\}=f^K{}_{IJ}(A^j_b,E^a_i)\mathcal{C}^Q_K+\mathcal{A}_{IJ}, \tag{6}$$

where $\mathcal{A}_{IJ}$ stands for the anomaly term which can appear due to the quantum modifications and the superscript 'Q' indicates that the constraints are quantum corrected. The consistency (closure of the algebra) requires that all $\mathcal{A}_{IJ}$ should vanish. Remarkably, the conditions, $\mathcal{A}_{IJ} = 0$, lead to restrictions on the form of the quantum corrections and determine them uniquely under natural assumptions.

The issue of anomaly freedom for the algebra of cosmological perturbations was extensively studied for inverse-triad corrections. It was demonstrated that this requirement can be fulfilled at first order in perturbations for scalar [17, 18], vector [19] and tensor perturbations [20]. Predictions for the power spectrum of cosmological perturbations were performed [21], leading to constraints on some parameters of the model by the use of observations of the cosmic microwave background radiation (CMB) [22]. It was also considered for holonomy corrections and vector modes in Ref. [23] and for scalar modes in Ref. [10] (the full analysis with inverse-triad and holonomy terms was performed in Ref. [24]). It was shown in Ref. [25] that there exists a single modification of the algebra structure that works for *all* kinds of modes, thus emphasizing the consistency of the theory. It is also important to underline that the matter content plays a role in removing degeneracies. Even if the calculations carried out in the above-mentioned articles are quite laborious, the guiding idea behind is very simple. Each time a $\bar{k}$ factor, defined as the mean value of the Ashtekar connection A_a^i, appears, it is replaced by

$$\bar{k} \to \frac{\sin(n\bar{\mu}\gamma\bar{k})}{n\bar{\mu}\gamma}, \tag{7}$$

where n is some unknown integer and $\bar{\mu}$ is the coordinate size of a loop. The full perturbations have to be calculated up to the desired order, the Poisson brackets are then explicitly calculated and the anomalies are cancelled by counter-terms required to vanish in the classical limit. The neat result is that the algebra of effective constraints is deformed with respect to its classical counterpart. It takes the following form:

$$\begin{aligned}
\{D[M^a], D[N^a]\} &= D[M^b\partial_b N^a - N^b\partial_b M^a],\\
\left\{D[M^a], S^Q[N]\right\} &= S^Q[M^a\partial_b N - N\partial_a M^a],\\
\left\{S^Q[M], S^Q[N]\right\} &= \Omega D\left[q^{ab}(M\partial_b N - N\partial_b M)\right],
\end{aligned}$$

where Ω is the deformation factor that plays a crucial role in the following. It is given by $\Omega = 1 - 2\rho/\rho_{\rm c}$ where ρ is the density of the Universe and $\rho_{\rm c}$ is the critical density expected to be close to the Planck density. In Lorentzian General Relativity $\Omega = 1$. When $\Omega < 0$ the structure of space-time becomes Euclidean. (Strictly speaking space-time is Lorentzian or Euclidean only if $\Omega = \pm 1$ but the most important properties regarding physical consequences, namely the existence of a causal structure and the general behavior of the solutions for wave equations, only depend on the sign of Ω and not on its precise value [13]. It therefore makes sense to speak of Lorentzian or Euclidean phases.)

Interestingly, this conclusion has strong links with results often postulated (for technical reasons, notably a better behavior of path integrals) in quantum cosmology, but it appears here as a real dynamical prediction of the theory. In standard quantum cosmology one usually deals with an amplitude

$$< \phi_2, t_2|\phi_1, t_1 >= \int d[\phi] e^{I[\phi]}, \tag{8}$$

where $I[\phi]$ is the action of the field configuration $\phi(x,t)$, and $d[\phi]$ is a measure on the space of field configurations. The integrand of Eq.(8) has a rapidly oscillating phase, and the path integral, in general, does not converge. This is why the time is rotated clockwise by $\pi/2$ so that $I[\phi] \to \tilde{I}[\phi] \equiv -iI[\phi]$. The integrand in the resulting Euclidean path integral is now exponentially damped, and the integral generically converges. Then, one can analytically continue the amplitude in the complex t-plane back to real values. Importantly, a quantum field theory machinery has been developed in this framework and the interested reader can, *e.g.*, consider Ref. [27]. Of course, there are also links with the Hartle-Hawking proposal [28]. But the Euclidean phase appears in the model considered in this article in a fundamentally dynamical way since the Poisson bracket between Hamiltonian constraints varies continuously from a positive to a negative expression. The "spirit" of the Hartle-Hawking proposal, translated in the framework considered here, has been studied in [12]. Importantly, the appearance of an Euclidean phase was also independently derived from another approach to LQC in Ref. [26]. Many quantum gravity approaches seem to predict the existence of a silent surface ($\Omega = 0$) where light cones are completely squeezed, on each "side" of the Euclidean phase. This is also a clear realization of the BKL conjecture (see, *e.g.* Ref. [29]). Arguments are given in Ref. [8] showing that the change from a hyperbolic to an elliptic type of equations in LQC should be understood as a true change of signature (that has been missed before because homogeneous models cannot probe it) and not just a tachyonic instability. It should also be emphasized that the deformed algebra approach is grounded in avoiding gauge issues. Many approaches make a gauge fixing. In most cases, gauge fixing before quantization is known to be harmless, but the situation is different in general relativity. The constraints we are considering are much more complicated functions than, for example, the Gauss constraint of Yang–Mills theories: it is therefore likely that the constraints receive significant quantum corrections. If the constraints are quantum corrected, the gauge transformations they generate are, as we have shown, not of the classical form. Gauge fixing before quantization might then be inconsistent because one would fix the gauge according to transformations which subsequently will be modified. In addition, in the present case, the dynamics is part of the gauge system. A consistent theory must therefore quantize gauge transformations and

the dynamics at once. It is not correct to fix one part (the gauge) in order to derive the second part (the dynamics) in an unrestricted way. The subtle consistency conditions associated with the covariance of general relativity are encoded in the first class nature of its system of constraints. Here, great care is taken in not breaking this consistency.

The equations of motion derived in this framework are still covariant under the deformed algebra replacing classical coordinate transformations. The corresponding quantum space-time structure is obviously not Riemannian (there is no line element in the usual sense), but has a well-defined canonical formulation using hypersurface deformations.

III. BACKGROUND EVOLUTION

At the background level, the change of signature cannot be probed/detected. This is obvious for two reasons. First, because the relative sign between temporal and spatial derivatives cannot be identified. Second, because the Poisson bracket between Hamiltonian constraints then trivially vanishes. The evolution of the cosmological background is studied at the effective level with holonomy corrections. The background geometry is described by the homogeneous, isotropic and flat configuration parametrized by the scale factor a. The dynamics of the background is governed by the quantum-corrected Friedmann equation

$$H^2 = \frac{\kappa}{3}\rho\left(1-\frac{\rho}{\rho_{\rm c}}\right), \tag{9}$$

derived in Ref. [30], where $H = \dot{a}/a$ is the Hubble rate in cosmic time, ρ is the energy density of the content of the universe and $\rho_{\rm c}$ denotes its maximal value attained at the bounce. The dot denotes a derivative w.r.t. cosmic time. Obviously, the physical interpretation of the background equations makes sense only in the Lorentzian phase, that is when $\rho < \rho_c/2$, but technically one can still determine the manifold structure for $\rho_c/2 < \rho < \rho_c$, that is in the Euclidean phase. An alternative view of our approach which solves all interpretation difficulties and which leads to the very same result, is to consider that there is no *real* change of signature: the background evolves in a standard way (although, of course, according to the modified Friedmann equation) and the change of sign of the Ω factor entering the propagation equation of perturbations is just a tachyonic instability, as well known to appear, for example, in Gauss-Bonnet gravity when the curvature invariant is non-minimally coupled with a scalar field. We prefer not to favor this view because, as detailed in [8], there are hints that the phenomenon is deeper but one is free to see things in this way. Planck units are used throughout this article with $m_{\rm Pl} = 1/\sqrt{G} \approx 1.22\cdot 10^{19}$ GeV. Furthermore, we consider a single massive scalar field, ϕ, with a quadratic potential $V = m^2\phi^2/2$, as the matter content of the Universe. This choice is made for simplicity. It allows easy comparisons with other works and generates a phase of slow-roll inflation. Even if this potential is not favored by current observational data [31], it still serves as a valuable toy model for studying the phase of inflation in different frameworks. Moreover, taking into account more subtle effects, e.g. the quantum gravitational corrections considered here, might improve the status of the quadratic potential in the light of the observational data.

Splitting the field $\phi = \bar{\phi} + \delta\phi$ into a background part, $\bar{\phi}$, and a perturbed part, $\delta\phi$, the Klein-Gordon equation for the background reads

$$\ddot{\bar{\phi}} + 3H\dot{\bar{\phi}} + m^2\bar{\phi} = 0. \tag{10}$$

A first analysis of this model has already been studied in Ref. [32]; a detailed analysis of the background equations can be found in Ref. [33]. Here, we only summarize the main features of the background dynamics. The field evolution can be characterized by two dynamical parameters [6], the potential energy parameter, x, and the kinetic energy parameter, y, defined as

$$x := \frac{m\bar{\phi}}{\sqrt{2\rho_{\rm c}}}, \qquad y := \frac{\dot{\bar{\phi}}}{\sqrt{2\rho_{\rm c}}}. \tag{11}$$

Then the total energy density can be written as $\rho = \rho_{\rm c}(x^2+y^2)$. Eqs. (9) and (10) can then be recast as

$$\begin{cases} \dot{H} &= -\kappa\rho_{\rm c}y^2\left(1-2x^2-2y^2\right), \\ \dot{x} &= my, \\ \dot{y} &= -3Hy - mx, \end{cases} \tag{12}$$

showing that there are two timescales involved in this system: one is given by $1/m$ and corresponds to the classical evolution of the field, the other one is $1/\sqrt{3\kappa\rho_{\rm c}}$ and corresponds to the quantum regime of the evolution. The ratio of these two timescales is

$$\Gamma := \frac{m}{\sqrt{3\kappa\rho_{\rm c}}}. \tag{13}$$

According to standard assumptions of slow-roll inflation with a quadratic potential, the value of the mass $m \simeq 1.2\times 10^{-6} m_{\rm Pl}$ is preferred in the light of the observational data from the Planck satellite (see Ref. [31]). The critical energy density at the bounce is given by $\rho_{\rm c} = 0.41\ m_{\rm Pl}^4$, which is exactly the upper bound of the spectrum of the energy density operator [3]. These values lead to $\Gamma \simeq 2\cdot 10^{-7}$. Hence, one can safely assume that $\Gamma \ll 1$, ensuring that the evolution splits into three phases: (i) a classical pre-bounce contracting phase, (ii) the bouncing phase and (iii) a classical expanding phase after the bounce (slow-roll inflation), see Ref. [33] for details. Initial conditions, $\{a_0, x_0, y_0\}$, are set in the remote past of the contracting phase when the energy density is very small compared to the critical energy density, *i.e.*

$$\sqrt{\frac{\rho_0}{\rho_{\rm c}}} \ll \Gamma. \tag{14}$$

It is convenient to use polar coordinates for the potential and kinetic energy parameters

$$x(t) = \sqrt{\frac{\rho}{\rho_{\rm c}}}\sin(mt+\theta_0), \tag{15}$$

$$y(t) = \sqrt{\frac{\rho}{\rho_{\rm c}}}\cos(mt+\theta_0), \tag{16}$$

where θ_0 is the initial phase between the share of potential energy and kinetic energy. In order to select different background evolutions independently of the small oscillatory behavior of the solutions, the following parametrization shall be used:

$$\sqrt{\frac{\rho_0}{\rho_{\rm c}}} = \frac{\Gamma}{\alpha}\left(1-\frac{\sin(2\theta_0)}{4\alpha}\right)^{-1}, \tag{17}$$

where α is a number large enough such that (14) holds. To each phase, θ_0, corresponds a specific value of the potential energy parameter at the bounce $x_{\rm B}$. As shown in Ref. [34], for a mass $m = 1.21\times10^{-6}m_{\rm Pl}$, the favored value for $x_{\rm B}$ is 3.55×10^{-6}. This solution for the background dynamics features only a tiny amount of deflation before the bounce as shown in Fig. 1. In general, we will chose the normalization of the scale factor at the bounce as $a_{\rm B}=1$. The plots and spectra are presented as functions of the number of e-folds $N := \pm\ln(a/a_{\rm B})$, that have to elapse until the bounce (negatively valued) and that have elapsed after the bounce (positively valued) respectively.

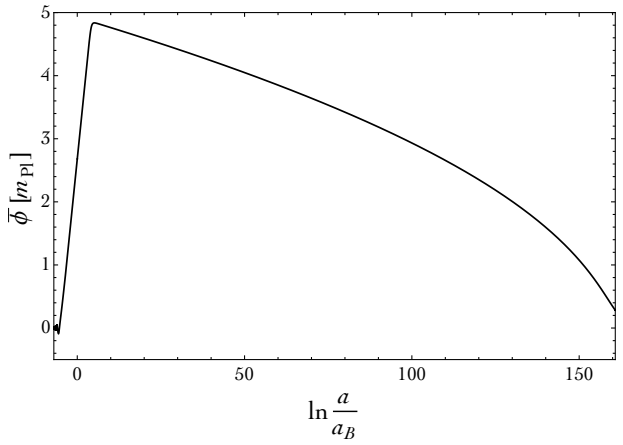

FIG. 1. Evolution of the scalar field as a function of the number of e-folds $N := \pm\ln a/a_{\rm B}$, with $m = 1.2\times10^{-6}m_{\rm Pl}$. The zero on the horizontal axis corresponds to the bounce when $a_{\rm B}=1$. This solution is such that $x_{\rm B}=3.55\times10^{-6}$ (obtained with $\alpha = 17\pi/4+1$ and $\theta_0 = 5.11$). The evolution is stopped at the end of inflation when $\phi = 1/\sqrt{4\pi}\ m_{\rm Pl}$.

IV. EQUATION OF MOTION FOR SCALAR MODES

The equation of motion for scalar modes in the deformed algebra approach is derived from the particular form of the Hamiltonian constraint. In Ref. [25], the gravitational part of the Hamiltonian constraint has been analyzed and reads (up to quadratic order)

$$H[N] = \int_\Sigma d^3x\left[\bar{N}\left(\mathcal{H}^{(0)}+\mathcal{H}^{(2)}\right)+\delta N\,\mathcal{H}^{(1)}\right], \tag{18}$$

where

$$2\kappa\,\mathcal{H}^{(0)} = -6\sqrt{\bar{p}}\bar{k}^2\ , \tag{19}$$

$$2\kappa\,\mathcal{H}^{(1)} = -4\sqrt{\bar{p}}\delta K^d_d - \frac{\bar{k}^2}{\sqrt{\bar{p}}}\delta E^d_d + \frac{2}{\sqrt{\bar{p}}}\partial^j\partial_c\delta E^c_j, \tag{20}$$

$$\begin{aligned}2\kappa\,\mathcal{H}^{(2)} = &-2\frac{\bar{k}}{\sqrt{\bar{p}}}\delta K^i_a\delta E^a_i\\ &+\sqrt{\bar{p}}\left(\delta^b_i\delta K^i_a\delta^a_j\delta K^j_b-\delta^a_i\delta K^i_a\delta^b_j\delta K^j_b\right)\\ &+\frac{1}{4}\frac{\bar{k}^2}{\bar{p}^{\frac{3}{2}}}\left(\delta^i_a\delta E^a_i\delta^j_b\delta E^b_j-2\delta^j_a\delta E^a_i\delta^i_b\delta E^b_j\right)\\ &+\frac{1}{\bar{p}^{\frac{3}{2}}}Y^{kjil}_{bdc}\ \epsilon^{ab}_k\ \partial_a\left(\delta E^d_j\partial_i\delta E^c_l\right)\\ &+\frac{1}{\bar{p}^{\frac{3}{2}}}Z^{cidj}_{ab}\ \left(\partial_c\delta E^a_i\right)\left(\partial_d\delta E^b_j\right).\end{aligned} \tag{21}$$

Here, $\bar{p}$ is the mean value of the densitized triad E^a_i and $\bar{k}$ was defined in Eq. (7). The term Z^{cidj}_{ab} depends on the kind of modes considered (scalar, vector or tensor):

$$Z^{cidj}_{ab} = \begin{cases}\delta_{ab}\delta^{ij}\delta^{cd} & \text{for tensor modes,}\\ 0 & \text{for vector modes,}\\ -\frac{1}{2}\delta^c_a\delta^d_b\delta^{ij} & \text{for vector modes.}\end{cases} \tag{22}$$

Lastly, Y^{kjil}_{bdc} is a complicated expression whose form is not relevant here. Based on this, the holonomy quantum corrections can be accounted for and the Mukhanov-Sasaki equation of motion for gauge-invariant perturbations can be calculated [10]. In conformal time it is given by

$$v_{\rm S}'' - \Omega\,\nabla^2 v_{\rm S} - \frac{z_{\rm S}''}{z_{\rm S}}v_{\rm S} = 0, \tag{23}$$

with

$$v_{\rm S} := \sqrt{\bar{p}}\left(\delta\phi+\frac{\bar{\phi}'}{\mathscr{H}}\Phi\right) \quad\text{and}\quad z_{\rm S} := \sqrt{\bar{p}}\,\frac{\bar{\phi}'}{\mathscr{H}}. \tag{24}$$

The variable Φ denotes the gauge invariant Bardeen potential taking into account the metric perturbations, whereas ϕ represents the massive scalar field. $\mathscr{H}$ is the conformal Hubble parameter. The Mukhanov equation of motion (23) reduces to the classical equation when $\Omega\to1$. Note that for FLRW cosmologies, in conformal time, $\sqrt{\bar{p}} = a$. On the quantum-modified background discussed in the previous section, we can evaluate the evolution of the Mukhanov variable $v_{\rm S}$. For simplicity we will omit the index 'S' in the following, assuming that it is clear that v denotes the scalar perturbation variable. Using the Fourier space decomposition of the $v(\mathbf{x},\eta)$ field,

$$v(\mathbf{x},\eta) = \int\frac{d^3k}{(2\pi)^{3/2}}v_{\mathbf{k}}(\eta)e^{i\mathbf{k}\cdot\mathbf{x}}, \tag{25}$$

one gets a set of ordinary differential equations for the Fourier components $v_{\mathbf{k}}$. Due to the isotropy of space, the $\mathbf{k}$-vector of $v_{\mathbf{k}}$ might be simplified to the absolute value dependence v_k, where $k := \sqrt{\mathbf{k}\cdot\mathbf{k}}$. The v_k function is called a mode function. Instead of using the conformal time dependence, it is often (due to technical reasons) convenient to switch to cosmic time t in the numerical computations. With $t = \int a \cdot d\eta$, the Mukhanov equation of motion reads

$$\ddot{v}_k + H\dot{v}_k + f_k^{(v)}(t)v_k = 0, \tag{26}$$

with $z = a\frac{\dot{\bar{\phi}}}{H}$ and

$$f_k^{(v)}(t) := \Omega\frac{k^2}{a^2} - \frac{\dot{z}}{z}H - \frac{\ddot{z}}{z}, \tag{27}$$

being the effective frequency term. In order to derive the primordial power spectrum after inflation one would have to solve Eq. (26) for every mode k for all times from $t_{\rm init}$ until $t_{\rm end}$ where $t_{\rm init}$ is the initial starting point, set in the remote past as we will see later, and $t_{\rm end}$ denotes the time at the end of the inflationary phase. This requires a numerical integration. However, the Mukhanov variable v, cannot be used for the whole integration because of a non-physical singularity occurring at the bounce. Let us describe how to bypass this difficulty by using the change of variable. We introduce $h_k := v_k/a$ for every k, so that (26) becomes

$$\ddot{h}_k + 3H\dot{h}_k + f_k^{(h)}(t)h_k = 0 \tag{28}$$

with

$$f_k^{(h)}(t) := \Omega\frac{k^2}{a^2} + m^2 + m^2\kappa\,\Omega\frac{\dot{\bar{\phi}}\bar{\phi}}{H} - 2\left(\frac{\dot{H}}{H}\right)^2 + \frac{\ddot{H}}{H}. \tag{29}$$

In the numerical computation this second order differential equation is replaced by the following first order system:

$$\begin{cases} \dot{h}_k &= (1/a)g_k, \\ \dot{g}_k &= -2Hg_k + f_k^{(h)}(t)a\ h_k. \end{cases} \tag{30}$$

The numerical integration of (30) is performed for $t \in [t_{\rm init}, t_{h\to\mathcal{R}}]$ where $t_{h\to\mathcal{R}}$ is before the bounce. Since the effective frequency terms, (29) or (27), depend on inverse powers of H, the differential equations have a generic singularity at the bounce, when the Hubble parameter vanishes. Nonetheless, this singularity is not physical, which can be seen by analyzing the physical scalar curvature,

$$\mathcal{R} := \frac{v}{z}. \tag{31}$$

Using this variable, one can rewrite Mukhanov's equation of motion in Fourier space as

$$\ddot{\mathcal{R}}_k - \left(3H + 2m^2\frac{\bar{\phi}}{\dot{\bar{\phi}}} + 2\frac{\dot{H}}{H}\right)\dot{\mathcal{R}}_k + \Omega\frac{k^2}{a^2}\mathcal{R}_k = 0. \tag{32}$$

When approaching the bounce, H tends to zero and Ω to minus one. It should be noticed that this equation is mathematically well behaved, even when $\Omega < 0$, that is in the Euclidean-like phase. Obviously, in the Euclidean phase, k loses its usual interpretation and the Fourier transformation has no intuitive physical sense. This is, however, already true on a Lorentzian curved manifold: the space/ time splitting – or positive/ negative frequency splitting – is, in general, ill defined: one usually relies on static boundaries that allow a physical choice. The "bet" of this study is fundamentally the same: quantities are defined in the remote past of the contracting branch when the signature is the usual one, and when quantum effects are negligible. Then, they are mathematically propagated through the bounce where they lose a clear meaning. Finally, the observables are computed in the expanding Lorentzian phase when physics is again under control. This is a questionable approach, but, in our opinion, a reasonable one at this stage.

During the bouncing phase, $\dot{\bar{\phi}} \simeq \sqrt{2\rho_{\rm c}} \gg m\bar{\phi}$, so that the equation of motion reduces to

$$\ddot{\mathcal{R}}_k - 2\frac{\dot{H}}{H}\dot{\mathcal{R}}_k - \frac{k^2}{a^2}\mathcal{R}_k \simeq 0. \tag{33}$$

According to the analytical expression for $\bar{\phi}$ and $\dot{\bar{\phi}}$ around the bounce developed in Ref. [33], this gives

$$\ddot{\mathcal{R}}_k - \frac{2}{t - t_{\rm B}}\dot{\mathcal{R}}_k - k^2\mathcal{R}_k \simeq 0, \tag{34}$$

when we restrict ourselves to the first order in $(t - t_{\rm B})$. The space of solutions to this differential equation is spanned by the two independent functions,

$$\mathcal{R}_k^{(1)} = \left[\sinh\left(k(t-t_{\rm B})\right) - k(t-t_{\rm B})\cosh\left(k(t-t_{\rm B})\right)\right],$$
$$\mathcal{R}_k^{(2)} = \left[\cosh\left(k(t-t_{\rm B})\right) - k(t-t_{\rm B})\sinh\left(k(t-t_{\rm B})\right)\right].$$

These solutions show an obviously regular behavior at the bounce. But it should be noticed that (32) runs into trouble away from the bounce due to the time derivative of the potential $\dot{\bar{\phi}}$ appearing in the denominator of the friction term. During the classical contracting and expanding phases, $\dot{\bar{\phi}}$ oscillates around a null value, causing the break-down of the numerical integration of the differential equation (32) of $\mathcal{R}$. For this reason one has to switch twice between Eq. (30) and Eq. (32) during the numerical computations. For $t \in [t_{\rm init}, t_{h\to\mathcal{R}}]$ and $t \in [t_{\mathcal{R}\to h}, t_{\rm end}]$, where $t_{h\to\mathcal{R}} < t_{\rm B} < t_{\mathcal{R}\to h}$, the differential equation for h, namely (30), must be used. Whereas for $t \in [t_{h\to\mathcal{R}}, t_{\mathcal{R}\to h}]$, it is the equation for $\mathcal{R}$, Eq. (32), that has to be integrated. The exact choice of the transition points is irrelevant as long as they do not approach one of the singularity points.

V. INITIAL CONDITIONS

The considered equations of motion for the scalar perturbations (Eq. (23) or Eq. (26)) might be considered – at the effective level – as the quantum ones. This is due to the presence of the factor Ω, being a result of the quantum gravitational effects. The quantum effects taken into account here are, however, only those which modify the background degrees of freedom. The inhomogeneous degrees might be (and are), treated classically in the perturbative regime under consideration. In order to see it, let us consider the extrinsic curvature K_a^i which is exponentiated to the form of a holonomy operator in the quantum theory. In the perturbative treatment we have $K_a^i = \bar{k}\delta_a^i + \delta K_a^i$, together with the condition $|\delta K_a^i|/\bar{k} \ll 1$. Path integration of K_a^i leads to a factor of the form $\gamma\bar{\mu}\bar{k}$ for the homogeneous contribution, which is of the order of unity in vicinity of the bounce. Full exponentiation of the background contribution to K_a^i must be, therefore, kept over the evolution through the bounce. However, this is not necessary for sufficiently small perturbations, for which the condition $\gamma\bar{\mu}|\delta K_a^i| \ll 1$ might be satisfied even at the bounce. This allows for the expansion of the holonomy up to a linear contribution in δK_a^i and treating the perturbative degrees of freedom in a classical manner.

As the phase space of the perturbative degrees of freedom is approximated by the classical one, the canonical quantization procedure for the modes might be applied. The canonical quantization is an approximation, which is valid only for sufficiently small amplitudes of δK_a^i and sufficiently large wavelengths (roughly greater than the Planck length) in the mode expansion. If the conditions are satisfied, the Fourier mode $v_{\mathbf{k}}(\eta)$ can be promoted to be an operator, such that in the Heisenberg picture

$$\hat{v}_{\mathbf{k}}(\eta) = v_k(\eta)\hat{a}_{\mathbf{k}} + v_k^*(\eta)\hat{a}_{-\mathbf{k}}^\dagger, \tag{35}$$

where $v_k(\eta)$ are the so-called mode functions satisfying the classical equation (26). The $\hat{a}_{\mathbf{k}}^\dagger$ and $\hat{a}_{\mathbf{k}}$ are the creation and annihilation operators respectively, satisfying $[\hat{a}_{\mathbf{k}}, \hat{a}_{\mathbf{q}}^\dagger] = \delta^{(3)}(\mathbf{k}-\mathbf{q})$. Using this commutation relation, one may show that the following condition

$$v_k\frac{dv_k^*}{d\eta} - v_k^*\frac{dv_k}{d\eta} = i, \tag{36}$$

called Wronskian condition, has to be satisfied in order to preserve the standard canonical structure.

Based on the above, the two-point correlation function for the scalar curvature field $\hat{\mathcal{R}}(\mathbf{x},\eta)$ in the vacuum state $|0\rangle$ is given by

$$\langle 0|\hat{\mathcal{R}}(\mathbf{x},\eta)\hat{\mathcal{R}}(\mathbf{y},\eta)|0\rangle = \int_0^\infty \frac{dk}{k}\mathcal{P}_S(k,\eta)\frac{\sin kr}{kr}, \tag{37}$$

where $r = |\mathbf{x}-\mathbf{y}|$ and the scalar power spectrum reads

$$\mathcal{P}_S(k,\eta) := \frac{k^3}{2\pi^2}\frac{|v_k(\eta)|^2}{z^2}. \tag{38}$$

The power spectrum carries all statistical information about the Gaussian scalar curvature field under consideration (non-linear effects are neglected in our analysis) and its determination for the LQC model discussed in the previous sections is a main goal of this study.

The equations of motion for the scalar mode functions $v_k(\eta)$ can be solved numerically, following the procedure presented in the previous section. For this purpose initial conditions for perturbations have to be set for every wavenumber k. In standard cosmology, it is common to set Cauchy initial conditions at some moment in time after the big bang singularity. In the present work, we set initial conditions in the pre-bounce phase. This is the natural choice if the bounce is a phenomenon to be really understood as resulting from a causal evolution of the Universe, with time flowing in a unique direction. In addition, in the remote past of the contracting branch, the Universe is classical and quantum effects do not play any important role. This seems both technically more convenient (since the quantum dominated region still represents a quite unknown field of physics) and physically better motivated. In particular, as discussed in the previous sections, it has been shown in Ref. [10] that the geometry of the universe in its quantum stage ($\rho > \rho_c/2$) might become Euclidean instead of being Lorentzian (the very notion of time obviously looses here its meaning). The physical consequences are still not perfectly well understood and setting initial conditions in the Euclidean phase would be the worst possible choice: we therefore focus on the classical contracting phase. Note that another proposal, studied in Refs. [12, 13], is to set initial conditions at the surface of silence (or in a "hybrid" way as advocated by a careful study of the Tricomi problem). We do not consider this hypothesis here.

The most simple and natural way to set initial conditions for a quantum oscillator is provided by the vacuum state $|0\rangle_k$ for every mode k at some given moment in time. This sets a clear Cauchy initial value problem. However, it is well known that the notion of vacuum in an arbitrary curved spacetime is ambiguous since the definition of the usual "instantaneous vacuum" is based on plane waves satisfying the differential equation of an harmonic oscillator with wavenumber k. In the case of scalar perturbations, as the effective frequency term depends non-trivially on time, it is more appropriate to use the Wentzel-Kramers-Brillouin (WKB) approximation and the so-called "adiabatic vacuum". In contrast with the ordinary instantaneous vacuum state, well known from quantum field theory, the adiabatic vacuum does not have to satisfy the differential equation of an harmonic oscillator in some limit. The instantaneous-vacuum state is recovered as the first term of the WKB expansion.

For scalar perturbations in LQC the equation of motion is given by Eq. (23). In conformal time, this equation resembles the differential equation of an oscillator,

$$v_k'' + k_{\rm eff}^2(\eta)v_{\rm k} = 0, \tag{39}$$

with a time-dependent wave number

$$k_{\rm eff}(\eta) := \sqrt{\Omega(\eta)k^2 - \frac{z''}{z}(\eta)}. \tag{40}$$

Recall that we set initial conditions in the remote past where $\Omega \sim 1$ is almost constant. Thus the Ω-factor actually plays no role when addressing the issue of initial conditions. The main idea of the WKB approximation is to use the following generic ansatz for the solutions to Eq. (39):

$$v_k(\eta) = c_1 \cdot e^{i(k_{\rm eff}T)\cdot W_k(\eta)} + c_2 \cdot e^{-i(k_{\rm eff}T)\cdot W_k(\eta)}, \tag{41}$$

where the values of constants c_1 and c_2 are constrained according to the Wronskian condition (36). In the WKB approximation the functions $W_k(\eta)$ are expanded in terms of some small parameter $(k_{\rm eff}T)^{-1}$ where T is the minimal time interval for which $k_{\rm eff}$, and its time derivatives, start to change substantially ($T \gg 1/k_{\rm eff}$). Then the WKB expansion reads

$$W_k(\eta) = \sum_{n=0}^{\infty} \left(\frac{i}{k_{\rm eff}T}\right)^n W_{k,n}(\eta). \tag{42}$$

Introducing this ansatz into Eq. (39), one gets the explicit expressions for the different orders, n, of $W_{k,n}$. The WKB approximation consists in truncating the series after the first order, leading to the approximated solution for the mode functions

$$\begin{aligned} v_k(\eta) = &\frac{c_1}{\sqrt{k_{\rm eff}(\eta)}} e^{i\int^\eta k_{\rm eff}(\tilde\eta)d\tilde\eta} \\ &+ \frac{c_2}{\sqrt{k_{\rm eff}(\eta)}} e^{-i\int^\eta k_{\rm eff}(\tilde\eta)d\tilde\eta}. \end{aligned} \tag{43}$$

Using the Wronskian condition (36), we find $|c_2|^2 - |c_1|^2 = 1/2$ as a condition that the free parameters c_1 and c_2 have to fulfill. The most convenient choice is $c_1 = 0$ and $c_2 = 1/\sqrt{2}$ which corresponds to a wave propagating in positive time direction. For this choice the mode function reads

$$v_k(\eta) = \frac{1}{\sqrt{2k_{\rm eff}(\eta)}} e^{-i\int^\eta k_{\rm eff}(\tilde\eta)d\tilde\eta}. \tag{44}$$

This represents a suitable choice because the mode function reduces to the Bunch-Davies vacuum in the UV limit ($k \to \infty$).

In order to check that this approach is valid, we plug this solution into Eq. (39) and find that it is actually an exact solution to

$$v_k'' + \left(k_{\rm eff}^2 - \frac{3}{4}\frac{(k_{\rm eff}')^2}{k_{\rm eff}^2} + \frac{1}{2}\frac{k_{\rm eff}''}{k_{\rm eff}}\right) v_k = 0. \tag{45}$$

Therefore, the solution (43) is valid as long as

$$\left|\frac{1}{2}\frac{k_{\rm eff}''}{k_{\rm eff}^3} - \frac{3}{4}\frac{(k_{\rm eff}')^2}{k_{\rm eff}^4}\right| \ll 1, \tag{46}$$

when the effective wavenumber, $k_{\rm eff}$, varies slowly. The appropriate initial conditions are then

$$v_k(\eta_{\rm init}) = \frac{1}{\sqrt{2k_{\rm eff}(\eta_{\rm init})}}, \tag{47}$$

$$\left.\frac{dv_k}{d\eta}\right|_{\eta=\eta_{\rm init}} = -\left(ik_{\rm eff} + \frac{1}{2}\frac{k_{\rm eff}'}{k_{\rm eff}}\right)\left.\frac{1}{\sqrt{2k_{\rm eff}}}\right|_{\eta=\eta_{\rm init}}, \tag{48}$$

where the exponential term can be neglected because it contributes only with an arbitrary phase. The initial moment $\eta_{\rm init}$ has to be chosen such that the WKB conditions are satisfied at this particular moment of time for all modes k. By analyzing $k_{\rm eff}(\eta)$ and its time derivatives, we can find an appropriate $\eta_{\rm init}$ in the remote past. For the numerical computations, the choice of $\eta_{\rm init}$ is therefore arbitrary as long as the condition (46) is fulfilled. The instantaneous vacuum can be used as well for setting initial conditions. The instantaneous vacuum choice relies on the minimal energy state of the system defined by the Hamiltonian. Therefore, the requirement

$$\left.\frac{k_{\rm eff}'}{(2k_{\rm eff})^{3/2}}\right|_{\eta=\eta_{\rm init}} = 0, \tag{49}$$

has to be satisfied (see Ref. [35] for instance). In fact, one can find that there exists $\eta_{\rm init}$ such that both conditions (46) and (49), are fulfilled. For reasons of comparability of the two approaches, we use this choice. In such a case, any difference between the two approaches is due to the higher order contribution to (48), which is present in case of the adiabatic vacuum-type normalization.

The conditions for the validity of both the instantaneous and WKB vacua depend strongly on the evolution of the cosmological term z''/z during the pre-bounce contracting phase. A direct calculation leads to

$$\begin{aligned} \frac{z''}{z} = -a^2\Bigg(&m^2 - 2H^2 + 2\kappa m^2\frac{\bar\phi\dot{\bar\phi}}{H} + \frac{7}{2}\kappa\Omega\dot{\bar\phi}^2 \\ &-\kappa^2\Omega^2\frac{\dot{\bar\phi}^4}{2H^2} - 3\kappa\frac{\dot{\bar\phi}^4}{\rho_{\rm c}}\Bigg). \end{aligned} \tag{50}$$

This expression is valid at all times. In order to analyze the shape of the effective potential it is convenient to divide the evolution into three background phases as mentioned in Sec. III. Then, analytical approximations for every phase can be used respectively. During the pre-bounce classical contracting phase, when $\rho(t) \ll \rho_{\rm c}$, the scalar field undergoes an oscillatory behavior with an amplitude proportional to $\sqrt{\rho(t)}$. The Hubble parameter H is proportional to $\sqrt{\rho}$ as well, whereas $\Omega \simeq 1$. Inserting these solutions into Eq. (50) yield terms which are proportional to different orders of $\sqrt{\rho}$. Averaging over the oscillatory contributions, which all have a characteristic oscillation time of $1/m$, gives

$$\begin{aligned} \left\langle\frac{z''}{z}\right\rangle = -a^2\Big(&m^2 - \alpha_1\sqrt{\kappa}m\sqrt{\rho(t)} + \alpha_2\kappa\rho(t) \\ &+ \alpha_3\kappa\rho_{\rm c}\left(\frac{\rho(t)}{\rho_{\rm c}}\right)^2\Big), \end{aligned} \tag{51}$$

where the constants α_i are determined by the averaged oscillations. Since the energy density is increasing for all times in the remote past, $\rho(t)$ becomes sufficiently small in the remote past. Thus the m^2-term will dominate for early times and therefore $z''/z \propto -m^2a^2$. On a logarithmic scale as a function of $\ln(a/a_{\rm B})$ like in Fig. 2 the absolute value of the effective potential is then given by a straight line with gradient -2 and with a $\ln(|z''/z|)$-intercept of $2\ln(a_{\rm B}m) = -27.26$. This result is obtained as well by a purely analytical analysis which is presented in Fig. 2. We use that the Hubble parameter H is approximated by $H(t) = H_0(1+\frac{3}{2}H_0t)^{-1}$ for the pre-bounce phase when neglecting the fast oscillations, where H_0 denotes the initial Hubble parameter. H_0 is determined by the mass and the parameter α, namely $H_0 = -m/3\alpha$. Integration leads to the analytical solution of the scale factor in the pre-bounce phase

$$a(t) = a_* \left(2 - \frac{m}{\alpha}t\right)^{\frac{2}{3}}, \tag{52}$$

where the prefactor a_* is the scale factor for $t = \alpha/m$. With this expression the analytical solution for $\ln|(z''/z)| = \ln a(t)^2m^2$ reads on the logarithmic scale

$$\ln\left|\frac{z''}{z}\right| = 2\ln a_* + \frac{4}{3}\ln\left(2 - \frac{m}{\alpha}t\right) + 2\ln m. \tag{53}$$

As a function of $\ln(a/a_{\rm B})$, one gets the red line on the left in Fig. 2. This analytic solution is valid until the energy density starts to dominate over the constant mass term in Eq. (51). The first term which is comparable to m^2 is proportional to $\sqrt{\rho}$. With the analytic solution of $\sqrt{\rho}$ in the pre-bounce phase,

$$\sqrt{\frac{\rho(t)}{\rho_{\rm c}}} = \frac{\Gamma\alpha^{-1}}{1 - \frac{1}{2\alpha}\left[mt + \frac{1}{2}\sin(2mt + 2\theta_0)\right]}, \tag{54}$$

we can compute the time when the $\sqrt{\rho}$-term crosses 'm^2' in its amplitude. The oscillation term in Eq. (54) is averaged over $T = 1/m$. This transition point is referred to $N_{\rm pre} := \ln(a_{\rm pre}/a_{\rm B}) = -5.38$ in the figure.
During the bouncing phase the potential energy parameter x, is very small compared to the kinetic potential parameter y, since we consider a kinetic bounce scenario. Then, in particular, $x^2 \ll y^2$ is satisfied during this phase and the Hubble parameter can be reduced to

$$H^2 \simeq \frac{\kappa\rho_{\rm c}}{3}y^2\left(1 - y^2\right). \tag{55}$$

The analytic solution for y around the bounce is given by $y(t) = (1+3\kappa\rho_{\rm c}(t-t_{\rm B})^2)^{-1/2}$, as presented in Ref. [33] and the scale factor is related to y via $a = a_{\rm B}\,|y|^{-1/3}$. With these approximations the expression for z''/z reduces to

$$\frac{z''}{z} = \frac{\kappa\rho_{\rm c}a_{\rm B}^2}{3}\frac{\left(-\left(\frac{a}{a_{\rm B}}\right)^2 + 23\left(\frac{a}{a_{\rm B}}\right)^{-4} - 4\left(\frac{a}{a_{\rm B}}\right)^{-10}\right)}{\left(\frac{a}{a_{\rm B}}\right)^6 - 1}.$$

Note that this expression is positively valued and diverges at the bounce. The absolute value of this expression on the logarithmic scale and as a function of $\ln(a/a_{\rm B})$ provides the red lines around the bounce in Fig. 2. These approximations are valid until x^2 becomes significant in comparison to y^2, let's say $x^2 > y^2/10$. The analytic solutions for x and y provide these transition points of validity respectively before and after the bounce, namely $N_{\rm preB} := \ln(a_{\rm preB}/a_{\rm B}) = -4.41$ and $N_{\rm postB} := \ln(a_{\rm postB}/a_{\rm B}) = 3.62$, as shown in Fig. 2.
During slow-roll inflation, $\Omega \simeq 1$ such that z''/z takes its classical expression. This leads to $z''/z = (2 + 6\epsilon_{\rm H} - 3\delta_{\rm H})/\eta^2$, with $\epsilon_{\rm H}$ and $\delta_{\rm H}$ the first and second Hubble flow functions, both much smaller than unity during inflation. Furthermore, $a \propto 1/\eta$ and therefore $\ln(z''/z) \propto 2\ln(a/a_{\rm B})$, see Fig. 2. In particular the effective potential is then given by $z''/z = \frac{1}{2}a^2H^2$. The curve can be approximated from the beginning of slow-roll inflation, *i.e.* when $t_{\rm i} = t_{\rm B} + f/m$ where f is an analytical expression related to the Lambert function and $t_{\rm B}$ is given analytically as well. For this time $a_{\rm i} = a_{\rm B}\Gamma^{-\frac{1}{3}}$ and the logarithm of the absolute value of the effective potential is given by $\ln|z''/z| = \ln(2/\eta^2) = \ln((1/2)a_{\rm i}^2H_{\rm i}^2)$. The value of the Hubble parameter $H_{\rm i}$ is given analytically as well, see Ref. [33]. The approximation is valid starting from $N_{\rm post} := \ln(a_{\rm post}/a_{\rm B}) = 5.53$. For the approximation we use that

$$H(t) = H_{\rm i}\left|1 - \frac{\epsilon\Gamma}{x_{\rm i}}m(t - t_{\rm i})\right| \tag{56}$$

during slow-roll inflation, where ϵ is the sign of the cosine of the phase parameter between the potential and kinetic energy parameters at the transition point between the pre-bounce and bouncing phases, and $x_{\rm i}$ is the value of the potential energy parameter at $t_{\rm i}$. Furthermore, the scale factor undergoes an exponential growth with coordinate time, namely

$$a(t) = a_{\rm i}e^{-\frac{H_{\rm i}}{2x_{\rm i}}(t-t_{\rm i})(\epsilon\Gamma m(t-t_{\rm i})-2x_{\rm i})}. \tag{57}$$

The analytic fit given by these two functions is displayed by the red line on the right side in Fig. 2. as a function of $\ln(a/a_{\rm B})$ with a provided by Eq. (57). The slight difference between numerical results and the analytical solution during slow-roll inflation is due to the fact that the analytical approximations for this phase goes back on approximations even for the pre-bounce phase. Hence, small differences are propagated.

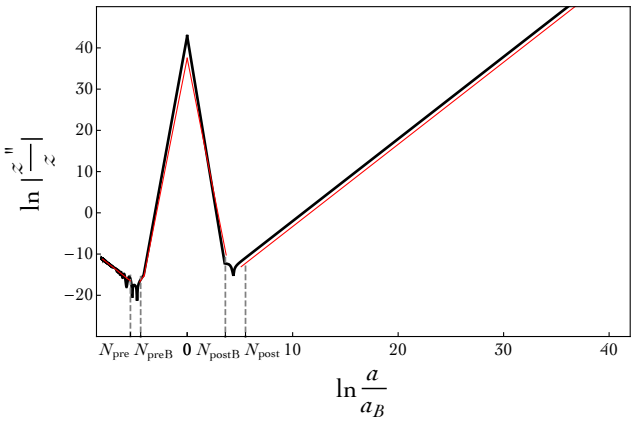

FIG. 2. Evolution of the cosmological term z''/z as a function of the number of e-folds $\ln(a/a_{\rm B})$, with $m = 1.2 \times 10^{-6} m_{\rm Pl}$. The parameters for the background are set as in Fig. 1. During the pre-bounce contracting phase and slow-roll inflation $\ln(z''/z) \propto \pm 2 \ln(a/a_{\rm B}) + const.$

VI. THE SCALAR POWER SPECTRUM

For scalar modes, the primordial power spectrum at the end of inflation is defined in terms of the mode functions by virtue of the definition (38). As we shall see in the next section, three ranges of wavenumbers can be identified, depending on how they compare to the effective potential z''/z: (i) the infrared regime, (ii) intermediate scales and (iii) the ultraviolet regime.

A. The infrared regime

The infrared limit (IR) of the primordial power spectrum corresponds to modes such that $k^2 \ll |z''/z|$ during the pre-bounce contracting phase. These modes are frozen during the bouncing phase and slow-roll inflation. The transition between the contracting phase and the bouncing phase occurs when $H \simeq -m/3$, as discussed in Ref. [33]. At the transition, the effective potential term z''/z is well approximated by a''/a, since $\dot{\bar{\phi}}/H$ remains nearly constant. This allows us to introduce the following IR scale (see Ref. [33]):

$$k_{\rm IR} := \frac{a_{\rm B}}{3\sqrt{2}} \left(m^2 \sqrt{3\kappa\rho_{\rm c}}\right)^{1/3} \approx 4.7 \times 10^{-5} m_{\rm Pl}, \qquad (58)$$

where the numerical value has been obtained for $m = 1.2 \times 10^{-6} m_{\rm Pl}$, $a_{\rm B} = 1$ and $\rho_{\rm c} = 0.41 m_{\rm Pl}^4$.
There is an important difference with respect to the case of tensor modes. For small enough values of k in the IR regime, the tensor power spectrum tends to be scale-invariant. This is due to the fact that initial conditions for tensor modes are set when *all* the modes of interest are sub-Hubble (or, more precisely, $k^2 \gg a''/a$). For the scalar modes, however, it is impossible to set appropriate initial conditions at a time when all relevant modes are such that $k^2 \gg |z''/z|$. Indeed, the conditions discussed in the previous section, (46) and (49), have to be satisfied as well respectively for the WKB and the instantaneous vacuum-type normalizations. In addition, the absolute value of the effective potential term keeps decreasing in the remote past of the contracting branch. It is possible to find a time $\eta_{\rm init}$, in the classical contracting phase, at which (i) the absolute value of the effective potential term z''/z is close to zero and (ii) the conditions of validity of the vacuum states are fulfilled. Nevertheless for the WKB vacuum, at this particular time, when $|z''/z|$ is minimal and condition (46) is satisfied, the effective potential does not strictly vanish, it is $|z''/z| = 2.1 \times 10^{-7} m_{\rm Pl}$, and therefore only the modes with $k > 4.5 \times 10^{-4} m_{\rm Pl}$ satisfy the condition $k^2 > |z''/z|$.

B. The ultraviolet regime

In the deformed algebra approach, the ultraviolet modes (UV) experience an exponential growth with increasing wavenumbers. This is due to the Ω-factor in front of the wavenumber in Eq. (32), which becomes negative near the bounce. When approaching the bounce, the friction term in Eq. (33), namely $\dot{H}/H = 1/(t - t_{\rm B})$, diverges. However, the approximate solution given in section IV shows that $\dot{\mathcal{R}}_k$ vanishes at the bounce, since its generic expression is given by

$$\dot{\mathcal{R}}_k = (t - t_{\rm B}) \left[c_1 {\rm ch}\left(k(t - t_{\rm B})\right) - c_2 {\rm sh}\left(k(t - t_{\rm B})\right)\right], \quad (59)$$

where c_1 and c_2 are numerical constants that have to be chosen in accordance to the initial state of the perturbations. Thus, the equation of motion (33) has no singularity, and $(\dot{H}/H)\dot{\mathcal{R}}_k \propto \sqrt{k}$. We are left with the differential equation of an harmonic oscillator, but with an imaginary frequency and a constant term, say $\beta\sqrt{k}$, such that $\ddot{\mathcal{R}}_k + \beta\sqrt{k} - k^2 \mathcal{R}_k = 0$. Close to the bounce the generic solution to this equation is

$$\mathcal{R}_k = \beta k^{-\frac{3}{2}} + \alpha_+ e^{kt} + \alpha_- e^{-kt}.$$

So, in the large k limit and close to the bounce the amplitude of scalar modes receives a real exponential contribution, which marks the Euclidean nature of the bounce ($\Omega < 0$). For large scales however, one has $\left|\Omega k^2\right| \ll |z''/z|$ around the bounce. The solutions for the mode functions are $\mathcal{R}_k(\eta) \sim A_k + B_k \int^\eta d\eta'/z^2(\eta')$, and the large-scale modes are thus qualitatively not affected by the Euclidean nature of the bounce. A similar behavior for the tensor modes was already discussed in Refs. [11] and [33].
The characteristic energy scale $k_{\rm UV}$ beyond which the effect of the Euclidean nature of the bounce qualitatively affects the evolution of the modes can be determined from an analysis of $k_{\rm eff}^2$ in Eq. (39). In vicinity of the bounce $\Omega \approx -1$ and $z''/z > 0$. Therefore, a given mode has an imaginary time-dependent wavenumber for a certain period around the bounce, *i.e.* '$k_{\rm eff}^2 < 0$'. This is what

we call the 'Euclidean phase' in this approach. However, the imaginary effective wavenumber only plays a role, if the interval of conformal time spend by the mode in this regime is large enough. Of course, in the Euclidean phase, it makes physically no sense to talk about time, the evolution parameter η however remains and quantifies the 'period' of the mode. If the mode spends more than one period in the region with complex effective wavenumber, $k^2_{\rm eff} < 0$, the mode will be amplified significantly. This is in accordance with the analytical solutions to the approximated differential equation around the bounce, (33), which show an hyperbolic behavior for $k(t - t_B) \gg 1$. This leads to the following condition for the energy scale $k_{\rm UV}$:

$$k_{\rm UV}\Delta\eta(k_{\rm UV}) \approx 1. \tag{60}$$

A direct analytical analysis of this condition gives the following expression

$$k_{\rm UV} \simeq a_{\rm B}\sqrt{\frac{2}{3}}\sqrt{\frac{\sqrt{2}}{2\sqrt{2}-1}}\sqrt{\kappa\rho_{\rm c}} \approx 2.3\ m_{\rm Pl}, \tag{61}$$

where the numerical value is obtained with use of $a_{\rm B} = 1$ and $\rho_{\rm c} = 0.41\ m^4_{\rm Pl}$.

C. Numerical Results

The scalar power spectrum is obtained by numerical integration of the equation of motion for the mode functions, respectively for the variable h and $\mathcal{R}$ for different phases in the time evolution, and the solution of the background equations (12). Initial conditions for the perturbations can be set according to the WKB approximation referring to the adiabatic vacuum, or with the instantaneous vacuum as shown in Sec. V. The initial conditions for the cosmological background are set in the contracting phase, such that the preferred value of the potential energy parameter x at the bounce is obtained. Note that the dynamics of the background and subsequently the shape of the power spectrum $\mathcal{P}_{\rm S}(k)$ are determined by the mass m of the scalar field, the value of the critical energy density $\rho_{\rm c}$ and the phase θ_0.

Our numerical results are shown in Fig. 3 and Fig. 4 which display the primordial power spectra for the scalar modes, choosing the adiabatic (WKB) vacuum as initial conditions (Fig. 3) and the instantaneous vacuum as initial conditions (Fig. 4). The three regions mentioned in the previous section ($k < k_{\rm IR}, k_{\rm IR} < k < k_{\rm UV}, k > k_{\rm UV}$) can be well identified in the spectra.

In the intermediate region ($k_{\rm IR} < k < k_{\rm UV}$), the spectrum follows a characteristic oscillating behavior observed also in case of the tensor modes (see Ref. [33]). For the values of $k > k_{\rm UV}$, the power spectrum is characterized by the exponential growth. This behavior should, however, be considered with care. First, the UV regime ($k > k_{\rm UV}$) corresponds to the modes which are trans-Planckian at the bounce. For such modes the effective description based on the continuous equations of motion might not be reliable. Second, the observed amplification is due to an instability related to the elliptic type of the equation of motion for perturbations in the Euclidean regime. The Cauchy initial value problem might not be valid for the modes with $k > k_{\rm UV}$ which are strongly affected by the Euclidean nature of the deep quantum regime.

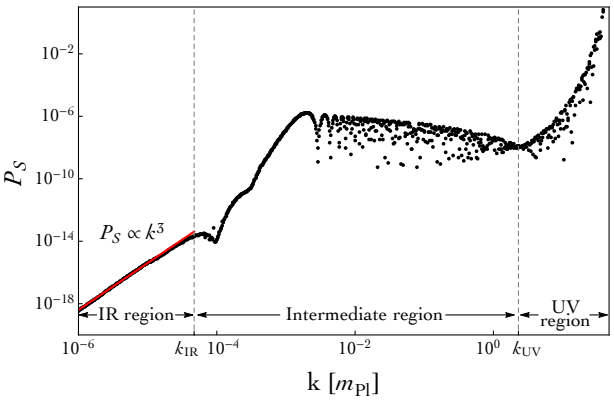

FIG. 3. Primordial power spectrum for scalar modes in the deformed algebra approach for $m = 1.2{\times}10^{-6}m_{\rm Pl}$ and the adiabatic vacuum for initial conditions in the pre-bounce (classical) contracting phase. The cosmological background is fixed such that $x_{\rm B} = 3.55 \times 10^{-6}$ and $a_{\rm B} = 1$ at the bounce.

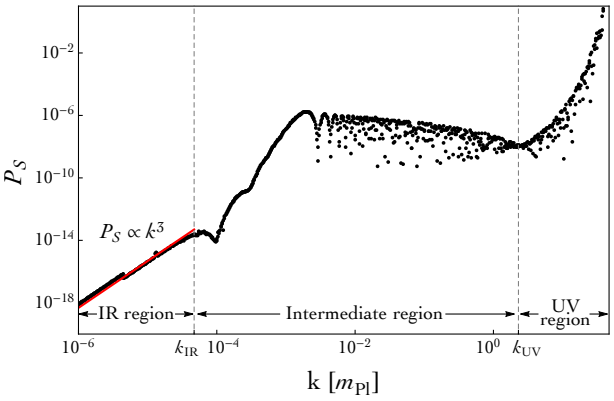

FIG. 4. Primordial power spectrum for scalar modes in the deformed algebra approach for $m = 1.2 \times 10^{-6}m_{\rm Pl}$ and the instantaneous vacuum for initial conditions in the pre-bounce (classical) contracting phase. The cosmological background is fixed such that $x_{\rm B} = 3.55 \times 10^{-6}$ and $a_{\rm B} = 1$ at the bounce.

The spectra for the adiabatic vacuum and the instantaneous vacuum choices are almost identical. The only difference is a slight enhancement in the IR region for the instantaneous vacuum-type normalization, in comparison to the adiabatic vacuum choice. This effect is due to the difference in $v'_k(\eta_{\rm init})$ for both types of initial conditions. At values of $k < k_{\rm IR}$, the shape of the spectra is mostly due to the initial super-Hubble vacuum normalization.

In this limit $k_{\rm eff} \simeq \sqrt{k^2 - \frac{z''}{z}} \approx$ const, is almost the same for every mode at this particular initial time, because $k^2 \ll \left|\frac{z''}{z}\right|$. Therefore, $\mathcal{P}_{\rm S}(k) = \frac{k^3}{2\pi^2}\frac{1}{2k_{\rm eff}z^2} \propto k^3$. The initial $\mathcal{P}_{\rm S}(k) \propto k^3$ behavior is preserved in the further evolution due to the super-Hubble nature of the modes. Only the absolute amplitude changes, which is a result of the time dependence of the z parameter.
Furthermore, it is worth stressing that at scales $k < k_{\rm UV}$ the power spectra computed in this paper qualitatively agree with those obtained in the so-called "dressed metric" approach to perturbations in LQC [36]. In that case the Ω-factor does not appear in front of the Laplace operator and the instabilities related to the Euclidean phase do not arise. Therefore, the corresponding spectrum at $k > k_{\rm UV}$ becomes nearly-scale invariant in the "dressed metric" approach, as in the standard inflationary picture.

We live the detailed associated phenomenology for a future study [37]. It is however important to stress that the spectrum derived in this article is basically in disagreement with data that are very precise for scalar modes. This rules out neither LQC in general nor the *deformed algebra* as a whole. But this shows that the set of specific hypotheses presented here is obviously in tension with measurements. Ruling out a given setting is useful for future quantum gravity investigations.

VII. DISCUSSION AND CONCLUSION

In this work, the primordial scalar power spectrum in the so-called "deformed algebra" approach to perturbations in loop quantum cosmology has been derived. Our considerations were focused on the model with a massive scalar field. The instantaneous and adiabatic vacuum-type initial conditions were imposed in the contracting phase. The non-trivial issue in the evolution of modes is their behavior in the Euclidean phase ($\Omega < 0$) surrounding the bounce. In this region, the equation of motion for the mode functions changes its type from hyperbolic to elliptic. In such a case, no preferred time direction exists. It is usually argued that a signature change implies instabilities because the oscillating time dependence '$\exp(\pm i\omega t)$' is replaced by an exponential '$\exp(\pm\omega t)$' one. The growing mode leads to an instability if initial values are chosen at some fixed t. The approach suggested in Ref. [13] precisely investigates how a boundary value problem for this kind of elliptic equations can eliminate the instability. This is, certainly, a path worth investigating. This article is devoted to the other hypothesis: considering seriously this real argument in the exponential function and investigate its physical consequences.
Even if the problem is not posed in the usual way for the partial differential equation in that case, reliable predictions can still be obtained for sufficiently low values of k in the Fourier space representation. More precisely, a characteristic scale $k_{\rm UV}$ discriminates between the modes which are amplified due to the imaginary effective wavenumber $k_{\rm eff}$ around the bounce. This is a mathematical consequence of the equation of motion in Fourier space. Of course, the physical interpretation as having or not enough "time" to oscillate and feel the quantum geometrical structure near the bounce is not possible without time. But this is not something fundamentally new or surprising in quantum cosmology/gravity. For the modes satisfying $k > k_{\rm UV}$, the elliptic nature of the equations becomes important, leading to an abnormal amplification of the power spectrum. The effect is the same as the one observed earlier in case of the tensor perturbations [11]. In turn, for $k < k_{\rm UV}$, that is for large wavelengths, the modes are not subject for a sufficiently long period to the negative effective potential, $k^2_{\rm eff} < 0$. Thus, the corresponding modes are not affected by the hyperbolic amplification, as discussed above. In the regime, $k_{\rm IR} < k < k_{\rm UV}$, a typical oscillatory behavior is observed. In the IR limit, the shape of the spectrum is determined by the initial vacuum normalization and scales as $\mathcal{P}_{\rm S}(k) \propto k^3$. This behavior is very different from the one observed in case of the tensor modes (see Ref. [33]), where the power spectrum becomes nearly-scale invariant while $k \to 0$. This is because the massive scalar field, oscillating in the contracting branch, effectively behaves as dust matter. As it is known, the freezing of massless modes during such an evolution leads to scale-invariance of the power spectrum, as for the case of tensor perturbations. For the scalar perturbations in a model with a massive scalar field the gauge-invariant degree of freedom $v_{\rm S}$ is explicitly massive leading to a breakdown of the scale-invariance.
Several points of the picture presented in this study still need to be addressed. First, the observational consequences of this calculations should be studied into the details. The key point for phenomenology is the knowledge of full duration of inflation. This is what translates coordinate wavenumbers used in this study into physical wavenumbers that can be compared with data. The number of inflationnary e-folds is in one-to-one correspondence with the value of the scalar field at the bounce which, itself, depends on the phase of the oscillations in the contracting branch. The higher the field value (and therefore the fraction of potential energy) at the bounce, the longer the inflation period and the smaller the physical scales at the bounce that are nowadays probed by astronomical observations. We leave a detailed phenomenological study for a future work, [37], but it is easy to guess from the primordial power spectrum derived in this study that the model as it is here investigated disagrees with data. It could simply be a consequence of the way modes with $k > 1$ are handled. But whatever the reason this problem should be stressed. Second, other proposals for setting initial conditions should also be considered. Here, the subtle issue of the very meaning of time in the Euclidean phase were deliberately ignored: modes were naively propagated through the Euclidean phase. A proper addressing of the well-posedness is crucial to obtain stable solutions in the $k > k_{\rm UV}$ regime (even if their

physical meaning is not clear due to the breakdown of validity of the effective equations under considerations) [38]. Furthermore, the matter content considered in this paper is no more favored by the observations of the cosmic microwave background radiation. A caraful analysis of different inflationary potentials would therefore be desirable. In particular, the Colemen-Weinberg potential with an unstable state may lead to inflationary spectra being in agreement with the up-to-date observational data. Such a change of the potential function would unavoidably affect our predictions regarding the shape of the power spectra.

ACKNOWLEDGMENTS

BB is supported by a grant from ENS Lyon. JM is supported by the Grant DEC-2014/13/D/ST2/01895 of the Polish National Centre of Science.

[1] C. Rovelli & F. Vidotto, *Covariant Loop Quantum Gravity*, Cambridge University Press (2014);
R. Gambini & J. Pullin, *A First Course in Loop Quantum Gravity*, Oxford, Oxford University Press (2011);
T. Thiemann, Lect. Notes Phys., **631**, 41 (2003);
T. Thiemann, *Modern Canonical Quantum General Relativity*, Cambridge, Cambridge University Press (2007);
C. Rovelli, *Quantum Gravity*, Cambridge, Cambridge University Press (2004);
C. Rovelli, Living Rev. Relativity, **1**, 1 (1998)

[2] A. Ashtekar and A. Barrau, arXiv:1504.07559;
A. Barrau, T. Cailleteau, J. Grain, J. Mielczarek, Class. Quantum Grav. **335**, 053001 (2014);
G. Calcagni, Annalen Phys. **525** (2013) 5, 323;
K. Banerjee, G. Calcagni, and M. Martin-Benito, SIGMA, **8**, 016 (2012);
M. Bojowald, *Quantum Cosmology*, Springer, New-York (2011);
A. Ashtekar, Gen. Rel. Grav. **41**, 707 (2009);
M. Bojowald, Living Rev. Rel. **11**, 4 (2008);
A. Ashtekar, M. Bojowald, & J. Lewandowski, Adv. Theor. Math. Phys. **7**, 233 (2003)

[3] A. Ashtekar, P. Singh, Class. Quantum Grav. **28**, 213001 (2011)

[4] J. Grain & A. Barrau, Phys. Rev. Lett. **102** 081301 (2009)

[5] J. Grain, T. Cailleteau, T. Cailleteau, & A. Gorecki, Phys. Rev. D **81** 024040 (2010)

[6] J. Mielczarek, T. Cailleteau, J. Grain, & A. Barrau, Phys. Rev. D **81** 104049 (2010)

[7] J. Grain, A. Barrau, T. Cailleteau, & J. Mielczarek, Phys. Rev. D **82** 123520 (2010)

[8] A. Barrau, M. Bojowald, G. Calcagni, J. Grain & M. Kagan, JCAP **1505** (2015) 05, 051

[9] M. Bojowald & G. M. Paily, Deformed General Relativity, Phys. Rev. D **87** 044044 (2013)

[10] T. Cailleteau, J. Mielczarek, A. Barrau & J. Grain, Class. Quantum Grav. 29 095010 (2012)

[11] L. Linsefors, T. Cailleteau, A. Barrau, & J. Grain, Phys. Rev. D **87** 107503 (2013)

[12] J. Mielczarek, L. Linsefors & A. Barrau, arXiv:1411.0272

[13] M. Bojowald & J. Mielczarek, JCAP **1508** (2015) 08, 052

[14] I. Agullo, A. Ashtekar, & W. Nelson, Class. Quantum Grav. **30**, 085014 (2013);
I. Agullo, A. Ashtekar, & W. Nelson, Phys. Rev. D **87**, 043507 (2013);
I. Agullo, A. Ashtekar, & W. Nelson, Phys. Rev. Lett. **109**, 251301 (2012)

[15] A. Ashtekar, W. Kaminski, & J. Lewandowski, Phys. Rev. D **79** 064030 (2009)

[16] H. Nicolai, K. Peeters & M. Zamaklar, Class. Quantum Grav. **22** R193 (2005)

[17] M. Bojowald, G. M. Hossain, M. Kagan & S. Shankaranarayanan, Phys. Rev. D **78** 063547 (2008)

[18] M. Bojowald, G. M. Hossain, M. Kagan & S. Shankaranarayanan, Phys. Rev. D **79** 043505 (2009)

[19] M. Bojowald & G. M. Hossain, Class. Quantum Grav. **24** 4801 (2007)

[20] M. Bojowald & G. M. Hossain, Phys. Rev. D **77** 023508 (2008)

[21] M. Bojowald & and G. Calcagni, JCAP 1103 032 (2011)

[22] M. Bojowald, G. Calcagni & S. Tsujikawa, JCAP 111 046 (2011)

[23] J. Mielczarek, T. Cailleteau, A. Barrau & J. Grain, Class. Quantum Grav. 29 085009 (2012)

[24] T. Cailleteau, L. Linsefors & A. Barrau Class. Quantum Grav. 31 125011 (2014)

[25] T. Cailleteau, A. Barrau, J. Grain, & F. Vidotto, Phys. Rev. D **86** 087301 (2012)

[26] E. Wilson-Ewing, Class. Quantum Grav. 29 085005 (2012)

[27] L.Z. Fang & R. Ruffini (ed.), *Quantum Cosmology*, World Scientific, 1987

[28] J.B. Hartle & S.W. Hawking, Phys. Rev. D **28**, 12, 2960 (1983)

[29] J. Mielczarek, Europhys. Lett. 108 4, 40003 (2014)

[30] A. Ashtekar, T. Pawlowski & P. Singh, Phys. Rev. D **74**, 084003 (2006)

[31] Planck Collaboration, arXiv:1502.01589 [astro-ph.CO]

[32] P. Singh, K. Vandersloot & G. V. Vereshchagin, Phys. Rev. D **74**, 043510 (2006)

[33] B. Bolliet, J. Grain, C. Stahl & A. Barrau, Phys. Rev. D **91** 084035 (2012)

[34] L. Linsefors & A. Barrau, arXiv:1301.1264v2 [gr-qc]

[35] V. F. Mukhanov & S. Winitzki, *Introduction to Quantum Effects in Gravity*, Cambridge University Press (2012);
S. A. Fulling, *Aspects of Quantum Field Theory in Curved Space-Time*, Cambridge Universtiy Press (1989);

[36] I. Agullo and N. A. Morris, arXiv:1509.05693 [gr-qc]

[37] B. Bolliet *et al.*, in preparation

[38] J. Mielczarek *et al.*, in preparation

Observational Exclusion of a Consistent Quantum Cosmology Scenario

Boris Bolliet,[1,*] Aurélien Barrau,[1] Julien Grain,[2,3] and Susanne Schander[1]

[1] *Laboratoire de Physique Subatomique et de Cosmologie, Université Grenoble-Alpes, CNRS/IN2P3 53, avenue des Martyrs, 38026 Grenoble cedex, France*

[2] *CNRS, Institut d'Astrophysique Spatiale, UMR8617, Orsay, France, F-91405*

[3] *Université Paris-Sud 11, Orsay, France, F-91405*

(Dated: November 3, 2015)

It is often argued that inflation erases all the information about what took place before it started. Quantum gravity, relevant in the Planck era, seems therefore mostly impossible to probe with cosmological observations. In general, only very *ad hoc* scenarios or hyper fine-tuned initial conditions can lead to observationally testable theories. Here we consider a well-defined and well motivated candidate quantum cosmology model that predicts inflation. Using the most recent observational constraints on the cosmic microwave background B modes, we show that the model is excluded for all its parameter space, without any tuning. Some important consequences are drawn for the *deformed algebra approach* to loop quantum cosmology. We emphasize that neither loop quantum cosmology in general nor loop quantum gravity are disfavored by this study but their falsifiability is established.

Introduction.—This Letter aims at giving a concrete example of a fully consistent quantum cosmology scenario with general relativity (GR) as its low-energy limit and leading to a standard phase of inflationary expansion of the Universe that is excluded by current experimental data. Although the considered model belongs to the loop quantum cosmology (LQC) framework, we emphasize from the beginning that the claim is not that loop quantum gravity (LQG) or LQC is excluded. The other way round: the fact that some specific settings within LQC are excluded demonstrates that the theory can fill the bridge between calculations and observations, which makes it an especially appealing quantum gravity proposal.

LQG is a non-perturbative background-independent quantization of GR [1–9] that relies on the Ashtekar variables, an SU(2)-valued connection and its conjugate densitized triads. The quantization is performed over the holonomies of the connections and the fluxes of the densitized triads. Important questions, in particular regarding the continuum limit of LQG, remain opened but important progresses have been achieved recently, see *e.g.* [10, 11].

LQC is a symmetry reduced version of LQG using cosmological symmetries. In LQC, the big bang is replaced by a big bounce due to repulsive quantum gravity effects close to the Planck density [12–22]. It is however important to underline that LQC has not yet been rigorously derived from LQG and remains an attempt to use LQG-like methods in the cosmological sector.

Although there is a general agreement on the background dynamics in LQC (modulo some issues on the best motivated initial conditions), there are different ways to implement LQG ideas at the level of cosmological perturbations. The most popular models are the *dressed metric approach*, the *hybrid quantization approach* and the *deformed algebra approach*. The *dressed metric* hypothesis [23–25] accounts for quantum fields propagating on a quantum background but lacks a proof of consistency taking into account the subtle gauge issues in gravity [10, 11]. The *hybrid quantization* formalism [26] nicely takes backreaction effects into account, but remains at a very early stage of development. In this work we focus on the *deformed algebra approach* [27] which is probably the most developed one and has generated a very large number of articles (see *e.g.* [28] and references therein).

The deformed algebra approach.—The fact that holonomies of the connections are the basic LQG variables can be accounted for, at the effective level, by the *standard holonomy correction* in the Hamiltonian constraint which consists in replacing the mean Ashtekar connection by a pseudo periodic function depending on the coordinate size of a loop (see *e.g.* [29–31] for seminal articles). The crucial point of the *deformed algebra approach* is to ensure that the resulting Poisson algebra remains consistent, so that Poisson brackets between quantum corrected constraints are proportional to a quantum corrected constraint. This algebraic structure has been derived for vector modes [32], scalar modes [33] and shown to be consistent for tensor modes [34]. Although requiring quite a lot of algebra, the main result is surprisingly simple and impressive in the way that there exists a *unique* solution to the anomaly freedom problem, which is far from being trivial. Furthermore, this procedure determines the lattice refinement scheme to be precisely the desired one, that is the so-called $\bar{\mu}$-scheme [35]. The resulting *anomaly free* algebra reads

$$\begin{aligned} \{D[M^a], D[N^a]\} &= D[M^b\partial_b N^a - N^b\partial_b M^a], \\ \{D[M^a], S[N]\} &= S[M^a\partial_b N - N\partial_a M^a], \\ \{S[M], S[N]\} &= \Omega D\left[q^{ab}(M\partial_b N - N\partial_b M)\right], \end{aligned} \tag{1}$$

where $N^a(M^a)$ and $N(M)$ are the shift and lapse functions, q^{ab} is the spatial metric, D and S are the holonomy-corrected diffeomorphism and hamiltonian

constraints, and $\Omega \equiv 1 - 2\rho/\rho_{\rm B}$ with ρ the density of the universe and $\rho_{\rm B}$ the critical density (close to the Planck density) which encodes deviations from standard GR. The algebra is elegant and simple. Furthermore it leads to a signature change close to the bounce which is somehow reminiscent of the Hartle-Hawking proposal [36]. When $\rho < (\rho_{\rm B}/2)$ the spacetime geometry is Lorentzian, but when $\rho > (\rho_{\rm B}/2)$, in the vicinity of the bounce, Ω becomes negative and the spacetime geometry becomes Euclidean. Strikingly, this effect has been found independently, still in LQC, in [37] and [38], the latter approach relying on a different approach based on "patches of universe" evolving independently in the longitudinal gauge.

Model and assumptions.—Here, we shall investigate the observational consequences of this effective signature change for cosmological perturbations near the big bounce, under some basic hypotheses: (i) we assume the universe to be filled with a massive scalar field, that is with a potential $V(\phi) = m^2\phi^2/2$, (ii) we restrict ourselves to spatially flat Friedmann-Lemaitre-Robertson-Walker cosmologies, (iii) we assume that initial conditions should be set in the remote past of the classical contracting branch of the universe for both the background and the perturbations, as expected from a truly causal evolution, (iv) we assume that initially the quantum field describing the metric perturbations is in the Minkowski vacuum state, which is well defined and non-ambiguous, (v) as argued in [23–25], we assume that the calculated perturbation power spectra make sense up to arbitrary small scales as long as the energy of the perturbations remains small when compared to the energy of the background, (vi) we do not consider backreaction effects. Each of these hypotheses can obviously be questioned. However, quite obviously too, each of them constitutes the most "natural", usual, and simple choice.

The metric perturbations are evolved from their initial vacuum state, in the contracting universe, toward some specific state, in the expanding branch, that can be computed numerically, allowing one to obtain the primordial power spectrum used as an input for cosmic microwave background (CMB) phenomenology.

The primordial tensor and scalar power spectra were derived in [39] and [40] respectively. Here, we focus on tensor modes that are better controlled (and are enough for our conclusion). The key point for phenomenology that we shall now investigate into more details is the duration of inflation since it allows one to convert the comoving wavenumbers, used in these studies, into physical scales probed by CMB experiments. Although, as demonstrated in [41], there exists a highly favored number of e-folds of inflation in this model, $N_{\rm tot} \simeq 140$, associated with a value of the scalar field at the bounce of about $\phi_{\rm B} \simeq 2.6\, m_{\rm Pl}$ with $m_{\rm Pl} \equiv 1/\sqrt{G}$, the conclusion we shall reach in the following remains true even for fine-tuned initial background conditions leading to a higher or smaller number of e-folds.

Observational constraints.—For CMB phenomenology, the scales of interest range between $k_{\rm min} = 10^{-6}\,{\rm Mpc}^{-1}$ and $k_{\rm max} = 1\,{\rm Mpc}^{-1}$. This range is referred to as the *observable window* of wavenumbers. The energy density at the bounce is associated to a wavenumber

$$k_{\rm B} \equiv a_{\rm B}\sqrt{\rho_{\rm B}}M_{\rm Pl}^{-1}, \tag{2}$$

where $\rho_{\rm B}$ has dimensions of $M_{\rm Pl}^4$, where this time $M_{\rm Pl} \equiv m_{\rm Pl}/\sqrt{8\pi}$ denotes the reduced Planck mass. The evolution of the amplitude of the fluctuations in the early universe depends on their size when compared to the horizon size (weighted by the Ω factor). Horizon-crossing is defined as the time when the wavelength of the considered perturbation equals the Hubble horizon. In particular, for the pivot scale $k_\star$, used to parametrize the primordial power spectra, this reads $k_\star = a_\star H_\star$, where $a_\star$ and $H_\star$ are the scale factor and the Hubble parameter at horizon-crossing during inflation. Clearly, possible footprints of LQC effects in the angular power spectrum of CMB anisotropies depend on the relative values of $k_\star$ and $k_{\rm B}$. This motivates the definition of a dimensionless function:

$$n(\rho_{\rm B}, \phi_{\rm B}) \equiv \ln(k_\star/k_{\rm B}). \tag{3}$$

The dependence upon the value of the scalar field at the bounce, $\phi_{\rm B}$, will appear explicitly in the following.

As shown in Fig. 1, the main characteristics of the spectrum we are considering in this study are [39]: (i) scale invariance for the infrared (IR) scales, *i.e.* $k \ll k_{\rm B}$, (ii) oscillations for the intermediate scales, *i.e.* $k \sim k_{\rm B}$, and (iii) an exponential growth for the ultraviolet (UV) scales, *i.e.* $k \gg k_{\rm B}$.

Let us now describe in more details how the scales affected by LQC effects compare to the present *observable window* of wavenumbers. The condition $k_{\rm B} \sim k_{\rm max}$ reads $n(\rho_{\rm B}, \phi_{\rm B}) \simeq -6.2$ when $k_{\rm max}$ is replaced with the numerical value given above. Our first goal is to analyze how such a condition can be fulfilled depending on the values of $\rho_{\rm B}$ and $\phi_{\rm B}$. Expanding the ratio $(k_\star/k_{\rm B})$ over the cosmic history, from the bounce until horizon-crossing, one gets

$$n(\rho_{\rm B}, \phi_{\rm B}) = N_{\rm tot} - N_\star + N_{\rm B} + \tfrac{1}{2}\ln(V_\star/3\rho_{\rm B}), \tag{4}$$

where $V_\star$ is the potential energy of the scalar field at horizon-crossing, $N_{\rm B}$ is the number of e-folds between the bounce and the start of inflation, $N_{\rm tot}$ is the total number of e-folds of the inflationary phase, and $N_\star$ is the number of e-folds of observable inflation, *i.e.* from horizon-crossing until the end of inflation. This number can in turn be calculated in terms of quantities related to the post-inflationary evolution of the universe as [42, 43]

$$\begin{aligned} N_\star = &-\ln(k_\star/k_0) + \tfrac{1}{4}\ln(\Omega_\gamma M_{\rm pl}^2/3H_0^2) - \tfrac{1}{12}\ln g_{\rm th} \\ &+ \tfrac{1}{12}\ln(\rho_{\rm th}/\rho_{\rm end}) + \tfrac{1}{2}\ln(V_\star/\sqrt{\rho_{\rm end}}M_{\rm pl}^2). \end{aligned} \tag{5}$$

In this formula, some parameters are known: $k_0 \equiv H_0/c$ with $H_0 = (67.31 \pm 0.96)\,\mathrm{km \cdot s^{-1} \cdot Mpc^{-1}}$, the pivot scale is $k_\star = 0.002\,\mathrm{Mpc}^{-1}$ by convention and the present radiation density of the universe is $\Omega_\gamma = 5.45 \times 10^{-5}$. Moreover one can safely assume $g_{\rm th} \sim 10^3$, accounting for the creation of new degrees of freedom during reheating. There remains three unknowns: (i) the potential energy at horizon-crossing, $V_\star = \frac{3}{2}\pi^2 A_{\rm s} r_\star M_{\rm Pl}^4$, for which there exists an upper bound due to observational constraints on both the amplitude of the scalar primordial power spectrum, $A_{\rm s}$, and the tensor-to-scalar ratio, $r_\star$, (ii) the energy scale of reheating, $\rho_{\rm th}$, (iii) the energy density at the end of inflation, $\rho_{\rm end}$, which should lie between $\rho_{\rm th}$ and $V_\star$, and can be expressed as $\rho_{\rm end} \simeq m^2 M_{\rm Pl}^2$ for a massive scalar field. However, as discussed in [44], most reasonable assumptions (if not all) over the different energy scales lead to take $N_\star$ between 50 and 60. We chose $N_\star = 60$ in the following to illustrate the procedure (the other extreme choice would not change the conclusion nor the following numerical estimates by more than ten percents). This sets all the unknowns since m can directly be expressed in terms of $N_\star$, leading to $m \simeq 1.2 \times 10^{-6}\, m_{\rm Pl}$ for $N_\star = 60$. The value of the mass can receive small LQC corrections [45] that play no role in our conclusion. Furthermore, now looking at (4) and using the analytical results of [46] one finds $N_{\rm B} = \frac{1}{3}\ln\Gamma$, where $\Gamma \equiv \sqrt{3\rho_{\rm B}}/(mM_{\rm Pl})$, and $N_{\rm tot} = \frac{1}{4}(\phi_{\rm i}/M_{\rm Pl})^2 - \frac{1}{2}$, with

$$\phi_{\rm i} = \phi_{\rm B} + \sqrt{\tfrac{2}{3}}\mathrm{Arcsinh}(\Gamma\sqrt{2/\mathrm{W}\,(z)}) \qquad (6)$$

the scalar field at the start of slow-roll inflation, where the argument of the Lambert W-function is

$$z \equiv 8\Gamma^2 \exp(\sqrt{6}\phi_{\rm B}/M_{\rm Pl}). \qquad (7)$$

Results.—In LQC, the critical energy density, $\rho_{\rm B}$, is related to the fundamental parameter of LQG, γ, the Barbero-Immirzi parameter, as $\rho_{\rm B} = 2\sqrt{3}M_{\rm Pl}^4/\gamma^3$ [25] (we do not, here, go into the subtlety of the area gap definition [47]). The standard value, $\gamma = 0.2375$, sets $\rho_{\rm B}$ to $0.41\, m_{\rm Pl}^4$. In fact, within the slow-roll approximation and for a massive scalar field, all quantities in (4) and (5) can be expressed in terms of $\phi_{\rm B}$, once $N_\star$ has been fixed. It is then easy to obtain the value $\phi_{\rm B}^+$ such that $n(\rho_{\rm B}, \phi_{\rm B}^+) = -6.2$. With the previous numerical values we find $\phi_{\rm B}^+ \simeq 1.1\, m_{\rm Pl}$ corresponding to $k_{\rm B} = 1\,\mathrm{Mpc}^{-1}$. This is far below the favored value of the scalar field at the bounce, $\phi_{\rm B} \simeq 2.6\, m_{\rm Pl}$, which leads to a physical wavenumber $k_{\rm B}$ much smaller than $k_\star$. More precisely, the favored value of the field leads to $k_{\rm B} \simeq 10^{-37} k_\star$. In other words, the scales of the primordial power spectrum that are probed by present measurements of the CMB anisotropies correspond to scales that were at the bounce much smaller than the characteristic scale of the bounce. This corresponds to the deep UV regime of the primordial power spectra presented in Fig. 1 [39, 41, 46], that is the one clearly excluded by data: the exponential growth of the amplitude of the power spectrum at these scales is ruled out by the CMB upper bound on B-modes ($r_{0.002} < 0.114$). Obviously, backreaction should be taken into account for a detailed prediction, but the general trend, that is perturbations becoming huge due to the real exponential factor associated with the change of signature of the metric, will anyway contradict the stringent upper bound coming from current observations.

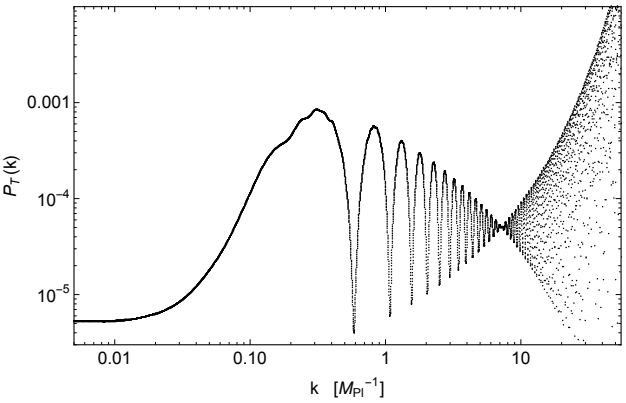

FIG. 1. Tensor primordial power spectrum predicted by the *deformed algebra approach* to cosmological perturbation in loop quantum cosmology. The data points were obtained from a numerical simulation (with mass $m = 1.2 \times 10^{-3}\, m_{\rm Pl}$ to improve the numerical stability on the exponential part).

With the natural measure defined in [41], the probability to escape this exclusion by having $k_{\rm max} < k_{\rm B}$, that is $\phi_{\rm B} < \phi_{\rm B}^+$ with $\phi_{\rm B}^+ \simeq 1.1\, m_{\rm Pl}$, is less than 10^{-8}. One could still focus on this specific case ($\phi_{\rm B} < \phi_{\rm B}^+$) by fine-tuning initial conditions for the background to this aim. (This is what is usually done in phenomenological studies of the *dressed metric approach* [48], requiring in addition $\phi_{\rm B} > 0.8\, m_{\rm Pl}$ so that the *observable window* falls just on the interesting part of the spectrum.) The key point we want to underline is that such a fine-tunning would not save the model. The *observable window* can fall in the "low k" part of the spectrum only if there is less inflation. The duration of inflation would need to be very close to its minimal value, $N_{\rm tot} \simeq 60$. However, a detailed numerical study shows that to achieve such a small amount of inflation the universe must go through a long phase of *deflation* (exponential decrease of the scale factor) before the bounce. This has a direct consequence on the primordial power spectrum: due to the specific dynamics of deflation, the nearly scale-invariant IR part of the spectrum is drastically amplified. Indeed, the equation of propagation in conformal time for a tensor mode v_k during deflation reduces to

$$v_k'' + (k^2 - 2\mathcal{H}^2)v_k = 0, \qquad (8)$$

where $\mathcal{H}$ is the conformal Hubble parameter. This equa-

tion is clearly unstable for the IR modes with $k < \sqrt{2}\mathcal{H}$. So even if the shape of the portion of the spectrum which would be observable is correct, its normalization would exceed the observational upper bound by orders of magnitude and the model would remain excluded. This has been numerically checked in details [49].

Finally, it is important to mention that, even if the exponential growth of the spectrum is arbitrarily removed, and initial conditions chosen so that the *observable window* falls exactly on the oscillatory part of the spectrum, the model would anyway hardly lead to a specific observational signature. This can be concluded from Fig. 2 where the CMB $C_\ell^{\rm BB}$ were explicitly calculated. The specific oscillatory behavior predicted for the primordial tensor power spectrum in LQC, which is the key prediction here, is smeared out by the cosmic evolution. The LQC spectrum would remain mostly undistinguishable from the standard prediction (GR) due to the cosmic variance.

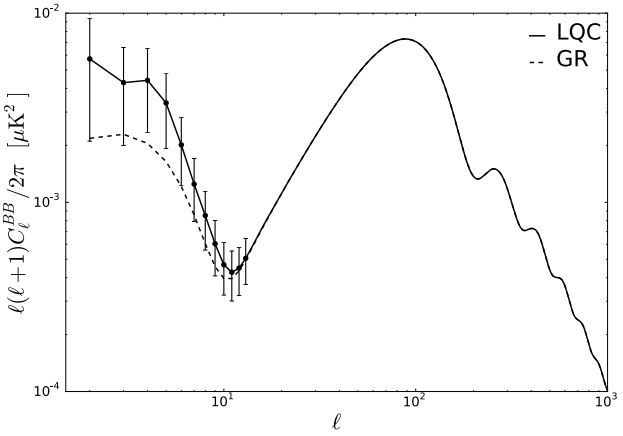

FIG. 2. Cosmic Microwave Background B modes angular power spectra (wihtout lensing) obtained with CLASS [50], using the best fit parameters for TT+LowP+Lensing in Table 4 of [51], for the primordial spectrum obtained in the *deformed algebra approach* with the exponential rise arbitrary removed and replaced by the red-tilted spectrum as predicted in standard inflation with $k_\star = 0.002\,\mathrm{Mpc}^{-1}$, $A_{\rm s} = 2.139 \times 10^{-9}$ and $r_{002} = 0.114$. The signal expected in standard general relativity corresponds to the dashed line. The error bars, shown for the first twelve multipoles, correspond to the cosmic variance. The specific oscillations in the primordial power spectrum are clearly washed out.

Discussion and conclusion.—There has recently been a number of new results on primordial perturbations within the *dressed metric approach* [45, 52, 53]. The associated primordial power spectra were compared to those from the *deformed algebra approach* in [46]. They share the same features in the IR regime (a slightly red-tilted spectrum) and at intermediate scales (oscillatory behavior), but their UV regimes are very different as there is no exponential amplification in the *dressed metric approach*. It is also worth emphasizing that the authors of the latter approach usually set initial conditions at the bounce, therefore avoiding by construction the effects of *deflation*.

Our main conclusion is that although the quantum cosmology model that is considered in this work is well-defined, well-motivated, has the standard Friedmann equation as its low-density limit and, even more importantly, leads to the required amount of inflation, it is excluded by current data. This illustrates with a concrete example that the usual statement claiming that "whatever happens before inflation cannot be probed" is incorrect. Cosmological tests of quantum gravity are now possible, even with mainstream models without any tuning of the parameters. However it is important to underline that only a very specific version of LQC is excluded: a universe filled with a massive scalar field, treated in the *deformed algebra approach*, with initial conditions set in the remote past before the bounce, no backreation, no anisotropies and no cutoff scale. This is, in itself, a substantial result to establish loop quantum cosmology as a predictive theory.

The work of B.B. was supported by a grant from ENS Lyon.

* Corresponding author: boris.bolliet@lpsc.in2p3.fr

[1] C. Rovelli and F. Vidotto, *Covariant Loop Quantum Gravity* (Cambridge Univ. Press, Cambridge, 2014).
[2] R. Gambini and J. Pullin, *A First Course in Loop Quantum Gravity* (Oxford Univ. Press, Oxford, 2011).
[3] C. Rovelli, *3rd Quantum Geometry and Quantum Gravity School*, PoS **QGQGS2011**, 003 (2011), arXiv:1102.3660 [gr-qc].
[4] P. Dona and S. Speziale, in *Gravitation Theorie et Experience. Troisime ecole de physique theorique de Jijel* (2013) pp. 89–140, arXiv:1007.0402 [gr-qc].
[5] T. Thiemann, in *271st WE-Heraeus Seminar on Aspects of Quantum Gravity: From Theory to Experiment Search Bad Honnef, Germany, February 25-March 1, 2002*, Vol. 631 (2003) pp. 41–135, arXiv:gr-qc/0210094 [gr-qc].
[6] T. Thiemann, *Modern canonical quantum general relativity*, Cambridge monographs on mathematical physics (Cambridge Univ. Press, Cambridge, 2007).
[7] C. Rovelli, *Quantum Gravity* (Cambridge Univ. Press, Cambridge, 2007).
[8] L. Smolin, in *3rd International Symposium on Quantum theory and symmetries (QTS3)* (2004) pp. 655–682, [Submitted to: Rev. Mod. Phys.(2004)], arXiv:hep-th/0408048 [hep-th].
[9] A. Perez, in *2nd International Conference on Fundamental Interactions (ICFI 2004) Domingos Martins, Espirito Santo, Brazil, June 6-12, 2004* (2004) arXiv:gr-

qc/0409061 [gr-qc].
[10] J. W. Barrett, R. J. Dowdall, W. J. Fairbairn, F. Hellmann, and R. Pereira, Class. Quant. Grav. **27**, 165009 (2010), arXiv:0907.2440 [gr-qc].
[11] M. Han, Phys. Rev. D **88**, 044051 (2013).
[12] A. Ashtekar and A. Barrau, (2015), arXiv:1504.07559 [gr-qc].
[13] A. Barrau, T. Cailleteau, J. Grain, and J. Mielczarek, Class. Quant. Grav. **31**, 053001 (2014), arXiv:1309.6896 [gr-qc].
[14] A. Barrau and J. Grain, (2014), arXiv:1410.1714 [gr-qc].
[15] I. Agullo and A. Corichi, (2013), arXiv:1302.3833 [gr-qc].
[16] G. Calcagni, Annalen Phys. **525**, 323 (2013), [Erratum: Annalen Phys.525,no.10-11,A165(2013)], arXiv:1209.0473 [gr-qc].
[17] M. Bojowald, Class. Quant. Grav. **29**, 213001 (2012), arXiv:1209.3403 [gr-qc].
[18] K. Banerjee, G. Calcagni, and M. Martin-Benito, SIGMA **8**, 016 (2012), arXiv:1109.6801 [gr-qc].
[19] A. Ashtekar and P. Singh, Class. Quant. Grav. **28**, 213001 (2011), arXiv:1108.0893 [gr-qc].
[20] M. Bojowald, Living Reviews in Relativity **11** (2008), 10.12942/lrr-2008-4.
[21] A. Ashtekar, Gen. Rel. Grav. **41**, 707 (2009), arXiv:0812.0177 [gr-qc].
[22] A. Ashtekar, M. Bojowald, and J. Lewandowski, Adv. Theor. Math. Phys. **7**, 233 (2003), arXiv:gr-qc/0304074 [gr-qc].
[23] I. Agullo, A. Ashtekar, and W. Nelson, Class.Quant.Grav. **30**, 085014 (2013), arXiv:1302.0254 [gr-qc].
[24] I. Agullo, A. Ashtekar, and W. Nelson, Phys. Rev. Lett. **109**, 251301 (2012), arXiv:1209.1609 [gr-qc].
[25] I. Agullo, A. Ashtekar, and W. Nelson, Phys. Rev. **D87**, 043507 (2013), arXiv:1211.1354 [gr-qc].
[26] L. C. Gomar, M. Martn-Benito, and G. A. M. Marugn, JCAP **1506**, 045 (2015), arXiv:1503.03907 [gr-qc].
[27] A. Barrau, M. Bojowald, G. Calcagni, J. Grain, and M. Kagan, JCAP **1505**, 051 (2015), arXiv:1404.1018 [gr-qc].
[28] M. Bojowald and G. M. Paily, Phys. Rev. **D86**, 104018 (2012), arXiv:1112.1899 [gr-qc].
[29] M. Bojowald, G. M. Hossain, M. Kagan, and S. Shankaranarayanan, Phys. Rev. D **82**, 109903 (2010).
[30] M. Bojowald and G. M. Hossain, Phys. Rev. D **77**, 023508 (2008).
[31] M. Bojowald, M. Kagan, P. Singh, H. H. Hernández, and A. Skirzewski, Phys. Rev. D **74**, 123512 (2006).
[32] J. Mielczarek, T. Cailleteau, A. Barrau, and J. Grain, Class. Quant. Grav. **29**, 085009 (2012), arXiv:1106.3744 [gr-qc].
[33] T. Cailleteau, J. Mielczarek, A. Barrau, and J. Grain, Class. Quant. Grav. **29**, 095010 (2012), arXiv:1111.3535 [gr-qc].
[34] T. Cailleteau, A. Barrau, J. Grain, and F. Vidotto, Phys. Rev. **D86**, 087301 (2012), arXiv:1206.6736 [gr-qc].
[35] A. Ashtekar, T. Pawlowski, and P. Singh, Phys. Rev. **D74**, 084003 (2006), arXiv:gr-qc/0607039 [gr-qc].
[36] J. B. Hartle and S. W. Hawking, Phys. Rev. D **28**, 2960 (1983).
[37] M. Bojowald and G. M. Paily, Phys. Rev. **D86**, 104018 (2012), arXiv:1112.1899 [gr-qc].
[38] E. Wilson-Ewing, Class. Quant. Grav. **29**, 215013 (2012), arXiv:1205.3370 [gr-qc].
[39] L. Linsefors, T. Cailleteau, A. Barrau, and J. Grain, Phys. Rev. **D87**, 107503 (2013), arXiv:1212.2852 [gr-qc].
[40] S. Schander, A. Barrau, B. Bolliet, L. Linsefors, and J. Grain, (2015), arXiv:1508.06786 [gr-qc].
[41] L. Linsefors and A. Barrau, Phys. Rev. **D87**, 123509 (2013), arXiv:1301.1264 [gr-qc].
[42] A. R. Liddle and D. H. Lyth, Phys.Rept. **231**, 1 (1993), arXiv:astro-ph/9303019 [astro-ph].
[43] P. Ade *et al.* (Planck), (2015), arXiv:1502.02114 [astro-ph.CO].
[44] A. R. Liddle and S. M. Leach, Phys. Rev. **D68**, 103503 (2003), arXiv:astro-ph/0305263 [astro-ph].
[45] I. Agullo and N. A. Morris, (2015), arXiv:1509.05693 [gr-qc].
[46] B. Bolliet, J. Grain, C. Stahl, L. Linsefors, and A. Barrau, Phys.Rev. **D91**, 084035 (2015), arXiv:1502.02431 [gr-qc].
[47] A. Ashtekar, B. Bonga, and A. Kesavan, Phys. Rev. **D92**, 044011 (2015), arXiv:1506.06152 [gr-qc].
[48] A. Ashtekar and D. Sloan, Gen. Rel. Grav. **43**, 3619 (2011), arXiv:1103.2475 [gr-qc].
[49] For initial conditions such that $N_{\rm tot} \simeq 60$ (corresponding to $\phi_{\rm B} \simeq 5\, M_{\rm Pl}$) the excess in the amplitude of the primordial tensor modes is about fourteen orders of magnitudes higher than the observational upper bound given by the tensor-to-scalar ratio.
[50] D. Blas, J. Lesgourgues, and T. Tram, JCAP **7**, 034 (2011), arXiv:1104.2933.
[51] P. A. R. Ade *et al.* (Planck), (2015), arXiv:1502.01589 [astro-ph.CO].
[52] B. Bonga and B. Gupt, (2015), arXiv:1510.00680 [gr-qc].
[53] A. Ashtekar and B. Gupt, (2015), arXiv:1509.08899 [gr-qc].

Some Conceptual Issues in Loop Quantum Cosmology

Aurélien Barrau* and Boris Bolliet†[1]

[1] *Laboratoire de Physique Subatomique et de Cosmologie, Université Grenoble-Alpes, CNRS/IN2P3 53, avenue des Martyrs, 38026 Grenoble cedex, France*

Loop quantum gravity is a mature theory. To proceed to explicit calculations in cosmology, it is necessary to make assumptions and simplifications based on the symmetries of the cosmological setting. Symmetry reduction is especially critical when dealing with cosmological perturbations. The present article reviews several approaches to the problem of building a consistent formalism that describes the dynamics of perturbations on a quantum spacetime and tries to address their respective strengths and weaknesses. We also review the main open issues in loop quantum cosmology.

GENERAL CONSIDERATIONS

In the strong curvature regime of general relativity (GR), quantum gravity should manifest itself as a resulting repulsive force. In cosmology, the total energy density of the universe is expected not to diverge and to remain smaller than an upper bound that can be guessed to be of the order of $\rho_{\rm max} \simeq m_{\rm Pl}^4$. The big bang singularity has to be reconsidered. Loop quantum gravity (LQG) suggests that the big bang is replaced by a bounce [1]. The resolution of the initial singularity is achieved in the sense that the operators corresponding to a complete family of Dirac observables, such as matter density, curvature invariant and anisotropic shears, all remain bounded in the physical Hilbert space. Then, the Hamiltonian constraint can in principle be solved, numerically if not exactly. The usual quantization procedure is the so called $\bar{\mu}$-scheme, which was proven to be exempt of infrared divergences. It uses the physical metric and, *e.g.*, a massless scalar field for modeling the energy content of the quantum Universe. The scalar field is also used as an internal time. The relationship between the quantum states, χ, and the classical geometrical data [2] , *i.e.* the metric tensor, has been formulated within two different approaches: (i) in the embedding approach the quantum phase space is embedded into a classical phase space, (ii) in the truncation approach one computes corrections to the classical dynamics by truncating the quantum phase space to low orders of moments only [3].

Note that the Wheeler-deWitt (WDW) theory is based on a continuous geometry, while in loop quantum cosmology (LQC) the quantum geometry is essentially discrete. Hence, the WDW theory is recovered at small spacetime curvature, but in general not for $\lambda \to 0$, where λ is the discreteness parameter. Actually, the continuous limit of LQC does not yield a physical theory [4].

*barrau@lpsc.in2p3.fr
†bolliet@lpsc.in2p3.fr

A first conceptual issue arises as it has been argued that given the current lack of control on higher-curvature corrections and dynamical inhomogeneities in LQC, evidence for a bounce at high density is, at present, only circumstantial [5]. Indeed, most studies are assuming Gaussian states or other specific forms of coherent or semi-classical wave functions. This is questionable in the high-density regime. Since strong quantum backreaction and higher-curvature terms (in addition to those coming from holonomies) are implicitly ignored by choosing a coherent state, it is not *a priori* fully guaranteed that all evidences for the existence of a bounce are reliable in loop quantum cosmology – setting aside the issue of signature change that we will review later.

We shall now address this objection and show why the bounce is a reliable and generic consequence of LQC. Most numerical studies have indeed focused on gaussian wave packets. These are parametrized by a volume at which the initial state is peaked, v^*, as well as its spread σ_v and the initial scalar field momentum, p_{φ_0}. Three subclasses were investigated numerically [6]: (i) WDW initial states, (ii) gaussians in volume and (iii) rotated WDW states. Recently, non sharply peaked states as well as non gaussian states were also considered [7]. A numerical scheme called CHIMERA [8] is being developed since 2013 at Louisiana State University in order to investigate the robustness of predictions in effective LQC. Presently, these numerical simulations all seem to confirm the robustness of the singularity resolution which was proven analytically for arbitrary states [9]. Moreover, further analytical studies showed that fluctuations around any given state are in tight control around the bounce [10–12].

The introduction of positive spatial curvature (spherical models) was dealt with in 2006 [13] and extended shortly after [14]. Since closed models also retain the classical recollapse predicted by GR, one is led to a cyclic cosmological scenario. The status of hyperbolic models ($k = -1$) is less clear but has also been mostly consistently addressed [15]. In addition, the robustness of the singularity resolution has also been checked for a negative [16] and a positive cosmological constant [17].

Ambiguities related to the quantization procedure for closed anisotropic LQC models were addressed [18]: in LQC there is a freedom in choosing between closed holonomies around loops (loop quantization) to define curvature, or open holonomies to define connection. For anisotropic models with non-trivial spatial curvature, loop quantization is not possible, while for the isotropic spherical FLRW model both quantizations schemes are available but are not equivalent. We refer the reader to the excellent recent review [19] (and references therein) for more details about anisotropic models and a clear introduction to the whole framework.

The effective equations derived in LQC and applied to the FLRW universe have already led to a large amount of phenomenological studies, making LQC one of the rare quantum gravity model that can be constrained by observations.

Measurements of the cosmic microwave background (CMB) anisotropy power spectrum are probing the early universe [20]. Within the inflationary paradigm, the seeds of the anisotropic features of the CMB light are the quantum fluctuations of the lowest energy state of a scalar field that filled the universe before radiation domination, during the inflationary phase. The calculation of the primordial power spectrum of these quantum fluctuations at the end of inflation is well known: if quantum fluctuations are generated during inflation, one expects a nearly scale invariant power spectrum slightly red tilted. After inflation, quantum fluctuations translate into density and pressure perturbations of the cosmological fluids (matter, radiation, dark matter and dark energy) which can be probed directly in the CMB angular power spectrum [21]. This prediction is in a very good agreement with CMB observations, although a higher level of accuracy is needed in order to conclude about the content of the primordial universe (*i.e.* one or several scalar fields, what exact shape for the potential, etc) and to definitely exclude alternative models. (It should be stressed that the aim of quantum cosmology might be less to suggest an "alternative model" to the standard paradigm than to provide it with a satisfactory foundation.) In LQC the past singularity is resolved. Therefore the quantum theory of cosmological perturbation can in principle be extended to the Planck era or even to the classical prebounce contracting universe [22–24]. This is the so-called LQC extension of the inflationary scenario.

For a flat FLRW universe, the LQC modified Friedmann equation is

$$H^2 = \frac{8\pi G}{3}\rho(1 - \frac{\rho}{\rho_{\rm B}}), \qquad (1)$$

while the equation expressing the local conservation of energy remains valid, $\dot{\rho} = -3H(\rho + P)$, with ρ and P the density and pressure of the cosmological fluid. For a single scalar field, φ, they read $\rho = \frac{1}{2}\dot{\varphi}^2 + V(\varphi)$ and $P = \frac{1}{2}\dot{\varphi}^2 - V(\varphi)$. If the potential energy dominates over the kinetic energy for a significant amount of time, the fluid has an effective equation of state which is close to '-1', allowing the universe to enter a phase of accelerated expansion.

Until 2013, the accuracy of CMB measurements was such that the simplest potential for the scalar field, $V(\varphi) = m^2\varphi^2/2$, was enough to account for the data. The LQC community has therefore focused on this simple model. However, the recent results of the Planck mission suggest that the quadratic potential is disfavored at a two sigma confidence level while the Starobinsky potential, $V(\varphi) \propto (1 - e^{-\sqrt{16\pi G/3}\varphi})$, seems to be the best alternative. An LQC analysis with this form of potential was performed recently [25]. The Starobinsky potential is based on a quadratic correction to the GR action[26]. As a matter of fact, it was shown [27] that LQC does not yield such a higher order curvature coupling: the action corresponding to the LQC bounce can only be written in terms of a non-metric theory with an action whose lowest order term beyond the Ricci scalar seems not to be quadratic. This approach however uses the effective modified Friedmann equation as a starting point and deriving the correct action from the full theory remains a challenge to be addressed in the years to come.

An estimation of the critical density, reached at the bounce, $\rho_{\rm B} \approx 0.41 m_{\rm Pl}^4$, is obtained when the Barbero-Immirzi parameter takes the standard numerical value suggested by black hole entropy calculation, *i.e.* $\gamma \approx 0.2375$. Once the energy density at the bounce is fixed, the background dynamics can be parametrized by a single number: the value of the scalar field at the bounce, $\varphi_{\rm B}$. Several questions have to be answered regarding the background before discussing further the dynamics of cosmological perturbations: (i) How likely is inflation to occur? (ii) Can the inflationary phase obtained in LQC last long enough so that the flatness and horizon problems are solved and the amplitude of the CMB angular spectrum explained? (iii) Are the scales probed by the CMB sensitive to the specific dynamics at the bounce?

Defining a consensual notion of probability in cosmology is still an open issue [28]. It can be argued [29] that there is no more ambiguity in LQC since there is in fact a precise time when the probability has to be evaluated, the bounce. Then, a consistent framework for the definition of probability can be built [30] and even be generalized to the covariant formulation of LQC [31]. Using the Liouville measure that corresponds to the Hamiltonian structure of LQC, the following conclusion was reached: the probability for the desired –*i.e.* in agreement with CMB measurements– slow roll not to occur in an LQC solution is less than three parts in a million. Hence a great deal of fine tuning would be necessary to avoid the

slow roll inflation that meets the CMB constraints: inflation is an attractor in LQC [32]. The rare dynamical trajectories that fail to meet the observational constraints are those which correspond to an extreme kinetic energy dominated bounce.

In parallel to this study, it was suggested [33] to adopt another viewpoint to the problem of measure: instead of setting initial data at the bounce, why not setting them in the remote past of the pre-bounce contracting branch of the universe and then compute the resulting probability distribution of $\varphi_{\rm B}$? It was claimed that in the remote past (*i.e.* when $\rho \ll \rho_{\rm B}$ and $H < 0$) it is the phase of the field, $\delta := \arctan(\dot{\varphi}/\sqrt{2V(\varphi)})$, that should be taken as the fundamental random variable with a flat probability distribution (the corresponding measure is preserved as long as $\rho \ll \rho_{\rm B}$). Quite surprisingly, this assumption translates into a probability distribution for $\varphi_{\rm B}$ that is highly peaked around a value that corresponds to a slow-roll inflation of about 140 e-folds. This would definitely be long enough to match the CMB constraints which require at least sixty e-folds of inflation.

In both cases, for initial conditions at the bounce or in the remote past, it seems well established that LQC leads to a long phase of slow-roll inflation shortly after the bounce (preceded by a brief phase of *super inflation*, with $\dot{H} > 0$). Except for initial conditions corresponding to a bounce preceded by a phase of deflation [34], the number of e-fold of superinflation, $N_{\rm B}$, as well as the total number of e-folds of inflation, $N_{\rm tot}$, can be expressed in terms of $\varphi_{\rm B}$ and $\rho_{\rm B}$ as $N_{\rm B} = \frac{1}{3}\ln\Gamma$, where $\Gamma := \sqrt{24\pi G\rho_{\rm B}}/m$, and $N_{\rm tot} = 2\pi G\varphi_{\rm i}^2 - \frac{1}{2}$, with

$$\varphi_{\rm i} \;=\; \varphi_{\rm B} + \sqrt{\tfrac{2}{3}}\,\mathrm{Arcsinh}(\Gamma\sqrt{2/\mathrm{W}\,(z)}) \qquad (2)$$

the scalar field at the start of slow-roll inflation, where the argument of the Lambert W-function is $z := 8\Gamma^2\exp(\sqrt{48\pi G}\varphi_{\rm B})$, for the quadratic potential. (Similar formulas can in principle be obtained for arbitrary potentials.) The important conceptual point we want to emphasize here is that the prediction of a long enough phase of inflation, which is a nice result, is actually *not* a prediction specific to the detailed structure of LQC. The '$w = -1$' effective equation of state is a strong attractor and the high probability for inflation to occur is only due to the large values of the energy density reached in the vicinity of the bounce. This condition, together with the existence of a scalar field with a reasonable potential, is basically enough to ensure an inflationary era. So LQC does indeed predict inflation as something "natural" but only in the sense that (in the isotropic setting) most trajectories goes through a high energy density state.

To conclude our general comments, we will discuss wether inflation predicted by LQC can have the required duration so that observable scales in the CMB correspond to scales that were affected by the specific dynamics of the bounce. On dimensional arguments, one might expect that the scales affected by quantum gravity effects have a wavenumber of order $k_{\rm B} \approx a_{\rm B}\sqrt{\rho_{\rm B}}m_{\rm Pl}^{-1}$, comparable to the radius of curvature at the bounce. (Actually, smaller scales can be also affected in the deformed algebra approach, and larger scales in the dressed metric approach, as we will explain later.) If the duration of inflation is too long, the scales "sensitive" to the bounce would now be super-Hubble. Within the inflationary paradigm, CMB experiments are sensitive to scales that exited the Hubble horizon at about sixty e-folds before the end of inflation and correspond to a physical wavenumber $k_\star \simeq 0.002\mathrm{Mpc}^{-1}$. Combining this information with the estimates of the number of e-folds of inflation in LQC, one is led to conclude that the value of the scalar field at the bounce must belong to a tiny range of values centered around the Planck mass for CMB experiments to be sensitive to LQC effects [35]. In a recent paper [36], this was studied in details, taking into account the degeneracy of the LQC parameters with the CMB parameters, namely the amplitude of the scalar primordial power spectrum and the tensor-to-scalar ratio. It was claimed [37] that an appropriate choice of the LQC parameters could in principle solve the anomalies observed for the large angular scales in the CMB. Such a choice would also lead to non-trivial predictions for the CMB polarization modes, as the observable scales in the CMB would be scales affected by the bounce (Planckian scales). However, this strategy holds at the price of adding a number of parameters: the Bogoliubov coefficients used to set the initial state of quantum fluctuations at the bounce [38]. In addition, conceptually, it is not clear that the prediction claimed for the polarized CMB is discriminant, because the scalar and polarized spectra are correlated. If the lack of power at large angular scales is due to a statistical fluctuation, it might very well also have imprints in the polarized spectrum too.

Finally, we note that the issue of the bounce has recently been investigated in the framework of group field theory [39]. Strikingly, the effective cosmological dynamics, emerging as the hydrodynamics of simple condensate states, leads to a bounce very similar to the one of LQC.

PERTURBATIONS

The background dynamics in LQC is well defined and compatible with data. This is a first success for the model. Going beyond this basic requirement implies to deal with perturbations in a consistent way. The task is highly non-trivial and different approaches, that we now briefly review, are being considered. We then adress the question of their advantages and drawbacks.

In a series of papers [40–42], a consistent formalism aimed at deriving the dynamics of cosmological perturbations propagating in a quantum background was developed. The starting point for the quantization is not the reduced phase space of the strictly homogeneous and isotropic background, $\Gamma_{\rm FLRW}$, but the reduced phase space of the perturbed FLRW space, $\tilde{\Gamma}$. It encapsulates both the homogeneous and isotropic degrees of freedom *and* the inhomogeneous degrees of freedom at first order in perturbation, $\tilde{\Gamma} = \Gamma_{\rm FLRW} \times \Gamma_{\rm pert}$, so that any quantum state can be written as the tensor product $\Psi(\nu, v_{\rm S(T)}, \varphi) = \Psi_{\rm FLRW}(\nu, \bar{\varphi}) \otimes \Psi_{\rm pert}(v_{\rm S}, v_{\rm T}, \bar{\varphi})$ with ν accouting for the homogeneous and isotropic degrees of freedom, and $v_{\rm S(T)}$ for scalar (tensor) perturbed degrees of freedom. The background quantization is performed using the usual loop quantization techniques for homogeneous and isotropic geometry. The seminal papers mostly focused on states that are sharply peaked, as usually studied in quantum cosmology, though the framework could be applied to any background state in principle. For the quantum background geometry, it is possible to define a metric operator,

$$\hat{g}_{\mu\nu}dx^\mu dx^\nu = \hat{H}^{-1}_{\rm FLRW}\ell^6\hat{a}^6(\bar{\varphi})\hat{H}^{-1}_{\rm FLRW}d\bar{\varphi}^2 - \hat{a}^2 d\vec{x}\cdot d\vec{x}, \quad (3)$$

with $\hat{H}_{\rm FLRW} = \hbar\sqrt{\Theta_{(\nu)}}$ the Hamiltonian operator of the isotropic and homogeneous background, and ℓ^3 the volume of the considered fiducial cell, while $\Theta_{(\nu)}$ is the difference operator. The dynamics of the physical perturbations is given by the second order part of the total Hamiltonian (still restricted to the square of the first order perturbations) raised as an operator. The action of the total Hamiltonian on the perturbed part of the Hilbert space does depend on the scale factor of the Universe. The quantization procedure for perturbations relies on techniques well understood for a test scalar field evolving on a quantum geometry [43]. The basic idea is the following. First, one considers the Hamiltonian operators, $-i\hbar\partial_{\bar{\varphi}}\Psi(\nu, v_{\rm S(T)}, \bar{\varphi}) = \left[\hat{H}_{\rm FLRW} + \hat{H}_{\rm pert}\right]\Psi(\nu, v_{\rm S(T)}, \bar{\varphi})$, and then switches to the interaction picture. Second, the factor ordering of $\hat{H}_{\rm pert}$ is chosen to be consistent with the factor ordering of the $\hat{g}_{\mu\nu}dx^\mu dx^\nu$ operator. For tensor perturbations (to illustrate the point) the quantum dynamics in the interaction picture reads

$$\begin{aligned}\Psi_{\rm FLRW}\otimes i\hbar\partial_{\bar{\varphi}}\Psi_{\rm pert} = \frac{1}{2}\int\frac{d^3k}{(2\pi)^3}\Bigg\{&32\pi G\left[\hat{H}^{-1}_{\rm FLRW}\Psi_{\rm FLRW}(\nu,\bar{\varphi})\right]\otimes\left[\left|\hat{\pi}_{{\rm T},\vec{k}}\right|^2\Psi_{\rm pert}(v_{\rm S(T)},\bar{\varphi})\right]\\ &+\frac{k^2}{32\pi G}\left[\hat{H}^{-1/2}_{\rm FLRW}\hat{a}^4(\bar{\varphi})\hat{H}^{-1/2}_{\rm FLRW}\Psi_{\rm FLRW}(\nu,\bar{\varphi})\right]\otimes\left[\left|\hat{v}_{{\rm T},\vec{k}}\right|^2\Psi_{\rm pert}(v_{\rm S(T)},\bar{\varphi})\right]\Bigg\},\end{aligned} \quad (4)$$

with $\left(\hat{v}_{{\rm T},\vec{k}}, \hat{\pi}_{{\rm T},\vec{k}}\right)$ the configuration and momentum operators for the perturbation degrees of freedom. Taking the scalar product of the above equation with $\Psi_{\rm FLRW}$ finally leads to the Schrödinger equation for the perturbation part of the wave function. The key point is the formal analogy between the quantum dynamics of perturbations evolving on a classical background and the quantum dynamics of the perturbations evolving on a fully quantum background. The quantum dynamics can be formally described as the dynamics of perturbations in a classical background but with a *dressed* metric, *i.e.*

$$i\hbar\partial_{\bar{\varphi}}\Psi_{\rm pert} = \frac{1}{2}\int\frac{d^3k}{(2\pi)^3}\left\{32\pi G(\tilde{p}_\varphi)^{-1}\left|\hat{\pi}_{{\rm T},\vec{k}}\right|^2\Psi_{\rm pert} + \frac{k^2}{32\pi G}(\tilde{p}_\varphi)^{-1}\tilde{a}^4(\bar{\varphi})\left|\hat{v}_{{\rm T},\vec{k}}\right|^2\Psi_{\rm pert}\right\}, \quad (5)$$

using the identification

$$(\tilde{p}_\varphi)^{-1} = \left\langle\hat{H}^{-1}_{\rm FLRW}\right\rangle \quad \text{and} \quad \tilde{a}^4 = \frac{\left\langle\hat{H}^{-1/2}_{\rm FLRW}\hat{a}^4(\bar{\varphi})\hat{H}^{-1/2}_{\rm FLRW}\right\rangle}{\left\langle\hat{H}^{-1}_{\rm FLRW}\right\rangle}. \quad (6)$$

This dressed metric $\tilde{g}_{\mu\nu}$ is *neither* equal to the classical metric nor equal to the metric traced by the sharply peaked background state. The final quantization of perturbations can be performed with standard techniques of

quantum field theory on curved spacetimes but using the dressed metric instead of the classical one. Scalar perturbations have also been calculated in this framework. The results are that the equations of motion for scalar and tensor perturbations have the same form as in the classical case,

$$Q_k'' + 2\left(\frac{\tilde{a}'}{\tilde{a}}\right) Q_k' + \left(k^2 + \tilde{U}\right) Q_k = 0, \tag{7}$$

$$h_k'' + 2\left(\frac{\tilde{a}'}{\tilde{a}}\right) h_k' + k^2 h_k = 0, \tag{8}$$

with Q_k a gauge-invariant variable for scalars, related to the Mukhanov-Sasaki variables via $Q_k = (v_{\mathrm{S},k}/a)$; $\tilde{U}$ is a dressed potential-like term given by

$$\tilde{U}(\bar{\varphi}) = \frac{\left\langle \hat{H}_{\mathrm{FLRW}}^{-1/2} \hat{a}^2(\bar{\varphi}) \hat{U}(\bar{\varphi}) \hat{a}^2(\bar{\varphi}) \hat{H}_{\mathrm{FLRW}}^{-1/2} \right\rangle}{\left\langle \hat{H}_{\mathrm{FLRW}}^{-1/2} \hat{a}^4(\bar{\varphi}) \hat{H}_{\mathrm{FLRW}}^{-1/2} \right\rangle}, \tag{9}$$

the quantum counterpart of

$$U(\bar{\varphi}) = a^2 \left(f V(\bar{\varphi}) - 2\sqrt{f} \partial_{\bar{\varphi}} V + \partial_{\bar{\varphi}}^2 V \right), \tag{10}$$

with $f := 24\pi G(\dot{\bar{\varphi}}^2/\rho)$ the fraction of kinetic energy. The power spectrum has been computed in this approach and is nearly scale-invariant, with a slight increase of power at large scales. In a subsequent study, it was understood that due to the freedom one has in selecting the initial state it is also possible to decrease the power at large scale, therefore leading to a better agreement with CMB data. An interesting conceptual point is that the reason why IR modes are affected by quantum gravity effects and not UV ones, as one could naively have expected, is clear and can be summarized as follows [22]. In LQC the curvature radius is bounded from below and takes its minium non-vanishing value R_{B} at the bounce. The UV modes, that have wavelengths smaller than R_{B} do not "feel" curvature and are in the Bunch-Davies vacuum. While IR modes do 'feel' curvature and can be amplified: they might not be in the Bunch-Davies vacuum at the onset of inflation.

The main other approach to perturbations in LQC is the "deformed algebra" approach. The constraints of general relativity form a first class system and this property is key to the consistency of the classical dynamics. It is not *a priori* clear whether this delicate consistency remains in effective theories that incorporate quantum corrections. The very notion of spacetime is supposed to emerge from solutions to the fundamental quantum gravity equations. The consistency of the effective quantum-corrected equations has to be ensured before they can be successfully solved. In some fields of physics, gauge fixing before quantization was shown to be harmless but the case of gravity is much more subtle and intricate than, say, Yang-Mills theories because dynamics is part of the gauge. In the deformed algebra approach this issue is addressed by building the algebra of constraints so that the constraints can be quantized without a classical specifications of gauge or observables. The deformed algebra approach is based on taking care of those gauge issues while embedding GR in a quantum framework.

Let us focus here on the holonomy corrections that are well defined and understood. The net effect of these corrections is encoded in the replacement

$$\bar{k} \to \mathbb{K}[n] := \frac{\sin(n\bar{\mu}\gamma\bar{k})}{n\bar{\mu}\gamma}, \tag{11}$$

where n is an unknown integer, $\bar{k}$ is the mean Ashtekar connection, and $\bar{\mu}$ is the coordinate size of a loop. The quantum-corrected constraints resulting from this substitution are renamed $\mathcal{C}_I^Q$. This replacement, motivated by the fundamental role given to holonomies in LQG, leads to the following algebraic structure:

$$\{\mathcal{C}_I^Q, \mathcal{C}_J^Q\} = f^K{}_{IJ}(A_b^j, E_i^a)\mathcal{C}_K^Q + \mathcal{A}_{IJ}, \tag{12}$$

where the $\mathcal{A}_{IJ}$ terms stand for anomalies and f_{IJ}^K are structure functions (and not anymore constants as in standard Yang-Mills theories). The consistency condition (that is the closure of the algebra) requires $\mathcal{A}_{IJ} = 0$. In turn, quite nicely, this condition imposes restrictions on the form of the quantum corrections, especially when matter is included in the Hamiltonian. Since the result is a modification of the algebra of constraints of spacetime, as it could be expected from the Hojman-Kuchar-Teitelboim theorem [44], the quantum structure is not a pseudo-Riemaniann spacetime with a metric in the usual sense. But it does have a well-defined *canonical* formulation using hypersurface deformations.

The conceptual strategy used to determine the algebraic structure can be summarized as follows. The quantum corrected constraints are explicitly calculated for the perturbations up to the desired order. Then, all the Poisson brackets are calculated, therefore exhibiting the anomaly terms. Counter-terms, required to vanish at the classical limit, are finally added to the expressions of constraints to ensure anomaly freedom. The resulting theory is consistent by construction but is also –maybe surprisingly– uniquely defined: the different unknown integers entering the game (that can be different from unity when one considers other terms than the $\bar{k}^2$ arising from the curvature of the connection) are all determined. Furthermore, although the calculations are intricate, the resulting algebra is simple and elegant. It involves a single structure function which encodes, at the effective level, all the quantum modifications:

$$\Omega = 1 - 2\rho/\rho_{\mathrm{B}}. \tag{13}$$

The algebra is then closed in a non-pertubative way. This method has been successful for vector [45] and scalar [46]

perturbations. It has aslo been shown that a single algebraic structure can be consistently written for *all* perturbations [47] (this has consequences for tensor modes that were forgotten in first studies), making the whole approach very appealing:

$$\{D[M^a], D[N^a]\} = D[M^b\partial_b N^a - N^b\partial_b M^a], \quad (14)$$
$$\{D[M^a], S^Q[N]\} = S^Q[M^a\partial_b N - N\partial_a M^a], \quad (15)$$
$$\{S^Q[M], S^Q[N]\} = \Omega D\left[q^{ab}(M\partial_b N - N\partial_b M)\right] \quad (16)$$

where D and S are the diffeomorphism and Hamiltonian constraints, N and M are lapse functions, N^a and M^a are shift functions, and the superscript Q indicates that the constraint is quantum corrected.

Beside its elegance, this algebra has a striking feature: it leads to a signature change close to the bounce. When $\rho < \rho_{\rm B}/2$ the spacetime structure is Lorentzian but when $\rho > \rho_{\rm B}/2$, in the vicinity of the bounce, Ω becomes negative and the spacetime structure becomes Euclidean. This is reminiscent of what is usually postulated in quantum cosmology, mostly for technical reasons (to improve the convergence of path integrals). In standard quantum cosmology one usually deals with an amplitude written as

$$< \varphi_2, t_2|\varphi_1, t_1 >= \int d[\varphi]e^{I[\varphi]}, \quad (17)$$

where $I[\varphi]$ is the action of the field configuration $\varphi(x,t)$, and $d[\varphi]$ is a measure on the space of field configurations. The integrand in (17) has a rapidly oscillating phase, and the path integral, in general, does not converge. This is why the time is rotated clockwise by $\pi/2$ so that $I[\varphi] \to \tilde{I}[\varphi] := -iI[\varphi]$. The integrand in the resulting Euclidean path integral is now exponentially damped, and the integral generically converges. Then, one can analytically continue the amplitude in the complex t-plane back to real values. Importantly, a quantum field theory machinery has been developed in this framework [48]. Recent reviews on quantum field theory on an Euclidean background can be found in [49, 50]. Although far from being fully understood (but QFT on a Lorentzian curved background is also not completely understood) the framework is basically consistent. There are also obvious links with the Hartle-Hawking proposal [51] but the Euclidean phase appears in the LQC model considered here in a fundamentally dynamical way since the Poisson bracket between Hamiltonian constraints varies continuously from a positive to a negative expression. This is the key conceptual point. This effect has also been found independently following different approaches within LQC [52, 53]. In particular, the first of these references relies on substantially different hypotheses (using a model of patches of universe evolving independently in the longitudinal gauge). The fact that it leads to the same result reinforces the credibility of the conclusion, we will come back to this point later. The resulting equation of motion is more complicated than in the "dressed metric" approach. For tensor modes, it reads

$$v_k''(\eta) + \left(\Omega k^2 - \frac{z_{\rm T}''}{z_{\rm T}}\right) v_k(\eta) = 0, \quad (18)$$

in conformal time, where the mode functions $z_{\rm T} := (a/\sqrt{\Omega})$ are related to the amplitude of the tensor modes of the metric perturbation h_k through $v_k = z_{\rm T}h_k/\sqrt{32\pi G}$. The evolution of the modes is not anymore driven only by the hierarchy between k^2 and $|a''/a|$. Due to the Ω-term, the situation is more complicated and several of new phenomena do appear, opening a wide phenomenology. Here, the ratio between the length scale associated with a mode and the curvature radius is not the only important number.

By definition there is no time in the Euclidean phase. The very meaning of "propagation of a mode" becomes unclear. However, the equation of motion in Fourier space, which reads for scalar modes

$$\ddot{\mathcal{R}}_k - \left(3H + 2m^2\frac{\bar{\varphi}}{\dot{\bar{\varphi}}} + 2\frac{\dot{H}}{H}\right)\dot{\mathcal{R}}_k + \Omega\frac{k^2}{a^2}\mathcal{R}_k = 0, \quad (19)$$

with $\mathcal{R} := v/z$, is mathematically well defined and has a regular solution even if there are singular points in the equation itself. The primordial power spectrum has been calculated and exhibits three regions. This approach implicitly assumes that the change of sign is in fact a kind of tachyonic instability and not a deep change of signature at the fundamental level of the structure of space-time. The case of a real change of signature requires news techniques that are briefly mentioned in the last part of this article whereas the instability case can be rigorously treated as done in [54]. The UV region is then characterized by an exponential growth of the spectrum whose origin is clearly grounded in the Euclidean phase. The intermediate region exhibits oscillations (that would be smeared out by the cosmic evolution). The IR region is mostly scale-invariant for tensor modes and blue for scalar modes. Whether we see the IR, the UV or the intermediate region in the CMB depends on the duration of inflation. If the number of e-folds is higher than the minimum required value, the observational window falls in the UV part, which is incompatible with data. This shows that quantum gravity can indeed be falsified by cosmological experiments, even when it predicts a long enough phase of inflation!

What are the conceptual differences between both approaches and the assumptions behind them[1]? Which

[1] The following arguments come partially from a discussion that

one is more reliable? Those questions are not easy to answer. The dressed metric approach is unquestionably more "quantum" as it addresses the essential question of dealing with a quantum field on a quantum background. In a way, the fundamental structure is given by the background wave function $\Psi_{\rm FLRW}$ and the dressed metric itself is only a manner of modeling how perturbations propagate. The background structure is not a smooth Riemannian metric, but a quantum geometry given by $\Psi_{\rm FLRW}$, which is consistent with the presence of perturbations since it has been checked that the backreaction they produce is negligible (consistency condition). However one still uses at some point (explicitly or implicitly) a line element $ds^2 = g_{\mu\nu}dx^\mu dx^\nu$, with $g_{\mu\nu}$ defined in terms of expectation values. For this to be meaningful, one would still have to demonstrate that $g_{\mu\nu}$, wherever it comes from, changes by standard (classical) coordinate transformations if one changes coordinates (or the gauge). Otherwise, $ds^2 = g_{\mu\nu}dx^\mu dx^\nu$ is not coordinate independent and not tensorial, and therefore loses its meaning. The problem is that the deformed algebra approach precisely shows that, in general, the classical transformations do not apply anymore when holonomy corrections are implemented consistently.

The basic question one can therefore ask about the dressed metric approach is whether it really goes beyond quantum field theory on curved spacetimes. If one has a background FLRW metric with a scale factor a and some scalar field φ, one can quantize any field on it, such as the gauge-invariant tensor modes. The background equations need not solve the classical Friedmann equation because quantum field theory can in principle be done on any Riemannian background, not just on one solving Einstein's equation. So even when one uses expectation values of minisuperspace operators, instead of the classical a and φ, one might still be within the setting of quantum field theory on a curved spacetime, rather than in quantum gravity. Gravity, even linearized, differs from fields on a background because it determines how the fields transform under coordinate transformations. This is what is meant by having a metric structure as opposed to just a background with fields lying over it. Quantum gravity in the linearized setting should, in general, differ from quantum field theory on curved spacetimes by deriving the existence of a corresponding structure with specific transformations. This is a key point and one must be careful of not implicitly assuming a classical background structure that has no reason to be correct in this framework.

There is *a priori* an infinite number of dynamical laws, all written with respect to different choices of time coordinates. They are classically equivalent to one another thanks to the symmetries we know GR enjoys, and one is therefore free to pick any one of these choices. In the dressed metric approach, when referring to a background gauge, by deparameterization, or by writing the mode dynamics in terms of coordinate invariant combinations of metric and matter perturbations, one might be implicitly using several time choices. It is only after these steps that a specific dynamics for background variables and perturbations can be obtained. Classically, those results do not depend on which coordinate choices are made, and the procedure is valid. But when one quantizes some (or all) relevant degrees of freedom, the equations are modified by quantum corrections of different kinds, and one is no longer guaranteed that the results do not depend on the choices made (that is, the theory may not be covariant or anomaly-free). What is crucial is the fact that the classical theory enjoys a symmetry which might be used in order to simplify the quantization procedure. When quantized or modified, the theory does not exhibit this symmetry anymore and the results might be gauge-dependent and therefore meaningless.

A possible answer is that the dressed metric approach does indeed go beyond quantum filed theory on a FLRW spacetime in the sense that perturbations now propagate on a quantum FLRW background. The evolution of perturbations is sensitive to the quantum nature of the background. It is sensitive not only to the fact that the peak of the wave function does not follow the classical evolution, but also to the quantum fluctuations. This, however, does not answer the consistency issue.

The other way round, one could wonder if the algebraic structure obtained in the deformed algebra approach is really unique. After all, there is no theorem proving that the values chosen for the free parameters entering the non-linear system under consideration are the only possible ones. And, indeed, they are probably not unique. Assumptions –although quite natural– need to be made in order to obtain a tractable solution.

A more serious criticism is the following. The theory of cosmological perturbations is a truncated theory in which one approximates the exact solutions by throwing away some terms in equations. It is clear that the most obvious way of doing it is to consider Einstein's equations, expand them around a given background, and keep terms up to first order in perturbations. It is then possible to recast the same dynamics in the Hamiltonian language. But the evolution of perturbations is not generated by a constraint. The full evolution is not generated by a single Hamiltonian. Rather, background evolution is dictated by a Hamiltonian H_0 (the index i in H_i refers to the considered order), and perturbations evolve on the top of this background according to their own Hamiltonian H_2. This dynamics differs from the

took place between I. Agullo, A. Barrau, M. Bojowald, and G. Calcagni.

one generated by the single Hamiltonian $H_0 + H_2$. Furthermore, perturbations are constrained by linear constraints such as the ones generated by H_1, but H_2 is not constrained to vanish. This suggests that the algebra of second order constraints might not play a fundamental role in the theory. One could follow a different approach and modify this setting by declaring that the dynamics is generated by the Hamiltonian $H_0 + H_2$ and that H_2 is also a constraint. The resulting equations of motion are different from the truncation of Einstein equations mentioned above as the new equations involve some backreaction. However is only involves part of the full backreatcion, which raises a consistency issue.

This issue could be addressed as follows. The classical constraint, playing the role of a starting point, reads $H[N] = 0$ (there are actually infinitely many constraints because the lapse function N is free, setting aside the diffeomorphism constraint). If this constraint is expanded, it remains a constraint. To second order, one can split it in two different terms: one that comes from varying the background lapse $\bar{N}$ (a single constraint $H_0 + H_2$) and one that comes from the variation with respect to $\delta N = N - \bar{N}$ (an infinite number of constraints H_1). For unique Hamiltonians H_0 and H_2 the background lapse has to be fixed and deparameterization can be used. The constraint $H_1 = 0$ is solved for the modes. However, this would not give the correct dynamics H_2: for general metric perturbations (no gauge fixing) there is more than one independent scalar degree of freedom left in H_2, even after solving the constraint $H_1 = 0$. It is possible to get rid of non-physical scalars either by fixing the gauge, or by rewriting H_2 in terms of gauge-invariant combinations of the scalar perturbations. In both cases, one refers to gauge transformations generated by H_1. Treating them as gauge transformations is consistent only if H_1 satisfies a closed first-class algebra. This is why the deformed algebra puts a specific emphasis on this point. The classical closure of this algebra relies on the background equations as well as the mode equations. If the background dynamics is modified by quantum effects, the algebra generated by H_1 is no longer guaranteed to close. It is however true that the dynamics generated by $H_0 + H_2$ can, in some background gauge, include a backreaction term and that there may be additional terms which are not taken into account into procedure. The important point is that this makes the system canonical, so the powerful methods of constrained systems can be used. In other words, this term is included for mathematical rather than physical reasons but it is correct to underline that a possible lack of physical consistency on this specific point still need to be addressed.

On the one hand, it should be emphasized that the main results of the deformed algebra approach have also been found independently following different paths. The holonomy corrections to the effective equations was considered in the longitudinal gauge [55]. The main result is that the equations of motion for the perturbations agree with the one of the deformed algebra. The algebraic structure is also similar, as the time derivative of the effective scalar constraint gives rise to a cosine multiplying the diffeomorphism constraint. In another work [56], the quantum theory on a lattice was studied so that long wavelength scalar perturbations in LQC could be accounted for, again using the longitudinal gauge. The commutators are explicitly calculated and taking the classical limit, and then the continuum limit, one recovers the considered algebra. Some support to the deformed algebra approach also comes from recent investigations of a linear redefinition of the constraints (with phase-space dependent coefficients) which can be used to eliminate structure functions, even Abelianizing the more-difficult part of the constraint algebra [57].

On the other hand, an analysis [58] of the quantization of cosmological perturbations in which one truncates the action up to second order in perturbations and looks at the whole symplectic system formed by zero-modes plus perturbations was performed. Perturbations are not treated as a test field on a background, as in the dressed metric approach, but backreaction up to the order considered is included. The model is here parametrized using only gauge-invariant quantities: it deals with the construction of approximate solutions of inhomogeneous cosmologies that effectively behave as approximate solutions of a homogeneous and isotropic model with a specific matter content, or even with geometric modifications [59, 60]. These solutions are far from being homogeneous, and the terms accounting for the matter or GR modifications have their origin in the collective behavior of the inhomogeneities. These solutions were constructed in the specific case of the hybrid quantization of the linearly polarized Gowdy model with three-torus topology, as an example of the fact that inhomogeneous quantum degrees of freedom can behave collectively to lead to a homogeneous description.

To conclude, let us emphasize that in spite of the conceptual and technical differences between the approaches we have presented, there are *universal* LQC features that appear at the phenomenological level (for tensor modes) in the IR and intermediate regions of the primordial power spectrum [34]. This is a pleasing and encouraging result.

OTHER OPEN CONCEPTUAL ISSUES

Ignoring the possible Euclidean phase around the bounce, we first come back to a simple question related to initial conditions. If the bounce is resulting from a causal evolution, there is no reason for initial conditions

–neither for the background nor for the perturbations– to be set at the bounce time. As advocated by the deformed algebra authors [61, 62], this is both causally unjustified and technically irrelevant since the bounce is probably the worst time (strong curvature regime) for setting initial conditions, especially when considering that the causal structure in the remote past of the contracting branch allows one to have a well defined vacuum state in the usual QFT sense. However, the way time flows is not obvious. It is perfectly allowed to assume that, starting from the bounce, time flows in two opposite directions, generating two *expanding* branches. In that case, putting initial conditions at the bounce is necessary. In principle both scenarios are distinguishable observationally as some extreme gravitational phenomena occurring in the contracting branch (first hypothesis, with only one time direction) might have footprints in the current universe [63].

Somehow related is also the question of the role of the cosmological constant (if the acceleration of the Universe is indeed due to a true cosmological constant) in the remote past of the contracting phase. When going backward in time, the universe inevitably becomes $\Lambda-$dominated at some point. This might be used to explain the matter content of the Universe by a purely geometrical origin and even lead to a cyclic scenario which does not suffer the problem of growth of inhomogeneities during the contracting phase [64].

In the case of an Euclidean phase, things are more complicated. Does it makes sense to "propagate" perturbations in the absence of time? This is possible if one interprets the effect as an instability in the equations of motion but the process is hard to understand if one really considers that there exists a true change of signature in the space-time structure. In fact, the naive propagation of perturbations across the bounce leads to a spectrum inconsistent with data [35]. This could be due to one of the numerous assumptions (isotropy, no backreaction, etc.) but it could also be an indication that the idea of propagating modes through an Euclidean phase does not make sense at all. An interesting alternative way of dealing with the same situation was suggested recently [65], taking advantage of the known mathematical treatment of the Tricomi problem. Conceptually it opens a whole new perspective for cosmology: the mixed-type partial differential equations for modes in this context lead to a nice balance between deterministic cyclic models and singular big bang models. There is no initial divergence, and yet initial data in the infinite past do not uniquely determine the entire space-time structure. For every mode, it is necessary to specify one function at the beginning of the expanding phase even if initial values for the contracting phase had already been chosen. Still, the normal derivative of the field is not free and may carry subtle but interesting information about the pre-big bang epoch.

A recent work suggested that time could emerge from a "SO(4) $\rightarrow$ SO(1,3)" symmetry breaking [66, 67]. By analogy with solid state physics, one could speculate that this transition, exhibited by the deformed algebra approach and other LQC studies mentioned before, is a result of the symmetry breaking at the level of the fundamental structure of spacetime. In particular, one could assume that the original SO(4) spacetime symmetry is broken into SO(3), where the residual SO(3) is the rotational symmetry of triads. The time direction could therefore be seen as the order parameter of the symmetry broken phase.

Another important issue is related to the cosmological shear. As the shear term is proportional to $1/a^6$ in the contracting branch, if a causal evolution viewpoint is adopted, anisotropies become significant at the bounce, when the scale factor reaches its minimal value. The effect of anisotropies on the duration of inflation was studied [62, 68] and it was shown [69] that if initial conditions are set at the bounce, there are many more solutions leading to a universe that does not resemble ours at all than to a universe with a standard classical limit. If initial conditions are set in the remote past of the contracting branch, the problem is automatically evaded by selecting a solution with the correct asymptotic behavior. Then, what should be the "initial" conditions for the shear? This is a delicate and important question. When dealing, for example, with the phase of the oscillations of the scalar field, a flat distribution can easily be chosen, especially because it is conserved in time. But there is no straightforward choice when the shear term is included, and the predictive power of the whole LQC approach depends crucially on this as the number of e-folds is strongly dependent on the anisotropies at the bounce.

In our opinion, the most important conceptual and technical issue is related to Planck length effects. In the black hole sector, it was recently suggested [70, 71] that too much emphasis was put on Planck length effects, neglecting Planck density effects. The situation is somehow reversed in cosmology. As explained in the first section of this article, the background dynamics at high density seems to be under a fairly good control. This is the main and less controversial result of LQC. However, when calculating the primordial spectra, one faces a Planck *length* problem. One possibility, used by the authors of the dressed metric approach, is to fine-tune initial conditions so that the amount of inflation just equals the required minimum. In that case, modes of physical interest are never trans-Planckian. However, for the vast majority of the parameter space (including

the value favored by the analysis with initial conditions in the past [33]) modes of physical interest are much smaller than the Planck length at the bounce time. This problem already exists in standard cosmology and is well known. However, it becomes much more important in the framework of a theory that predicts that there is nothing smaller length than the Planck length (This statement is rigorous about surfaces only, it is actually much less clear for lengths and depends on the chosen operator.) Otherwise stated, the question is: in the purely classical (far from the bounce) contracting branch of the Universe, what happens to a photon blue-shifted to the Planck length? It is possible that the dressed metric approach automatically accounts for such effects through its quantum field on a quantum background treatment. But the physical interpretation of values of wavenumbers higher that the Planck scale –and they are 30 orders of magnitude higher in a typical case– is still to be understood. In the deformed algebra approach, this point is clearly not taken into account at this stage. It probably could be accounted for by modified dispersion relations. This makes sense as the LQC deformation of the GR algebra naturally leads to such effects. This will however in general raise new conceptual issues as complex frequencies would then enter the game.

Finally, we would like to mention that the problems of quantum-to-classical transition (the measurement problem) and entropy production are rarely addressed in the framework of LQC. They should be faced in future studies.

The issues presented in this article are in no way suggesting that LQC fails as an effective quantum cosmological formalism. In fact, the abundance of questions being addressed is a positive sign showing that LQC is an active and healthy field of research, with motivating challenges for the years to come.

[1] A. Ashtekar, T. Pawlowski and P. Singh, *Phys. Rev. Lett.* **96** (2006) 141301, arXiv:gr-qc/0602086 [gr-qc].

[2] A. Ashtekar and T. A. Schilling (1997) arXiv:gr-qc/9706069 [gr-qc].

[3] M. Bojowald, D. Brizuela, H. H. Hernandez, M. J. Koop and H. A. Morales-Tecotl, *Phys. Rev.* **D84** (2011) 043514, arXiv:1011.3022 [gr-qc].

[4] A. Ashtekar and P. Singh, *Class. Quant. Grav.* **28** (2011) 213001, arXiv:1108.0893 [gr-qc].

[5] A. Barrau, M. Bojowald, G. Calcagni, J. Grain and M. Kagan, *JCAP* **1505** (2015) 051, arXiv:1404.1018 [gr-qc].

[6] P. Diener, B. Gupt and P. Singh, *Class. Quant. Grav.* **31** (2014) 105015, arXiv:1402.6613 [gr-qc].

[7] P. Diener, B. Gupt, M. Megevand and P. Singh, *Class. Quant. Grav.* **31** (2014) 165006, arXiv:1406.1486 [gr-qc].

[8] P. Diener, B. Gupt and P. Singh, *Class. Quant. Grav.* **31** (2014) 025013, arXiv:1310.4795 [gr-qc].

[9] A. Ashtekar, A. Corichi and P. Singh, *Phys. Rev.* **D77** (2008) 024046, arXiv:0710.3565 [gr-qc].

[10] A. Corichi and P. Singh, *Phys. Rev. Lett.* **100** (2008) 161302, arXiv:0710.4543 [gr-qc].

[11] A. Corichi and E. Montoya, *Phys. Rev.* **D84** (2011) 044021, arXiv:1105.5081 [gr-qc].

[12] W. Kaminski and T. Pawlowski, *Phys. Rev.* **D81** (2010) 084027, arXiv:1001.2663 [gr-qc].

[13] A. Ashtekar, T. Pawlowski, P. Singh and K. Vandersloot, *Phys. Rev.* **D75** (2007) 024035, arXiv:gr-qc/0612104 [gr-qc].

[14] L. Szulc, W. Kaminski and J. Lewandowski, *Class. Quant. Grav.* **24** (2007) 2621, arXiv:gr-qc/0612101 [gr-qc].

[15] K. Vandersloot, *Phys. Rev.* **D75** (2007) 023523, arXiv:gr-qc/0612070 [gr-qc].

[16] E. Bentivegna and T. Pawlowski, *Phys. Rev.* **D77** (2008) 124025, arXiv:0803.4446 [gr-qc].

[17] T. Pawlowski and A. Ashtekar, *Phys. Rev.* **D85** (2012) 064001, arXiv:1112.0360 [gr-qc].

[18] A. Corichi and A. Karami, *Phys. Rev.* **D84** (2011) 044003, arXiv:1105.3724 [gr-qc].

[19] I. Agullo and A. Corichi (2013) arXiv:1302.3833 [gr-qc].

[20] Planck Collaboration (P. A. R. Ade *et al.*) (2015) arXiv:1502.01589 [astro-ph.CO].

[21] A. R. Liddle and D. H. Lyth, *Phys.Rept.* **231** (1993) 1, arXiv:astro-ph/9303019 [astro-ph].

[22] A. Ashtekar and A. Barrau (2015) arXiv:1504.07559 [gr-qc].

[23] J. Grain and A. Barrau, *Phys. Rev. Lett.* **102** (2009) 081301, arXiv:0902.0145 [gr-qc].

[24] J. Mielczarek, T. Cailleteau, J. Grain and A. Barrau, *Phys. Rev.* **D81** (2010) 104049, arXiv:1003.4660 [gr-qc].

[25] B. Bonga and B. Gupt (2015) arXiv:1510.04896 [gr-qc].

[26] A. A. Starobinsky, *Phys. Lett.* **B91** (1980) 99.

[27] G. J. Olmo and P. Singh, *JCAP* **0901** (2009) 030, arXiv:0806.2783 [gr-qc].

[28] J. S. Schiffrin and R. M. Wald, *Phys. Rev.* **D86** (2012) 023521, arXiv:1202.1818 [gr-qc].

[29] A. Ashtekar and D. Sloan, *Gen. Rel. Grav.* **43** (2011) 3619, arXiv:1103.2475 [gr-qc].

[30] D. A. Craig and P. Singh, *Class. Quant. Grav.* **30** (2013) 205008, arXiv:1306.6142 [gr-qc].

[31] D. Craig and P. Singh, The Vertex Expansion in the Consistent Histories Formulation of Spin Foam Loop Quantum Cosmology, in *14th Marcel Grossmann Meeting on Recent Developments in Theoretical and Experimental General Relativity, Astrophysics, and Relativistic Field Theories (MG14) Rome, Italy, July 12-18, 2015*, (2016). arXiv:1603.09671 [gr-qc].

[32] P. Singh, K. Vandersloot and G. V. Vereshchagin, *Phys. Rev.* **D74** (2006) 043510, arXiv:gr-qc/0606032 [gr-qc].

[33] L. Linsefors and A. Barrau, *Phys. Rev.* **D87** (2013) 123509, arXiv:1301.1264 [gr-qc].

[34] B. Bolliet, J. Grain, C. Stahl, L. Linsefors and A. Barrau, *Phys.Rev.* **D91** (2015) 084035, arXiv:1502.02431 [gr-qc].

[35] B. Bolliet, A. Barrau, J. Grain and S. Schander (2015) arXiv:1510.08766 [gr-qc].

[36] I. Agullo and N. A. Morris (2015) arXiv:1509.05693 [gr-qc].

[37] A. Ashtekar and A. Barrau, *Class. Quant. Grav.* **32** (2015) 234001, arXiv:1504.07559 [gr-qc].

[38] I. Agullo, W. Nelson and A. Ashtekar, *Phys. Rev.* **D91** (2015) 064051, arXiv:1412.3524 [gr-qc].

[39] D. Oriti, L. Sindoni and E. Wilson-Ewing (2016) arXiv:1602.08271 [gr-qc].

[40] I. Agullo, A. Ashtekar and W. Nelson, *Class.Quant.Grav.* **30** (2013) 085014, arXiv:1302.0254 [gr-qc].

[41] I. Agullo, A. Ashtekar and W. Nelson, *Phys. Rev. Lett.* **109** (2012) 251301, arXiv:1209.1609 [gr-qc].

[42] I. Agullo, A. Ashtekar and W. Nelson, *Phys. Rev.* **D87** (2013) 043507, arXiv:1211.1354 [gr-qc].

[43] A. Ashtekar, W. Kaminski and J. Lewandowski, *Phys. Rev.* **D79** (2009) 064030, arXiv:0901.0933 [gr-qc].

[44] S. A. Hojman, K. Kuchar and C. Teitelboim, *Annals Phys.* **96** (1976) 88.

[45] J. Mielczarek, T. Cailleteau, A. Barrau and J. Grain, *Class. Quant. Grav.* **29** (2012) 085009, arXiv:1106.3744 [gr-qc].

[46] T. Cailleteau, J. Mielczarek, A. Barrau and J. Grain, *Class. Quant. Grav.* **29** (2012) 095010, arXiv:1111.3535 [gr-qc].

[47] T. Cailleteau, A. Barrau, J. Grain and F. Vidotto, *Phys. Rev.* **D86** (2012) 087301, arXiv:1206.6736 [gr-qc].

[48] R. Laflamme, *Phys. Lett.* **B198** (1987) 156.

[49] F. Strocchi, *Int. Ser. Monogr. Phys.* **158** (2013) 1.

[50] F. Guerra (2005) arXiv:math-ph/0510087 [math-ph].

[51] J. B. Hartle and S. W. Hawking, *Phys. Rev. D* **28** (Dec 1983) 2960.

[52] E. Wilson-Ewing, *Class. Quant. Grav.* **29** (2012) 215013, arXiv:1205.3370 [gr-qc].

[53] M. Bojowald and G. M. Paily, *Phys. Rev.* **D86** (2012) 104018, arXiv:1112.1899 [gr-qc].

[54] S. Schander, A. Barrau, B. Bolliet, L. Linsefors, J. Mielczarek and J. Grain, *Phys. Rev.* **D93** (2016) 023531, arXiv:1508.06786 [gr-qc].

[55] E. Wilson-Ewing, *Class. Quant. Grav.* **29** (2012) 085005, arXiv:1108.6265 [gr-qc].

[56] E. Wilson-Ewing, *Class. Quant. Grav.* **29** (2012) 215013, arXiv:1205.3370 [gr-qc].

[57] M. Bojowald, S. Brahma and J. D. Reyes, *Phys. Rev.* **D92** (2015) 045043, arXiv:1507.00329 [gr-qc].

[58] L. C. Gomar, M. Martin-Benito and G. A. M. Marugan, *JCAP* **1506** (2015) 045, arXiv:1503.03907 [gr-qc].

[59] B. Elizaga Navascus, M. Martn-Benito and G. A. Mena Marugn, *Phys. Rev.* **D91** (2015) 024028, arXiv:1409.2927 [gr-qc].

[60] B. Elizaga Navascus, M. Martn-Benito and G. A. Mena Marugn, *Phys. Rev.* **D92** (2015) 024007, arXiv:1504.08152 [gr-qc].

[61] L. Linsefors and A. Barrau, *Phys. Rev.* **D87** (2013) 123509, arXiv:1301.1264 [gr-qc].

[62] L. Linsefors and A. Barrau, *Class. Quant. Grav.* **32** (2015) 035010, arXiv:1405.1753 [gr-qc].

[63] W. Nelson and E. Wilson-Ewing, *Phys. Rev.* **D84** (2011) 043508, arXiv:1104.3688 [gr-qc].

[64] A. Barrau and L. Linsefors, *JCAP* **1412** (2014) 037, arXiv:1406.3706 [gr-qc].

[65] M. Bojowald and J. Mielczarek, *JCAP* **1508** (2015) 052, arXiv:1503.09154 [gr-qc].

[66] J. Mielczarek, *Springer Proc. Phys.* **157** (2014) 555, arXiv:1207.4657 [gr-qc].

[67] J. Mielczarek (2012) arXiv:1212.3527 [gr-qc], [AIP Conf. Proc.1514,81(2012)].

[68] B. Gupt and P. Singh, *Class. Quant. Grav.* **30** (2013) 145013, arXiv:1304.7686 [gr-qc].

[69] L. Linsefors and A. Barrau, *Class. Quant. Grav.* **31** (2014) 015018, arXiv:1305.4516 [gr-qc].

[70] C. Rovelli and F. Vidotto, *Int. J. Mod. Phys.* **D23** (2014) 1442026, arXiv:1401.6562 [gr-qc].

[71] H. M. Haggard and C. Rovelli, *Phys. Rev.* **D92** (2015) 104020, arXiv:1407.0989 [gr-qc].

Chapter III

Black holes in quantum gravity

Recently, there has been a growing interest in black hole phenomenology for two good reasons: the discovery of gravitational waves by the LIGO/VIRGO collaboration in 2015 and the theoretical developments of quantum gravity. As was obtained within different quantum gravity approaches, there is a strong belief that quantum gravity effects could manifest themselves outside the event horizon of black holes.

In this Chapter, we start by recalling the basics properties of black holes in GR: the Schwarzschild metric in section III.1, the different types of black holes that are considered in astrophysics are presented in section III.2, the thermal properties of the event horizon are reviewed in section III.3. Section III.4 is dedicated to a review of the work of Rovelli and Haggard [81] regarding the black hole to white hole transition in Loop Quantum Gravity. This is the basis for our phenomenological work, reported in the last section III.5.

III.1 The Schwarzschild solution

Black holes are the pure geometrical realization of spherically symmetric solutions to Einstein's field equations. Space-time around a (static) black hole is described by the Schwarzschild metric. The corresponding line element is

$$ds^2 = \left(1 - \frac{r_s}{r}\right) dt^2 - \left(1 - \frac{r_s}{r}\right)^{-1} dr^2 - r^2 d\Omega^2, \quad \text{with} \quad r_s \equiv 2Gm, \tag{III.1}$$

the Schwarzschild radius and $d\Omega^2$ the metric of the unit sphere. Hence, the gravitational field (i.e. the metric components) manifestly diverges on two hyper-surfaces, at $r = 0$ and at $r = r_s$. The singularity at $r = r_s$ is a coordinate singularity: the Kretschmann scalar does not diverge and a change of coordinate, for instance to Kruskal coordinate, may regularize the metric. However, the singularity at $r = 0$ is a space-time singularity where curvature diverges and space and time can no longer be described by standard GR. Not being singular, the Schwarzschild surface, $r = r_s$, is still associated with a unique physical phenomenon. As can be seen in (III.1), for an in-falling observer, space and time interchange their role at the crossing of the Schwarzschild sphere. Then, the distance r to the central singularity becomes the time parameter. But, nothing can stop or reverse the flow of time: the observer's journey inevitably ends at the space-time singularity. In fact, even light can not escape. For instance, a star with the mass of the sun but with a radius smaller than three kilometers would be invisible. For this reason, the Schwarzschild sphere is called an event horizon. Interestingly, such effect was already apprehended by Laplace and Michell in the eighteenth century within the Newtonian theory, based on the notion of escape velocity. (In Newtonian physics, the minimal velocity needed for an object to escape the gravitational attraction of a massive body of mass m at distance r is precisely $v = \sqrt{2Gm/r}$.) The Schwarzschild solution was obtained by Schwarzschild in 1916, generalized to

spinning black holes by Kerr in 1963, to charged black holes by Newman in 1965 and the term 'Black Hole' was coined by Wheeler in 1968.

III.2 Black holes in Nature

Black holes generically form after gravitational collapse of matter. There are two main situations in which a black hole is believed to form. The gravitational collapse of a star that has ended its fusion cycle (stellar black holes) and the gravitational collapse of entire regions of the sky when the density perturbation field $\delta\rho/\rho$ becomes of order one (primordial black holes, stellar clusters, gas clouds). The mass range spanned by stellar black holes lies between a few and a few dozens of solar masses. The gravitational waves GW150914 detected by LIGO were certainly emitted following the coalescence of two stellar black holes with masses around thirty solar masses [60].

Primordial black holes may have masses as light as the Planck mass, i.e. $10^{-5}g$, up to a million solar masses depending on when they form. Several scenarios for primordial black holes (PBH) formations have been developed. Their common features are that PBH are more likely to form during the first moments of the universe: during reheating or at the early stage of radiation dominations. Then, their mass is roughly given by the *Hubble horizon mass* at the time they form,

$$m \approx \rho\,(ct)^3 \approx \frac{(ct)^3}{G}H^2 \approx \frac{c^3 t}{G} \approx 10^{15}\mathrm{g}\left(\frac{t}{10^{-23}\mathrm{s}}\right). \tag{III.2}$$

Hence, lighter PBH are formed at early times. Planck mass PBH would have formed around a few Planck seconds after the big bang, while PBH forming at nucleosynthesis, $t = 1$s, would have a mass $m \approx 10^5 M_\odot$. I refer to [80] and [79]for details. By accretion of the surrounding matter, a stellar black hole or a PBH can substantially increase its mass, however certainly not by many orders of magnitudes (see [50] and references therein). Still, it is remarkable that the mass spectrum of black holes is surprisingly wide: there is only very few physical systems that 'exist' over so many orders of magnitudes (with respect to their energy scale or size).

Thanks to very-long-baseline interferometry (VLBI) methods, there are observational evidences for supermassive black holes (MBH) located at the centers of several galaxies. These may originate from PBH as suggested by exotic models, or perhaps, more realistically, from the collapse of a dense gas cloud followed by accretion [26]. The most famous one is the radio source SgrA* in the nuclear star cluster in the central light years of the Milky Way. The radio emission pattern of SgrA* is indeed consistent with that of a rotating ionized gas around a MBH of about $4.4 \times 10^6 M_\odot$. In fact, current observations rule out all plausible astrophysical alternatives to a MBH [75]. Forthcoming astronomical observations of the Milky Way center even have the potential to probe the strong curvature of GR, in the vicinity of the Schwarzschild radius of SgrA*, by tracking the orbiting stars [94]. Most recent observation are at the level of about six Schwarzschild radii [95].

The phenomenology of the event horizon of black holes is the subject of this chapter, and the main question we are interested in is: Can quantum gravity affect the history of a black hole and have an impact on the physical phenomena occurring near the horizon?

III.3 The event horizon: a door to quantum gravity

In 1974, Stephen Hawking was able to derive one of the major predictions of theoretical physics of the last decades [83]. Building on the earlier work by Bekenstein, he found that the horizon of a black hole of mass m, constantly radiates a thermal distribution of particles at temperature

$$T_{\mathrm{H}} = \frac{\hbar c^3}{8\pi G k_{\mathrm{B}} m}. \tag{III.3}$$

As a black hole radiates, it evaporates. In other words, the area, A, of its event horizon shrinks until it disappears. Actually, the results obtained by Bekenstein and Hawking show that black holes may be seen as thermodynamical systems, completely described by a few *macroscopic* parameters (no-heir theorem [58]). As put by Rovelli, this can be heuristically appreciated by noticing that: "a black hole is a system with a horizon that screens information, precisely as the description of a system by macroscopic parameters does". For a Kerr-Newman black hole, the *macroscopic* parameters are its mass, m, the area of the event horizon, A, its charge Q and its angular momentum J. The first law of black hole thermodynamics, relates the variation of the mass to the area of the event horizon, the charge and the angular momentum as

$$\delta m = \tfrac{1}{4} T_{\text{H}} \delta A + \omega \delta J + \phi \delta Q, \tag{III.4}$$

where ω is the angular velocity of the horizon and ϕ the electric potential. While the entropy (Bekenstein-Hawking) of a black hole is simply

$$S_{\text{BH}} = \tfrac{1}{4} A. \tag{III.5}$$

Hence, for a black hole at thermal equilibrium, the second law implies $\delta A > 0$. Hawking's results illustrates beautifully the unification of thermodynamics, gravity and the quantum theory. A derivation of the entropy of black holes from statistical physics is an important test for a quantum theory of gravity.

This exercise has been carried out successfully in Loop Quantum Gravity, the problem is that there seem to still be an ambiguity for the correct manner to arrive at the Bekenstein Hawking result (III.5). In particular, some argue that the Bekenstein-Hawking entropy can be recovered in LQG provided one sets the Barbero Immirzi parameter to a precise value $\gamma = 0.274$ [118], while others argue that one can arrive at the black hole entropy formula in a γ independent way [36, 30, 84]. This has quite important consequences for Loop Quantum Cosmology, as the peculiar features of the bouncing scenario depend strongly on the value of γ. See for instance [29] where the author consider a LQC model with a complex Barbero Immirzi parameter, $\gamma = i$.

Closing this parenthesis, and back to black hole phenomenology, we see that due to Hawking evaporation, black holes are potentially an important source of energy release in the cosmos. A simple calculation shows that a black hole of mass m evaporates completely in a time

$$\tau\,(m) \approx 10^{64} \left(\frac{m}{M_{\odot}}\right)^{3} \text{yr}. \tag{III.6}$$

In particular, a primordial black hole with a mass smaller than 10^{15}g would already have evaporated today and released all its energy in the form of Hawking radiation. This phenomenon can alter the cosmic history of the universe, especially the properties of the cosmic microwave background leading for instance to spectral distortions of the CMB temperature spectrum [55]. Hawking evaporation can also contribute to the γ ray background or even explain intense γ ray burst [50]. In turn, these astrophysical effects can be used, in light of the present measurements, in order to set constraints on the abundance of PBH in our universe and address the question of the fraction of the dark matter that could be in the form of PBH [51].

III.4 Black hole to white hole transition

In 2014, Carlo Rovelli, Francesca Vidotto, Hal Haggard and Aurélien Barrau proposed an evolution scenario for black holes that allows a black to white hole transition. The idea is that quantum gravitational effects may leak outside the Schwarzschild radius so that in-falling matter would avoid ending its journey into the central singularity but rather bounce out. Consider an observer at distance r_{obs} from the center $r = 0$ of a spherical collapsing shell of matter. With the Schwarzschild metric (III.1),

one can compute the time it takes for the collapsing shell to reach the radius $r < r_{\rm obs}$, as measured by the observer's clock. It is given by

$$\tau_{\rm obs} = \sqrt{1-\frac{r}{r_{\rm obs}}}\left\{(r_{\rm obs}-r) - r_{\rm s}\ln\left(\frac{r-r_{\rm s}}{r_{\rm obs}-r_{\rm s}}\right)\right\}, \tag{III.7}$$

where $r_{\rm s}$ is the Schwarzschild radius given in (III.1). Hence, the observer sees the shell slowing down as it gets closer and closer to the horizon. At the observer's location, the Kretschmann scalar is constant, $R^{abcd}R_{abcd} = 48r_{\rm s}^2/r_{\rm obs}^6$, and so is the curvature $\mathcal{R} \approx r_{\rm s}/r_{\rm obs}^3$. For an observer located far away from the Schwarzschild radius, $r_{\rm obs} \gg r_{\rm s}$, the curvature is vanishingly small and one expects no quantum gravity effect to happen at such distances. Even for an observer close to the Schwarzschild radius $r_{\rm obs} \gtrsim r_{\rm s}$, the curvature is $\mathcal{R} \approx 1/r_{\rm s}^2$ and one would naively expect that quantum gravity, which would become significant at curvature $\mathcal{R}_{\rm QG} = 1/\ell_{\rm Pl}^2$, does not have much chance to play any role. Indeed, forming the ratio

$$\mathcal{R}/\mathcal{R}_{\rm QG} = \ell_{\rm Pl}^2/r_{\rm s}^2 = m_{\rm Pl}^2/m^2, \tag{III.8}$$

we find that it is extremely small compared to one for, say, a solar mass black hole with $m \approx 10^{38} m_{\rm Pl}$. It is here that Rovelli and Haggard proposed in [81] to take something else into consideration: cumulative effects of quantum gravitational origin integrated over the time, $\tau_{\rm obs}$, of the event as seen by the observer at distance $r_{\rm obs}$. Then, on dimensional grounds, the relevant parameter for classicality is not $\mathcal{R}/\mathcal{R}_{\rm QG}$, but rather

$$x \equiv (\mathcal{R}/\mathcal{R}_{\rm QG}) \times (\tau_{\rm obs}/\tau_{\rm Pl})^n . \tag{III.9}$$

And we can now ask: at which distance from the horizon quantum gravitational effect may become manifest? This happens for the observer at the distance $r_{\rm QG}$ which maximizes x. Taking the derivative of x with respect to $r_{\rm obs}$ and equating it to zero one finds $r_{\rm QG} = r_{\rm s}\left(1+\frac{1}{6}n\right)$ in the limit $r \to r_{\rm s}$. Then, requiring $x \approx 1$ one finds a precise value for r which corresponds to a time $\tau = \alpha\,(m/m_{\rm Pl})^{2/n}$ where α is a numerical constant of order unity. There are good reasons to assume $n = 1$, as explained in [81]. This yields

$$r_{\rm QG} = \tfrac{7}{6} r_{\rm s}, \quad \text{and} \quad \tau = \alpha\,(m/m_{\rm Pl})^2 . \tag{III.10}$$

We conclude that quantum gravity may affect the *exterior* of a black hole ($r_{\rm QG} > r_{\rm s}$) after a time of order m^2. Quantum gravity effects leaking outside the Schwarzschild radius have been discussed recently by a number of authors belonging to diverse quantum gravity communities, *e.g.* Mazur and Mottola's gravitational condensate stars [117], firewalls [13] or Gidding's metric fluctuations [76]. The latter two being motivated by solutions to the famous information loss paradox for black holes.

In what follows, I shall focus on a scenario motivated by Loop Quantum Gravity: singularity resolution and transition amplitude from black to white hole. Indeed, the final step undertaken by Haggard and Rovelli is to suggest that these leaking quantum gravity effects lead to the avoidance of the singularity. The in-falling shell of matter bounces out due to quantum gravity, analogous to the bouncing scenario for the universe in loop quantum cosmology. In classical GR, the singularity theorems of Hawking and Penrose do not allow for the existence of a solution to Einstein's equation featuring a black hole to white hole transition. However, it is strongly expected that quantum gravity may allow such situation. Considerable efforts are being deployed in this direction by Rovelli, Christodolou and Speziale. They are currently developing the tools to compute the transition amplitude from two quantum geometrical state that would realize this transition in Loop Quantum Gravity [57]. The final goal is to derive the relationship between the mass of the "bouncing black hole" and the bouncing time τ, maybe confirming the educated guess $\tau \propto m^2$. These bouncing black holes have been called Planck Stars in the literature. If the educated guess, $\tau \propto m^2$, proves to be correct, the phenomenology of Planck Stars becomes very rich: they bounce before they have time to evaporate via Hawking radiation ($\tau \propto m^3$). Then, we can hope to detect the radiation emitted subsequently to the bounce in the form of cosmic rays, or spectral distortions of the CMB radiation.

III.5 Results and articles

In the remainder of this chapter I report two articles were we studied the the detectability of Planck stars based on cosmic ray measurements, under different assumptions.

In the first article, *Phenomenology of bouncing black holes in quantum gravity: a closer look*, we consider different values of bouncing time by varying the proportionality constant α (called k in the articles) in the relationship (III.10) between the time and the mass of the Planck star. We show that, in general, the observationally interesting Planck stars have a small mass (compared to the solar mass).

Indeed, the Planck stars of interest are the one which have already bounced. So they would correspond to primordial black holes formed during the early universe. We consider two different scenarios for the outgoing emission following the bounce. In both scenario, the energy is released spontaneously all at once, unlike for Hawking evaporation. However, in the first scenario we consider a radiation emitted at a wavelength $\lambda \sim m$, while in the second scenario we assume that the outgoing radiation is still at the temperature of the collapsing matter that formed the Planck star. In this case, the Planck Star is literally a time machine that sends a patch of the primordial universe to the future, while the surrounding space has had time to cool down by many orders of magnitudes due to the expansion of the universe. Given the size of the present detectors (telescopes), and accounting for the possible absorption of the radiation by scattering with the cosmic infrared background, we study the study the maximal distance at which a single Planck Star may be seen. Finally, we consider the situation of a diffuse background of cosmic rays coming from a distribution of Planck stars after we have specified a mass spectrum for these objects.

In the second article, *Bouncing black holes in quantum gravity and the Fermi gamma-ray excess*, we ask wether the gamma ray excess coming from the galactic center could be explained by the Planck Star scenario. The answer is yes and in addition, the signal corresponding to Planck stars has a redshift dependency that may be used to discriminate between the Planck Star hypothesis and other astrophysical sources.

Phenomenology of bouncing black holes in quantum gravity: a closer look

Aurélien Barrau,[1,*] Boris Bolliet,[1,†] Francesca Vidotto,[2,‡] and Celine Weimer[1,§]

[1] *Laboratoire de Physique Subatomique et de Cosmologie, Université Grenoble-Alpes, CNRS-IN2P3 53,avenue des Martyrs, 38026 Grenoble cedex, France*

[2] *Radboud University, Institute for Mathematics, Astrophysics and Particle Physics Mailbox 79, P.O. Box 9010, 6500 GL Nijmegen, The Netherlands*

(Dated: February 22, 2016)

It was recently shown that black holes could be bouncing stars as a consequence of quantum gravity. We investigate the astrophysical signals implied by this hypothesis, focusing on primordial black holes. We consider different possible bounce times and study the integrated diffuse emission.

I. THE MODEL

A new possible window for observing quantum gravitational effects has been recently pointed out in [1] (some details were refined in [2]). The idea is grounded on a result of loop cosmology [3]: when matter or radiation reaches the Planck density, quantum gravity generates a sufficient pressure to counterbalance the classically attractive gravitational force. In a black hole, matter's collapse could stop before the central singularity is formed. The standard event horizon of the black hole can be replaced by an apparent horizon [4] which is locally equivalent to an event horizon, but from which matter can eventually bounce out. The model is not specific to loop quantum gravity (for instance a similar scenario can be realized in asymptotic safety [5]). The case of non-singular black holes has been investigated by many authors [6–24].

A heuristic description of the model we are studying can be given as follows. When the density of matter becomes high enough, quantum gravity effects generate sufficient pressure to compensate the matter's weight, the collapse ends, and matter bounces out. A collapsing "black hole" might avoid sinking into the $r = 0$ singularity, as much as an electron in a Coulomb potential does not sink all the way into $r = 0$ because of quantum mechanical effects. The picture is close to Giddings's remnant scenario [25] but with a macroscopic remnant developing into a white hole.

The phenomenology associated with this scenario was considered in [26], opening the fascinating possibility to detect quantum gravity effects far below the Planck energy. It was shown there that primordial black holes (PBHs) could generate a signal in the 100 MeV range, possibly compatible with very fast gamma-ray bursts [27]. Observability is made possible by the amplification due to the large ratio of the black hole lifetime over the Planck time [28].

The scenario was developed in [29] with the discovery of an explicit metric satisfying Einstein's equations everywhere outside the quantum region. The model describes a quantum tunneling from a classical in-falling black hole to a classical emerging white hole. The process is seen in extreme "slow motion" from the outside because of the huge time dilatation inside the gravitational potential: this is why massive black holes would appear to us as long living black holes. Only light black holes –as primordial black holes– are expected to yield observational signatures of this model because the time required for the bounce to occur can then be smaller that the current age of the Universe.

Outside the horizon, the quantum effects are small at any time but their time integration can lead to important cumulative effects leading to a dramatic revision of the usual scenario. After a sufficiently long time, the black hole can tunnel to a white hole. This phenomenon is similar to the cosmological bounce studied in loop quantum cosmology [30] where a contracting universe tunnels into an expanding one.

Some authors have considered the possibility that the matter collapsing inside a black hole could bounce out in a different universe, namely with a different future asymptotic region. The scenario we are considering is simpler and more conservative: the white hole "fireworks" emerging from the bouncing black hole takes place where the black hole is. The crucial point demonstrated in [29] is that such a simple minimal evolution is *possible*: the white hole horizon can be in the future of the black hole horizon, bounding the same external Schwarzschild region with nothing dramatic happening in the surrounding universe. This unexpected possibility is obtained by carving out the relevant solution from a double covering of the Kruskal metric (where the black hole horizon is in the future of the white hole horizon). This scenario opens the possibility that signals from exploding black

*Electronic address: aurelien.barrau@cern.ch
†Electronic address: boris.bolliet@ens-lyon.fr
‡Electronic address: fvidotto@science.ru.nl
§Electronic address: celinew@kth.se

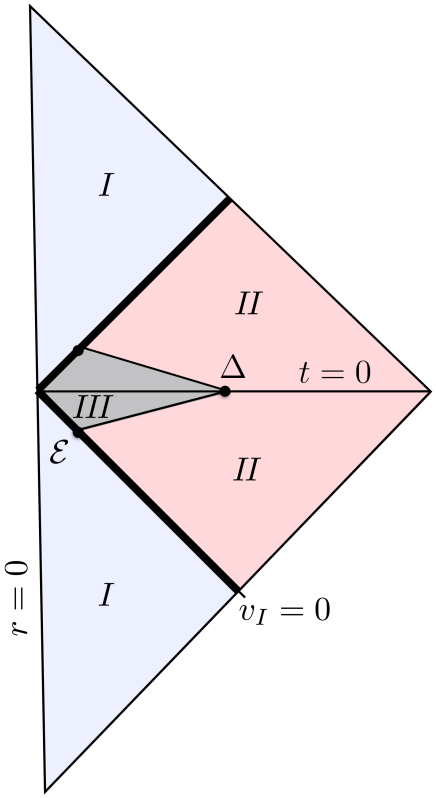

FIG. 1: Penrose diagram of a bouncing black hole, from [29].

holes can be detected and keeps the number of hypotheses at its minimum.

The metric found in [29] is indeed locally isometric to the Kruskal solution (outside the quantum region), but it is, actually, a portion of a double cover of the Kruskal solution. Fig. 1 represents a bouncing star where the "$t = 0$" hyperplane is the surface of reflection of the time reversal symmetry in the simplified case of a collapsing null shell. There are two important points (detailed definitions are given in [29]), Δ and $\mathcal{E}$: the point Δ at $t = 0$ is the maximal extension in space of the region where the Einstein field equations are violated, whereas point $\mathcal{E}$ is the first moment in time where this happens. Region (I), inside the bouncing shell, must be flat by Bhirkoff's theorem. Region (II), again by Bhirkoff's theorem, must be a portion of the maximal extension of the Schwarzschild metric for a mass M. Region (III) is where quantum gravity becomes non-negligible.

Because of spherical symmetry, one can use coordinates (u, v, θ, ϕ) with u and v null coordinates in the r-t plane and the metric is determined by two functions:

$$ds^2 = -F(u,v)dudv + r^2(u,v)(d\theta^2 + \sin^2\theta d\phi^2). \quad (1)$$

In these coordinates (in this case called Kruskal–Szekeres coordinates), the Kruskal metric is obtained by taking

$$F(u,v) = \frac{32M^3}{r} e^{\frac{r}{2m}}, \quad (2)$$

with r the function of (u, v) defined by

$$\left(1 - \frac{r}{2m}\right) e^{\frac{r}{2M}} = uv. \quad (3)$$

The region of interest is bounded by a constant $v = v_o$ null line drawn thicker in Figure 1. This constant is a fundamental parameter of the metric under consideration. The key result of [29] is that, by gluing the different parts of the effective metric, and computing the minimal time for quantum gravitational effects to pile up in the region outside the horizon, one obtains an estimate for the bounce duration:

$$\tau = -8m \ln v_o > \tau_q = 4p\, M^2, \quad (4)$$

where p was estimated in [29] to be of the order of 0.05. We use Planck units where $G = \hbar = c = 1$. The bounce time is therefore proportional to M^2, whereas the time of the Hawking evaporation is proportional to M^3. Let us write the actual bounce time as $x\tau_q$ with $x > 1$. This leads to

$$\tau = 4kM^2 \quad (5)$$

with $k \equiv xp > 0.05$. As the Hawking evaporation is assumed (in this model) to be a small dissipative process that can be neglected at first order, k cannot be taken arbitrarily large. If k is too large the bouncing time becomes comparable to the Hawking time and the model fails. Therefore, there exists a given interval (which, in principle, depends on M) of values of k for which the scenario is consistent. Unfortunately, this interval is very large. In this article we investigate all possibilities by considering the whole range of the possible values of k, yielding different characteristics for the observable signals.

The basic phenomenology was investigated in [31] where k was assumed to take its smallest possible value, that corresponds to the shortest bounce. The aim of the present article is to go beyond this first study, following in two directions. First, we generalize the previous results by varying k. The assumption that the bounce time remains smaller than the Hawking time is supported by the "firewall argument" presented in [1], in the sense that it allows to solve the information paradox without requiring something particular to happen at the horizon (the equivalence principle is therefore respected). We study in detail the maximal distance at which a single black-hole bounce can be detected. Second, we go beyond the "single event detection" and consider the diffuse emission produced by a distribution of bouncing black holes on cosmological scales.

II. SINGLE EVENT DETECTION

For detection purposes, we are interested in black holes with a lifetime that is less than the age of our universe. Therefore, for a PBH detected today, this condition translates into $\tau = t_H$ where t_H is the Hubble time.

This fixes the mass M, as a function of the parameter k (defined in the previous section). In all the considered cases, M remains very small compared to a solar mass and would correspond to PBHs possibly formed in the early Universe. Although no PBH has been detected to date, various mechanisms for their production shortly after the Big Bang have been suggested (see, *e.g.*, [33] for an early detailed calculation and [34] for a review). Although their number density might be way too small for direct detection, the production of PBHs remains a quite generic prediction of cosmological physics either directly from density perturbations –possibly enhanced by phase transitions– or through exotic phenomena like the collapse of string loops generated by string self-intersections or collisions of bubbles of false vacua.

The energy (and amplitude) of the signal emitted in the quantum gravity model considered here remains an open issue. As suggested in [31] and to remain general, we consider two possible signals of different origins. The first one, referred to as the *low energy* signal, is determined by dimensional arguments. The white hole horizon from which matter emerges has size $L \approx 2M$ and its emission, in the metric studied in [29], is instantaneous. It is natural to expect that the signal of an exploding object includes a component with a wavelength equal to its size. This is the main scale of the problem and it fixes an expected wavelength for the emitted radiation: $\lambda \approx L$. At this stage no detailed astrophysical model is available for this component. It should be noticed that although the instantaneous Hawking radiation is also emitted with a wavelength of order $L \approx 2M$, the Hawking evaporation is a quasi-continuous process while the phenomenon we are considering here is a tunneling-like phenomenon: a sudden explosion where the entire energy of the hole is emitted together. The two phenomena are therefore very different when considering the time integrated spectra. The signal we are considering, in particular, is different from what was investigated in [32], except for some particular values of k. This has been studied in [26]. We assume that particles are emitted at the prorata of their number of internal degrees of freedom. (This is also the case for the Hawking spectrum in the optical limit, *i.e.* when the greybody factors describing the backscattering probability are spin-independent.)

The second signal, referred to as the *high energy* component, has a very different origin. Consider the history of the matter emerging from a white hole: it comes from the bounce of the matter that formed the black hole by collapsing. In most scenarios there is a direct relation between the initial mass M of a PBH and the temperature of the Universe when it was formed (see [35] for a review). The black hole mass, M, should be of the order of the horizon mass[1], M_H:

$$M \sim M_H \sim t. \tag{6}$$

The cosmic time t is related to the temperature of the Universe T by

$$t \approx 0.3 g_*^{-\frac{1}{2}} T^{-2}, \tag{7}$$

where $g_* \approx 100$ is the number of degrees of freedom. Once k is fixed, M is fixed (by $\tau \approx t_H$) and T is therefore known. As the process is time-symmetric, what comes out from the white hole should be what went in the black hole, re-emerging at the same energy: a blackbody spectrum at temperature T. Intuitively, the bouncing black hole plays the role of a "time machine" that sends the primordial universe radiation to the future: while the surrounding space has cooled down to 2.7K, the high-energy radiation emerges from the white hole with its original energy.

When the parameter k is taken larger than its smallest possible value, which is fixed by the requirement that quantum effects are important enough to lead to a bounce, the bounce time becomes larger for a given mass. If this time is assumed to be equal to the Hubble time (or slightly less if we focus on black holes bouncing far away), this means that the mass has to be smaller. The resulting energy will then be higher for both the *low energy* and the *high energy* signals, but for different reasons. In the first case, this is because of the smaller size of the hole, leading to a smaller emitted wavelength. In the second case, the reason is a bit more subtle: the primordial black hole has to be formed earlier, when the Hubble mass was smaller, and the temperature of the Universe was therefore higher. Importantly, we will show later that although both signals vary in the same "direction" as a function of k, they do not have the same k-dependence.

The first question to be addressed is the maximal distance at which one could observe a bouncing black hole. We focus on emitted photons as, unlike charged cosmic-rays, they travel in straight lines and therefore allow for a precise determination of the event location. When k varies from its minimum value (≈ 0.05, determined for the quantum effects to cumulate and the bounce to take place) to its maximum value ($\approx 10^{22}$, determined for the bounce time to remain smaller than Hawking time), the energy of the emitted signal varies over many orders of magnitude.

The resulting detectability depends on several factors:

- *The size of the detector (and its detection efficiency).* In the infrared, ultra-violet, X-rays and

[1] Other more exotic models, *e.g.* collisions of cosmic strings or collisions of bubbles associated with different vacua, can lead to different masses at a given cosmic time. We will not consider them in this study.

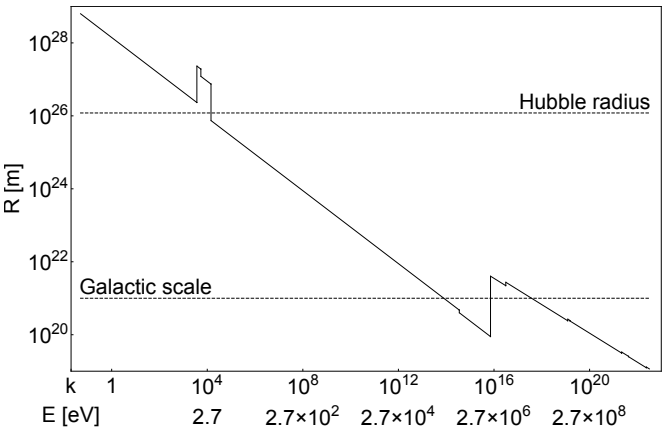

FIG. 2: Maximum distance at which a bouncing black hole can be detected in the *low energy* channel as a function of the parameter k (the associated signal energy is also given). The upper horizontal dashed line represents the Hubble radius and the lower one represents the Galactic scale.

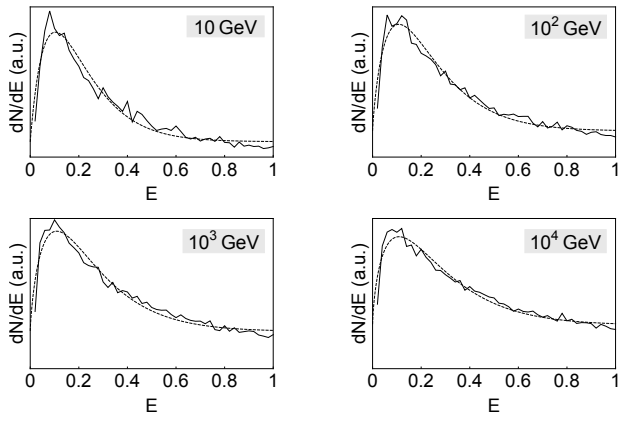

FIG. 3: Histograms of gamma-rays produced by jets of quarks at 10, 100, 1000, and 10000 GeV. The smooth curves are the fits used in the following analysis whereas the other curve is the output of the Monte-Carlo simulation with 10000 events. The energies of the x axis are given in GeV.

soft gamma-rays, only satellites can be used as the atmosphere is not transparent. This fixes the size around an order of magnitude close to a meter. In the optical domain, larger ground-based telescopes are available (around ten meters). For hard gamma-rays the size of the instrument is no longer relevant, what matters is the size of the Cherenkov shower induced by the high-energy photon. This increases the size to roughly a hundred meters.

- *The absorption during the propagation over cosmological distances.* Although some subtleties do appear at several energies, the Universe is mostly transparent up to TeV energies where pair production of leptons becomes possible through interactions with the cosmic infrared background $\gamma_{TeV} + \gamma_{IR} \to e^+ + e^-$. The absorption is basically exponential above the threshold energy (corresponding to twice the electron mass in the center-of-mass frame of the interaction).

- *The number of measured photons required for the detection to be statistically significant,* that is to be several standard deviations above the background fluctuations. This is also energy-dependent. For example, although a few synchronous measured gamma-rays are enough for a detection in the 100 GeV range –where the background is very low– many more are required in the optical band. Not only because the diffuse background is much higher at lower energies, but also because measurements require a substantial integration time that makes the determination of the accurate arrival timing impossible. We have only used crude approximations for the galactic and extragalactic backgrounds assuming that the line of sight aways lies outside the galactic plane. A more careful analysis would be important in the future.

Figure 2 represents the maximum distance at which a bouncing black hole can be seen in the *low energy* channel, calculated by taking into account all the above-mentioned phenomena. Several effects of different origins can be observed. The large step around $k = 10^4$ is associated with the larger size of ground based optical telescopes. The little steps decreasing the distance are associated with the fact that the mean energy of the signal emitted by the bouncing black hole becomes higher than the mass of a new particle: this new particle can then be emitted and if it does not decay into photons, the percentage of produced photons inevitably decreases (and so does the maximum distance). An important step in the opposite direction occurs around $k = 10^{16}$. This is due to the fact that quarks begin to be emitted. Then, the most important source of gamma-rays emitted by the bouncing black hole is no longer the direct emission –that is photons emitted as such by the PBH– but instead the one coming from the decay of neutral pions (whose lifetime is negligible here) produced in the fragmentation process of the emitted partons. To take this into account, we have used the Pythia program [36], which is a standard tool for the generation of events in high-energy collisions, comprising a coherent set of physics models for the evolution from a few-body hard process to complex multiparticle final states. It incorporates a large number of hard processes, models for initial and final state parton showers, matching and merging methods between hard processes and parton showers, multiparton interactions, beam remnants, string fragmentation and particle decays. It is based on the Lund model [37]. Although most previous approaches have used cruder analytical approximations, this way of treating the quark and gluon emission is

not new and was also implemented in the study of hadron production by primordial black holes: as soon as the black hole temperature becomes higher than the quantum chromodynamics (QCD) confinement scale, those processes inevitably have to be taken into account [38]. In a high-energy hadronic process, a very large number of pions can be generated. As nearly each neutral pion will decay into two photons, this mechanism –called "indirect" or "secondary" emission– will, by far, dominate the gamma-ray production. In Fig. 2, little steps increasing the maximum distance can also be seen. They are due to the fact that the available energy reaches a new threshold corresponding to the possible emission of a new quark –because the black hole size becomes smaller than its inverse mass– that will produce gamma-rays in its hadronization. This leads to more gamma-rays (whereas at lower energies, or lower values of k, the emission of new particles was only associated with a lower gamma-ray rate).

Figure 3 shows the histograms obtained using Pythia for different jet energies. The smooth curves corresponds to the fits used in the analysis. It is interesting to note that increasing the available energy increases the number of generated gamma-rays and the mean energy of the histogram but not the position of the peak in the distribution which is associated with π^0 particles generated at rest in the galactic frame.

Figure 4 represents the maximum distance at which a bouncing black hole can be seen in the *high energy* channel. The lower curve represents the direct emission of gamma-rays and the higher one represents gamma-rays coming from the decay of unstable hadrons. As expected, the latter dominates. For this signal, there is no threshold effect associated with masses as the effective temperature of the process is in any case well above the QCD confinement scale.

The largest distance is given, for any k, by $d = inf\{d_{hor}, sup\{d_{direct}, d_{decay}\}\}$ where d_{decay} is the maximum distance for the photons associated with the secondary emission while d_{direct} is the one associated with the direct emission and d_{hor} is the horizon at the considered energy. Photons cannot come from arbitrary long distance and are limited by an effective horizon ranging from around a Gpc for photons in the 100 GeV - 1 TeV range to a few Mpc at 100 TeV because of their interactions with the diffuse background. Above this energy, interactions with the CMB become possible and the horizon can decrease to a few kpc only around 1000 TeV. This effect does not happen for the indirect emission which takes place at a lower energy where the Universe is quite transparent. Although the effective surface of detectors (due to Cherenkov showers) is much higher at high energy this does not compensate for the limited flux. The flux is small at high energy for two reasons. First, because it is associated with smaller PBH masses, making the total energy available smaller. Second, because the energy carried out by each emitted photon is higher, making their number smaller even for the same total available energy.

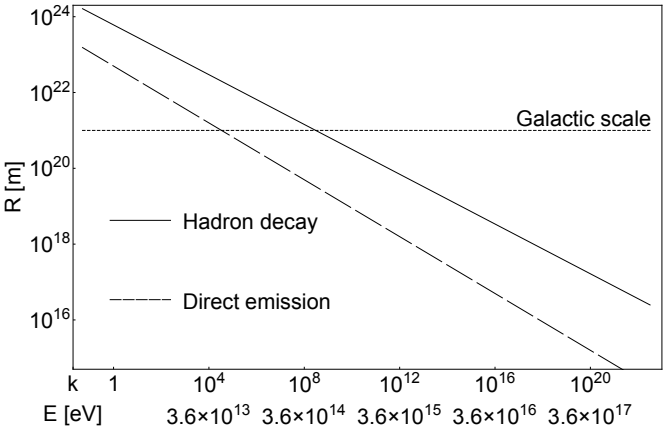

FIG. 4: Maximum distance at which a bouncing black hole can be detected in the *high energy* channel as a function of the parameter k (the associated signal energy is also given). The horizontal dashed line represents the Galactic scale. The lower line corresponds to the direct emission and the upper one to the decay of unstable hadrons produced by jets of quarks and gluons. Interestingly, the slope is not exactly the same for both signals.

It is interesting to investigate analytically the k dependence of both signals. In both cases, one can use the following approximation for the relationship between time and redshift:

$$t \approx \frac{2H_0^{-1}}{3\Omega_\Lambda^{1/2}} \sinh^{-1}\left[\left(\frac{\Omega_\Lambda}{\Omega_M}\right)^{\frac{1}{2}}(1+z)^{-\frac{3}{2}}\right], \qquad (8)$$

where H_0 is the Hubble constant, Ω_Λ is the normalized dark energy density, and Ω_M is the normalized matter density. Requiring this time to be equal to the bounce time $4kM^2$ leads, for the measured *low energy* signal, to

$$\lambda_{low}^{meas} \approx 2\,(1+z)\sqrt{\frac{H_0^{-1}}{6k\Omega_\Lambda^{1/2}} \sinh^{-1}\left[\left(\frac{\Omega_\Lambda}{\Omega_M}\right)^{\frac{1}{2}}(1+z)^{-\frac{3}{2}}\right]}. \qquad (9)$$

The same reasoning can be applied to the *high energy* signal. To fix orders of magnitude, one can write $\lambda \approx \frac{2\pi}{k_B T}$ where k_B is the Boltzmann constant and T is the temperature of the Universe at the formation time. Gathering everything, this leads to

$$\lambda_{high}^{meas} \approx \frac{2\pi}{k_B T} \frac{(1+z)}{(0.3 g_*^{-1})^{\frac{1}{2}}} \left[\frac{H_0^{-1}}{6k\Omega_\Lambda^{1/2}} \sinh^{-1} \left[\left(\frac{\Omega_\Lambda}{\Omega_M} \right)^{\frac{1}{2}} (1+z)^{-\frac{3}{2}} \right] \right]^{\frac{1}{4}}. \quad (10)$$

Although the mean wavelength does decrease as a function of k in both cases, it does not follow the same general behavior. It scales with $k^{-\frac{1}{2}}$ for the low energy component and as $k^{-\frac{1}{4}}$ for the high energy one.The following conclusions can be drawn:

- The *low energy* channel leads to a better single-event detection than the *high energy* channel. Although a lower energy dilutes the signal in a higher astrophysical background, this effect is over-compensated by the larger amount of photons.
- The difference of maximal distances between the *low-* and *high energy* channels decreases for higher values of k, *i.e.* for longer black-hole lifetimes.
- In the *low energy* channel, for the smaller values of k, a single bounce can be detected arbitrary far away in the Universe.
- In all cases, the distances are large enough and experimental detection is far from being hopeless.

III. INTEGRATED EMISSION

In addition to the instantaneous spectrum emitted by a single bouncing black hole, it is interesting to consider the possible diffuse background due to the integrated emission of a population of bouncing black holes. Formally, the number of measured photons detected per unit time, unit energy and unit surface, can be written as:

$$\frac{dN_{mes}}{dEdtdS} = \int \Phi_{ind}((1+z)E, R) \cdot n(R) \cdot A(E) \cdot f(E,R) dR, \quad (11)$$

where $\Phi_{ind}(E,R)$ denotes the individual flux emitted by a single bouncing black hole at distance R and at energy E, $A(E)$ is the angular acceptance of the detector multiplied by its efficiency, $f(E,R)$ is the absorption function, and $n(R)$ is the number of black holes bouncing at distance R per unit time and volume. The distance R and the redshift z entering the above formula are linked. The integration has to be carried out up to cosmological distances and it is therefore necessary to use exact results behind the linear approximation. The energy is also correlated with R as the distance fixes the bounce time of the black hole which, subsequently, fixes the emitted energy.

It is worth considering the $n(R)$ term in more details. If one denotes by $\frac{dn}{dMdV}$ the initial differential mass spectrum of primordial black holes per unit volume, it is possible to define $n(R)$ as:

$$n(R) = \int_{M(t)}^{M(t+\Delta t)} \frac{dn}{dMdV} dM, \quad (12)$$

leading to

$$n(R) \approx \frac{dn}{dMdV} \frac{\Delta t}{8k}, \quad (13)$$

where the mass spectrum is evaluated for the mass corresponding to a time $(t_H - \frac{R}{c})$. The shape of the mass spectrum obviously depends on the details of the formation mechanism (see [39] for a review on PBHs and inflation). As an example, we shall assume that primordial black holes are directly formed by the collapse of density fluctuations with a high-enough density contrast in the early Universe. The initial mass spectrum is then directly related to the equation of state of the Universe at the formation epoch. It is given by [33, 40]:

$$\frac{dn}{dMdV} = \alpha M^{-1-\frac{1+3w}{1+w}}, \quad (14)$$

where $w = p/\rho$. In a matter-dominated universe the exponent $\beta \equiv -1 - \frac{1+3w}{1+w}$ takes the value $\beta = -5/2$. The normalization coefficient α will be kept unknown as it depends on the details of the black hole formation mechanism. For a sizeable amount of primordial black holes to form, the power spectrum normalized on the CMB needs to be boosted at small scales. The formula given above might therefore be correct only within a limited interval of masses. The idea is that the mass spectrum takes a high enough value in the relevant range whereas it is naturally suppressed at small masses by inflation. We will neither study those questions here (focusing on the shape of the resulting emission), nor the normalisation issues which depend sensitively on the bounds of the mass spectrum, that are highly model-dependent. As this part of the study is devoted to the investigation of the shape of the signal, the y axis on the figures are not normalized. As we show below, the shape of the signal is quite independent on the shape of the mass spectrum, so Eq. 14 does not play any significant role for the computed spectra.

This is illustrated in Fig. 5 where different hypothesis for the exponent β are displayed. The electromagnetic spectrum induced by the distribution of bouncing black holes is almost exactly the same. Only one case ($\beta = -5/2$, corresponding to $w = 1/3$) is therefore

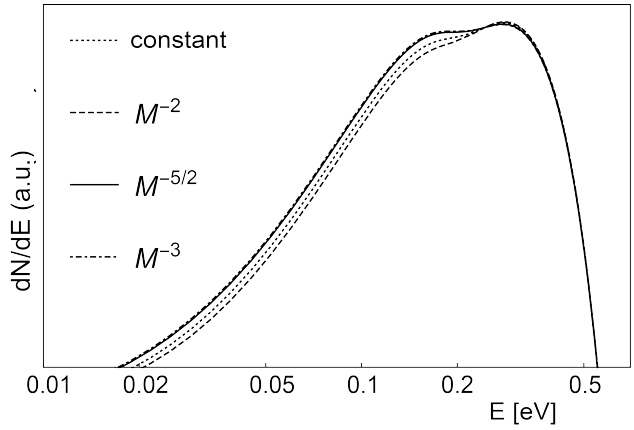

FIG. 5: *Low energy* channel signal calculated for different mass spectra. As the mass spectrum is not normalized, the units of the y axis are arbitrary.

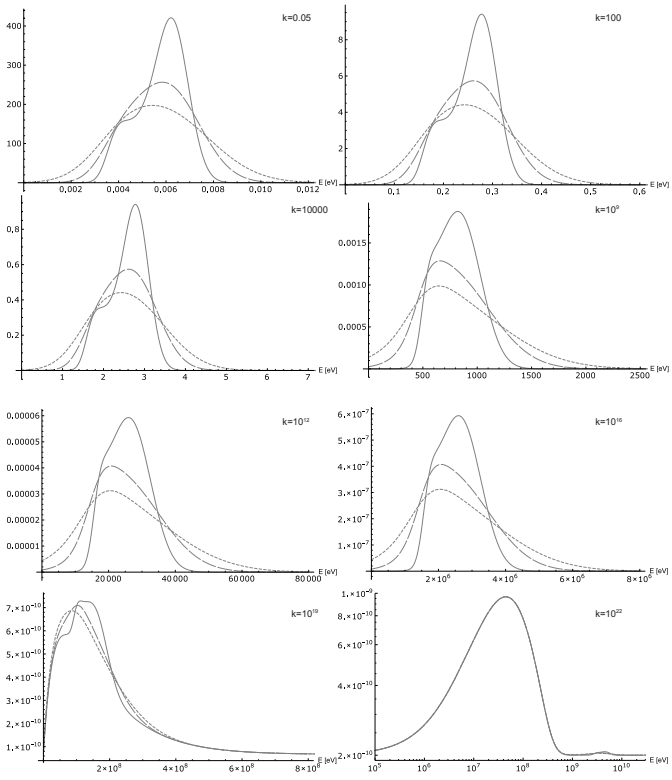

FIG. 6: Electromagnetic signal expected, in the *low-energy* channel, from a distribution of bouncing black holes respectively with $k = 0.05$, $k = 100$, $k = 10000$, $k = 10^5$, $k = 10^{12}$, $k = 10^{16}$, $k = 10^{19}$, $k = 10^{22}$. The plain line corresponds to $\sigma = 0.1E$, the dashed line to $\sigma = 0.2E$ and the dotted line to $\sigma = 0.3E$, where E is the mean energy of emitted signal. As the mass spectrum is not normalized, the units of the y axis are arbitrary.

considered in the following, leading to generic results. The black holes are assumed to be uniformly distributed in the Universe, which is a meaningful hypothesis as long as we deal with cosmological distances[2].

Once again, we consider the two different channels for the emitted signal. Let us begin with the *low energy* signal. The issues about the different components of the emitted photons, presented in the preceding section, are still accounted for in this part. Figure 6 displays the resulting signal on Earth for values of the parameter k varying from 0.05 (minimum) to 10^{22} (maximum) by carrying out the numerical integration of Eq. 11. The smallest value of k minimizes the bounce time whereas the largest one makes it comparable to the Hawking time. The last plot of Fig. 6 is in double logarithmic scale to improve the readability. On this plot, it is easy to distinguish the direct emission (on the right side) from the emission due to the decay of pions produced by the fragmentation of parton jets (on the left side). Obviously, the second strongly dominates. For smaller values of k, there is a little "bump" in the signal which is due to the non-linear redshift-distance relation leading to a kind of "accumulation" of the signal. In principle, by construction of the model, the direct emission is nearly monochromatic. This is however obviously an approximation and we have therefore considered three possible relative widths for the signal : $\sigma/E = 0.1$, $\sigma/E = 0.2$ and $\sigma/E = 0.3$ where E is the mean energy of emitted quanta. Those three hypotheses are displayed on the plots of Fig. 6.

We have also considered the *high energy* signal coming from radiation re-emitted at the energy at which it was absorbed in the early universe. In this case, the situation is better controlled as the spectrum of the signal is accurately known: it is simply given by a blackbody law at the temperature T of the plasma filling the Universe at the formation time of the black hole. As the shape of the signal is very weakly dependent on the value of k, we have just displayed the two extreme cases ($k = 0.05$ and $k = 10^{22}$) in Fig. 7 and Fig. 8. As it can be seen on the plots, the emission is strongly dominated by the gamma-rays coming from decaying neutral pions.

For both the *low energy* and the *high energy* signals the integration effect does not change much the signal as it would be expected from a single bouncing black hole. This is due to a "redshift-compensation" effect. When considering a black hole bouncing far away, the mean energy of its emitted signal (in its rest frame) is smaller for both the *low energy* and the *high energy* cases but, as explained before, for different reasons. In the first case,

[2] The local distribution of primordial black hole is expected to match dark-matter distribution.

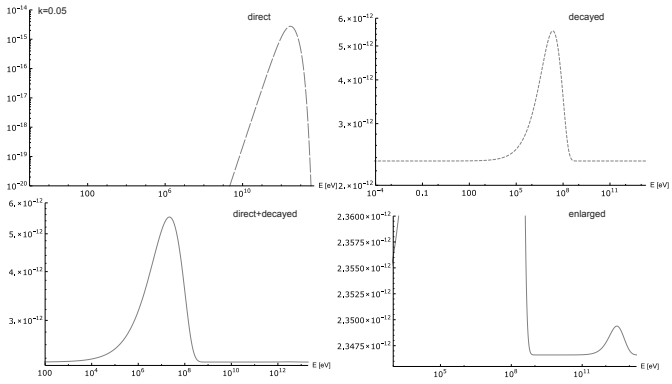

FIG. 7: Electromagnetic signal expected, in the *high-energy* channel, from a distribution of bouncing black holes with $k = 0.05$. The upper left plot corresponds to the direct emission, the upper right plot to the gamma-rays coming from the decay of neutral pions produced by jets of quarks. The lower left plot is the full signal. The lower right plot is a zoom on the direct emission part of the spectrum.

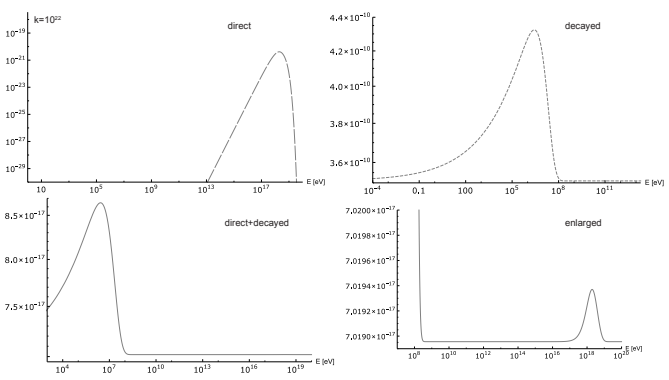

FIG. 8: Electromagnetic signal expected, in the *high-energy* channel, from a distribution of bouncing black holes with $k = 10^{22}$. The upper left plot corresponds to the direct emission, the upper right plot to gamma-rays coming from the decay of neutral pions produced by jets of quarks. The lower left plot is the full signal. The lower right plot is a zoom on the direct emission part of the spectrum.

this is because a black hole observed now and bouncing far away has a smaller lifetime, so that its initial mass is therefore smaller and so is its radius. As the emission wavelength is controlled by the size of the black hole, the emitted signal has a higher energy. It should also be underlined that the more distant the black hole, the smaller the number of emitted photons. This is not only because the total available energy (given by the mass of he black hole) is smaller but also because the individual energy of each photon is, in addition, higher. For the second case, the *high energy* emission, a black hole bouncing far away also has a smaller lifetime, hence a smaller initial mass: it was formed earlier in the history of the Universe (in the "standard" formation scenario we are considering), when the plasma was hotter. The emitted signal (which is the same as the absorbed one in this case) is higher in energy as well. In both cases, this higher emitted energy is partially compensated by the redshift, therefore reducing the distortion induced by the integration effect.

The conclusion is that the shape of the signal might be used as an observational signature of its specific origin in the *high energy* case. It looks indeed like a slightly distorted (by the redshift-distance integration) blackbody law that is not to be expected from any other known astrophysical effect. In the *low energy* case, the situation is less clear as the accurate shape (in particular width) on the signal is unknown but, still, quite generic features do appear in the figures, leading to some hope for detection.

It is still impossible to normalize these plots so as to compare them with the astrophysical background, whose spectral energy density roughly scales as $E^{-1/2}$, as this entirely depends on the percentage of dark matter made by PBHs and, more importantly, on the arbitrary choice of the bounds on the mass spectrum.

IV. CONCLUSION

The possibility that black holes are bouncing objects, suggested by quantum-gravity arguments, should be taken seriously. We have studied the individual bounce detectability and the integrated signal for all possible values of the bounce time. Some characteristic features emerge.

This study should be pushed forward in two directions. On the theoretical side, it would be very interesting to compute the quantum transition amplitudes between the contracting classical black hole solution and the expanding classical white hole solution [41]. Explicit models of quantum gravity, *e.g.* loop quantum gravity, do, in principle, make this calculation possible.

On the phenomenological side, it would be important to consider not only photons but also charged cosmic-rays that should be emitted by bouncing black holes as well. New experimental data are being made available (in particular by the AMS experiment onboard the International Space Station) and any predicted excess could be detectable in the near future. Although the signal looses its directionality and is confined to smaller scales, the enhancement by the galactic magnetic field could lead to promising detection perspectives. Finally, it would also be interesting to use known constraints on primordial black holes to investigate how they should be revised in this model, for different values of the k parameter.

[1] C. Rovelli & F. Vidotto, "Planck Stars", *Int. J. Mod. Phys. D 23* **12** (2014) 1442026.

[2] T. De Lorenzo, C. Pacilio, C. Rovelli, and S. Speziale, "On the Effective Metric of a Planck Star", *Gen. Rel. Grav.* **47** (2015) 41.

[3] A. Ashtekar, T. Pawlowski, and P. Singh, "Quantum Nature of the Big Bang", *Phys. Rev. Lett.* **96** (2006) 141301.

[4] A. Ashtekar & M. Bojowald, "Black hole evaporation: A paradigm", *Class. Quant. Grav.* **22** (2005) 3349.

[5] F. Saueressig, N. Alkofer, G. D'Odorico, and F. Vidotto, "Black holes in asymptotically safe gravity", *PoS* FFP **14** (2015) 174.

[6] J. M. Bardeen, " Non-singular general-relativistic gravitational collapse", in *Proc. Int. Conf. GR5, Tbilisi*, 174, 1968.

[7] V. P. Frolov and G. A. Vilkovisky, "Spherically Symmetric Collapse in Quantum Gravity", *Phys. Lett. B* **106** (1981) 307.

[8] T. A. Roman and P. G. Bergmann, "Stellar collapse without singularities?", *Phys. Rev. D* **28** (1983) 1265.

[9] R. Casadio, "Quantum gravitational fluctuations and the semiclassical limit", *Int. J. Mod. Phys. D* **9** (2000) 511.

[10] E. Ayon-Beato and A. Garcia, "The Bardeen model as a nonlinear magnetic monopol", *Phys. Lett. D* **493** (2000) 149.

[11] P. O. Mazur and E. Mottola, "Gravitational condensate stars: An alternative to black holes", gr-qc/0109035.

[12] I. Dymnikova, "Cosmological term as a source of mass", *Class. Quant. Grav.* **19** (2002) 725.

[13] S. A. Hayward, "Formation and evaporation of regular black holes", *Phys. Rev. Lett.* **96** (2006) 31103.

[14] L. Modesto, *Loop quantum black hole*, *Class. Quant. Grav.* **23** (2006) 5587.

[15] M. Visser, C. Barcelo, S. Liberati and S. Sonego, "Small, dark, and heavy: But is it a black hole?", PoSBHGRS (2008) 010.

[16] L. Modesto and P. Nicolini, "Charged rotating noncommutative black holes", *Phys. Rev. D* **82** (2010) 104035.

[17] B. Carr, L. Modesto, and I. Prémont-Schwarz,"Generalized Uncertainty Principle and Self-dual Black Holes", arXiv:1107.0708.

[18] K. Falls, D. F. Litim and A. Raghuraman, *Black Holes and Asymptotically Safe Gravity*, Int. J. Mod. Phys. A **27** (2012) 1250019

[19] C. Bambi and L. Modesto, "Rotating regular black holes", *Phys. Lett. B* **721** (2013) 329.

[20] C. Bambi, D. Malafarina and L. Modesto, "Non-singular quantum-inspired gravitational collapse", *Phys. Rev. D* **88** (2013) 044009.

[21] V. P. Frolov, "Information loss problem and a 'black hole' model with a closed apparent horizon", arXiv:1402.5446

[22] L. Mersini-Houghton, "Backreaction of hawking radiation on a gravitationally collapsing star i: Black holes?", *Phys. Lett. B* **16** (2014) 06.

[23] C. Bambi, D. Malafarina and L. Modesto, "Terminating black holes in asymptotically free quantum gravity", *Eur. Phys. J. C* **74** (2014) 2767.

[24] V. P. Frolov, "Mass-gap for black hole formation in higher derivative and ghost free gravity", *Phys. Rev. Lett.* **115** (2015), 051102.

[25] S. Giddings, "Black holes and massive remnants ", *Phys. Rev. D* **46** (1992) 1347.

[26] A. Barrau & C. Rovelli, "Planck Star Phenomenology", *Phys. Lett. B.* **739** (2014) 405.

[27] E. Nakar, "Short-Hard Gamma-Ray Bursts", *Physcis Report* **442** (2007) 166.

[28] G. Amelino-Camelia, "Quantum Spacetime Phenomenology" *Living Rev. Rel.* 16 (2013) 5.

[29] J.M. Haggard & C. Rovelli, "Black hole fireworks: quantum-gravity effects outside the horizon spark black to white hole tunneling ", *Phys. Rev. D* **92** (2015) 104020.

[30] A. Ashtekar, T. Pawlowski, and P. Singh. "Quantum nature of the big bang", *Phys. Rev. Lett.* **96** (2006)141301.

[31] A. Barrau, C. Rovelli, and F. Vidotto , "Fast Radio Bursts and White Hole Signals", *Phys. Rev. D. 90* **12** (2014) 127503.

[32] D.B. Cline, S. Otwinowski, B. Czerny, and A. Janiuk, "Does Very Short Gamma Ray Bursts originate from Primordial Black Holes? Review", arXiv:1105.5363

[33] B. J. Carr, "The primordial black hole mass spectrum,"*Astrophys. J.* **201** (1975) 1.

[34] A.M. Green, "Primordial Black Holes: sirens of the early Universe", arXiv:1403.1198 [gr-qc].

[35] B.J. Carr, K. Kohri, Y. Sendouda, and J. Yokoyama, "New cosmological constraints on primordial black holes", *Phys. Rev. D.*, **81** (2010) 104019.

[36] T. Sjöstrand *et al.*, "An Introduction to PYTHIA 8.2", arXiv:hep-ph/0212122.

[37] B. Andersson, S. Mohanty, and F. Soderberg ,"Recent developments in the Lund model", arXiv:1410.3012.

[38] J.H. MacGibbon & B.R. Webber, "Quark- and gluon-jet emission from primordial black holes: The instantaneous spectra", *Physical Review D* **41** (1990) 3052.

[39] B.J. Carr, J.H. Gilbert, and J.E. Lidsey, "Black hole relics and inflation: Limits on blue perturbation spectra ", *Physical Review D* **50** (1994) 4853.

[40] J.H. MacGibbon & B.J. Carr, "Cosmic rays from primordial black holes", *Astrophysical J.* **371** (1991) 447.

[41] C. Rovelli, "Planck stars and fast radio bursts", talk at the 3rd EFI winter conference on Quantum Gravity, Tux (2015)

Bouncing black holes in quantum gravity and the Fermi gamma-ray excess

Aurélien Barrau,[1,*] Boris Bolliet,[1,†] Marrit Schutten,[1,2,‡] and Francesca Vidotto[2,§]

[1] *Laboratoire de Physique Subatomique et de Cosmologie, Université Grenoble-Alpes, CNRS-IN2P3 53,avenue des Martyrs, 38026 Grenoble cedex, France*

[2] *Radboud University, Institute for Mathematics, Astrophysics and Particle Physics, Mailbox 79, P.O. Box 9010, 6500 GL Nijmegen, The Netherlands.*

(Dated: June 28, 2016)

Non-perturbative quantum-gravity effects can change the fate of black holes and make them bounce in a time scale shorter than the Hawking evaporation time. In this article, we show that this hypothesis can account for the GeV excess observed from the galactic center by the *Fermi* satellite. By carefully taking into account the secondary component due to the decay of unstable hadrons, we show that the model is fully self-consistent. This phenomenon presents a specific redshift-dependance that could allow to distinguish it from other astrophysical phenomena possibly contributing to the GeV excess.

INTRODUCTION

The Planck scale is currently out of reach from any direct local experiment by a factor of approximately 10^{15}. It is therefore hard to test quantum gravity. Many efforts have however been devoted to quantum gravity phenomenology in the last decade (see, *e.g.*, [1–3] and references therein for some general arguments) and it is not unreasonable to expect measurable consequences. Most efforts in the recent years have focused on the early Universe or on modified dispersion relations impacting the propagation of gamma-rays on huge distances. In this article, we focus on a recent result associated with black holes physics, first exposed in [4]. The main idea is grounded in a robust result of loop quantum cosmology: quantum gravity might manifest itself in the form of an effective pressure that counterbalances the classically attractive gravity when matter reaches the Planck density [5]. For a black hole, this means that matter's collapse could stop before the central singularity forms. The classical singularity is replaced in the quantum theory by a phase of maximum density – a "Planck star" [4]. The absence of the central singularity allows for the dynamical trapping horizon (shrinking of light surfaces) to be converted in an anti-trapping horizon (expanding of light surfaces), that releases matter and eventually disappears. This is a non-pertubartive quantum-gravity process that tunnels a classical black hole into a classical white hole. Because of the gravitational redshift, the process is almost instantaneous in proper time but appears as very long if measured by an external distant observer.

The viability of the model is supported by the existence of a classical metric satisfying the Einstein equations outside the spacetime region where matter collapses into a black hole and then emerges from a white hole[1] [7]. This can be achieved without violating causality nor the semiclassical approximation, as quantum effects piles up outside the horizon over a very long time.

The time quantum effects take to pile up outside the horizon determines the lifetime of the black hole, and its phenomenology. This was first investigated in [8] for a long lifetime (comparable but shorter than the Hawking evaporation time). Further studies in [9] and [10] were developed considering a wider range of possible lifetimes and the integrated signal coming from a diffuse emission.

The tunneling process connects two classically disconnected solutions. Einstein equations should therefore be violated during the evolution, but the model allows for a violation that takes place only over a finite region. This is where full quantum gravity dominates[2]. This process seems to be quite generically allowed for a wide range of viable quantum theories of gravity. Interestingly, in covariant loop quantum gravity (LQG) it is possible to perform the calculation of the tunneling amplitudes [14] that provides an estimation of the black-hole lifetime.

In this work, we address the puzzle posed by the observation by the *Fermi* telescope of a GeV photon excess, coming from the galactic center. Different explanations – including standard astrophysical sources – have been considered to explain it. Here we investigate whether bouncing (primordial) black holes could explain this specific excess and if this hypothesis has specific features that could allow to distinguish it from more conventional explanations.

In the first part, we briefly explain what are the pa-

[1] A modifications was suggested in [6] where the scenario was made asymmetric, with a black hole phase longer than the white hole one. Such a modification overcomes complications coming from a possible instability in the white-hole phase.

[2] A possibility could be to study an effective metric associated with this finite region, as originally done by Hayward [11]. See [12] for recent results in this direction, recently extended to rotating metrics [13].

rameters of the model and their possible values. In the second part, we present the way we have calculated and modeled the gamma-ray emission from bouncing black holes. In the third part we show the fit to the GeV *Fermi* excess we are interested in. In the fourth part, we suggest ways to discriminate our model from other possible explanations and normalize the masse spectrum. Some prospects are then discussed in the conclusion.

PARAMETERS OF THE MODEL

A precise astrophysical model for the emission from a bouncing black hole is not available, but heuristic arguments lead to consider two different emission mechanisms [9]. One, designated as the *low-energy* component, is grounded in a simple and conservative dimensional analysis. The mean energy of the emitted signal is assumed to be such that the corresponding wavelength matches the size of the horizon. This is a reasonable expectation, agreeing with the Hawking spectrum. The other one, designated as the *high-energy* component, has a smaller wavelength and depends on the conditions at which the black hole formed. In the model, the matter forming the black hole reemerges rapidly in the white-hole phase. The gravitational blueshift felt by radiation in the contracting phase is precisely compensated by the very same amount of redshift in the expanding phase.

If the considered model is correct, the bounce should take place for all kinds of black holes, but observable effects become experimentally accessible only for primordial black holes (PBHs), *i.e.* black holes that formed in the early universe with a potentially wide mass spectrum. In particular, they can form with with masses smaller than the Solar mass so that their bouncing time can be of the order of the age of the Universe (more massive black holes would require much more than the Hubble time to bounce and nothing would be visible). Studying the phenomenology of bouncing black holes, we are interested only by primordial black holes. Many different processes that can lead to the formation of black holes in the early Universe were suggested, see, *e.g.*, [15] for a recent review. In the simplest models, PBHs form by collapse of over-dense regions. Given the mass of a black hole, its formation time is then (approximately) known and so is the spectrum of the radiation that collapsed to form it – and that will emerge from the bounce in the *high-energy* component of the signal considered here.

The most important parameter of the model is the bouncing time of black holes. It can be written as [7]

$$\tau = 4kM^2, \tag{1}$$

in Planck units, where M is the mass of the black hole and k is a free parameter. This is a key-point: the bounce time scales as M^2 whereas the Hawking evaporation requires a time of order M^3. The parameter k is bounded from below at the value $k_{min} = 0.05$ which ensures that the quantum effects do pile up enough to appear outside of the black hole horizon so that the bounce can take place. It is also bounded from above at a value $k_{max}(M)$ which translates the fact that the bouncing time needs to be smaller than the Hawking time[3], otherwise the black hole would disappear before bouncing and the evaporation could not be considered anymore as a small correction associated with a dissipative process, as assumed in the model.

A signal detected today comes from black holes that have lived for a time equal to the Hubble time t_H. Fixing the lifetime to t_H, Eq. (1) gives the corresponding mass of the bouncing black hole, that determines the energy of the emitted radiation. We ask the following question: is there an allowed value of k such that this emission can explain the GeV excess observed by the *Fermi* telescope? We note immediately that the GeV energy scale is far below any possible contribution coming from the high-energy component of our model: even for the smaller possible value of k the emitted energy is of order a TeV. On the other hand, the low-energy component can indeed match the observed signal. Our analysis therefore focuses on this component. To have an emitted energy of the order of 1 GeV, that is of order $10^{-19}E_{Pl}$, the size of the black hole should be of the order of $10^{19}l_{Pl}$ and its mass of the oder $M \sim 10^{19}M_{Pl}$. The Hubble time is $t_H \sim 10^{60}t_{Pl}$. Requiring the Hubble time to be equal to the bouncing time leads to $k \sim 10^{22}$. How does this compare with the Hawking time? The Hawking time is roughly $t_{Haw} \sim 10^3M^3$, that is of the order of $10^{60}t_{Pl}$ for the mass we are interested in. This is of the same order of magnitude than the bouncing time[4]. This is therefore a quite interesting situation from the theoretical point of view in the sense that the required value of the parameter is not random or arbitrary in the (very large) allowed interval but a near-extremal one.

To summarize, the *high-energy* component of the signal emitted by bouncing black holes cannot explain the *Fermi* excess but the *low-energy* component might do so

[3] More precisely, the bounce time is constrained to be smaller than "Page time" at which the black holes would have lost half of its mass by Hawking evaporation because this time signs the entrance in the full quantum gravity regime [16].

[4] In our study we disregard the mass loss due to Hawking evaporation. In fact, even if the bouncing time considered here is comparable with the Hawking one, Hawking radiation decreases the mass of the black hole only by a small amount without changing its order of magnitude.

if the free parameter k is chosen near its highest possible value.

MODELING OF THE GAMMA-RAY EMISSION

Whatever the details of the emission mechanism, as soon as fundamental particles are emitted at energies higher than the QCD confinement scale, quarks and gluons are emitted and do fragmentate into subsequent hadrons. For a bouncing black hole emitting quanta with energies greater than, say, 100 MeV, it is required to consider not only the primary (*i.e.* direct) emission of gamma-rays but also the secondary component, due to the decay of unstable hadrons produced by fragmentation. This has been studied with analytical approximations for evaporating black holes in [17, 18]. In this work we use a full Monte Carlo analysis based the "Lund" PYTHIA code (with some scaling approximations in the low energy range) [19] to determine the normalized differential fragmentation functions $dg(\epsilon, E)/d\epsilon$, where E is the quark energy and ϵ is the photon energy. This takes into account a large number of physical aspects, including hard and soft interactions, parton distributions, initial- and final-state parton showers, multiple interactions, fragmentation and decay.

For all energies, we have found that the obtained spectra can be well fitted by a function

$$f(E,\epsilon) = \frac{a\epsilon^b}{\pi\gamma}\left[\frac{\gamma^2}{(\epsilon-\epsilon_0)^2+\gamma^2}\right] e^{-\left(\frac{4\epsilon}{E}\right)^3}, \qquad (2)$$

with $a = 50.7$, $b = 0.847$, $\gamma = 0.0876$ and $\epsilon_0 = 0.0418$ if the energies are given in GeV. The low-energy peak of the spectrum is well approximated by a Cauchy function. It is then roughly a power law, followed by an exponential cutoff around the initial jet energy.

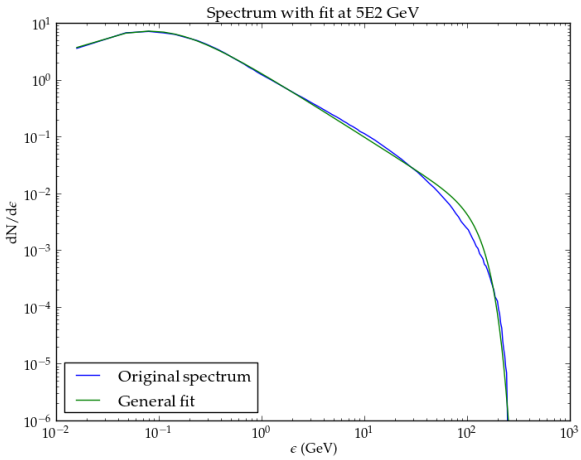

FIG. 1. Spectrum of gamma-rays generated by 5×10^2 GeV jets. The green histogram corresponds to the output of the simulation and the blue curve to the analytical fit.

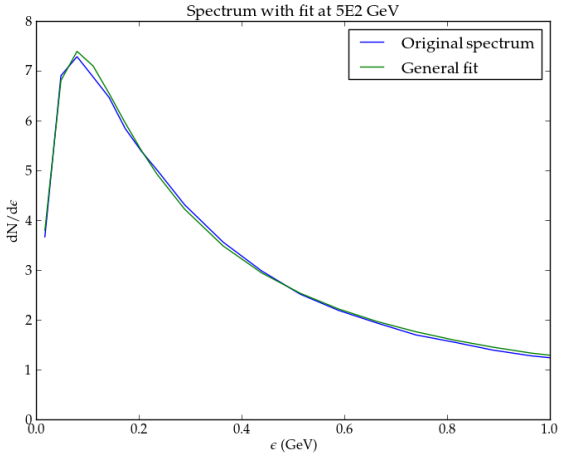

FIG. 2. Zoom on the low-energy part of the spectrum of gamma-rays generated by 5×10^2 GeV jets. The green histogram corresponds to the output of the simulation and the blue curve to the analytical fit.

As soon as the jet reaches an energy much higher that the associated quark mass, the result does not depend substantially on the quark type. Depending on the mean energy E of the primary component, the number of types of emitted quarks – that is with $m < E$ – is accounted for. The normalisation is chosen to be consistent with the primary emission.

For the *low-energy* component, the shape of the primary signal is not completely determined by the model. We have used a Gaussian function, centered on the energy estimated in the previous Section, with a relative width taken as the second free parameter of the model.

Its exact value depends on the details of the astrophysical phenomena occurring during the bounce and this is far beyond the scope of this study. The full signal can be written as

$$Ae^{-\frac{(\epsilon-E)^2}{2\sigma^2}} + 3N\sqrt{2\pi}A\sigma f(E,\epsilon), \tag{3}$$

where N is the number of species of quarks with $m < E$.

For the *high-energy* component, which is irrelevant for this study but potentially interesting for other works, the same strategy can be followed. The primary component is then a Planck law and the full signal can be written as

$$A\frac{\epsilon^2}{e^{E/T}-1} + 36AT^3\zeta(3)f(E,\epsilon). \tag{4}$$

Interestingly, this formula can also be used to model the full spectrum of an evaporating black hole since the Hawking spectrum is also very close to a Planck law.

FITTING FERMI DATA

The *Fermi* Gamma-ray Space Telescope is a space observatory being used for gamma-ray astronomy observations from low Earth orbit. Its main instruments are the Large Area Telescope (LAT), intended to perform an all-sky survey studying astrophysical and cosmological phenomena, and the Gamma-ray Burst Monitor (GBM), used to study transients.

An excess in the *Fermi*-LAT data has been reported within the inner 10 arcmin of the Galactic center (see, *e.g.*, [20–22]) and up to larger galactic latitudes (see, *e.g.*, [23–26]). A huge number of works have been published on possible explanations. Our opinion is that an astrophysical origin, notably associated with millisecond pulsars, is the most convincing one (see, *e.g.*, [27]). It is however not fully satisfactory and dark-matter like hypotheses are worth being considered (see, *e.g.*, [23]). Here we investigate whether this signal can be due to bouncing black holes.

We stress that the explanation we suggest is specifically associated with the quantum gravity scenario considered in this work. The time integrated spectrum of black holes evaporating by the usual Hawking process is scaling as E^{-3} and there is no way it can account for the *Fermi* excess. As explained before, two parameters are required to fully determine the low-energy component of bouncing black holes: their bouncing time and the width of the primary Gaussian. The best fit (with a near-extremal bouncing time) is shown in Fig. 3. The agreement with data is good, with a χ^2 per degree of freedom of 1.05. Notice that what is plotted here is not the differential spectrum but the spectral energy density ($\epsilon^2 dN/d\epsilon$), as used for most experimental publications. The key point we want to stress is that although the number of secondary gamma-rays is higher than the number of primary gamma-rays, their spectral energy density is much lower. This is of utmost importance for this study: as the background has a basically constant spectral energy density, this means that the anomaly can be accounted for without any spurious excess in the 10-100 MeV range, where is situated the peak of the secondary component. This peak remains much below the background and the signal can be explained with no contradiction with the data.

This also shows why the *high-energy* component cannot be used to explain the excess. The energy of its primary component is in all cases too high and its secondary component would not have a high enough spectral energy density.

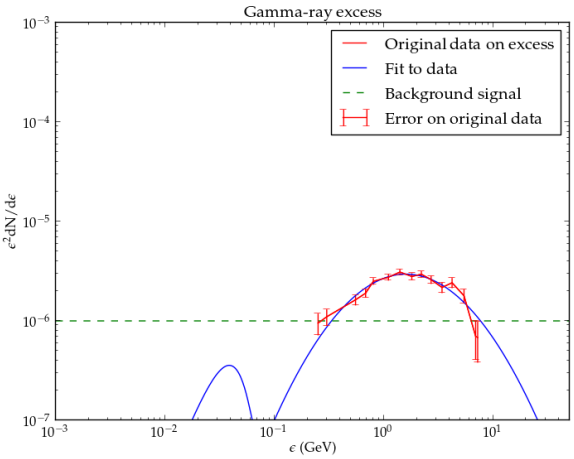

FIG. 3. Best fit to the *Fermi* excess with bouncing black holes.

DISCRIMINATION WITH DARK MATTER AND MASS SPECTRUM

The model presented in this work is unquestionably quite exotic when compared with astrophysical hypotheses. But the important point is than it can, in principle, be distinguished both from astrophysical explanations and from other "beyond the Standard Model" scenarios. The reason for that is a peculiar redshift dependance. When looking at a galaxy at redshift z, the measured energy of the signal emitted either by decaying WIMPS or by astrophysical objects will be $E/(1+z)$ if the rest-frame energy is E. But this is not true for the bouncing black holes signal. The reason for this is that black holes that have bounced far away and are observed now must have a shorter bouncing time and therefore a smaller mass. Their emission energy – in the low energy channel we are considering in this article – is therefore higher and this

partly compensates for the redshift effect. Following [9], we can write down the observed wavelength of the signal from a host galaxy at redshift z, taking into account both the expansion of the universe and the change of bouncing time, as:

$$\lambda_{obs}^{BH} \sim \frac{2Gm}{c^2}(1+z) \quad \times \quad \sqrt{\frac{H_0^{-1}}{6\,k\Omega_\Lambda^{1/2}}\ \sinh^{-1}\left[\left(\frac{\Omega_\Lambda}{\Omega_M}\right)^{1/2}(z+1)^{-3/2}\right]}, \tag{5}$$

where we have reinserted the Newton constant G and the speed of light c; H_0, Ω_Λ and Ω_M being the Hubble constant, the cosmological constant, and the matter density. On the other hand, for standard sources, the measured wavelength is just related to the observed wavelength by

$$\lambda_{obs}^{other} = (1+z)\lambda_{emitted}^{other}\ . \tag{6}$$

The redshift dependence specific of our model makes it possibly testable against other proposals. Obviously, detecting such a signal from far away galaxies is challenging but we hope this work might motivate some experimental prospects for the next generation of gamma-ray satellites.

The order of magnitude of the number of bouncing black holes in the galactic-center region required to account for the observed flux is around 100 per second. The associated mass is negligible when compared to the expected dark matter density, even when integrated over a long time interval. If the mass spectrum of primordial black holes was known, which is not the case, in principle it would be possible to fix the total mass associated with bouncing black holes. As a reasonable toy model, let us assume that the mass spectrum is given by

$$\frac{d^2N}{dMdV} = pM^{-\alpha}. \tag{7}$$

If the number of exploding black holes required to explain the data on a time interval $d\tau$ is N_{exp}, one can estimate the associated mass variation

$$dM = \frac{d\tau}{8kM}. \tag{8}$$

Calling M_0 the mass corresponding to a black hole exploding today, one then gets

$$N_{exp} = \int_{M_0}^{M_0+dM} pM^{-\alpha}dM\,. \tag{9}$$

This allows, in principe, to determine p and therefore to normalize the spectrum.

CONCLUSION

Black holes could bounce once they have reached the "Planck star" stage. This can be seen as a tunneling into an expanding explosive phase. The process appears generic in quantum gravity. In this article, we have shown that this phenomenon could explain the GeV excess measured by the *Fermi* satellite. This would open the fascinating possibility to observe (non perturbative) quantum gravity processes at energies 19 orders of magnitude below the Planck scale. Interestingly, the explanation we suggest is fully self-consistent in the sense that the hadronic "noise" due to decaying pions remains much below the observed background. Unquestionably, there are other – less exotic – ways to explain the *Fermi* excess. But the important point we have made is that this model has a specific redshift dependance which, in principle, can lead to a clear signature for future experiments. On the theoretical side, the important next step would be to fix the free parameter of the model from the full theory so that the energy of the signal is fixed from first principle and not anymore tuned to fit the data (see [28] for a recent step in this direction). Another interesting possible improvement would be to take into account the distribution of actual bouncing times for individual black holes around the mean time τ fixed by the theory.

ACKNOWLEDGMENTS

B.B. is supported by a grant from ENS-Lyon. F.V. is supported by a Veni grant from the Netherlands Organisation for Scientific Research (NWO).

* Electronic address: Aurelien.Barrau@cern.ch
† Electronic address: Bolliet@lpsc.in2p3.fr
‡ Electronic address: M.Shutten@students.ru.nl
§ Electronic address: F.Vidotto@science.ru.nl

[1] S. Liberati and L. Maccione, J. Phys. Conf. Ser. **314**, 012007 (2011), 1105.6234.
[2] S. Hossenfelder and L. Smolin, Phys. Canada **66**, 99 (2010), 0911.2761.
[3] G. Amelino-Camelia, Living Rev. Rel. **16**, 5 (2013), 0806.0339.
[4] C. Rovelli and F. Vidotto, Int. J. Mod. Phys. **D23**, 1442026 (2014), 1401.6562.
[5] A. Ashtekar, T. Pawlowski, and P. Singh, Phys. Rev. Lett. **96**, 141301 (2006), gr-qc/0602086.
[6] T. De Lorenzo and A. Perez (2015), 1512.04566.
[7] H. M. Haggard and C. Rovelli, Phys. Rev. **D92**, 104020 (2015), 1407.0989.
[8] A. Barrau and C. Rovelli, Phys. Lett. **B739**, 405 (2014), 1404.5821.
[9] A. Barrau, C. Rovelli, and F. Vidotto, Phys. Rev. **D90**, 127503 (2014), 1409.4031.
[10] A. Barrau, B. Bolliet, F. Vidotto, and C. Weimer, JCAP **1602**, 022 (2016), 1507.05424.
[11] S. A. Hayward, Phys. Rev. Lett. **96**, 031103 (2006), gr-qc/0506126.

[12] T. D. Lorenzo, C. Pacilio, C. Rovelli, and S. Speziale, General Relativity and Gravitation (2015), Volume 47 (2014), 1412.6015, URL http://arxiv.org/abs/1412.6015.
[13] T. D. Lorenzo, A. Giusti, and S. Speziale, General Relativity and Gravitation 48 (March 2016) (2015), 1510.08828, URL http://arxiv.org/abs/1510.08828.
[14] M. Christodoulou, C. Rovelli, S. Speziale, and I. Vilensky (2016), 1605.05268.
[15] A. M. Green (2014), 1403.1198, URL http://arxiv.org/abs/1403.1198.
[16] A. Almheiri, D. Marolf, J. Polchinski, and J. Sully, JHEP **02**, 062 (2013), 1207.3123.
[17] J. H. MacGibbon and B. R. Webber, Phys. Rev. **D41**, 3052 (1990).
[18] J. H. MacGibbon, Phys. Rev. **D44**, 376 (1991).
[19] T. Sjstrand, S. Ask, J. R. Christiansen, R. Corke, N. Desai, P. Ilten, S. Mrenna, S. Prestel, C. O. Rasmussen, and P. Z. Skands, Comput. Phys. Commun. **191**, 159 (2015), 1410.3012.
[20] D. Hooper and L. Goodenough, Phys. Lett. **B697**, 412 (2011), 1010.2752.
[21] K. N. Abazajian and M. Kaplinghat, Phys. Rev. **D86**, 083511 (2012), [Erratum: Phys. Rev.D87,129902(2013)], 1207.6047.
[22] C. Gordon and O. Macias, Phys. Rev. **D88**, 083521 (2013), [Erratum: Phys. Rev.D89,no.4,049901(2014)], 1306.5725.
[23] T. Daylan, D. P. Finkbeiner, D. Hooper, T. Linden, S. K. N. Portillo, N. L. Rodd, and T. R. Slatyer, Phys. Dark Univ. **12**, 1 (2016), 1402.6703.
[24] F. Calore, I. Cholis, and C. Weniger, JCAP **1503**, 038 (2015), 1409.0042.
[25] D. Hooper and T. R. Slatyer, Phys. Dark Univ. **2**, 118 (2013), 1302.6589.
[26] W.-C. Huang, A. Urbano, and W. Xue (2013), 1307.6862.
[27] R. Bartels, S. Krishnamurthy, and C. Weniger, Phys. Rev. Lett. **116**, 051102 (2016), 1506.05104.
[28] M. Christodoulou, C. Rovelli, S. Speziale, and I. Vilensky (2016), 1605.05268, URL http://arxiv.org/abs/1605.05268.

Chapter IV

Dark energy and modified gravity Theories

This chapter is dedicated to my work related to the late acceleration of the universe. We consider the possibility that this acceleration is due to dark energy or modifications to Einstein's theory of gravity, beyond the cosmological constant. With the forthcoming large scale surveys, the challenge is to be able to discriminate between different dark sector theories and to identify the 'best' models with two criteria in mind: non-contradiction with data and simplest set of assumptions to explain the widest set of phenomena. Currently, the 'best' model is the ΛCDM cosmology but many alternative are being explored.

The unified framework for classifying and constraining dark sector theories that constitutes the first part of this chapter is the so-called e*quation of state approach to cosmological perturbations in the dark sector* (EoS). It was introduced in 2013 by Battye and Pearson [25]. I was involved in the latest development of the EoS approach and I have obtained two crucial results so far:

- To prove that the EoS approach, formally defined by Battye and Pearson, can be used efficiently to describe the dynamics of perturbations in the dark sector: I obtained the expressions of the dark sector anisotropic stress and entropy perturbation in $f(\mathcal{R})$ gravity.
- To build a numerical code where, through the implementation of the EoS approach, any modified gravity and dark energy proposal can, in principle, be incorporated straightforwardly. I wrote a modified version of CLASS [105], named `class_eos`, which is, to this date, operational for $f(\mathcal{R})$ gravity and wCDM. The code is publicly available on the internet[1].

My theoretical work on $f(\mathcal{R})$ gravity was published in 2016 and the article is reported in section IV.4.1. However, the other numerical and phenomenological results on the EoS approach, which constitute most of the material presented in this chapter, are still unpublished.

This is also the case for my research project on the thermal Sunyaev Zel'dovich (tSZ) power spectrum, the subject of section IV.7. Although still unpublished, it constitutes one of my main achievements in these last three years: for the first time, we give a conservative constraint on the equation of state for dark energy, $w_{\rm de}$, extracted from the SZ data of the Planck mission.

In section IV.1, I review our current knowledge of dark energy and give a brief overview of dark sector theories and the scope of my work. Then, I start be recalling the main steps leading to the dynamical equations for both background cosmology and perturbations. I introduce gauge invariant notations that enable working in both the synchronous and conformal Newtonian gauge at the same time. I describe how I have implemented the perturbed fluid equations for dark energy in a Boltzmann code and developed the numerical code `class_eos`. Based on numerical simulations and analytical approximations, I discuss some important phenomenological facts related to dark sector perturbations, especially in $f(\mathcal{R})$ theories and quintessence models, *i.e.* models with $w_{\rm de} \neq 1$ and a speed of sound $c^2_{s,\rm de} = 1$. The chapter ends on the SZ constraints on $w_{\rm de}$ in section IV.7.

[1] https://github.com/borisbolliet

IV.1 Overview

Most of our knowledge regarding the present observed accelerated expansion of the universe is related to the background evolution in time, which amounts to the measure of the dark energy density parameter, $\Omega_{\rm de}$, and the equation of state parameter $w_{\rm de} = P_{\rm de}/\rho_{\rm de}$, where $P_{\rm de}$ and $\rho_{\rm de}$ are the pressure and energy density of the dark energy component. These quantities are extracted from three main observables: the CMB temperature anisotropy, standard rulers (Baryon Acoustic Oscillations) and standard candles (Type Ia supernovae). Studying the change of the angular size of standard rulers, or the luminosity of standard candles, with respect to redshift provides a way to extract the values of $\Omega_{\rm de}$ and $w_{\rm de}$. But just as for the CMB data, there is a strong degeneracy between these two parameters and, in particular, the value of the Hubble parameter today. A combination of data sets, with Supernovae and BAO data, can help breaking these degeneracies and gives the following 68% constraints [7]:

$$\Omega_{\rm de} = 0.6911 \pm 0.0062 \quad \text{and} \quad w_{\rm de} = -1.019^{+0.075}_{-0.080} \tag{IV.1}$$

In the simplest case (ΛCDM) the dark energy component is a mere cosmological constant, Λ, which is equivalent to a perfect fluid with $w = -1$ and a constant energy density $\rho = \Lambda$. So far this model is the 'best' at explaining present data. Indeed, it contains less free parameters than any other models and its predictions are matching all cosmological observations to the present accuracy of our measurements. Nevertheless, although the ΛCDM is successful, it is not the only viable dark energy models. In order to discriminate between different models and rule out some of them from observational constraints, one needs to go beyond the background dynamics and investigate how a given model affects the growth of cosmological perturbations. Indeed, most of dark sector proposals can mimic a cosmological constant for the background expansion of the universe. In this case, modifications to general relativity are only manifest in observables related to cosmological perturbations.

The next generation of surveys (LSST, EUCLID, DES, WFIRST) will considerably improve the constraints on dark energy and the growth of structure. For instance, the LSST forecast for the equation of state parameter $w_{\rm de}$ is a relative standard deviation of about five percents [112], compared to thirty percents for CMB alone [7]. With the forthcoming data, we want to be able to discriminate between different dark energy models by confronting them to observations within the same phenomenological framework. This will enable us to answer the question: which is the 'best' model?

The most well known examples of theories that go beyond general relativity are f(R) gravity and quintessence. In $f(R)$ gravity, the Einstein-Hilbert action contains not only the Ricci scalar $\mathcal{R}$, but also higher order terms through an arbitrary function, $f(\mathcal{R})$. In quintessence models, a minimally coupled scalar field with an arbitrary potential is added to the Einstein-Hilbert action. In addition to those models, a special emphasis is presently placed on Horndeski theories because they constitute a wider set of extensions of general relativity that can be studied under the same umbrella. Indeed, the Lagrangian of a Horndeski theory is by definition a sub-class of the most generic Lagrangian involving a non-minimally coupled scalar field and leading to at most second order equations of motions. Relaxing the requirement of having second order equations of motion, but preserving isotropy and homogeneity at the background level as well as the weak equivalence principle, one finds an even larger set of modified gravity models, referred to as Effective Field Theory, with a generic Lagrangian containing nine arbitrary functions of time [78]. Finally, there has been a large number of phenomenological parameterizations of dark energy where the dark energy is seen as a fluid with diverse hydrodynamical and thermodynamical properties [102]. For example: the wCDM class of models, the $\{w_0, w_a\}$ parametrization, or elastic dark energy [24]. As a matter of fact, the wide variety of modified gravity models can be recast as a dark energy fluid [103]. This will be illustrated in this chapter with $f(\mathcal{R})$ gravity and Horndeski theories.

A considerable amount of work has already been done regarding the parametrization of departure from GR and constraints on the dark sector parameter space from cosmological probes. Currently, the

best constraints are obtained from Redshift-space distortions (RSD) and baryon acoustic oscillations (BAO) measurements. Redshift space distortions refer to the distortions of the peculiar velocity field of galaxies generated by clustering. Baryon acoustic oscillations are the small oscillations in the matter power spectrum that result from the dragging of baryons by radiation, before decoupling. These two observables can be measured by analyzing the correlations of the positions and velocities of a large number of galaxies. The most compelling galaxy surveys for BAO and RSD are WiggleZ [61] and SDSS-BOSS [140].

Galaxy weak lensing (WL) is also a promising probe for testing the LCDM paradigm. This time, one studies the correlations between the apparent ellipticity of galaxies. The shape of a visible galaxy appears to us as lensed image of the source, due to galaxy clusters located on the way of the light we receive on Earth. The two-point correlation function of the ellipticity of galaxies is therefore directly related to the gravitational potential integrated over the line of sight. Using this tool, it is possible to set competitive constraints on the dark sector. The most recent galaxy survey aimed at measuring galaxy weak lensing is CFHTLenS [74].

The Planck 2015 article on dark energy and modified gravity [6] presents a thorough analysis of dark sector constraints based on these measurements, sensitive to the evolution of cosmological perturbations in the recent universe (BAO, RSD, WL and CMB lensing). As of today, it has been possible to set constrains on most dark sector proposals. However, a comparison between the different models remains to be done. This is the long term objective of my work in the domain.

I am convinced that the EoS approach is *the* appropriate formalism to discuss dark energy and modified gravity models in a unified way. In addition, I am hopeful that the code I am presently developing (class_eos) will eventually become a powerful tool to confront these models with observational data.

IV.2 The effective fluid description of dark energy

By placing non-GR terms of the action for gravity to the right hand side of the field equations, one is allowed to recast dark energy or modifications to gravity as an effective fluid: *the dark sector fluid*. This is the subject of this section.

IV.2.1 The field equations

The action for (metric theories of) gravity with matter can be written as

$$\mathcal{S} = \int \mathrm{d}^4\mathrm{x}\sqrt{-|g|}\,\{\mathcal{L}_\mathrm{m} + \mathcal{L}_\mathrm{ds}\} \quad \text{with} \quad |g| = \det\left(g_{\mu\nu}\right), \tag{IV.2}$$

where $g = g_{\mu\nu}\mathrm{d}\mathrm{x}^\mu \otimes \mathrm{d}\mathrm{x}^\nu$ is the metric tensor, and $\mathcal{L}_\mathrm{m}$ and $\mathcal{L}_\mathrm{ds}$ are the Lagrangian for matter and the dark sector. Here, by matter we mean baryons, photons, neutrinos and dark matter. By dark sector we mean either a cosmological constant, dark energy or any modification to GR. The components of the stress-energy tensors of matter, T, and the dark sector, D, are given by

$$T_{\mu\nu} \equiv -\frac{2}{\sqrt{-|g|}}\frac{\delta}{\delta g^{\mu\nu}}\left(\sqrt{-|g|}\mathcal{L}_\mathrm{m}\right) \quad \text{and} \quad D_{\mu\nu} \equiv -\frac{2}{\sqrt{-|g|}}\frac{\delta}{\delta g^{\mu\nu}}\left(\sqrt{-|g|}\mathcal{L}_\mathrm{ds}\right). \tag{IV.3}$$

The variation of the action (IV.2) with respect to the metric, g, yields the field's equations:

$$G = T + D \quad \text{with} \quad G = R - \tfrac{1}{2}\mathcal{R}g, \tag{IV.4}$$

where G is the Einstein tensor, R is the Ricci tensor and $\mathcal{R} \equiv g^{\mu\nu}R_{\mu\nu}$ the Ricci scalar. In the next subsection we review several calculation tricks and present the Bianchi identity.

IV.2.2 Technical "aparté" and conservation laws

To obtain (IV.4) one has to use a few important formulas from the calculus of variations, in particular

$$\delta\left(\sqrt{-|g|}\right) = \frac{1}{2}\sqrt{-g}g^{\mu\nu}\delta g_{\mu\nu} \tag{IV.5}$$

which is a direct consequence of $\delta\det[\mathrm{A}] = \det[\mathrm{A}]\,\mathrm{tr}\left[\mathrm{A}^{-1}\delta\mathrm{A}\right]$ for any invertible matrix A. But also,

$$g^{\mu\nu}\delta g_{\mu\nu} = -g_{\mu\nu}\delta g^{\mu\nu} \quad \text{and} \quad \delta g^{\mu\nu} = -g^{\mu\alpha}g^{\nu\beta}\delta g_{\alpha\beta}, \tag{IV.6}$$

as well as

$$\int \mathrm{d}^4\mathrm{x}\delta\mathcal{R} = \int \mathrm{d}^4\mathrm{x}R_{\mu\nu}\delta g^{\mu\nu} \tag{IV.7}$$

which is true whenever δg has compact support (see Choquet-Bruhat [56] p. 52). A crucial geometrical identity is the Bianchi identity (Bianchi 1902, Ricci 1880), as it ensures the covariant conservation of Einstein's tensor. In abstract notations:

$$\nabla G = 0, \tag{IV.8}$$

where ∇ is the Levi-Civita connection (torsion free and metric compatible). Note that in this case the components of the covariant derivative of a generic tensor F are

$$\nabla_\mu F^{\mu_1..\mu_p}_{\nu_1..\nu_q} = \partial_\mu F^{\mu_1..\mu_p}_{\nu_1..\nu_q} + \Gamma^{\mu_i}_{\mu\sigma}F^{\mu_1..\mu_{i-1}\sigma\mu_{i+1}..\mu_p}_{\nu_1..\nu_q} - \Gamma^{\sigma}_{\mu\nu_i}F^{\mu_1..\mu_p}_{\nu_1..\nu_{i-1}\sigma\nu_{i+1}..\nu_p}, \tag{IV.9}$$

where the coefficient, $\Gamma^\gamma_{\alpha\beta}$, are the Christoffel symbols

$$\Gamma^\gamma_{\alpha\beta} = \tfrac{1}{2}g^{\gamma\sigma}\left(\partial_\beta g_{\sigma\alpha} + \partial_\alpha g_{\sigma\beta} - \partial_\sigma g_{\alpha\beta}\right). \tag{IV.10}$$

Since the stress-energy tensor of matter is also conserved due to the local conservation of energy,

$$\nabla T = 0, \tag{IV.11}$$

any viable dark sector must have

$$\nabla D = 0 \tag{IV.12}$$

as it follows from the field's equation and the Bianchi identity. Equation (IV.12) is central as its different projections yield the differential equations which determine the dynamics of the background cosmology (homogeneous equations) and cosmological perturbations (inhomogeneous equations).

IV.2.3 Homogeneous equations

With the assumption that the background space-time is spatially flat, homogeneous and isotropic, the metric is conformally related to the Minkowski metric: $g_{\mu\nu} = a^2\eta_{\mu\nu}$, where a is the scale-factor and $\eta = \mathrm{diag}\,(-1,1,1,1)$ the Minkowski metric. At the homogeneous level, the scale factor is therefore the only geometrical degree of freedom.

The 3+1 split

A time-like unit vector, u, orthogonal to the three dimensional spatial sub-manifold can be used to rewrite the metric as (3+1 split)

$$g = \gamma - u \otimes u. \tag{IV.13}$$

where γ is the spatial metric. By construction, one has

$$u^\mu u_\mu = -1, \quad u^\mu\gamma_{\mu\nu} = 0, \quad \text{and} \quad \gamma^\mu_\nu = u^\mu u_\nu + \delta^\mu_\nu, \tag{IV.14}$$

where δ^μ_ν is the Dirac delta. The components of the extrinsic curvature of the spatial slices are, by definition, $K_{\mu\nu} = \nabla_\mu u_\nu$. A short and instructive calculation shows that extrinsic curvature, K, is spatial:

$$\begin{aligned} u^\mu u^\nu K_{\nu\mu} &= u^\mu u^\nu \nabla_\mu u_\nu = u^\mu \nabla_\mu \left(u^\nu u_\nu\right) - u^\mu u_\nu \nabla_\mu u^\nu = u^\mu \nabla_\mu \left(u^\nu u_\nu\right) - u^\mu u_\nu K^\nu_\mu \\ &= -u^\mu u^\nu K_{\nu\mu} = 0. \end{aligned} \tag{IV.15}$$

The extrinsic curvature measures the expansion rate of the spatial slices and shall appear in all the conservation equations.

From the stress-energy tensors to perfect fluids

Just as any rank two tensors, the background matter and dark sectors stress-energy tensors may be decomposed as

$$T = \rho_{\rm m} u \otimes u + P_{\rm m} \gamma, \quad \text{and} \quad D = \rho_{\rm ds} u \otimes u + P_{\rm ds} \gamma, \tag{IV.16}$$

where $\rho_{\rm m,ds}$ and $P_{\rm m,ds}$ are the energy density and pressure of the effective matter and dark energy fluids.

Let us denote by U a generic stress-energy tensor, so

$$U \equiv T \,\text{or}\, D. \tag{IV.17}$$

The energy density and pressure are actually the 'time' and 'space' projections of the stress-energy tensor:

$$\rho = u^\mu u^\nu U_{\mu\nu} \quad \text{and} \quad P = \tfrac{1}{3} \gamma^{\mu\nu} U_{\mu\nu}. \tag{IV.18}$$

For the flat FLRW metric there are two natural choices for the time-like vector u_μ, the so-called *Hubble flow*. These two choices correspond to either conformal time $u = -a{\rm d}\tau$ or to coordinate time $u = -{\rm d}t$. In both cases the spatial metric is

$$\gamma = a^2 \delta_{ij} {\rm dx}^i \otimes {\rm dx}^j. \tag{IV.19}$$

Hence, on the spatial slice, the geometry is conformally Euclidean.

FLRW geometrical data

To write the FLRW Einstein tensors and covariant derivatives, one needs the expressions of the Christoffel symbols. In conformal time, they are

$$\Gamma^0_{00} = aH, \quad \Gamma^0_{ij} = aH\delta_{ij}, \quad \Gamma^i_{0j} = aH\delta^i_j, \quad \Gamma^i_{00} = 0, \quad \Gamma^k_{ij} = 0, \quad \Gamma^0_{0i} = 0. \tag{IV.20}$$

These can be used to express the Ricci scalar, Ricci and Einstein tensors, as well as the extrinsic curvature:

$$\mathcal{R} = 12H^2 + 6\dot{H}, \tag{IV.21}$$

$$R = -3\left(H^2 + \dot{H}\right) u \otimes u + \left(3H^2 + \dot{H}\right) \gamma, \tag{IV.22}$$

$$G = 3H^2 u \otimes u - \left(3H^2 + 2\dot{H}\right) \gamma, \tag{IV.23}$$

$$K = H\gamma. \tag{IV.24}$$

In these expressions, a dot denotes a derivative with respect to time $dt = ad\tau$ (and not to conformal time[1]).

[1] In fact, for a scalar quantity φ one has $\dot{\varphi} = u^\mu \nabla_\mu \varphi = u^0 \nabla_0 \varphi = \frac{1}{a}\partial_\tau \varphi = \partial_t \varphi$.

The field equations

Comparing (IV.23) with (IV.16), using the field's equations (IV.4), we obtain the Friedmann equation (projection along $u \otimes u$) and the expression of the pressure in terms of H and $\dot{H}$ (projection on γ). We recast these equations as

$$\Omega_{\rm m} + \Omega_{\rm de} = 1, \quad \text{and} \quad w_{\rm m}\Omega_{\rm m} + w_{\rm de}\Omega_{\rm de} = \tfrac{2}{3}\epsilon_{\rm H} - 1, \tag{IV.25}$$

where we have introduced the density parameters Ω, the background equation of state parameters w, and the 'slow-roll' parameter $\epsilon_{\rm H}$, defined as

$$\Omega \equiv \frac{\rho}{3H^2}, \quad w \equiv \frac{P}{\rho}, \quad \text{and} \quad \epsilon_{\rm H} \equiv -\frac{\dot{H}}{H^2}. \tag{IV.26}$$

Note that $\Omega_{\rm m} = \Omega_{\rm b} + \Omega_\gamma + \Omega_\nu + \Omega_{\rm c}$, where the subscript 'b' denotes baryons, 'γ' for photons, 'ν' for neutrinos and 'c' for cold dark matter. Let us use brackets to denote the sum over matter species. Hence, for an arbitrary quantity A we may write

$$\langle A \rangle \equiv A_{\rm b} + A_\gamma + A_\nu + A_{\rm c}. \tag{IV.27}$$

For instance, with this notation, the effective equation of state for the matter sector is given by $w_{\rm m} = \langle w_{\rm m}\Omega_{\rm m} \rangle / \Omega_{\rm m}$.

Adiabatic sound speed and local conservation of energy

Another important quantity that will appear in the analysis of cosmological perturbations is the *adiabatic sound speed* defined as

$$c_a^2 \equiv \frac{dP}{d\rho} = w - \frac{\dot{w}}{3H\,(1+w)}, \tag{IV.28}$$

where we used the time projection of the conservation equation (IV.12) for the second equality. Indeed, for a generic stress energy tensor, $u^\nu \nabla_\mu U^\mu_\nu = 0$, yields

$$\dot{\rho} = -3H\,(\rho + P) \tag{IV.29}$$

for both matter and dark sector. This equation expresses the local conservation of energy: for a fluid with positive pressure the energy density decreases as the universe expands. Note that the space projections of the conservation equation, $\gamma^{\lambda\nu}\nabla_\mu U^\mu_\nu$, are identically zero due to homogeneity and isotropy.

Useful formulas

Before studying the dynamics of perturbations, we give some useful relations for the background functions. The derivative of the density parameter is

$$\Omega_{\rm i}' = -3\,(1 + w_{\rm i})\,\Omega_{\rm i} + 2\epsilon_{\rm H}\Omega_{\rm i} \quad \text{with} \quad {\rm i} \in \{{\rm m}, {\rm de}\}\,, \tag{IV.30}$$

where a prime denotes a logarithmic derivative with respect the scale factor. Then the derivative of the 'slow-roll' parameter is given by

$$\epsilon_{\rm H}' = \tfrac{3}{2}\sum \left(w_{\rm i}\Omega_{\rm i}' + w_{\rm i}'\Omega_{\rm i}\right) = \sum \left\{3\epsilon_{\rm H} w_{\rm i} - \tfrac{9}{2}\,(1 + w_{\rm i})\,c_{a,{\rm i}}^2\right\}\Omega_{\rm i} \tag{IV.31}$$

At this stage, we introduce another background function which will help simplifying the expressions of the equations of state for perturbations:

$$\bar{\epsilon}_{\rm H} \equiv -\frac{\mathcal{R}'}{6H^2} = \epsilon_{\rm H}' + 4\epsilon_{\rm H} - 2\epsilon_{\rm H}^2. \tag{IV.32}$$

In the next section, we consider the linear perturbations of the field equations (IV.4) and conservation equations (IV.11)-(IV.12), in order to obtain the dynamics of cosmological perturbations.

IV.2.4 Inhomogeneous equations

The linear perturbation to the conservation equation (IV.11)-(IV.12) yields the *perturbed fluid equations*. For clarity, I decided to split this section into several little paragraphs corresponding to each step of the derivation.

General perturbed fluid equations

Starting with $\delta\left(\nabla_\mu U^\mu_\nu\right) = 0$ one finds

$$\nabla_\mu\left(\delta U^\mu_\nu\right) + U^\alpha_\nu \delta\Gamma^\mu_{\alpha\mu} - U^\mu_\alpha \delta\Gamma^\alpha_{\mu\nu} = 0. \tag{IV.33}$$

There are two types of ingredients in this equation, namely the perturbed stress-energy tensor, δU^μ_ν, and the perturbed Christoffel symbols, $\delta\Gamma^\alpha_{\mu\nu}$. After a lengthy calculation these can be expressed in terms of the perturbed metric, δg, as

$$\delta\Gamma^\gamma_{\alpha\beta} = \tfrac{1}{2} g^{\gamma\sigma}\left(\nabla_\beta \delta g_{\sigma\alpha} + \nabla_\alpha \delta g_{\sigma\beta} - \nabla_\sigma \delta g_{\alpha\beta}\right). \tag{IV.34}$$

Perturbed velocity field

Before writing the perturbed stress-energy tensor, we first note that the perturbed Hubble flow is a spatial quantity since $\delta u^\mu u_\mu = 0$. So we can define a perturbed velocity field as

$$v \equiv \delta u^\mu \partial_\mu, \tag{IV.35}$$

which is also spatial, by construction.

Perturbed stress-energy tensor

Then, the first order perturbation of the mixed type components of the stress-energy tensor can be written as

$$\delta U^\mu_\nu = \delta\rho u^\mu u_\nu + 2\left(\rho + P\right) v^{(\mu} u_{\nu)} + \delta P \gamma^\mu_\nu + P\Pi^\mu_\nu, \tag{IV.36}$$

where $\delta\rho$ is the *density perturbation*, δP is the *perturbed pressure* and Π is the so-called perturbed *anisotropic stress*.

The density perturbation corresponds to the time projection of the perturbed stress-energy tensor, the perturbed pressure to the space projection, the perturbed velocity to the space-time projection and the anisotropic stress to the spatial symmetric trace-free projection. Therefore, given a generic stress-energy energy tensor U, the perturbed fluid quantities can be obtained via

$$\delta\rho = u_\mu u^\nu \delta U^\mu_\nu, \quad \delta P = \tfrac{1}{3}\gamma^\mu_\nu \delta U^\nu_\mu, \quad \left(\rho + P\right) v^\mu = -u_\nu \gamma^{\mu\lambda} \delta U^\nu_\lambda, \tag{IV.37}$$

and

$$P\Pi^{\mu\nu} = \perp^{\mu\nu}{}_{\alpha}{}^{\beta} \delta U^\alpha_\beta \quad \text{with} \quad \perp^{\mu\nu}_{\alpha\beta} = \gamma^\mu_\alpha \gamma^\nu_\beta - \tfrac{1}{3}\gamma^{\mu\nu}\gamma_{\alpha\beta}, \tag{IV.38}$$

the components of the spatial traceless projection operator, $\perp$.

Euler and conservation equations for perturbations

The local conservation of energy for the perturbed fluid is expressed through the time projection of the perturbed conservation equation (IV.33), while its projection on the spatial slices gives the Euler equation,

$$\dot{\delta\rho} + K\left(\delta\rho + \delta P\right) + \left(\rho + P\right)\bar{\nabla}_\mu v^\mu + \rho u^\alpha \delta\Gamma^\mu_{\alpha\mu} + u^\nu U^\mu_\alpha \delta\Gamma^\alpha_{\mu\nu} = 0, \tag{IV.39}$$

$$\left(\rho + P\right)\dot{v}_\mu + \left(\dot{\rho} + \dot{P} + \tfrac{4}{3}K\left(\rho + P\right)\right)v_\mu + \bar{\nabla}_\mu \delta P + P\gamma^\nu_\mu \bar{\nabla}_\sigma \Pi^\sigma_\nu + u^\lambda u_\beta \delta\Gamma^\beta_{\lambda\mu} = 0. \tag{IV.40}$$

where a dot means $u^\mu\nabla_\mu$ and $\bar{\nabla}_\sigma \equiv \gamma^\mu_\sigma \nabla_\mu$. Our next step is to become more specific by choosing conformal time *i.e.* $u = -a\mathrm{d}\tau$ and fixing the gauge for the metric perturbation. By fixing the gauge we mean specifying a coordinate system in which the perturbations to the metric are defined. Then we will move to Fourier space and write the perturbed fluid equations as they are usually implemented in Boltzmann codes.

Metric perturbation and the SVT decomposition

The most generic metric perturbation can be written as

$$\delta g = a^2\left\{\Phi \mathrm{d}\tau\otimes\mathrm{d}\tau + w_i \mathrm{d}\tau\otimes\mathrm{d}x^i + h_{ij}\mathrm{d}x^i\otimes\mathrm{d}x^j\right\}. \tag{IV.41}$$

The 'vector' $w = w_i\mathrm{d}x^i$ (which is, properly speaking, a one-form) can be decomposed into a longitudinal part (the gradient of a scalar, W) and a transverse part (a divergence-less vector, $B = B_i\mathrm{d}x^i$),

$$w_i = \partial_i W + B_i. \tag{IV.42}$$

Now, let $A = A_{ij}\mathrm{d}x^i\otimes\mathrm{d}x^j$ be a generic tensor in Euclidean space. For instance, $A_{ij} = h_{ij}$ the spatial part of the perturbed metric, or $A_{ij} = \Pi_{ij}$ the anisotropic stress. Recall that the three-dimensional cartesian basis for symmetric two-forms contains six basis matrices, namely $\mathrm{d}x^{(i}\otimes\mathrm{d}x^{j)}$ for $i,j\in\{1,2,3\}$. Without loss of generality, let us assume a fluctuation propagating along the x^1 direction. A useful way to rewrite the cartesian basis is the scalar-vector-tensor (SVT) decomposition. Indeed, since the field equations are linear and isotropic, the scalar, vector and tensor perturbations evolve independently. The basis matrices of the SVT decomposition are

$$\begin{array}{lllllllll} t &=& \delta_{ij}\mathrm{d}x^i\otimes\mathrm{d}x^j, & v^1 &=& 2\mathrm{d}x^{(1}\otimes\mathrm{d}x^{2)}, & e^+ &=& \mathrm{d}x^2\otimes\mathrm{d}x^2 - \mathrm{d}x^3\otimes\mathrm{d}x^3, \\ \sigma &=& \left(\delta^1_i\delta^1_j - \tfrac{1}{3}\delta_{ij}\right)\mathrm{d}x^i\otimes\mathrm{d}x^j, & v^2 &=& 2\mathrm{d}x^{(1}\otimes\mathrm{d}x^{3)}, & e^\times &=& 2\mathrm{d}x^{[2}\otimes\mathrm{d}x^{3]}. \end{array} \tag{IV.43}$$

So our generic tensor A can be decomposed as

$$A = \tfrac{1}{3}\mathrm{tr}\left(A\right)t + A_\parallel\sigma + A_1 v^1 + A_2 v^2 + A_+ e^+ + A_\times e^\times. \tag{IV.44}$$

The coefficients of the decomposition of A onto the SVT basis matrices are easily obtained by projections, for instance $A_\parallel = \frac{3}{2}\mathrm{tr}\left(A\cdot\sigma\right)$.

Perturbed anisotropic stress

The anisotropic stress is traceless so its expansion reads as

$$\Pi = \Pi^{\mathrm{S}}\sigma + \boldsymbol{\Pi}^{\mathbf{V}}\boldsymbol{v} + \boldsymbol{\Pi}^{\mathbf{T}}\boldsymbol{e}, \tag{IV.45}$$

where we omitted the distinction between v^1, v^2 on one hand, and e^+,$e^\times$ on the other hand since both degrees of freedom obey the same equations as we shall see later. We used bold symbols to emphasize that there are still two independent degrees of freedom for both vector and tensor perturbations.

Degrees of freedom counting

Therefore, the anisotropic stress contains five degrees of freedom. In addition, there are also three scalar $\left\{\delta\rho, \delta P, \nabla_i v^i\right\}$ and two vector (the two transverse components of the perturbed velocity) fluid degrees of freedom. Hence the perturbed stress-energy tensor has ten degrees of freedom.

In the SVT basis, the metric perturbation (IV.41) is

$$\delta g = a^2 \left\{\Phi \mathrm{d}\tau \otimes \mathrm{d}\tau + w_i \mathrm{d}\tau \otimes \mathrm{d}x^i + \tfrac{1}{3} h t + h_{\parallel}\sigma + \boldsymbol{h}^{\mathbf{V}}\boldsymbol{v} + \boldsymbol{h}^{\mathbf{T}}\boldsymbol{e}\right\}, \tag{IV.46}$$

where $h \equiv \delta^{ij} h_{ij}$. The SVT decomposition owes its name to the symmetry properties of the scalar, vector and tensor degrees of freedom which we do not discuss here but that may be found in any good textbook on cosmology, e.g. [96]. We see from (IV.46) that the perturbed metric contains four scalar $\left\{\Phi, W, h, h_{\parallel}\right\}$, four vector $\left\{B_i, h_1^{\mathrm{V}}, h_2^{\mathrm{V}}\right\}$ (since B_i is divergence-less it has to be transverse and therefore lies on ∂_2 and ∂_3) and two tensor degrees of freedom so we recover the ten degrees of freedom of a four by four symmetric matrix.

The need for an equation of state

In the treatment of the background dynamics (homogeneous equations), the metric and stress energy tensors initially have ten degrees of freedom each. Homogeneity and isotropy reduces tremendously the number of degrees of freedom, leaving only the scale factor, the total pressure and energy density. Finally, with the two field equations (IV.25) one is still left with one degree of freedom. To close the system and solve the dynamics it is necessary to provide another 'constraint' equation: the equation of state $w = P/\rho$. The same applies for perturbations. Before discussing this topic at the inhomogeneous level we must make an important remark regarding the 'gauge' choice.

Gauge fixing

By writing the perturbed metric (IV.46), we implicitly chose a coordinate system.

Say we change the time parametrization as $\tau \mapsto \tau + \xi$, where ξ is infinitesimal and can be treated as a perturbation. Then the density field changes according to $\rho(\tau) \mapsto \rho(\tau + \xi) = \rho(\tau) + \rho'\xi$, hence a fictious scalar 'gauge' perturbation, $\rho'\xi$, has appeared and is only due to our time re-parametrization.

Similarly, a change of spatial coordinate leads to fictious perturbations. An infinitesimal spatial transformation can be parametrized by a vector $\xi^i = \nabla^i \xi + s^i$, with $\nabla_i s^i = 0$, which would therefore lead to one scalar (associated with ξ) and two vector (associated with s^i) fictious perturbations.

A generic change of coordinates may therefore introduce two scalar and two vector fictious fluctuations. In order to remove fictious perturbations, one has to 'fix' the gauge *i.e.* the coordinate system. For instance, we could chose the time coordinate so that the density perturbation is always zero (*uniform density gauge*), $\delta\rho = 0$, and also set $W = 0$ (see (IV.42)) to completely fix the gauge for scalar perturbations.

Once the gauge is fixed, computations can be safely done but observables have to be *gauge invariant* quantities in the sense that their numerical values should not depend on the choice of the coordinate system.

Equations of state for perturbations

Scalar perturbations are described by four metric and four fluid degrees of freedom. Like we just saw, two of them shall be set to zero once a choice for the coordinate system is made (gauge fixing). The two perturbed fluid equations and two of the four 'scalar' perturbed field equations[2] then reduce the number of degrees of freedom by four. One is left with two scalar degrees of freedom that have to be

[2]The other two are redundant with Bianchi identities.

specified in order to solve the dynamics. This can be done by specifying the perturbed pressure and scalar anisotropic stress in terms of the other scalar degrees of freedom,

$$\delta P = \delta P\left(\delta\rho, \Phi, h, h_{\parallel}, W, \nabla_i v^i\right), \tag{IV.47}$$

$$\Pi^{\mathrm{S}} = \Pi^{\mathrm{S}}\left(\delta\rho, \Phi, h, h_{\parallel}, W, \nabla_i v^i\right). \tag{IV.48}$$

Following the same reasoning for vector and tensor perturbations, one finds that in both cases there remains two unconstrained degrees of freedom, which can be chosen to be the two vector and the two tensor anisotropic stresses:

$$\boldsymbol{\Pi}^{\mathbf{V}} = \boldsymbol{\Pi}^{\mathbf{V}}\left(\boldsymbol{h}^{\mathbf{V}}, B_i, \boldsymbol{\theta}^{\mathbf{V}}\right) \quad \text{and} \quad \boldsymbol{\Pi}^{\mathbf{T}} = \boldsymbol{\Pi}^{\mathbf{T}}\left(\boldsymbol{h}^{\mathbf{T}}\right), \tag{IV.49}$$

where B_i is the divergence-less part of the 'time-space' metric perturbation and $\boldsymbol{\theta}^{\mathbf{V}}$ is the vectorial part of the perturbed velocity field. In analogy with the equation of state for homogeneous quantities, $P = w\rho$, the previous expressions (IV.47), (IV.48) and (IV.49) are *equations of state for perturbations.* Our goal is to obtain equations of state for dark sector perturbations, given a specific dark sector theory.

Fourier modes

The strategy is to carry the calculations in both the conformal Newtonian gauge and the synchronous gauge, in Fourier space, and then identify gauge invariant combination of the perturbed degrees of freedom to finally obtain a system of equation written in a gauge invariant manner. For the Fourier transform, we use the following convention

$$A\left(\mathbf{x}, \tau\right) = \int \mathrm{d}^3\mathbf{k} A\left(\mathbf{k}, \tau\right) \exp\left(i\mathbf{k}\cdot\mathbf{x}\right). \tag{IV.50}$$

For instance, the divergence of the perturbed velocity field expands as

$$\begin{aligned}\nabla_a v^a\left(\mathbf{x}, \tau\right) &= \nabla_a\left\{\int \mathrm{d}^3\mathbf{k} v^a\left(\mathbf{k}, \tau\right)\exp\left(i\mathbf{k}\cdot\mathbf{x}\right)\right\} = \int \mathrm{d}^3\mathbf{k} i k_a v^a\left(\mathbf{k}, \tau\right)\exp\left(i\mathbf{k}\cdot\mathbf{x}\right)\\ &= \int \mathrm{d}^3\mathbf{k} k^2\theta\left(\mathbf{k}, \tau\right)\exp\left(i\mathbf{k}\cdot\mathbf{x}\right),\end{aligned} \tag{IV.51}$$

where we defined the rescaled Fourier modes of the divergence of the velocity field as

$$\theta\left(\mathbf{k}, \tau\right) \equiv \frac{ik_a}{k^2} v^a\left(\mathbf{k}, \tau\right). \tag{IV.52}$$

This quantity, along with the perturbed density field $\delta\rho$, constitutes the main scalar degree of freedom for which we provide an evolution equation.

Conformal and synchronous gauges

In the conformal Newtonian gauge (CNG), we set w_i and $h_{\parallel}$ to zero and in the synchronous gauge (SG) wet w_i and the time-time degree of freedom of the perturbed metric to zero. To recapitulate,

$$\delta g = a^2\left\{-2\psi \mathrm{d}\tau\otimes\mathrm{d}\tau - 2\phi\delta_{ij}\mathrm{d}x^i\otimes\mathrm{d}x^j + \boldsymbol{h}^{\mathbf{V}}\boldsymbol{v} + \boldsymbol{h}^{\mathbf{T}}\boldsymbol{e}\right\} \quad \text{in the CNG.} \tag{IV.53}$$

$$\delta g = a^2\left\{\left[\tfrac{1}{3}h\delta_{ij} + h_{\parallel}\sigma_{ij}\right]\mathrm{d}x^i\otimes\mathrm{d}x^j + \boldsymbol{h}^{\mathbf{V}}\boldsymbol{v} + \boldsymbol{h}^{\mathbf{T}}\boldsymbol{e}\right\} \quad \text{in the SG,} \tag{IV.54}$$

As a consequence of setting w_i to zero and due to the perturbed field equations, one can show that the vectorial part of the velocity field has to vanish, $B_i = 0 \Rightarrow \boldsymbol{\theta}^{\mathbf{V}} = 0$. This means that the vector anisotropic stress may only depend on the metric perturbations $\boldsymbol{h}^{\mathbf{V}}$.

In fact, there is a residual gauge freedom in the synchronous gauge. This is a subtle point. One way of seeing it is by noting that in this gauge the coordinate system is defined by free falling 'observers' (δg has no time components) so, to prevent two observers' trajectories from intersecting with each other, one must specify an appropriate foliation of hyper-surface of constant time. In general we set those hyper-surfaces to be such as the CDM fluid is at rest:

$$\theta_c = 0 \text{ in the synchronous gauge.} \tag{IV.55}$$

I skip the straightforward but lengthy calculations of the perturbed Christoffel symbols and the perturbed Einstein's tensor in Fourier space.

Conventions and notations

In what follows a prime will denote a logarithmic derivative with respect the scale factor and we will use two dimensionless quantities in place of the modulus of the wavenumber, k, defined bellow

$$(\cdots)' \equiv \frac{d(\cdots)}{d\ln a}, \quad \mathrm{K} \equiv \frac{k}{aH}, \quad g_{\mathrm{K}} \equiv 1 + \frac{\mathrm{K}^2}{3\epsilon_{\mathrm{H}}}. \tag{IV.56}$$

We shall recombine the metric perturbations into the new variables $\{W, X, Y, Z\}$ and the fluid perturbations into $\left\{\Delta, \hat{\Theta}, \Gamma, \Pi\right\}$ that we define hereafter. First, we introduce

$$T \equiv \begin{cases} h_{\parallel}' / \left(2\mathrm{K}^2\right) & \text{in the synchronous gauge,} \\ 0 & \text{in the conformal Newtonian gauge.} \end{cases} \tag{IV.57}$$

In fact, T is proportional to the infinitesimal time-like vector field that enables to go from the CNG to the SG via a coordinate transformation. Let $\hat{x}^\mu$ be the coordinates in the SG and x^μ the coordinates in the CNG. Then, $\hat{x}^i = x^i$ and $\hat{x}^0 = x^0 + \xi$ with $\xi = (T/H)$.

Then, the new set of metric perturbations $\{W, X, Y, Z\}$ is defined as

$$Y \equiv \begin{cases} T' + \epsilon_{\mathrm{H}} T & \text{in the synchronous gauge,} \\ \psi & \text{in the conformal Newtonian gauge,} \end{cases} \tag{IV.58}$$

$$Z \equiv \begin{cases} \eta - T & \text{in the synchronous gauge,} \\ \phi & \text{in the conformal Newtonian gauge,} \end{cases} \tag{IV.59}$$

$$X \equiv Z' + Y, \tag{IV.60}$$

$$W \equiv X' - \epsilon_{\mathrm{H}} (X + Y). \tag{IV.61}$$

Note that $\{W, X, Y, Z\}$ are gauge invariant and dimensionless quantities. Their numerical value is independent of the coordinate system. One the other hand, the new dimensionless and gauge invariant perturbed fluid variables are defined as

$$\Delta \equiv \delta + 3H(1+w)\theta, \quad \hat{\Theta} \equiv 3(1+w)\{H\theta + T\}, \quad \text{and} \quad w\Gamma \equiv \frac{\delta P}{\rho} - c_a^2 \delta. \tag{IV.62}$$

They are the gauge invariant density and velocity perturbations, and the entropy perturbation respectively.

Entropy perturbation and sound speed

Let us pause for a moment on the entropy perturbation, to express it in terms of gauge invariant quantities. The sound speed, c_s^2, is defined as the ratio between the pressure and density perturbation in the rest-frame of the fluid (denoted with a subscript 'rf'), *i.e.* where its perturbed velocity field is zero):

$$c_s^2 \equiv \frac{\delta P^{\rm rf}}{\delta \rho^{\rm rf}}. \tag{IV.63}$$

The perturbed pressure and density fields in a frame where the fluid has a velocity θ are given by

$$\delta P = \delta P^{\rm rf} - 3\left(1+w\right)\rho c_a^2 H\theta, \tag{IV.64}$$
$$\delta \rho = \delta \rho^{\rm rf} - 3\left(1+w\right)\rho H\theta. \tag{IV.65}$$

So, the entropy perturbation becomes

$$\begin{aligned} w\Gamma &= \frac{\delta P^{\rm rf}}{\rho} - 3\left(1+w\right)c_a^2 H\theta - c_a^2\delta \\ &= c_s^2\delta^{\rm rf} - 3\left(1+w\right)c_a^2 H\theta - c_a^2\delta \\ &= \left(c_s^2 - c_a^2\right)\left\{\delta + 3\left(1+w\right)H\theta\right\} \\ &= \left(c_s^2 - c_a^2\right)\Delta. \end{aligned} \tag{IV.66}$$

In other words, the entropy perturbation is almost equivalent to the sound speed c_s^2.

Perturbed fluid equations in gauge invariant notations

With these notations, the perturbed fluid equations can be recast in an elegant manner as

$$\Delta' - 3w\Delta - 2w\Pi^{\rm S} + g_{\rm K}\epsilon_{\rm H}\hat{\Theta} = 3\left(1+w\right)X, \tag{IV.67}$$
$$\hat{\Theta}' + 3\left(c_a^2 - w + \tfrac{1}{3}\epsilon_{\rm H}\right)\hat{\Theta} - 3c_a^2\Delta - 2w\Pi^{\rm S} - 3w\Gamma = 3\left(1+w\right)Y. \tag{IV.68}$$

Perturbed field equations in gauge invariant notations

The perturbed field equations, $\delta G = \delta U$, can be recast in the same fashion as

$$-\tfrac{2}{3}{\rm K}^2 Z = \Omega\Delta, \tag{IV.69}$$
$$2X = \Omega\hat{\Theta}, \tag{IV.70}$$
$$\tfrac{2}{3}W + 2\left(1+c_a^2\right)X - \tfrac{2}{9}{\rm K}^2 Y + \tfrac{2}{9}\left(1+3c_a^2\right){\rm K}^2 Z = \Omega w\Gamma, \tag{IV.71}$$
$$\tfrac{1}{3}{\rm K}^2\left(Y - Z\right) = \Omega w\Pi^{\rm S}, \tag{IV.72}$$

for scalar modes, while in the vector and tensor sectors one finds

$$\tfrac{1}{6}\boldsymbol{h}^{\mathbf{V}\prime\prime} + \left(\tfrac{1}{2} - \tfrac{1}{6}\epsilon_{\rm H}\right)\boldsymbol{h}^{\mathbf{V}\prime} = \Omega w\boldsymbol{\Pi}^{\mathbf{V}}, \tag{IV.73}$$
$$\tfrac{1}{6}\boldsymbol{h}^{\mathbf{T}\prime\prime} + \left(\tfrac{1}{2} - \tfrac{1}{6}\epsilon_{\rm H}\right)\boldsymbol{h}^{\mathbf{T}\prime} + \tfrac{1}{3}{\rm K}^2\boldsymbol{h}^{\mathbf{T}} = \Omega w\boldsymbol{\Pi}^{\mathbf{T}}. \tag{IV.74}$$

Solving the dynamics

The dynamics of vector and tensor perturbations is quite straightforward since the matter sector has

$$\boldsymbol{\Pi}^{\mathbf{V}}_{\mathbf{m}} = \boldsymbol{\Pi}^{\mathbf{T}}_{\mathbf{m}} = 0, \tag{IV.75}$$

and there are only two equations to be solved, namely (IV.73) and (IV.74). This can be done once initial conditions for $\boldsymbol{h}^{\mathbf{T}}$, $\boldsymbol{h}^{\mathbf{T}\prime}$ and $\boldsymbol{h}^{\mathbf{V}\prime}$ are given and the equations of state state for dark sector perturbations (IV.49) are known. The RHS of (IV.73) and (IV.74) then reduces to

$$\Omega w \boldsymbol{\Pi}^{\mathbf{V}} = \Omega_{\rm de} w_{\rm de} \boldsymbol{\Pi}^{\mathbf{V}}_{\mathbf{de}} \left(\boldsymbol{h}^{\mathbf{V}\prime}, \boldsymbol{h}^{\mathbf{V}\prime\prime} \right), \tag{IV.76}$$

$$\Omega w \boldsymbol{\Pi}^{\mathbf{V}} = \Omega_{\rm de} w_{\rm de} \boldsymbol{\Pi}^{\mathbf{T}}_{\mathbf{de}} \left(\boldsymbol{h}^{\mathbf{T}}, \boldsymbol{h}^{\mathbf{T}\prime}, \boldsymbol{h}^{\mathbf{T}\prime\prime} \right). \tag{IV.77}$$

More work is necessary for the scalar perturbations. The different fluid components have to be treated separately.

Cold dark matter

The easiest case is the CDM fluid, as the equations of state are trivial:

$$w_{\rm c} = w_{\rm c} \Pi^{\rm S}_{\rm c} = w_{\rm c} \Gamma_{\rm c} = 0. \tag{IV.78}$$

For the CDM fluid the perturbed fluid equation are

$$\Delta'_{\rm c} + g_{\rm K} \epsilon_{\rm H} \hat{\Theta}_{\rm c} = 3X, \tag{IV.79}$$

$$\hat{\Theta}'_{\rm c} + \epsilon_{\rm H} \hat{\Theta}_{\rm c} = 3Y. \tag{IV.80}$$

Baryons

The sound speed in the baryonic fluid is non-zero therefore the equations of state are

$$w_{\rm b} = w_{\rm b} \Pi^{\rm S}_{\rm b} = 0 \quad \text{and} \quad w_{\rm b} \Gamma_{\rm b} = c^2_{s,{\rm b}} \Delta_{\rm b}. \tag{IV.81}$$

The origin of a non-vanishing entropy perturbation is due to their coupling with photons through Thomson scattering. Here, for the sake of clarity in our discussion, we only give a simplistic version of the equations of propagation in the standard matter sector and assume that the stress energy tensor of photons and baryons are conserved separately (which is true after recombination and therefore in the period of interest since we are eventually concerned with dark sector perturbations whose evolution affects the gravitational potentials only at late time). For baryons the perturbed fluid equations are

$$\Delta'_{\rm b} + g_{\rm K} \epsilon_{\rm H} \hat{\Theta}_{\rm b} = 3X, \tag{IV.82}$$

$$\hat{\Theta}'_{\rm b} + \epsilon_{\rm H} \hat{\Theta}_{\rm b} - 3 c^2_{s,{\rm b}} \Delta_{\rm b} = 3Y. \tag{IV.83}$$

Relativistic species: photons and neutrinos

For photons and neutrinos the equations of state at the background level are simple:

$$w_\gamma = w_\nu = \tfrac{1}{3}, \tag{IV.84}$$

however the expressions of the anisotropic stresses and entropy perturbations are more intricate. One has to consider the phase space distribution of particles and solve the Boltzmann equation for the distribution functions. I refer the reader to [113] for a complete treatment. Denoting both photons and neutrinos with a subscript 'r' (relativistic species), the equations of motion are

$$\Delta'_{\rm r} - \Delta_{\rm r} - \tfrac{2}{3} \Pi^{\rm S}_{\rm r} + g_{\rm K} \epsilon_{\rm H} \hat{\Theta}_{\rm r} = 4X, \tag{IV.85}$$

$$\hat{\Theta}'_{\rm r} + \epsilon_{\rm H} \hat{\Theta}_{\rm r} - \Delta_{\rm r} - 2w \Pi^{\rm S}_{\rm r} - 3 w_{\rm r} \Gamma_{\rm r} = 4Y. \tag{IV.86}$$

Dark sector perturbations

For a dark sector consisting of a cosmological constant, $w_{\rm de} = -1$, the dark sector fluid perturbations are identically zero. But for a generic dark sector fluid they are not and the equations of propagation are

$$\Delta'_{\rm de} - 3w_{\rm de}\Delta_{\rm de} - 2w_{\rm de}\Pi^{\rm S}_{\rm de} + g_{\rm K}\epsilon_{\rm H}\hat{\Theta}_{\rm de} = 3\left(1+w_{\rm de}\right)X, \tag{IV.87}$$

$$\hat{\Theta}'_{\rm de} + 3\left(c^2_{a,{\rm de}} - w_{\rm de} + \tfrac{1}{3}\epsilon_{\rm H}\right)\hat{\Theta}_{\rm de} - 3c^2_{a,{\rm de}}\Delta_{\rm de} - 2w_{\rm de}\Pi^{\rm S}_{\rm de} - 3w_{\rm de}\Gamma_{\rm de} = 3\left(1+w_{\rm de}\right)Y. \tag{IV.88}$$

The projections of the dark sector stress-energy tensor can be used to extract the expressions of the anisotropic stress and entropy perturbations in terms of the dark sector fluid perturbations $\left\{\Delta_{\rm de}, \hat{\Theta}_{\rm de}\right\}$ and the metric variables $\{W, X, Y, Z\}$. Then one can use the perturbed field equations to express the metric variables in terms of the matter and dark sector fluid variables.

Therefore the dark sector equations of state for scalar perturbations can always be written in the following manner

$$\begin{aligned}
w_{\rm de}\Pi^{\rm S}_{\rm de} &= c_{\Pi\Delta_{\rm de}}\Delta_{\rm de} + c_{\Pi\Theta_{\rm de}}\hat{\Theta}_{\rm de} \\
&+ c_{\Pi\Delta_{\rm m}}\left\langle\frac{\Omega_{\rm m}}{\Omega_{\rm de}}\Delta_{\rm m}\right\rangle + c_{\Pi\Delta_{\rm m}}\left\langle\frac{\Omega_{\rm m}}{\Omega_{\rm de}}\hat{\Theta}_{\rm m}\right\rangle + c_{\Pi\Pi_{\rm m}}\left\langle\frac{\Omega_{\rm m}}{\Omega_{\rm de}}w_{\rm m}\Pi^{\rm S}_{\rm m}\right\rangle, \\
w_{\rm de}\Gamma_{\rm de} &= c_{\Gamma\Delta_{\rm de}}\Delta_{\rm de} + c_{\Gamma\Theta_{\rm de}}\hat{\Theta}_{\rm de} \\
&+ c_{\Gamma\Delta_{\rm m}}\left\langle\frac{\Omega_{\rm m}}{\Omega_{\rm de}}\Delta_{\rm m}\right\rangle + c_{\Gamma\Theta_{\rm m}}\left\langle\frac{\Omega_{\rm m}}{\Omega_{\rm de}}\hat{\Theta}_{\rm m}\right\rangle + c_{\Gamma\Gamma_{\rm m}}\left\langle\frac{\Omega_{\rm m}}{\Omega_{\rm de}}w_{\rm m}\Gamma_{\rm m}\right\rangle.
\end{aligned} \tag{IV.89}$$

These constitute the most generic form of the equations of state for dark sector perturbations. A specific dark sector theory determines the coefficients $c_{\Pi X}$ and $c_{\Gamma X}$ in terms of background quantities.

IV.2.5 Numerical implementation of the EoS for dark sector perturbations

The set of differential equations (IV.79)-(IV.86) is solved numerically in the perturbation module of CLASS [105] after the integration of the background equations (Friedmann equation and conservation equations for each fluid specie). I have added in CLASS the dark sector equations of motion for the gauge invariant density, $\Delta_{\rm de}$, (IV.87) and the velocity perturbations, $\hat{\Theta}_{\rm de}$, (IV.88).

Initial conditions

Since dark energy becomes significant at late time, we set initial conditions in matter domination some time before matter-dark energy equality around redshift of about one hundred. Our generic choice is $a_{\rm ini} = 10^{-2}$ with

$$\Delta_{\rm de}\left(a_{\rm ini}\right) = 0 \quad \text{and} \quad \hat{\Theta}_{\rm de}\left(a_{\rm ini}\right) = 0. \tag{IV.90}$$

In fact, the specific initial values for $\Delta_{\rm de}$ and $\hat{\Theta}_{\rm de}$ are not important as dark sector perturbations tend to converge rapidly towards an attractor that depends on the behavior of the matter sector. This point is illustrated in $f(\mathcal{R})$ gravity on figure 2. For an effective dark energy fluid given by a $\{w_0, w_{\rm a}\}$ parametrization I refer to [21].

Filling the total stress energy tensor

Before each step of integration, we collect the matter fluid variables $\langle\Delta_{\rm m}\rangle$, $\left\langle\hat{\Theta}_{\rm m}\right\rangle$, $\langle\Pi^{\rm S}_{\rm m}\rangle$ and $\langle\Gamma_{\rm m}\rangle$ which are readily available in CLASS. Then they are used to get the dark sector anisotropic stress and entropy perturbation. One has to take care of the definitions and conventions of CLASS which differs from the

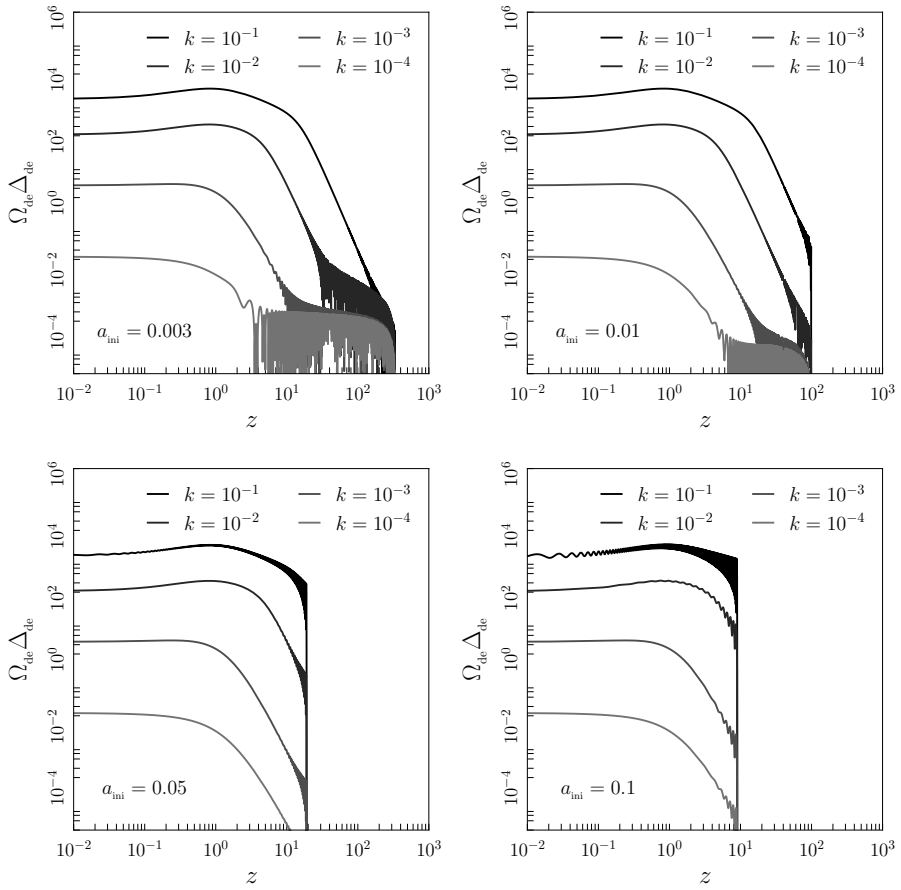

Figure 2: Time evolution of the rescaled dark sector density perturbation $\Omega_{\rm de}\Delta_{\rm de}$ in $f(\mathcal{R})$ gravity as we vary the initial time (or scale factor), $a_{\rm ini}$, at which dark sector perturbations are 'turned on'. Other parameters were set to $B_0 = 1$, $w_{\rm de} = -1$, with $h = 0.673$ and $\Omega_{\rm m}^0 = 0.315$. With these parameters, dark energy-matter equality occurs at $a_\Lambda \simeq 0.77$. The different initial scale factors are: $a_{\rm ini} = 0.003$ (top left); $a_{\rm ini} = 0.01$ (top right); $a_{\rm ini} = 0.05$ (bottom left); $a_{\rm ini} = 0.1$ (bottom right). In each panel we present the evolution of the over-density for four wavenumbers between $k = 10^{-1}\,{\rm Mpc}^{-1}$ and $k = 10^{-4}\,{\rm Mpc}^{-1}$. These results were obtained with `class_eos`.

conventions adopted here. In particular, the total matter anisotropic stress and entropy perturbations are obtained via

$$\langle w_{\rm m}\Pi_{\rm m}^{\rm S}\rangle = -\tfrac{3}{2}\left\langle (1+w_{\rm m})\,\sigma_{\rm m}^{\rm CLASS}\right\rangle \quad \text{and} \quad \langle w_{\rm m}\Gamma_{\rm m}\rangle = \frac{\langle \delta P_{\rm m}\rangle}{\rho_{\rm m}} - c_{a,{\rm m}}^2\,\langle \delta_{\rm m}\rangle\,, \tag{IV.91}$$

where $\sigma_{\rm m}^{\rm CLASS}$ is the anisotropic stress in the conventions of CLASS. The *effective* adiabatic sound-speed of the matter sector is given by

$$c_{a,{\rm m}}^2 = \frac{w_{\rm m}\Omega_{\rm m} + \left\langle w_{\rm m}^2\Omega_{\rm m}\right\rangle}{(1+w_{\rm m})\,\Omega_{\rm m}}, \tag{IV.92}$$

as can be shown by a short calculation. Moreover the perturbed velocity in CLASS is related to ours via $\theta^{\rm CLASS} = \left(k^2/a\right)\theta$.

Then, we update the total stress energy tensor with the dark sector contribution

$$\delta\rho_{\rm tot} = \langle\delta\rho_{\rm m}\rangle + \delta\rho_{\rm de}, \tag{IV.93}$$
$$(\rho_{\rm tot}+P_{\rm tot})\,\theta^{\rm CLASS}_{\rm tot} = \langle(\rho_{\rm m}+P_{\rm m})\,\theta^{\rm CLASS}_{\rm m}\rangle + \tfrac{1}{3}{\rm K}^2 aH\rho_{\rm de}\Theta_{\rm de}, \tag{IV.94}$$
$$(\rho_{\rm tot}+P_{\rm tot})\,\sigma^{\rm CLASS}_{\rm tot} = \langle(\rho_{\rm m}+P_{\rm m})\,\sigma^{\rm CLASS}_{\rm m}\rangle - \tfrac{2}{3}w_{\rm de}\Pi^{\rm S}_{\rm de}, \tag{IV.95}$$
$$\delta P_{\rm tot} = \langle\delta P_{\rm m}\rangle + \delta P_{\rm de}. \tag{IV.96}$$

These perturbed fluid quantities can be combined and fed to the RHS of the perturbed field equations (IV.69)-(IV.72) to deduce the metric perturbations $\{W, X, Y, Z\}$ and in particular X and Y which are the source terms of the dark sector perturbed fluid equations. These two first order differential equation can then be solved numerically by CLASS in exactly the same way as the ones for the other matter species.

IV.3 The Equation of State for perturbations in Horndeski models

We shall now present the equations of state for dark sector perturbations for the most general class of scalar-tensor theories which are Lorentz invariant and have at most second order equations of motion.

IV.3.1 Horndeski Lagrangian

This class of models is based on the Horndeski Lagrangian density

$$\mathcal{L}_{\rm ds} = \sum_{i=2}^{5}\mathcal{L}_i \tag{IV.97}$$

where

$$\begin{aligned}
&\mathcal{L}_2 \equiv G_2(\varphi,{\rm X}),\\
&\mathcal{L}_3 \equiv G_3(\varphi,{\rm X})\,\Box\varphi,\\
&\mathcal{L}_4 \equiv G_4(\varphi,{\rm X})\,\mathcal{R} + G_{4{\rm X}}(\varphi,{\rm X})\left[(\Box\varphi)^2 - \varphi_{;\mu\nu}\varphi^{;\mu\nu}\right],\\
&\mathcal{L}_5 \equiv G_5(\varphi,{\rm X})\,G_{\mu\nu}\varphi^{;\mu\nu} - \tfrac{1}{6}G_{5{\rm X}}(\varphi,{\rm X})\left[(\Box\varphi)^3 + 2\varphi^{\nu}_{;\mu}\varphi^{\alpha}_{;\nu}\varphi^{\mu}_{;\alpha} - 3\varphi_{;\mu\nu}\varphi^{;\mu\nu}\,\Box\varphi\right],
\end{aligned} \tag{IV.98}$$

where the G_i's are four arbitrary functions and where we used the following definitions and notations for the kinetic term and the covariant derivatives

$${\rm X} \equiv \tfrac{1}{2}\nabla_\mu\nabla^\mu\varphi, \quad \varphi_{;\mu\nu} \equiv \nabla_\mu\nabla_\nu\varphi, \quad \varphi^{\nu}_{;\mu} \equiv \nabla_\mu\nabla^\nu\varphi, \quad G_{i{\rm X}} \equiv \frac{\partial G_i}{\partial {\rm X}}. \tag{IV.99}$$

Most of the well-known dark energy models can be formulated in this context, such as quintessence, k-essence, kinetic gravity braiding and $f(\mathcal{R})$ gravity. To recover $k-$essence one has to set $G_3 = G_5 = 0$ and $G_4 = (1/2)$. Quintessence then corresponds to a specific form for G_2, namely $G_2 = \frac{1}{2}\dot\varphi^2 - V(\varphi)$. Finally, $f(\mathcal{R})$ gravity, *i.e.* $\mathcal{L}_{\rm ds} = F(\mathcal{R})$, is recovered in this formalism with $G_3 = G_5 = 0$, $G_4 = \frac{1}{2}F_\mathcal{R}$ and $G_2 = \frac{1}{2}(F - \mathcal{R}F_\mathcal{R})$, with the scalar field given by $\varphi \equiv \sqrt{3/2}\ln F_\mathcal{R}$.

IV.3.2 The alpha functions and the generic EoS

After performing a $3+1$ split, the freedom in the choice of the functions G_i's is recast into four time-dependent functions $\left\{M_\star^2, \alpha_{\rm B}, \alpha_{\rm K}, \alpha_{\rm T}\right\}$. These are linear combination of the G_i's and their derivatives and have a clear phenomenological interpretation [28, 162]. For convenience, we also define

$$\alpha_{\rm M} \equiv 2\frac{M_\star'}{M_\star}, \quad \mu \equiv \frac{M_{PL}^2}{M_\star^2} \quad \text{and} \quad \nu \equiv \alpha_{\rm K}\alpha\mu - 1, \tag{IV.100}$$

with

$$\alpha \equiv \left(\alpha_{\rm K} + 6\alpha_{\rm B}^2\right)^{-1}. \tag{IV.101}$$

In terms of these functions, the coefficients appearing in the equations of state for dark sector perturbations (IV.89) are given by

$$\begin{aligned}
c_{\Pi\Delta_{\rm de}} &= -\tfrac{1}{2} g_0\left({\rm K}\right) g_1\left({\rm K}\right) \\
c_{\Pi\Theta_{\rm de}} &= \tfrac{1}{12}\alpha\left[\alpha_{\rm T} - \alpha_{\rm M}\right]{\rm K}^2 g_0\left({\rm K}\right) \\
c_{\Pi\Delta_{\rm m}} &= -\tfrac{1}{2}\mu\alpha_{\rm T} + \tfrac{1}{2}\left[\mu - 1\right] g_0\left({\rm K}\right) g_1\left({\rm K}\right) \\
c_{\Pi\Theta_{\rm m}} &= \left[1 - \mu + 3\mu\alpha_{\rm B}^2\left\{\alpha_{\rm T} - \alpha_{\rm M}\right\}\right]{\rm K}^2 g_0\left({\rm K}\right) \\
c_{\Pi\Pi_{\rm m}} &= \mu - 1
\end{aligned} \tag{IV.102}$$

for the anisotropic stress and

$$\begin{aligned}
c_{\Gamma\Delta_{\rm de}} &= g_0\left({\rm K}\right) g_2\left({\rm K}\right) - c_{a,{\rm de}}^2 \\
c_{\Gamma\Theta_{\rm de}} &= -\tfrac{1}{3} g_0\left({\rm K}\right) g_3\left({\rm K}\right) + c_{a,{\rm de}}^2 \\
c_{\Gamma\Delta_{\rm m}} &= \left[1 - \mu\right] g_0\left({\rm K}\right) g_2\left({\rm K}\right) + \beta\mu + \nu c_{a,{\rm m}}^2 \\
c_{\Gamma\Theta_{\rm m}} &= \tfrac{1}{3}\left[\mu - 1\right] g_0\left({\rm K}\right) g_3\left({\rm K}\right) - \tfrac{1}{3}\mu g_0\left({\rm K}\right) g_4\left({\rm K}\right) - \nu c_{a,{\rm m}}^2 \\
c_{\Gamma\Gamma_{\rm m}} &= \nu
\end{aligned} \tag{IV.103}$$

for the entropy perturbation. Here, we have introduced

$$\beta \equiv \tfrac{1}{3}\alpha\left[\alpha_{\rm K}\alpha_{\rm M} - 6\alpha_{\rm B}^2 + \left(\alpha_{\rm K} - 6\alpha_{\rm B}\right)\left(\alpha_{\rm T} - \alpha_{\rm M}\right)\right], \tag{IV.104}$$

as well as the five scale dependent functions

$$g_0\left({\rm K}\right) = \left(\gamma_0 + \alpha_{\rm B}^2{\rm K}^2\right)^{-1} \tag{IV.105}$$

$$g_i\left({\rm K}\right) = \gamma_0\gamma_i + \bar{\gamma}_i{\rm K}^2 \quad i \in \{1, .., 4\} \tag{IV.106}$$

where

$$\begin{aligned}
\gamma_0 &= -\tfrac{3}{4}\alpha_{\rm K}\mu\left(1 + w_{\rm m}\right)\Omega_{\rm m} + \tfrac{1}{2}\alpha^{-1}\epsilon_{\rm H} \\
\gamma_1 &= \alpha_{\rm T}, \\
\gamma_2 &= \mathcal{C}_s^2 + \tfrac{1}{3}\alpha_{\rm T} - 4\alpha_{\rm B}\alpha - 2\alpha\mathcal{D} + 2\left(1 + \alpha_{\rm B}\right)\left(\alpha_{\rm T} - \alpha_{\rm M}\right)\alpha \\
\gamma_3 &= \frac{1}{2\epsilon_{\rm H} - 3\mu\left(1 + w_{\rm m}\right)\Omega_{\rm m}}\Big\{2\epsilon_{\rm H} + 2\bar{\epsilon}_{\rm H} - \mu\alpha_{\rm M} + \\
&\qquad + 9\mu\left(1 + w_{\rm m}\right)\Omega_{\rm m}\left[2\alpha_{\rm B}^2\alpha\left(3 + \alpha_{\rm M}\right) - \alpha_{\rm K}c_{a,{\rm m}}^2 + 2\alpha_{\rm B}\alpha\mathcal{D}\right]\Big\} \\
\gamma_4 &= \alpha_{\rm K}\alpha_{\rm M}\alpha - 18\alpha_{\rm B}^2\alpha - 6\alpha_{\rm B}\alpha\mathcal{D}
\end{aligned} \tag{IV.107}$$

and

$$\begin{aligned}
\bar{\gamma}_1 &= \alpha_{\rm B}^2\alpha_{\rm T} + \alpha_{\rm B}\left(\alpha_{\rm T} - \alpha_{\rm M}\right) \\
\bar{\gamma}_2 &= \alpha_{\rm B}^2\mathcal{C}_s^2 + \tfrac{1}{3}\alpha_{\rm B}^2\alpha_{\rm T} + \tfrac{1}{3}\alpha_{\rm B}\left(\alpha_{\rm T} - \alpha_{\rm M}\right) \\
\bar{\gamma}_3 &= -\alpha_{\rm B}^2 - \tfrac{1}{6}\left(\alpha_{\rm T} - \alpha_{\rm M}\right)\left(6\alpha_{\rm B} - \alpha_{\rm K}\right) + \alpha_{\rm B}\alpha\left(\alpha_{\rm K}'\alpha_{\rm B} - 2\alpha_{\rm K}\alpha_{\rm B}'\right) \\
\bar{\gamma}_4 &= \beta\alpha_{\rm B}^2
\end{aligned} \tag{IV.108}$$

with

$$\begin{aligned}\mathcal{C}_s^2 &= 2\alpha\left(1+\alpha_{\rm B}\right)\left[\epsilon_{\rm H}+\alpha_{\rm M}-\alpha_{\rm T}-\alpha_{\rm B}-\alpha_{\rm B}\alpha_{\rm T}\right]-2\alpha_{\rm B}'-3\mu\left(1+w_{\rm m}\right)\Omega_{\rm m},\\ \mathcal{D} &= \tfrac{3}{4}\gamma_1^{-1}\alpha_{\rm K}\alpha_{\rm B}\mu\left(1+w_{\rm m}\right)\Omega_{\rm m}\left[3c_{a,{\rm m}}^2+\left(3+\alpha_{\rm M}\right)\right]\\ &\quad-\tfrac{1}{4}\gamma_1^{-1}\left(\alpha_{\rm K}'\alpha_{\rm B}-2\alpha_{\rm K}\alpha_{\rm B}'\right)\left[3\mu\left(1+w_{\rm m}\right)\Omega_{\rm m}-2\epsilon_{\rm H}\right]-\tfrac{1}{2}\gamma_1^{-1}\alpha_{\rm B}\alpha^{-1}\left(4\epsilon_{\rm H}-\bar{\epsilon}_{\rm H}\right).\end{aligned}\tag{IV.109}$$

This determines completely the EoS for perturbations in the dark sector. The α functions can either be deduced from a specific modified gravity model or from a phenomenological parametrization.

IV.3.3 Phenomenological parametrization

A common choice is to set the alpha functions proportional to the dark energy density parameter [162],

$$\alpha_{\rm M}\left(a\right)=\alpha_{\rm K}^0\Omega_{\rm de}\left(a\right),\quad \alpha_{\rm K}\left(a\right)=\alpha_{\rm K}^0\Omega_{\rm de}\left(a\right),\quad \alpha_{\rm B}\left(a\right)=\alpha_{\rm B}^0\Omega_{\rm de}\left(a\right),\quad \alpha_{\rm T}\left(a\right)=\alpha_{\rm T}^0\Omega_{\rm de}\left(a\right),\tag{IV.110}$$

with $\left\{\alpha_{\rm M}^0,\alpha_{\rm K}^0,\alpha_{\rm B}^0,\alpha_{\rm T}^0\right\}$ some numbers that are the values of these functions today.

One also needs to specify $M_{\star,{\rm ini}}^2$, the present value of $M_\star^2$, in order to deduce $M_\star^2\left(a\right)$ via the integration of $\alpha_{\rm M}$. Such parametrization implies that the time evolution of $\Omega_{\rm de}$ is known.

A simple way to to determine the time evolution of $\Omega_{\rm de}$ is to demand a constant equation of state, $w_{\rm de}=w_0$, or the $\left\{w_0,w_{\rm a}\right\}$ parametrization with $w\left(a\right)=w_0+w_{\rm a}\left(1-a\right)$. Then, given some observational data, it is possible to extract constraints on the dark sector parameter space.

IV.3.4 Quintessence and wCDM models

Let us now illustrate the other possibility, that is a modified gravity model belonging to the Horndeski class of theories. The simplest one is certainly quintessence, i.e. a scalar field φ with a potential $V\left(\varphi\right)$ such as the background equation of state is constant or given by the $\left\{w_0,w_{\rm a}\right\}$ parametrization. Then, one easily finds the alpha functions and dark sector EoS:

$$\text{[wCDM and quintessence]}\quad\begin{cases}\alpha_{\rm M}=0, & \alpha_{\rm K}=3\left(1+w_{\rm de}\right)\Omega_{\rm de},\\ \alpha_{\rm B}=0, & \alpha_{\rm T}=0,\quad M_\star^2=1,\end{cases}\Rightarrow\begin{cases}w_{\rm de}\Pi_{\rm de}^{\rm S}=0\\ w_{\rm de}\Gamma_{\rm de}=\left(c_{s,{\rm de}}^2-c_{a,{\rm de}}^2\right)\Delta_{\rm de}\end{cases}\tag{IV.111}$$

Note that properly speaking, wCDM can have arbitrary $w_{\rm de}$ and $c_{s,{\rm de}}^2$, while for quintessence the sound speed has to be the speed of light $c_{s,{\rm de}}^2=1$.

IV.3.5 $f\left(\mathcal{R}\right)$ modifications to gravity

We shall now focus on $f\left(\mathcal{R}\right)$ gravity, which, in spite of being observationally unfavored and of suffering from conceptual problems, presents the advantages of being a non-trivial modification to gravity that can be studied analytically to some extent. The Lagrangian for $f\left(\mathcal{R}\right)$ gravity (in the metric formalism) is

$$\mathcal{L}_{\rm ds}=\mathcal{R}+f\left(\mathcal{R}\right),\tag{IV.112}$$

and leads to

$$\text{[}f\left(\mathcal{R}\right)\text{ gravity]}\quad\begin{cases}\alpha_{\rm M}=f_{\mathcal{R}}'/\left(1+f_{\mathcal{R}}\right), & \alpha_{\rm K}=0,\\ \alpha_{\rm B}=f_{\mathcal{R}}'/2\left(1+f_{\mathcal{R}}\right), & \alpha_{\rm T}=0,\quad M_\star^2=\left(1+f_{\mathcal{R}}\right).\end{cases}\tag{IV.113}$$

The coefficients entering the equations of state for scalar perturbations are given by

$$
\begin{aligned}
c_{\Pi\Delta_{\rm de}} &= \frac{\mathrm{K}^2}{3g_{\mathrm{K}}\epsilon_{\mathrm{H}}}, & c_{\Gamma\Delta_{\rm de}} &= \zeta_{\rm de} - \frac{\bar{\epsilon}_{\mathrm{H}}}{3g_{\mathrm{K}}\epsilon_{\mathrm{H}}}\left(\frac{2(1+f_{\mathcal{R}})}{f'_{\mathcal{R}}} - 1\right),\\
c_{\Pi\Theta_{\rm de}} &= -\frac{\mathrm{K}^2}{3g_{\mathrm{K}}\epsilon_{\mathrm{H}}}\frac{f'_{\mathcal{R}}}{2(1+f_{\mathcal{R}})}, & c_{\Gamma\Theta_{\rm de}} &= -\zeta_{\rm de},\\
c_{\Pi\Delta_{\rm m}} &= \frac{\mathrm{K}^2}{3g_{\mathrm{K}}\epsilon_{\mathrm{H}}}\frac{f_{\mathcal{R}}}{1+f_{\mathcal{R}}}, & c_{\Gamma\Delta_{\rm m}} &= \zeta_{\rm m} - \frac{\bar{\epsilon}_{\mathrm{H}}}{3g_{\mathrm{K}}\epsilon_{\mathrm{H}}}\left(\frac{2f_{\mathcal{R}}}{f'_{\mathcal{R}}} - 1\right),\\
c_{\Pi\Theta_{\rm m}} &= -\frac{\mathrm{K}^2}{3g_{\mathrm{K}}\epsilon_{\mathrm{H}}}\frac{f'_{\mathcal{R}}}{2(1+f_{\mathcal{R}})}, & c_{\Gamma\Theta_{\rm m}} &= -\zeta_{\rm m},\\
c_{\Pi\Pi_{\rm m}} &= -\frac{\mathrm{K}^2}{3g_{\mathrm{K}}\epsilon_{\mathrm{H}}}\frac{f_{\mathcal{R}}}{1+f_{\mathcal{R}}}, & c_{\Gamma\Gamma_{\rm m}} &= -1.
\end{aligned}
\tag{IV.114}
$$

where

$$
\zeta_{\rm i} \equiv \frac{g_{\mathrm{K}}\epsilon_{\mathrm{H}} - \bar{\epsilon}_{\mathrm{H}}}{3g_{\mathrm{K}}\epsilon_{\mathrm{H}}} - c^2_{a,{\rm i}}, \quad \text{with} \quad {\rm i} \in \{{\rm m}, {\rm de}\}\,. \tag{IV.115}
$$

The equations of state in the vector and tensor sectors are simple:

$$
w_{\rm de}\boldsymbol{\Pi}^{\mathbf{V}}_{\mathbf{de}} = -\frac{1}{6\Omega_{\rm de}}\left[f_{\mathcal{R}}\boldsymbol{h}^{\mathbf{V}\prime\prime} + \left\{f'_{\mathcal{R}} + (3-\epsilon_{\mathrm{H}})\,f_{\mathcal{R}}\right\}\boldsymbol{h}^{\mathbf{V}\prime}\right], \tag{IV.116}
$$

$$
w_{\rm de}\boldsymbol{\Pi}^{\mathbf{T}}_{\mathbf{de}} = -\frac{1}{6\Omega_{\rm de}}\left[f_{\mathcal{R}}\boldsymbol{h}^{\mathbf{T}\prime\prime} + \left\{f'_{\mathcal{R}} + (3-\epsilon_{\mathrm{H}})\,f_{\mathcal{R}}\right\}\boldsymbol{h}^{\mathbf{T}\prime} + f_{\mathcal{R}}\mathrm{K}^2\boldsymbol{h}^{\mathbf{T}}\right]. \tag{IV.117}
$$

The dynamics of vector and tensor perturbations, in $f(\mathcal{R})$ gravity or wCDM models, are not discussed in this manuscript. Vector perturbations do not present much interest since it is difficult to build a cosmological scenario that would generate vector perturbations to an observable level. Primordial vector perturbations are exponentially diluted by inflation, as can be deduced from the absence of a term proportional to $\boldsymbol{h}^{\mathbf{V}}$ in their equation of motion (IV.73). Tensor perturbations are more interesting, due to the last term in the RHS of Eq. (IV.117) which generates an effective mass term in their equation of evolution. The associated phenomenology was studied recently in [14] for primordial tensor perturbations, and in [153] for astrophysical gravitational waves.

IV.4 Phenomenology of cosmological perturbations in $f(\mathcal{R})$ gravity

Since dark sector perturbations become significant around matter-dark energy equality, when the matter sector is dominated by cold dark matter, we can safely assume that the matter sector is pressure-less, $w_m = c^2_{a,{\rm m}} = 0$, with no anisotropic stress nor entropy perturbation, $w_{\rm m}\Pi^{\rm S}_{\rm m} = w_{\rm m}\Gamma_{\rm m} = 0$. Then, from the field equations, one gets

$$
\epsilon_{\mathrm{H}} = \tfrac{3}{2}\left(1 + w_{\rm de}\Omega_{\rm de}\right), \qquad \text{and} \qquad \epsilon'_{\mathrm{H}} = \tfrac{9}{2}\left(1+w_{\rm de}\right)\left(w_{\rm de} - c^2_{a,{\rm de}}\right)\Omega_{\rm de}. \tag{IV.118}
$$

Hence, during matter domination, when $\Omega_{\rm de} \ll 1$ and assuming that the equation of state parameter remains bounded $w_{\rm de} = \mathcal{O}(1)$, one has $\epsilon'_{\mathrm{H}} = \bar{\epsilon}'_{\mathrm{H}} = 0$ and $\epsilon_{\mathrm{H}} = \bar{\epsilon}_{\mathrm{H}} = 3/2$. This has important consequences for the $f(\mathcal{R})$ function.

Indeed, the time-time projection of the effective stress-energy tensor corresponding to $f(\mathcal{R})$ gravity leads to

$$
\Omega_{\rm de} = -\frac{f}{6H^2} + (1-\epsilon_{\mathrm{H}})\,f_{\mathcal{R}} - f'_{\mathcal{R}}. \tag{IV.119}
$$

Noticing that $f_{\mathcal{R}} = (f'/\mathcal{R}')$, this equation can be recast into a second order differential equation on $f(\mathcal{R})$,

$$
f'' + \left(3\epsilon_{\mathrm{H}} - 1 - \frac{\bar{\epsilon}'_{\mathrm{H}}}{\bar{\epsilon}_{\mathrm{H}}}\right)f' - \bar{\epsilon}_{\mathrm{H}}f = 6H^2\bar{\epsilon}_{\mathrm{H}}\Omega_{\rm de}. \tag{IV.120}
$$

This equation holds for any $f(\mathcal{R})$ gravity theory and at any time during the expansion history. Hence, during matter domination in virtue of what we just saw, it reduces to

$$
f'' + \tfrac{7}{2}f' - \tfrac{3}{2}f = 3\rho^0_{\rm de}e^{-3\int(1+w_{\rm de})dN}, \quad \text{when} \quad \Omega_{\rm de} \ll 1 \quad \text{and} \quad w_{\rm de} = \mathcal{O}(1)\,, \tag{IV.121}
$$

where $N \equiv \ln a$ and $\rho_{\rm de}^0$ is the value of dark energy density today. The set of solutions to (IV.121) is a linear combinations of power laws plus a particular solution associated with the RHS. One gets

$$f(a) = b_+ a^{n_+} + b_- a^{n_-} + f_{\rm part}(a), \quad \text{with} \quad n_\pm = \frac{7}{4}\left(-1 \pm \sqrt{1+\frac{24}{7}}\right). \tag{IV.122}$$

The decaying mode, $b_- a^{n_-}$, is not admissible as it breaks the viability condition $\lim_{a\to 0} f_{\mathcal{R}} = 0$ (see [64] for details), hence its amplitude has to be set to zero, $b_- = 0$. Note that $n_+ \simeq 3.89$. So, once a $f(\mathcal{R})$ model has been specified, and therefore the time evolution of $w_{\rm de}$ and $f_{\rm part}$ are known, there remains a freedom in the choice of b_+ to select a solution to (IV.121). A more convenient quantity to parametrize the set of solutions is B_0, the present value of the quantity

$$B \equiv -\frac{f_{\mathcal{R}}'}{\epsilon_{\rm H}(1+f_{\mathcal{R}})}. \tag{IV.123}$$

There is a one-to-one correspondence between b_+ and B_0. In our modified version of CLASS, the user specifies a $f(\mathcal{R})$ function and asks for a value of B_0, then the code explores a range of b_+ solving (IV.121), between $a_{\rm ini}$ and today, until the value of b_+ that leads to the desired value of B_0.

The range of wave numbers of interest for cosmological observables lies between $10^{-4}{\rm Mpc}^{-1}$ and $10{\rm Mpc}^{-1}$. For those modes, one always has ${\rm K} \gg 1$ between $z = 0$ and $z \simeq 100$. So let us study the dynamics of dark sector sub-horizon modes. For simplicity, we assume that the equation of state is constant, i.e. $c^2_{a,{\rm de}} = w_{\rm de}$. In this regime, the equations of state for scalar perturbations take a very simple form,

$$w_{\rm de}\Pi^{\rm S}_{\rm de} = \Delta_{\rm de}, \tag{IV.124}$$

$$w_{\rm de}\Gamma_{\rm de} = \left\{\tfrac{1}{3} - w_{\rm de} + \frac{{\rm M}^2}{{\rm K}^2}\right\}\Delta_{\rm de} + \tfrac{1}{3}\Omega_{\rm m}\Delta_{\rm m}, \quad \text{with} \quad {\rm M}^2 \equiv \frac{2\bar{\epsilon}_{\rm H}}{\epsilon_{\rm H}}B^{-1}, \tag{IV.125}$$

and the perturbed fluid equations reduce to

$$\Delta_{\rm m}' = -\tfrac{1}{3}{\rm K}^2\hat{\Theta}_{\rm m}, \qquad \hat{\Theta}_{\rm m}' = -\epsilon_{\rm H}\hat{\Theta}_{\rm m} + 3Y, \tag{IV.126}$$

$$\Delta_{\rm de}' = -\tfrac{1}{3}{\rm K}^2\hat{\Theta}_{\rm de}, \qquad \hat{\Theta}_{\rm de}' = -\epsilon_{\rm H}\hat{\Theta}_{\rm de} + 3\left(1+\frac{{\rm M}^2}{{\rm K}^2}\right)\Delta_{\rm de} + \frac{\Omega_{\rm m}}{\Omega_{\rm de}}\Delta_{\rm m}. \tag{IV.127}$$

Using the field equations (IV.69)-(IV.72), these can be rewritten as a system of two coupled second order differential equations for $\Delta_{\rm m}$ and $\Delta_{\rm de}$,

$$\Delta_{\rm m}'' + (2-\epsilon_{\rm H})\Delta_{\rm m}' - \tfrac{3}{2}\Omega_{\rm m}\Delta_{\rm m} = -\tfrac{3}{2}\Omega_{\rm de}\Delta_{\rm de}, \tag{IV.128}$$

$$\Delta_{\rm de}'' + (2-\epsilon_{\rm H})\Delta_{\rm de}' + \left({\rm K}^2+{\rm M}^2\right)\Delta_{\rm de} = -\tfrac{1}{3}\frac{\Omega_{\rm m}}{\Omega_{\rm de}}{\rm K}^2\Delta_{\rm m}. \tag{IV.129}$$

Again, this holds for any $f(\mathcal{R})$ model in both matter and dark energy domination as long as $w_{\rm de}$ is constant and the matter sector is pressure-less. Nonetheless, the extension to varying $w_{\rm de}$ is straightforward and should not affect the subsequent conclusions.

Deep inside matter domination when $\epsilon_{\rm H} = 3/2$ and $\Omega_{\rm de} \ll \Omega_{\rm m} \simeq 1$, the matter perturbation is insensitive to the dark sector and grows as $\Delta_{\rm m} \sim a$ as can be deduced from (IV.128). Moreover, the gravitational potential Y and Z (or ϕ and ψ in the CNG) are equal. The dark sector perturbation $\Delta_{\rm de}$ oscillates at a time dependent frequency $\omega = \sqrt{{\rm K}^2+{\rm M}^2}$ rapidly converging towards the attractor

$$\Delta_{\rm de} = -\frac{1}{3}\frac{{\rm K}^2}{{\rm K}^2+{\rm M}^2}\frac{\Omega_{\rm m}}{\Omega_{\rm de}}\Delta_{\rm m} = \frac{1}{3\Omega_{\rm de}}\frac{2{\rm K}^2}{2{\rm K}^2+3{\rm M}^2}{\rm K}^2 Z, \tag{IV.130}$$

where we used (IV.69) for the second equality. This confirms that the specific values for the initial dark sector perturbations are not important, as long as they are initially small compared to matter

perturbations. For all $f(\mathcal{R})$ models M^2 always dominates over K^2 at sufficiently early time and therefore the frequency of the oscillations becomes independent of the wavenumber. Indeed during matter domination K is decreasing with redshift z,

$$\mathrm{K}' = \mathrm{K}\,(\epsilon_{\mathrm{H}} - 1) \quad \text{and} \quad \epsilon_{\mathrm{H}} = 3/2 \quad \Rightarrow \mathrm{K}^2 \sim z^{-1}, \tag{IV.131}$$

while M^2 generically increases. This can be seen easily in the case of a constant w_{de} since then the particular solution in (IV.122) dominates at early time and goes as $f_{\mathrm{part}}(a) \sim a^{-3(1+w_{\mathrm{de}})}$, so that $f_{\mathcal{R}} \sim f'_{\mathcal{R}} \sim a^{-3w_{\mathrm{de}}}$ and

$$\mathrm{M}^2 = -\frac{3}{f'_{\mathcal{R}}} \sim z^{-3w_{\mathrm{de}}} \quad \text{with} \quad w_{\mathrm{de}} < 0 \quad \text{and} \quad \epsilon_{\mathrm{H}} = \bar{\epsilon}_{\mathrm{H}} = 3/2. \tag{IV.132}$$

As a side remark, we conclude from (IV.129) that if M^2 (or B) is negative at early time the dark sector perturbations are unstable during matter domination since the frequency ω would become imaginary.

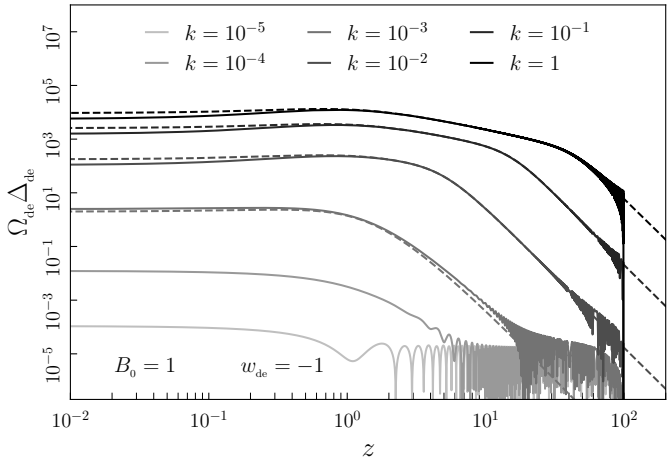

Figure 3: Time evolution of the rescaled dark sector density perturbation $\Omega_{\mathrm{de}}\Delta_{\mathrm{de}}$ in $f(\mathcal{R})$ gravity. Parameters were set to $B_0 = 1$, $w_{\mathrm{de}} = -1$, with $h = 0.673$ and $\Omega_{\mathrm{m}}^0 = 0.315$. With these parameters, dark energy-matter equality occurs at $a_\Lambda \simeq 0.77$. The initial scale factor in $a_{\mathrm{ini}} = 0.01$. We show the evolution of the over-density for four wavenumbers between $k = 10^{-1}\,\mathrm{Mpc}^{-1}$ and $k = 10^{-4}\,\mathrm{Mpc}^{-1}$. The dashed lines represent the attractor given in Eq. (IV.130) corresponding to each wavenumber. These results were obtained with `class_eos`.

Figure 3 presents the time evolution of dark sector perturbations in $f(\mathcal{R})$ gravity. The dynamics for dark sector perturbations starts at $z = 100$. The evolution is plotted for six wavenumbers, ranging from $k = 10^{-5}\mathrm{Mpc}^{-1}$ to $k = 1\mathrm{Mpc}^{-1}$. As predicted, the dark energy over-density oscillates at early time and converges towards the attractor (IV.130) corresponding to the dashed lines on the figure. For the largest wave-length modes, $k < 10^{-3}\mathrm{Mpc}^{-1}$, the attractor is no longer a correct description of the dynamics as these modes are not sub-Hubble. Also, during dark energy domination for $z \lesssim 1$ the dark energy over-density departs slightly from the attractor: at late time the coefficient in front of $\hat{\Theta}_{\mathrm{de}}$ in the EoS may no longer be negligible (compared to one) if $B_0 \sim 1$, however we did not take this into account in our previous approximations.

The presence of non-zero dark sector perturbations affects the evolution of the gravitational potential and therefore the cosmological observables such as the matter power spectrum, weak lensing or the

CMB temperature anisotropy. In what follows, I have reported my article on the treatment of $f(\mathcal{R})$ gravity within the EoS approach where we study the impact of dark sector perturbations on the gravitational potential. After the article, this section continues with a discussion on parametrized post-Friedmann parameters, a comparison between $f(\mathcal{R})$ gravity and wCDM (or quintessence) models, and finally a presentation of the influence of $f(\mathcal{R})$ gravity on the late integrated Sachs-Wolf effect.

$f(\mathcal{R})$ gravity as a dark energy fluid

Richard A. Battye*
Jodrell Bank Centre for Astrophysics, School of Physics and Astronomy, The University of Manchester, Manchester M13 9PL, U.K.

Boris Bolliet†
Laboratoire de Physique Subatomique et de Cosmologie, Université Grenoble-Alpes, CNRS/IN2P3 53, avenue des Martyrs, 38026 Grenoble cedex, France

Jonathan A. Pearson‡
School of Physics and Astronomy, University of Nottingham, Nottingham NG7 2RD, U.K.

(Dated: August 20, 2015)

We study the equations for the evolution of cosmological perturbations in $f(\mathcal{R})$ and conclude that this modified gravity model can be expressed as a dark energy fluid at background and linearised perturbation order. By eliminating the extra scalar degree of freedom known to be present in such theories, we are able to characterise the evolution of the perturbations in the scalar sector in terms of equations of state for the entropy perturbation and anisotropic stress which are written in terms of the density and velocity perturbations of the dark energy fluid and those in the matter, or the metric perturbations. We also do the same in the much simpler vector and tensor sectors. In order to illustrate the simplicity of this formulation, we numerically evolve perturbations in a small number of cases.

I. INTRODUCTION

In the past few years there has been a growing realisation that dark energy [1] and modified gravity theories [2] models need to be confronted with observational data in a systematic way. This has generated interest in constructing frameworks and formalisms for comparing models, or classes of models, to data as opposed to testing individual models. There are number of approaches which have been developed to do this including the Effective Field Theory for dark energy [3–6], Parametrized Post Friedmann framework [7–10], and the Equation of State for perturbations (EoS) [11–13]. These very similar ideas correspond to parameterizations at the level of the perturbed action, perturbed gravitational field equations, and the perturbed dark energy fluid equations, respectively. In this paper we will concentrate on the EoS approach.

Each of these parameterization schemes can be used in two different ways. The first is to construct arbitrary dark sector theories and the second is to map from a given model to the observationally combinations. In the latter of these —"model-mapping" — EoS approach prescribed how micro-physical degree of freedoms in the model combine to affect the evolution of quantities such as densities and velocity fields that are related to observables in terms of equations of state for the gauge invariant entropy and anisotropic stresses. Using the former approach preliminary constraints have been discussed in [14–16] based on presently available cosmological data including that from the Cosmic Microwave Background (CMB), weak lensing and redshift space distortions (RSDs).

One of the most popular modified gravity theories is the $f(R)$ class of models [17, 18]. The $f(\mathcal{R})$ models of gravity are constructed by replacing the Ricci scalar in the Einstein-Hilbert action by an arbitrary function of the Ricci scalar $f(\mathcal{R})$. Such models are well known to lead to an extra scalar degree of freedom and it has been shown, for example in [19–21], that observationally acceptable models can be constructed.

In this paper we provide expressions for the equations of state for perturbations which completely characterize the linearized perturbations in $f(\mathcal{R})$ modified gravity, including the scalar, vector, and tensor modes. Essentially we will model-map this theory into the EoS formalism. In doing this we show that the $f(\mathcal{R})$ modification to General Relativity (GR) can be formulated as a dark energy fluid at background order —something which is well known — and also at first order in perturbations. As well as providing a physical interpretation and allowing these models to be included under the umbrella of the EoS formalism, we will see that writing the theory in this way can allow for a

*Electronic address: richard.battye@manchester.ac.uk
†Electronic address: boris.bolliet@ens-lyon.fr
‡Electronic address: j.pearson@nottingham.ac.uk

very simple inclusion in codes, such as `CAMB`, used to calculate cosmological observables.

II. BACKGROUND FIELD EQUATIONS

The $f(\mathcal{R})$ models of gravity are characterized by the action

$$S = \tfrac{1}{2}\int \mathrm{d}^4x\,\sqrt{-g}\,\{\mathcal{R} + f(\mathcal{R})\} + S_{\rm m}, \tag{2.1}$$

where $\mathcal{R}$ is the Ricci scalar and $S_{\rm m}$ is the action describing the standard matter fields. Natural units, $c = \hbar = M_{\rm Pl} = 1$, are used throughout this paper. Varying the action (2.1) with respect to the space-time metric $g_{\mu\nu}$ yields the field equations,

$$G_{\mu\nu} = T_{\mu\nu} + U_{\mu\nu}, \tag{2.2}$$

where $G_{\mu\nu}$ is the Einstein tensor and $T_{\mu\nu}$ is the stress-energy tensor of the standard matter fields. All contributions due to $f(\mathcal{R})$ are packaged into the extra-term $U_{\mu\nu}$, which we call the stress-energy tensor of the dark sector, explicitly formulated as

$$U_{\mu\nu} \equiv \tfrac{1}{2} f g_{\mu\nu} - (R_{\mu\nu} + g_{\mu\nu}\Box - \nabla_\mu\nabla_\nu)\, f_{\mathcal{R}}, \tag{2.3}$$

where $R_{\mu\nu}$ is the Ricci tensor, and $f_{\mathcal{R}} \equiv \frac{df}{d\mathcal{R}}$. Direct calculation shows that $U_{\mu\nu}$ is covariantly conserved, $\nabla^\mu U_{\mu\nu} = 0$, as is required by the conservation of the matter energy-momentum tensor, $T_{\mu\nu}$. The background geometry is assumed to be isotropic and spatially flat, with a line element written as $ds^2 = -dt^2 + a(t)^2\,\delta_{ij}dx^i dx^j$, where $a(t)$ is the scale factor. Instead of the first and second order time derivative of the Hubble parameter, H, we use the dimensionless parameters[1]

$$\epsilon_{\rm H} \equiv -\frac{H'}{H}, \qquad \bar{\epsilon}_{\rm H} \equiv -\frac{\mathcal{R}'}{6H^2}, \tag{2.4}$$

where the prime denotes derivative with respect to $d/d\ln a$. The dark sector can be viewed as a fluid, with energy density $\rho_{\rm de} \equiv \frac{1}{a^2}U_{00}$ and pressure $P_{\rm de} \equiv \frac{1}{3a^2}\delta^{ij}U_{ij}$. The field equations (2.2) can be recast as

$$\Omega_{\rm m} + \Omega_{\rm de} = 1, \qquad w_{\rm m}\Omega_{\rm m} + w_{\rm de}\Omega_{\rm de} = \tfrac{2}{3}\epsilon_{\rm H} - 1, \tag{2.5}$$

where $\Omega_{\rm i} = \frac{\rho_{\rm i}}{3H^2}$ and $w_{\rm i} \equiv P_{\rm i}/\rho_{\rm i}$ for ${\rm i} \in \{{\rm m}, {\rm de}\}$. From (2.3), the density and equation of state parameters of the $f(\mathcal{R})$ fluid are explicitly given by

$$\Omega_{\rm de} = -\frac{f}{6H^2} + (1-\epsilon_{\rm H})f_{\mathcal{R}} - f'_{\mathcal{R}}, \tag{2.6a}$$

$$w_{\rm de} + 1 = -\frac{1}{3\Omega_{\rm de}}\left(2\epsilon_{\rm H} f_{\mathcal{R}} + (1+\epsilon_{\rm H})f'_{\mathcal{R}} - f''_{\mathcal{R}}\right). \tag{2.6b}$$

The case of a cosmological constant is recovered when $f(\mathcal{R}) = -2\Lambda$, for which (2.2) reduces to the standard Einstein's field equations. Note that (2.6a) is actually a second order differential equation for the function $f(\mathcal{R})$ since $f_{\mathcal{R}} = f'/\mathcal{R}'$. When the equation of state parameters, $w_{\rm i}$'s, are taken to be constant, this equation can be integrated leading to the so-called designer $f(\mathcal{R})$, see [22] for details.

III. GAUGE INVARIANT FORMALISM FOR LINEAR PERTURBATIONS

The dynamics of linear perturbations is written in Fourier space, in both the synchronous and conformal Newtonian gauges. Instead of the coordinate wavenumber that appears in the Fourier transform, k, a reduced dimensionless wavenumber will be used,

$$\mathrm{K} \equiv \frac{k}{aH}, \tag{3.1}$$

[1] With these notation the Ricci scalar reads $\mathcal{R} = 12H^2(1 - \frac{1}{2}\epsilon_{\rm H})$. Furthermore, $\bar{\epsilon}_{\rm H}$ and $\epsilon_{\rm H}$ are related through $\bar{\epsilon}_{\rm H} = \epsilon'_{\rm H} + 4\epsilon_{\rm H} - 2\epsilon_{\rm H}^2$.

so that $\mathrm{K} \ll 1$ and $\gg 1$ can be used identify the sub-(super)-horizon regimes. In the synchronous gauge, the non-zero metric perturbations are $\delta g_{ij} = a^2 h_{ij}$. In an orthonormal basis $\{\hat{k}, \hat{l}, \hat{m}\}$ in k-space, the spatial matrix h_{ij} is further decomposed as $h_{ij} = \frac{1}{3}h\delta_{ij} + h_{\parallel}\sigma_{ij} + h^{\mathrm{V}} \cdot v_{ij} + h^{\mathrm{T}} \cdot e_{ij}$, where the notations $h^{\mathrm{V(T)}}$ contain the two vector (tensor) polarization states (the dot product is to be understood as a sum over the polarization states). Instead of h, we use the combination $6\eta \equiv h_{\parallel} - h$. The basis matrices are $\sigma_{ij} = \hat{k}_i\hat{k}_j - \frac{1}{3}\delta_{ij}$ for the longitudinal traceless mode, $v^{(1)}_{ij} = 2\hat{k}_{(i}\hat{l}_{j)}$ and $v^{(2)}_{ij} = 2\hat{k}_{(i}\hat{m}_{j)}$ for the vector modes and $e^{\times}_{ij} = 2\hat{l}_{[i}\hat{m}_{j]}$, $e^{+}_{ij} = \hat{l}_i\hat{l}_j - \hat{m}_i\hat{m}_j$ for the tensor modes. In the conformal Newtonian gauge, the scalar modes are given by $\delta g_{00} = -2a^2\psi$ and $\delta g_{ij} = -2a^2\phi\delta_{ij}$, while the tensor and vector modes remain the same in both gauges). An additional scalar degree of freedom arises at the perturbative level from the non-vanishing $f'_{\mathcal{R}}$, given by

$$\chi \equiv -\frac{f'_{\mathcal{R}}}{\bar{\epsilon}_{\mathrm{H}}}\frac{\delta\mathcal{R}}{6H^2}. \tag{3.2}$$

This feature was pointed out in [23] and is a manifestation of the well-known connection between $f(\mathcal{R})$ theories and non-minimally coupled scalar-tensor theories [24, 25]. Actually, $f'_{\mathcal{R}}$ constitutes the first non-trivial contribution of an arbitrary function of the Ricci scalar since a linear or affine $f(\mathcal{R})$ can always be recast as standard GR with a rescaled Newton constant [22].

Our results are presented simultaneously in both the synchronous and conformal Newtonian gauges thanks to a new set of variables presented below: W, X, Y, Z for the GR sector and $\hat{\chi}, \hat{\chi}', \hat{\chi}''$ for the $f(\mathcal{R})$ sector. The introduction of this set of variables is motivated by the gauge transformation rules that are recalled in Appendix A. Quantities denoted with the subscript 'S' ('C') are evaluated in the synchronous (conformal Newtonian) gauge.

Symbol	**Synchronous gauge**	**Conformal Newtonian gauge**
T	$\frac{h'_{\parallel}}{2\mathrm{K}^2}$	0
Y	$T' + \epsilon_{\mathrm{H}}T$	ψ
Z	$\eta - T$	ϕ
X	$Z' + Y$	$Z' + Y$
W	$X' - \epsilon_{\mathrm{H}}(X + Y)$	$X' - \epsilon_{\mathrm{H}}(X + Y)$
$\hat{\chi}$	$\chi_s + f'_{\mathcal{R}}T$	χ_c
$\hat{\chi}'$	$\chi'_s + (f''_{\mathcal{R}} - \epsilon_{\mathrm{H}}f'_{\mathcal{R}})T$	$\chi'_c - f'_{\mathcal{R}}\psi$
$\hat{\chi}''$	$\chi''_s - \epsilon_{\mathrm{H}}\chi'_s + (f'''_{\mathcal{R}} - 3\epsilon_{\mathrm{H}}f''_{\mathcal{R}} + (4\epsilon_{\mathrm{H}} - \bar{\epsilon}_{\mathrm{H}})f'_{\mathcal{R}})T$	$\chi''_c - \epsilon_{\mathrm{H}}\chi'_c - f'_{\mathcal{R}}\psi' - 2(f''_{\mathcal{R}} - \epsilon_{\mathrm{H}}f'_{\mathcal{R}})\psi$

(3.3)

Let us emphasize that $\hat{\chi}'$ and $\hat{\chi}''$ are not just the first and second derivatives of $\hat{\chi}$, but are degrees of freedom in their own right. Using these gauge invariant variables, the first order perturbation of the Ricci scalar reads $\delta\mathcal{R} = -6H^2(W + 4X - \frac{1}{3}K^2(Y - 2Z) - \bar{\epsilon}_{\mathrm{H}}T)$. The fact that T appears explicitly in the expression of $\delta\mathcal{R}$ indicates that this is not a gauge invariant quantity, and hence that χ defined in (3.2) is also not gauge invariant. However, $\hat{\chi}$ defined in the table above is gauge invariant and it can be written in terms of the geometric perturbations as

$$\hat{\chi} = \frac{f'_{\mathcal{R}}}{\bar{\epsilon}_{\mathrm{H}}}\left\{W + 4X - \tfrac{1}{3}\mathrm{K}^2(Y - 2Z)\right\}, \tag{3.4}$$

which is valid in both gauges, when W, X, Y and Z are replaced by the corresponding expressions presented in the table.

A generic stress-energy tensor, $D^{\mu}{}_{\nu}$, can be decomposed into

$$\delta D^{\mu}{}_{\nu} = (\rho\delta + \delta P)\, u^{\mu}u_{\nu} + (\rho + P)\,(u_{\nu}\delta u^{\mu} + u^{\mu}\delta u_{\nu}) + \delta P\delta^{\mu}{}_{\nu} + P\Pi^{\mu}{}_{\nu}, \tag{3.5}$$

where the density contrast is $\delta \equiv \delta\rho/\rho$, the Hubble flow is parametrized by $u_{\nu} = (-1, \vec{0})$ in coordinate time, and $\delta u_{\nu} = (0, \delta u_i)$ is the perturbed velocity field whose scalar mode is $\theta \equiv \frac{\mathrm{i}k^j\delta u_j}{k^2}$.

Instead of δ and θ, we make an extensive use of the dimensionless variables

$$\Delta \equiv \delta + 3\,(1 + w)\,H\theta, \qquad \Theta \equiv 3\,(1 + w)\,H\theta. \tag{3.6}$$

In the same way as for the geometric perturbations, it is possible to form gauge invariant combinations of the perturbed fluid variables:

Symbol	**Synchronous gauge**	**Conformal Newtonian gauge**
$\hat{\Theta}$	$\Theta_s + 3\,(1 + w)\,T$	Θ_c
$\delta\hat{P}$	$\delta P_s + P'_s T$	δP_c

(3.7)

The gauge invariant pressure perturbation, $\delta\hat{P}$, is packaged into the gauge invariant entropy perturbation,

$$w\Gamma = \frac{\delta\hat{P}}{\rho} - \frac{dP}{d\rho}\left(\Delta - \hat{\Theta}\right). \tag{3.8}$$

The anisotropic stress is the spatial traceless part of the stress-energy tensor. In the same way as the metric perturbation, it decomposes into one scalar, $\Pi^{\rm S}$, two vector, $\Pi^{\rm V}$, and two tensor modes, $\Pi^{\rm T}$. Note that our θ and $\Pi^{\rm S}$ differ from $\theta^{\rm MB}$ and σ (anisotropic stress) defined in [26] by $\theta^{\rm MB} = \frac{k^2}{a}\theta$ and $(\rho + P)\sigma = -\frac{2}{3}P\Pi^{\rm S}$.

The generic perturbed fluid equations which follow from the conservation of the stress-energy tensor, $\delta(\nabla^\mu D_{\mu\nu}) = 0$, are

$$\Delta' - 3w\Delta - 2w\Pi^{\rm S} + g_{\rm K}\epsilon_{\rm H}\hat{\Theta} = 3\,(1+w)\,X, \tag{3.9a}$$

$$\hat{\Theta}' + 3(\tfrac{dP}{d\rho} - w + \tfrac{1}{3}\epsilon_{\rm H})\hat{\Theta} - 3\tfrac{dP}{d\rho}\Delta - 2w\Pi^{\rm S} - 3w\Gamma = 3\,(1+w)\,Y, \tag{3.9b}$$

where

$$g_{\rm K} \equiv 1 + \frac{{\rm K}^2}{3\epsilon_{\rm H}}. \tag{3.10}$$

The field equations (2.2) expanded to linear order in perturbations, $\delta G_{\mu\nu} = \delta T_{\mu\nu} + \delta U_{\mu\nu}$, yield

$$-\tfrac{2}{3}{\rm K}^2 Z = \Omega_{\rm m}\Delta_{\rm m} + \Omega_{\rm de}\Delta_{\rm de}, \tag{3.11a}$$

$$2X = \Omega_{\rm m}\hat{\Theta}_{\rm m} + \Omega_{\rm de}\hat{\Theta}_{\rm de}, \tag{3.11b}$$

$$\tfrac{2}{3}W + 2X - \tfrac{2}{9}{\rm K}^2\,(Y - Z) = \Omega_{\rm m}(\delta\hat{P}_{\rm m}/\rho_{\rm m}) + \Omega_{\rm de}(\delta\hat{P}_{\rm de}/\rho_{\rm de}), \tag{3.11c}$$

$$\tfrac{1}{3}{\rm K}^2\,(Y - Z) = \Omega_{\rm m}w_{\rm m}\Pi^{\rm S}_{\rm m} + \Omega_{\rm de}w_{\rm de}\Pi^{\rm S}_{\rm de}, \tag{3.11d}$$

$$\tfrac{1}{6}h^{\rm V\prime\prime} + (\tfrac{1}{2} - \tfrac{1}{6}\epsilon_{\rm H})h^{\rm V\prime} = \Omega_{\rm m}w_{\rm m}\Pi^{\rm V}_{\rm m} + \Omega_{\rm de}w_{\rm de}\Pi^{\rm V}_{\rm de}, \tag{3.11e}$$

$$\tfrac{1}{6}h^{\rm T\prime\prime} + (\tfrac{1}{2} - \tfrac{1}{6}\epsilon_{\rm H})h^{\rm T\prime} + \tfrac{1}{3}{\rm K}^2 h^{\rm T} = \Omega_{\rm m}w_{\rm m}\Pi^{\rm T}_{\rm m} + \Omega_{\rm de}w_{\rm de}\Pi^{\rm T}_{\rm de}. \tag{3.11f}$$

The first equation (3.11a) enables to write ${\rm K}^2 Z$ in terms of the $\Delta_{\rm i}$'s, while the second equation (3.11b) constitutes the expression of the metric perturbation X in terms of the perturbed fluid variables $\hat{\Theta}_{\rm i}$'s. The variables $\{W, X, Y, Z, \hat{\chi}, \hat{\chi}', \hat{\chi}'', h^{\rm V,T}\}$, which are linear combinations of the metric perturbations and their time derivatives, are called the *geometric perturbations*. The variables $\left\{\Delta_{\rm i}, \hat{\Theta}_{\rm i}, \delta\hat{P}_{\rm i}, \Gamma_{\rm i}, \Pi^{\rm S,V,T}_{\rm i}\right\}$ with ${\rm i} \in \{{\rm m}, {\rm de}\}$, which are linear combinations of the different projections of a perturbed stress-energy tensor, are called the *perturbed fluid variables*.

IV. EQUATION OF STATE FOR PERTURBATIONS

Equations of state for perturbations (EoS) constitute expressions for the entropy perturbation, $\Gamma_{\rm de}$, and the anisotropic stresses, $\Pi^{\rm S,V,T}_{\rm de}$, that are constructed out of the perturbed metric degrees of freedom, the matter fluid variables, and the dark density and velocity divergence fields. Once these expressions are provided, the equations governing cosmological perturbations explicitly closes. Schematically, for the scalar sector in synchronous gauge, we are looking to obtain expressions of the form

$$\Gamma_{\rm de} = \Gamma_{\rm de}(\delta_{\rm de}, \theta_{\rm de}, h', \eta, \ldots, \delta_{\rm m}), \qquad \Pi^{\rm S}_{\rm de} = \Pi^{\rm S}_{\rm de}(\delta_{\rm de}, \theta_{\rm de}, h', \eta, \ldots, \delta_{\rm m}), \tag{4.1}$$

where the list of arguments shown is not exhaustive and can include derivatives, for example. Certain classes of equation of state have already been worked out (see [12, 13] for kinetic gravity braiding models, [27] for coupled Horndeski theories, [28] for generalised scalar-tensor theories and [29–31] for relativistic elastic and viscoelastic material models).

The simplest way to understand this approach is in the vector and tensor sectors of the theory. If one assumes that there are no extra vector and tensor degrees of freedom (which is the case in $f(\mathcal{R})$ theories), then the anisotropic stresses can only be functions of the metric variables. Focusing on tensor modes, the only tensor field available is the tensor mode of the metric perturbation, $h^{\rm T}$, and its time derivatives (which we will limit to second order). The most general form of $\Pi^{\rm T}_{\rm de}$ would then be given by

$$\Pi^{\rm T}_{\rm de} = \mathcal{T}_1 h^{\rm T\prime\prime} + \mathcal{T}_2 h^{\rm T\prime} + \mathcal{T}_3 h^{\rm T}, \tag{4.2}$$

where the $\{\mathcal{T}_i\}$ are a set of dimensionless functions of space and time, that do not depend on the perturbed field quantities. Often one can deduce that these can be limited to just being functions of time only for specific theories. A similar expression could be written for the vector sector.

In $f(\mathcal{R})$ gravity, the expansion to first order in perturbations of the dark sector stress-energy tensor is

$$\begin{aligned}\delta U_{\mu\nu} &= -f_{\mathcal{R}}\delta R_{\mu\nu} + \tfrac{1}{2}f\delta g_{\mu\nu} + \tfrac{1}{2}g_{\mu\nu}f_{\mathcal{R}}\delta\mathcal{R} - f_{\mathcal{R}\mathcal{R}}R_{\mu\nu}\delta\mathcal{R} \\ &\quad +\delta\left(\nabla_\mu\nabla_\nu f_{\mathcal{R}}\right) - \left(\Box f_{\mathcal{R}}\right)\delta g_{\mu\nu} - g_{\mu\nu}\delta\left(\Box f_{\mathcal{R}}\right). \end{aligned} \tag{4.3}$$

This allows us to isolate the perturbed fluid variables for the $f(\mathcal{R})$ dark sector theory [32]. The tensor and vector projections of (4.3) readily constitute the EoS for $\Pi^{\mathrm{V}}_{\mathrm{de}}$ and $\Pi^{\mathrm{T}}_{\mathrm{de}}$,

$$\Omega_{\mathrm{de}}w_{\mathrm{de}}\Pi^{\mathrm{V}}_{\mathrm{de}} = -\tfrac{1}{6}f_{\mathcal{R}}h^{\mathrm{V}\prime\prime} - \tfrac{1}{6}\left\{(3-\epsilon_{\mathrm{H}})f_{\mathcal{R}} + f'_{\mathcal{R}}\right\}h^{\mathrm{V}\prime}, \tag{4.4a}$$

$$\Omega_{\mathrm{de}}w_{\mathrm{de}}\Pi^{\mathrm{T}}_{\mathrm{de}} = -\tfrac{1}{6}f_{\mathcal{R}}h^{\mathrm{T}\prime\prime} - \tfrac{1}{6}\left\{(3-\epsilon_{\mathrm{H}})f_{\mathcal{R}} + f'_{\mathcal{R}}\right\}h^{\mathrm{T}\prime} - \tfrac{1}{6}f_{\mathcal{R}}\mathrm{K}^2h^{\mathrm{T}}. \tag{4.4b}$$

As expected these are of the form (4.2) and the coefficients are just functions of time except for the explicit dependence on K^2 in the final term in the expression for $\Pi^{\mathrm{T}}_{\mathrm{de}}$.

The scalar projections yield the following expressions:

$$\Omega_{\mathrm{de}}\Delta_{\mathrm{de}} = -g_{\mathrm{K}}\epsilon_{\mathrm{H}}\hat{\chi} + f'_{\mathcal{R}}X + \tfrac{2}{3}f_{\mathcal{R}}\mathrm{K}^2Z, \tag{4.5a}$$

$$\Omega_{\mathrm{de}}\hat{\Theta}_{\mathrm{de}} = \hat{\chi}' - \hat{\chi} - 2f_{\mathcal{R}}X, \tag{4.5b}$$

$$\begin{aligned}\Omega_{\mathrm{de}}(\delta\hat{P}_{\mathrm{de}}/\rho_{\mathrm{de}}) &= \tfrac{1}{3}\hat{\chi}'' + (\tfrac{2}{3} - \tfrac{1}{3}\epsilon_{\mathrm{H}})\hat{\chi}' - \left(1 - \tfrac{1}{3}\epsilon_{\mathrm{H}} - \tfrac{2}{9}\mathrm{K}^2\right)\hat{\chi} \\ &\quad -\tfrac{2}{3}f_{\mathcal{R}}W - 2(f_{\mathcal{R}} + \tfrac{1}{3}f'_{\mathcal{R}})X + \tfrac{2}{9}f_{\mathcal{R}}\mathrm{K}^2\left(Y - Z\right), \end{aligned} \tag{4.5c}$$

$$\Omega_{\mathrm{de}}w_{\mathrm{de}}\Pi^{\mathrm{S}}_{\mathrm{de}} = -\tfrac{1}{3}\mathrm{K}^2\hat{\chi} - \tfrac{1}{3}f_{\mathcal{R}}\mathrm{K}^2\left(Y - Z\right). \tag{4.5d}$$

From now on, the standard matter fluid will be assumed to have vanishing anisotropic stress and entropy perturbation, $\Pi^{\mathrm{S}}_{\mathrm{m}} = \Gamma_{\mathrm{m}} = 0$ which is the case for a CDM fluid. When those are they are non-zero, the procedure presented below is easily generalized, with additional terms proportional to $\Pi^{\mathrm{S}}_{\mathrm{m}}$ and Γ_{m}. In the last equation (4.5d), $\Pi^{\mathrm{S}}_{\mathrm{de}}$ can be eliminated with (3.11d), providing the expression of Y in terms of Z and $\hat{\chi}$,

$$Y = Z - \tfrac{1}{1+f_{\mathcal{R}}}\hat{\chi}, \tag{4.6}$$

valid for all K. Therefore, the dark sector anisotropic stress is simply

$$\Omega_{\mathrm{de}}w_{\mathrm{de}}\Pi^{\mathrm{S}}_{\mathrm{de}} = \tfrac{1-g_{\mathrm{K}}}{1+f_{\mathcal{R}}}\epsilon_{\mathrm{H}}\hat{\chi}. \tag{4.7}$$

Equation (4.5a), combined to (3.11a) and (3.11b), enables to write $\hat{\chi}$ in terms of the Δ_{i}'s and $\hat{\Theta}_{\mathrm{i}}$'s,

$$\hat{\chi} = -\tfrac{\Omega_{\mathrm{de}}}{g_{\mathrm{K}}\epsilon_{\mathrm{H}}}\Delta_{\mathrm{de}} - \tfrac{f_{\mathcal{R}}}{g_{\mathrm{K}}\epsilon_{\mathrm{H}}}\left\{\Omega_{\mathrm{de}}(\Delta_{\mathrm{de}} - \tfrac{f'_{\mathcal{R}}}{2f_{\mathcal{R}}}\hat{\Theta}_{\mathrm{de}}) + \Omega_{\mathrm{m}}(\Delta_{\mathrm{m}} - \tfrac{f'_{\mathcal{R}}}{2f_{\mathcal{R}}}\hat{\Theta}_{\mathrm{m}})\right\}. \tag{4.8}$$

With (4.7, 4.8) one obtains the EoS for the anisotropic stress:

$$w_{\mathrm{de}}\Pi^{\mathrm{S}}_{\mathrm{de}} = \tfrac{1}{3g_{\mathrm{K}}\epsilon_{\mathrm{H}}}\mathrm{K}^2\left\{\Delta_{\mathrm{de}} - \tfrac{f'_{\mathcal{R}}}{2(1+f_{\mathcal{R}})}\hat{\Theta}_{\mathrm{de}} + \tfrac{\Omega_{\mathrm{m}}}{\Omega_{\mathrm{de}}}\tfrac{f_{\mathcal{R}}}{1+f_{\mathcal{R}}}\Delta_{\mathrm{m}} - \tfrac{\Omega_{\mathrm{m}}}{\Omega_{\mathrm{de}}}\tfrac{f'_{\mathcal{R}}}{2(1+f_{\mathcal{R}})}\hat{\Theta}_{\mathrm{m}}\right\}. \tag{4.9}$$

In order to deduce the entropy perturbation as an equation of state, one might begin with the expression for $\delta\hat{P}_{\mathrm{de}}$ in (4.5c), and then eliminate $\hat{\chi}$ and its time-derivatives, as in [12]. This involved differentiation of (4.5a) or (4.5b) to obtain $\hat{\chi}''$, and $\hat{\chi}'$. However, this strategy eventually leads to the perturbed fluid equation (3.9b) and hence a tautology, and therefore an alternative strategy is required. The starting point is the field equation (3.11c). On the right-hand-side of (3.11c), the pressure perturbations $\delta\hat{P}_{\mathrm{de}}$ and $\delta\hat{P}_{\mathrm{m}}$ are replaced in favor of the Γ_{i}'s with (3.8). On the left-hand-side of (3.11c), W is replaced in terms of the geometric perturbations X, Y, Z and $\hat{\chi}$ with (3.4). As before, X is written in terms of the $\hat{\Theta}_{\mathrm{i}}$'s with (3.11b). Furthermore, with (4.6) and (4.8), Y can be expressed with Z and the perturbed fluid variables Δ_{i}'s and $\hat{\Theta}_{\mathrm{i}}$'s. After these replacements, the geometric perturbations only appear within K^2Z which can be replaced with the Δ_{i}'s with (3.11a). Eventually, the EoS for the dark sector entropy perturbation is obtained as

$$\begin{aligned}w_{\mathrm{de}}\Gamma_{\mathrm{de}} &= \left[\zeta_{\mathrm{de}} - \tfrac{\bar{\epsilon}_{\mathrm{H}}}{3g_{\mathrm{K}}\epsilon_{\mathrm{H}}}\tfrac{2(1+f_{\mathcal{R}})-f'_{\mathcal{R}}}{f'_{\mathcal{R}}}\right]\Delta_{\mathrm{de}} - \zeta_{\mathrm{de}}\hat{\Theta}_{\mathrm{de}} \\ &\quad +\tfrac{\Omega_{\mathrm{m}}}{\Omega_{\mathrm{de}}}\left[\zeta_{\mathrm{m}} - \tfrac{\bar{\epsilon}_{\mathrm{H}}}{3g_{\mathrm{K}}\epsilon_{\mathrm{H}}}\tfrac{2f_{\mathcal{R}}-f'_{\mathcal{R}}}{f'_{\mathcal{R}}}\right]\Delta_{\mathrm{m}} - \tfrac{\Omega_{\mathrm{m}}}{\Omega_{\mathrm{de}}}\zeta_{\mathrm{m}}\hat{\Theta}_{\mathrm{m}} \end{aligned} \tag{4.10}$$

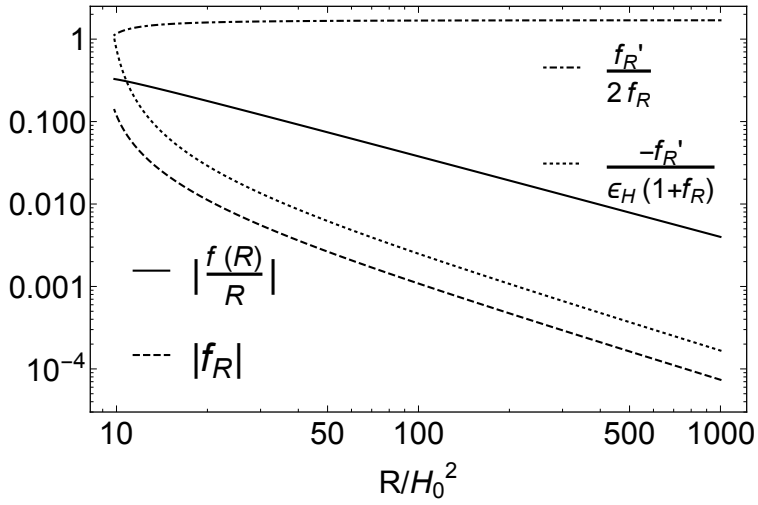

Figure 1: Evolution of some relevant $f(\mathcal{R})$ quantities that appear as coefficients in the EoS for the dark sector anisotropic stress (4.9) and entropy perturbation (4.10), for a designer $f(\mathcal{R})$ that mimics Λ-CDM ($w_{\rm de} = -1$) with $B_0 = 1$. When these are negative valued, their absolute value is plotted in order to accommodate the logarithmic scale.

where

$$\zeta_{\rm i} \equiv \frac{g_{\rm K}\epsilon_{\rm H} - \bar{\epsilon}_{\rm H}}{3g_{\rm K}\epsilon_{\rm H}} - \frac{dP_{\rm i}}{d\rho_{\rm i}}. \tag{4.11}$$

Note that when the matter fluid is pressure-less and $w_{\rm de} = -1$, then $\bar{\epsilon}_{\rm H} = \epsilon_{\rm H}$ and therefore

$$\zeta_{\rm de} = \tfrac{4g_{\rm K}-1}{3g_{\rm K}}, \qquad \zeta_{\rm m} = \tfrac{g_{\rm K}-1}{3g_{\rm K}}. \tag{4.12}$$

Equations (4.9) and (4.10), as well as (4.4a, 4.4b) for the vector and tensor sectors, are the main result of this paper. They constitute the EoS for perturbations in $f(R)$ gravity expressed in a gauge invariant way. One could choose to express the EoS in terms of the dark sector perturbed fluid variables and the geometric perturbations X, Y and Z. For the entropy perturbation, this is achieved by replacing $\Delta_{\rm m}$ and $\hat{\Theta}_{\rm m}$ in (4.10) with (3.11a) and (3.11b). The dark sector EoS for perturbations are then expressed in a 'self-consistent' way, which does not depend explicitly on the perturbed fluid variables of the other fluid components

$$w_{\rm de}\Pi^{\rm S}_{\rm de} = \tfrac{1}{3\Omega_{\rm de}}{\rm K}^2(Y-Z), \tag{4.13a}$$

$$w_{\rm de}\Gamma_{\rm de} = -\tfrac{dP_{\rm de}}{d\rho_{\rm de}}(\Delta_{\rm de} - \hat{\Theta}_{\rm de}) + \tfrac{2}{3}\tfrac{\bar{\epsilon}_{\rm H}}{\Omega_{\rm de}}\tfrac{1+f_{\mathcal{R}}}{f'_{\mathcal{R}}}(Z-Y) - \tfrac{2}{3\Omega_{\rm de}}(X + \tfrac{1}{3}{\rm K}^2 Z). \tag{4.13b}$$

The coefficients that play an important role in the EoS are either proportional to $f_{\mathcal{R}}$, $\frac{2f_{\mathcal{R}}}{f'_{\mathcal{R}}}$ and

$$B \equiv -\tfrac{f'_{\mathcal{R}}}{\epsilon_{\rm H}(1+f_{\mathcal{R}})}, \tag{4.14}$$

or its inverse. Their evolution in the case of a designer $f(\mathcal{R})$ with $w_{\rm de} = -1$ is plotted in figure 1. In order to illustrate some of the applications of the EoS formalism and the gauge invariant notations, we shall now describe the procedure for solving the linear perturbations in $f(\mathcal{R})$ gravity.

V. DYNAMICS OF LINEAR PERTURBATION IN $f(\mathcal{R})$ GRAVITY

The dynamics of vector and tensor perturbations is straightforward to deduce and therefore we will only focus on the scalar sector. The dynamics of the scalar perturbations can be specified by writing the four perturbed fluid equations (3.9), plus one evolution equation for the geometric perturbation Z which follows from the definition of the gauge invariant notations (3.3),

$$Z' = X - Y, \tag{5.1}$$

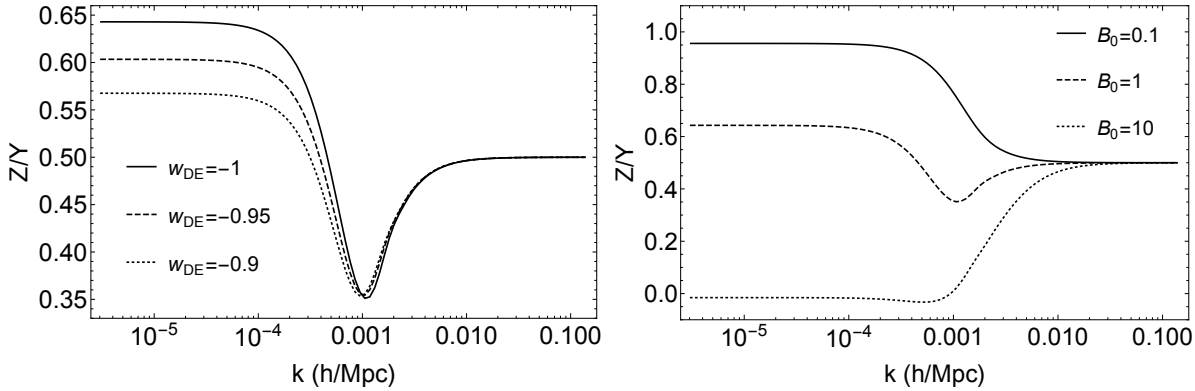

Figure 2: Spectrum of the ratio Z/Y (or $-\Phi/\Psi$ in the notation of [22]) for different values of the equation of state parameter when $B_0 = 1$ (left) and different designer $f(\mathcal{R})$ scenarios parametrized by B_0 and with $w_{\rm de} = -1$ (right). On the x-axis, the wavenumber is written in units 'h/Mpc', where $h = 0.73$ is the reduced Hubble constant.

where X and Y are given in (3.11b, 4.6-4.8) in terms of the perturbed fluid variables. In fact, the system of five differential equations is overdetermined: when $\mathrm{K} = 0$, the field equation (3.11a) can be used to express $\Delta_{\rm de}$ in terms of $\Delta_{\rm m}$; and when $\mathrm{K} \neq 0$, the same equation gives Z in terms of the $\Delta_{\rm i}$'s. This approach is powerful and elegant: it provides an efficient way to solve the linear perturbation in $f(R)$ gravity, and the phenomenology becomes transparent through the interpretation of the fluid variables.

Before proceeding to this analysis, let us note that an essential feature of linear perturbation in $f(\mathcal{R})$ gravity can be deduced from (4.6), when $\hat{\chi}$ is replaced by its expression (3.4) in terms of the geometric perturbations,

$$B\mathrm{K}^2(Y - 2Z) = 3BW + 12BX + 3\tfrac{\bar{\epsilon}_{\rm H}}{\epsilon_{\rm H}}(Y - Z), \tag{5.2}$$

where B is defined in (4.14). Since the geometric perturbations $\{W, X, Y, Z\}$ shall remain bounded during their evolution, it appears that for K larger than $B^{-1/2}$ the ratio Z/Y is driven to $1/2$, as illustrated in figure 2 in the case of a designer $f(\mathcal{R})$.

Let us consider the case of a matter fluid with $w_{\rm m} = \Pi^{\rm S}_{\rm m} = \Gamma_{\rm m} = 0$, along with a designer $f(\mathcal{R})$ fluid that mimics Λ-CDM ($w_{\rm de} = -1$). The function $f(\mathcal{R})$ is determined by (2.6a). As shown in [22], the different solutions to (2.6a) can by parametrized by the single number B, defined in (4.14), evaluated today[2] when $a_0 = 1$ (analytical expressions for $f(\mathcal{R})$ are available in some regimes [33]). For the numerical simulation we have chosen $B_0 = 1$, and we have set the initial conditions for the perturbations at redshift $z = 100$, when $B \ll 1$. At such high curvature, during the matter dominated era, the initial conditions for the perturbations must follow from the general relativistic expectation in order to be consistent with CMB observations. Hence, initially $\Delta_{\rm de} = \hat{\Theta}_{\rm de} = 0$ and $\Omega_{\rm m}\Delta_{\rm m} = -\frac{2}{3}\mathrm{K}^2 Z$, $\Omega_{\rm m}\hat{\Theta}_{\rm m} = 2X$, with $X = Y = Z$. As mentioned before, the five relevant dynamical equations are

$$\begin{aligned}
\Delta'_{\rm de} &= -3\Delta_{\rm de} - g_{\rm K}\epsilon_{\rm H}\hat{\Theta}_{\rm de} - 2\Pi^{\rm S}_{\rm de}, & \qquad \Delta'_{\rm m} &= -g_{\rm K}\epsilon_{\rm H}\hat{\Theta}_{\rm m} + 3X,\\
\hat{\Theta}'_{\rm de} &= -3\Delta_{\rm de} - \epsilon_{\rm H}\hat{\Theta}_{\rm de} - 2\Pi^{\rm S}_{\rm de} - 3\Gamma_{\rm de}, & \qquad \hat{\Theta}'_{\rm m} &= -\epsilon_{\rm H}\hat{\Theta}_{\rm m} + 3Y,\\
Z' &= X - Y,
\end{aligned} \tag{5.3}$$

where X and Y are replaced with (3.11b, 4.6-4.8) in terms of the perturbed fluid variables, while $\Pi^{\rm S}_{\rm de}$ and $\Gamma_{\rm de}$ are given in (4.9) and (4.10). Recall that in the conformal Newtonian gauge, $Z = \phi$ and $Y = \psi$ in our notations that follow [26], while $Z = -\Phi$ and $Y = \Psi$ in Song-Hu-Sawicki notation [22]. With this strategy we have successfully reproduced the results presented in figure 2 of [22], see figure 3.

Alternatively one could have favored the geometric perturbations instead of the perturbed fluid variables. The way the equations have been written makes it straightforward to go from one picture to the other. Let us pick the conformal Newtonian gauge in order to illustrate this point. In the conformal Newtonian gauge, $\hat{\chi}' = \chi'_c - f'_{\mathcal{R}}Y$ (see section III). Therefore, equation (4.5b) combined to (4.6) and (5.1) yields a first order differential equation for the

[2] A subscript '0' means that the quantity is evaluated today.

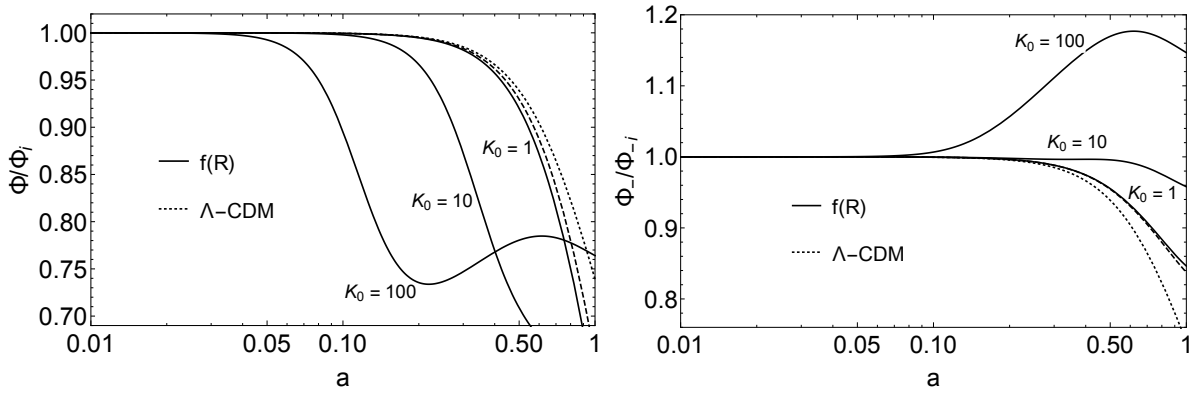

Figure 3: Evolution of the metric perturbations $\Phi = -Z$ (left) and $\Phi_- = -\frac{Y+Z}{2}$ (right) for the ΛCDM expansion history ($w_{\rm de} = -1$, $\Omega^0_{\rm de} = 0.76$). The dotted lines correspond to the ΛCDM scenario without $f(\mathcal{R})$. In this case the amplitudes of the perturbed potentials Φ and Φ_- do not depend on the wavenumber. The black lines correspond to a $f(\mathcal{R})$ scenario that mimics the cosmological constant ($w_{\rm de} = -1$, $B_0 = 1$). The amplitudes of the metric perturbations are now sensitive to the wavenumber $\mathrm{K}_0 = \frac{k}{H_0}$. Even the infrared limit, $K_0 = 0$, represented by the dashed curves closest to the dotted lines, there is a disagreement with the ΛCDM predictions.

geometric perturbation Y. The differential equation for X is simply provided by (3.4), where $\hat{\chi}$ is replaced with (4.6) and W with its definition, $W = X' - \epsilon_{\rm H}(X + Y)$. Hence, the resulting set of equations to be solved is

$$\begin{aligned} X' &= (\epsilon_{\rm H} - 4)X - \tfrac{1+f_{\mathcal{R}}-g_{\rm K}f'_{\mathcal{R}}}{f'_{\mathcal{R}}}\epsilon_{\rm H}Y + \tfrac{1+f_{\mathcal{R}}+2(1-g_{\rm K})f'_{\mathcal{R}}}{f'_{\mathcal{R}}}\epsilon_{\rm H}Z, \qquad \Delta'_{\rm m} = -g_{\rm K}\epsilon_{\rm H}\Theta_{\rm m} + 3X, \\ Y' &= -X - 2\tfrac{f'_{\mathcal{R}}}{1+f_{\mathcal{R}}}Y - \tfrac{1+f_{\mathcal{R}}-f'_{\mathcal{R}}}{1+f_{\mathcal{R}}}Z + \tfrac{1}{1+f_{\mathcal{R}}}\Omega_{\rm m}\Theta_{\rm m}, \qquad \Theta_{\rm m}' = -\epsilon_{\rm H}\Theta_{\rm m} + 3Y, \\ Z' &= X - Y, \end{aligned} \tag{5.4}$$

valid in the conformal Newtonian gauge, where $Z = \phi, Y = \psi$ and $X = \phi' + \psi$. From here, the results in the synchronous gauge can be obtained using the gauge transformation rules.

The last strategy would be to consider only the dark sector fluid variables and geometrical perturbations, eliminating $\Theta_{\rm m}$ in the equation for Y in (5.4) with (3.11b) and taking the perturbed fluid equations for the dark sector. The resulting set of equations is

$$\begin{aligned} X' &= \tfrac{1+f_{\mathcal{R}}-g_{\rm K}f'_{\mathcal{R}}}{f'_{\mathcal{R}}(1+f_{\mathcal{R}})}\epsilon_{\rm H}\chi + (\epsilon_{\rm H} - 4)X + (2 - g_{\rm K})\epsilon_{\rm H}Z, \qquad \Theta_{\rm de}' = -3\Delta_{\rm de} - \epsilon_{\rm H}\Theta_{\rm de} - 2\Pi^{\rm S}_{\rm de} - 3\Gamma_{\rm de}, \\ Z' &= \tfrac{1}{1+f_{\mathcal{R}}}\chi + X - Z, \qquad \Delta'_{\rm de} = -3\Delta_{\rm de} - g_{\rm K}\epsilon_{\rm H}\Theta_{\rm de} - 2\Pi^{\rm S}_{\rm de}, \\ \chi' &= \Omega_{\rm de}\Theta_{\rm de} + \tfrac{1+f_{\mathcal{R}}-f'_{\mathcal{R}}}{1+f_{\mathcal{R}}}\chi + 2f_{\mathcal{R}}X + f'_{\mathcal{R}}Z, \end{aligned} \tag{5.5}$$

with $\Pi^{\rm S}_{\rm de}$ and $\Gamma_{\rm de}$ given in (4.13). In much of the previous work, the linear perturbation in $f(\mathcal{R})$ gravity have been solved with equations analogous to (5.5), with the difference that $\Delta_{\rm de}$ and $\hat{\Theta}_{\rm de}$ are replaced with $\Delta_{\rm m}$ and $\hat{\Theta}_{\rm m}$, thanks to the field equations (3.11), see [23].

We argue that the EoS approach (5.3) provides a clearer set of equations which can be solved and interpreted in an easier way. For instance, the stability of the metric perturbation in the high curvature regime, as discussed in [22], can be straightforwardly seen in (5.3). When $B \ll 1$ (high curvature), from a quick look at the EoS (4.9, 4.10) we can see that

$$\Pi^{\rm S}_{\rm de} = -\tfrac{1}{3g_{\rm K}\epsilon_{\rm H}}\mathrm{K}^2\Delta_{\rm de}, \qquad \Gamma_{\rm de} = -\tfrac{2}{3g_{\rm K}\epsilon_{\rm H}B}\Delta_{\rm de}. \tag{5.6}$$

By considering the second derivative of the perturbed fluid variable $\Delta_{\rm de}$ from (5.3) in the high curvature regime, one is left with a second order differential equation which can be recast as

$$\Delta''_{\rm de} + (3 - \tfrac{2}{3g_{\rm K}\epsilon_{\rm H}}\mathrm{K}^2)\Delta'_{\rm de} + \tfrac{2}{B}\Delta_{\rm de} = \tfrac{2}{B}F(\Delta_{\rm m}, \hat{\Theta}_{\rm m}). \tag{5.7}$$

Therefore if $B < 0$, the perturbed fluid variable $\Delta_{\rm de}$ does not converge toward the particular solution, $\Delta_{\rm de} = F(\Delta_{\rm m}, \hat{\Theta}_{\rm m})$, but diverges exponentially, see [22] for a detailed discussion.

When a model of $f(\mathcal{R})$ gravity is specified analytically, the EoS for $\Gamma_{\rm de}$ and $\Pi_{\rm de}$ (4.9, 4.10) are easily obtained from a direct calculation of $f_{\mathcal{R}}$ and $f'_{\mathcal{R}}$. For instance, the Hu-Sawicki-Strarobinsky model [21, 34, 35],

$$f(\mathcal{R}) \equiv -2\Lambda \frac{\left(\frac{\mathcal{R}}{m^2}\right)^{2n}}{1+\left(\frac{\mathcal{R}}{m^2}\right)^{2n}}, \tag{5.8}$$

commonly used as an alternative to the cosmological constant, leads to the following expressions for $f_{\mathcal{R}}$ and $f'_{\mathcal{R}}$,

$$f_{\mathcal{R}} = 2n \frac{1-\left(\frac{\mathcal{R}}{m^2}\right)^{2n}}{1+\left(\frac{\mathcal{R}}{m^2}\right)^{2n}} \frac{f(\mathcal{R})}{\mathcal{R}}, \tag{5.9a}$$

$$f'_{\mathcal{R}} = 2n(2n+1) \frac{\frac{2n-1}{2n+1}+\left(\frac{\mathcal{R}}{m^2}\right)^{4n}}{1+2\left(\frac{\mathcal{R}}{m^2}\right)^{2n}+\left(\frac{\mathcal{R}}{m^2}\right)^{4n}} \frac{\mathcal{R}'}{\mathcal{R}} \frac{f(\mathcal{R})}{\mathcal{R}}. \tag{5.9b}$$

Another interesting case is when the dark energy fluid is dominating ($\Omega_{\rm m}=0$, $\Omega_{\rm de}=1$). Then the equation of state parameter reduces to

$$1+w_{\rm de} = \tfrac{2}{3}\epsilon_{\rm H}. \tag{5.10}$$

This case is relevant not only for the present acceleration but also when studying inflationary scenarios based on $f(\mathcal{R})$ modifications to GR. In particular, when the slow-roll conditions are fulfilled, $\epsilon_{\rm H} \ll 1$ and $\epsilon'_{\rm H} \ll \epsilon_{\rm H}$, one gets

$$\frac{dP_{\rm de}}{d\rho_{\rm de}} = -1 \qquad \text{and} \qquad \zeta_{\rm de} = \tfrac{4}{3}\frac{g_{\rm K}-1}{g_{\rm K}}. \tag{5.11}$$

with $\epsilon'_{\rm H} = 2\epsilon_{\rm H}^2$ and $\bar{\epsilon}_{\rm H} = 4\epsilon_{\rm H}$ (see footnote 1). With no other fluid than the $f(\mathcal{R})$ fluid, the perturbed field equations (3.11) provide very simple relationship between the geometric perturbations and the perturbed fluid variables: $-\frac{2}{3}{\rm K}^2 Z = \Delta_{\rm de}$ and $2X = \hat{\Theta}_{\rm de}$. For the most popular Starobinsky's proposal [36] for primordial acceleration,

$$f(\mathcal{R}) = \frac{\mathcal{R}^2}{6M^2}, \tag{5.12}$$

one finds $f_{\mathcal{R}} = \frac{2}{3\epsilon_{\rm H}} - \frac{1}{3}$, $f'_{\mathcal{R}} = -\frac{4}{3}$ with $\epsilon_{\rm H} = \frac{M^2}{6H^2}$, as well as $g_{\rm K} = 1 + \frac{2k^2}{a^2M^2}$. So that the expressions for the anisotropic stress and the entropy perturbation become

$$w_{\rm de}\Pi^{\rm S}_{\rm de} = \tfrac{g_{\rm K}-1}{g_{\rm K}}\left(\Delta_{\rm de} + \epsilon_{\rm H}\hat{\Theta}_{\rm de}\right), \tag{5.13a}$$

$$w_{\rm de}\Gamma_{\rm de} = \tfrac{4}{3g_{\rm K}}\left\{(g_{\rm K} + \tfrac{1+\epsilon_{\rm H}}{\epsilon_{\rm H}})\Delta_{\rm de} + (g_{\rm K}-1)\,\hat{\Theta}_{\rm de}\right\}. \tag{5.13b}$$

These simple expressions can be plugged into the perturbed fluid equations (3.9) in order to solve the dynamics of linear perturbations during Starobinsky inflation, in the conformal Newtonian gauge or synchronous gauge.

VI. DISCUSSION

The EoS approach for dark sector perturbations has been discussed in details for (i) generalised k-essence theories, where the generic Lagrangian is $\mathcal{L}_{\rm de}(\phi,\chi)$, with $\chi \equiv -\frac{1}{2}\nabla^\mu\phi\nabla_\mu\phi$, and (ii) for theories in which the dark sector Lagrangian only contains the metric tensor $\mathcal{L}_{\rm de}(g_{\mu\nu})$, see [29, 30]. In these two cases the gauge invariant equations of state were found to be

$$w_{\rm de}\Pi^{\rm S}_{\rm de} = 0, \qquad w_{\rm de}\Gamma_{\rm de} = (c_{\rm S}^2 - w_{\rm de})\Delta_{\rm de}, \tag{6.1}$$

where $c_{\rm S}^2$ is the sound speed in the effective dark sector fluid, and

$$w_{\rm de}\Pi^{\rm S}_{\rm de} = -\tfrac{3}{2}(c_{\rm S}^2 - w_{\rm de})\left\{\Delta_{\rm de} - \hat{\Theta}_{\rm de} - 3(1+w_{\rm de})Z\right\}, \qquad w_{\rm de}\Gamma_{\rm de} = 0, \tag{6.2}$$

respectively.

We have presented the EoS approach to cosmological perturbations in $f(\mathcal{R})$ gravity. After reviewing the formalism for describing the evolution of linear perturbation in $f(\mathcal{R})$ gravity, we have exhibited three equivalent ways to solve

their dynamics. In previous work, linear perturbation equations in $f(\mathcal{R})$ gravity are solved in the geometric picture (5.4). Using the EoS approach (5.3-5.5) appears to have some advantages over the geometrical approach (5.4) because all the $f(\mathcal{R})$ modification can be implemented in the dynamics by simply adding a new fluid species at the perturbed level, rather than modifying the whole set of equation for the geometrical variables.

The main results of this paper are the equations of state for $\Gamma_{\rm de}$ and $\Pi_{\rm de}$ (4.4, 4.9, 4.10, 4.13). In these expressions the entropy perturbation and the anisotropic stresses are specified either in terms of the perturbed fluid variables of the dark sector and standard matter fluid, $\Pi^{\rm S}_{\rm de}=\Pi^{\rm S}_{\rm de}(\Delta_{\rm de},\hat{\Theta}_{\rm de},\Delta_{\rm m},\hat{\Theta}_{\rm m})$ and $\Gamma_{\rm de}=\Gamma_{\rm de}(\Delta_{\rm de},\hat{\Theta}_{\rm de},\Delta_{\rm m},\hat{\Theta}_{\rm m})$, or the perturbed fluid variables of the dark sector and the geometrical perturbations, $\Pi^{\rm S}_{\rm de}=\Pi^{\rm S}_{\rm de}(Y,Z)$ and $\Gamma_{\rm de}=\Gamma_{\rm de}(\Delta_{\rm de},\hat{\Theta}_{\rm de},X,Y,Z)$, thanks to the field equations (3.11). An important point is the extra degree of freedom, $\hat{\chi}$, induced by a non-trivial $f(\mathcal{R})$ modification to GR, is absent of these expressions. The elimination of this internal degree of freedom is the essence of the procedure.

In order to illustrate the EoS formalism we have presented the EoS in the scalar sector for three different cases: (i) the designer $f(\mathcal{R})$ in the high curvature regime (5.6), (ii) the analytical Hu-Sawicki-Starobinsky model for dark energy (5.9; to be plugged into 4.9, 4.10); and (iii) the Starobinsky proposal for inflation (5.13).

Acknowledgements

JAP is supported by the STFC Consolidated Grant ST/J000426/1. BB is supported by a grant from ENS de Lyon.

Appendix A: Gauge transformation rules

Any expression written in the conformal Newtonian gauge can by translated into the synchronous gauge and vice versa. The relationship between both gauges can be seen as an infinitesimal coordinate transformation, with a specific four vector d^μ characterizing the change of coordinate [26]. The time-like component of d^μ is

$$d^0 = \frac{a^2 \dot{h}_\parallel}{2k^2}. \tag{A1}$$

It is related to T introduced in section III by $T = Hd^0$. The dot denotes derivative with respect to coordinate time. The transformation rules for the metric perturbations, from the conformal Newtonian gauge to the synchronous gauge are

$$\begin{aligned} \psi &= \dot{d}^0, \\ \phi &= \eta - Hd^0, \\ \dot{\phi} + H\psi &= \dot{\eta} - \dot{H}d^0, \\ \ddot{\phi} + H\dot{\psi} + 2\dot{H}\psi &= \ddot{\eta} - \ddot{H}d^0. \end{aligned} \tag{A2}$$

For the fluid perturbations, the transformation rules are

$$\begin{aligned} \delta_c &= \delta_s + \frac{\dot{\rho}}{\rho} d^0, \\ \theta_c &= \theta_s + d^0, \\ \delta P_c &= \delta P_s + \dot{P} d^0, \\ \Pi_c{}^{\mathrm{S,V,T}} &= \Pi_s{}^{\mathrm{S,V,T}}, \end{aligned} \tag{A3}$$

where the subscripts 'c' and 's' hold for conformal Newtonian gauge and synchronous gauge respectively. For χ and its time derivatives the transformation rules are obtained from its definition in terms of the first order perturbation of the Ricci scalar (3.2)

$$\begin{aligned} \chi_c &= \chi_s + \dot{f}_\mathcal{R} d^0, \\ \dot{\chi}_c - \dot{f}_\mathcal{R}\psi &= \dot{\chi}_s + \ddot{f}_\mathcal{R} d^0, \\ \ddot{\chi}_c - \dot{f}_\mathcal{R}\dot{\psi} - 2\ddot{f}_\mathcal{R}\psi &= \ddot{\chi}_s + \dddot{f}_\mathcal{R} d^0. \end{aligned} \tag{A4}$$

Writing these relations with T instead of d^0 and the 'prime' derivative instead of the 'dot' derivative leads to the definition of the gauge invariant notations of section III.

[1] E. J. Copeland, M. Sami, and S. Tsujikawa, *Dynamics of dark energy*, *Int.J.Mod.Phys.* **D15** (2006) 1753–1936, [hep-th/0603057].

[2] T. Clifton, P. G. Ferreira, A. Padilla, and C. Skordis, *Modified Gravity and Cosmology*, *Phys.Rept.* **513** (2012) 1–189, [arXiv:1106.2476].

[3] J. K. Bloomfield, E. E. Flanagan, M. Park, and S. Watson, *Dark energy or modified gravity? An effective field theory approach*, *JCAP* **1308** (2013) 010, [arXiv:1211.7054].

[4] J. Gleyzes, D. Langlois, F. Piazza, and F. Vernizzi, *Essential Building Blocks of Dark Energy*, *JCAP* **1308** (2013) 025, [arXiv:1304.4840].

[5] F. Piazza and F. Vernizzi, *Effective Field Theory of Cosmological Perturbations*, *Class.Quant.Grav.* **30** (2013) 214007, [arXiv:1307.4350].

[6] J. Bloomfield, *A Simplified Approach to General Scalar-Tensor Theories*, *JCAP* **1312** (2013) 044, [arXiv:1304.6712].

[7] C. Skordis, *Consistent cosmological modifications to the Einstein equations*, *Phys.Rev.* **D79** (2009) 123527, [arXiv:0806.1238].

[8] T. Baker, P. G. Ferreira, C. Skordis, and J. Zuntz, *Towards a fully consistent parameterization of modified gravity*, *Phys.Rev.* **D84** (2011) 124018, [arXiv:1107.0491].

[9] T. Baker, P. G. Ferreira, and C. Skordis, *The Parameterized Post-Friedmann Framework for Theories of Modified Gravity: Concepts, Formalism and Examples*, *Phys.Rev.* **D87** (2013) 024015, [arXiv:1209.2117].

[10] P. G. Ferreira, T. Baker, and C. Skordis, *Testing general relativity with cosmology: a synopsis of the parametrized post-Friedmann approach*, .

[11] R. A. Battye and J. A. Pearson, *Effective action approach to cosmological perturbations in dark energy and modified gravity*, *JCAP* **1207** (2012) 019, [arXiv:1203.0398].

[12] R. A. Battye and J. A. Pearson, *Parametrizing dark sector perturbations via equations of state*, *Phys.Rev.* **D88** (2013), no. 6 061301, [arXiv:1306.1175].

[13] R. A. Battye and J. A. Pearson, *Computing model independent perturbations in dark energy and modified gravity*, *JCAP* **1403** (2014) 051, [arXiv:1311.6737].

[14] B. Soergel, T. Giannantonio, J. Weller, and R. A. Battye, *Constraining dark sector perturbations II: ISW and CMB lensing tomography*, arXiv:1409.4540.

[15] R. A. Battye, A. Moss, and J. A. Pearson, *Constraining dark sector perturbations I: cosmic shear and CMB lensing*, arXiv:1409.4650.

[16] **Planck** Collaboration, P. Ade *et. al.*, *Planck 2015 results. XIV. Dark energy and modified gravity*, arXiv:1502.0159.

[17] T. P. Sotiriou and V. Faraoni, *f(R) Theories Of Gravity*, *Rev.Mod.Phys.* **82** (2010) 451–497, [arXiv:0805.1726].

[18] A. De Felice and S. Tsujikawa, *f(R) theories*, *Living Rev. Rel.* **13** (2010) 3, [arXiv:1002.4928].

[19] W. Hu and I. Sawicki, *Models of f(R) cosmic acceleration that evade solar system tests*, *Phys. Rev. D* **76** (Sept., 2007) 064004, [arXiv:0705.1158].

[20] S. Appleby and R. Battye, *Do consistent F(R)F(R) models mimic general relativity plus Λ?*, *Physics Letters B* **654** (Oct., 2007) 7–12, [arXiv:0705.3199].

[21] A. A. Starobinsky, *Disappearing cosmological constant in f(R) gravity*, *Soviet Journal of Experimental and Theoretical Physics Letters* **86** (Oct., 2007) 157–163, [arXiv:0706.2041].

[22] Y.-S. Song, W. Hu, and I. Sawicki, *The Large Scale Structure of f(R) Gravity*, *Phys.Rev.* **D75** (2007) 044004, [astro-ph/0610532].

[23] R. Bean, D. Bernat, L. Pogosian, A. Silvestri, and M. Trodden, *Dynamics of Linear Perturbations in f(R) Gravity*, *Phys.Rev.* **D75** (2007) 064020, [astro-ph/0611321].

[24] T. Faulkner, M. Tegmark, E. F. Bunn, and Y. Mao, *Constraining f(R) Gravity as a Scalar Tensor Theory*, *Phys.Rev.* **D76** (2007) 063505, [astro-ph/0612569].

[25] T. P. Sotiriou, *f(R) gravity and scalar-tensor theory*, *Class.Quant.Grav.* **23** (2006) 5117–5128, [gr-qc/0604028].

[26] C.-P. Ma and E. Bertschinger, *Cosmological perturbation theory in the synchronous and conformal Newtonian gauges*, *Astrophys.J.* **455** (1995) 7–25, [astro-ph/9506072].

[27] J. Bloomfield and J. Pearson, *Simple implementation of general dark energy models*, *JCAP* **1403** (2014) 017, [arXiv:1310.6033].

[28] J. Gleyzes, D. Langlois, and F. Vernizzi, *A unifying description of dark energy*, arXiv:1411.3712.

[29] R. A. Battye and A. Moss, *Cosmological Perturbations in Elastic Dark Energy Models*, *Phys.Rev.* **D76** (2007) 023005, [astro-ph/0703744].

[30] R. A. Battye and J. A. Pearson, *Massive gravity, the elasticity of space-time, and perturbations in the dark sector*, *Phys. Rev. D* **88** (Oct., 2013) 084004, [arXiv:1301.5042].

[31] J. A. Pearson, *Material models of dark energy*, *Annalen Phys.* **526** (2014), no. 7-8 318–339, [arXiv:1403.1213].

[32] J.-c. Hwang, *Cosmological perturbations in generalised gravity theories: formulation*, *Class. Quantum Grav.* **7** (1990) 1613–1631, [arXiv:1002.4928].

[33] J.-h. He and B. Wang, *Revisiting $f(R)$ gravity models that reproduce ΛCDM expansion*, *Phys.Rev.* **D87** (2013), no. 2 023508, [arXiv:1208.1388].

[34] S. A. Appleby, R. A. Battye, and A. A. Starobinsky, *Curing singularities in cosmological evolution of F(R) gravity*, *JCAP* **1006** (2010) 005, [arXiv:0909.1737].

[35] W. Hu and I. Sawicki, *Models of f(R) Cosmic Acceleration that Evade Solar-System Tests*, *Phys.Rev.* **D76** (2007) 064004, [arXiv:0705.1158].

[36] A. A. Starobinsky, *A New Type of Isotropic Cosmological Models Without Singularity*, *Phys. Lett.* **B91** (1980) 99–102.

IV.4.2 Parametrized Post Friedmann Parameters

The parametrized pos-Friedmann (PPF) formalism is currently the most widely used parametrization of departure from standard GR [20]. There are two dimensionless parameters, which depend on time and scale. The first one, μ, measures the modification to the Poisson equation (IV.69). It is defined via

$$\Omega_{\rm m}\Delta_{\rm m} = -\tfrac{2}{3}\mu\left(a,k\right)\mathrm{K}^2 Z \tag{IV.133}$$

In $f\left(\mathcal{R}\right)$ gravity, using Eq. (IV.130) which can be re-written as a relation between the gauge invariant matter density perturbation $\Delta_{\rm m}$ and the gravitational potential Z, we find

$$\mu\left(a,k\right) = \frac{3\left(\mathrm{K}^2+\mathrm{M}^2\right)}{2\mathrm{K}^2+3\mathrm{M}^2}. \tag{IV.134}$$

The second parameter, denoted η, is known as the gravitational slip and measures the presence of a non-zero anisotropic stress or equivalently a difference between the gravitational potentials:

$$\eta\left(a,k\right) \equiv \frac{Z}{Y} \tag{IV.135}$$

To obtain η in $f\left(\mathcal{R}\right)$ gravity, we use (IV.72) and (IV.124) and form the ratio between the potentials Z and Y. One finds

$$\eta\left(a,k\right) = \frac{2\mathrm{K}^2+3\mathrm{M}^2}{4\mathrm{K}^2+3\mathrm{M}^2}. \tag{IV.136}$$

With the perturbed field's equations, μ and η can be rewritten in terms of the dark sector fluid variables, in a model independent manner, as

$$\mu\left(a,k\right) = \left(1+\frac{\Omega_{\rm de}\Delta_{\rm de}}{\Omega_{\rm m}\Delta_{\rm m}}\right)^{-1} \quad \text{and} \quad \eta\left(a,k\right) = \left(1-2\frac{\Omega_{\rm m}w_{\rm m}\Pi^{\rm S}_{\rm m}+\Omega_{\rm de}w_{\rm de}\Pi^{\rm S}_{\rm de}}{\Omega_{\rm m}\Delta_{\rm m}+\Omega_{\rm de}\Delta_{\rm de}}\right)^{-1} \tag{IV.137}$$

The expressions of μ and η given in (IV.134) and (IV.136) for $f\left(\mathcal{R}\right)$ gravity are quite general. We recall that they are valid for the modes of interest, in both matter (CDM) and dark energy domination, when the dark energy equation of state parameter is slowly varying $c^2_{a,\rm de} \simeq w_{\rm de}$ and remains bounded $w_{\rm de} = \mathcal{O}\left(1\right)$, and when B stays small compared to unity (or $\mathrm{M}^2 \gg 1$) so that the anisotropic stress is well approximated by (IV.124).

The expressions of the PPF, (IV.134) and (IV.136), enable a clear discussion on the phenomenology of dark sector perturbations in $f\left(\mathcal{R}\right)$ gravity. Two regimes for the behavior of sub-horizon modes, $\mathrm{K}^2 \gg 1$, can be identified: (i) the *GR regime* at early time, when $\mathrm{K}^2 \ll \mathrm{M}^2$, and (ii) the *scalar-tensor regime* (ST) at late time, when $\mathrm{K}^2 \gg \mathrm{M}^2$ and with $\mathrm{M}^2 \gg 1$. In both phases, the PPF parameters tend to scale independent constants:

$$\text{GR regime } \left(\mathrm{K}^2 \ll \mathrm{M}^2\right): \qquad \mu\left(a,k\right) = 1 \qquad \eta\left(a,k\right) = 1, \tag{IV.138}$$

$$\text{ST regime } \left(\mathrm{K}^2 \gg \mathrm{M}^2\right): \qquad \mu\left(a,k\right) = 3/2 \qquad \eta\left(a,k\right) = 1/2. \tag{IV.139}$$

Remarkably, the limits of $\mu$and η in the ST regime do not depend on the particular $f\left(\mathcal{R}\right)$ function. Nevertheless, the transition between the GR and ST regime happens at different time for different scales, *i.e.* when $\mathrm{K}^2 \approx \mathrm{M}^2$, and therefore depends on the particular $f\left(\mathcal{R}\right)$ model via the time evolution of M^2.

For the largest wavenumbers, the transition from the GR to the ST regime occurs during matter domination, while for smaller wavenumbers (larger scales) it can occur during dark energy domination, or may not take place at all, if B_0 is small enough. Indeed, if B_0 is so small that M^2 is always large

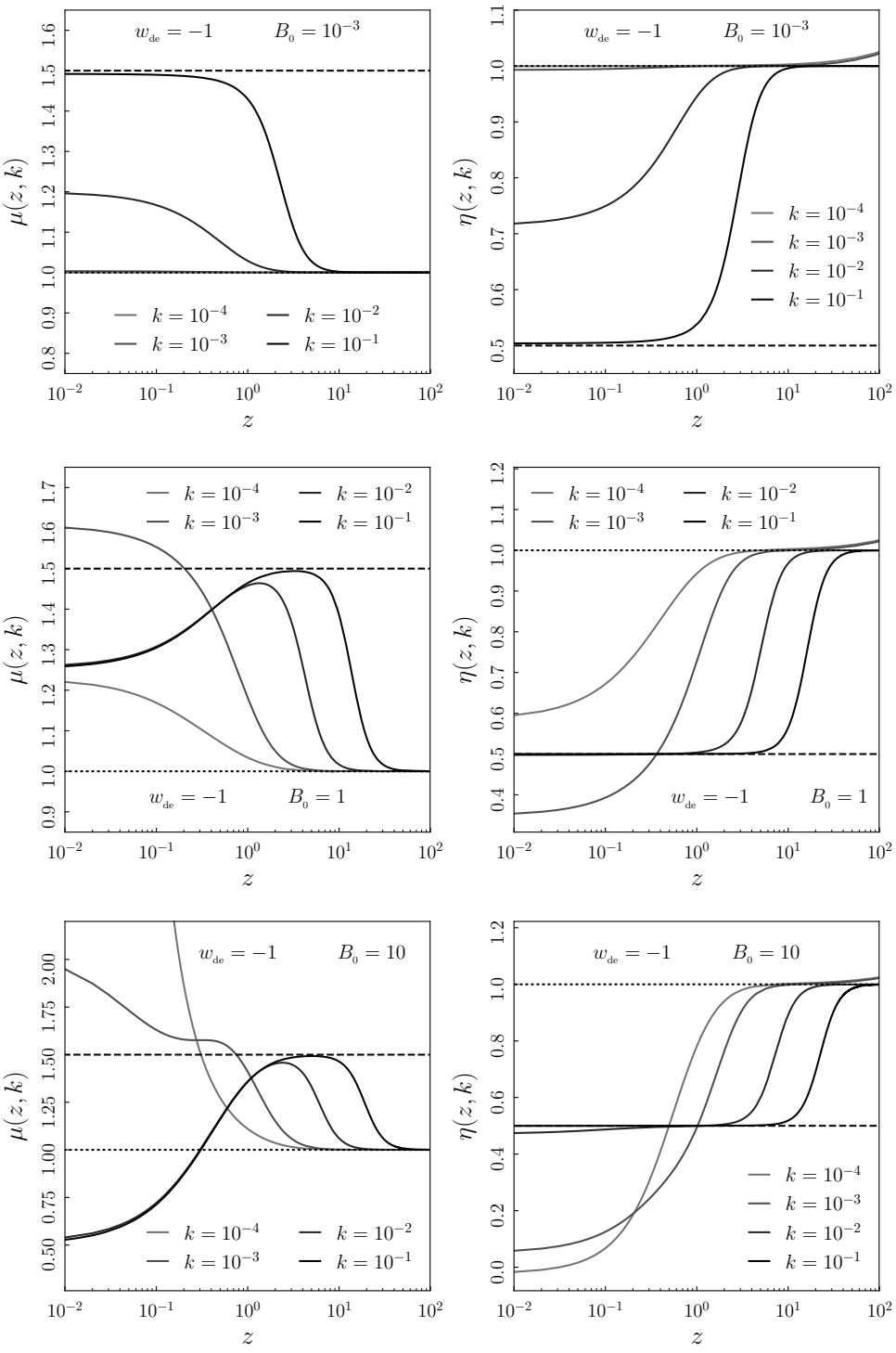

Figure 4: The post-Friedmann parameters μ (left column) and η (right column) defined in Eq. (IV.133)-(IV.135), in $f(\mathcal{R})$ gravity for several values of the parameter B_0 until redshift $z = 100$. The background cosmology was set to $w_{de} = -1$, $h = 0.673$ and $\Omega_m^0 = 0.315$. With these parameters, dark energy-matter equality occurs at $a_\Lambda \simeq 0.77$. The dashed lines are the scalar-tensor (ST) regime expectations ($\mu = 3/2$, $\eta = 1/2$), while the dotted lines are the ΛCDM expectations ($\mu = \eta = 1$). The three different $f(\mathcal{R})$ models shown here have: $B_0 = 10^{-3}$ (top); $B_0 = 1$ (middle); $B_0 = 10$ (bottom). In each panel, we present the results for four wavenumbers ranging from $k = 10^{-4}\,\mathrm{Mpc}^{-1}$ to $k = 10^{-1}\,\mathrm{Mpc}^{-1}$. Computation were carried out with `class_eos`.

compared to K^2 for all scales of interest, the dynamics remains in the GR regime and one recovers the dynamics of a simple wCDM model. This is the case for the smallest wavenumbers on the top panels of figure 4 where $B_0 = 10^{-3}$.

Figure 4 illustrates the evolution of the post-Friedmann parameters μ and η with respect to redshift for different $f(\mathcal{R})$ models and different wavenumbers in the range $10^{-4} - 10^{-1}\mathrm{Mpc}^{-1}$. Each panel corresponds to a different $f(\mathcal{R})$ function. All of the $f(\mathcal{R})$ models presented on this figure are mimicking a cosmological constant at the background level: the equation of state for the effective dark energy fluid is always $w_{\mathrm{de}} = -1$. The different $f(\mathcal{R})$ function are characterized by the parameter B_0 introduced in (IV.123), which ranges from 10^{-3} in the top panels to 10 in the bottom panels. The dotted lines are the standard GR expectations, $\mu = \eta = 1$, and the dashed lines are the ST limits $\mu = 3/2$ and $\eta = 1/2$. At high redshift, $z \approx 10^2$, the perturbations start in the GR regime and progressively transit to the ST regime depending on the wavenumber k. For small B_0 (top panel) the transition to the ST regime only occurs for the smallest scales, while for large B_0 (bottom panel) all the modes depart from the GR regime at low redshift. When B_0 is large the ST regime does not last until today because at low redshift M^2 becomes small and the dynamics in no longer well described by Eq. (IV.128) and (IV.129).

IV.4.3 Comparison with wCDM models and quintessence

The effective fluid description for wCDM and quintessence depends on two parameters, the equation of state at the background level w_{de} and the sound speed of the dark sector fluid, see subsection IV.2.4. In quintessence the sound speed is always one (in natural units). For a generic wCDM dark sector it may take any positive value. There is no restriction regarding the equation of state parameter w_{de}, which may be constant or time-dependent.

The phenomenological analysis we did for $f(\mathcal{R})$ gravity can be done for perturbations in wCDM. The effective dark sector fluid has no anisotropic stress and the entropy perturbation is given by the simple expression of Eq. (IV.111). Neglecting the matter anisotropic stress and entropy perturbation, and for sub-horizon modes, $\mathrm{K}^2 \gg 1$, we find the following differential equations for matter and dark sector density perturbations:

$$\Delta_{\mathrm{m}}'' + (2 - \epsilon_{\mathrm{H}})\,\Delta_{\mathrm{m}}' - \tfrac{3}{2}\Omega_{\mathrm{m}}\Delta_{\mathrm{m}} = \tfrac{3}{2}\Omega_{\mathrm{de}}\Delta_{\mathrm{de}}, \tag{IV.140}$$

$$\Delta_{\mathrm{de}}'' + (2 - \epsilon_{\mathrm{H}})\,\Delta_{\mathrm{de}}' + \left\{\mathrm{K}^2 c_{s,\mathrm{de}}^2 - \tfrac{3}{2}(1 + w_{\mathrm{de}})\,\Omega_{\mathrm{de}}\right\}\Delta_{\mathrm{de}} = \tfrac{3}{2}(1 + w_{\mathrm{de}})\,\Omega_{\mathrm{m}}\Delta_{\mathrm{m}}. \tag{IV.141}$$

Moreover, the PPF parameters are easily obtained with Eq. (IV.137),

$$\eta(a,k) = 1 \quad \text{and} \quad \mu(a,k) = 1 - \tfrac{3}{2}\tfrac{(1+w_{\mathrm{de}})\Omega_{\mathrm{de}}}{\mathrm{K}^2 c_{s,\mathrm{de}}^2}. \tag{IV.142}$$

The only non-trivial cases are a vanishingly small sound speed, $c_{s,\mathrm{de}}^2 \ll 1$, or an extremely large equation of state parameter, $w_{\mathrm{de}} \gg 1$. This would lead to significant corrections to the Poisson equation, parametrized by μ, but would not generate any gravitational slip η as the anisotropic stress is identically zero. Although they may be motivated by some Dirac-Born-Infeld theories [104], we will not discuss these specific cases. The reader is also referred to [21] for a phenomenological analysis.

Here, we shall only consider wCDM models with $|w_{\mathrm{de}}|, c_{s,\mathrm{de}}^2 \sim 1$. For this specific class of models the dynamics of perturbations can not depart significantly from GR since $\eta = 1$ and $\mu = 1 + \mathcal{O}\left(\Omega_{\mathrm{de}}/\mathrm{K}^2\right)$.

However, if $w_{\mathrm{de}} \neq 1$ the background evolution may have a significant impact on the growth of matter perturbations. For instance, if w_{de} is closer to zero, dark energy becomes dominant earlier than if $w_{\mathrm{de}} = -1$. Therefore, matter perturbations have less time to grow and the amplitude of the matter power spectrum is decreased, as can be seen on figure 9.

The comparison between the dynamics of perturbations in wCDM and other dark sector models is instructive: it enables to disentangle the effects of the background evolution from the effects of non standard equations of state for dark sector perturbations.

In the next subsection we turn back to $f(\mathcal{R})$ models and their influence on the CMB temperature anisotropy.

IV.4.4 Late integrated Sachs Wolfe effect

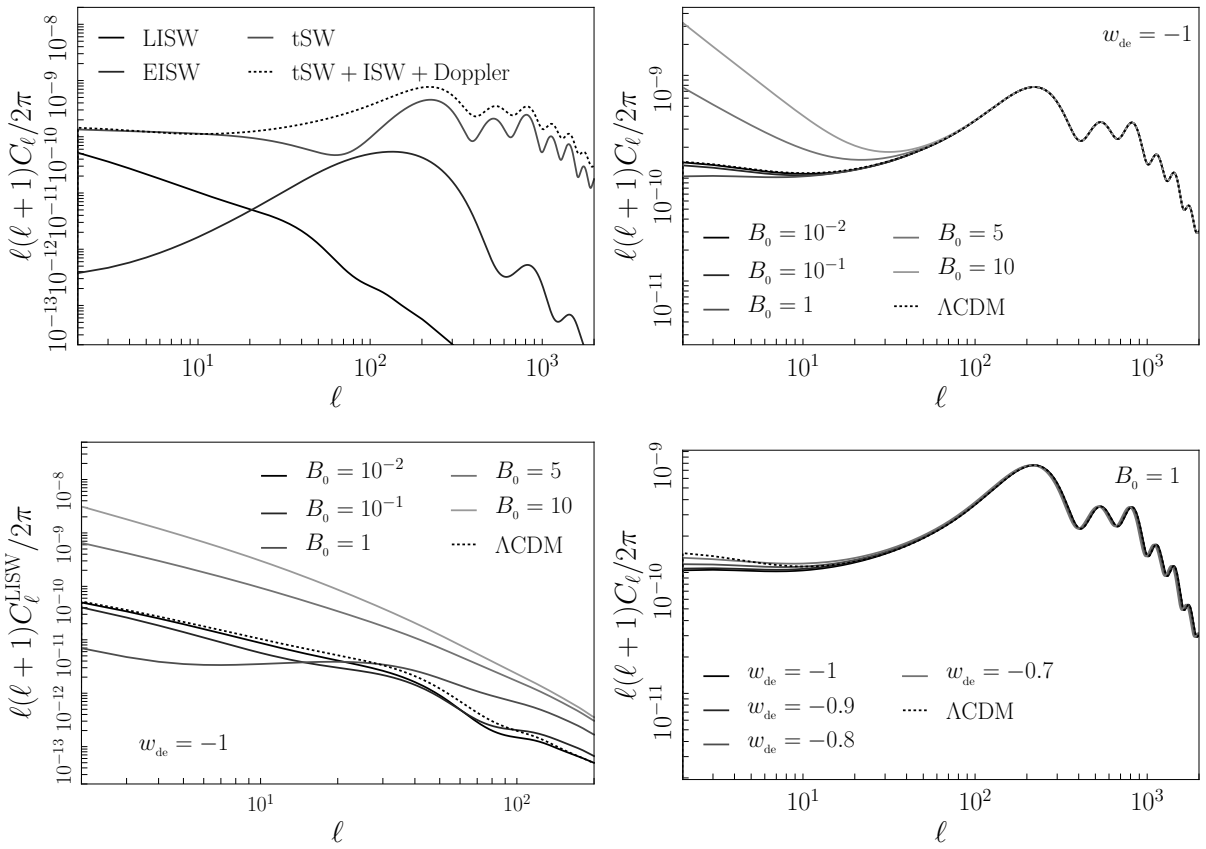

Figure 5: The different contributions to the temperature angular anisotropy power spectrum of the cosmic microwave background (top left) and effects of $f(\mathcal{R})$ gravity (other panels). Cosmological parameters were set to $h = 0.673$ and $\Omega_{\rm m}^0 = 0.315$ (other parameters set to Planck TT+lowP 2015 best-fit values). The top left panel shows the late integrated Sachs-Wolfe (LISW), the early integrated Sachs-Wolfe (EISW) and the temperature Sachs-Wolfe contributions (tSW) as well as the three combined with the Doppler contribution (dotted line). On the top-right panel the total angular power spectrum is shown for four $f(\mathcal{R})$ gravity models with B_0 ranging from 10^{-2} to 10 and $w_{\rm de} = -1$, while on the bottom-right panel B_0 is kept fixed to unity and $w_{\rm de}$ is varied from -1 to -0.7. The bottom-left panel illustrates to effect of $f(\mathcal{R})$ gravity on the LISW contribution for different values of B_0, and $w_{\rm de} = -1$. The dotted line represents the ΛCDM prediction. These computations were carried out with `class_eos`.

At the time of decoupling, $z \simeq 1100$, baryon acoustic oscillations are printed into the temperature anisotropy of the CMB photons. Then, the photons travel across the line of sight, falling and climbing out of the potential wells created by the density fluctuations.

This generates a particular structure to the CMB temperature anisotropy power spectrum known as the *integrated Sachs-Wolf effect* (ISW): since the curvature perturbations are time dependent the blue shift of the photon's temperature associated with the 'fall' is not exactly compensated by the redshift associated with the 'rising' of the photons out of the potential wells. More precisely, the ISW contribution to the CMB anisotropy is given by an integral of the time derivative of the sum of the gravitational potentials, $Z' + Y'$ (or $\phi' + \psi'$), along the line of sight, between decoupling and today.

When the gravitational potentials are constant, the contribution is vanishingly small. There are two epochs when Y and Z are varying, leading to two distinct contributions to the ISW effect: just after decoupling (*Early ISW effect*, EISW) and during Λ domination at late time (*Late ISW effect*, LISW).

At the time of decoupling dark sector perturbations are totally negligible. So, the only way dark sector perturbations can have an impact on the CMB temperature anisotropy is via the LISW effect. A detailed analysis of the LISW effect shows that it plays a significant role only for low multipoles of the CMB spectrum. For details I refer to [106]. The LISW effect is maximal for the smallest observable wavenumbers, typically $k \lesssim 10^{-3}\mathrm{Mpc}^{-1}$, and results in a tilt of the Sachs-Wolfe plateau of the CMB temperature anisotropy power spectrum.

In the top left panel of figure 5, the different contributions to the total CMB temperature anisotropy are presented with different line styles. The different contributions are the LISW and ISW effects that we discussed, as well as the so-called temperature Sachs-Wolfe (tSW) and Doppler contributions. These two contributions are closely related to the physics of decoupling, as explained in [106], and are therefore not affected by dark sector perturbations. The tSW and Doppler contributions largely dominate the CMB anisotropy at high multipoles $\ell \gtrsim 500$, the EISW effect contributes significantly around $\ell \simeq 100$ and the LISW effect is important for $\ell \lesssim 50$ or $k \lesssim 10^{-3}\mathrm{Mpc}^{-1}$. Hence, if the large-wavelength modes spend a significant amount of time outside the GR regime ($\mu, \eta \neq 1$) between horizon entry and today, the LISW effect can be boosted significantly and lead to important modifications of the Sachs-Wolf plateau of the CMB.

In $f(\mathcal{R})$ gravity, based on our previous analysis, one can be more specific and predict the lower bound for B_0 that corresponds to a noticeable modulation of the CMB temperature anisotropy. A departure of the CMB temperature anisotropy from the expectations of a wCDM model with $c^2_{s,\mathrm{de}} = \mathcal{O}(1)$, due to dark sector perturbations, may be significant only if

$$B_0 \gtrsim \left.\frac{2\bar{\epsilon}_{\mathrm{H}}}{\epsilon_{\mathrm{H}}}\right|_{a=1} \left(\frac{H_0}{kc}\right)^2 \simeq 2\times 10^{-4} \quad \text{with,} \;\; \Omega^0_{\mathrm{de}} = 0.7, \;\; \text{and} \;\; H_0 = 67\,\mathrm{km\,s^{-1}\,Mpc^{-1}}, \tag{IV.143}$$

where c is the velocity of light. Indeed, this condition expresses that the mode corresponding to $k = 10^{-3}\mathrm{Mpc}^{-1}$ has just entered the ST regime ($\mu = 3/2$ and $\eta = 1/2$) today. Nevertheless, it also means that modes with a smaller k remain unaffected by $f(\mathcal{R})$ gravity. So, this condition is quite weak. Demanding that modes with $k = 10^{-4}\mathrm{Mpc}^{-1}$ enter the ST regime at present leads to $B_0 \gtrsim 2\times 10^{-2}$.

As shown on the bottom left panel of figure 5, the LISW contribution indeed starts departing from the LCDM expectation (dashed line) for $B_0 \approx 10^{-2}$. On the top right panel, we show the CMB temperature anisotropy power spectrum for $f(\mathcal{R})$ models that mimic LCDM ($w_{\mathrm{de}} = -1$) but with different values of B_0. For $B_0 = 10$ the amplitude of the dipole increases by one order of magnitude compared to LCDM. This can be used to extract constraints on the upper bound for B_0 from CMB data. However, these constraints can not be compelling because at such low multipole the CMB temperature anisotropy signal necessarily has a large variance (cosmic variance), $\sigma/C_\ell = \sqrt{2/(2\ell+1)}$. The Planck collaboration obtained $B_0 < 0.79$ at 95% CL from CMB only [6].

Like we shall see in the next sections, more compelling observables are the matter power spectrum (BAO) and weak lensing observables (galaxy and CMB weak lensing) as they probe the evolution of the gravitational potentials (and not just their time derivatives) all the way between decoupling and today. For $f(\mathcal{R})$ gravity, with data coming from BAO and weak lensing, the value of B_0 is constrained to be less than 10^{-4} [6, 71], four orders of magnitudes smaller than with CMB only.

Something that has not been studied so far in the $f(\mathcal{R})$ literature is the degeneracy between B_0 and the effective fluid equation of state $w_{\rm de}$. The bottom right panel of figure 5 shows the CMB temperature anisotropy power spectrum for various $f(\mathcal{R})$ models with the same B_0 but different $w_{\rm de}$. We see that at low multipoles, the model with $B_0 = 1$ and $w_{\rm de} = -0.7$ is undistinguishable from LCDM. It indicates that B_0 and $w_{\rm de}$ can not be constrained separately. I am currently investigating this topic with Richard Battye and Francesco Pace.

IV.5 Observational probes I: The matter power spectrum

In this section we study the impact of dark sector perturbations on the growth of matter perturbations and the matter power spectrum. The matter power spectrum, or equivalently the two-point correlation function in position space, is one of the main observables that will be measured by the next generation of surveys (WFIRST, LSST, EUCLID). Therefore, understanding the role of the dark sector for the evolution of the large scale structure of the universe is one of the most urgent challenge for theoretical cosmology.

We start by reviewing the treatment of gaussian random fields in IV.5.1 and give the definition of the matter power spectrum. In subsection IV.5.2, we analyze how the growth rate and growth index for matter perturbation are affected by the dark sector. This helps us to study the effects of the dark sector on the matter power spectrum, the subject of the last subsection IV.5.3.

IV.5.1 Homogeneous and isotropic Gaussian random fields

A random field $\Delta(\mathbf{x}) \in \mathbb{C}$ is *homogenous* and *isotropic* if it is invariant under translations and rotations respectively. Mathematically, this translates into

$$\Delta(\mathbf{x}+\mathbf{y}) = \Delta(\mathbf{x}), \tag{IV.144}$$
$$\Delta(\mathrm{R}\mathbf{x}) = \Delta(\mathbf{x}), \tag{IV.145}$$

where $\mathrm{R} \in \mathrm{SO}(3)$ and $\mathbf{x}, \mathbf{y} \in \mathbb{R}^3$. For a homogeneous and isotropic random field, the two-point correlation function in position space $\xi(\mathbf{x}, \mathbf{y}) \in \mathbf{R}$ can only depend on the absolute value of the difference between the spatial points $\mathbf{x}$ and $\mathbf{y}$,

$$\xi(|\mathbf{x}-\mathbf{y}|) \equiv \langle \Delta(\mathbf{x}) \Delta^\star(\mathbf{y}) \rangle, \tag{IV.146}$$

where the brackets denote the ensemble average over all the spatial points separated by the distance $|\mathbf{x}-\mathbf{y}|$.

The two-point correlation function in Fourier space is related to the power spectrum, $P(k)$, and to the two-point function in position space via

$$\begin{aligned}
\langle \Delta(\mathbf{k}_1) \Delta^\star(\mathbf{k}_2) \rangle &= \int\int \mathrm{d}^3x \mathrm{d}^3y e^{i\mathbf{x}\cdot\mathbf{k}_1} e^{-i\mathbf{y}\cdot\mathbf{k}_2} \langle \Delta(\mathbf{x}) \Delta^\star(\mathbf{y}) \rangle, \\
&= \int\int \mathrm{d}^3x \mathrm{d}^3y e^{i\mathbf{x}\cdot\mathbf{k}_1} e^{-i\mathbf{y}\cdot\mathbf{k}_2} \xi(|\mathbf{x}-\mathbf{y}|), \\
&= \int\int \mathrm{d}^3x \mathrm{d}^3y e^{i\mathbf{x}\cdot\mathbf{k}_1} e^{i\mathbf{y}\cdot(\mathbf{k}_1-\mathbf{k}_2)} \xi(|\mathbf{x}|), \\
&= (2\pi)^3 \delta(\mathbf{k}_1-\mathbf{k}_2) P(|\mathbf{k}_1|),
\end{aligned} \tag{IV.147}$$

where

$$P(k) = \int \frac{\mathrm{d}^3\mathbf{r}}{(2\pi)^3} \xi(x) \exp(i\mathbf{k}\cdot\mathbf{x}) \quad \text{and} \quad \xi(x) = \int \mathrm{d}\mathbf{k} P(k) \exp(i\mathbf{k}\cdot\mathbf{x}) \tag{IV.148}$$

We say that $\Delta(\mathbf{x})$ is a *Gaussian* random field when it obeys a Gaussian statistics. Having in mind cosmological perturbations and galaxy surveys, we will be interested in Gaussian random fields, with zero expectation value, averaged over spherical volumes of some radius R. Let us denote this quantity $\bar{\Delta}(R)$, the *smoothed* random field, which itself is a Gaussian random field with zero expectation value. The probability density function of $\bar{\Delta}(R)$ is given by

$$\rho\left(\bar{\Delta}; R\right) = \frac{1}{\sqrt{2\pi}\sigma(R)} \exp\left(-\frac{\bar{\Delta}^2}{2\sigma^2(R)}\right), \tag{IV.149}$$

where the root mean square (RMS) of $\bar{\Delta}$ is obtained from the power spectrum via

$$\sigma^2(R) = \int_0^\infty \frac{dk}{k} \frac{k^3}{2\pi^2} P(k) W(kR)^2, \quad \text{with} \quad W(x) = \frac{3}{x^3}(\sin x - x\cos x) \tag{IV.150}$$

the Fourier transform of the top-hat window function divided by $\frac{4}{3}\pi R^3$ [38, 73], see also [142]. The RMS, $\sigma^2(R)$, is therefore the volume average of the power spectrum.

For instance, the cosmological parameter σ_8 is defined as the dispersion of the averaged matter over-density field over a sphere of radius $8\,h^{-1}$Mpc. This is about half the distance between the Virgo Cluster and the Milky Way. It is a crucial parameter that measures the growth of structure, i.e. the amplitude of clustering.

To close this parenthesis, we note that the power spectrum of the matter over-density is normalized to the primordial power spectrum of curvature perturbations so that

$$P(k) \equiv \frac{2\pi^2}{k^3} \Delta_{\rm m}^2 \mathcal{P}_{\mathcal{R}}(k), \quad \text{with} \quad \mathcal{P}_{\mathcal{R}}(k) \equiv A_s \left(\frac{k}{k_\star}\right)^{n_s - 1}. \tag{IV.151}$$

Hence, σ_8 is directly related to A_s, the amplitude of the primordial power spectrum at the pivot scale, $\mathcal{P}_{\mathcal{R}}(k_\star)$ with $k_\star = 0.05\,\mathrm{Mpc}^{-1}$ for the Planck mission, and to the present value of the matter over-density field $\Delta_{\rm m}$. See Eq. (75) of [100] for more details.

For a given dark sector theory, we saw that dark sector perturbations may affect the evolution of $\Delta_{\rm m}$. Hence, the matter power spectrum (IV.151) and the growth of structure can differ significantly from the LCDM expectation. The goal of the next section is to get some insight on this phenomenon, using the growth rate and growth index.

IV.5.2 Growth rate and growth index for matter perturbations

For sub-Hubble modes, at sufficiently late time during matter domination when the matter sector can be safely assumed to be CDM dominated, with no anisotropic stress nor entropy perturbation, the equation of evolution for the gauge invariant matter over-density can be written as

$$\Delta_{\rm m}'' + (2 - \epsilon_{\rm H})\Delta_{\rm m}' - \tfrac{3}{2}\varepsilon(a,k)\Omega_{\rm m}\Delta_{\rm m} = 0, \quad \text{with} \quad \varepsilon(a,k) = \frac{1}{\mu\eta}. \tag{IV.152}$$

Recall that with pressure-less matter sector $\epsilon_{\rm H} = \frac{3}{2}(1 + w_{\rm de}\Omega_{\rm de})$. To arrive at Eq. (IV.152), one starts with the perturbed fluid equations (IV.67)-(IV.68), and replaces the gravitational potential in terms of the post-Friedmann parameters defined in (IV.133) and (IV.135).

The *linear growth function* D is then defined via

$$\Delta_{\rm m}(a) = D(a)\Delta_{\rm m}(a=1), \tag{IV.153}$$

and naturally obeys the same equation as $\Delta_{\rm m}$. The most recent galaxy surveys such as BOSS and WiggleZ, as well as the next generation of surveys (WFIRST, EUCLID, LSST), are able to probe the redshift dependence of clustering. This corresponds to measuring the linear growth function, since

$$\sigma_8(a) = \sigma_8 D(a). \tag{IV.154}$$

Measurements of the matter over-density from galaxy surveys are biased: the observed galaxies are not a faithful tracer of the linear matter power spectrum. The positions of galaxies are resulting from a highly non-linear and complex formation process. Hence, one has to use bias parameters to link galaxy observables to the total matter over-density [66].

To break the important degeneracy between the linear growth function D and the bias parameters, spectroscopic surveys measure the position of galaxies *and* their velocity (associated with the so-called redshift-space distortions, RSD [93]). The velocity perturbations is related to the density perturbation through the continuity equation IV.67, which, in the case of sub-Hubble modes and pressure-less matter, leads to

$$\vartheta = -\mathrm{f}\Delta_{\mathrm{m}}, \quad \text{with} \quad \mathrm{f} \equiv \frac{D'}{D} \tag{IV.155}$$

the *growth rate* of matter perturbations, and where ϑ is the Fourier transform of the divergence of the peculiar velocity field $\vec{u}$ in units of the comoving Hubble velocity, *i.e.* $\vec{u} = \vec{v}/aH$ and $\vartheta = \vec{\nabla}\vec{u}$. Therefore, the parameter that is best determined is not $\sigma_8(a)$ but rather the parameter combination

$$\mathrm{f}\sigma_8(a) \equiv \frac{d\sigma_8(a)}{d\ln a}, \tag{IV.156}$$

as proposed by Song and Percival in [144]. For the latest measurements of this parameter combination see [7, 61] and [39] for details on the formalism. Another important reference is [139] where the authors explore departure from GR by considering different functional forms of $\varepsilon(a,k)$ that appears in (IV.152) and confront them to BAO and RSD data.

From Eq. (IV.152), it is straightforward to arrive at the equation of evolution for the growth rate:

$$\mathrm{f}' + \mathrm{f}^2 + (2 - \epsilon_{\mathrm{H}})\,\mathrm{f} = \tfrac{3}{2}\varepsilon(a,k)\,\Omega_{\mathrm{m}}. \tag{IV.157}$$

For completeness, we also give the differential equation for the *rescaled* growth function $g(a)$:

$$g'' + \left(\tfrac{5}{2} - \tfrac{3}{2}w_{\mathrm{de}}\Omega_{\mathrm{de}}\right)g' + \tfrac{3}{2}\left(1 - \varepsilon + [\varepsilon - w_{\mathrm{de}}]\,\Omega_{\mathrm{de}}\right)g = 0, \quad \text{with} \quad g(a) \equiv D(a)/a \tag{IV.158}$$

where we have replaced ϵ_{H} with its expression given bellow Eq. (IV.152). As can be easily deduced from Eq. (IV.152), deep inside the matter era but after matter-radiation equality ($\epsilon_{\mathrm{H}} = 3/2$, $\mu = \eta = \varepsilon = 1$) the growth function is simply proportional to the scale factor a so that $g$is constant. Thus, appropriate initial conditions for Eq. (IV.158) are $g(a_{\mathrm{ini}}) = 1$ and $g'(a_{\mathrm{ini}}) = 0$, with *e.g.* $a_{\mathrm{ini}} = 10^{-2}$.

As we shall see, in LCDM the growth rate is well approximated by $\mathrm{f} \approx \Omega_{\mathrm{m}}^{6/11}$, independently of the wavelength of the perturbation. This motivates the definition of the *growth index*,

$$\gamma \equiv \frac{\log \mathrm{f}}{\log \Omega_{\mathrm{m}}}. \tag{IV.159}$$

With our previous results one can easily arrive at the following differential equations for the growth index:

$$\gamma' + \tfrac{3w_{\mathrm{de}}\Omega_{\mathrm{de}}}{\log(1-\Omega_{\mathrm{de}})}\gamma + \tfrac{(1-\Omega_{\mathrm{de}})^{\gamma}}{\log(1-\Omega_{\mathrm{de}})} - \tfrac{3}{2}\varepsilon\tfrac{(1-\Omega_{\mathrm{de}})^{1-\gamma}}{\log(1-\Omega_{\mathrm{de}})} = \tfrac{3w_{\mathrm{de}}\Omega_{\mathrm{de}}-1}{2\log(1-\Omega_{\mathrm{de}})}. \tag{IV.160}$$

Measurements of the growth function, the growth rate and the growth index are expected to be a key step for discriminating between dark sector theories. Remarkably, the effects of the dark sector on the growth of structure are completely absorbed into the parameter ε defined in (IV.152), which itself depends on the dark sector anisotropic stress and over-density.

Equations (IV.152)-(IV.160) hold for any dark sector model, provided ε is expressed with the corresponding $\mu$and η. For the models we discussed previously one finds

$$f(\mathcal{R}) \text{ gravity}: \quad \varepsilon(a,k) = \frac{4\mathrm{K}^2 + 3\mathrm{M}^2}{3\left(\mathrm{K}^2 + \mathrm{M}^2\right)}, \tag{IV.161}$$

$$\text{quintessence, wCDM with } \mathrm{c}^2_{\mathrm{s,de}} = \mathcal{O}(1),\ \Lambda\text{CDM}: \quad \varepsilon(a,k) = 1. \tag{IV.162}$$

The differential equation (IV.160) is highly non-trivial as γ appears as an exponent in several terms, however it simplifies significantly when $\Omega_{\rm de} = o(1)$. This includes the matter domination but also a significant portion of the dark energy era. Equation (IV.160) can then be linearized with $\log(1-\Omega_{\rm de}) \simeq -\Omega_{\rm de}$ and $(1-\Omega_{\rm de})^x \simeq 1 - x\Omega_{\rm de}$. One finds

$$\gamma' + \left(1 - 3w_{\rm de} + \tfrac{3}{2}\varepsilon\right)\gamma = \tfrac{3}{2}\left(\tfrac{1-\varepsilon}{\Omega_{\rm de}} + \varepsilon - w_{\rm de}\right), \tag{IV.163}$$

In the GR regime, *i.e.* when dark energy is negligible and dark sector perturbations had no time to grow ($\varepsilon \approx 1$), the solution to this equation does not depend on the wavenumber and is constant in time:

$$\gamma_{w\rm CDM} \equiv \frac{3(1-w_{\rm de})}{5-6w_{\rm de}}. \tag{IV.164}$$

When we set $w_{\rm de} = -1$, the ΛCDM expectation is recovered, namely $\gamma_{\Lambda\rm CDM} \equiv 6/11$. (Note that since the term multiplying γ in the LHS of (IV.163) is positive, the constant of integration for the solution to the homogeneous equation has to be set to zero, in order to avoid a non-realistic divergence of the growth index at early time.)

After a mode has transitioned into the modified gravity regime ($\varepsilon \neq 1$), we can also write the stable solution to IV.163 as

$$\gamma_{\rm MG} = \frac{3(1-\varepsilon)}{2+3\varepsilon}\frac{1}{\Omega_{\rm de}} + \frac{3(\varepsilon - w_{\rm de})}{2+3\varepsilon-6w_{\rm de}}. \tag{IV.165}$$

For instance, consider the ST regime in $f(\mathcal{R})$ gravity, with $w_{\rm de} = -1$ and $\Omega^0_{\rm de} = 0.69$. Then, with $\varepsilon = 4/3$ we find $\gamma_{\rm MG} = 0.342$ in a very good agreement with our numerical results (which is $\gamma_{\rm MG} = 0.365$ as shown in figure IV.168) in spite of the fact that we extrapolate Eq. (IV.165) until redshift $z = 0$.

A comparison between figure 6 and 7 clearly indicates that the growth rate, or indirectly the growth index, can be used to detect potential departure from the standard LCDM growth of structure. In figure 6 and 7, we present the growth index versus redshift for $z \lesssim 4$, that is the maximal redshift of galaxy surveys[1], for four different scales ranging from $k = 10^{-1}\,{\rm Mpc}^{-1}$ to $k = 10^{-4}\,{\rm Mpc}^{-1}$, and three different equation of state parameters: $w_{\rm de} = -1, -0.9, -0.8$ on the left, middle and right panels respectively. Figure 6 corresponds to the $f(\mathcal{R})$ dark sector effective fluid, and figure 7 to a wCDM model with unit sound speed.

The LCDM growth index evolution can be seen on the left panel of figure 7. We see that for k between 10^{-4} and $10^{-2}\,{\rm Mpc}^{-1}$, the growth index is indeed fairly scale independent and well approximated by $\gamma_{\Lambda\rm CDM}$ (dashed line), however for smaller wavelength modes the growth index can depart significantly from the LCDM limit. The reason for this discrepancy is that these modes have entered the Hubble horizon before matter-radiation equality so that the corresponding fluctuations are affected by the dynamics of the radiation dominated era, not accounted for in our analysis. Nevertheless, even the perturbations on the smallest scales ($k = 10^{-1}\,{\rm Mpc}^{-1}$) end up with the same growth index as other scales, a few percents above $\gamma_{\Lambda\rm CDM}$, during dark energy domination.

Both wCDM models presented on the middle and right panel of figure 7 follow the same qualitative description. In addition, we note that even a small change in the value of the equation of state parameter, namely $w_{\rm de} = -0.9$ or $w_{\rm de} = -0.8$ has a strong impact on the growth index for perturbations on the largest scales ($k = 10^{-4}\,{\rm Mpc}^{-1}$) , although these can not be probed by galaxy surveys. (Our analysis did not allow to predict this behavior because we restricted ourselves to sub-horizon modes, while $k = 10^{-4}\,{\rm Mpc}^{-1}$ typically corresponds to a mode entering the horizon during dark energy domination.)

The growth index is, however, drastically different in $f(\mathcal{R})$ gravity. Manifestly, from figure 6, the only common feature between wCDM and $f(\mathcal{R})$ is that a change in the equation of state parameter

[1] Although bright isolated objects may be seen at redshift $z \approx 4$ with Euclid, LSST or WFIRST, it is true that LSS properties will only be probed up to $z \approx 2$.

$w_{\rm de}$ affects mostly the largest scales. Apart from that, the redshift evolution of the growth index in $f(\mathcal{R})$ gravity is very peculiar: the growth index for fluctuations on scales that had time to transit towards the ST regime during matter domination is scale independent, well modeled by Eq. (IV.165) with $\varepsilon = 4/3$ (dashed line on the figure), and becomes negative above redshift $z \sim 1$. This has an important effect on the quantity $f\sigma_8$. In figure 8 we show the current measurements of $f\sigma_8$ by WiggleZ [40], 6dFGRS [34] and SDSS [128] against the expectations for this quantity in $f(\mathcal{R})$ gravity.

The conclusion of this subsection is that dark sector theories can be constrained with galaxy survey measurements of $f\sigma_8$ versus redshift. Given this data, and a specific dark sector proposal, one can compute numerically the expected time evolution of $f\sigma_8$ within the model, using `class_eos` (as illustrated on figure 6 for $f(\mathcal{R})$ gravity). With the appropriate likelihood, we can then perform a MCMC exploration of the dark sector parameter space with `MontePython` and extract new constraints, similarly to the analysis of [139]. See [114] for an Euclid forecast of dark sector constraints up to redshift $z = 2$.

In the next subsection we discuss some aspects of the phenomenology associated with the matter power spectrum in modified gravity theories and dark energy.

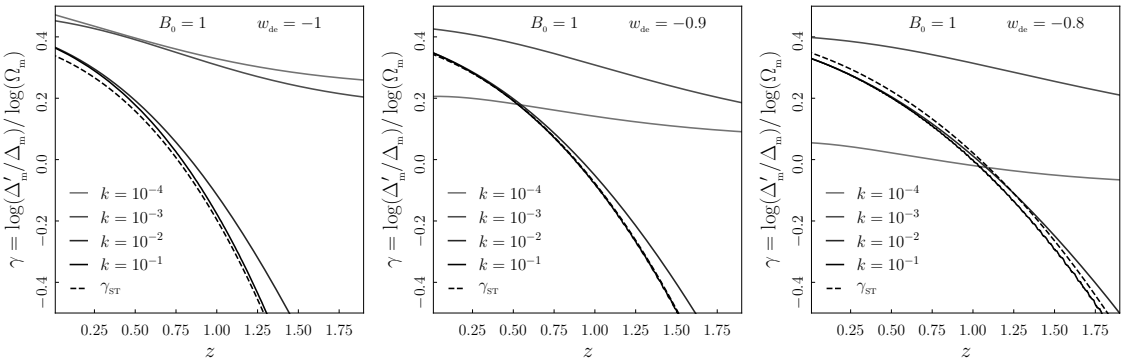

Figure 6: The growth index in $f(\mathcal{R})$ gravity until redshift $z = 1.75$ for several equation of state parameters with $B_0 = 1$, $h = 0.673$ and $\Omega_{\rm m}^0 = 0.315$, computed with `class_eos`: $w_{\rm de} = -1$ (left); $w_{\rm de} = -0.9$ (middle); $w_{\rm de} = -0.8$ (right). The dashed line is the growth index obtained analytically in Eq. (IV.165) with $\varepsilon = 4/3$, *i.e.* scalar-tensor (ST) expectation. The results are shown for four wavenumbers ranging from $k = 10^{-4}\,{\rm Mpc}^{-1}$ to $k = 10^{-1}\,{\rm Mpc}^{-1}$.

IV.5.3 The matter power spectrum in $f(\mathcal{R})$ gravity and wCDM models

The matter power spectrum can not be measured directly by observing the surrounding matter. Indeed, the matter power spectrum computed in cosmological perturbation theory refer to the power spectrum of the *total* matter over-density including dark matter and baryons. Our telescopes can detect just tiny fraction of the baryonic matter of the cosmos: the one that corresponds to visible galaxies and luminous dust clouds, which, as we said, are the result of highly non-linear processes. Thus the two-point correlation functions associated to these objects are necessarily biased. A summary of the different phenomenons involved in the formation of large scale structures is very well presented in [129]. In spite of this, marginalizing over the bias parameters, galaxy surveys can set some constraints on the amplitude of clustering.

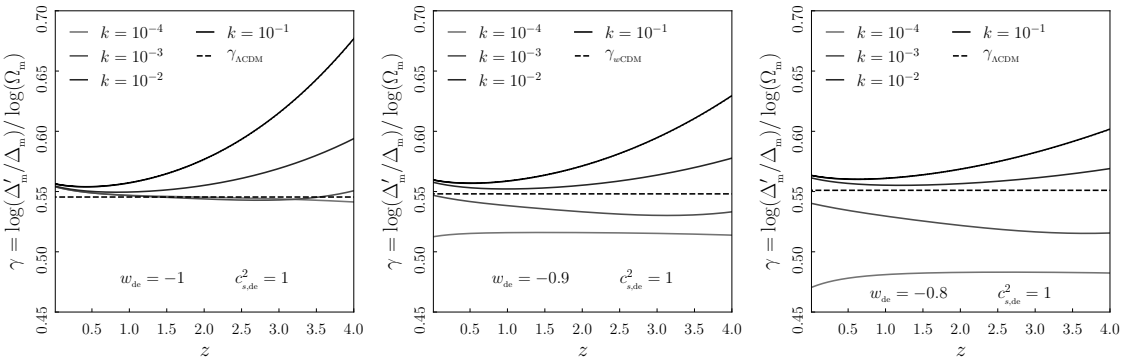

Figure 7: The growth index in wCDM models until redshift $z = 4$ for several equation of state parameters, with $c^2_{s,\mathrm{de}} = 1$, $h = 0.673$ and $\Omega^0_\mathrm{m} = 0.315$, computed with `class_eos`: $w_\mathrm{de} = -1$ (left); $w_\mathrm{de} = -0.9$ (middle); $w_\mathrm{de} = -0.8$ (right). The dashed line is the growth index obtained analytically in Eq. (IV.165) with $\varepsilon = 1$, *i.e.* the ΛCDM expectation. The results are shown for four wavenumbers ranging from $k = 10^{-4}\,\mathrm{Mpc}^{-1}$ to $k = 10^{-1}\,\mathrm{Mpc}^{-1}$.

Independently of galaxy surveys, the amplitude of the total matter power spectrum can also be extracted from CMB data, in particular the power spectrum of the thermal Sunyaev Zel'dovich effect that we discuss extensively in section IV.7. Galaxy weak lensing, the main subject of section IV.6, is also a promising tool for measuring σ_8.

From visible galaxies and clusters of galaxies one can build estimators of the galaxy power spectrum, which provides us with some valuable information on the total matter power spectrum. The most important pieces of information that can be extracted are: (i) the asymptotic behavior of the power spectrum, or its *shape*, and (ii) the baryon acoustic oscillations (BAO). Both features were observed first by the SDSS collaboration. The measurement of the shape of the power spectrum is reported in the 2003 seminal paper [148], where, in combination with the WMAP data, the SDSS team was able to extract percent level constraints on the cosmological parameters, opening the era for precision cosmology.

The matter power spectrum, defined in (IV.151), has three regimes with respect to the scale of the fluctuations. On the largest scales, super-Hubble modes with $k < 10^{-4}\,\mathrm{Mpc}^{-1}$, the matter over-density which is sourced by the curvature perturbation remains constant, frozen to its primordial amplitude. The scale dependence is simply given by that of the primordial power spectrum, divided by k^3. Since the primordial power spectrum is nearly scale invariant we therefore expect $P(k) \sim k^{-3}$ for these modes. But obviously, such scales are not observables (at least no via observable probes based on two-point correlation functions[2]).

The part of the power spectrum that can be probed by current CMB and LSS data corresponds to sub-Hubble scales and has two branches. The first one corresponds to scales that entered the Hubble horizon before matter-radiation equality and the second regime corresponds to scales that entered the Horizon after matter-radiation equality, in the more recent universe. Matter-radiation equality occurs at redshift $z_\mathrm{eq} \sim 5 \times 10^3$, corresponding to $k_\mathrm{eq} = a_\mathrm{eq} H_\mathrm{eq} \approx 10^{-2}\,\mathrm{Mpc}^{-1}$. This scale separates the two branches of the power spectrum.

For $k \gtrsim k_\mathrm{eq}$, the matter fluctuation had time to grow since the radiation dominated era. A careful analysis leads to $P(k) \sim k^{-3}\,[\ln(k)]^2$ at the end of radiation domination for these small scale fluctuations. Then, the effect of the subsequent matter (and dark energy) domination is to enhance this branch of the power spectrum but in a scale invariant manner. Indeed, we saw that the equation of

[2]The study of the higher order statistical properties of the CMB and LSS could, in principle, give us some insights on supper-Hubble scales *e.g.* the squeezed limit of the CMB bispectrum.

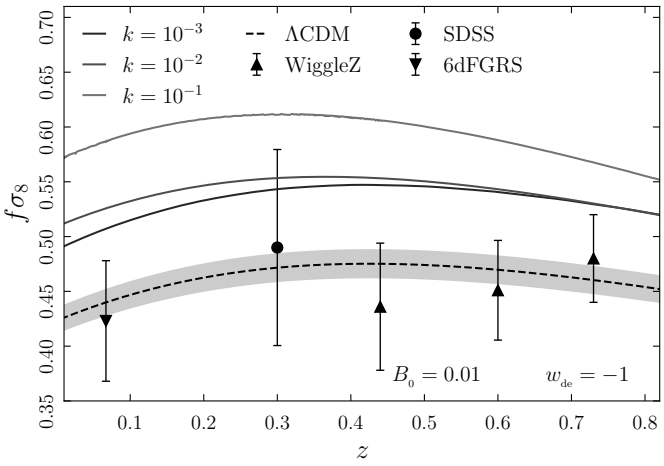

Figure 8: The parameter fσ_8 as measured by various redshift surveys until redshift $z \simeq 0.8$: downward triangle (6dFGRS, [34]); circle (SDSS LRG, [128]); triangle (WiggleZ, [40]). The grey band shows the range allowed at 95% C.L. by the Planck TT+lowP+lensing data, assuming the ΛCDM model. The dashed line corresponds from the best-fit extracted from the Planck TT+lowP+lensing data. The grey lines are the theoretical expectation for a $f(\mathcal{R})$ gravity model with $B_0 = 1$ and which mimics ΛCDM at the background level ($w_{de} = -1$). Unlike in ΛCDM, fσ_8 is scale-dependent in $f(\mathcal{R})$ gravity. Therefore we present our results for three wavenumbers ranging from $k = 10^{-4}\,\mathrm{Mpc}^{-1}$ to $k = 10^{-1}\,\mathrm{Mpc}^{-1}$. These computations were performed with `class_eos`.

evolution for the sub-Horizon matter over-density IV.152 does not depend on the wavenumber (in the LCDM scenario).

For $k \lesssim k_{eq}$, the scale dependence of the power spectrum is essentially set by the horizon entry: during matter domination $\Delta_m \sim a$, so that modes entering the horizon early have time to grow more than modes entering the horizon at later time. More precisely, between horizon entry and the end of matter domination, the fluctuation for the mode with wavenumber k is amplified by a factor proportional to $a_\star^{-1}$ where the star denote horizon entry, defined via $k = a_\star H_\star$. Since $H_\star \propto a_\star^{-3/2}$ during matter domination, one finds $a_\star \propto k^{-2}$ and consequently $P(k) \sim k$. During dark energy domination, these modes are sub-Hubble and continue to evolve independently of the wave-number: the power spectrum is enhanced in a scale independent way (in the LCDM scenario).

Our analysis on the evolution of the growth index in modified gravity can help us to explore the effects of dark sector perturbations on the matter power spectrum. Recall that the growth rate is defined as $f = \Delta_m'/\Delta_m$ and the growth index, γ, via $D = \Omega_m^\gamma$. In the regime, $\Omega_{de} = o(1)$ we get

$$\Delta_m' = (1 - \gamma\Omega_{de})\,\Delta_m. \tag{IV.166}$$

Assuming that the growth index varies slowly with time, $\gamma' \ll \gamma$, (in fact this assumption holds because the solution to IV.160 without RHS is set to zero for the reasons given in section IV.5.2) we can use IV.160 to rewrite IV.166as

$$\Delta_m' = \left\{\frac{6\varepsilon - 1}{2 + 3\varepsilon} - \frac{3(\varepsilon - w_{de})}{2 + 3\varepsilon - 6w_{de}}\Omega_{de}\right\}\Delta_m. \tag{IV.167}$$

With $\Omega_{de} \propto a^{-3w_{de}}$ and assuming that ε is slowly varying too, Eq. (IV.167) is easily integrated and yields

$$\Delta_m \propto \left\{1 + \frac{\varepsilon - w_{de}}{(2 + 3\varepsilon)\,w_{de} - 6w_{de}^2}\Omega_{de}\right\} a^{\frac{6\varepsilon - 1}{2 + 3\varepsilon}}. \tag{IV.168}$$

For ΛCDM, $\varepsilon = 1$ and $w_{\rm de} = -1$, so one recovers $\Delta_{\rm m}^{\Lambda{\rm CDM}} \sim a$. When $\varepsilon = 1$, for a wCDM fluid with $c^2_{s,{\rm de}} = \mathcal{O}(1)$, quintessence, or in the GR regime for $f(\mathcal{R})$ gravity perturbations we get

$$\Delta_{\rm m}^{w{\rm CDM}} \propto \left\{1 + \tfrac{1}{3w_{\rm de}}\gamma_{w{\rm CDM}}\Omega_{\rm de}\right\} a, \tag{IV.169}$$

where $\gamma_{w{\rm CDM}}$ is positive and given in IV.164. Therefore, the growth of matter perturbations is practically unaffected by the dark sector but does receive an extra contribution. We can quantify this extra contribution by forming the ratio $(P^{w{\rm CDM}}/P^{\Lambda{\rm CDM}}) \equiv (\Delta_{\rm m}^{w{\rm CDM}}/\Delta_{\rm m}^{\Lambda{\rm CDM}})^2$. One finds,

$$\frac{P^{w{\rm CDM}}}{P^{\Lambda{\rm CDM}}} = 1 + \tfrac{2}{3w_{\rm de}}\left\{\gamma_{w{\rm CDM}} + w_{\rm de}\gamma_{\Lambda{\rm CDM}}\right\}\Omega_{\rm de}, \tag{IV.170}$$

$$= 1 + \frac{4}{11}\frac{1+w_{\rm de}}{w_{\rm de}}\left\{\frac{w_{\rm de} - \frac{11}{12}}{w_{\rm de} - \frac{5}{6}}\right\}\Omega_{\rm de}. \tag{IV.171}$$

This is the extra contribution to the matter power spectrum at linear order in $\Omega_{\rm de}$. The term between brackets in the second equality is always positive for a negative $w_{\rm de}$. Then, for $w_{\rm de} > -1$ the total contribution is always negative, decreasing power in the matter density perturbation compared to LCDM. On the contrary, for phantom models, *i.e.* $w_{\rm de} < -1$, the matter power spectrum shifts to higher amplitudes compared to LCDM.

On figure 9, we present the matter power spectrum computed with `class_eos` in several wCDM models with constant equation of state parameters between -1.4 and -0.6. Qualitatively, formula (IV.171) gives the correct trend, as can be appreciated on the right panel where we plotted the ratio of the power spectrum with the LCDM expectation. On small scales, typically the ones that enter horizon during matter domination (where our approximations hold) the wCDM power spectrum is shifted in a scale independent manner, towards higher amplitude for more negative $w_{\rm de}$ and towards lower amplitude for less negative $w_{\rm de}$, compared to LCDM.

Quantitatively, formula (IV.171) is not satisfying: the analytical results differ from the numerical simulations by about twenty percent. Its regime of validity is indeed limited to $\Omega_{\rm de} = o(1)$, corresponding to redshift $z \gtrsim 1$. Hence, we do not expect it to be a faithful description of the *present* matter power spectrum.

For $f(\mathcal{R})$ gravity, analytical results for the matter power spectrum are even more intricate to obtain because $\varepsilon(a,k) = (1/\mu\eta)$ depends strongly on time and the wavenumber, as illustrated in figure 4. But looking at the functional form of ε given in Eq. (IV.161) we can yet understand a few things. Indeed, for large wavenumbers ($k \gtrsim 10^{-2}{\rm Mpc}^{-1}$), modes enter the modified gravity (ST) regime before matter-radiation equality. The larger the wavenumber, the earlier the mode is in the ST regime. In the ST regime, $\varepsilon \simeq 4/3$ so that during after matter-radiation equality (but before dark energy domination) one has $\Delta_{\rm m} \sim a^{1.2}$, for a $f(\mathcal{R})$ gravity model with $w_{\rm de} = -1$. Thus, clustering is quicker for the modes in the ST regime compared to LCDM ($\Delta_{\rm m} \sim a$ during matter domination) and the power spectrum is boosted in a scale dependent way as small scale fluctuations spend more time in the modified gravity regime.

In figure 10 we show the power spectrum calculated with `class_eos` in $f(\mathcal{R})$ gravity, for various values of the B_0 parameter and $w_{\rm de}$. The top right panel clearly illustrates the scale dependent boost of the power spectrum, with more power for small scales. The parameter B_0 was fixed for the bottom panel, so one can appreciate the weak dependence of the power spectrum on the equation of state parameter $w_{\rm de}$. Curiously, the effect of $w_{\rm de}$ is 'inverted' compared to our previous analysis of wCDM models. This time, less negative $w_{\rm de}$ tend to increase the amplitude of clustering at small scales. Such effect is however difficult to describe analytically, it certainly depends on the particular type of $f(\mathcal{R})$ function being considered.

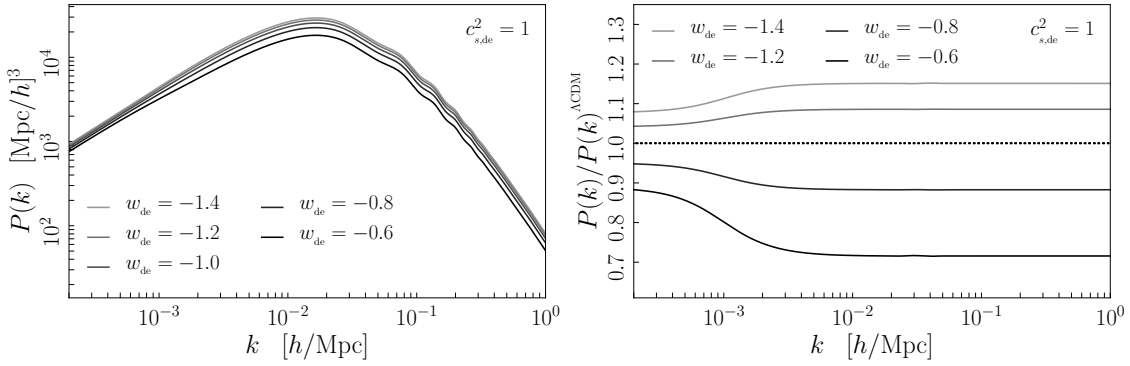

Figure 9: Matter power spectrum in wCDM for different equation of state parameters, $-1.1 \leq w_{\mathrm{de}} \leq -0.8$, with unit sound speed ($c^2_{s,\mathrm{de}} = 1$). Other parameters were set to $h = 0.673$, $A_s = 2.2 \times 10^{-9}$, $n_s = 0.97$ and $\Omega^0_{\mathrm{m}} = 0.315$. The left panel shows the linear matter power spectrum, while the right panel shows its ratio with the ΛCDM prediction as a function of the wavenumber. Computations were performed with `class_eos`.

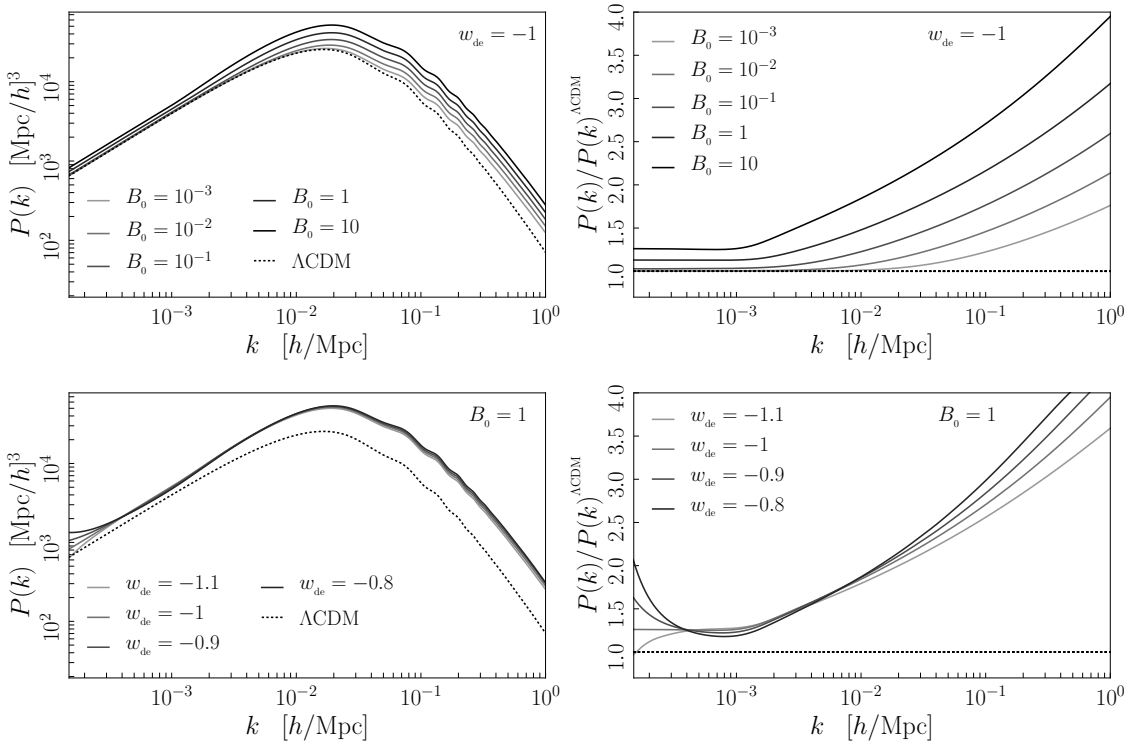

Figure 10: Matter power spectrum in $f(\mathcal{R})$ gravity for different equation of state parameters w_{de} with $B_0 = 1$ (top panel) and different B_0 with $w_{\mathrm{de}} = 1$ (bottom panel). Other parameters were set to $h = 0.673$, $A_s = 2.2 \times 10^{-9}$, $n_s = 0.97$ and $\Omega^0_{\mathrm{m}} = 0.315$. The left columns shows the linear matter power spectrum, while the right column shows its ratio with the ΛCDM prediction as a function of the wavenumber. Computations were performed with `class_eos`.

IV.6 Observational probes II: Weak lensing

In this section, I describe how the matter power spectrum $P(k)$, which gives the power of density perturbation in Fourier space, can be translated into the galaxy shear correlation function $\xi_{\pm}(\theta)$ in angular space. The galaxy shear correlation function is a direct observable extracted from galaxy shape catalogues, such as the one produced by the Canada-France-Hawaii Telescope Lensing Survey [74]. Details regarding weak lensing can be found in [98] and [22]. Towards the end of the section, I also briefly discuss CMB weak lensing Hanson et al. [82].

IV.6.1 The lensing potential

A small perturbation of the gravitational field on the FLRW background is parametrized by the gravitational potentials as

$$ds^2 = -(1+2\psi)\,dt^2 + (1-2\phi)\,dx^2. \tag{IV.172}$$

When $\phi, \psi \ll 1$, the perturbation may act as a refractive medium for light rays. Indeed, on the light cone ($ds^2 = 0$) the phase velocity of the light ray becomes

$$v = \left(\frac{1+2\psi}{1-2\phi}\right)^{\frac{1}{2}} = 1 + 2\Phi_{\rm WL}, \quad \text{with} \quad \Phi_{\rm WL} \equiv \frac{\phi+\psi}{2} = \frac{Z+Y}{2} \tag{IV.173}$$

the so-called *Weyl potential*[1], where Z and Y are the gauge invariant notations introduced on page 107. We note that, in terms of the PPF parameters μ and η of section IV.4.2 and the gauge invariant matter over-density in Fourier space $\Delta_{\rm m}$, the Weyl potential can be written as

$$\Phi_{\rm WL} = -\frac{3}{2}\Sigma\frac{\Omega_{\rm m}\Delta_{\rm m}}{\mathrm{K}^2} = -\frac{3}{2}\Sigma\frac{\Omega^0_{\rm m}\Delta_{\rm m}}{k^2 a}, \quad \text{with} \quad \Sigma \equiv \frac{1+\eta}{2\mu\eta}. \tag{IV.174}$$

Let us first consider a point source emitting light. In order to minimize their travel, the light rays bend when going across a gravitational perturbation. The deflection angle, $\delta\boldsymbol{\alpha}$, between the ingoing and out going light ray is expressed in terms of the Weyl potential as

$$\delta\boldsymbol{\alpha} = 2\nabla_\perp \Phi_{\rm WL}\delta r. \tag{IV.175}$$

It is the gradient of the 'refractive index' normal to the direction of propagation, r, where both $\nabla_\perp$ and δr are expressed in comoving coordinate. In the flat FLRW universe, the deflection angle $\delta\boldsymbol{\alpha}$ can be translated into a (comoving) separation vector

$$\mathrm{d}\mathbf{x} = \left(\chi - \chi'\right)\delta\boldsymbol{\alpha}, \tag{IV.176}$$

where χ is the comoving distance to the source and χ' the comoving distance to the lens (non-zero gravitational potential). The separation vector measures the distance between the source and its apparent location in the sky.

Next, we consider an extended source. The effect described above results in an apparent stretching or shrinking of the image of the source. Let $\boldsymbol{\theta}$ be the angle under which the source appears to the observer, and $\boldsymbol{\beta}$ the same angle in case of no lensing effect. Then the deflection angle $\boldsymbol{\alpha} \equiv \boldsymbol{\beta} - \boldsymbol{\theta}$ is given by [97]

$$\boldsymbol{\alpha} = -2\int_0^\chi \mathrm{d}\chi' \frac{\chi-\chi'}{\chi}\left\{\nabla_\perp\Phi_{\rm WL}\left(\chi'\boldsymbol{\theta}, \chi'\right) - \nabla_\perp\Phi_{\rm WL}\left(0, \chi'\right)\right\}, \tag{IV.177}$$

where the first argument of $\nabla_\perp\Phi_{\rm WL}$ is transverse to the line of sight.

[1] The *Weyl potential* actually refers to a class of solution to Einstein's field equations which are static and axisymmetric. In the weak field limit, these solutions are equivalent to IV.172.

The amplification matrix is then defined as

$$\boldsymbol{A} = \mathbf{1} + (\partial\boldsymbol{\alpha}/\partial\boldsymbol{\theta})\,. \tag{IV.178}$$

It is the Jacobian of the mapping from the lensed image to the unlensed image of the source. So $A_{ij} = \delta_{ij} - \partial_i\partial_j\Psi$, where Ψ is the *lensing potential*

$$\Psi(\boldsymbol{\theta}, \chi) = 2\int_0^\chi \mathrm{d}\chi' \frac{\chi - \chi'}{\chi}\Phi_{\mathrm{WL}}\left(\chi'\boldsymbol{\theta}, \chi'\right), \tag{IV.179}$$

and partial derivatives are in $\boldsymbol{\theta}$ space. The amplification matrix is decomposed into its trace (twice the *convergence* κ), a transverse part, $\epsilon_\times$, and a traceless tangential component, ϵ_t. These constitutes the two components of the *shear* $\boldsymbol{\epsilon} \equiv (\epsilon_t, \epsilon_\times)$.

The convergence κ is associated with an overall change of the source image, while the shear $\boldsymbol{\epsilon}$ is associated with a distortion effect. The shear is often written as a complex number,

$$\boldsymbol{\epsilon} = \epsilon_t + i\epsilon_\times = |\epsilon| \exp(2i\varphi)\,, \tag{IV.180}$$

where $|\epsilon|$ is the shear amplitude and φ the complex phase between the transverse and tangential modes. Note that the shear vector, is a spin-two object (in analogy to gravity waves, see [122] p. 954).

In terms of the Euclidean basis in the plane of the image $\{\boldsymbol{\partial}_1, \boldsymbol{\partial}_2\}$, the shear decomposes as

$$\boldsymbol{\epsilon} = \epsilon_t \mathbf{e}_+ + \epsilon_\times \mathbf{e}_\times, \tag{IV.181}$$

where $\mathbf{e}_+$ and $\mathbf{e}_\times$ are expressed in terms of the dual basis one-forms $\{\mathbf{dx}_1, \mathbf{dx}_2\}$ as

$$\mathbf{e}_+ \equiv \mathbf{dx}_1 \otimes \mathbf{dx}_1 - \mathbf{dx}_2 \otimes \mathbf{dx}_2, \text{ and } \mathbf{e}_\times \equiv \mathbf{dx}_1 \otimes \mathbf{dx}_2 + \mathbf{dx}_2 \otimes \mathbf{dx}_1. \tag{IV.182}$$

With these tools, we shall now describe how the ellipticity of galaxy shapes can be employed to probe the Weyl potential.

IV.6.2 The ellipticity of galaxies

The unlensed image of a galaxy is an ellipse, characterized by its major axis a and minor axis b. The orientation of the major axis, in the plane transverse to the propagation of the light rays, is denoted ω. We define the complex (unlensed) ellipticity of a galaxy as

$$\boldsymbol{\varepsilon}^{\mathrm{S}} \equiv \frac{a-b}{a+b}\exp(2i\omega)\,. \tag{IV.183}$$

Then the observed (lensed) ellipticity of the galaxy is given by (linear regime)

$$\boldsymbol{\varepsilon} = \boldsymbol{\varepsilon}^{\mathrm{S}} + \boldsymbol{\epsilon}, \tag{IV.184}$$

where $\boldsymbol{\epsilon}$ is the lensing shear written as complex number (IV.180).

The typical fluctuation of the unlensed ellipticity of individual galaxies, *i.e.* the noise, is $\sigma \sim 0.3$, while the RMS of the lensing shear due to large scale structure lensing, *i.e.* the signal, is $s \sim 0.03$ [97]. Hence, to achieve a significant signal-to-noise ratio one needs a catalogue of at least several thousands of galaxy (signal/noise $= s\sqrt{N}/\sigma$).

Since galaxies have, *a priori*, no preferred orientation, the expectation value of $\boldsymbol{\varepsilon}^{\mathrm{S}}$ for a large galaxy survey, is zero. The Weyl potential being a gaussian random field, its expectation value is also zero, which implies $\langle\boldsymbol{\epsilon}\rangle = 0$, see (IV.179). Hence, the expectation value of the observed shear, $\boldsymbol{\varepsilon}$ of Eq. (IV.184), a gaussian random field with zero mean value, must vanish too.

The key observables to measure the weak lensing effect are associated to the dispersion of $\boldsymbol{\varepsilon}$. They are the *two-point shear correlation functions*,

$$\xi_{\pm}(\boldsymbol{\theta}) \equiv \langle \boldsymbol{\epsilon}\boldsymbol{\epsilon} \rangle = \frac{\sum w_i w_j \left[\epsilon_t(\mathbf{x}_i)\,\epsilon_t(\mathbf{x}_j) \pm \epsilon_\times(\mathbf{x}_i)\,\epsilon_\times(\mathbf{x}_j)\right]}{\sum w_i w_j}, \tag{IV.185}$$

where w_i are weights that depend on the quality of the data, $\boldsymbol{\theta} = |\mathbf{x}_i - \mathbf{x}_j|$ is the angular separation of the pair of galaxies (i, j), and $\epsilon_{t,\times}$ are the observed shear components of the previous section after a rotation into the reference frame joining each pair of galaxy, see [86] for a rigorous treatment.

In the next subsection we link the two-point shear correlation functions (IV.185) to the projected power spectrum of the Weyl potential.

IV.6.3 Power spectrum of the lensing shear

From the definition of the amplification matrix, A in Eq. (IV.178), in Fourier space, the *convergence* reads as $\kappa = \frac{1}{2}\ell^2\Psi$, where ℓ is the norm of the wavenumber transverse to the line of sight, $\boldsymbol{\ell} \equiv \ell_1\boldsymbol{\partial}_2 + \ell_2\boldsymbol{\partial}_2$ (the Fourier-conjugate of $\boldsymbol{\theta}$) and Ψ is the lensing potential defined in Eq. (IV.179). The shear components are $\epsilon_t = \frac{1}{2}\left(\ell_1^2 - \ell_2^2\right)\Psi$ and $\epsilon_\times = \ell_1\ell_2\Psi$ in Fourier space. So, we have a simple relation that relates the shear (IV.180) to the lensing potential and the convergence:

$$\boldsymbol{\epsilon}(\boldsymbol{\ell}) = \left\{\tfrac{1}{2}\left(\ell_1^2 - \ell_2^2\right) + \ell_1\ell_2\right\}\Psi = \frac{(\ell_1 + i\ell_2)^2}{\ell}\kappa(\boldsymbol{\ell}) = e^{2i\varphi}\kappa(\boldsymbol{\ell}), \tag{IV.186}$$

where φ is the phase of $\ell_1 + i\ell_2$.

Then, the *shear power spectrum* is simply the power spectrum of the convergence, $P^\epsilon = P^\kappa$, defined by (IV.147), which gives

$$\left\langle \kappa(\boldsymbol{\ell})\,\kappa^\star\left(\boldsymbol{\ell}'\right)\right\rangle = (2\pi)^3\,\delta\left(\boldsymbol{\ell} - \boldsymbol{\ell}'\right)P^\kappa(\ell). \tag{IV.187}$$

Then, the correlation functions in position space $\xi_\pm(\theta)$ can be written as the Hankel transform of the convergence power spectrum:

$$\xi_\pm(\theta) = \frac{1}{2\pi}\int \mathrm{d}\ell J_\pm(\ell\theta)\,P^\kappa(\ell), \tag{IV.188}$$

where J_+ and J_- are the zeroth and fourth order Bessel functions respectively (see [97] and [22] for the details).

Finally, using (IV.179) and accounting for the source galaxy distribution per redshift bin i, $n_i(\chi)\,\Delta\chi = n_i(z)\,\Delta z_i$, the convergence power spectrum can be written in terms of the *power spectrum of the Weyl potential*, $P_{\Phi_{\rm WL}}$, as

$$P^\kappa_{i,j}(\ell) = 2\pi^2\ell\int\frac{\mathrm{d}\chi}{\chi}g_i(\chi)\,g_j(\chi)\,P_{\Phi_{\rm WL}}(\ell/\chi, \chi), \tag{IV.189}$$

where we used the Limber approximation, $\ell = \chi\theta$. In this expression, we have recast the $\chi' - \chi$ terms of Eq. (IV.179) into the *lensing efficiency* defined as

$$g_i(\chi) \equiv \int_\chi^{\chi_{\rm lim}}\mathrm{d}\chi' n_i(\chi')\,\frac{\chi' - \chi}{\chi'}, \tag{IV.190}$$

where $\chi_{\rm lim}$ is the comoving distance of the furthest galaxy in the survey [6].

Note that when considering sources at different redshift, the shear correlation functions (IV.188) shall also bear indices relative to the redshift bin. Then, this correlation functions relative to redshift bins have to be understood as measuring the correlation between the shear of a galaxy in the redshift bin i to the shear of a galaxy in the redshift bin j.

In the gauge invariant notations defined on page 107, the power spectrum of the Weyl potential is

$$P_{\Phi_{\rm WL}} \equiv \left\{\frac{Z+Y}{2}\right\}^2 \mathcal{P}_{\mathcal{R}} = \frac{9}{4}\Omega_{\rm m,0}^2 H_0^4 \frac{1}{k^4 a^2}\Delta_{\rm m}^2 \mathcal{P}_{\mathcal{R}}\Sigma^2, \tag{IV.191}$$

with Σ defined in Eq. (IV.174), $\mathcal{P}_{\mathcal{R}}$ the primordial power spectrum and where a subscript '0' means that the quantity is evaluated today. In the second equality we have used Einstein's field equations (IV.4).

Recalling (IV.151) and re-inserting (IV.191) into (IV.189), we arrive at the expression of the lensing power spectrum in terms of the matter power spectrum $P(k)$ evaluated at $k = \ell/\chi$ and at redshift z (corresponding to comoving distance χ)

$$P_{i,j}^{\kappa}(\ell) = \frac{9}{4}\Omega_{\rm m,0}^2 H_0^4 \int \frac{{\rm d}\chi}{a^2} g_i(\chi)\, g_j(\chi)\, P(\ell/\chi, \chi)\, \Sigma^2(\ell/\chi, \chi)\,, \tag{IV.192}$$

This motivates the definition of an *effective power spectrum*:

$$P_{\rm eff}(k) \equiv \Sigma^2 P(k)\,, \tag{IV.193}$$

where the gauge invariant function Σ can be expressed in terms of the perturbed fluid variables as

$$\Sigma(a,k) = 1 + \frac{\Omega_{\rm de}\Delta_{\rm de}}{\Omega_{\rm m}\Delta_{\rm m}} - \frac{\Omega_{\rm de} w_{\rm de}\Pi_{\rm de}^{\rm S}}{\Omega_{\rm m}\Delta_{\rm m}} - \frac{\Omega_{\rm m} w_{\rm m}\Pi_{\rm m}^{\rm S}}{\Omega_{\rm m}\Delta_{\rm m}}. \tag{IV.194}$$

The lensing power spectrum (IV.192) and the shear correlation functions (IV.185), measured in galaxy surveys, are actually a probe of the dark sector over-density and anisotropic stress projected along the line of sight. We can use this fact in order to set constraints on dark sector theories. Before moving to this topic, since the forthcoming surveys LSST and EUCLID will primarily measure galaxy lensing, let us say a few words on the CFHTLenS survey. This will give some insight on what EUCLID and LSST will be about.

IV.6.4 The CFHT Lensing Survey

The Canada-France-Hawaii Telescope Lensing Survey (CFHTLenS) [86, 74], has explored 154 square degree of the sky (about the size of Ursa Minoris) measuring lensing shear and photometric redshift in the five frequency bands (u-g-r-i-z). The collaboration has about thirty members and the telescope (3.6m mirror) is located in Hawaii.

The *median redshift* of the the survey is $z_{\rm m} = 0.70$, from redshift 0.2 to 1.3, with about 11 galaxies per square arc-minute. The redshift of a galaxy, or more exactly of a Spectral Energy Distribution (SED), is obtained with the Bayesian Photometric redshift (BPZ) method [31]. The redshift interval is split into six bins of width $\Delta z \sim 0.2$.

The angular range consists in five bins equally spaced in $\log\theta$ between $1 < \theta < 35$ arc-minute (the full-moon viewed from Earth is about 30 arc-minute). The shape of the SED, the ellipticity that enters (IV.185), is also measured via a bayesian method described in [121].

The shear data coming from the early-type galaxies is contaminated by *intrinsic galaxy alignment* ($\langle\boldsymbol{\epsilon}^{\rm S}\rangle \neq 0$) as described in [87]. The main cause of intrinsic galactic alignment is that the galaxy ellipticity is correlated to the gravitational 'tidal' field in which it forms [88]. For the late-type galaxy (the so-called blue sample of CFHTLenS) the intrinsic alignment signal is consistent with zero, and so we shall use this better quality data set for cosmological parameter extraction.

A *redshift probability distribution* is associated to each of the six redshift bins: there is always a non-zero probability that a galaxy whose best-fit redshift falls in the first redshift bin, actually *is* in

the third bin. The redshift probability distribution, $p(z)$, a by-product of the BPZ analysis, can be converted into the *effective number density of galaxy* for a given redshift bin:

$$n(\chi) = \frac{dz}{d\chi} p(z), \tag{IV.195}$$

where χ is the conformal distance corresponding to redshift z. This is the quantity entering the lensing efficiency (IV.190), and is taken as the normalized effective number of sources per redshift bin. Note that the six redshift bins are defined so that the effective number of galaxies in each bin is equal. For the blue dataset[2], this number is $\sim 6 \times 10^7$ galaxies per steradian per bin. For illustrative purpose, the redshift probability distributions relative to each redshift bin of CFHTLenS is presented in figure 11.

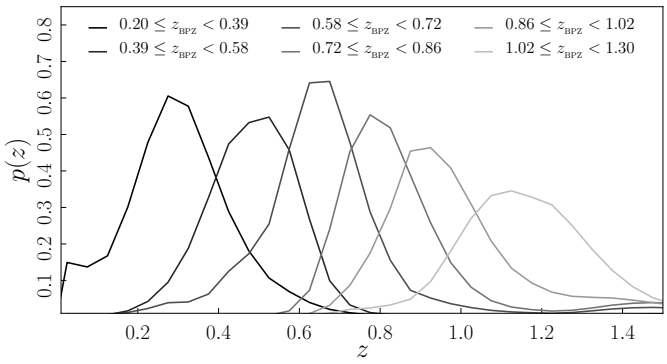

Figure 11: The redshift probability distribution $p(z)$ defined in Eq. (IV.195), for the six redshift bins of the CFHTLenS blue galaxy dataset [87]. The notation $z_{\rm BPZ}$ refers to the redshift as estimated by the Bayesian Photometric Redshift (BPZ) method [31].

The data for the shear correlation functions (IV.185) comes as a vector of 210 data point: 5 angular bins times 21 pairs of redshift bins times 2 functions (ξ_+ and ξ_-), supplemented by a 210×210 covariance matrix. The blue dataset of CFHTLenS and the covariance matrix are available in the current version of `MontePython`.

In figure 12, the best-fit ΛCDM model to the CFHTLenS data is presented in the top panel. It corresponds to $\sigma_8(\Omega_{\rm m}/0.27)^{0.46} = 0.774^{+0.032}_{-0.041}$. We have just reported the shear correlation function ξ_+ relative to the last two redshift bins of the survey (see figure 11). See [87] for a complete overview of the data and cosmological parameter constraints. On this plot, the model does not seem to fit very well the data point, but this is just due to the fact that we are looking at only five data points (over the 210 that are fitted).

Weak lensing is an effect that probes the frontier of the non-linear regime of general relativity. It involves the small scales of the matter power spectrum, the ones that correspond to the large scale structure of the cosmos. It is therefore important to include as much non-linear physics as possible into the theoretical calculations to predict the shear correlation function, which are eventually compared to data (see figure (12)).

Of course, as we rely on a Bayesian analysis for the parameter extraction, we have to find a balance between computation time and faithfulness of our models compared to reality. This balance depends on the accuracy one has to achieve given a certain dataset. In the next subsection we discuss the key aspects of the non-linear modeling of gravitational collapse.

[2] cfhtlens_xipm_6bin_blu

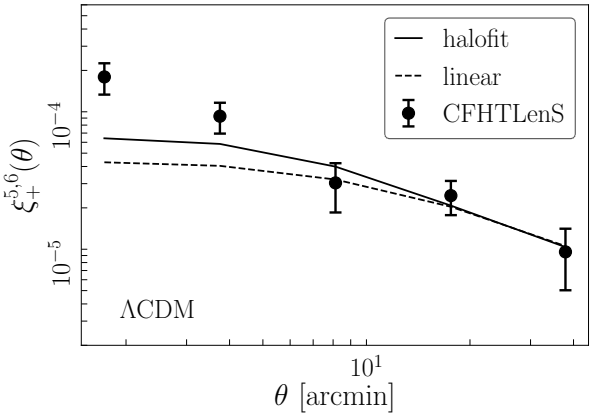

Figure 12: The two point shear correlation function relative to the last two redshift bins ($0.86 \leq z_{\rm BPZ} < 1.02$ and $0.86 \leq z_{\rm BPZ} < 1.02$) of the CFHTLenS survey for the blue galaxy dataset [87], plotted against the best-fit ΛCDM model calculated with `class`. The dashed line corresponds to linear perturbation theory while the solid line accounts for non-linearity treated with the `halofit` module. The cosmological parameters were set so that $\sigma_8(\Omega_{\rm m}/0.27)^{0.46} = 0.774$, the best-fit value quoted by the CFHTLenS team.

IV.6.5 The non-linear power spectrum

Exploring the non-linear regime of the dynamics of cosmological perturbations is a whole research area. A seminal analysis was presented in [142], introducing the so-called *halo model* or `Halofit` based on N-body simulations. It was then refined throughout the years [147].

Gravitational collapse of cosmological perturbations leads to the formation and clustering of galaxies. Observables associated to the mass and redshift distributions of galaxy clusters may be used to probe the primordial power spectrum of fluctuations, provided we have a clear understanding of the linear to non-linear transition of the dynamical system.

As we saw, during matter domination in LCDM cosmology, when the perturbations are small, $\Delta \ll 1$, the temporal and spatial evolution of the over-density field can be trivially separated,

$$\Delta(\mathbf{x}, t) = D(t)\, \Delta(\mathbf{x}, t_0)\,, \tag{IV.196}$$

where $D(t)$ is a time dependent function, the growth function. This is a typical feature of the linear regime and renders the dynamics easy to solve. However, as the perturbation grows, higher order perturbation theory shall be used [33]. One can say that fluctuation enters the non-linear regime as soon as the dispersion of the linear density field, $\sigma^2(R)$ given in (IV.150), becomes comparable to unity. This defines a time dependent non-linear scale and wavenumber, $k_{\rm NL}$.

Beyond the non-linear scale, the halo model suggests to interpret the density field as a the sum of contributions due to isolated dark matter halos. Clustering is a collective phenomenon characterized by a correlation length. Beyond this scale, typically $k_{\rm NL} \approx 0.2\,{\rm Mpc}^{-1}$, fluctuations enter the non-linear regime. The non-linear over-density is defined as

$$\Delta_{\rm NL}(k) \equiv \lim_{k \gtrsim k_{\rm NL}} \Delta(k)\,. \tag{IV.197}$$

In the halo-model, the non-linear power spectrum is decomposed into two parts:

$$\Delta^2_{\rm NL} = \Delta^2_{\rm Q} + \Delta^2_{\rm H}, \tag{IV.198}$$

where $\Delta^2_{\rm Q}$ is the power associated to the localization of the halos (the so-called quasi linear term) and $\Delta^2_{\rm H}$ measures the correlation between halos (the two-halos term). These two terms are parametrized

as follows

$$\Delta^2_{\rm Q} = \Delta^2_{\rm L}\left[\frac{\left\{1+\Delta^2_{\rm L}\right\}^{\beta_n}}{1+\alpha_n\Delta^2_{\rm L}}\right]\exp\left\{-\tfrac{1}{4}\left(\frac{k}{k_{\rm NL}}\right)-\tfrac{1}{8}\left(\frac{k}{k_{\rm NL}}\right)^2\right\}, \tag{IV.199}$$

$$\Delta^2_{\rm H} = \frac{\tilde{\Delta}^2_{\rm H}}{1+\mu_n\left(\frac{k}{k_{\rm NL}}\right)^{-1}+\nu_n\left(\frac{k}{k_{\rm NL}}\right)^{-2}}, \quad \text{with } \tilde{\Delta}^2_{\rm H} = \frac{a_n\left(\frac{k}{k_{\rm NL}}\right)^{f_3}}{1+\sigma_n\left(\frac{k}{k_{\rm NL}}\right)^{f_1}+\delta_n\left(\frac{k}{k_{\rm NL}}\right)^{f_2}}, \tag{IV.200}$$

where all the free parameters are estimated through large N-body simulations [142, 62, 147].

Non-linear corrections are also essential for a precise modeling of the galaxy weak lensing potential and the lensing shear correlation functions. These observables are indeed probing the smallest cosmological scales.

In figure 13 we compare the power spectrum calculated using the `halofit` module of `class` with its linear counterpart. On the left panel, the non-linear power spectrum is plotted as a solid line and the linear power spectrum as a dashed line. For wavenumbers smaller than roughly $k_{\rm NL} = 0.2h{\rm Mpc}^{-1}$ both power spectra agree. Indeed, this corresponds to modes that enter the horizon in the recent universe, near or after matter-radiation equality. The corresponding fluctuations do not have enough time to enter the non-linear regime. However, for smaller scales, the ratio between the non-linear and linear over-density increases quickly, up to a factor of ten for wavenumbers larger than $40\,h{\rm Mpc}^{-1}$ (corresponding to the smallest scales probed by galaxy weak lensing). This can be seen explicitly on the right panel of the same figure, where we plotted the ratio $\Delta_{m,{\rm NL}}/\Delta_{\rm m}$ versus k.

Figure 14 shows the ratio $\Delta_{m,{\rm NL}}/\Delta_{\rm m}$ versus k evaluated at several redshifts. Early in the matter dominated era, at $z = 7$, we see that non-linear corrections are only significant for the smallest scales ($k \sim 40\,h{\rm Mpc}^{-1}$) but their contribution remains at the level of a small fraction of the over-density computed within linear perturbation theory. At later time, bellow $z \approx 5$, we see that the non-linear corrections can not be ignored for all wavenumbers larger than $k_{\rm NL}$, and they naturally keep increasing with time.

Thus, we conclude that non-linear corrections to the matter power spectrum and the correlation functions of LSS must be included in theoretical models used to predict observables associated with galaxy surveys. These non-linear corrections are estimated from N-body simulations, which assume a fiducial cosmological model for the expansion of the universe and the dynamics of cosmological perturbations. In general the fiducial cosmology is LCDM, based on standard GR.

It is still unclear and ambiguous wether modifications to gravity would lead to a substantial change of the non-linear corrections. Some have actually argued that the results of N-body simulations including $f(\mathcal{R})$ gravity are better reproduced by linear perturbation theory than by the `halofit` module, see Dossett et al. [71] and reference therein. This seems to me a crucial point to be addressed in details, because a rigorous comparison between dark sector theories confronted to forthcoming LSS data will rely on non-linear perturbation theory to a great extent. Serious research on this particular topic has only started very recently Winther et al. [160].

The next subsection is dedicated to a brief review of CMB weak lensing, before we finally discuss the effects of dark sector perturbations on lensing observables.

IV.6.6 Weak lensing of the cosmic microwave background

The weak lensing of the CMB photons by clusters of galaxies along the line of sight between decoupling and today is potentially a compelling probe for modified gravity. Indeed, this observable bears the imprints of the physics of the late evolution of the universe, when it becomes dark energy dominated.

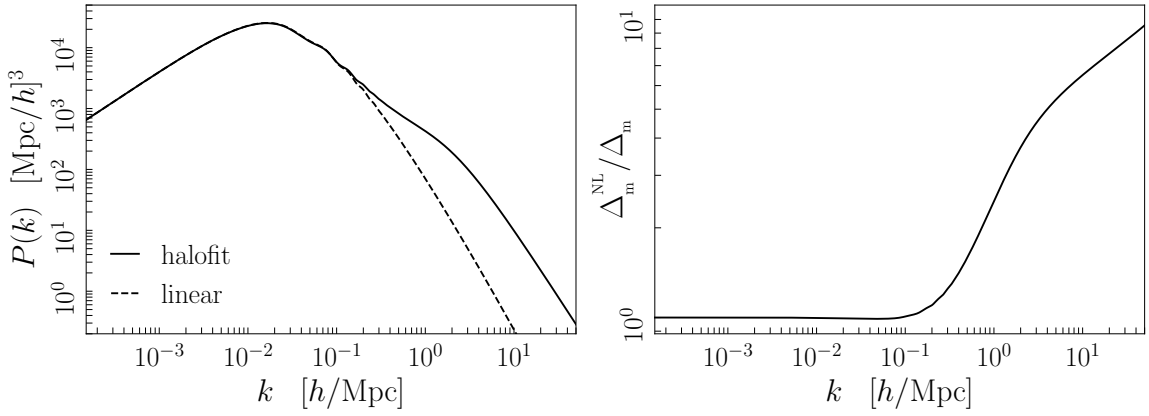

Figure 13: The matter power spectrum resulting from linear perturbation theory compared with the non-linear corrected power spectrum. The non-linear contribution is treated with the `halofit` module of `class`. The left panel shows the matter power spectrum and the right panel shows the ratio between the linear and non-linear power spectra. Cosmological parameters were set to their Planck TT+lowP 2015 best-fit values.

Weak lensing has the effect of a remapping of the CMB photon's temperature anisotropy field,

$$\tilde{T}(\mathbf{x}) = T(\mathbf{x} + \boldsymbol{\alpha}), \tag{IV.201}$$

where $\mathbf{x}$ is a direction in the sky and $\boldsymbol{\alpha}$ is the deflection angle arising from lenses on the line of sight, see Eq. IV.177.

The formalism is the same as in section IV.6.1, but this time the maximal comoving distance for the integration of the lensing potential is the comoving distance of decoupling, $\chi_\star$, and the angular size $\boldsymbol{\theta}$ is the angular separation between two directions in the sky where the temperature anisotropy of the CMB is measured.

The lensing power spectrum can be expanded into harmonic space and translated into an angular power spectrum in harmonic space which can be expressed as [82]

$$C_\ell^{\phi\phi} = 16\pi \int \frac{dk}{k} \mathcal{P}_\mathcal{R}(k) \left[\int_0^{\chi_\star} d\chi \left\{ \frac{Z+Y}{2} \right\} j_\ell(k\chi) \left\{ \frac{\chi_\star - \chi}{\chi_\star \chi} \right\} \right]^2, \tag{IV.202}$$

where $j_\ell(k\chi)$ is a spherical Bessel function and where we used our gauge invariant notations Z and Y defined on page 107.

At first order in $C_\ell^{\phi\phi}$, the lensed angular anisotropy power spectrum is given by

$$C_\ell^{\tilde{T}\tilde{T}} = \left(1 - \ell^2 R^\phi\right) C_\ell^{TT} + \int \frac{d^2\boldsymbol{\ell}'}{(2\pi)^2} \left[\boldsymbol{\ell}' \cdot (\boldsymbol{\ell} - \boldsymbol{\ell}')\right]^2 C_{|\boldsymbol{\ell}-\boldsymbol{\ell}'|}^{\phi\phi} C_{\ell'}^{TT} \tag{IV.203}$$

where C_ℓ^{TT} is the unlensed CMB temperature power spectrum and

$$R^\phi \equiv \frac{1}{2} \left\langle |\boldsymbol{\alpha}|^2 \right\rangle = \frac{1}{4\pi} \int \frac{d\ell}{\ell} \ell^4 C_\ell^{\phi\phi} \tag{IV.204}$$

is half the root mean squared of the deflection angle, typically of order 10^{-7} [108]. At large angular scales, the term proportional to R^ϕ and the second term on the RHS of (IV.203) almost cancel out. However at smaller angular scales, this terms which is actually a convolution of the CMB unlensed

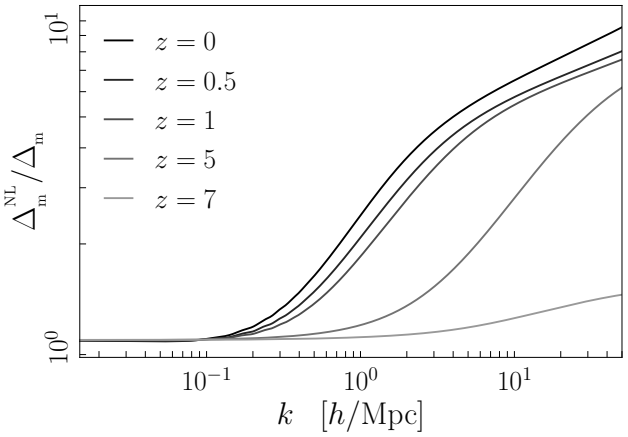

Figure 14: The scale dependence of ratio between the linear ($\Delta_{\rm m}$) and non-linear matter over-density ($\Delta_{\rm m}^{\rm NL}$) at different redshifts. Non-linear evolution is treated with the `halofit` module of `class`. Cosmological parameters were set to their Planck TT+lowP 2015 best-fit values.

power spectrum by $C_\ell^{\phi\phi}$ has the effect of smoothing the acoustic peaks. In the large ℓ limit, since the primordial temperature anisotropy becomes negligible due to diffusion damping, the lensed CMB power spectrum becomes proportional to $C_\ell^{\phi\phi}$.

In figure 15 we compare the lensed and unlensed angular power spectrum of the CMB temperature anisotropy. The left panel shows the dimensionless power spectra. The lensed power spectrum is shown as a solid line and the unlensed power spectrum as a dashed line. This illustrates the smoothing of the acoustic peak and the increase of power at small angular scales. On the right panel we show the relative difference between both power spectra up to $\ell = 3000$.

The lensing power spectrum in Eq. (IV.202) involves the integration of the gravitational potentials along the line of sight. One can use Eq. (IV.191) and express it in terms of the effective power spectrum (IV.193), that is the dark sector anisotropic stress, $\Pi_{\rm de}^{\rm S}$, and dark sector over-density, $\Delta_{\rm de}$.

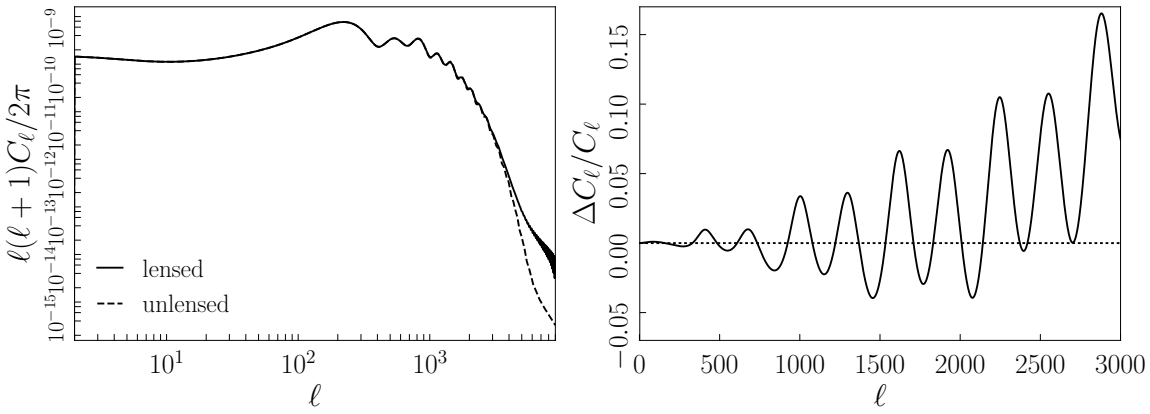

Figure 15: Comparison between the lensed and unlensed angular power spectra of the temperature anisotropy of the cosmic microwave background. These were computed using `class`. Cosmological parameters were set to their Planck TT+lowP 2015 best-fit values. On the left-panel the lensed power spectrum is depicted as a solid line and the unlensed power spectrum is shown as a dashed line. The right-panel presents the relative difference between the lensed and unlensed spectra until multipole $\ell = 3000$.

IV.6.7 The dark sector as a lens

In the previous subsections we have described how the lensing of the CMB anisotropy and the lensing of galaxy shapes by large scale structures can be measured and modeled theoretically. We have seen that lensing observables are sensitive to the Weyl potential (IV.173). With Einstein equations (IV.4), the Weyl potential can be expressed in terms of the PPF parameters $\mu$and η as in (IV.174) or in terms of dark sector perturbed fluid variables (IV.194). Hence, in some sense, lensing observables are a direct probe of dark sector perturbations.

Both the lensing power spectrum of the CMB $C_\ell^{\phi\phi}$ and the shear correlation functions for the ellipticity of galaxies $\xi_\pm(\theta)$ can be written as an integral of the effective power spectrum defined in (IV.193). The effective power spectrum is proportional to the gauge invariant function Σ^2 given in (IV.194).

In most numerical codes, such as the standard version of `class`, the shear correlation functions are computed by integration of the matter power spectrum $P(k)$, instead of the effective power spectrum $P_{\rm eff}(k) = \Sigma^2 P(k)$. This is valid within the LCDM scenario, because in this case $\Sigma^2 = 1$. However, when one deals with modified gravity or dark energy models, the function Σ^2 can be significantly different from one.

On figure 16 we show Σ^2 as a function of the wavenumber calculated with `class_eos`. On the left panel we present the results for several $f(\mathcal{R})$ gravity models, parametrized by B_0, that mimic LCDM at the background level ($w_{\rm de} = -1$). For all models, we see that the departure from $\Sigma^2 = 1$ is larger for small wavenumbers, reaching $\Sigma^2 \sim 30$ for $B_0 = 10$. On small scales, Σ^2 appears to approach unity as k becomes larger. Indeed, for small scales we saw in section IV.4 that the anisotropic stress is well approximated by $w_{\rm de}\Pi^{\rm S}_{\rm de} = \Delta_{\rm de}$ and consequently $\Sigma^2 \approx 1$, see Eq. (IV.194). On the right panel, we present the same quantity in wCDM models with constant equations of state parameters ranging from $w_{\rm de} = -1.4$ to $w_{\rm de} = -0.6$, and unit sound speed. In all cases, Σ^2 remains close to unity. Departure from unity starts to arise only for $k \lesssim 10^{-2} h{\rm Mpc}^{-1}$.

Note that $\Sigma^2 = 1$ does not mean that lensing observables are unaffected by the dark sector. Like

we saw in the previous section, dark sector perturbations have a significant impact on the dynamics of matter perturbations and therefore the matter power spectrum, that enters the calculation of these observables, is generally modified compared its LCDM expectation. The point is that when $\Sigma^2 \neq 1$ there are more modifications due to the dark sector to account for in the calculation of lensing observables.

On figure 17 we present the shear correlation function $\xi_+(\theta)$, relative to the last two redshift bins of CFHTLenS, for different $f(\mathcal{R})$ gravity (left panel) and wCDM (right panel) models. Figure 18 illustrates the lensing power spectrum of the CMB anisotropy in $f(\mathcal{R})$ gravity. The LCDM expectation is shown as a dashed line. The interpretation of these results follows the same lines as our discussion of the matter power spectrum in subsection IV.5.3.

In these calculation, we saw that non-linear corrections have to be included. To do this in `class_eos`, we first compute the matter power spectrum and the dark sector perturbed fluid variables with the linear perturbation equations. Then, we use `halofit` to get $\Delta_{\rm m}^{\rm NL}$, and $\hat{\Theta}_{\rm m}^{\rm NL}$ with the perturbed fluid equation (IV.68). Last, we can compute Σ^2 with Eq. (IV.194) and using the EoS for the anisotropic stress (IV.89) where we carefully replace $\Delta_{\rm m}$ and $\hat{\Theta}_{\rm m}$ by their non-linear corrected values $\Delta_{\rm m}^{\rm NL}$ and $\hat{\Theta}_{\rm m}^{\rm NL}$.

This procedure accounts for non-linearity in the matter sector, but assumes that dark sector perturbation can be treated linearly all the way to $z = 0$. Wether this is a valid assumption is still an open question.

To close this Chapter on dark energy, we focus on wCDM models and present a new constraint on the equation of state parameter for dark energy, $w_{\rm de}$, based on the Sunyaev Zel'dovich effect data obtained by Planck

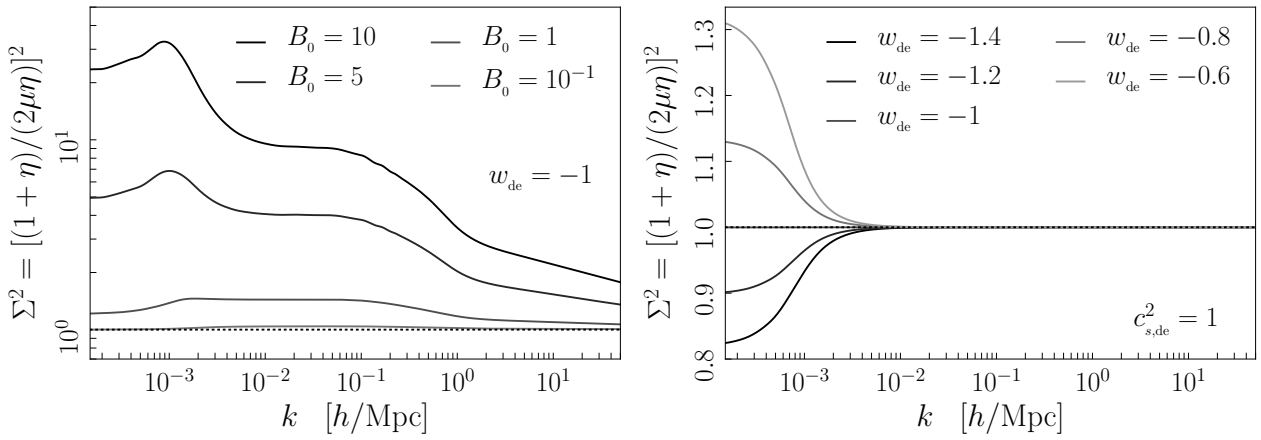

Figure 16: The scale dependence of the gauge invariant function Σ^2 defined in Eq. (IV.174) at redshift $z = 0$ in $f(\mathcal{R})$ gravity for several values of B_0 with $w_{\rm de} = -1$ (left-panel) and in wCDM models, with unit sound speed ($c^2_{s,\rm de} = 1$), for several values of $w_{\rm de}$ (right-panel). Cosmological parameters were set to their Planck TT+lowP 2015 best-fit values. The ΛCDM expectation is $\Sigma^2 = 1$. Computations were performed with `class_eos`.

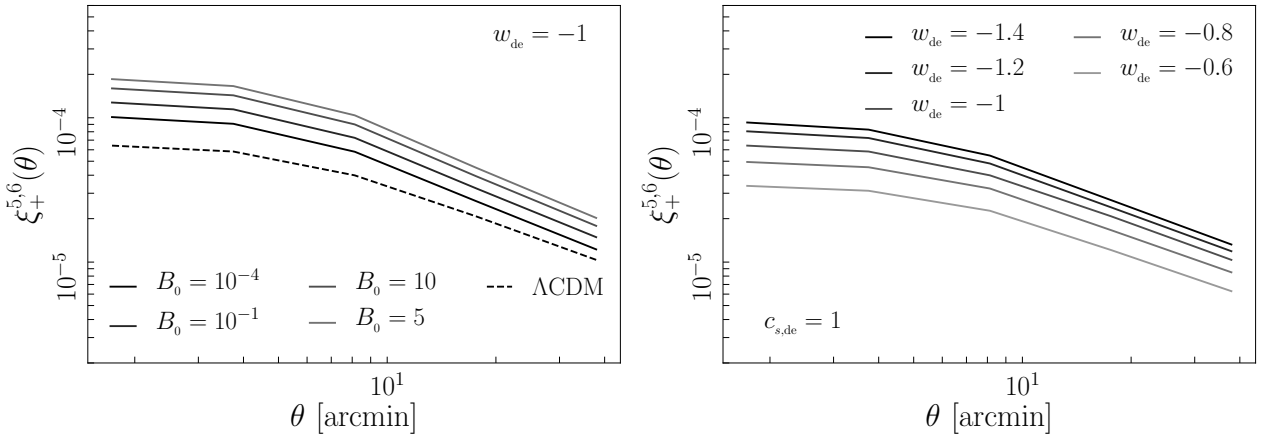

Figure 17: The two point shear correlation function relative to the last two redshift bins ($0.86 \leq z_{\rm BPZ} < 1.02$ and $0.86 \leq z_{\rm BPZ} < 1.02$) of the CFHTLenS survey for the blue galaxy dataset [87], in $f(\mathcal{R})$ gravity and in wCDM models with unit sound speed, computed with `class_eos`. On the left-panel four $f(\mathcal{R})$ functions that mimic ΛCDM ($w_{\rm de} = -1$) were considered, with B_0 ranging from 10^{-4} to 5. The ΛCDM prediction is depicted as a dashed line. On the right-panel we show the results for five w CDM models with $w_{\rm de}$ between -1.4 and -0.6. The cosmological parameters were set so that $\sigma_8(\Omega_{\rm m}/0.27)^{0.46} = 0.774$ in the ΛCDM scenario (the best-fit value quoted by the CFHTLenS team).

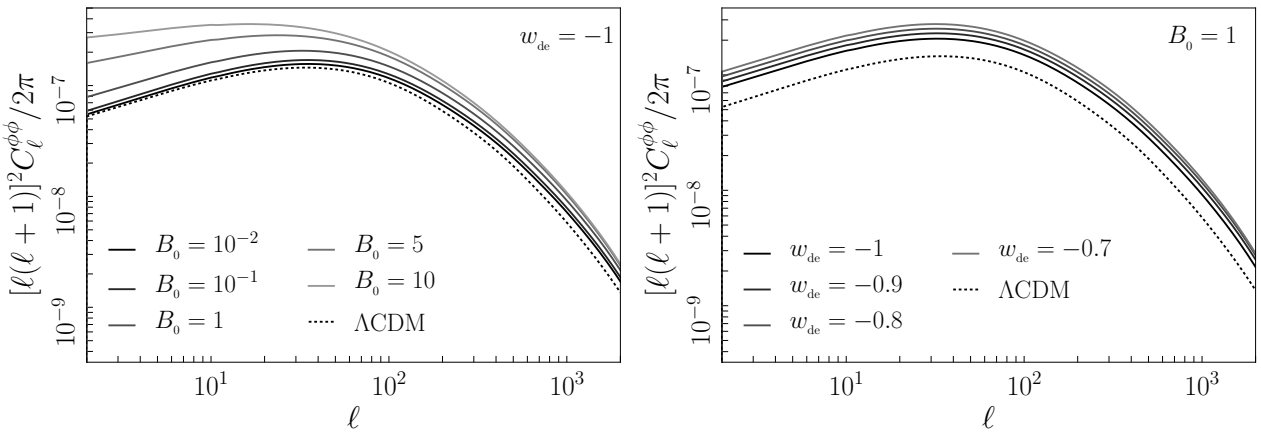

Figure 18: The lensing power spectrum of the cosmic microwave background in $f(\mathcal{R})$ gravity. Cosmological parameters were set to their Planck TT+lowP 2015 best-fit values. The dashed line represents the ΛCDM prediction. On the left-panel we have set $w_{\rm de} = -1$ and considered five values of B_0 between 10^{-2} and 10. On the right-panel we set $B_0 = 1$ and vary $w_{\rm de}$ between -0.7 and -1. These results were obtained with `class_eos`.

IV.7 Observational probes III: the thermal Sunyaev Zel'dovich effect

In this last section, I describe my work related to the use of the Sunyaev Zel'dovich (SZ) effect as a cosmological probe. This research was carried out in collaboration with Barbara Comis, Eiichiro Komatsu and Juan Macias-Perez.

IV.7.1 The Sunyaev Zel'dovich effect

The SZ effect was first described by Sunyaev and Zel'dovich in 1972 [146]. It refers to a small distortion of the cosmic microwave background due to the inverse Compton scattering of the CMB photons off the electrons in the intra-cluster medium (ICM), the hot gas surrounding galaxy clusters. The ICM is assumed to be a diffuse plasma at hydrostatic equilibrium within the dark matter potential wells, *i.e.* the *dark matter halos*, where the galaxy clusters are located. Because of the SZ effect, the CMB spectrum receives a small boost in energy of the order of $k_{\rm B}T_{\rm e}/m_{\rm e}c^2 \approx 1{\rm mK}$, where $k_{\rm B}T_{\rm e} \sim 10{\rm keV}$ is the electron gas temperature and $m_{\rm e}$ is the electron rest-mass.

The SZ effect is frequency dependent: at a frequency larger than the cross-over frequency $\nu \simeq 217{\rm GHz}$, the intensity of the CMB is increased while it is decreased for smaller frequencies.

We can identify two components to the SZ effect. One that is due to the internal motion of the electrons, the so-called thermal SZ effect (tSZ), and the one caused by the bulk motion of the gas when the cluster is moving with respect to the CMB rest-frame, the so-called kinetic SZ effect (kSZ). The contribution from the kSZ effect is al least one order of magnitude smaller than the tSZ effect, when we compare the angular anisotropy power spectra of the CMB temperature anisotropy associated with each component. Therefore we ignore the kSZ effect in this analysis.

If we assume the electrons in the gas to be non-relativistic, the frequency dependence of the tSZ effect is described by the spectral function

$$g_\nu\left(x\right) = x\coth\left(x/2\right) - 4, \quad \text{with} \quad x = \frac{h\nu}{k_{\rm B}T_{\rm CMB}}. \tag{IV.205}$$

Then, the temperature of the CMB photons is shifted by

$$\frac{\Delta T}{T_{\rm CMB}} = g_\nu y, \tag{IV.206}$$

where the Compton-y parameter contains the information relative to the thermal structure of the ICM,

$$y \equiv \int {\rm d}s \frac{n_{\rm e}k_{\rm B}T_{\rm e}}{m_{\rm e}c^2}\sigma_{\rm T} = \int {\rm d}s \frac{P_{\rm e}}{m_{\rm e}c^2}\sigma_{\rm T}, \tag{IV.207}$$

where $\sigma_{\rm T} \simeq 6.65 \times 10^{-25}{\rm cm}^2$ is the Thomson cross-section, $n_{\rm e}$ and $P_{\rm e}$ are the electron number density and pressure, respectively, and ds is the line element along the line of sight. In words, the amplitude of the SZ effect is given by the integrated pressure of the ICM along the line of sight.

IV.7.2 Data from the Planck 2015 full sky survey

The main product of the Planck mission are temperature maps of the CMB at angular resolutions from 33 arcmin to 5 arcmin, with nine frequency bands centered at 30, 44, 70, 100, 143, 217, 353, 545 and 857 GHz. Based on the tSZ spectral signature (IV.205), it is possible to extract two types of information from the Planck maps.

First, one can apply a series of algorithms described in [4] to identify individual clusters. The Planck collaboration reported several hundreds of resolved clusters (RC) up to redshift $z \simeq 1$ and within the mass range $10^{14} - 10^{15}{\rm M}_\odot$. The mass of a candidate cluster is not directly accessible. It is deduced

from a scaling relation between the integrated Compton-y contribution over the solid angle spanned by the cluster,

$$Y \equiv \int y d\Omega \tag{IV.208}$$

and the *over-density mass* M_{500}. Given a an over-density mass, the *scale radius* r_{500} is obtained by inverting the relation

$$M_{500} \equiv \frac{4\pi}{3} \left[500\rho_{\rm c}\left(z\right)\right] r_{500}^3, \tag{IV.209}$$

where

$$\rho_{\rm c}\left(z\right) \equiv \frac{3H^2\left(z\right)}{8\pi G}, \tag{IV.210}$$

is the critical density of the universe at redshift z. So, r_{500} is the radius of the sphere within which the mean mass over-density of the cluster is 500 times the critical density. The scaling-relation used in the Planck analysis is shown in Eq. (7) of [4].

By neglecting all contributions due to non-gravitational processes, assuming spherical collapse for the dark matter halo and hydrostatic equilibrium of the gas within the dark matter gravitational potential, a simple model to relate the physical parameters of clusters can be built (Kaiser 1986). The integrated Compton parameter Y can be related to the cluster total mass M through a simple power law. The $Y - M$ relation can then be tested against data and simulations [63].

However, Not only hydrostatical equilibrium may not be reached, due to non-thermal pressure in the halo [141], there may also be issues related with systematics of the X-ray observations that can affect the mass estimate. To account for these facts, a free parameter, known as the hydrostatic equilibrium bias $B_{\rm HSE}$, is introduced in order to translate M_{500} (and r_{500}) into the 'true' halo mass (and scale-radius). As we shall see, the hydrostatic equilibrium mass bias will play a crucial role in our analysis.

Apart from the cluster catalogue, the wide sky coverage and the multiple frequency bands of the Planck mission allows to compute the all-sky Compton parameter y-map. This is done using the Modified Internal Linear Combination Algorithm (MILCA, [92]) and Needlet Independent Linear Combination (NILC, [136]) methods for components separation. Then, the statistical properties of the Compton y parameter can be analyzed in harmonic space, in a way similar to the CMB temperature maps. We shall consider the tow-points correlator that yields the angular anisotropy power spectra of the y-maps in harmonic space, $C_\ell^{y^2}$. Note that even low mass or not individually resolved clusters also contribute to this observable, although they can not be detected individually. Higher oder correlators have also been considered in recent works [8], but we chose to not discuss them here.

To estimate the angular power spectrum of the y-maps (NILC/MILCA) it is necessary to correct for the beam convolution as well as statistical noise due to mode-coupling induced by masking foreground-contaminated sky regions. For the SZ data, this is done by exploiting the `XSPECT` method [151] that uses cross-power spectra between different y-maps.

IV.7.3 Foreground contributions to the y-map

The final power spectrum obtained with this procedure does not contain exclusively the contribution from the tSZ effect associated with galaxy clusters, $C_\ell^{\rm tSZ}$. It also contains a significant contribution from several foregrounds: the cosmic infrared background (CIB), radio sources (RS) and infrared point sources (IR). Moreover, on small angular scales ($\ell \gtrsim 1400$) the y^2 power spectrum is dominated by correlated noise (CN). The frequency dependence of the power spectra for these foregrounds can be accurately estimated using the Full Focal Plane (FFP6) simulations [134] and physically motivated models [5]. Nevertheless, their normalizations remain undetermined and have to be treated as free parameters.

Therefore, for the measured power spectrum $\hat{C}_\ell^{y^2}$, we assume a four components model:

$$C_\ell^{y^2} = C_\ell^{\rm tSZ} + A_{\rm CIB} C_\ell^{\rm CIB} + A_{\rm IR} C_\ell^{\rm IR} + A_{\rm RS} C_\ell^{\rm RS} + A_{\rm CN} C_\ell^{\rm CN}, \tag{IV.211}$$

where $C_\ell^{\rm CIB}$, $C_\ell^{\rm IR}$, $C_\ell^{\rm RS}$, $C_\ell^{\rm CN}$ are the foreground contaminants, tabulated and reported in table 12. In our notations, a hat refers to the measured signal and no hat refer to the model.

Since correlated noise largely dominates over other foregrounds and the tSZ component at high multipoles, its amplitude can be set by fitting the signal at $\ell = 2742$:

$$A_{\rm CN} = \hat{C}_{2742}^{y^2} / C_{2742}^{\rm CN} = 0.903, \tag{IV.212}$$

as can be computed with the numerical values in the last line of table (12). This leaves three undetermined foreground parameters, namely $A_{\rm CIB}$, $A_{\rm IR}$ and $A_{\rm RS}$.

Nonetheless, a crucial information can be extracted from the catalogue of confirmed clusters detected via the SZ effect: the power spectrum of the combined foregrounds can not be larger than the difference between the measured total power spectrum, $\hat{C}_\ell^{y^2}$, and the power spectrum associated with the projection of the SZ signal from resolved clusters on the y-map, $C_\ell^{\rm RC}$. If we neglect systematic and statistical uncertainties, this means that the foreground amplitudes have to satisfy the following inequality:

$$A_{\rm CIB} C_\ell^{\rm CIB} + A_{\rm IR} C_\ell^{\rm IR} + A_{\rm RS} C_\ell^{\rm RS} + A_{\rm CN} C_\ell^{\rm CN} < \hat{C}_\ell^{y^2} - C_\ell^{\rm RC}. \tag{IV.213}$$

As we shall see, we will make use of this condition in our maximum likelihood analysis for the determination of cosmological parameters based on the Planck 2015 SZ data.

IV.7.4 Maximum likelihood analysis

Our ultimate objective is to use the SZ information contained in the y-maps in order to set constraints on cosmological parameters. To do so, we sample the parameter space via the Monte Carlo Markov Chain (MCMC) method and extract the joint posterior probability distributions for the input parameters.

The tSZ power spectrum $C_\ell^{\rm tSZ}$ is modeled analytically, following Komatsu and Seljak [101]. It is sensitive to the cosmological parameters, in particular: the reduced Hubble constant $h = (H_0/100)$; σ_8 the amplitude of clustering within a sphere of $8h^{-1}$Mpc; the matter density parameter $\Omega_{\rm m} = 1 - \Omega_{\rm de}$ and the equation of state parameter of dark energy $w_{\rm de}$.

The universe is assumed to be spatially flat with an effective number of ultra-relativistic species $N_{\rm eff} = 3.046$. The *input* cosmological parameters that are varied are: the amplitude of the primordial power spectrum of scalar curvature perturbations A_s; the spectral index of the primordial power spectrum n_s; the optical depth at re-ionization $\tau_{\rm reio}$; the angular size of the sound horizon at decoupling θ_s; the reduced density parameter of baryons $\Omega_{\rm b}h^2$; the reduced density parameter of cold dark matter $\Omega_{\rm c}h^2$ and $w_{\rm de}$. Hence, h, σ_8 and $\Omega_{\rm m}$ are obtained as *derived* parameters.

In addition, the amplitude of the tSZ power spectrum strongly depends on the hydrostatic equilibrium bias $B_{\rm HSE}$, via the pressure profile of the ICM. Therefore, $B_{\rm HSE}$ is also treated as an input varying parameter in this analysis. To recap, the parameter space has dimension $n = 11$:

$$\underbrace{A_s, n_s, \tau_{\rm reio}, \theta_s, \Omega_{\rm b}h^2, \Omega_{\rm c}h^2, w_{\rm de}, B_{\rm HSE}}_{C_\ell^{\rm tSZ}\text{: } slow \text{ param.}}, \underbrace{A_{\rm CIB}, A_{\rm IR}, A_{\rm RS}}_{C_\ell^{\rm FG}\text{: } fast \text{ param.}} \tag{IV.214}$$

with 8 *slow* parameters which affect the amplitude of the tSZ power spectrum, and 3 *fast* parameters that set the amplitude of the foregrounds. The sampling is performed with `Montepython` [19] using the Cholesky decomposition method for an optimal treatment of fast and slow parameters [107].

	min.	max.		min.	max.		min.	max.
$10^9 A_s$	1.8	2.7	$\Omega_b h^2$	0.0199	0.0245	$A_{\rm CIB}$	0	10
n_s	0.8	1	$\Omega_c h^2$	0.09	0.15	$A_{\rm IR}$	0	10
$\tau_{\rm reio}$	0.04	0.12	$w_{\rm de}$	-2	-0.5	$A_{\rm RS}$	0	10
$100\theta_s$	1.03	1.05	$B_{\rm HSE}$	1.11	1.67			

Table 1: Uniform priors imposed on the input parameter space for the MCMC analysis.

Weak uniform priors are imposed on the varying parameters to avoid the sampling of unrealistic regions of the parameter space. These priors are reported in table 1. For each parameter, the allowed range of value is wide enough so that changing the upper or lower bound does not affect the posterior probability distributions.

The data for the total y^2 power spectrum is deduced from the y-map of the Planck survey, discussed in the previous subsections. It is the same as the one used for the MCMC analysis carried out by the Planck collaboration, described in [8]. We refer to this analysis as the *Planck 2015 analysis* (PL15). For completeness, the measured power spectrum $\hat{C}_\ell^{y^2}$ data points and error bars $\sigma_\ell^{y^2}$ are reported in table 12 at the end of this section.

At low multipoles, the signal is contaminated by emissions from the galactic dust, while at high multipoles, the signal is dominated by correlated noise. Hence, the likelihood calculation is restricted to the multipole range $10 \leq \ell_{\rm eff} \leq 959.5$. The effective multipoles, $\ell_{\rm eff}$, are at the middle of the bins used in the Planck 2015 analysis. The bin sizes were chosen by minimizing the correlations between adjacent bins at low multipole and by maximizing the signal-to-noise ratio at high multipole [2].

In addition to the uniform priors of table 1, we used a rejection criterion for the amplitudes of the foreground components. Like we saw, there is an upper bound for the combined foregrounds fixed by the power spectrum of the y-map obtained by projecting the confirmed clusters pf the Planck 2015 SZ catalogues, $C_\ell^{\rm RC}$. At each new proposed values for the foreground amplitudes $\{A_{\rm CIB}, A_{\rm IR}, A_{\rm RS}\}$, we ensure that inequality (IV.213) is satisfied for the seven multipole bins between $\ell_{\rm eff} = 257.5$ and $\ell_{\rm eff} = 1247.5$, otherwise the point is rejected. Above $\ell_{\rm eff} = 1247.5$ the power spectrum $C_\ell^{\rm RC}$ is affected by the resolution of the $y-$map and can not be used. Bellow $\ell_{\rm eff} = 257.5$, statistical and systematic uncertainties are important and (IV.213) is no longer applicable. The data $C_\ell^{\rm RC}$ and error bars $\sigma_\ell^{\rm RC}$ for the power spectrum of the projected resolved clusters is reported in table 12, see [2, 8] for details.

At each step of the MCMC sampling, the likelihood is computed according to

$$-\ln\mathcal{L} = \tfrac{1}{2}\chi^2 \quad \text{with} \quad \chi^2 \equiv \sum_{a\leq a'} \left(C^{y^2}_{\ell^a_{\rm eff}} - \hat{C}^{y^2}_{\ell^a_{\rm eff}}\right) \left[M^{-1}\right]_{aa'} \left(C^{y^2}_{\ell^{a'}_{\rm eff}} - \hat{C}^{y^2}_{\ell^{a'}_{\rm eff}}\right), \tag{IV.215}$$

where a, a' are indices for the multipole bins running from $a = 1$ ($\ell_{\rm eff} = 10$) to $a = 18$ ($\ell_{\rm eff} = 959.5$), $C^{y^2}_{\ell^a_{\rm eff}}$ is the model y^2 power spectrum, $\hat{C}^{y^2}_{\ell^a_{\rm eff}}$ are the data points and M is the binned covariance matrix.

Unlike in the Planck 2015 analysis, our covariance matrix accounts for the non-gaussian contributions, *i.e.* auto-correlations and correlations between multipole bins, arising from the tSZ *trispectrum* calculation. Hence, the coefficient of the covariance matrix relative to multipole bins a and a' reads as

$$M_{aa'} = \left(\sigma^{y^2}_{\ell^a_{\rm eff}}\right)^2 \delta_{aa'} + \frac{\ell^a_{\rm eff}\left(\ell^a_{\rm eff}+1\right)\ell^{a'}_{\rm eff}\left(\ell^{a'}_{\rm eff}+1\right)}{4\pi^2}\frac{T_{aa'}}{4\pi f_{\rm sky}}, \tag{IV.216}$$

where $\sigma^{y^2}_{\ell^a_{\rm eff}}$ are the measured error bars (third column of table 12), $f_{\rm sky} = 0.47$ is the Planck sky coverage, and $T_{aa'}$ is the binned trispectrum whose computation is detailed hereafter.

IV.7.5 Analytical model for the thermal Sunyaev Zel'dovich power spectrum and trispectrum

In this subsection we describe our model for the computation of the tSZ power spectrum and trispectrum. The main ingredients are the mass function that gives the number density of dark matter halos (clusters) as a function of their mass and redshift, the pressure profile of the ICM and the linear power spectrum of matter and dark matter fluctuations. We consider only the 1-halo contribution, as the 2-halo term is not significant given the precision of the current data, see *e.g.* [91]. Our derivation follows [101]. For the numerical calculations of the tSZ power spectrum and trispectrum, I have developed a version of `class` augmented with a tSZ module. The code is dubbed `class_sz` and is available on the internet[1] along with the likelihood module written for the MCMC sampling in `MontePython`. The new tSZ module of `class_sz` is based on routines originally written by Eiichiro Komatsu[2].

The angular power spectrum of the Compton parameter is calculated via an integration over mass and redshift of the two dimensional Fourier transform of the Compton y parameter multiplied by the differential number density of dark-matter halos of mass $n(M,z)$. To translate the Fourier transform of the Compton y parameter into harmonic space we use the Limber approximation, $k \equiv \ell/d_{\rm A}$ where $d_{\rm A}(z)$ is the physical angular diameter distance at redshift z. Then, we use Eq. (IV.207) in order to express y_ℓ in terms of the pressure profile of the ICM, $P_{\rm e}(x)$ with $x \equiv r/r_{500}$ where r is the radial distance to the center of the halo and r_{500} is the scale-radius introduced in Eq. (IV.209). Hence, one has

$$y_\ell = 4\pi \int_0^{+\infty} {\rm d}r r^2 y(r) \frac{\sin(kr)}{kr} = \frac{\sigma_{\rm T}}{m_{\rm e}c^2} \frac{4\pi r_{500}}{\ell_{500}^2} \int_0^{+\infty} {\rm d}x x^2 \frac{\sin(\ell x/\ell_{500})}{\ell x/\ell_{500}} P_{\rm e}(x)\,, \tag{IV.217}$$

where $\ell_{500} \equiv d_{\rm A}/r_{500}$. And the tSZ power spectrum is finally given by

$$C_\ell^{\rm tSZ} = \int_{z_{\rm min}}^{z_{\rm max}} {\rm d}z \frac{dV}{dz} \int_{\ln M_{\rm min}}^{\ln M_{\rm max}} d\ln M \frac{dn}{d\ln M} \left|y_\ell(M,z)\right|^2, \tag{IV.218}$$

where V is the comoving volume of the universe per steradian. Its derivative with respect to redshift is expressed as

$$\frac{dV}{dz} = (1+z)^2 d_{\rm A}(z)^2 cH_0/H(z)\,. \tag{IV.219}$$

The integration over redshift is carried out numerically with a simple trapezoidal rule from $z_{\rm min} = 0$ and up to $z_{\rm max} = 6$. (At higher redshift the number density of halos is vanishingly small.) The integration over the mass is performed using a gaussian quadrature method within the mass range determined by

$$M_{\rm min} = 10^{11} h^{-1} {\rm M}_\odot \quad \text{and} \quad M_{\rm max} = 10^{15} h^{-1} {\rm M}_\odot. \tag{IV.220}$$

The integral of the ICM pressure profile is done with Romberg integration method. For the pressure profile, a standard generalized Navarro-Frenk-White (NFW) functional is used:

$$P_{\rm e}(x) = C \times P_0 (c_{500} x)^{-\gamma} \left[1 + (c_{500} x)^\alpha\right]^{(\gamma-\beta)/\alpha}, \tag{IV.221}$$

where C is a dimension-full quantity that depends on the over-density mass M_{500} (via the $Y - M$ scaling relation). It is given by

$$C = 1.65\,(h/0.7)^2 (H/H_0)^{8/3} \left[\frac{M_{500}}{3\times 10^{14}\,(0.7/h)\,{\rm M}_\odot}\right]^{2/3+0.12} {\rm eV\,cm^{-3}}. \tag{IV.222}$$

The reader is referred to Appendix D of [99] for details. The values of $\{\gamma, \alpha, \beta, P_0, c_{500}\}$ are set to their best-fit values for the Planck 2013 analysis of clusters X-ray data [133]. They are reported in table 2.

	P_0	c_{500}	γ	α	β
Arnaud *et al.* 2013	6.41	1.81	0.31	1.33	4.13
Arnaud *et al.* 2010	8.13	1.16	0.33	1.06	5.48

Table 2: Best fit parameters for a generalized Navarro-Frenk-White pressure profile (third line of table 1 of [133] for the 2013 values, and Eq. B2 of [15] for 2010 values).

The differential number density of halos in Eq. (IV.218) is written as

$$\frac{dn\left(M,z\right)}{d\ln M}=-\tfrac{1}{2}f\left(\sigma\right)\frac{\rho_{\rm m}\left(z_{\rm min}\right)}{M}\frac{d\ln\sigma^2}{d\ln M} \tag{IV.223}$$

where σ^2 is the variance of the matter over-density field over a sphere of radius $R\left(M,z\right)\equiv\left[3M/4\pi\rho_{\rm m}\left(z\right)\right]^{1/3}$, *i.e.*

$$\sigma^2\left(M,z\right)\equiv\int_0^\infty\frac{dk}{k}\frac{k^3}{2\pi^2}P\left(k,z\right)W\left(kR\right)^2 \tag{IV.224}$$

where $P\left(k\right)$ is the linear matter power spectrum and W is the top-hat window function, and $f\left(\sigma\right)$ is the so-called *halo mass function* (HMF) whose parametrization can be deduced from N-body simulations.

To simplify the task of accounting for the redshift dependency, the term involving σ^2 can be factorized as

$$\sigma^2\left(M,z\right)=\sigma^2\left(M,z_{\rm min}\right)\times\left[D\left(z_{\rm min}\right)/D\left(z\right)\right]^2 \tag{IV.225}$$

where $D\left(z\right)$ is the linear growth rate for matter perturbations discussed in section IV.5.2 and in section 5.5 of [100]. Then, instead of $\sigma^2\left(M,z\right)$, one can introduce an auxiliary variable, $\nu\left(M,z\right)$, defined via

$$\nu\left(M,z\right)=\delta_{\rm crit}^2/\sigma^2\left(M,z\right)=\left[D\left(z_{\rm min}\right)/D\left(z\right)\right]^2\times\delta_{\rm crit}^2/\sigma^2\left(R_M\right) \tag{IV.226}$$

where

$$\sigma^2\left(R_M\right)\equiv\sigma^2\left(M,z_{\rm min}\right)\quad\text{with}\quad R_M\equiv\left[3M/4\pi\rho_{\rm m}\left(z_{\rm min}\right)\right]^{1/3}, \tag{IV.227}$$

and where we used Eq. (IV.225) for the second equality. In addition, $\delta_{\rm crit}=1.6865$ is the critical over-density for spherical collapse [149]. Since the mass function, now a function of ν, is parametrized in terms of the over-density mass M_{200m}, we apply a chain rule:

$$\begin{aligned}\frac{dn\left(M,z\right)}{d\ln M}&=\frac{d\ln M_{200m}}{d\ln M}\frac{dn\left(M_{200m},z\right)}{d\ln M_{200m}}\\&\approx\frac{d\ln M_{200m}}{d\ln M}\frac{1}{8\pi R_{M_{200m}}^3}\frac{d\ln\sigma^2}{d\ln R_{M_{200m}}}f\left(\nu\right),\quad\text{with}\quad R_{M_{200m}}\equiv\left[3M_{200m}/4\pi\rho_{\rm m}\left(z_{\rm min}\right)\right]^{1/3}\end{aligned} \tag{IV.228}$$

where $\nu:=\nu\left(M_{200m},z\right)$ is obtained from (IV.226) and where we used $\left(d\ln M_{200m}/d\ln M\right)\approx 1$ for the second equality [70].

In fact, to write $dn/d\ln M$ in this manner, an interpolation of $\sigma^2\left(M_{200m},z_{\rm min}\right)=\sigma^2\left(R_{M_{200m}}\right)$ is needed for all masses M_{200m} (so one can deduce ν and subsequently $f\left(\nu\right)$) and a similar interpolation

[1] https://github.com/borisbolliet
[2] http://wwwmpa.mpa-garching.mpg.de/~komatsu/CRL/clusters/szpowerspectrumdks/

for $d\ln\sigma^2/d\ln R_{M_{200m}}$. To obtain the interpolating functions, given the linear matter power spectrum $P(k)$ computed at $z = z_{\rm min}$, we evaluate $\sigma^2(R_{M_{200m}})$ at various radii $R_{M_{200m}}$ between

$$R^{\rm min}_{M_{200m}} = 0.0034h^{-1}{\rm Mpc}\ (M_1 \simeq 1.8\times10^4{\rm M}_\odot)\ \text{ and }\ R^{\rm max}_{M_{200m}} = 54.9h^{-1}{\rm Mpc}\ (M_2 \simeq 7.5\times10^{16}{\rm M}_\odot) \tag{IV.229}$$

At each $R_{M_{200m}}$ within this range, the integral (IV.224) is performed with Romberg's method. Eventually, the interpolation for σ^2 and its derivative with respect to R_{200m} is obtained in terms of Chebyshev polynomials.

The parameterizations for both the differential number density of halos and the NFW pressure profile involve the over-density masses M_{200m} and M_{500}, but not the true halo mass M. To translate M into an over-density, the strategy is to start with the assumption the ICM to be at hydrostatic equilibrium, so that the virial theorem applies and M can be interpreted as the *virial* mass $M_{\rm vir}$. As shown by N-body simulations, virialized dark matter halos have the important property to be well described by a NFW density profile

$$\rho_{\rm NFW}(r) = \frac{\rho_{\rm s}}{(r/r_{\rm s})\,(1+r/r_{\rm s})^2},\quad \text{with}\quad r_{\rm s}\equiv r_{\rm vir}/c_{\rm vir}, \tag{IV.230}$$

where $\rho_{\rm s}$ and $r_{\rm s}$ are the characteristic density and scale of the halo, and where $r_{\rm vir}$ and $c_{\rm vir}$ are the virial radius and concentration parameters. When this is the case, any over-density mass M_δ can be calculated from the virial mass $M_{\rm vir}$, through the non-linear relation

$$M_\delta = M_{\rm vir}\frac{m(r_\delta/r_{\rm s})}{m(c_{\rm vir})},\quad \text{with}\quad m(x)\equiv\ln(1+x) - x/(1+x)\,. \tag{IV.231}$$

Thus, one needs to specify $r_{\rm vir}$ and $c_{\rm vir}$ in order to determine $r_{\rm s}$. Note that

$$r_{200m}\equiv M_{\rm vir}^{1/3}\left\{\frac{4\pi}{3}\left[200\times\rho_{\rm m}(z)\right]\right\}^{-1/3} \tag{IV.232}$$

is defined in terms of matter density and not the critical density, unlike r_{500} given in Eq. (IV.209). For a virial mass $M_{\rm vir}$, the concentration parameter $c_{\rm vir}$ at redshift z is accurately modeled by the fitting formula [72]:

$$c_{\rm vir} = 7.85\,(1+z)^{-0.71}\left(\frac{M_{\rm vir}}{2\times10^{12}h^{-1}{\rm M}_\odot}\right)^{-0.81}. \tag{IV.233}$$

Moreover, the virial radius $r_{\rm vir}$ at redshift z can be obtained from the relation [44]:

$$M_{\rm vir} = \frac{4\pi}{3}\left[\Delta_{\rm c}(z)\,\rho_{\rm c}(z)\right]r_{vir}^3,\quad \text{with}\quad \Delta_{\rm c}(z)\equiv 18\pi^2 - 82\left[\Omega_{\rm m}(z)-1\right] - 39\left[\Omega_{\rm m}(z)-1\right]^2. \tag{IV.234}$$

So, from (IV.234), (IV.233) and $r_{\rm s}\equiv r_{\rm vir}/c_{\rm vir}$, one can get M_δ with Eq. (IV.231). Numerically, Eq. (IV.231) is solved for M_δ with Brent's root finding algorithm. Finally, to account for the fact that the dark matter halo may not be virialized ($M\neq M_{\rm vir}$), the over-density mass is rescaled using the hydrostatic equilibrium bias $B_{\rm HSE}$ discussed in section IV.7.2. Precisely, the over-density mass obtained with the above procedure is rescaled as $M_\delta := M_\delta/B_{\rm HSE}$. Note that this rescaling actually plays no role for the differential number density of halos, since it involves logarithmic derivatives with respect to $\ln M$. However, it is important to take into account for the pressure profile of the ICM. Hence, the only over-density mass that has to be rescaled is M_{500}.

In our analysis we have considered three different parameterizations of the halo mass function $f(\sigma)$. We used the Bocquet *et al.* 2015 (B15) calibration obtained with the `Magneticum` simulations, that captures the impact of baryons [41], as our main model. For comparison with the Planck 2015 analysis, we have run some MCMC chains with the Tinker *et al.* 2008 (T08) parametrization which is based

Bocquet *et al.* 2015 (B15)			
A_0	0.228	A_z	0.285
a_0	2.15	a_z	−0.058
b_0	1.69	b_z	−0.366
c_0	1.30	c_z	−0.045

Tinker *et al.* 2008 (T08)			
A_0	0.186	A_z	−0.14
a_0	1.47	a_z	−0.06
b_0	2.57	b_z	−0.484
c_0	1.19	c_z	0

Tinker *et al.* 2010 (T10)			
α_0	0.368	α_z	0
β_0	0.589	β_z	0.2
γ_0	0.864	γ_z	−0.01
η_0	−0.243	η_z	0.27
φ_0	−0.729	φ_z	−0.08

Table 3: Parameters for the mass function B15 (second line 'Hydro' in table 2 of [41] v3), T08 (first line of table 2 in [150]) and T10 (Eq. 8 and first line of table 4 of [149]).

on `GADGET2` simulations [150]. The third model we have implemented in `class_sz` is the Tinker *et al.* 2010 (T10) calibration, an updated version of T08 [149] that enforces the normalization of the mass function to $\int_0^\infty dM_{200m} dn/d\ln M_{200m} = \rho_c$, the critical density of the universe. The corresponding HMF are expressed as

$$\text{B15 and T08}: \qquad f(\sigma) = A\left[\left(\frac{\sigma}{b}\right)^{-a} + 1\right]\exp\left(-\frac{c}{\sigma^2}\right), \quad \text{with} \quad \sigma = \delta_{\rm crit}/\sqrt{\nu}, \tag{IV.235}$$

$$\text{T10}: \qquad f(\nu) = \alpha\left[1 + \left(\beta^2\nu\right)^{-\varphi}\right]\nu^{\eta}\exp\left(-\gamma\frac{\nu}{2}\right)\sqrt{\nu}. \tag{IV.236}$$

In these expressions, the parameters (all letters except σ and ν) are all redshift dependent. The redshift dependency is parametrized via $p = p_0\,(1+z)^{p_z}$ for a parameter $p = A, a, b,$ etc. The best-fit values to the numerical simulations, for "p_0 and p_z", are reported in table 3.

The trispectrum $T_{\ell\ell'}$ of the Compton y parameter is assumed to be dominated by the tSZ effect contribution. Its computation follows the same procedure as the tSZ power spectrum, with the fourth power of the y parameter in the integrand:

$$T_{\ell\ell'} = \int_{z_{\rm min}}^{z_{\rm max}} {\rm d}z \frac{dV}{dz} \int_{\ln M_{\rm min}}^{\ln M_{\rm max}} d\ln M \frac{dn}{d\ln M} \left|y_\ell(M,z)\right|^2 \left|y_{\ell'}(M,z)\right|^2. \tag{IV.237}$$

For the eighteen multipole bins of our analysis, the *binned* trispectrum that enters the covariance matrix (IV.216) is

$$T_{aa'} = \sum_{\ell\in a}\sum_{\ell'\in a'} \frac{T_{\ell\ell'}}{N_a N_{a'}}, \tag{IV.238}$$

where a and a' denotes two multipole bins containing respectively N_a and $N_{a'}$ multipoles.

Both amplitudes of the power spectrum and trispectrum of the SZ effect are sensitive to the cosmological parameters h, $\Omega_{\rm m}$, σ_8 and to the hydrostatic equilibrium bias $B_{\rm HSE}$. In principle, at each step of the MCMC sampling, when a new set of cosmological parameters is proposed, the trispectrum should be computed simultaneously to the power spectrum in order to deduce the likelihood value (IV.215). Numerically, the calculation of the trispectrum is time consuming: for instance for eighteen multipole bins, there are one hundred and seventy one trispectrum terms to compute. In addition, since the trispectrum is of order four with respect to the Compton parameter, the numerical precision

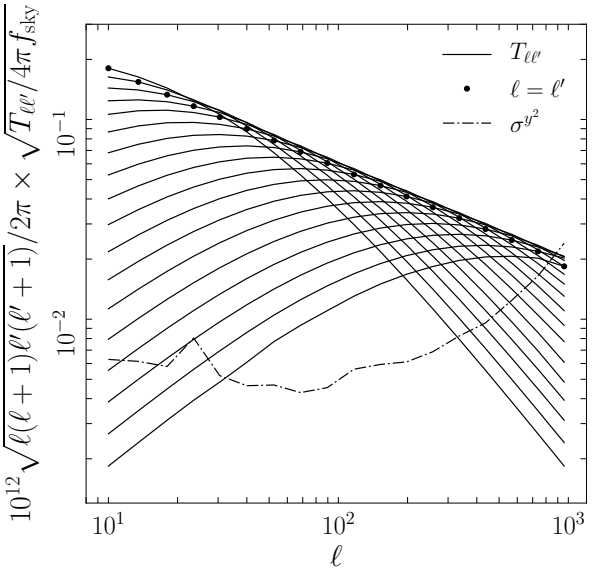

Figure 19: Reference trispectrum used in our MCMC analysis, computed with `class_sz` using Arnaud *et al.* 2013 pressure profile, B15 mass function, with $B_{\rm HSE}$, A_s and $\Omega_{\rm c}h^2$ set to their best-fit values from the analysis without trispectrum (tSZ-Ref. in table 5), and other cosmological parameters set to Planck 2015 TT+lowP mean values, see table 4.

has to be improved significantly[3] to get an accurate evaluation of $T_{\ell\ell'}$. The requirement for a higher numerical accuracy leads to a substantial increment of the computing time too. When it takes about fifteen minutes (on two threads running in parallel) to obtain all the components of the trispectrum in the eighteen multipole bins, it takes only fifteen seconds for the power spectrum computation.

To avoid calculating the trispectrum at each proposed set of varying parameters, we use a unique 'reference' trispectrum for the whole analysis. The 'reference' trispectrum is calculated for the parameters set to their best-fit values of an analysis without trispectrum. In figure 19, the normalized reference trispectrum (solid lines) is shown against the measured error bars (dotted dashed line). At low multipoles, the non-gaussian part of the covariance matrix due to the trispectrum can be more than one order of magnitude larger than the gaussian contribution. The reference trispectrum was computed using the best-fit values for an analysis where A_s and $\Omega_{\rm c}h^2$ were allowed to vary and the other cosmological parameters set to the mean Planck TT+lowP 2015 mean values in the baseline model ($w_{\rm de} = -1$), see table 4, and the hydrostatic equilibrium bias was set to $B_{\rm HSE} = 1.25$. A file that contains the data for the reference trispectrum is also available on the `class_sz` webpage.

Before presenting our results and how they compare with other analysis, we investigate the influence of cosmological parameters and the hydrostatic equilibrium bias on the tSZ power spectrum. This enables us to determine the parameter combination that is best measured from the y-map data.

IV.7.6 Influence of cosmological parameters and hydrostatic bias on the tSZ power spectrum

The effects of the cosmological parameters on the tSZ power spectrum, in addition to the hydrostatic equilibrium bias $B_{\rm HSE}$, is illustrated in figure 20. The optical depth at reionization, $\tau_{\rm reio}$, has a negligible

[3] In particular, we find that the order of extrapolation in the Romberg method for the integration of the ICM pressure profile (**??**) has to be set to $K = 2$ in order to obtain a numerically stable estimate (for the computation of the tSZ power spectrum it can be set to $K = 6$, which renders the code about ten times faster than the original fortran code written by Eiichiro Komatsu with $K = 5$).

	Planck TT+lowP 2015		Planck TT+lowP 2013	
	best-fit	68% C.L.	best-fit	68% C.L.
$\Omega_c h^2$	0.11977	0.1197 ± 0.0022	0.12029	0.12029 ± 0.0031
$\Omega_b h^2$	0.022242	0.02222 ± 0.00023	0.022068	0.02207 ± 0.00033
$100\theta_s$	1.041058	1.04105 ± 0.00046	1.04139	1.04148 ± 0.00066
$\tau_{\rm reio}$	0.0781	0.078 ± 0.019	0.0925	$0.089^{+0.012}_{-0.014}$
$10^9 A_s$	2.199	$2.198^{+0.076}_{-0.085}$	2.215	2.23 ± 0.16
n_s	0.9658	0.9655 ± 0.0062	0.9624	0.9616 ± 0.0094

Table 4: Planck TT+lowP 2015 and 2013 best-fit, mean values and 68% C.L. standard deviations for the six cosmological parameters. These can be found on the Planck Legacy Archive website.

influence on the amplitude of the tSZ power spectrum (less than one percent relative variation for $0.04 \leq \tau_{\rm reio} \leq 0.12$) and therefore it is not shown on the figure. In each panel, we have varied a single parameter, keeping the others fixed.

For the multipole range of interest ($\ell < 10^3$), the equation of state of dark energy $w_{\rm de}$ (top right panel) and the spectral index n_s (bottom left panel) have a minor effect on the amplitude of the tSZ power spectrum, but are related to the shape of $C_\ell^{\rm tSZ}$. However, the hydrostatic equilibrium bias $B_{\rm HSE}$ (top left), the parameter σ_8 (not explicitly shown on the figure but directly related to A_s presented in the bottom-right panel) and the matter density parameter $\Omega_{\rm m}$, via $\Omega_c h^2$ (middle-right panel) are determining for the amplitude of the tSZ power spectrum (and trispectrum). The reduced Hubble parameter h also has an important effect on the amplitude of $C_\ell^{\rm tSZ}$ up to $\ell \approx 10^3$.

We find that the scaling of the tSZ power spectrum is well approximated by

$$C_\ell^{\rm tSZ} \propto \sigma_8^{8.1} \Omega_{\rm m}^{3.2} B_{\rm HSE}^{-3.2} h^{-1.7} \quad \text{for} \quad \ell \lesssim 10^3, \tag{IV.239}$$

in agreement with [2] for the scaling with σ_8 and $\Omega_{\rm m}$, but now accounting for $B_{\rm HSE}$ and h. This means that the parameter combination that is best measured by experiments probing the tSZ power spectrum at multipoles $\ell \lesssim 10^3$ is

$$F \equiv \sigma_8 \, (\Omega_{\rm m}/B_{\rm HSE})^{3/8} \, h^{-1/5}. \tag{IV.240}$$

This is the parameter combination that we will systematically quote in the remainder of this section. Note that for clarity and similar to [8], we opted for a replacement of the decimal numbers in Eq. (IV.239) with the closest integers. The parameter F differs from the parameters quoted in previous works [8, 91], *i.e.* $\sigma_8 \Omega_{\rm m}^{3/8}$. It has the advantage of accounting for the degeneracy between the amplitude of the tSZ power spectrum and the hydrostatic bias and Hubble parameter.

IV.7.7 Revisiting the Planck 2015 tSZ power spectrum analysis

The Planck 2015 analysis (PL15) used T08 mass function, the Arnaud *et al.* 2010 pressure profile (see table 2) allowing σ_8 and $\Omega_{\rm m}$ to vary with other parameters set to their Planck 2013 TT+lowP best-fit values reported in table 4. Two MCMC analysis were carried out by the Planck collaboration. First, with an hydrostatic equilibrium bias set to $B_{\rm HSE} = 1.25$ ($b = 0.2$ in the notations of [8]). Second, with $B_{\rm HSE} = 1.67$ (corresponding to $b = 0.4$). In both cases, the trispectrum was not included, so that the covariance matrix (IV.216) only had a gaussian contribution coming from the measured error bars σ^{y^2}.

We have performed an analysis with the same settings, without trispectrum and $B_{\rm HSE} = 1.25$, however we were unable to reproduce the Planck 2015 constraints for all parameters. The marginalized

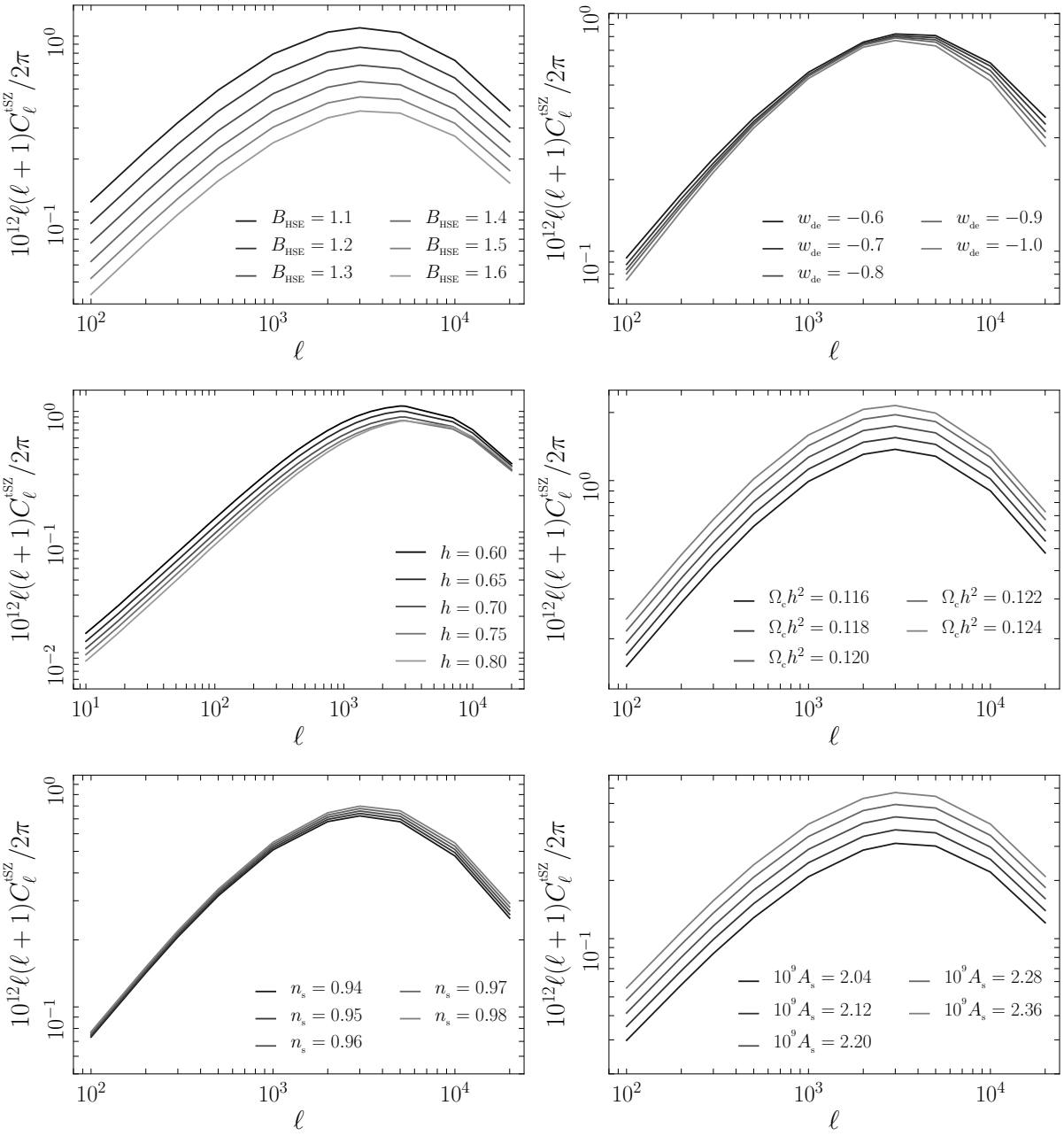

Figure 20: Influence of various parameters on the tSZ power spectrum: hydrostatic equilibrium bias $B_{\rm HSE}$ (top left); equation of state of dark energy (top right); reduced Hubble parameter h (middle left); reduced cold-dark-matter density parameter $\Omega_c h^2$ (middle right); spectral index n_s (bottom left) and amplitude of primordial curvature perturbations A_s (bottom right). The influence of the optical depth at reionization $\tau_{\rm reio}$ is negligible and therefore not shown. When $\Omega_c h^2$ was varied, the Hubble parameter was set to $h = 0.6731$. When h was varied, σ_8 and $\Omega_{\rm m}$ were kept constant. These calculations were carried out with `class_sz` .

posterior probability distributions for the foreground parameters are practically the same, but our analysis disagrees with Planck 2015 by more than two standard deviations for the parameter $\sigma_8\,(\Omega_\mathrm{m}/0.28)^{3/8}$. Our results and reference values for $\sigma_8\,(\Omega_\mathrm{m}/0.28)^{3/8}$ and the parameter combination F defined in Eq. (IV.240) are reported in table 5. In particular, we have re-analyzed the Planck 2015 chains with `MontePython` as well as the CMB chains Planck 2015 TT+lowP to discuss a possible tension that was mentioned in [8] between CMB and tSZ data on the determination of $\sigma_8\Omega_\mathrm{m}^{3/8}$.

To identify the origin of the discrepancy between our determination of F (fourth line of table 5) and that of PL15 (first two lines of table 5), we have run several sets of MCMC chains starting with the PL15 settings and then gradually changed the pressure profile to Arnaud *et al.* 2013, the mass function to B15 and the cosmology to Planck 2015 TT+lowP mean values for the fixed parameters. This led to our reference analysis without trispectrum (last line of table 5) whose posterior probability distribution for F completely overlaps with the one corresponding to the PL15 settings. It shows that the difference between the pressure profiles (Arnaud *et al.* 2013 and 2009), the mass functions (B15 and T08) and the cosmological parameters (2013 best-fit values and 2015 mean values) has a negligible impact on the joint posterior probability distribution. This can be seen explicitly on figure 21, where the yellow contours that correspond to the PL15 settings (fourth line of table 5) are overlapping the red contours that correspond to our 'reference' analysis without trispectrum (fifth line of table 5). The figure also illustrates the robustness of the constraints on the foreground parameters A_CIB, A_IR and A_RS for which there is a good agreement between the Planck chains and our different analysis without trispectrum.

The only difference between the PL15 analysis and our analysis is the conversion between the virial mass and the over-density mass M_{200m} that enters the mass function in the computation of the tSZ power spectrum. We used a method involving the concentration parameter c_vir while the Planck collaboration chose to use a different procedure that relies on the tabulation of M_{200m} versus M_vir, however I am not aware of the details of this procedure and can not comment further on this discrepancy. We trust our computation of the tSZ power spectrum more than PL15 because it agrees perfectly with the results published in recent related peer-reviewed articles [70, 91] and in the seminal work of Komatsu and Seljak [101], nevertheless it is important to clarify this point.

The Planck collaboration mentioned a possible tension between CMB and tSZ constraints for $\sigma_8\,(\Omega_\mathrm{m}/0.28)^{3/8}$ [8, 2]. Indeed, the CMB chains yield $\sigma_8\,(\Omega_\mathrm{m}/0.28)^{3/8} = 0.87 \pm 0.02$ while with a bias set to $B_\mathrm{HSE} = 1.25$ ($b = 0.2$ in the notations of [8]), the preferred value from N-body simulations [150], the PL15 analysis gives $\sigma_8\,(\Omega_\mathrm{m}/0.28)^{3/8} = 0.80 \pm 0.01$. There are at least two facts that indicate that arguing for a tension between tSZ and CMB is not well motivated. First, if we account for the degeneracy with the hydrostatic bias and Hubble parameter, and quote the parameter $F \equiv \sigma_8\,(\Omega_\mathrm{m}/B_\mathrm{HSE})^{3/8}\,h^{-1/5}$ instead of $\sigma_8\,(\Omega_\mathrm{m}/0.28)^{3/8}$ the tension is lessened: PL15 ($b = 0.2$) gives $F = 0.494 \pm 0.006$ and the CMB, assuming $b = 0.2$, yields $F = 0.535 \pm 0.014$. So, the tension is now at the two-sigma level, instead of the four standard deviations discrepancy for $\sigma_8\,(\Omega_\mathrm{m}/0.28)^{3/8}$. Second, the Planck 2015 analysis did not include the trispectrum in the covariance matrix. This has a significant impact on the width of the marginalized posterior probability distributions for the parameter F and the foreground amplitudes. For comparison between the analysis with and without trispectrum, we have reported the contours of the analysis with trispectrum in black on figure 21. In addition to this, as can be seen on the figure, the Planck chains (PL15) have manifestly not converged.

In the next section we discuss the inclusion of the trispectrum in the analysis and its consequences on the constraints of the foreground parameters and the cosmological parameters through F.

IV.7.8 Results for the tSZ analysis with trispectrum

Using the same trispectrum at each step of the MCMC sampling is an assumption that can be questioned. Indeed, the amplitude of the trispectrum scales quadratically with $\sigma_8^{8.1}\Omega_\mathrm{m}^{3.2}B_\mathrm{HSE}^{-3.2}h^{-1.7}$. If

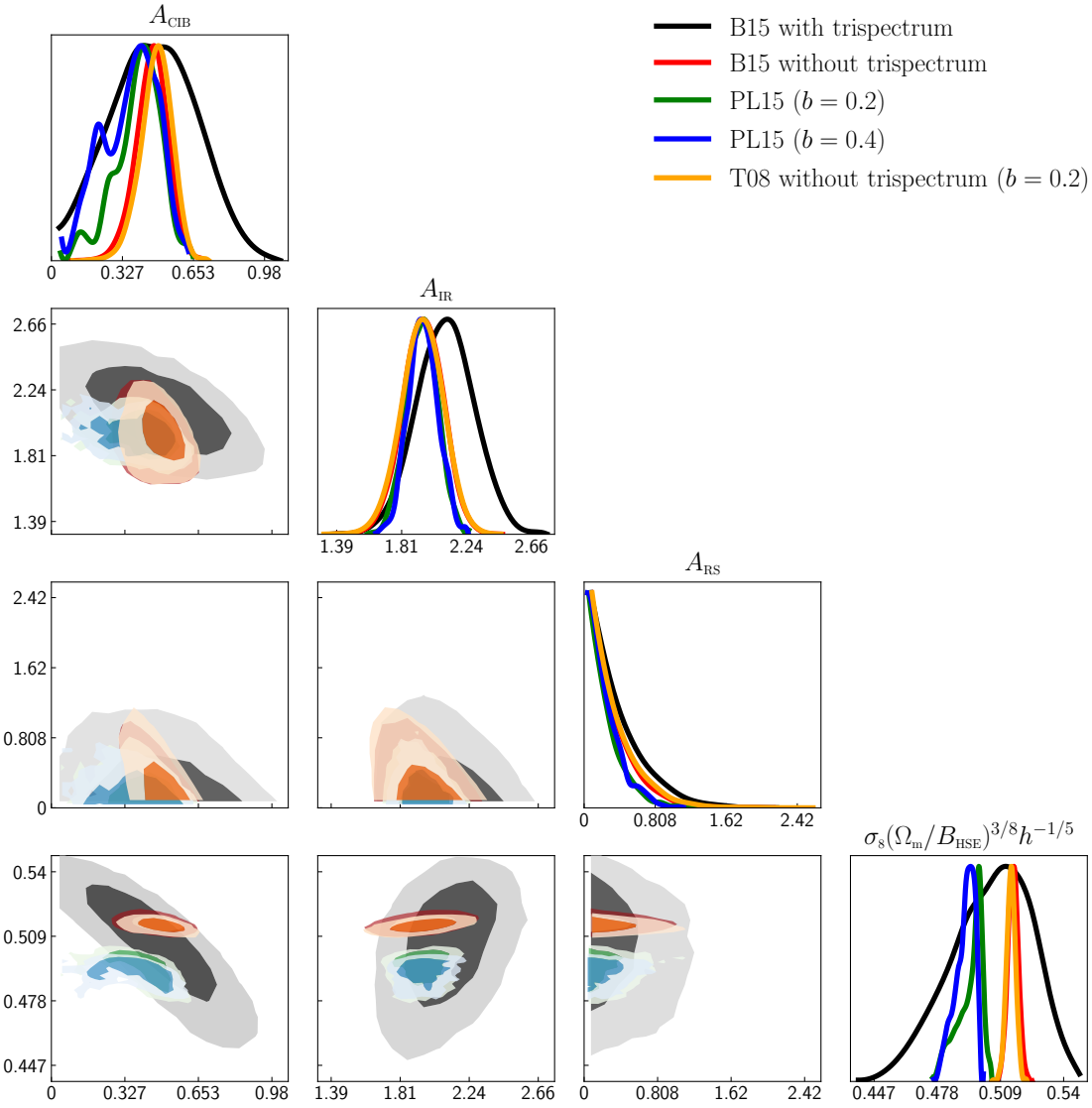

Figure 21: Projected (1D and 2D) joint posterior probability distribution from several MCMC analysis, fitting the Planck y^2 power spectrum obtained from the all-sky y-map: our analysis with B15 mass function with trispectrum (black contours) and without trispectrum "tSZ-Ref." (red contours); our analysis with T08 mass function and the same settings as the Planck 2015 analysis (PL15) with the hydrostatic bias set to $B_{\rm HSE} = 1.25$ ($b = 0.2$). The Planck 2015 chains with $B_{\rm HSE} = 1.67$ ($b = 0.4$) and $B_{\rm HSE} = 1.25$ ($b = 0.2$) re-analyzed with `MontePython` correspond to the blue and green contours respectively. See table 5 for details and numerics.

	F	$\sigma_8\,(\Omega_{\rm m}/0.28)^{3/8}$
PL15 ($B_{\rm HSE}=1.25$)	0.494 ± 0.006	0.80 ± 0.01
PL15 ($B_{\rm HSE}=1.67$)	0.491 ± 0.005	0.89 ± 0.01
CMB TT+lowP	0.513 ± 0.014	0.87 ± 0.02
PL15 settings (T08, $B_{\rm HSE}=1.25$) ..	0.514 ± 0.002	0.836 ± 0.005
tSZ-Ref. no $T_{\ell\ell'}$ (B15, varying $B_{\rm HSE}$)	0.515 ± 0.003	0.86 ± 0.04

Table 5: Constraints (68% CL) on the parameter combinations $\sigma_8\,(\Omega_{\rm m}/0.28)^{3/8}$ and $F\equiv\sigma_8\,(\Omega_{\rm m}/B_{\rm HSE})^{3/8}\,h^{-1/5}$. The first two lines are the Planck tSZ 2015 chains of [8]. The third line corresponds to the Planck CMB 2015 chains TT+lowP [7]. (In order to bring the CMB TT+lowP posterior to the central value $F=0.513$ the hydrostatic equilibrium bias was set to $B_{\rm HSE}=1.40$.) The fourth line is an analysis with $B_{\rm HSE}=1.25$ and PL15 setting: Arnaud *et al.* 2010 pressure profile, T08 mass function, with $A_{\rm CIB}$, $A_{\rm IR}$, $A_{\rm RS}$, $B_{\rm HSE}$, A_s and $\Omega_{\rm c}h^2$ varying, other cosmological parameters set to Planck 2013 TT+lowP best-fit values. The fifth line is our reference analysis without trispectrum: Arnaud *et al.* 2013 pressure profile, B15 mass function, with $A_{\rm CIB}$, $A_{\rm IR}$, $A_{\rm RS}$, $B_{\rm HSE}$, A_s and $\Omega_{\rm c}h^2$ varying, other cosmological parameters set to Planck 2015 TT+lowP mean values.

the trispectrum was calculated at each step, its amplitude would become small for parameters yielding a small power spectrum. Then, the degeneracy with the foreground parameters would decrease. Conversely, for parameters yielding a large power spectrum, the amplitude of the trispectrum would increase, leading to a greater degeneracy with the foreground amplitudes.

To address this issue into some extent, we performed additional analysis with two different trispectra. Recall that the analysis with the reference trispectrum, calculated with parameters set to the values given in the first column of table 6 (with B15 mass function, Arnaud et al 2013 pressure profile, Planck 2015 TT+lowP cosmology) yields $F=0.504^{+0.024}_{-0.017}$ at 68% confidence level. We considered a 'low' trispectrum that corresponds to a model with $F=0.487$ (lower 68% C.L. value) and a 'high' trispectrum for which $F=0.528$ (upper 68% C.L. value).

Note that the 'low' trispectrum, $T^{\rm low}_{\ell\ell'}$, can be obtained by setting the hydrostatic equilibrium bias to $B_{\rm HSE}=1.5937$ (and for the 'high' trispectrum $T^{\rm high}_{\ell\ell'}$ the bias has to be set to $B_{\rm HSE}=1.3090$) while other parameters are set to the best-fit values of the analysis with the reference trispectrum (second column of table 6).

The contours for the analysis with $T^{\rm low}_{\ell\ell'}$, $T^{\rm high}_{\ell\ell'}$ and $T^{\rm ref}_{\ell\ell'}$ are presented in figure 22. The marginalized posterior probability distributions for $A_{\rm IR}$ and $A_{\rm RS}$ are the same for the three analysis. However, the CIB amplitude and F are affected by a change in the amplitude of the trispectrum. The 'low' trispectrum (green contours) leads to a mean value for F which is larger than the one obtained with the reference trispectrum (red contours) by roughly two percent. This difference is of the same magnitude for the 'high' trispectrum (black contours). At the extreme, the relative difference is 2.5% when we compare the means of the posterior probability distributions for F between the 'high' and the 'low' trispectrum. Since the width of the 68% C.L interval on F for the reference trispectrum represents about 7% of the mean value, we conclude that accounting for the variation of the trispectrum at each step of the MCMC sampling can not change the constraints on F and $A_{\rm CIB}$ by more than a few percents.

Moreover, the 'low' trispectrum, corresponding to a low power spectrum, leads to a higher value of F compared to the analysis with $T^{\rm ref}_{\ell\ell'}$. If the trispectrum would then be updated, its amplitude would increase and lead towards smaller values of F. The same reasoning holds for the 'high' trispectrum:

	tSZ-Ref. no $T_{\ell\ell'}$		tSZ-Ref. with $T_{\ell\ell'}$	
	best fit	68% C.L.	best fit	68% C.L.
$\Omega_c h^2$	0.11018	/	0.12812	/
$10^9 A_{\rm s}$	2.54050	/	1.82977	/
$B_{\rm HSE}$	1.24928	/	1.40915	/
$A_{\rm CIB}$	0.48346	0.461 ± 0.007	0.52462	0.47 ± 0.21
$A_{\rm IR}$	1.97698	1.95 ± 0.14	2.11226	2.1 ± 0.2
$A_{\rm RS}$	0.02102	$0.28^{+0.06}_{-0.28}$	0.01835	$0.35^{+0.07}_{-0.35}$
χ^2	28.62	/	18.92	/
F	0.513	0.515 ± 0.003	0.515	$0.504^{+0.024}_{-0.017}$

Table 6: Best-fit and 68% CL interval for the varying parameters of the analysis without trispectrum (left) and with trispectrum (right), and constraint on the derived parameter $F \equiv \sigma_8 \, (\Omega_{\rm m}/B_{\rm HSE})^{3/8} \, h^{-1/5}$. These analysis have B15 mass function, Arnaud et al 2013 pressure profile and fixed cosmological parameters set to Planck 2015 TT+lowP mean values.

$T^{\rm high}_{\ell\ell'}$ leads to a small F, which would decrease the trispectrum amplitude, if it was updated, leading to higher values of F. Hence, both qualitatively and quantitatively, it seems perfectly acceptable to use a fixed 'reference' trispectrum for the entire sampling.

The most realistic trispectrum can in principle be obtained iteratively: starting with an analysis using an over-estimated trispectrum, one gets a small value of F, dubbed F_n. Then, a new trispectrum corresponding to F_n can be computed, and a second analysis using this new trispectrum can be performed, yielding a larger value of F, dubbed F_{n+1}. Based on what we discussed in the previous paragraphs, it is easy to see that the sequence $\{F_n\}$, obtained with this procedure, is convergent. Then, the 'best' trispectrum is the one that corresponds to $\lim_{n\to\infty} F_n$. The fact that the analysis we carried out with $T^{\rm ref}_{\ell\ell'}$ led to a best-fit value of F very close to the one used to compute $T^{\rm ref}_{\ell\ell'}$, ($F = 0.515$ and $F = 0.513$, see table 6) is an indication that our reference trispectrum is well chosen.

The large non-gaussian contribution to the covariance matrix due to the trispectrum, omitted in the Planck 2015 analysis [8], was first pointed out by Horowitz and Seljak in [91]. They used the data points for the tSZ power spectrum, $C^{\rm tSZ}_\ell$, that were calculated in the Planck analysis by correcting for the foreground contribution estimated from the PL15 analysis (without trispectrum), see figure 17 of [8]. The goal of their project was mainly to study the consequences of AGN and supernovae feedbacks on the amplitude of the tSZ effect. These feedbacks are associated with the possible gas emission from AGN and supernovae, in light halos, reaching beyond the virial radius. Numerical simulations have shown that taking these physical processes into account leads to a decrease of the high multipole tSZ contribution from halos below a certain critical mass, $M_{\rm crit}$. They performed a MCMC analysis of the parameter space (σ_8, $M_{\rm crit}$) and eventually marginalized over $M_{\rm crit}$ to obtain $\sigma_8 = 0.831^{+0.024}_{-0.013} \, (\Omega_{\rm m}/0.31)^{0.4}$. Unlike us, they did not take into account the degeneracy between the tSZ power spectrum and foregrounds in their work. Neither did they consider the influence of the hydrostatic equilibrium bias on the estimated amplitude of the tSZ power spectrum. Our analysis tSZ-Ref. with trispectrum yields

$$\sigma_8 = 0.820^{+0.040}_{-0.030} \, (\Omega_{\rm m}/0.31)^{0.4} \, (B_{\rm HSE}/1.40)^{-0.4} \, (h/0.6774)^{-1/5} \, , \qquad \text{(IV.241)}$$

where the numerics in the denominators are motivated by the cosmological setting of the analysis

of Horowitz and Seljak, *i.e.* $\Omega_{\rm m} = 0.31$ and $h = 0.6774$. We obtain significantly larger error bars, which we attribute to the degeneracy between the tSZ and CIB amplitudes. The Planck 2015+BAO +JLA+H_0 joint constraint on the amplitude of clustering is $\sigma_8 = 0.8159 \pm 0.0086$, while ACT gives $\sigma_8 = 0.796 \pm 0.18$. Our results are consistent with the aforementioned constraints on σ_8 within 68%CL and can be accommodated to match exactly any of those constraints by a tuning of the hydrostatic bias. We also note that our different determination of the CIB amplitude would have a substantial impact on Horowitz and Seljak constraint (although difficult to quantify without re-performing their analysis).

The foreground amplitudes as determined by our analysis tSZ-Ref. with trispectrum are

$$A_{\rm CIB} = 0.47 \pm 0.21, \quad A_{\rm IR} = 2.1 \pm 0.2, \quad A_{\rm RS} = 0.35^{+0.07}_{-0.35}, \tag{IV.242}$$

(also reported in table 6) while the values quoted by the Planck collaboration are $A_{\rm CIB} = 0.29^{+0.34}_{-0.20}$, $A_{\rm IR} = 1.97^{+0.20}_{-0.30}$, $A_{\rm RS} = 0.01^{+0.70}_{-0.01}$ [8]. The estimated infrared (IR) and radio (RS) point sources contribution agree well, however, we find a significantly larger CIB contribution than the Planck 2015 analysis. Again, this is due to the enhanced degeneracy between the CIB and tSZ amplitudes caused by the trispectrum.

Figure 23 shows the impact of the foreground contributions and the tSZ amplitude (via the parameter F) on the total y^2 power spectrum, against the Planck 2015 data points derived from the y-map. The RS and IR amplitudes are well constrained thanks to the multipole dependency of the corresponding signals: a large RS contribution would generate a 'bump' in the y^2 power spectrum around $\ell = 100$ and a large RS contribution would lead to a faster growth of the y^2 power spectrum on small angular scales. Nevertheless, the CIB signal has a shape that is hardly distinguishable from the tSZ contribution. This is why F and $A_{\rm CIB}$ are strongly degenerated, see the contours in *e.g.* figure 22. Hence, the rejection criterion based on the lower bound for the tSZ contribution deduced from the projection of the SZ cluster catalogue on the y-map, see Eq. (IV.213), is crucial in the analysis with trispectrum as it cuts the large values of $A_{\rm CIB}$ and allows for a realistic estimation of the parameter.

Our main result is

$$F = 0.504^{+0.024}_{-0.017} \ \ (\text{mean} \pm 68\%\text{CL}) \ \ \text{and} \ \ F = 0.515 \ \ (\text{best} - \text{fit}), \tag{IV.243}$$

as reported in table 6. The CMB TT+lowP 2015 joint posterior distribution on σ_8 and $\Omega_{\rm m}$ can be matched to our best-fit value of F, provided one sets the hydrostatic bias to $B_{\rm HSE} = 1.40$, then the CMB gives $F = 0.513 \pm 0.014$. Remarkably, the Weighting the Giants determination of the hydrostatic bias is centered around this value[4]: $B_{\rm HSE} = 1.43 \pm 0.13$. Moreover, the best-fit value of the hydrostatic equilibrium bias from our analysis tSZ Ref. with trispectrum is $B_{\rm HSE} = 1.41$. These may not be mere coincidences, but valuable clues in support of an hydrostatic $B_{\rm HSE} \approx 1.40$ (or $b \approx 0.3$).

The best-fit parameters for the analysis tSZ Ref. with trispectrum are shown in table 6. The corresponding $C_\ell^{y^2}$ is shown on figure 24 against Planck y^2 data and ACT/SPT tSZ measurements at $\ell = 3000$. The foreground dominate over the tSZ contribution after $\ell = 300$, as can be seen on the left panel. The right panel shows the best-fit and 68%CL region for the tSZ power spectrum against ACT/SPT data points. The ACT/SPT information is not included in our likelihood, therefore it is interesting to notice that our best-fit Planck tSZ model falls exactly on top of the data points. (The magnitude of the error bars are also in a fairly good agreement.) However, one must be aware that the analytical model for the tSZ power spectrum at high multipoles is not well trusted because of uncertainties in the pressure profiles at the core of halos. Recent numerical y-map simulations continue to find a substantially larger tSZ power spectrum at $\ell \gtrsim 10^3$ than the analytical models such as the one used in our analysis [70].

[4] $(1 - b) = 0.698 \pm 0.062$ in the notation of [154].

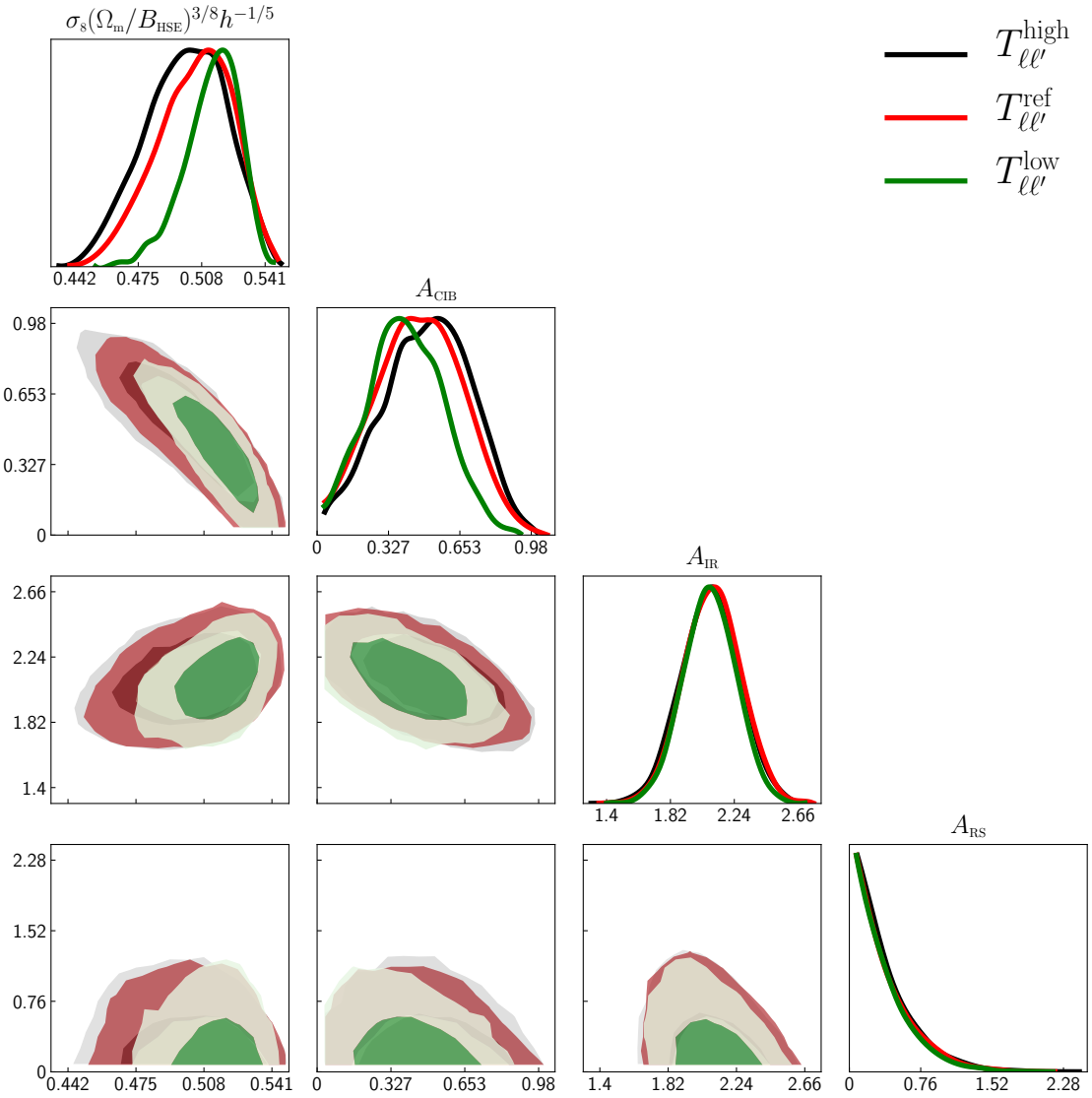

Figure 22: Projected (1D and 2D) joint posterior probability distribution from three analysis with same settings, but different trispectrum amplitudes. The red contours correspond to the analysis "tSZ-Ref" with trispectrum, yielding $F = 0.515$ (best-fit value, see table 6). The black contours were obtained with an over-estimated trispectrum, $T^{high}_{\ell\ell'}$, and the green contours with an under-estimated trispectrum, $T^{low}_{\ell\ell'}$ (see text in subsection IV.7.8 for details).

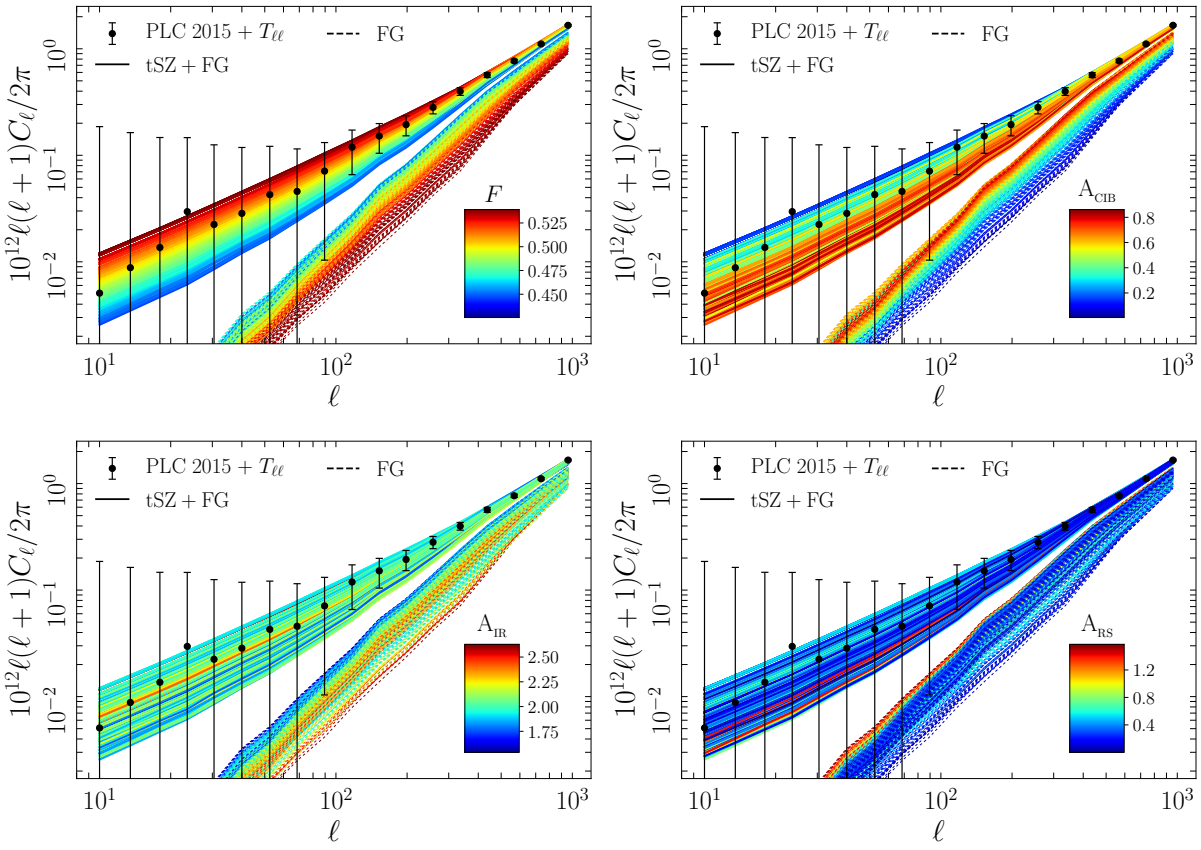

Figure 23: Distribution of models for $C_\ell^{y^2}$ (solid lines) and foreground estimate (dashed line) with respect to the parameters $F \equiv \sigma_8 \left(\Omega_m/B_{HSE}\right)^{3/8} h^{-1/5}$ (top left) and the foreground amplitudes A_{CIB} (top right), A_{IR} (bottom left) and A_{RS} (bottom right) against Planck 2015 SZ data with the non-gaussian contributions (trispectrum) added to the measured error bars. For this figure we only considered the models corresponding to last 500 steps of the MCMC analysis "tSZ-Ref." with trispectrum (see table 6).

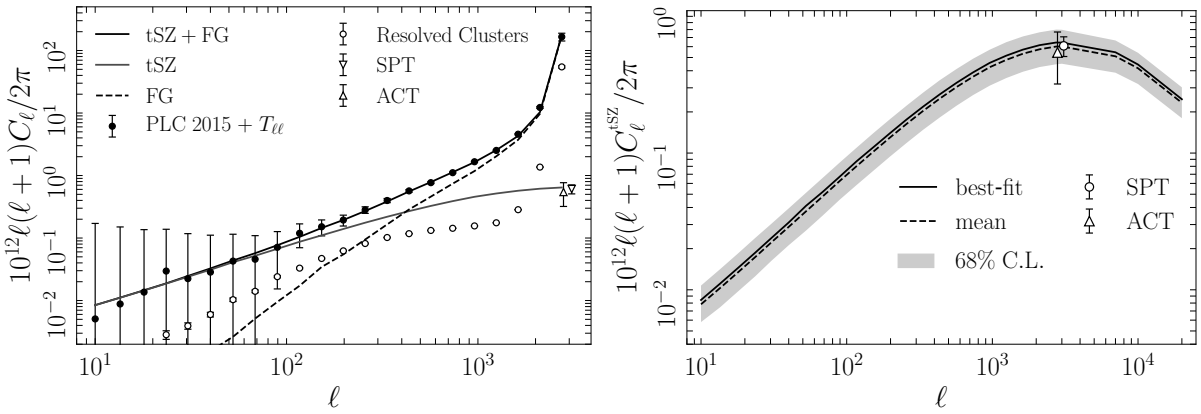

Figure 24: Best-fit models for the y^2 power spectrum, $C_\ell^{y^2}$ (solid black line on the left panel), the combined foregrounds (dashed line on the left panel) and the tSZ power spectrum, $C_\ell^{\rm tSZ}$ (grey line on the left panel and black line on the right panel), plotted against Planck 2015 y^2 power spectrum (including the trispectrum contribution to the error bars) and ACT/SPT tSZ data points at $\ell = 3000$. The y^2 power spectrum obtained by projection of the Planck SZ cluster catalogue on the y-map is show with empty circles. It can not be trusted above $\ell \approx 10^3$ due to the resolution of the Planck y-maps and beam properties. On the right panel the dashed line is for the $C_\ell^{\rm tSZ}$ model computed using the mean values of the "tSZ-Ref" analysis with trispectrum (see table 6). The gray region shows the 68% CL allowed region.

IV.7.9 Constraints on the equation of state of dark energy

To end this thesis, I present a new way of constraining the equation of state for dark energy, independent from other known measurements, based on the SZ cosmological data (all sky y-map) and an independent determination of the Hubble parameter.

The `class_sz` code allows for an easy exploration of the cosmological parameter space in the light of the SZ data. We carried out an analysis were the six base cosmological parameters, the equation of state for dark energy $w_{\rm de}$, the hydrostatic equilibrium bias, and the three foreground amplitudes were sampled from the uniform priors reported in table 1. The contours are shown in black on figure 25. Although $w_{\rm de}$ seems to be de-correlated from the parameter combination $F \equiv \sigma_8 \left(\Omega_{\rm m}/B_{\rm HSE}\right)^{3/8} h^{-1/5}$ (the joint posterior in the $F - w_{\rm de}$ plane is a straight open region), there is an important degeneracy between $w_{\rm de}$ and the other cosmological parameters σ_8, $\Omega_{\rm m}$ and $h = H_0/100$. To break these degeneracies and extract a constraint on $w_{\rm de}$, we allowed ourselves to use three independent priors on $10^9 A_s e^{-2\tau_{\rm reio}}$, $\tau_{\rm reio}$ and h reported in table 7.

The prior on $10^9 A_s e^{-2\tau_{\rm reio}}$ is motivated by the latest Planck CMB data, which constrains well and unambiguously the amplitude of primordial curvature perturbations combined with the optical depth. First, we have checked that $k = 0.05{\rm Mpc}^{-1}$ is indeed the pivot scale for Planck data, in the sense that the chains with running spectral index lead to the smallest error bars on n_s at this value of the wavenumber. Then, we have analyzed the Planck chains for four different settings: (i) flat ΛCDM universe, (ii) curved ΛCDM, (iii) flat wCDM universe and (iv) flat ΛCDM with massive neutrinos. From those chains, we read out the constraints on $10^9 A_s e^{-2\tau_{\rm reio}}$ and deduce a model independent normalization prior: $10^9 A_s e^{-2\tau_{\rm reio}} = 1.878 \pm 0.014$. To further reduce the degeneracy, we also set a gaussian prior on the optical depth at reionization $\tau_{\rm reio} = 0.06 \pm 0.01$ that is a good compromise between the different measurements of last decade [7, 99]. The last prior we imposed is a gaussian prior for the Hubble parameter deduced from up to date time-delay cosmography measurements of quasars:

	Gaussian priors
h	0.72 ± 0.03
$10^9 A_s e^{-2\tau_{\rm reio}}$	1.878 ± 0.014
$\tau_{\rm reio}$	0.06 ± 0.01

Table 7: Gaussian priors imposed on the parameters h, $10^9 A_s e^{-2\tau_{\rm reio}}$ and $\tau_{\rm reio}$ (in order to break the degeneracy between $w_{\rm de}$ and other cosmological parameters in the tSZ wCDM analysis). The prior on h is from [32] (quasars time delay), the prior on $A_s e^{-2\tau_{\rm reio}}$ was obtained from the Planck chains (see table 8) and the prior on the optical depth is a compromise between the different measurements over the last decade.

	$10^9 A_s e^{-2\tau_{\rm reio}}$
$\Omega_{\rm k} = 0$ and $w = -1$	1.880 ± 0.014
$\Omega_{\rm k} \neq 0$ and $w = -1$	1.872 ± 0.014
$\Omega_{\rm k} = 0$ and $w \neq -1$	1.880 ± 0.014
$\Omega_{\rm k} = 0$ and $w = -1$ and $m_\nu > 0$	1.881 ± 0.014
Normalization prior	1.878 ± 0.014

Table 8: The constraints on $10^9 A_s e^{-2\tau_{\rm reio}}$, with pivot scale $k = 0.05{\rm Mpc}^{-1}$, are read out of four sets of Planck 2015 chains (corresponding to the first four lines of the table) in order to deduce the Planck 2015 model independent *normalization* prior on this parameter combination.

$h = 0.72 \pm 0.03$, see [32] for details. This prior on the Hubble parameter is completely independent from CMB constraints.

Our results, best-fit values and 68%CL interval, are reported in table 11. For the tSZ wCDM analysis, without priors on h, $10^9 A_s e^{-2\tau_{\rm reio}}$ and $\tau_{\rm reio}$, we obtain $F = 0.493^{+0.024}_{-0.018}$ very similar to the result of the analysis with priors, dubbed tSZ+H_0, for which we get

$$F = 0.498^{+0.025}_{-0.016}. \tag{IV.244}$$

So, the use of the three priors aforementioned has no significant impact on the determination of F. This is because F is a parameter that accounts for the degeneracy with the Hubble parameter and the amplitude of fluctuations via σ_8. The constraints on the amplitudes of the foreground contributions CIB, IR and RS, to the y^2 power spectrum are also left unchanged from the tSZ to the tSZ+H_0 analysis. As can be seen by looking at the red contours of figure 25, the prior on H_0 determines the marginalized posterior distributions for $w_{\rm de}$, σ_8 and $\Omega_{\rm m}$. Their estimates from the tSZ+H_0 analysis are:

$$w_{\rm de} = -1.22^{+0.16}_{-0.14}, \quad \sigma_8 = 0.850 \pm 0.050, \quad \Omega_{\rm m} = 0.281 \pm 0.026. \tag{IV.245}$$

The 68% CL intervals are relatively large, alleviating any possible tension with the CMB. To enable a proper comparison with the CMB constraints, we use a *compressed* likelihood in order to get the TT+lowP+lensing+H_0 joint posterior probability distribution. This technique of compressed likelihood applied to dark energy related data was initiated in [124]. It is based on the fact that the information contained in the Planck chains for a given model universe (flat, curved, ΛCDM, etc.) can be efficiently recast in the form of a low dimensional covariance matrix for a small set of well chosen

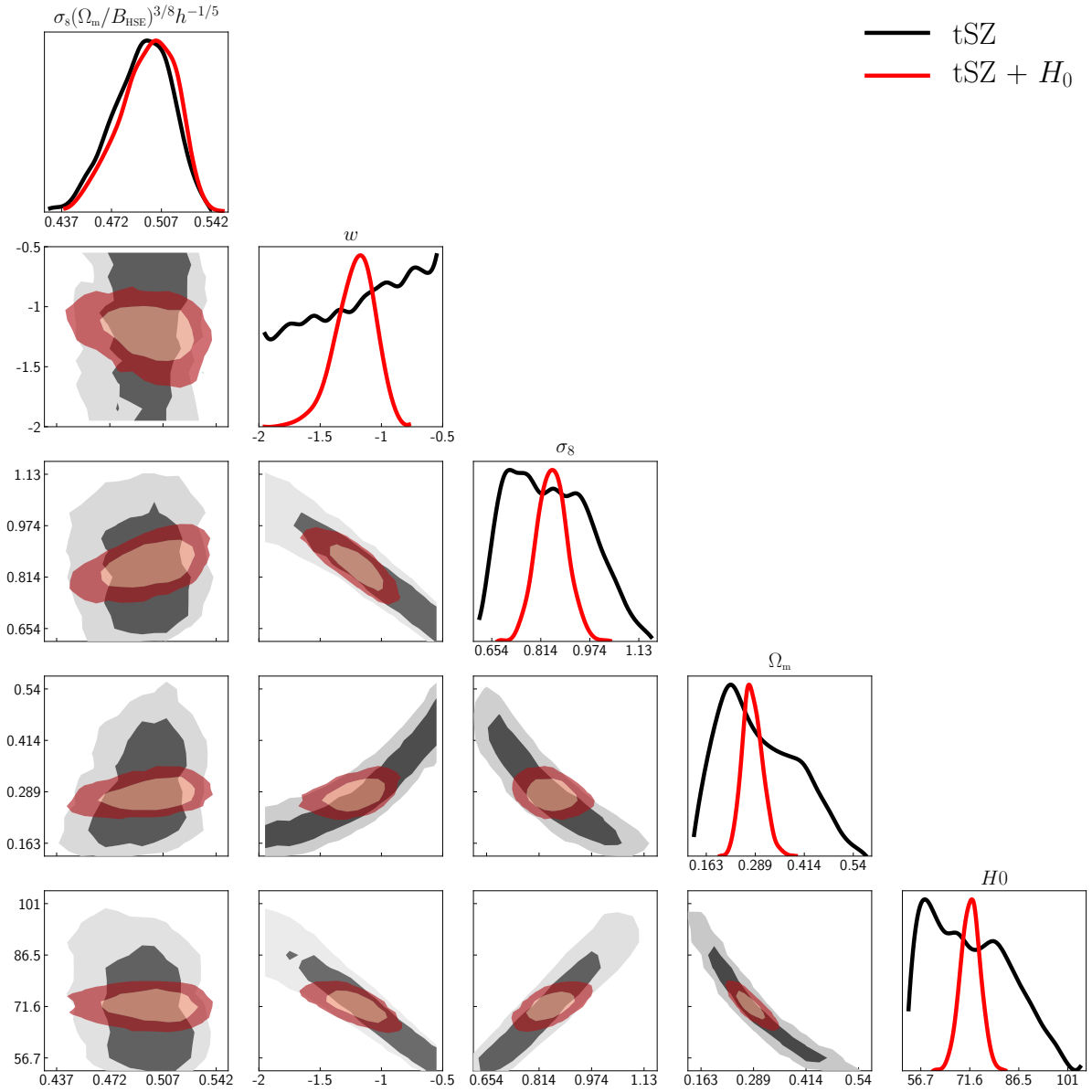

Figure 25: Projected (1D and 2D) joint posterior probability distribution as obtained from the "tSZ" analysis (all parameters varying including the hydrostatic bias, with trispectrum, B15 mass function and Arnaud *et al.* 2013 pressure profile) and the "tSZ + H_0" analysis for which we imposed priors on h, $A_s e^{-2\tau_{\rm reio}}$ and $\tau_{\rm reio}$ (see table 7). Numerics for the best-fit and mean values, and the 68% C.L. intervals, are reported in table 11.

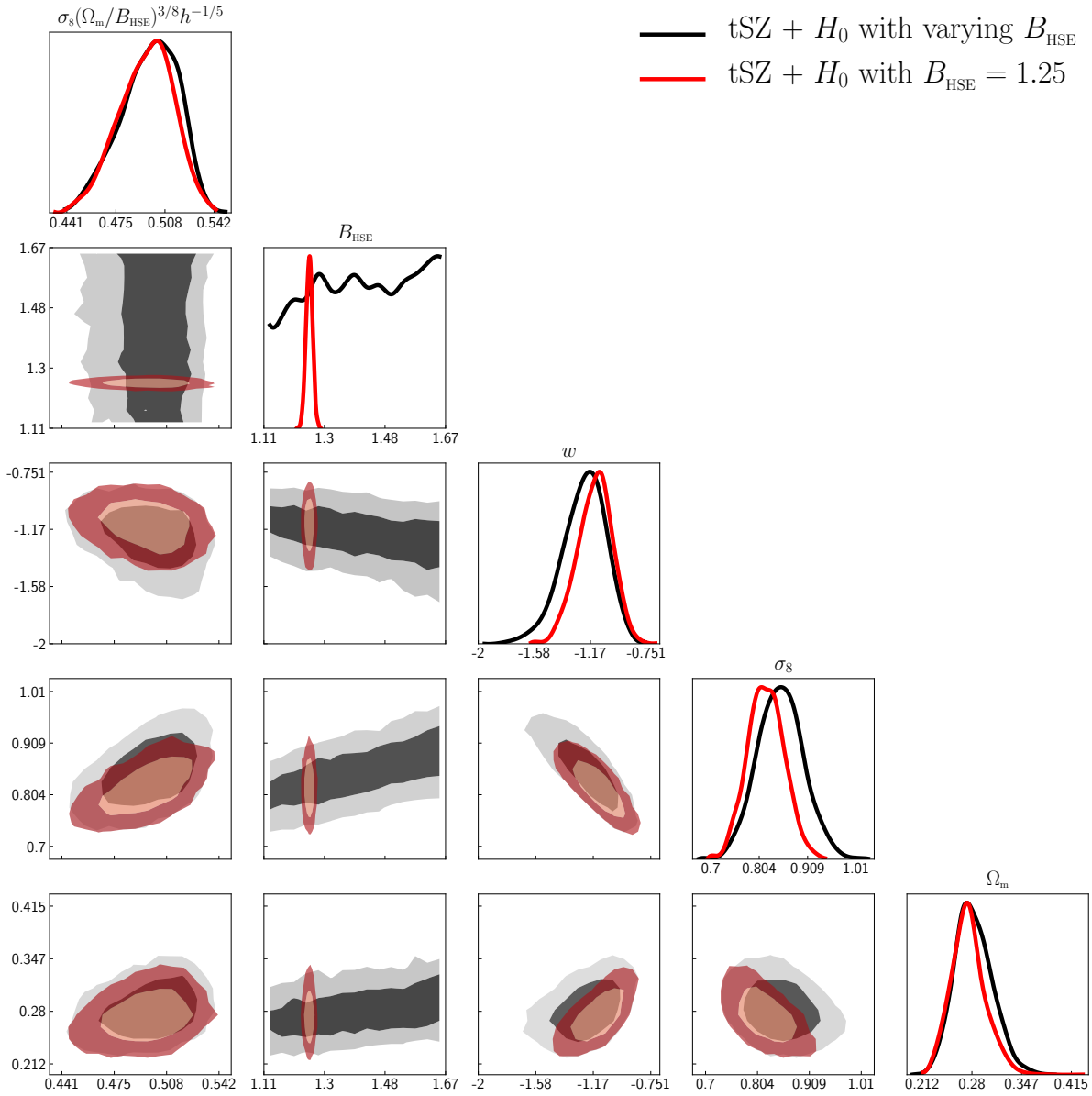

Figure 26: Projected (1D and 2D) joint posterior probability distribution as obtained from the "tSZ+H_0" analysis: all parameters varying, with trispectrum, B15 mass function and Arnaud *et al.* 2013 pressure profile, priors on h, $A_s e^{-2\tau_{\rm reio}}$ and $\tau_{\rm reio}$ (see table 7). Black contours are for the analysis with varying hydrostatic equilibrium bias and red contours for the analysis with $B_{\rm HSE} = 1.25$ ($b = 0.2$).

	68% C.L.	$\Omega_{\rm b}h^2$	$10^9 A_{\rm s}$	$n_{\rm s}$	R	$\ell_{\rm A}$
$\Omega_{\rm b}h^2$	0.02228 ± 0.00024	1	0.39	0.61	−0.66	−0.44
$10^9 A_{\rm s}$	2.1108 ± 0.0713	0.39	1	0.60	−0.58	−0.37
$n_{\rm s}$	0.9681 ± 0.0057	0.61	0.60	1	−0.85	−0.45
R	1.7447 ± 0.0068	−0.66	−0.58	−0.85	1	0.51
$\ell_{\rm A}$	301.70 ± 0.14	−0.44	−0.37	−0.45	0.51	1

Table 9: Normalized compressed likelihood for the Planck 2015 TT+lowP+lensing (wCDM) chains. The first column gives the the mean values and 68%CL standard deviations. The last five columns are the coefficients D_{ij} of the normalized covariance matrix. The shift parameter R is defined in Eq. (IV.246).

cosmological parameter combinations. The requirement is that the marginalized posterior probability distribution for the proposed parameter combination has to be well approximated by a Gaussian. Then, it is not necessary to re-do the analysis of the Planck observational data, one can use the compressed likelihood instead. Following [157], we constructed the compressed covariance matrix relative to the Planck 2015 wCDM chains for the TT+lowP+lensing likelihood. The essential parameter combinations that encapsulate the information associated with the background cosmology are the shift parameters, R, and the angular scale of the sound horizon at last scattering $\ell_{\rm A}$. They are given by

$$R \equiv \sqrt{\Omega_{\rm m} H_0^2}\, D_{\rm A}\left(z_\star\right)/c, \qquad \ell_{\rm A} \equiv \pi D_{\rm A}\left(z_\star\right)/r_* = \pi/\theta_s, \tag{IV.246}$$

where $z_\star$ is the decoupling redshift, $D_{\rm A}\left(z\right)$ is the comoving angular diameter distance, $r_\star$ is the comoving size of the sound horizon at decoupling and θ_s is the corresponding comoving angular size. In addition, we also use parameters that carry information relative to the dynamics of perturbations, namely: A_s, n_s and $\Omega_b h^2$, leading to a 5x5 covariance matrix for the compressed likelihood.

In table 9, we give the *normalized* covariance matrix coefficients, D_{ij}, corresponding to the compressed likelihood. At each step of the MCMC, we compute

$$\chi^2_{\rm CMB} = \sum_{i,j=1}^{5} \left(P - \bar{P}\right)_i \left[C^{-1}\right]_{ij} \left(P - \bar{P}\right)_j, \tag{IV.247}$$

where $P \equiv \left\{\Omega_{\rm b}h^2, A_{\rm s}, n_{\rm s}, R, \ell_{\rm A}\right\}$ contains the proposed values of the parameters and $\bar{P}$ contains the mean values of the parameters deduced from the wCDM TT+lowP+lensing chains. They are reported in the first column of the table along with the 68% standard deviations σ_i which enter the covariance matrix coefficients

$$C_{ij} = \sigma_i \sigma_j D_{ij}. \tag{IV.248}$$

Then, to obtain the current χ^2 value for TT+lowP+lensing+H_0 (also denoted CMB+H_0) is given by

$$\chi^2 = \chi^2_{\rm CMB} + \chi^2_{\rm H_0} \tag{IV.249}$$

where $\chi^2_{\rm H_0}$ corresponds to the priors on h, $10^9 A_s e^{-2\tau_{\rm reio}}$ and $\tau_{\rm reio}$ (see table 7). Resulting contours are shown on figure 27. The black contours are from the Planck chains, the red contours are obtained with the compressed likelihood only and the green contours include the priors on h, $10^9 A_s e^{-2\tau_{\rm reio}}$ and $\tau_{\rm reio}$ in addition to $\chi^2_{\rm CMB}$. This latter analysis is also referred to as CMB+H_0 on figure 28. The degeneracy between the parameters σ_8, $w_{\rm de}$ and $\Omega_{\rm m}$ is qualitatively the same for CMB (black and red

	$F \equiv \sigma_8 \left(\Omega_{\rm m}/B_{\rm HSE}\right)^{3/8} h^{-1/5}$	$w_{\rm de}$
tSZ (ΛCDM)	$0.504^{+0.024}_{-0.017}$	/
tSZ (wCDM)	$0.493^{+0.024}_{-0.018}$	/
tSZ (wCDM) + H_0	$0.498^{+0.025}_{-0.016}$	$-1.22^{+0.16}_{-0.14}$
tSZ (wCDM, $B_{\rm HSE} = 1.25$) + H_0	$0.495^{+0.022}_{-0.017}$	$-1.13^{+0.14}_{-0.13}$
CMB (TT+lowP, ΛCDM)	0.513 ± 0.014	/
CMB (TT+lowP+lensing, wCDM)	$0.475^{+0.016}_{-0.028}$	$-1.41^{+0.26}_{-0.46}$
CMB (*compressed* likelihood)	$0.480^{+0.024}_{-0.017}$	/
CMB (*compressed* likelihood) + H_0	$0.489^{+0.009}_{-0.011}$	$-1.12^{+0.11}_{-0.10}$
CMB (*compressed* likelihood) + H_0	$0.510^{+0.010}_{-0.011}$ ($B_{\rm HSE} = 1.25$)	$-1.12^{+0.11}_{-0.10}$

Table 10: Constraints (68% CL) on $F \equiv \sigma_8 \left(\Omega_{\rm m}/B_{\rm HSE}\right)^{3/8} h^{-1/5}$. The first four lines (tSZ) show the constraint from the MCMC analysis fitting the Planck 2015 SZ data (with B15 mass function, Arnaud *et al.* 2013 pressure profile for the computation of the tSZ power spectrum) including the trispectrum contribution into the covariance matrix. The last five lines (CMB) show the results relative to the Planck 2015 CMB data (for these CMB analysis, we used $B_{\rm HSE} = 1.40$ in order to quote a value for F, except the last one where we used $B_{\rm HSE} = 1.25$). The notation "$+H_0$" refers to the analysis where we imposed the priors on h, $A_s e^{-2\tau_{\rm reio}}$ and $\tau_{\rm reio}$ (see table 7).

contours on figure 27) and tSZ (black contours on figure 25) . However, in the CMB joint posterior probability distributions there is an additional degeneracy between σ_8, $w_{\rm de}$, $\Omega_{\rm m}$ and the parameter F. The CMB+H_0 analysis yields:

$$w_{\rm de} = -1.12^{+0.11}_{-0.10}, \quad \sigma_8 = 0.844 \pm 0.030, \quad \Omega_{\rm m} = 0.275 \pm 0.024, \tag{IV.250}$$

in a good agreement with tSZ+H_0 , see Eq. IV.245. Contours from both analysis are shown together on figure 28. Note that for the CMB+H_0 , CMB or compressed likelihood analysis, the numerical values for F are obtained with the hydrostatic bias set to $B_{\rm HSE} = 1.40$ and $B_{\rm HSE} = 1.25$. There is no tension between the CMB and tSZ constraints: the 68% CL regions overlap significantly, if not completely (see red and black on figure 28). The tSZ+H_0 constraints on $w_{\rm de}$ is weaker than the CMB+H_0 constraint.

If we assume that the hydrostatic bias is well measured and its value is close to the one favored by N-body simulations, $B_{\rm HSE} \simeq 1.25$ the constraints on $w_{\rm de}$ is substantially tighter and in a very good agreement with the CMB+H_0 constraint. We find

$$w_{\rm de} = -1.13^{+0.14}_{-0.13}, \quad \sigma_8 = 0.819 \pm 0.041, \quad \Omega_{\rm m} = 0.275 \pm 0.025. \tag{IV.251}$$

This shows that the SZ power spectrum is a compelling probe for dark energy, as efficient as CMB lensing. Our important results are recapitulated in table 10.

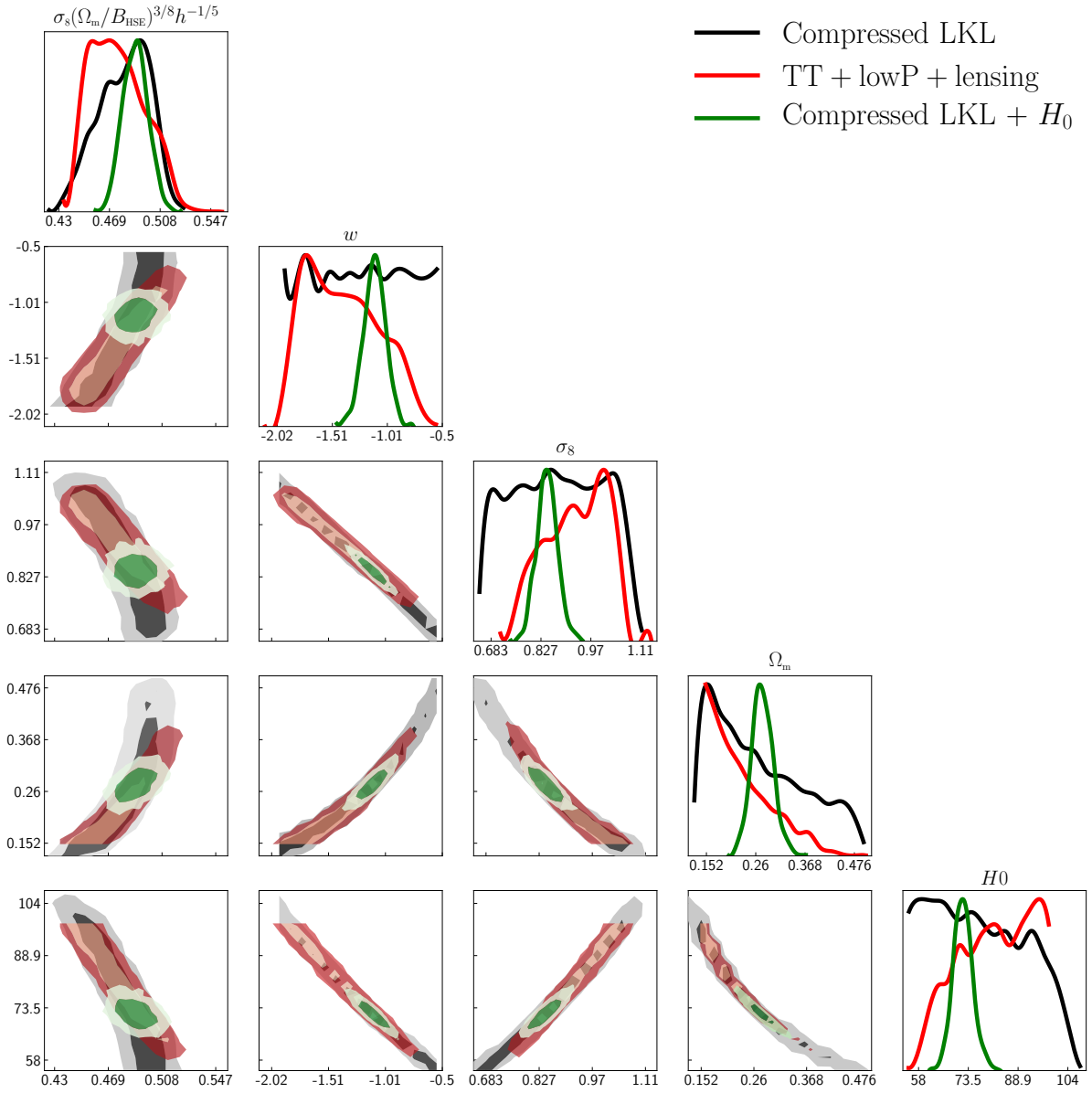

Figure 27: Projected (1D and 2D) joint posterior probability distribution as obtained from the Planck 2015 TT+lowP+lensing wCDM chains (red contours) available on the Planck Legacy Archive website, the compressed likelihood technique (black contours) that reproduces well the joint distribution of the Planck chains, and the analysis where we used the compressed likelihood along with the priors on h, $A_s e^{-2\tau_{\rm reio}}$ and $\tau_{\rm reio}$ (green contours, see table 7). Numerics for the best-fit and mean values, and the 68% C.L. intervals, for "TT+lowP+lensing" (red) and "Compressed LKL+H_0" (green) are reported in table 11 in the CMB and CMB+H_0 columns respectively. We used $B_{\rm HSE} = 1.40$ in order to show contours for $F \equiv \sigma_8 \, (\Omega_{\rm m}/B_{\rm HSE})^{3/8} \, h^{-1/5}$.

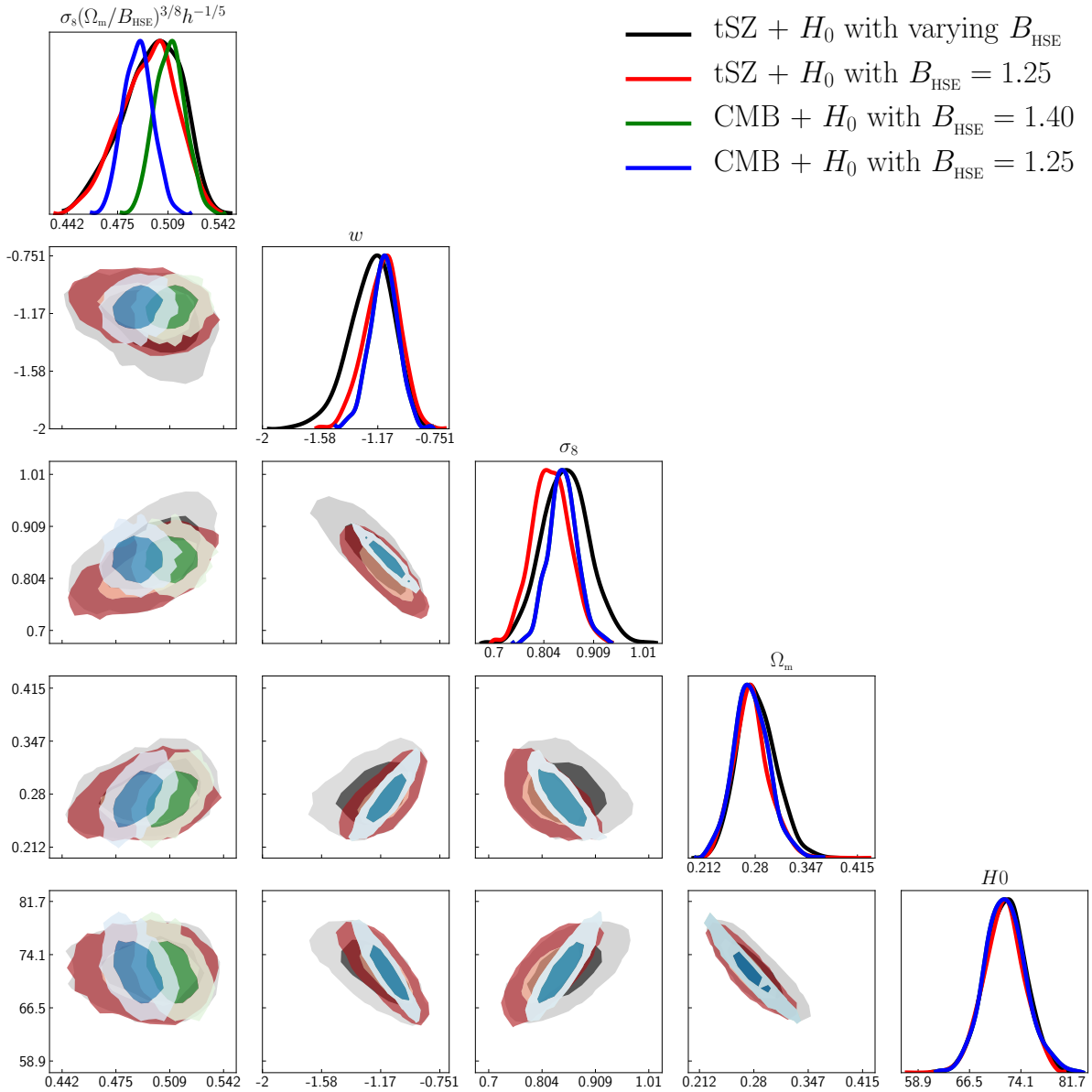

Figure 28: Projected (1D and 2D) joint posterior probability distribution as obtained from the tSZ+H_0 (black contours) analysis and CMB+H_0 (red contours) analysis. For details on the tSZ+H_0 analysis, see figure 25. The analysis CMB+H_0 corresponds to "Compressed LKL+H_0" on figure 27 (green contours) .

	tSZ		tSZ + H_0		CMB	CMB + H_0
	best fit	68% C.L.	best fit	68% C.L.	68% C.L.	68% C.L.
$B_{\rm HSE}$	1.11134	/	1.2378	/	/	/
$A_{\rm CIB}$	0.41784	0.49 ± 0.21	0.53632	0.46 ± 0.21	/	/
$A_{\rm IR}$	2.36527	2.12 ± 0.20	2.2238	2.12 ± 0.19	/	/
$A_{\rm RS}$	0.04056	$0.35^{+0.21}_{-0.35}$	0.018717	$0.35^{+0.21}_{-0.35}$	/	/
$\Omega_c h^2$	0.11481	/	0.11908	0.1218 ± 0.0063	0.1183 ± 0.0020	0.1178 ± 0.0018
$\Omega_b h^2$	0.02109	/	0.023221	/	0.02229 ± 0.00024	0.02230 ± 0.00024
$100\theta_{\rm s}$	1.03579	/	1.0354	/	1.04129 ± 0.00048	1.04130 ± 0.00048
$\tau_{\rm reio}$	0.05795	/	0.062499	0.06 ± 0.01	0.059 ± 0.018	0.06 ± 0.01
$10^9 A_{\rm s}$	1.93527	/	2.1184	2.12 ± 0.04	2.11 ± 0.07	2.12 ± 0.04
$n_{\rm s}$	0.90074	/	0.80792	/	$0.9681^{+0.0054}_{-0.0062}$	$0.9681^{+0.0049}_{-0.0052}$
$w_{\rm de}$	-0.54463	/	-1.2254	$-1.22^{+0.16}_{-0.14}$	$-1.41^{+0.26}_{-0.46}$	$-1.12^{+0.11}_{-0.10}$
σ_8	0.62190	/	0.81193	0.850 ± 0.050	$0.924^{+0.120}_{-0.067}$	0.844 ± 0.030
$\Omega_{\rm m}$	0.47524	/	0.26886	0.281 ± 0.026	$0.224^{+0.034}_{-0.090}$	0.275 ± 0.24
h	0.53608	/	0.72924	0.72 ± 0.03	> 0.76	0.72 ± 0.03
χ^2	18.70	/	20.05	/	/	/
F	0.512	$0.493^{+0.024}_{-0.018}$	0.488	$0.498^{+0.025}_{-0.016}$	$0.475^{+0.016}_{-0.028}$	$0.489^{+0.009}_{-0.011}$

Table 11: Results for the MCMC analysis assuming a wCDM cosmology. Varying parameters are all parameters above σ_8 with priors reported in table 1. (Other parameters are *derived* parameters and in the last line $F \equiv \sigma_8 \left(\Omega_{\rm m}/B_{\rm HSE}\right)^{3/8} h^{-1/5}$.) In the column "tSZ" we present the best-fit and 68%CL intervals for the tSZ analysis with trispectrum, B15 mass function and Arnaud *et al.* 2013 pressure profile. The column "tSZ + H_0" are the results after we imposed priors on h, $A_s e^{-2\tau_{\rm reio}}$ and $\tau_{\rm reio}$ (see table 7). The last two columns present the CMB constraints. Numerics in the "CMB" columns are taken from the extensive tables that can be found on the Planck Legacy Archive website, under the section base_w_plik_HMTT_lowTEB_post_lensing (the corresponding chains are also available on the website). To get the CMB + H_0 constraints we used the *compressed* likelihood technique. The values of F for the CMB columns are obtained with $B_{\rm HSE} = 1.40$.

$\ell_{\rm eff}$	$C_\ell^{y^2}$	$\sigma_\ell^{y^2}$	$C_\ell^{\rm RC}$	$\sigma_\ell^{\rm RC}$	$C_\ell^{\rm CIB}$	$C_\ell^{\rm RS}$	$C_\ell^{\rm IR}$	$C_\ell^{\rm CN}$
10	0.00508	0.00629	0.000421	0.000160	0.000000	0.000043	0.000007	0.000001
13.5	0.00881	0.00615	0.000710	0.000192	0.000000	0.000142	0.000024	0.000001
18	0.01363	0.00579	0.001251	0.000254	0.000000	0.000296	0.000048	0.000002
23.5	0.02961	0.00805	0.002837	0.000446	0.000000	0.000400	0.000073	0.000004
30.5	0.02241	0.00521	0.003933	0.000460	0.000902	0.000541	0.000111	0.000006
40	0.02849	0.00464	0.005969	0.000510	0.002010	0.001056	0.000224	0.000010
52.5	0.04276	0.00468	0.010318	0.000672	0.003119	0.001647	0.000449	0.000018
68.5	0.04580	0.00429	0.014045	0.000699	0.006278	0.002787	0.000837	0.000030
89.5	0.07104	0.00454	0.024061	0.000896	0.012242	0.004306	0.001400	0.000052
117	0.11914	0.00562	0.032976	0.000936	0.021584	0.006842	0.002701	0.000089
152.5	0.15150	0.00594	0.04710	0.00102	0.045915	0.011264	0.004721	0.000153
198	0.19390	0.00611	0.06238	0.00104	0.070582	0.016744	0.008115	0.000262
257.5	0.28175	0.00687	0.08173	0.00103	0.119786	0.027345	0.014618	0.000456
335.5	0.39837	0.00824	0.101911	0.000978	0.211686	0.043275	0.024893	0.000815
436.5	0.56743	0.00958	0.117412	0.000860	0.332863	0.070587	0.051570	0.001503
567.5	0.76866	0.01242	0.132234	0.000769	0.434931	0.115356	0.107293	0.002934
738	1.1101	0.0165	0.143214	0.000642	0.602030	0.154926	0.197053	0.006334
959.5	1.6614	0.0240	0.156202	0.000544	0.754733	0.207200	0.361713	0.016171
1247.5	2.5217	0.0417	0.175341	0.000492	1.029014	0.287652	0.681036	0.054883
1622	4.5851	0.0987	0.283969	0.000900	1.357567	0.410274	1.295272	0.301480
2109	12.269	0.401	1.36368	0.00365	1.850146	0.657659	2.534448	3.738250
2742	165.6	23.6	54.69	2.31	2.629002	1.117189	4.545315	183.267263

Table 12: Planck 2015 data points and error bars for the y^2 power spectrum from the all-sky y-map, $C_\ell^{y^2}$, the SZ resolved cluster catalogue $C_\ell^{y^2}$, and models for the foreground contributions: cosmic infrared background (CIB), infrared sources (IR) and radio sources (RS). Data points were taken from [8]. The last column is the correlated noise of the instrument, see [151]. The numerical values correspond to the rescaled dimensionless power spectra $10^{12}\ell\,(\ell+1)\,C_\ell/2\pi$ and error bars. Only the first eighteen multipole bins (up to $\ell = 959.5$) are fitted in our MCMC analysis. The last data point at $\ell_{\rm eff} = 2742$ is used for the determination of the correlated noise amplitude.

Conclusion and Outlook

Motivated by the promising theory of Loop Quantum Gravity, in the first part of this thesis, we have investigated two extensions of General Relativity. We have explored the possible observational consequences of the bouncing scenario in Loop Quantum Cosmology and of the Planck Star hypothesis for black holes.

We have shown that the imprints of a quantum bounce can be present in the temperature anisotropy power spectrum of the CMB. The CMB data can actually be used to exclude consistent quantum cosmological models, such as a particular setting of the deformed algebra (effective constraints) approach to perturbations in LQC.

For black holes, we considered the idea of quantum effects leaking outside the horizon. The Planck Star model, that realizes a black hole to white hole transition via quantum tunneling, was shown to be a potential explanation to the Fermi gamma ray excess. We also predicted that the radiation emitted by these 'bouncing' black holes can have a unique signature due to the peculiar redshift dependency of the phenomenon.

Observations of black holes (gravitational wave interferometry or via the trajectories of surrounding luminous objects) and the measurements of the statistical properties of the large scale structure of the universe are the two main windows on quantum gravity. Hopefully, the increasing accuracy of observational data will soon allow us to probe the quantum properties of space-time in both directions.

In the second part of the thesis, we focused on the recent acceleration of the universe. We reviewed the theory of cosmological perturbations and proposed a powerful framework aimed at deriving the phenomenological consequences of a wide range of dark sector theories in a unified way. The 'equation of state' description of dark energy was implemented numerically into a modified version of the CLASS code. Then, we could study the impact of dark sector perturbations onto several observables: the late integrated Sachs Wolfe effect, CMB weak lensing, the matter power spectrum, the galaxy shear correlation function and redshift space distortions. Finally, in the last section of the manuscript, we obtained a new determination of the equation of state parameter of dark energy from the latest measurement of the Sunyaev Zel'dovich power spectrum.

Since SDSS and WMAP almost twenty years ago, there has not been any major advancement in our understanding of the expansion of the universe. Even after the Planck mission, the properties of dark energy and dark matter remain largely unknown.

However, there is no doubt that within ten years, the next generation of galaxy surveys (EUCLID, LSST, WFIRST) will have corroborated the ΛCDM model, by proving that dark energy is a cosmological constant, or will have disproved it by showing that dark energy is dynamical.

Bibliography

[1] Georges Aad et al. Observation of a new particle in the search for the Standard Model Higgs boson with the ATLAS detector at the LHC. *Phys. Lett.*, B716:1–29, 2012. doi: 10.1016/j.physletb.2012.08.020.

[2] P. A. R. Ade et al. Planck 2013 results. XXI. Power spectrum and high-order statistics of the Planck all-sky Compton parameter map. *Astron. Astrophys.*, 571:A21, 2014. doi: 10.1051/0004-6361/201321522.

[3] P. A. R. Ade et al. Planck 2015 results. XVII. Constraints on primordial non-Gaussianity. *Astron. Astrophys.*, 594:A17, 2016. doi: 10.1051/0004-6361/201525836.

[4] P. A. R. Ade et al. Planck 2015 results. XXIV. Cosmology from Sunyaev-Zeldovich cluster counts. *Astron. Astrophys.*, 594:A24, 2016. doi: 10.1051/0004-6361/201525833.

[5] P. A. R. Ade et al. Planck 2015 results. XXIII. The thermal Sunyaev-Zeldovich effect–cosmic infrared background correlation. *Astron. Astrophys.*, 594:A23, 2016. doi: 10.1051/0004-6361/201527418.

[6] P. A. R. Ade et al. Planck 2015 results. XIV. Dark energy and modified gravity. *Astron. Astrophys.*, 594:A14, 2016. doi: 10.1051/0004-6361/201525814.

[7] P. A. R. Ade et al. Planck 2015 results. XIII. Cosmological parameters. *Astron. Astrophys.*, 594:A13, 2016. doi: 10.1051/0004-6361/201525830.

[8] N. Aghanim et al. Planck 2015 results. XXII. A map of the thermal Sunyaev-Zeldovich effect. *Astron. Astrophys.*, 594:A22, 2016. doi: 10.1051/0004-6361/201525826.

[9] Ivan Agullo, Abhay Ashtekar, and William Nelson. A Quantum Gravity Extension of the Inflationary Scenario. *Phys. Rev. Lett.*, 109:251301, 2012. doi: 10.1103/PhysRevLett.109.251301.

[10] Ivan Agullo, Abhay Ashtekar, and William Nelson. Extension of the quantum theory of cosmological perturbations to the Planck era. *Phys. Rev.*, D87(4):043507, 2013. doi: 10.1103/PhysRevD.87.043507.

[11] Ivan Agullo, Abhay Ashtekar, and William Nelson. The pre-inflationary dynamics of loop quantum cosmology: Confronting quantum gravity with observations. *Class. Quant. Grav.*, 30:085014, 2013. doi: 10.1088/0264-9381/30/8/085014.

[12] Ivan Agullo, Abhay Ashtekar, and Brajesh Gupt. Phenomenology with fluctuating quantum geometries in loop quantum cosmology. 2016.

[13] Ahmed Almheiri, Donald Marolf, Joseph Polchinski, and James Sully. Black Holes: Complementarity or Firewalls? *JHEP*, 02:062, 2013. doi: 10.1007/JHEP02(2013)062.

[14] Luca Amendola, Guillermo Ballesteros, and Valeria Pettorino. Effects of modified gravity on B-mode polarization. *Phys. Rev.*, D90:043009, 2014. doi: 10.1103/PhysRevD.90.043009.

[15] M. Arnaud, G. W. Pratt, R. Piffaretti, H. Böhringer, J. H. Croston, and E. Pointecouteau. The universal galaxy cluster pressure profile from a representative sample of nearby systems (REXCESS) and the Y_{SZ} - M_{500} relation. , 517:A92, July 2010. doi: 10.1051/0004-6361/200913416.

[16] Abhay Ashtekar and Brajesh Gupt. Generalized effective description of loop quantum cosmology. *Phys. Rev.*, D92(8):084060, 2015. doi: 10.1103/PhysRevD.92.084060.

[17] Abhay Ashtekar and Brajesh Gupt. Quantum Gravity in the Sky: Interplay between fundamental theory and observations. *Class. Quant. Grav.*, 34(1):014002, 2017. doi: 10.1088/1361-6382/34/1/014002.

[18] Abhay Ashtekar, Tomasz Pawlowski, and Parampreet Singh. Quantum Nature of the Big Bang: Improved dynamics. *Phys. Rev.*, D74:084003, 2006. doi: 10.1103/PhysRevD.74.084003.

[19] B. Audren, J. Lesgourgues, K. Benabed, and S. Prunet. Conservative constraints on early cosmology with MONTE PYTHON. *JCAP*, 2:001, February 2013. doi: 10.1088/1475-7516/2013/02/001.

[20] Tessa Baker, Pedro G. Ferreira, and Constantinos Skordis. The Parameterized Post-Friedmann framework for theories of modified gravity: concepts, formalism and examples. *Phys. Rev.*, D87 (2):024015, 2013. doi: 10.1103/PhysRevD.87.024015.

[21] Guillermo Ballesteros and Julien Lesgourgues. Dark energy with non-adiabatic sound speed: initial conditions and detectability. *JCAP*, 1010:014, 2010. doi: 10.1088/1475-7516/2010/10/014.

[22] Matthias Bartelmann and Peter Schneider. Weak gravitational lensing. *Phys. Rept.*, 340:291–472, 2001. doi: 10.1016/S0370-1573(00)00082-X.

[23] Nicola Bartolo, Matteo Fasiello, Sabino Matarrese, and Antonio Riotto. Large non-Gaussianities in the Effective Field Theory Approach to Single-Field Inflation: the Bispectrum. *JCAP*, 1008: 008, 2010. doi: 10.1088/1475-7516/2010/08/008.

[24] R. A. Battye and A. Moss. Cosmological perturbations in elastic dark energy models. *Phys. Rev. D*, 76(2):023005, July 2007. doi: 10.1103/PhysRevD.76.023005.

[25] Richard A. Battye and Jonathan A. Pearson. Parametrizing dark sector perturbations via equations of state. *Phys. Rev.*, D88(6):061301, 2013. doi: 10.1103/PhysRevD.88.061301.

[26] Mitchell C. Begelman, Marta Volonteri, and Martin J. Rees. Formation of supermassive black holes by direct collapse in pregalactic halos. *Mon. Not. Roy. Astron. Soc.*, 370:289–298, 2006. doi: 10.1111/j.1365-2966.2006.10467.x.

[27] Jacob D. Bekenstein. Relativistic gravitation theory for the MOND paradigm. *Phys. Rev.*, D70:083509, 2004. doi: 10.1103/PhysRevD.70.083509,10.1103/PhysRevD.71.069901. [Erratum: Phys. Rev.D71,069901(2005)].

[28] Emilio Bellini and Ignacy Sawicki. Maximal freedom at minimum cost: linear large-scale structure in general modifications of gravity. *JCAP*, 1407:050, 2014. doi: 10.1088/1475-7516/2014/07/050.

[29] Jibril Ben Achour, Julien Grain, and Karim Noui. Loop Quantum Cosmology with Complex Ashtekar Variables. *Class. Quant. Grav.*, 32:025011, 2015. doi: 10.1088/0264-9381/32/2/025011.

[30] Jibril Ben Achour, Amaury Mouchet, and Karim Noui. Analytic Continuation of Black Hole Entropy in Loop Quantum Gravity. *JHEP*, 06:145, 2015. doi: 10.1007/JHEP06(2015)145.

[31] N. Benítez. Bayesian Photometric Redshift Estimation. *Astrophys. J.*, 536:571–583, June 2000. doi: 10.1086/308947.

[32] Jose Luis Bernal, Licia Verde, and Adam G. Riess. The trouble with H_0. *JCAP*, 1610(10):019, 2016. doi: 10.1088/1475-7516/2016/10/019.

[33] F. Bernardeau, S. Colombi, E. Gaztanaga, and R. Scoccimarro. Large scale structure of the universe and cosmological perturbation theory. *Phys. Rept.*, 367:1–248, 2002. doi: 10.1016/S0370-1573(02)00135-7.

[34] F. Beutler, C. Blake, M. Colless, D. H. Jones, L. Staveley-Smith, G. B. Poole, L. Campbell, Q. Parker, W. Saunders, and F. Watson. The 6dF Galaxy Survey: z≈ 0 measurements of the growth rate and σ_8. *Mon. Not. Roy. Astron. Soc.*, 423:3430–3444, July 2012. doi: 10.1111/j.1365-2966.2012.21136.x.

[35] Fedor L. Bezrukov and Mikhail Shaposhnikov. The Standard Model Higgs boson as the inflaton. *Phys. Lett.*, B659:703–706, 2008. doi: 10.1016/j.physletb.2007.11.072.

[36] Eugenio Bianchi. Entropy of Non-Extremal Black Holes from Loop Gravity. 2012.

[37] Eugenio Bianchi and Carlo Rovelli. Why all these prejudices against a constant? 2010.

[38] David Blais, Torsten Bringmann, Claus Kiefer, and David Polarski. Accurate results for primordial black holes from spectra with a distinguished scale. *Phys. Rev.*, D67:024024, 2003. doi: 10.1103/PhysRevD.67.024024.

[39] C. Blake, S. Brough, M. Colless, C. Contreras, W. Couch, S. Croom, T. Davis, M. J. Drinkwater, K. Forster, D. Gilbank, M. Gladders, K. Glazebrook, B. Jelliffe, R. J. Jurek, I.-H. Li, B. Madore, D. C. Martin, K. Pimbblet, G. B. Poole, M. Pracy, R. Sharp, E. Wisnioski, D. Woods, T. K. Wyder, and H. K. C. Yee. The WiggleZ Dark Energy Survey: the growth rate of cosmic structure since redshift z=0.9. *Mon. Not. Roy. Astron. Soc.*, 415:2876–2891, August 2011. doi: 10.1111/j.1365-2966.2011.18903.x.

[40] C. Blake, S. Brough, M. Colless, C. Contreras, W. Couch, S. Croom, D. Croton, T. M. Davis, M. J. Drinkwater, K. Forster, D. Gilbank, M. Gladders, K. Glazebrook, B. Jelliffe, R. J. Jurek, I.-h. Li, B. Madore, D. C. Martin, K. Pimbblet, G. B. Poole, M. Pracy, R. Sharp, E. Wisnioski, D. Woods, T. K. Wyder, and H. K. C. Yee. The WiggleZ Dark Energy Survey: joint measurements of the expansion and growth history at z < 1. *Mon. Not. Roy. Astron. Soc.*, 425:405–414, September 2012. doi: 10.1111/j.1365-2966.2012.21473.x.

[41] Sebastian Bocquet, Alex Saro, Klaus Dolag, and Joseph J. Mohr. Halo mass function: Baryon impact, fitting formulae and implications for cluster cosmology. *Mon. Not. Roy. Astron. Soc.*, 456(3):2361–2373, 2016. doi: 10.1093/mnras/stv2657.

[42] Robert Brandenberger and Patrick Peter. Bouncing Cosmologies: Progress and Problems. 2016. doi: 10.1007/s10701-016-0057-0.

[43] Matvei Bronstein. Republication of: Quantum theory of weak gravitational fields. *General Relativity and Gravitation*, 44(1):267–283, 2012. ISSN 1572-9532. doi: 10.1007/s10714-011-1285-4. URL http://dx.doi.org/10.1007/s10714-011-1285-4.

[44] G. L. Bryan and M. L. Norman. Statistical Properties of X-Ray Clusters: Analytic and Numerical Comparisons. *Astrophys. J.*, 495:80–99, March 1998. doi: 10.1086/305262.

[45] Thomas Cailleteau and Aurelien Barrau. Gauge invariance in Loop Quantum Cosmology : Hamilton-Jacobi and Mukhanov-Sasaki equations for scalar perturbations. *Phys. Rev.*, D85: 123534, 2012. doi: 10.1103/PhysRevD.85.123534.

[46] Thomas Cailleteau, Aurelien Barrau, Julien Grain, and Francesca Vidotto. Consistency of holonomy-corrected scalar, vector and tensor perturbations in Loop Quantum Cosmology. *Phys. Rev.*, D86:087301, 2012. doi: 10.1103/PhysRevD.86.087301.

[47] Thomas Cailleteau, Jakub Mielczarek, Aurelien Barrau, and Julien Grain. Anomaly-free scalar perturbations with holonomy corrections in loop quantum cosmology. *Class. Quant. Grav.*, 29: 095010, 2012. doi: 10.1088/0264-9381/29/9/095010.

[48] Thomas Cailleteau, Linda Linsefors, and Aurelien Barrau. Anomaly-free perturbations with inverse-volume and holonomy corrections in Loop Quantum Cosmology. *Class. Quant. Grav.*, 31:125011, 2014. doi: 10.1088/0264-9381/31/12/125011.

[49] S. Capozziello, S. Nojiri, and S.D. Odintsov. Unified phantom cosmology: Inflation, dark energy and dark matter under the same standard. *Physics Letters B*, 632(5–6):597 – 604, 2006. ISSN 0370-2693. doi: http://dx.doi.org/10.1016/j.physletb.2005.11.012. URL http://www.sciencedirect.com/science/article/pii/S0370269305016254.

[50] B. J. Carr, Kazunori Kohri, Yuuiti Sendouda, and Jun'ichi Yokoyama. New cosmological constraints on primordial black holes. *Phys. Rev.*, D81:104019, 2010. doi: 10.1103/PhysRevD.81.104019.

[51] Bernard Carr, Florian Kuhnel, and Marit Sandstad. Primordial Black Holes as Dark Matter. *Phys. Rev.*, D94(8):083504, 2016. doi: 10.1103/PhysRevD.94.083504.

[52] Sean M. Carroll. The Cosmological constant. *Living Rev. Rel.*, 4:1, 2001. doi: 10.12942/lrr-2001-1.

[53] Serguei Chatrchyan et al. Observation of a new boson at a mass of 125 GeV with the CMS experiment at the LHC. *Phys. Lett.*, B716:30–61, 2012. doi: 10.1016/j.physletb.2012.08.021.

[54] Clifford Cheung, Paolo Creminelli, A. Liam Fitzpatrick, Jared Kaplan, and Leonardo Senatore. The Effective Field Theory of Inflation. *JHEP*, 03:014, 2008. doi: 10.1088/1126-6708/2008/03/014.

[55] Jens Chluba. Science with CMB spectral distortions. In *Proceedings, 49th Rencontres de Moriond on Cosmology: La Thuile, Italy, March 15-22, 2014*, pages 327–334, 2014. URL https://inspirehep.net/record/1298250/files/arXiv:1405.6938.pdf.

[56] Y. Choquet-Bruhat. *General Relativity and the Einstein Equations*. Oxford Mathematical Monographs. OUP Oxford, 2008. ISBN 9780199230723. URL https://books.google.fr/books?id=slA4CFfIpHAC.

[57] Marios Christodoulou, Carlo Rovelli, Simone Speziale, and Ilya Vilensky. Planck star tunneling time: An astrophysically relevant observable from background-free quantum gravity. *Phys. Rev.*, D94(8):084035, 2016. doi: 10.1103/PhysRevD.94.084035.

[58] Piotr T. Chrusciel, Joao Lopes Costa, and Markus Heusler. Stationary Black Holes: Uniqueness and Beyond. *Living Rev. Rel.*, 15:7, 2012. doi: 10.12942/lrr-2012-7.

[59] James M. Cline, Christophe Grojean, and Geraldine Servant. Cosmological expansion in the presence of extra dimensions. *Phys. Rev. Lett.*, 83:4245, 1999. doi: 10.1103/PhysRevLett.83.4245.

[60] LIGO Scientific Collaboration and Virgo Collaboration. Gw151226: Observation of gravitational waves from a 22-solar-mass binary black hole coalescence. *Phys. Rev. Lett.*, 116:241103, Jun 2016. doi: 10.1103/PhysRevLett.116.241103. URL http://link.aps.org/doi/10.1103/PhysRevLett.116.241103.

[61] Carlos Contreras et al. The WiggleZ Dark Energy Survey: measuring the cosmic growth rate with the two-point galaxy correlation function. 2013. doi: 10.1093/mnras/sts608. [Mon. Not. Roy. Astron. Soc.430,924(2013)].

[62] Asantha Cooray and Ravi K. Sheth. Halo models of large scale structure. *Phys. Rept.*, 372: 1–129, 2002. doi: 10.1016/S0370-1573(02)00276-4.

[63] Antonio C. da Silva, Scott T. Kay, Andrew R. Liddle, and Peter A. Thomas. Hydrodynamical simulations of the sunyaev-zel'dovich effect: cluster scaling relations and x-ray properties. *Mon. Not. Roy. Astron. Soc.*, 348:1401, 2004. doi: 10.1111/j.1365-2966.2004.07463.x.

[64] Antonio De Felice and Shinji Tsujikawa. f(R) theories. *Living Rev. Rel.*, 13:3, 2010. doi: 10.12942/lrr-2010-3.

[65] C. Deffayet, Xian Gao, D. A. Steer, and G. Zahariade. From k-essence to generalised Galileons. *Phys. Rev.*, D84:064039, 2011. doi: 10.1103/PhysRevD.84.064039.

[66] Vincent Desjacques, Donghui Jeong, and Fabian Schmidt. Large-Scale Galaxy Bias. 2016.

[67] Bryce S. DeWitt. Quantum theory of gravity. ii. the manifestly covariant theory. *Phys. Rev.*, 162:1195–1239, Oct 1967. doi: 10.1103/PhysRev.162.1195. URL http://link.aps.org/doi/10.1103/PhysRev.162.1195.

[68] R. H. Dicke. Mach's principle and invariance under transformation of units. *Phys. Rev.*, 125: 2163–2167, 1962. doi: 10.1103/PhysRev.125.2163.

[69] Peter Diener, Brajesh Gupt, and Parampreet Singh. Numerical simulations of a loop quantum cosmos: robustness of the quantum bounce and the validity of effective dynamics. *Class. Quant. Grav.*, 31:105015, 2014. doi: 10.1088/0264-9381/31/10/105015.

[70] Klaus Dolag, Eiichiro Komatsu, and Rashid Sunyaev. SZ effects in the Magneticum Pathfinder Simulation: Comparison with the Planck, SPT, and ACT results. *Mon. Not. Roy. Astron. Soc.*, 463(2):1797–1811, 2016. doi: 10.1093/mnras/stw2035.

[71] Jason Dossett, Bin Hu, and David Parkinson. Constraining models of f(R) gravity with Planck and WiggleZ power spectrum data. *JCAP*, 1403:046, 2014. doi: 10.1088/1475-7516/2014/03/046.

[72] Alan R. Duffy, Joop Schaye, Scott T. Kay, and Claudio Dalla Vecchia. Dark matter halo concentrations in the Wilkinson Microwave Anisotropy Probe year 5 cosmology. *Mon. Not. Roy. Astron. Soc.*, 390:L64, 2008. doi: 10.1111/j.1745-3933.2008.00537.x. [Erratum: Mon. Not. Roy. Astron. Soc.415,L85(2011)].

[73] Daniel J. Eisenstein and Wayne Hu. Power spectra for cold dark matter and its variants. *Astrophys. J.*, 511:5, 1997. doi: 10.1086/306640.

[74] T. Erben, H. Hildebrandt, L. Miller, L. van Waerbeke, C. Heymans, H. Hoekstra, T. D. Kitching, Y. Mellier, J. Benjamin, C. Blake, C. Bonnett, O. Cordes, J. Coupon, L. Fu, R. Gavazzi, B. Gillis, E. Grocutt, S. D. J. Gwyn, K. Holhjem, M. J. Hudson, M. Kilbinger, K. Kuijken, M. Milkeraitis, B. T. P. Rowe, T. Schrabback, E. Semboloni, P. Simon, M. Smit, O. Toader, S. Vafaei, E. van Uitert, and M. Velander. Cfhtlens: the canada-france-hawaii telescope lensing survey - imaging data and catalogue products. *Mon. Not. Roy. Astron. Soc.*, 433:2545–2563, August 2013. doi: 10.1093/mnras/stt928.

[75] R. Genzel, F. Eisenhauer, and S. Gillessen. The Galactic Center massive black hole and nuclear star cluster. *Reviews of Modern Physics*, 82:3121–3195, October 2010. doi: 10.1103/RevModPhys.82.3121.

[76] Steven B. Giddings. Possible observational windows for quantum effects from black holes. *Phys. Rev.*, D90(12):124033, 2014. doi: 10.1103/PhysRevD.90.124033.

[77] S. L. Glashow. Partial Symmetries of Weak Interactions. *Nucl. Phys.*, 22:579–588, 1961. doi: 10.1016/0029-5582(61)90469-2.

[78] Jérôme Gleyzes, David Langlois, and Filippo Vernizzi. A unifying description of dark energy. *Int. J. Mod. Phys.*, D23(13):1443010, 2015. doi: 10.1142/S021827181443010X.

[79] Anne M. Green. Primordial Black Holes: sirens of the early Universe. *Fundam. Theor. Phys.*, 178:129–149, 2015. doi: 10.1007/978-3-319-10852-0_5.

[80] Anne M. Green, Andrew R. Liddle, Karim A. Malik, and Misao Sasaki. A New calculation of the mass fraction of primordial black holes. *Phys. Rev.*, D70:041502, 2004. doi: 10.1103/PhysRevD.70.041502.

[81] Hal M. Haggard and Carlo Rovelli. Quantum-gravity effects outside the horizon spark black to white hole tunneling. *Phys. Rev.*, D92(10):104020, 2015. doi: 10.1103/PhysRevD.92.104020.

[82] D. Hanson, A. Challinor, and A. Lewis. Weak lensing of the CMB. *General Relativity and Gravitation*, 42:2197–2218, September 2010. doi: 10.1007/s10714-010-1036-y.

[83] S. W. Hawking. Particle Creation by Black Holes. *Commun. Math. Phys.*, 43:199–220, 1975. doi: 10.1007/BF02345020. [,167(1975)].

[84] Pierre Heidmann, Hongguang Liu, and Karim Noui. Semiclassical analysis of black holes in loop quantum gravity: Modeling Hawking radiation with volume fluctuations. *Phys. Rev.*, D95(4):044015, 2017. doi: 10.1103/PhysRevD.95.044015.

[85] W. Heisenberg. Über den anschaulichen inhalt der quantentheoretischen kinematik und mechanik. *Zeitschrift für Physik*, 43(3):172–198, 1927. ISSN 0044-3328. doi: 10.1007/BF01397280. URL http://dx.doi.org/10.1007/BF01397280.

[86] C. Heymans, L. Van Waerbeke, L. Miller, T. Erben, H. Hildebrandt, H. Hoekstra, T. D. Kitching, Y. Mellier, P. Simon, C. Bonnett, J. Coupon, L. Fu, J. Harnois Déraps, M. J. Hudson, M. Kilbinger, K. Kuijken, B. Rowe, T. Schrabback, E. Semboloni, E. van Uitert, S. Vafaei, and M. Velander. CFHTLenS: the Canada-France-Hawaii Telescope Lensing Survey. *Mon. Not. Roy. Astron. Soc.*, 427:146–166, November 2012. doi: 10.1111/j.1365-2966.2012.21952.x.

[87] C. Heymans, E. Grocutt, A. Heavens, M. Kilbinger, T. D. Kitching, F. Simpson, J. Benjamin, T. Erben, H. Hildebrandt, H. Hoekstra, Y. Mellier, L. Miller, L. Van Waerbeke, M. L. Brown, J. Coupon, L. Fu, J. Harnois-Déraps, M. J. Hudson, K. Kuijken, B. Rowe, T. Schrabback,

E. Semboloni, S. Vafaei, and M. Velander. CFHTLenS tomographic weak lensing cosmological parameter constraints: Mitigating the impact of intrinsic galaxy alignments. *Mon. Not. Roy. Astron. Soc.*, 432:2433–2453, July 2013. doi: 10.1093/mnras/stt601.

[88] Christopher M. Hirata and Uros Seljak. Intrinsic alignment-lensing interference as a contaminant of cosmic shear. *Phys. Rev.*, D70:063526, 2004. doi: 10.1103/PhysRevD.82.049901,10.1103/PhysRevD.70.063526. [Erratum: Phys. Rev.D82,049901(2010)].

[89] Jan Holland and Stefan Hollands. A small cosmological constant due to non-perturbative quantum effects. *Class. Quant. Grav.*, 31:125006, 2014. doi: 10.1088/0264-9381/31/12/125006.

[90] Gregory Walter Horndeski. Second-order scalar-tensor field equations in a four-dimensional space. *Int. J. Theor. Phys.*, 10:363–384, 1974. doi: 10.1007/BF01807638.

[91] Benjamin Horowitz and Uroš Seljak. Cosmological constraints from thermal Sunyaev Zeldovich power spectrum revisited. 2016.

[92] G. Hurier, J.F. Macias-Perez, and S.R. Hildebrandt. MILCA, a modified internal linear combination algorithm to extract astrophysical emissions from multifrequency sky maps. *Astronomy and Astrophysics - A&A*, 558:A118, 2013. doi: 10.1051/0004-6361/201321891. URL http://hal.in2p3.fr/in2p3-00498624. 8 pages.

[93] Dragan Huterer et al. Growth of Cosmic Structure: Probing Dark Energy Beyond Expansion. *Astropart. Phys.*, 63:23–41, 2015. doi: 10.1016/j.astropartphys.2014.07.004.

[94] Tim Johannsen. Sgr A* and General Relativity. *Class. Quant. Grav.*, 33(11):113001, 2016. doi: 10.1088/0264-9381/33/11/113001.

[95] Michael D. Johnson et al. Resolved Magnetic-Field Structure and Variability Near the Event Horizon of Sagittarius A*. *Science*, 350(6265):1242–1245, 2015. doi: 10.1126/science.aac7087.

[96] C. Kiefer. *Quantum Gravity*. International Series of Monographs on Physics. OUP Oxford, 2007. ISBN 9780199212521. URL https://books.google.fr/books?id=zLDRIqgjrW4C.

[97] Martin Kilbinger. Cosmology with cosmic shear observations: a review. *Rept. Prog. Phys.*, 78: 086901, 2015. doi: 10.1088/0034-4885/78/8/086901.

[98] Martin Kilbinger, Catherine Heymans, Marika Asgari, Shahab Joudaki, Peter Schneider, Patrick Simon, Ludovic Van Waerbeke, Joachim Harnois-Déraps, Hendrik Hildebrandt, Fabian Köhlinger, Konrad Kuijken, and Massimo Viola. Precision calculations of the cosmic shear power spectrum projection. 02 2017. URL https://arxiv.org/abs/1702.05301.

[99] E. Komatsu, K. M. Smith, J. Dunkley, C. L. Bennett, B. Gold, G. Hinshaw, N. Jarosik, D. Larson, M. R. Nolta, L. Page, D. N. Spergel, M. Halpern, R. S. Hill, A. Kogut, M. Limon, S. S. Meyer, N. Odegard, G. S. Tucker, J. L. Weiland, E. Wollack, and E. L. Wright. Seven-year Wilkinson Microwave Anisotropy Probe (WMAP) Observations: Cosmological Interpretation. *Astrophys. J. Suppl.*, 192:18, February 2011. doi: 10.1088/0067-0049/192/2/18.

[100] E. Komatsu et al. Five-Year Wilkinson Microwave Anisotropy Probe (WMAP) Observations: Cosmological Interpretation. *Astrophys. J. Suppl.*, 180:330–376, 2009. doi: 10.1088/0067-0049/180/2/330.

[101] Eiichiro Komatsu and Uros Seljak. The Sunyaev-Zel'dovich angular power spectrum as a probe of cosmological parameters. *Mon. Not. Roy. Astron. Soc.*, 336:1256, 2002. doi: 10.1046/j.1365-8711.2002.05889.x.

[102] Martin Kunz. The phenomenological approach to modeling the dark energy. *Comptes Rendus Physique*, 13:539–565, 2012. doi: 10.1016/j.crhy.2012.04.007.

[103] Martin Kunz and Domenico Sapone. Dark Energy versus Modified Gravity. *Phys. Rev. Lett.*, 98:121301, 2007. doi: 10.1103/PhysRevLett.98.121301.

[104] D. Langlois, S. Renaux-Petel, D.A. Steer, and T. Tanaka. Primordial Fluctuations and Non-Gaussianities in Multifield Dirac-Born-Infeld Inflation. *Physical Review Letters*, 101: 061301, August 2008. doi: 10.1103/PhysRevLett.101.061301. URL http://hal.in2p3.fr/in2p3-00294691. 4 pages.

[105] J. Lesgourgues. The Cosmic Linear Anisotropy Solving System (CLASS) I: Overview. *ArXiv e-prints*, April 2011.

[106] Julien Lesgourgues. Cosmological Perturbations. In *Proceedings, Theoretical Advanced Study Institute in Elementary Particle Physics: Searching for New Physics at Small and Large Scales (TASI 2012): Boulder, Colorado, June 4-29, 2012*, pages 29–97, 2013. doi: 10.1142/9789814525220_0002. URL https://inspirehep.net/record/1220222/files/arXiv:1302.4640.pdf.

[107] Antony Lewis. Efficient sampling of fast and slow cosmological parameters. *Phys. Rev.*, D87(10): 103529, 2013. doi: 10.1103/PhysRevD.87.103529.

[108] Antony Lewis and Anthony Challinor. Weak gravitational lensing of the cmb. *Phys. Rept.*, 429: 1–65, 2006. doi: 10.1016/j.physrep.2006.03.002.

[109] Andrew R Liddle and Samuel M Leach. How long before the end of inflation were observable perturbations produced? *Phys. Rev.*, D68:103503, 2003. doi: 10.1103/PhysRevD.68.103503.

[110] Linda Linsefors and Aurelien Barrau. Duration of inflation and conditions at the bounce as a prediction of effective isotropic loop quantum cosmology. *Phys. Rev.*, D87(12):123509, 2013. doi: 10.1103/PhysRevD.87.123509.

[111] Hongguang Liu, Karim Noui, Edward Wilson-Ewing, and David Langlois. Effective loop quantum cosmology as a higher-derivative scalar-tensor theory. 2017.

[112] LSST Science Collaboration, P. A. Abell, J. Allison, S. F. Anderson, J. R. Andrew, J. R. P. Angel, L. Armus, D. Arnett, S. J. Asztalos, T. S. Axelrod, and et al. LSST Science Book, Version 2.0. *ArXiv e-prints*, December 2009.

[113] Chung-Pei Ma and Edmund Bertschinger. Cosmological perturbation theory in the synchronous and conformal Newtonian gauges. *Astrophys. J.*, 455:7–25, 1995. doi: 10.1086/176550.

[114] Elisabetta Majerotto et al. Probing deviations from General Relativity with the Euclid spectroscopic survey. *Mon. Not. Roy. Astron. Soc.*, 424:1392–1408, 2012. doi: 10.1111/j.1365-2966.2012.21323.x.

[115] Juan Martin Maldacena. The Large N limit of superconformal field theories and supergravity. *Int. J. Theor. Phys.*, 38:1113–1133, 1999. doi: 10.1023/A:1026654312961. [Adv. Theor. Math. Phys.2,231(1998)].

[116] Killian Martineau, Aurélien Barrau, and Susanne Schander. Detailed investigation of the duration of inflation in loop quantum cosmology for a Bianchi-I universe with different inflaton potentials and initial conditions. *Phys. Rev.*, D95(8):083507, 2017. doi: 10.1103/PhysRevD.95.083507.

[117] Pawel O. Mazur and Emil Mottola. Gravitational condensate stars: An alternative to black holes. 2001.

[118] Krzysztof A. Meissner. Black hole entropy in loop quantum gravity. *Class. Quant. Grav.*, 21: 5245–5252, 2004. doi: 10.1088/0264-9381/21/22/015.

[119] Jakub Mielczarek. Signature change in loop quantum cosmology. *Springer Proc. Phys.*, 157: 555–562, 2014. doi: 10.1007/978-3-319-06761-2_77.

[120] M. Milgrom. A modification of the Newtonian dynamics as a possible alternative to the hidden mass hypothesis. *Astrophys. J.*, 270:365–370, July 1983. doi: 10.1086/161130.

[121] L. Miller, C. Heymans, T. D. Kitching, L. van Waerbeke, T. Erben, H. Hildebrandt, H. Hoekstra, Y. Mellier, B. T. P. Rowe, J. Coupon, J. P. Dietrich, L. Fu, J. Harnois-Déraps, M. J. Hudson, M. Kilbinger, K. Kuijken, T. Schrabback, E. Semboloni, S. Vafaei, and M. Velander. Bayesian galaxy shape measurement for weak lensing surveys - III. Application to the Canada-France-Hawaii Telescope Lensing Survey. *Mon. Not. Roy. Astron. Soc.*, 429:2858–2880, March 2013. doi: 10.1093/mnras/sts454.

[122] C.W. Misner, K.S. Thorne, and J.A. Wheeler. *Gravitation*. Number ptie. 3 in Gravitation. W. H. Freeman, 1973. ISBN 9780716703440. URL https://books.google.fr/books?id=w4Gigq3tY1kC.

[123] Viatcheslav F. Mukhanov and G. V. Chibisov. Quantum Fluctuations and a Nonsingular Universe. *JETP Lett.*, 33:532–535, 1981. [Pisma Zh. Eksp. Teor. Fiz.33,549(1981)].

[124] Pia Mukherjee, Martin Kunz, David Parkinson, and Yun Wang. Planck priors for dark energy surveys. *Phys. Rev.*, D78:083529, 2008. doi: 10.1103/PhysRevD.78.083529.

[125] Yoichiro Nambu. Quasi-particles and gauge invariance in the theory of superconductivity. *Phys. Rev.*, 117:648–663, Feb 1960. doi: 10.1103/PhysRev.117.648. URL http://link.aps.org/doi/10.1103/PhysRev.117.648.

[126] Stefan Nobbenhuis. Categorizing different approaches to the cosmological constant problem. *Found. Phys.*, 36:613–680, 2006. doi: 10.1007/s10701-005-9042-8.

[127] Stefan Nobbenhuis. *The Cosmological Constant Problem, an Inspiration for New Physics*. PhD thesis, Utrecht U., 2006. URL https://inspirehep.net/record/725276/files/Thesis_1977_Nobbenhuis.pdf.

[128] Akira Oka, Shun Saito, Takahiro Nishimichi, Atsushi Taruya, and Kazuhiro Yamamoto. Simultaneous constraints on the growth of structure and cosmic expansion from the multipole power spectra of the SDSS DR7 LRG sample. *Mon. Not. Roy. Astron. Soc.*, 439:2515–2530, 2014. doi: 10.1093/mnras/stu111.

[129] D. Parkinson, S. Riemer-Sørensen, C. Blake, G. B. Poole, T. M. Davis, S. Brough, M. Colless, C. Contreras, W. Couch, S. Croom, D. Croton, M. J. Drinkwater, K. Forster, D. Gilbank, M. Gladders, K. Glazebrook, B. Jelliffe, R. J. Jurek, I.-h. Li, B. Madore, D. C. Martin, K. Pimbblet, M. Pracy, R. Sharp, E. Wisnioski, D. Woods, T. K. Wyder, and H. K. C. Yee. The WiggleZ Dark Energy Survey: Final data release and cosmological results. *Phys. Rev. D*, 86(10):103518, November 2012. doi: 10.1103/PhysRevD.86.103518.

[130] S. Perlmutter et al. Measurements of Omega and Lambda from 42 high redshift supernovae. *Astrophys. J.*, 517:565–586, 1999. doi: 10.1086/307221.

[131] Patrick Peter and Sandro D. P. Vitenti. The simplest possible bouncing quantum cosmological model. *Mod. Phys. Lett.*, A31(21):1640006, 2016. doi: 10.1142/S021773231640006X.

[132] Patrick Peter, Emanuel J. C. Pinho, and Nelson Pinto-Neto. A Non inflationary model with scale invariant cosmological perturbations. *Phys. Rev.*, D75:023516, 2007. doi: 10.1103/PhysRevD.75.023516.

[133] Planck Collaboration, P. A. R. Ade, N. Aghanim, M. Arnaud, M. Ashdown, F. Atrio-Barandela, J. Aumont, C. Baccigalupi, A. Balbi, A. J. Banday, and et al. Planck intermediate results. V. Pressure profiles of galaxy clusters from the Sunyaev-Zeldovich effect. *Astron. Astrophys.*, 550: A131, February 2013. doi: 10.1051/0004-6361/201220040.

[134] Planck Collaboration, P. A. R. Ade, N. Aghanim, M. Arnaud, M. Ashdown, J. Aumont, C. Baccigalupi, A. J. Banday, R. B. Barreiro, J. G. Bartlett, and et al. Planck 2015 results. XII. Full focal plane simulations. , 594:A12, September 2016. doi: 10.1051/0004-6361/201527103.

[135] Lisa Randall and Raman Sundrum. An Alternative to compactification. *Phys. Rev. Lett.*, 83: 4690–4693, 1999. doi: 10.1103/PhysRevLett.83.4690.

[136] M. Remazeilles, J. Delabrouille, and J.-F. Cardoso. CMB and SZ effect separation with constrained Internal Linear Combinations. *mnras*, 410:2481–2487, February 2011. doi: 10.1111/j.1365-2966.2010.17624.x.

[137] Adam G. Riess et al. Observational evidence from supernovae for an accelerating universe and a cosmological constant. *Astron. J.*, 116:1009–1038, 1998. doi: 10.1086/300499.

[138] Carlo Rovelli and Lee Smolin. Discreteness of area and volume in quantum gravity. *Nucl. Phys.*, B442:593–622, 1995. doi: 10.1016/0550-3213(95)00150-Q,10.1016/0550-3213(95)00550-5. [Erratum: Nucl. Phys.B456,753(1995)].

[139] Lado Samushia et al. The clustering of galaxies in the SDSS-III Baryon Oscillation Spectroscopic Survey: measuring growth rate and geometry with anisotropic clustering. *Mon. Not. Roy. Astron. Soc.*, 439(4):3504–3519, 2014. doi: 10.1093/mnras/stu197.

[140] Siddharth Satpathy et al. The clustering of galaxies in the completed SDSS-III Baryon Oscillation Spectroscopic Survey: On the measurement of growth rate using galaxy correlation functions. *Submitted to: Mon. Not. Roy. Astron. Soc.*, 2016.

[141] Xun Shi and Eiichiro Komatsu. Analytical model for non-thermal pressure in galaxy clusters. *Mon. Not. Roy. Astron. Soc.*, 442(1):521–532, 2014. doi: 10.1093/mnras/stu858.

[142] R. E. Smith, J. A. Peacock, A. Jenkins, S. D. M. White, C. S. Frenk, F. R. Pearce, P. A. Thomas, G. Efstathiou, and H. M. P. Couchmann. Stable clustering, the halo model and nonlinear cosmological power spectra. *Mon. Not. Roy. Astron. Soc.*, 341:1311, 2003. doi: 10.1046/j.1365-8711.2003.06503.x.

[143] Lee Smolin. MOND as a regime of quantum gravity. 2017.

[144] Yong-Seon Song and Will J. Percival. Reconstructing the history of structure formation using Redshift Distortions. *JCAP*, 0910:004, 2009. doi: 10.1088/1475-7516/2009/10/004.

[145] Alexei A. Starobinsky. A New Type of Isotropic Cosmological Models Without Singularity. *Phys. Lett.*, B91:99–102, 1980. doi: 10.1016/0370-2693(80)90670-X.

[146] R. A. Sunyaev and Y. B. Zeldovich. The Observations of Relic Radiation as a Test of the Nature of X-Ray Radiation from the Clusters of Galaxies. *Comments on Astrophysics and Space Physics*, 4:173, November 1972.

[147] Ryuichi Takahashi, Masanori Sato, Takahiro Nishimichi, Atsushi Taruya, and Masamune Oguri. Revising the Halofit Model for the Nonlinear Matter Power Spectrum. *Astrophys. J.*, 761:152, 2012. doi: 10.1088/0004-637X/761/2/152.

[148] Max Tegmark et al. Cosmological parameters from SDSS and WMAP. *Phys. Rev.*, D69:103501, 2004. doi: 10.1103/PhysRevD.69.103501.

[149] J. L. Tinker, B. E. Robertson, A. V. Kravtsov, A. Klypin, M. S. Warren, G. Yepes, and S. Gottlöber. The Large-scale Bias of Dark Matter Halos: Numerical Calibration and Model Tests. *Astrophys. J.*, 724:878–886, December 2010. doi: 10.1088/0004-637X/724/2/878.

[150] Jeremy L. Tinker, Andrey V. Kravtsov, Anatoly Klypin, Kevork Abazajian, Michael S. Warren, Gustavo Yepes, Stefan Gottlober, and Daniel E. Holz. Toward a halo mass function for precision cosmology: The Limits of universality. *Astrophys. J.*, 688:709–728, 2008. doi: 10.1086/591439.

[151] M. Tristram, J. F. Macias-Perez, C. Renault, and D. Santos. Xspect, estimation of the angular power spectrum by computing cross power spectra. *Mon. Not. Roy. Astron. Soc.*, 358:833, 2005. doi: 10.1111/j.1365-2966.2005.08760.x.

[152] Shinji Tsujikawa. Quintessence: A Review. *Class. Quant. Grav.*, 30:214003, 2013. doi: 10.1088/0264-9381/30/21/214003.

[153] Jaakko Vainio and Iiro Vilja. f(R) gravity constraints from gravitational waves. 2016.

[154] Anja von der Linden et al. Robust Weak-lensing Mass Calibration of Planck Galaxy Clusters. *Mon. Not. Roy. Astron. Soc.*, 443(3):1973–1978, 2014. doi: 10.1093/mnras/stu1423.

[155] B. Wang, E. Abdalla, F. Atrio-Barandela, and D. Pavon. Dark Matter and Dark Energy Interactions: Theoretical Challenges, Cosmological Implications and Observational Signatures. *Rept. Prog. Phys.*, 79(9):096901, 2016. doi: 10.1088/0034-4885/79/9/096901.

[156] Qingdi Wang, Zhen Zhu, and William G. Unruh. How the huge energy of quantum vacuum gravitates to drive the slow accelerating expansion of the Universe. *Phys. Rev.*, D95(10):103504, 2017. doi: 10.1103/PhysRevD.95.103504.

[157] Yun Wang and Mi Dai. Exploring uncertainties in dark energy constraints using current observational data with Planck 2015 distance priors. *Phys. Rev.*, D94(8):083521, 2016. doi: 10.1103/PhysRevD.94.083521.

[158] J. A. Wheeler. Geons. *Phys. Rev.*, 97:511–536, 1955. doi: 10.1103/PhysRev.97.511.

[159] Edward Wilson-Ewing. Testing loop quantum cosmology. 2016.

[160] Hans A. Winther et al. Modified Gravity N-body Code Comparison Project. *Mon. Not. Roy. Astron. Soc.*, 454(4):4208–4234, 2015. doi: 10.1093/mnras/stv2253.

[161] Ya B Zel'dovich. The cosmological constant and the theory of elementary particles. *Soviet Physics Uspekhi*, 11(3):381, 1968. URL http://stacks.iop.org/0038-5670/11/i=3/a=A13.

[162] Miguel Zumalacárregui, Emilio Bellini, Ignacy Sawicki, and Julien Lesgourgues. hiclass: Horndeski in the Cosmic Linear Anisotropy Solving System. 2016.